Oxidative Medicine and Cellular Longevity

Modulation of Oxidative Stress: Pharmaceutical and Pharmacological Aspects 2018

Lead Guest Editor: Luciano Saso
Guest Editors: Tomris Ozben and Robert Smith

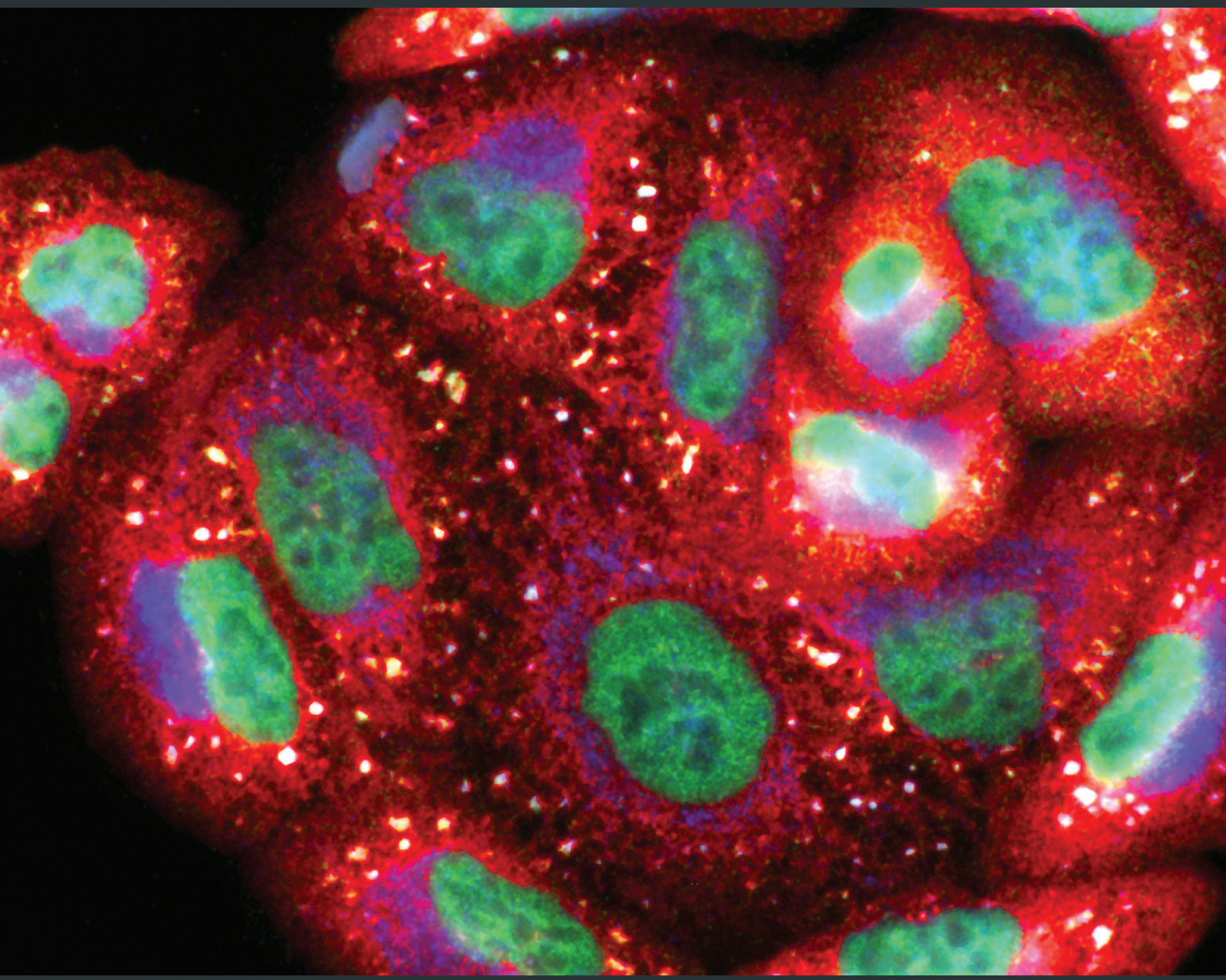

Modulation of Oxidative Stress: Pharmaceutical and Pharmacological Aspects 2018

Oxidative Medicine and Cellular Longevity

Modulation of Oxidative Stress: Pharmaceutical and Pharmacological Aspects 2018

Lead Guest Editor: Luciano Saso
Guest Editors: Tomris Ozben and Robert Smith

Editorial Board

Contents

Hindawi
Oxidative Medicine and Cellular Longevity
Volume 2019, Article ID 6380473, 3 pages
https://doi.org/10.1155/2019/6380473

Editorial

Modulation of Oxidative Stress: Pharmaceutical and Pharmacological Aspects 2018

Robert E. Smith,[1] **Tomris Ozben**,[2] **and Luciano Saso**[3]

[1]*Park University, 8700 River Park Drive, Parkville, MO 64152, USA*
[2]*Department of Biochemistry, Akdeniz University Medical Faculty Campus, Dumlupinar Street, 07070 Antalya, Turkey*
[3]*Department of Physiology and Pharmacology "Vittorio Erspamer", Sapienza University of Rome, Piazzale Aldo Moro 5, 00185 Rome, Italy*

Correspondence should be addressed to Robert E. Smith; robert.smith@fda.hhs.gov

Received 5 June 2019; Accepted 9 June 2019; Published 3 July 2019

Chronic, low-grade, smoldering inflammation (also called parainflammation) can lead to cardiovascular and neurodegenerative diseases, as well as many types of cancer [1]. It can be caused by obesity, metabolic syndrome, and even periodontal disease. One of the articles in this special issue tells how adding antioxidants to dental materials can help to prevent oxidative stress in gingival fluid ("Influence of Dental Restorations on Oxidative Stress in Gingival Crevicular Fluid" (E. Taso et al.)).

Still, inflammation has been one of the most misunderstood aspects of health when viewed with reductionist thinking [1, 2]. Part of the misunderstanding was based on the assumption that the effects of inflammation on model organisms such as baker's yeast (*Saccharomyces cerevisiae*), the fruit fly *Drosophila melanogaster*, mice, rats, and dogs can tell us what also happens in humans. That is, caloric restriction without starvation has extended the lifespans of these organisms. It was thought that restricting the consumption of calories by reducing the consumption of proteins, fats, and carbohydrates reduced the total metabolic rate and the production of reactive oxygen and nitrogen species (RONS) and free radicals. This led to the free radical theory of aging, in which it was proposed that the accumulation of damage caused by free radicals causes aging and eventually death. Note that most authors use the term ROS (reactive oxygen species), instead of RONS. Still, some ROS or RONS (like nitric oxide or NO) have a reactive nitrogen, rather than a reactive oxygen. This free radical theory encouraged people to eat foods that have a high antioxidant capacity. So, *in vitro* tests for total antioxidant capacity emerged. They were based on measuring the destruction of oxidized test compounds by reacting directly with the antioxidants in foods [1, 2].

However, as scientists and physicians learned more about human nutrition, they realized that the caloric restriction that worked for other organisms did not work for humans [1, 2]. This required changing the paradigm from reductionist thinking to systems thinking. It is important to use systems thinking and realize that inflammation can be not just a cause or a symptom of many diseases, but it is also essential for good health. Inflammation, like so much else in the body, must be carefully controlled [1, 2].

Even though vitamins A and C as well as CoQ10 can react directly with RONS and destroy them, other antioxidants seldom do this [1, 2]. Most antioxidants (especially phenolic compounds) do not work by reacting directly with RONS and free radicals. They exert their health effects by first activating the transcription factor nuclear erythroid 2 like factor-2 (Nrf2), which then induces the transcription of endogenous antioxidant response elements (AREs). Nrf2 controls the expression of AREs by binding to their promoter regions. The combined system is called the Nrf2/ARE antioxidant signaling system [1, 2].

The Nrf2/ARE signaling system can prevent cardiovascular disease (CVD) by preventing smoldering inflammation [1–3]. It also helps prevent neurodegenerative diseases and limit the damage caused by ischemia during a stroke. One of the articles in this issue ("C_{60} Fullerene Prevents Restraint

Stress-Induced Oxidative Disorders in Rat Tissues: Possible Involvement of the Nrf2/ARE-Antioxidant Pathway" (O. O. Gonchar et al.)) describes how a type of fullerene (also known as Buckminsterfullerenes and Buckyballs) containing 60 carbons (C_{60} fullerene) can prevent stress-induced oxidative disorders by activating the Nrf2/ARE antioxidant system. It is interesting to note that C_{60} fullerene has two opposite properties regarding RONS or ROS [4]. When exposed to visible light, it can produce ROS, making it suitable for photodynamic therapy. It can also downregulate the production of ROS in cells, making a neuroprotective agent. It can also be used as a drug delivery system. In one system, C_{60} fullerene was conjugated with the popular and effective anticancer drug, doxorubicin. C_{60} fullerene is used for targeted drug delivery to reduce the cardiomyopathy that occurs frequently when doxorubicin is used without C_{60} fullerene. It also breaks links that are sensitive to ROS, enabling the release of doxorubicin into cancer cells [4].

A completely different substance, uric acid, was shown to protect against the deadly effects of oxidative stress caused by ischemia-reperfusion, as described in another article in this issue ("Uric Acid Protects against Focal Cerebral Ischemia/Reperfusion-Induced Oxidative Stress via Activating Nrf2 and Regulating Neurotrophic Factor Expression" (B. Ya et al.)). It provides this protection by activating the Nrf2/ARE system, which was already known to play a critical role in ischemic stroke [5].

Another article in this issue ("Modulation of Hippocampal Antioxidant Defense System in Chronically Stressed Rats by Lithium" (N. Popović et al.)) tells how a widely used drug to treat bipolar disorders (lithium) exerts its therapeutic effects, in part by increasing the activity of some of the enzymes that are activated by Nrf2. This reduces the oxidative stress in the hippocampus [5]. This adds another mechanism to the previously described ability of lithium to inhibit inositol monophosphatase and glycogen synthase kinase-3 [6, 7].

Oxidative stress is also prevalent in children suffering from autism spectrum disorder (ASD). It alters the shape of erythrocytes and reduces oxidative stress ("Oxidative Stress in Autistic Children Alters Erythrocyte Shape in the Absence of Quantitative Protein Alterations and of Loss of Membrane Phospholipid Asymmetry" (A. Bolotta et al.)). Oxidative stress is reduced due to the activity of the antioxidant enzyme peroxiredoxin-2 (Prx2), which is upregulated by Nrf2 [1–3].

Not only the brain but also the eyes can be affected by oxidative stress, as described in another article in this series ("Sodium Ferulate Attenuates Lidocaine-Induced Corneal Endothelial Impairment" (G. Jiang and T. Fan)). When lidocaine is used as an anesthetic in cataract surgery, it can cause corneal thickening, opacification, and loss of corneal endothelial cells. When sodium ferulate is included, the toxicity of lidocaine is reduced. Ferulate activates the Nrf2/ARE system [1–3].

Oxidative stress can also affect stem cells. Another article in this series ("Pharmacological Regulation of Oxidative Stress in Stem Cells" (J. Lee et al.)) describes how the redox state of a stem cell affects the balance between self-renewal and differentiation. Hematopoietic stem cells (HSCs) are adult stem cells that form blood cells that are needed to replace the ones that die. They stay in hypoxic niches in the bone marrow, which protects them from oxidative stress. As a result, they can maintain their ability to self-renew. HSCs need to be protected from excess ROS but need continuous ROS production at low levels to maintain their biological function. Since stem cells are also important in replacing damaged tissues in regenerative medicine, attempts are being made to regulate oxidative stress in them through pharmacology. There are radioprotective substances and drugs that can protect stem cells in the liver from injury due to the use of radiation therapy. Melatonin, alpha-lipoic acid, and conjugated 5-methoxytryptamine-α-lipoic acid decrease the concentration of ROS in hematopoietic cells by inhibiting NADPH oxidase 4 (NOX4), which is upregulated by the Nrf2/ARE system. There is also an FDA-approved prescription drug, amifostine, that is a ROS scavenger and radioprotective drug. In addition, cyclosporine A inhibits ROS production that is linked to cyclophilin D. This increased the yield of hematopoietic stem cells obtained from the bone marrow and cord blood.

Alpha-lipoic acid is a popular dietary supplement [8–10]. It is used to treat diabetic polyneuropathy, obesity, and related metabolic disorders, as well as to help prevent vascular disease, hypertension, and inflammation. When given in combination with L-carnosine, zinc, and B vitamins, alpha-lipoic acid improved fasting glucose and insulin resistance and decreased the level of glycosylated hemoglobin (Hb_{A1C}) [11]. However, in an article in this issue ("The Effect of 600 mg Alpha-lipoic Acid Supplementation on Oxidative Stress, Inflammation, and RAGE in Older Adults with Type 2 Diabetes Mellitus" (V. M. Mendoza-Núñez et al.)), alpha-lipoic acid by itself (at a dose of 600 mg/day for six months) did not have a significant antioxidant or anti-inflammatory effect.

Oxidative damage can also occur in the lungs, leading to respiratory diseases. One article in this series describes the role of the Nrf2/ARE system and compounds that activate it ("Role of Nrf2 and Its Activators in Respiratory Diseases" (Q. Liu et al.)). Activators of Nrf2 can help prevent bronchopulmonary dysplasia, respiratory infections, acute respiratory stress syndrome, chronic obstructive pulmonary disease (COPD), asthma, idiopathic pulmonary fibrosis, and lung cancer. Activated Nrf2 can also protect against infection by the respiratory syncytial virus (RSV), which decreases Nrf2 activity when the RSV is active. In addition, sulforaphane in broccoli, curcumin in turmeric, and epigallocatechin gallate (EGCG) in green tea can help to protect against damage that is done by infection by the influenza A virus.

The use of a tourniquet can cause damage due to ischemia-reperfusion. One of the articles in this issue ("The Possible Pathophysiological Outcomes and Mechanisms of Tourniquet-Induced Ischemia-Reperfusion Injury during Total Knee Arthroplasty" (P. Leurcharusmee et al.)) tells how a mixture of ischemic preconditioning, vitamin C, and propofol (a popular general anesthetic) protected against oxidative and inflammatory damage.

Infection by the hepatitis C virus leads to oxidative stress in the acute and persistent phases of infection, as described in

another article in this series ("Counteraction of HCV-Induced Oxidative Stress Concurs to Establish Chronic Infection in Liver Cell Cultures" (S. Anticoli et al.)). On the other hand, a reduced environment emerges during the chronic phase of infection, as the concentration of ROS decreases and the activity of the antioxidant enzyme, glutathione reductase, increases.

In another article in this series, flavonoids from silymarin (a seed extract of *Silybum marianum* (L.) Gaertn.) were shown to increase systemic and hepatic bilirubin concentrations and lower lipoperoxidation in mice ("Isolated Silymarin Flavonoids Increase Systemic and Hepatic Bilirubin Concentrations and Lower Lipoperoxidation in Mice" (J. Ŝuk et al.)). Even though bilirubin (the end product of heme catabolism) has been thought of as primarily a toxic catabolite and a sign of liver dysfunction, it is a potent antioxidant that has anti-inflammatory, antiproliferative, antigenotoxic, and antiaging properties. Bilirubin is also an agonist of the peroxisome proliferator-activated receptor-α (PPARα), a master regulator of lipid metabolism that inhibits the development of atherosclerosis, plaque rupture, and thrombus formation [12].

In another article in this series, a new potential antitumor agent and coumarin derivative was synthesized and characterized ("Synthesis and Characterization of 3-(1-((3,4-Dihydroxyphenethyl)amino)ethylidene)-chroman-2,4-dione as a Potential Antitumor Agent" (D. S. Dimić et al.)). It was active against carcinoma cell lines, especially the MCF7 breast carcinoma.

In conclusion, this issue contains a variety of articles about the pharmaceutical and pharmacological aspects of the modulation of oxidative stress.

Conflicts of Interest

The guest editors declare that they have no conflict of interest regarding the publication of this special issue.

Robert E. Smith
Tomris Ozben
Luciano Saso

References

[1] R. E. Smith, *Systems Thinking in Medicine and New Drug Discovery Volume Two*, Cambridge Scholars Publishing, Newcastle upon Tyne, 2018.

[2] R. E. Smith, "The effects of dietary supplements that overactivate the Nrf2/ARE system," *Current Medicinal Chemistry*, vol. 26, 2019print.

[3] R. E. Smith, K. Tran, C. C. Smith, M. McDonald, P. Shejwalker, and K. Hara, "The role of the Nrf2/ARE antioxidant system in preventing cardiovascular diseases," *Diseases*, vol. 4, no. 4, p. 34, 2016.

[4] H. Kazemzadeh and M. Mozafari, "Fullerene-based delivery systems," *Drug Discovery Today*, vol. 24, no. 3, pp. 898–905, 2019.

[5] L. Liu, L. M. Locascio, and S. Doré, "Critical role of Nrf2 in experimental ischemic stroke," *Frontiers in Pharmacology*, vol. 10, no. 153, p. 31, 2019.

[6] W. R. Sherman, A. L. Leavitt, M. P. Honchar, L. M. Hallcher, and B. E. Phillips, "Evidence that lithium alters phosphoinositide metabolism: chronic administration elevates primarily D-*myo*-inositol-1-phosphate in cerebral cortex of the rat," *Journal of Neurochemistry*, vol. 36, no. 6, pp. 1947–1951, 1981.

[7] A. Saiardi and A. W. Mudge, "Lithium and fluoxetine regulate the rate of phosphoinositide synthesis in neurons: a new view of their mechanisms of action in bipolar disorder," *Translational Psychiatry*, vol. 8, no. 1, p. 175, 2018.

[8] A. E. Huerta, M. Fernández-Galilia, P. L. Prieto-Hontoria, J. A. Martínez, and M. J. Moreno-Aliaga, "Alpha-lipoic acid: a dietary supplement with therapeutic potential for obesity and related metabolic disorders," in *Chapter 2.10 in Nonvitamin and Nonmineral Nutritional Supplements*, S. Mohammed and A. S. Silva, Eds., Academic Press, London, 2019.

[9] K. P. Shay, R. F. Moreau, E. J. Smith, A. R. Smith, and T. M. Hagen, "Alpha-lipoic acid as a dietary supplement: molecular mechanisms and therapeutic potential," *Biochimica et Biophysica Acta (BBA) - General Subjects*, vol. 1790, no. 10, pp. 1149–1160, 2009.

[10] N. Nguyen and J. K. Takemoto, "A case for alpha-lipoic acid as an alternative treatment for diabetic polyneuropathy," *Journal of Pharmacy & Pharmaceutical Sciences*, vol. 21, no. 1s, pp. 192–199s, 2018.

[11] G. Derosa, A. D'Angelo, D. Romano, and P. Maffioli, "A clinical trial about a food supplement containing α-lipoic acid on oxidative stress markers in type 2 diabetic patients," *International Journal of Molecular Sciences*, vol. 17, no. 11, article 1802, 2016.

[12] S. Li, B. Yang, Y. Du et al., "Targeting PPARα for the treatment and understanding of cardiovascular diseases," *Cellular Physiology and Biochemistry*, vol. 51, no. 6, pp. 2760–2775, 2018.

Hindawi
Oxidative Medicine and Cellular Longevity
Volume 2019, Article ID 3276958, 12 pages
https://doi.org/10.1155/2019/3276958

Research Article

The Effect of 600 mg Alpha-lipoic Acid Supplementation on Oxidative Stress, Inflammation, and RAGE in Older Adults with Type 2 Diabetes Mellitus

Víctor Manuel Mendoza-Núñez,[1] **Beatriz Isabel García-Martínez**,[1] **Juana Rosado-Pérez**,[1] **Edelmiro Santiago-Osorio**,[2] **José Pedraza-Chaverri**,[3] **and Vicente Jesús Hernández-Abad**[4]

[1]*Research Unit on Gerontology, FES Zaragoza, National Autonomous University of Mexico, Mexico City, Mexico*
[2]*Hematopoiesis and Leukemia Laboratory, Research Unit on Cell Differentiation and Cancer, FES Zaragoza, National Autonomous University of Mexico, Mexico City, Mexico*
[3]*Department of Biology, Faculty of Chemistry, National Autonomous University of Mexico (UNAM), Mexico City 04510, Mexico*
[4]*Pharmaceutical Research Laboratory, FES Zaragoza, National Autonomous University of Mexico, Mexico City, Mexico*

Correspondence should be addressed to Víctor Manuel Mendoza-Núñez; mendovic@unam.mx

Received 29 August 2018; Revised 22 November 2018; Accepted 26 May 2019; Published 12 June 2019

Guest Editor: Robert Smith

Alpha-lipoic acid (ALA) has been used as a dietary supplement at different doses in patients with diabetes mellitus type 2 (T2DM) due to its antioxidant, anti-inflammatory, and hypoglycemic effects. However, the reports on the effects of ALA are controversial. For this reason, the purpose of the present study was to determine the effect of 600 mg/day of ALA on the markers of oxidative stress (OxS) and inflammation and RAGE in older adults with T2DM. A quasiexperimental study was carried out with a sample of 135 sedentary subjects (98 women and 37 men) with a mean age of 64 ± 1 years, who all had T2DM. The sample was divided into three groups: (i) experimental group (EG) with 50 subjects, (ii) placebo group (PG) with 50 subjects, and control group (CG) with 35 subjects. We obtained the following measurements in all subjects (pre- and posttreatment): glycosylated hemoglobin (HbA1c), receptor for advanced glycation end products (RAGE), 8-isoprostane, superoxide dismutase (SOD), glutathione peroxidase (GPx), total antioxidant status (TAS), and inflammatory (CRP, TNF-α, IL-6, IL-8, and IL-10) markers. Regarding the effect of ALA on HbA1c, a decrease was observed in the EG (baseline 8.9 ± 0.2 vs. posttreatment 8.6 ± 0.3) and the PG (baseline 8.8 ± 0.2 vs. posttreatment 8.4 ± 0.3) compared to the CG (baseline 8.8 ± 0.3 vs. six months 9.1 ± 0.3) although the difference was not statistically significant ($p < 0.05$). There was a statistically significant decrease ($p < 0.05$) in the blood concentration of 8-isoprostane in the EG and PG with respect to the CG (EG: baseline 100 ± 3 vs. posttreatment 57 ± 3, PG: baseline 106 ± 7 vs. posttreatment 77 ± 5, and CG: baseline 94 ± 10 vs. six months 107 ± 11 pg/mL). Likewise, a statistically significant decrease ($p < 0.05$) in the concentration of the RAGE was found in the EG (baseline 1636 ± 88 vs. posttreatment 1144 ± 68) and the PG (baseline 1506 ± 97 vs. posttreatment 1016 ± 82) compared to CG (baseline 1407 ± 112 vs. six months 1506 ± 128). A statistically significant decrease was also observed in all markers of inflammation and in the activity of SOD and GPx in the CG with respect to the EG and PG. Our findings suggest that the administration of ALA at a dose of 600 mg/day for six months has a similar effect to that of placebo on oxidative stress, inflammation, and RAGE in older adults with T2DM. Therefore, higher doses of ALA should be tried to have this effect. This trial is registered with trial registration number ISRCTN13159380.

1. Introduction

Oxidative stress (OxS) is a biochemical imbalance that is propitiated by excessive production of reactive oxygen and nitrogen species, which provoke oxidative damage to biomolecules and cannot be counteracted by antioxidative systems. This is an important factor that contributes to aging and the development of several diseases, including type 2 diabetes mellitus (T2DM) [1, 2]. For several decades, it has been shown that OxS and the chronic inflammatory process are involved in the physiopathological mechanisms of T2DM [3]. In this sense, the chronic hyperglycemia that is present in T2DM activates several unusual metabolic pathways in organisms, such as the sorbitol pathway (or that of aldose reductase), nonenzymatic protein glycosylation, glucose autooxidation, modification of protein kinase C activity, pseudohypoxia, lipoprotein-altered metabolism, and cytokine-associated alteration. All these pathways generate reactive oxygen species (ROS) and, consequently, OxS [4]. Likewise, several studies have shown that aging and/or T2DM increases the synthesis and secretion of cytokines, such as interleukin 6 (IL-6), tumor necrosis factor-alpha (TNF-α), and free radicals. These are all recognized as factors that increase the risk of disease-related complications [4, 5]. In this regard, our research group showed that aging in the context of diabetes increases the production of OxS and causes inflammation [6].

For this reason, some therapeutic supplements have been proposed with antioxidant and anti-inflammatory properties, such as vitamins A, C, E; omega 3 and 6 fatty acids; coenzyme Q10; melatonin; and alpha-lipoic acid [7–9].

Alpha-lipoic acid (ALA) is an amphipathic substance, which is synthesized in the mitochondria of plants and animals from octanoic acid and cysteine as a sulfur donor through the reactions catalyzed by the enzyme lipoic acid synthase. The participation of ALA in oxidative metabolism is essential. [7] ALA chemically exists in two enantiomeric forms R and S although only the R isoform acts as a cofactor in the oxidant metabolism, since it binds through an amide bond to the amino group of the lysine residues. This allows it to form a lipoamide, which is a cofactor of the enzymes, pyruvate dehydrogenase and α-ketoglutarate dehydrogenase [10, 11].

Several studies have demonstrated the antioxidant, anti-inflammatory, and hypoglycemic properties of ALA [12–15]. Furthermore, ALA has been shown to have a positive effect on the OxS linked with aging [16]. For this reason, the aim of the present study was to determine the effect of 600 mg/day of ALA on some markers of OxS and inflammation and RAGE in older adults with T2DM.

2. Materials and Methods

2.1. Design and Subjects. A quasiexperimental study was carried out with a sample of 135 sedentary subjects (98 women and 37 men) with a mean age of 64 ± 1 years, who all had T2DM. The age range of the subjects was 60–74 years. All participants gave their written informed consent for the inclusion in the study. The investigation protocol was approved by the Ethics Committee of the Universidad Nacional Autónoma de México (UNAM) Zaragoza Campus (25/11/SO/3.4.3). It was also registered in International Standard Randomised Controlled Trial Number (ISRCTN13159380) [17]. We have used some protocols and standardized techniques by our research group [18].

2.2. Inclusion Criteria. All subjects were independent and had a medical diagnosis of type 2 diabetes mellitus for one to three years without complications or comorbidity and were under medical treatment in a public hospital: (i) body mass index < 35; (ii) medicines: all patients taking two tablets of glibenclamide/metformin (5/500 mg) per day as a hypoglycemic treatment and not taking antioxidant supplements (vitamins or minerals) nor anti-inflammatory drugs for at least 6 months prior to initiation of or during the study; (iii) habits: no smoking, no frequent alcoholic drinks (less than two drinks or beers per week), or no drug addictions (marijuana, cocaine and others) in the last three years; and (iv) sedentary: all participants who reported that they do not exercise regularly during the last year.

2.3. Study Sample. We invited 200 older adults who were under medical supervision for type 2 diabetes mellitus in a public hospital in Mexico City. In this regard, 47 did not meet the inclusion criteria and 18 did not agree to participate in the study, for the reason that they did not have time for the follow-up meetings every four weeks for the delivery of the medication, self-report of health status, registration of secondary reactions, and reinforcement for therapeutic adherence.

In Figure 1, we outlined the study. All participants were assigned to the following study groups: (i) the experimental group (EG) with 50 individuals, (ii) the placebo group (PG) also with 50 individuals, and the control group (CG) with only 35 individuals. The assignment of the EG and PG was randomized. EG received 600 mg of racemic alpha-lipoic acid (two capsules of 300 mg per day), PG received two capsules containing microcrystalline cellulose (295 mg) plus magnesium stearate (5 mg) of pharmaceutical presentation similar to that of the treatment, and CG did not receive any treatment. Alpha-lipoic acid and placebo capsules were manufactured by ProductosMedix®. Also, the control group (CG) with 35 subjects was added for the aim of assessing the placebo effect.

The medication contained in the treatment capsules provided by ProductosMedix® was analyzed by polarimetry, obtaining a specific rotation of 0° (the mixture contained 50 : 50 of R and S enantiomers).

The treatment was self-administered orally in a daily base. The EG and PG were instructed to record adverse reactions. We had the same personal contact with the three groups. All groups had a monthly meeting with the research team. In this meeting, the subjects were informed about a lifestyle conducive to successful aging (ageism, active aging, healthy aging, mental and social functioning, healthy feeding, physical exercise and aging, mild cognitive impairment, and depression). Likewise, the placebo and treatment groups

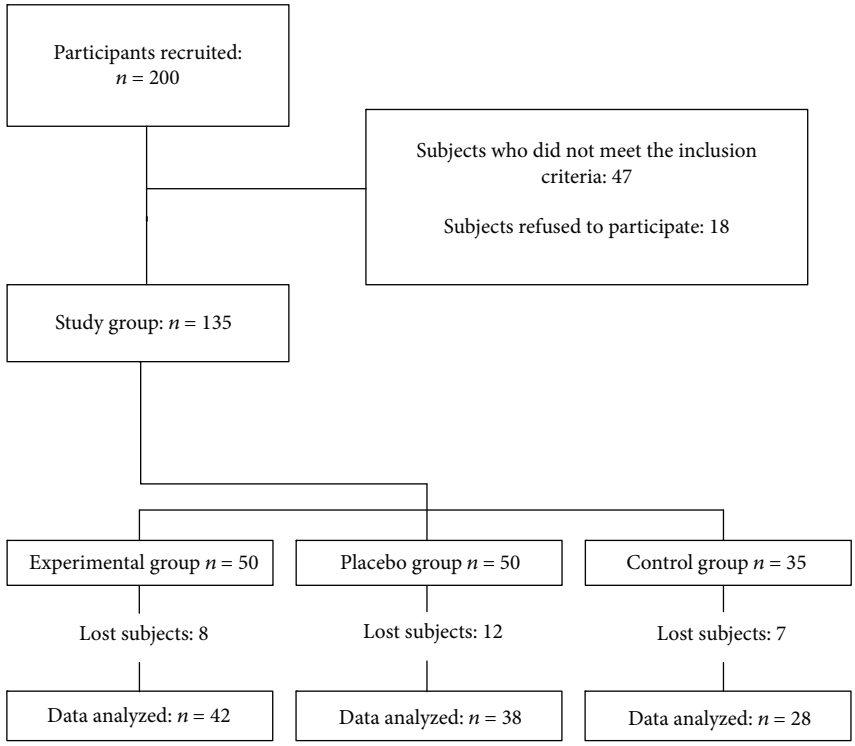

Figure 1: Outline of the study.

were informed about the antioxidant effects of alpha-lipoic acid (ALA).

The following measurements were performed in the three study groups: blood pressure, anthropometric measurements, glycosylated hemoglobin (HaA1c), biochemical parameters (lipid profile, glucose, albumin, and uric acid), blood concentration of 8-isoprostane, superoxide dismutase and glutathione peroxidase of red blood cells, inflammatory cytokines, receptor of advanced glycation end products (RAGE), and plasma concentration of ALA. All measurements were performed at baseline and after six months.

2.4. Dietary Intake. All participants were given a guide on the amount and type of food they could consume: recommended consumption of 2500 kcal per day. In this sense, all kilocalories of 50% carbohydrate consumption, 30% fat, and 20% protein were considered, in addition to an intake of 1500 mL of water. Regarding carbohydrates, the foods to be eaten per day were 3 tortillas/boiled rice or pasta and, regarding proteins, fish and chicken (daily) and red meats twice a week. Daily consumption of boiled and raw vegetables (chayote, broccoli, squash, green beans, and carrots) was recommended. The fruits allowed were papaya, melon, apple, oranges, guavas, strawberries, and grapes. The prohibited foods were all kinds of bread, soft drinks, sugar (natural and artificial sweeteners), and fruit juices or canned juices. Each month, they were insisted on the importance of following the guide of food consumption that was provided to them.

The caloric intake was measured by 24 h dietary total recall [19].

2.5. Anthropometric Measurements. The anthropometric measurements of weight, height, and waist circumference were obtained following a standardized protocol after recording the clinical history and conducting the physical examination. Weight was measured while the subject was wearing underwear and a hospital smock and was in a fasting state (after evacuation). A Torino® scale (Tecno Lógica Mexicana, Mexico City, Mexico), calibrated before each measurement, was used. Height was obtained with an aluminum cursor stadiometer graduated in millimeters. The subject was barefoot with the back and head in contact with the stadiometer in the Frankfurt horizontal plane. The body mass index (BMI) was calculated by dividing weight (kg) by height squared (m^2). Waist circumference (cm) was measured to the nearest 0.5 cm with a tape measure at the umbilical scar level [18].

2.6. Blood Pressure. Blood pressure (BP) was measured following the standardized protocol according to the Official Mexican Norm (Norma Official Mexicana) [20]. Using a mercurial manometer at both arms, BP was registered before the treatment (BP Baseline) and six months after (BP six months); measurements were taken in the morning in a fasted condition or 2 hours after breakfast in the sitting and standing positions. Subjects with pseudohypertension were identified by applying the Osler technique (feeling the radial pulse when the manometer registered values above the true systolic pressure). Blood pressure was taken by medical technicians who attended training sessions to standardize the procedures. The technicians were supervised to avoid possible biases in measurement.

2.7. Blood Sampling and Biochemical Analyses. Blood samples were collected before and after the treatment at six months in the three groups (EG, PG, and CG) by venipuncture after a 10 h fasting period and placed in vacutainer/siliconized test tubes without anticoagulant for biochemical determinations (glucose, urate, albumin, lipid profile, and inflammatory cytokines) and with heparin for glycosylated hemoglobin determination and oxidative stress tests.

Glucose, urate, albumin, cholesterol, triglycerides, and HDL-C concentration levels were determined using a Merck Vitalab Eclipse autoanalyzer (Merck, Dieren, The Netherlands). In particular, glucose levels were measured by the glucose oxidase method, and urate levels by the uricase colorimetric method. Albumin levels were measured with the bromocresol green technique.

The low-density lipoproteins (LDL cholesterol) were calculated by the Friedewald equation: LDL = total cholesterol – (triglycerides/5 + HDL)[21]. The C-reactive protein was measured in serum by immunoturbidimetric assay.

Glycosylated hemoglobin (HbA1c) was measured in a whole blood sample with an immunoturbidimetric assay with an automated Selectra Junior clinical chemistry analyzer.

High and normal control sera were included as quality controls (Randox Laboratories Ltd.). The intra- and interassay variation coefficients were less than 5% for all determinations.

2.8. Isoprostane Blood Concentration. 8-Isoprostane level was measured in plasma samples using ELISA (Cayman, USA) following the manufacturer's instructions (Catalog No. 516351). This assay is based on the competition between 8-isoprostane and an 8-isoprostane-acetylcholinesterase (AChE) conjugate (8-Isoprostane Tracer) for a limited number of 8-isoprostane-specific rabbit antiserum binding sites. Because the concentration of the 8-Isoprostane Tracer is held constant while the concentration of 8-isoprostane varies, the amount of the 8-Isoprostane Tracer that is able to bind to the rabbit antiserum will be inversely proportional to the concentration of 8-isoprostane in the well. This rabbit antiserum-8-isoprostane (either free or tracer) complex binds to the rabbit IgG mouse monoclonal antibody that has been previously attached to the well. The plate is washed to remove any unbound reagents, and then, Ellman's Reagent (which contains the substrate to AChE) is added to the well. The product of this enzymatic reaction has a distinct yellow color and absorbs strongly at 412 nm. The intensity of this color, determined spectrophotometrically, is proportional to the amount of 8-isoprostane.

2.9. Plasma Total Antioxidant Status. Plasma total antioxidant status levels were quantified using 2,2′-azino-bis(3-ethylbenzthiazoline-6-sulfonic acid) (ABTS) (Randox Laboratories Ltd.), which is incubated with a peroxidase to produce the radical cation $ABTS^+$. The bluish green staining of the $ABTS^+$ cation is relatively stable and measured at 600 nm; antioxidants present in the plasma cause the suppression of this color production to a degree that is proportional to the concentration. The kinetics reaction was measured with a Shimadzu UV-1601 spectrophotometer (Shimadzu, Kyoto, Japan).

2.10. Red Blood Cell Superoxide Dismutase. In this method, superoxide radicals are generated by employing xanthine and xanthine oxidase. The formed radical reacts with 2-(4-iodophenyl)-3-(4-nitrophenol)-5-phenyltetrazolium chloride to form a red formazan color, which is measured at 505 nm. The superoxide dismutase (SOD) in the sample causes the inhibition of this reaction; the SOD activity is proportional to the degree of inhibition of the reaction (Randox Laboratories Ltd.). Kinetics were measured with a Shimadzu UV-1601 spectrophotometer (Shimadzu Kyoto, Japan).

2.11. Red Blood Cell Glutathione Peroxidase. The glutathione peroxidase (GPx) catalyzes glutathione (GSH) oxidation by cumene hydroperoxide. In the presence of glutathione reductase (GR) and nicotinamide adenine dinucleotide phosphate (NADPH), oxidized GSH is immediately converted into the reduced form with a concomitant oxidation of NADPH to $NADP^+$ (Randox Laboratories Ltd.). The decrease in absorbance is measured at 340 nm; we used a Shimadzu UV-1601 spectrophotometer (Shimadzu).

We calculated the SOD/GPx ratio and the antioxidant gap (AOGAP) using the following equation: AOGAP = (TAS-[(albumin(mmol) × 0.69) + uric acid(mmol)]) [22]

2.12. Receptor for Advanced Glycation End Products (RAGE). RAGE concentrations were measured by RAGE (DRG00, Quantikine; R&D System Inc., Minneapolis, MN, USA) according to the manufacturer's protocol. For this assay, a monoclonal antibody for human RAGE is used, which has been bound to the bottom of each well. After the correct addition of reagents, standards, and samples, the RAGE-anti RAGE reaction occurs, and after the corresponding incubations and washings, the optical density of the complex formed is read in a microplate reader set at 450 nm. The RAGE concentration is directly proportional to the intensity of the color developed by the RAGE-substrate complex.

2.13. Inflammatory Cytokines and C-reactive Protein (CRP). Aliquots of serum sample were assayed by flow cytometry (CBA Kit, Human Inflammatory Cytokine, BD) to determine the levels of interleukin (IL)-1β, IL-6, IL-8, IL-10, and tumor necrosis factor-alpha (TNF-α) [23]. For the measurement of CRP, particles coated with anti-human CRP antibodies were used, which were agglutinated by CRP molecules present in the serum samples analyzed. Since the agglutination causes changes in the absorbance proportionally to the concentration of CRP and after comparison with a calibrator, it was possible to determine the exact concentration of the protein. The test was carried out on the Selectra Junior-automated equipment, under a turbidimetric principle, using a commercial kit from Spinreact (CRP TURBI 1107101L).

2.14. Measurement of ALA Plasma Concentration. ALA was quantified by high-performance liquid chromatography (HPLC) coupled to electrochemical detection. 1 mL of acetonitrile was added to each sample and centrifuged at 3000 rpm for 5 minutes to precipitate the proteins. The supernatant was separated and placed into a solid phase extraction cartridge (Hypersep, Thermo Scientific™). Then, the supernatant was washed with 3 mL of methanol followed by

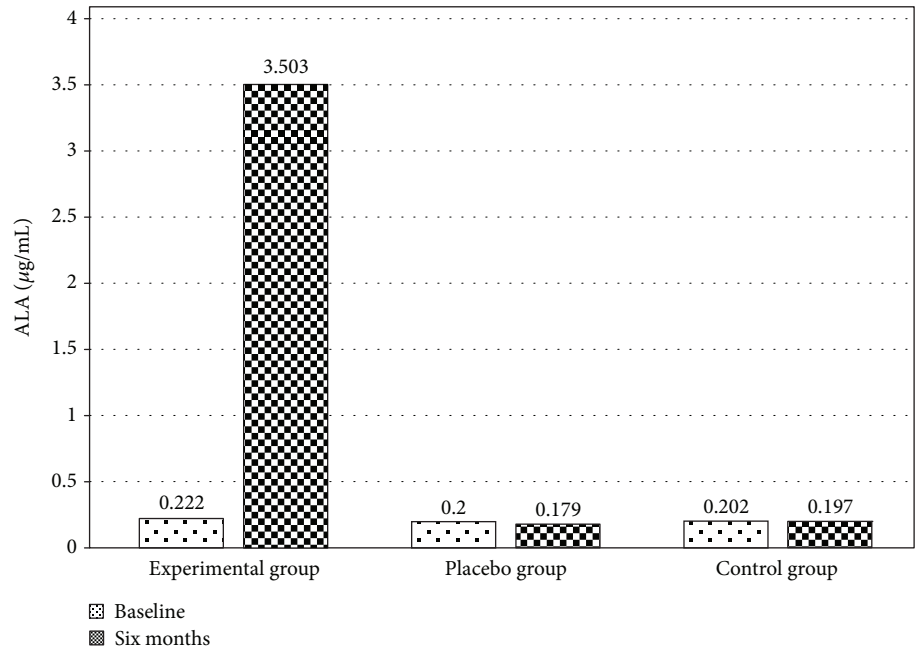

Figure 2: Plasma concentration of alpha-lipoic acid (ALA) before and after treatment in the study groups. A significant increase in the concentration of ALA was observed in the experimental group (before 0.222 ± 0.03 vs. after $3.503 \pm 0.2\mu$g/mL) compared to the placebo (before 0.2 ± 0.02 vs. after $0.179 \pm 0.03\mu$g/mL) and control groups (before 0.202 ± 0.04 vs. after $0.197 \pm 0.03\mu$g/mL). The values represent mean + standard error. Repeated measure analysis of variance. $p < 0.01$.

2 mL of acetate buffer solution (0.01 M, pH = 4). The eluate was collected into a clean tube and dried under nitrogen stream at room temperature. The residue was reconstituted with 1 mL of mobile phase (methanol/0.01 M acetate buffer (pH = 4) (60 : 40 *v*/*v*) and injected into the chromatograph (KnauerSmartline) coupled to an electrochemical detector (Recipe EC3000) in a direct current (DC) mode at the detector potential of 1000 mV under the following conditions: mobile phase pumped at a flow rate of 1 mL·min^{-1}, temperature of 25°C, and pressure of 1500 PSI. The chromatographic separation was carried out on a Hypersil Gold C18 column of 150 mm × 4.5 mm and 5 μm particle size (Thermo Scientific ™). A chromatogram to each sample was obtained, and the area under curve was calculated. Afterwards, all areas under the curve obtained from samples were interpolated in a standard curve to calculate ALA concentration [24].

2.15. Statistical Analysis. The statistical analysis of the data was done as follows: First, a descriptive analysis was performed to calculate the means and standard error (SE) of the outcomes over time. Second, a repeated measure multivariate analysis of variance was conducted to investigate the effects of the ALA on the changes of biochemical parameters, oxidative stress, and proinflammatory markers over time. The between-subject factor was each group (i.e., the experimental group versus the placebo and control groups), and the within-subject factor was time (baseline versus six months) [25], after Dunnett's post hoc test was done. Likewise, a correlation analysis between ALA concentration with oxidative stress and inflammation markers and RAGE was carried out. In the present study, the significance level (α) was set at <0.05 for all statistical analyses. We used the statistical analysis program IBM SPSS Statistics 20.0.

3. Results

3.1. ALA Plasma Concentration. Figure 2 shows the blood ALA concentration of the participants in the experimental group (EG) (baseline 0.222 ± 0.03 vs. posttreatment $3.503 \pm 0.2\mu$g/mL), placebo group (PG) (baseline 0.2 ± 0.02 vs. posttreatment $0.179 \pm 0.03\mu$g/mL), and control group (CG) (baseline 0.202 ± 0.04 vs. after six months $0.197 \pm 0.03\mu$g/mL). Statistically significant differences were observed in the EG with respect to PG and CG after the treatment ($p < 0.01$).

3.2. Caloric Intake, Anthropometric Measurements, and Blood Pressure. All subjects had a caloric intake between 3,000 and 3,500 kcal per day pre- and posttreatment, considering 50 to 60% of carbohydrates, 30 to 40% of fats, and 20 to 30% of proteins.

The data on the body mass index and blood pressure did not show statistically significant differences between the groups after six months of treatment ($p > 0.05$) (Table 1).

3.3. Biochemical Parameters. Regarding the biochemical parameters, a statistically significant increase was observed in the blood HDL concentration in the EG (baseline 48 ± 1 vs. posttreatment 54 ± 2 mg/dL) and PG (baseline 46 ± 2 vs. posttreatment 51 ± 2 mg/dL) compared to the CG (baseline 64 ± 2 vs. six months 58 ± 3 mg/dL; $p < 0.05$). We also found a statistically significant increase in the concentration of total cholesterol in the CG (baseline 198 ± 10 vs. six months

Table 1: Body mass index and blood pressure by the study group.

Variable	Experimental ($n = 42$)		Placebo ($n = 38$)		Control ($n = 28$)	
	Baseline	Posttreatment	Baseline	Posttreatment	Baseline	Six months
Age (years)	63 ± 1		64 ± 1		66 ± 1	
BMI (kg/m^2)	28.69 ± 0.64	28.32 ± 0.63	28.96 ± 1.03	28.83 ± 0.70	29.70 ± 0.98	29.44 ± 1.43
SBP (mmHg)	124 ± 3	126 ± 3	126 ± 3	127 ± 2	136 ± 3	136 ± 3
DBP (mmHg)	78 ± 2	77 ± 2	77 ± 2	77 ± 2	79 ± 2	81 ± 2

BMI: body mass index; SBP: systolic blood pressure; DBP: diastolic blood pressure. Repeated measure analysis of variance. $p > 0.05$.

Table 2: Biochemical parameters at baseline and posttreatment by the study group.

Variable	Experimental ($n = 42$)		Placebo ($n = 38$)		Control ($n = 28$)	
	Baseline	Posttreatment	Baseline	Posttreatment	Baseline	Six months
Hemoglobin (g/dL)	14.1 ± 0.3	13.8 ± 0.3	13.8 ± 0.3	13.6 ± 0.3	14.4 ± 0.3	14.7 ± 0.3
Hematocrit (%)	42 ± 1	41 ± 1	41 ± 1	40 ± 1	42 ± 1	42 ± 1
Glucose (mg/dL)	156 ± 9	147 ± 8	153 ± 7	145 ± 8	149 ± 12	159 ± 13
Urea (mg/dL)	35 ± 2	35 ± 2	34 ± 2	35 ± 2	35 ± 2	35 ± 2
Creatinine (mg/dL)	0.65 ± 0.02	0.78 ± 0.03	0.64 ± 0.02	0.82 ± 0.03	0.70 ± 0.06	0.59 ± 0.07
Uric acid (mg/dL)	4.4 ± 0.2	4.0 ± 0.2	4.8 ± 0.2	4.2 ± 0.2	4.1 ± 0.4	4.0 ± 0.2
Cholesterol (mg/dL)	180 ± 8	180 ± 9	176 ± 7	158 ± 8	198 ± 10	215 ± 8*
Triglycerides (mg/dL)	152 ± 12	145 ± 12	142 ± 11	155 ± 13	150 ± 15	161 ± 14
HDL-C (mg/dL)	48 ± 1	54 ± 2	46 ± 2	51 ± 2	64 ± 2	58 ± 3*
Albumin (g/dL)	4.6 ± 0.1	4.6 ± 0.1	4.5 ± 0.1	4.6 ± 0.1	4.5 ± 0.1	4.5 ± 0.1
HbA1c (%)	8.9 ± 0.2	8.6 ± 0.3	8.8 ± 0.2	8.4 ± 0.3	8.8 ± 0.3	9.1 ± 0.3

HDL-C: high-density lipoprotein cholesterol; HbA1c: glycosylated hemoglobin. The values represent mean + standard error. Repeated measure analysis of variance. Dunnett's post hoc test. *$p < 0.05$.

215 ± 8 mg/dL) compared to the EG (baseline 180 ± 8 vs. posttreatment 180 ± 9 mg/dL) and PG (baseline 176 ± 7 vs. posttreatment 158 ± 8 mg/dL) ($p < 0.05$). Regarding the effect of ALA on HbA1c, a decrease was observed in the EG (baseline 8.9 ± 0.2 vs. posttreatment 8.6 ± 0.3) and the PG (baseline 8.8 ± 0.2 vs. posttreatment 8.4 ± 0.3) compared to the CG (baseline 8.8 ± 0.3 vs. six months 9.1 ± 0.3) although the difference was not statistically significant ($p = 0.20$). There were no significant changes in the rest of the biochemical parameters (Table 2).

3.4. OxS Markers and RAGE. There was a statistically significant decrease ($p < 0.05$) in the blood concentration of 8-isoprostane in the EG and PG with respect to the CG (EG: baseline 100 ± 3 vs. posttreatment 57 ± 3, PG: baseline 106 ± 7 vs. posttreatment 77 ± 5, CG: baseline 94 ± 10 vs. six months 107 ± 11 pg/mL). We also observed a statistically significant decrease in the activity of SOD in the CG (baseline 182 ± 2 vs. six months 172 ± 1 IU/L, $p < 0.05$) compared to the EG (baseline 178 ± 1 vs. posttreatment 177 ± 1 IU/L) and PG (baseline 176 ± 1 vs. posttreatment 172 ± 1 IU/L). Likewise, there was a statistically significant decrease in the activity of the GPx in the CG (baseline 9531 ± 815 vs. six months 6223 ± 613 IU/L, $p < 0.05$) compared to the EG (baseline 8409 ± 507 vs. posttreatment 9694 ± 458 UI/L) and PG (baseline 8273 ± 575 vs. posttreatment 8691 ± 355 UI/L). Consequently, these changes were reflected in a statistically significant increase ($p < 0.05$) in the SOD/GPx ratio in the CG. Likewise, a statistically significant decrease ($p < 0.05$) in the concentration of the RAGE was found in the EG (baseline 1636 ± 88 vs. posttreatment 1144 ± 68) and the PG (baseline 1506 ± 97 vs. posttreatment 1016 ± 82) compared to CG (baseline 1407 ± 112 vs. six months 1506 ± 128). There were no statistically significant differences in TAS and AOGAP (Table 3).

3.5. Inflammatory Cytokines and CRP. The blood concentration of all the inflammatory cytokines measured (IL-1β, IL-6, IL-8, IL-10, and TNF-α) and CRP showed a statistically significant increase in CG after six months ($p < 0.05$) with respect to the EG and PG (Table 4).

3.6. Correlation between ALA and OxS Markers. A positive correlation was observed between the blood concentration of ALA with the activity of the SOD ($r = 0.279$, $p < 0.01$) and the GPx ($r = 0.249$, $p < 0.05$). Furthermore, the blood concentration of ALA had a negative correlation with the concentration of 8-isoprostane ($r = -0.247$, $p < 0.05$) (Table 5).

Table 3: Oxidative stress markers at baseline and posttreatment by the study group.

Markers	Experimental ($n = 42$)		Placebo ($n = 38$)		Control ($n = 28$)	
	Baseline	Posttreatment	Baseline	Posttreatment	Baseline	Six months
8-Isoprostane (pg/mL)	100 ± 3	57 ± 3	106 ± 7	77 ± 5	94 ± 10	107 ± 11*
SOD (UI/L)	178 ± 1	177 ± 1	176 ± 1	172 ± 1	182 ± 2	172 ± 1*
GPx (UI/L)	8409 ± 507	9694 ± 458	8273 ± 575	8691 ± 355	9531 ± 815	6223 ± 613*
TAS (μmol/L)	1045 ± 27	986 ± 24	1144 ± 34	951 ± 34	1107 ± 51	1060 ± 52
AOGAP (μmol/L)	796 ± 20	729 ± 21	843 ± 29	702 ± 27	978 ± 49	883 ± 58
SOD/GPx	0.024 ± 0.001	0.020 ± 0.001	0.026 ± 0.002	0.021 ± 0.001	0.026 ± 0.004	0.031 ± 0.002*
RAGE	1636 ± 88	1144 ± 68	1506 ± 97	1016 ± 82	1407 ± 112	1506 ± 128*

SOD: superoxide dismutase; GPx: glutathione peroxidase; TAS: total antioxidant status; AOGAP: antioxidant gap; SOD/GPx: SOD/GPx ratio; RAGE: receptor for advanced glycation end products; SE: standard error. Values are the means ± SE. Repeated measure analysis of variance. Dunnett's post hoc test. *$p < 0.05$.

Table 4: Inflammatory markers at baseline and posttreatment by the study group.

Markers	Experimental ($n = 42$)		Placebo ($n = 38$)		Control ($n = 28$)	
	Baseline	Posttreatment	Baseline	Posttreatment	Baseline	Six months
CRP (mg/dL)	0.26 ± 0.04	0.26 ± 0.04	0.25 ± 0.04	0.29 ± 0.05	0.25 ± 0.05	0.37 ± 0.06*
TNF-α (pg/mL)	6.56 ± 0.20	6.48 ± 0.20	6.62 ± 0.17	6.66 ± 0.16	7.99 ± 0.24	8.87 ± 0.25*
IL-10 (pg/mL)	3.31 ± 0.17	3.41 ± 0.19	3.07 ± 0.09	3.16 ± 0.05	2.96 ± 0.11	3.58 ± 0.10*
IL-6 (pg/mL)	5.07 ± 0.23	5.06 ± 0.21	5.27 ± 0.19	5.24 ± 0.31	5.17 ± 0.19	6.13 ± 0.17*
IL-1β (pg/mL)	9.46 ± 0.27	9.30 ± 0.18	9.51 ± 0.20	9.45 ± 0.12	9.78 ± 0.23	10.96 ± 0.20*
IL-8 (pg/mL)	16.20 ± 0.9	15.61 ± 1.0	17.20 ± 1.4	16.74 ± 1.2	15.5 ± 0.75	18.10 ± 1.57*

CRP: C-reactive protein; TNF-α: tumor necrosis factor-alpha; IL-10: interleukin 10; IL-6: interleukin 6; IL-1β: interleukin 1β; IL-8: interleukin 8; SE: standard error. Values are the means ± SE. Repeated measure analysis of variance. Dunnett's post hoc test. *$p < 0.05$.

3.7. Correlation between ALA and Inflammatory Markers. The blood concentration of ALA had a negative correlation with TNF-α ($r = -0.250$, $p < 0.05$), IL-6 ($r = -0.249$, $p < 0.05$), and IL-1β ($r = -0.329$, $p < 0.01$) (Table 6).

4. Discussion

Alpha-lipoic acid (ALA) is synthesized *de novo* in the body from fatty acid and cysteine in low quantities. Therefore, it is important to consume exogenous sources of ALA to have a therapeutic effect. In this regard, it has been shown that ALA is found abundantly in animal tissues, being located mainly in THE viscera, such as THE heart, liver, and kidneys. However, it is also found in high concentrations in vegetables, such as broccoli, spinach, tomatoes, peas, potatoes, and rice bran [26, 27]. However, to fully utilize its antioxidant, anti-inflammatory, and hypoglycemic properties, a racemic mixture available in capsules was prepared from a commercial product provided by ProductosMedix®. In this sense, it has been demonstrated that the gastrointestinal absorption of ALA depends on the timing of ingestion as there is a greater absorption of the compound if it is administered 30 minutes before or 2 hours after food intake. It has also been shown that the absorption of ALA is enantioselective since the R isoform is absorbed more efficiently than S [28–30].

Several studies have shown a therapeutic effect of ALA with doses of 300–1800 mg per day administered for three months up to four years. In this regard, we decided to administer 600 mg per day of ALA for six months in the present study, which took the evidence of effectiveness and safety for the elderly population into consideration [31–39].

Among the beneficial health effects of taking ALA supplements, it has been observed that the administration of ALA is capable of promoting the synthesis of nitric oxide. In this regard, it has been proposed that ALA stimulates the PI3K/Akt signaling pathway, with Akt being responsible for the phosphorylation and subsequent activation of eNOS (NO synthase), an enzyme that catalyzes the conversion of L-arginine and O_2 in citrulline with NO release [9]. This is a molecule that is responsible for regulating the elasticity of the walls of blood vessels and improving endothelial function, which results in a decrease in blood pressure. In addition, ALA reduces the levels of reactive oxygen species, which also favors endothelial function and subsequently lowers blood pressure [31]. However, no statistically significant differences were observed after treatment with ALA in our study. In this sense, our findings are similar to that reported in the systematic review published by Mohammadi et al., who found that the administration of ALA at doses of 300–1800 mg/day has no effect on arterial hypertension [40].

Table 5: Correlation between ALA, HbA1c, RAGE, and oxidative stress markers after six months.

	ALA	HbA1c	RAGE	SOD	GPx	TAS	AOGAP	SOD/GPx	8-ISOP
r									
ALA	1	0.084	-0.100	0.279	0.249	0.038	0.006	-0.180	-0.247
HbA1c		1.000	-0.020	-0.131	-0.041	0.017	0.061	-0.004	0.157
RAGE			1.000	-0.084	-0.302	-0.245	-0.069	0.290	-0.026
SOD				1.000	0.134	0.119	0.165	-0.076	-0.109
GPx					1.000	-0.060	-0.020	-0.828	-0.145
TAS						1.000	0.649	0.137	0.187
AOGAP							1.000	0.047	0.079
SOD/GPx								1.000	0.139
8-ISOP									1.000
p									
ALA		0.402	0.329	0.005	0.012	0.702	0.952	0.077	0.017
HbA1c			0.845	0.194	0.690	0.862	0.546	0.969	0.134
RAGE				0.415	0.003	0.014	0.504	0.005	0.810
SOD					0.186	0.233	0.103	0.457	0.303
GPx						0.546	0.841	0.000	0.170
TAS							0.000	0.177	0.068
AOGAP								0.653	0.453
SOD/GPx									0.200
8-ISOP									

ALA: alpha-lipoic acid; HbA1c: glycosylated hemoglobin; RAGE: receptor for advanced glycation end products; SOD: superoxide dismutase; GPx: glutathione peroxidase; TAS: total antioxidant status; AOGAP: antioxidant gap; SOD/GPx: SOD/GPx ratio; 8-ISOP: 8-isoprostane.

Table 6: Correlation between ALA and inflammatory markers after six months.

	ALA	TNF-α	IL-10	IL-6	IL-1β	IL-8	CRP
r							
ALA	1	-0.250	0.041	-0.249	-0.329	0.067	-0.100
TNF-α		1.000	0.289	0.188	0.574	0.126	0.030
IL-10			1.000	0.370	0.361	0.222	-0.010
IL-6				1.000	0.230	0.154	0.290
IL-1β					1.000	0.136	0.003
IL-8						1.000	0.085
CRP							1.000
p							
ALA		0.014	0.694	0.019	0.001	0.545	-0.100
TNF-α			0.005	0.076	0.000	0.249	0.775
IL-10				0.000	0.000	0.041	0.922
IL-6					0.028	0.169	0.006
IL-1β						0.213	0.977
IL-8							0.440
CRP							

ALA: alpha-lipoic acid; TNF-α: tumor necrosis factor-alpha; IL-10: interleukin 10; IL-6: interleukin 6; IL-1β: interleukin 1β; IL-8: interleukin 8; CRP: C-reactive protein.

On the other hand, it has been observed that the administration of ALA decreases the body weight and, consequently, the BMI in both animals and humans. In this regard, although the precise mechanisms are unknown, it has been suggested that ALA participates in the modulation of some pathways that are involved in energy homeostasis, the synthesis and oxidation of lipids, and the elimination of cholesterol through the liver. One of these pathways involves the protein kinase being activated by adenosine monophosphate (AMPK). It is known that AMPK integrates both hormonal and nutrient signals in the hypothalamus, which gives it a functional role in behavior that is related to food consumption and energy expenditure. Likewise, it has been suggested that ALA has an anorectic effect, which is more evident during the first two weeks of supplementation and gradually dissipates over time [41, 42]. In this regard, no statistically significant differences were observed in the BMI after treatment with ALA in our study, which is in contrast to previously reported results as researchers found that the administration of ALA induces a moderate loss of body weight and a statistically significant decrease in the BMI. However, this effect was observed with higher doses of ALA (1200 mg/day and 1800 mg/day) [42–44] compared to the 600 mg/day administered in our investigation. Likewise, it is important to point out that time is another determining factor since the anorectic effect only occurs during the first weeks as mentioned above.

Regarding the effect of ALA on lipid metabolism, it has been pointed out that it reduces lipogenesis at the peripheral level by increasing the β-oxidation of fatty acids and improving the energy expenditure of the whole body [45, 46]. In this sense, a statistically significant increase in blood HDL concentration was observed in the EG after

treatment ($p < 0.05$) in our study although this increase was also observed in the PG, which suggests that the administration of ALA at a dose of 600 mg/day has an effect on HDL that is similar to placebo. In this regard, similar findings were reported by Khabbazi et al. in a study conducted in patients with renal failure, who were given 600 mg/day of ALA for eight weeks [47]. In addition, Koh et al. did not observe statistically significant changes in the HDL blood concentration in obese adults, who consumed 1200 and 1800 mg/day of ALA for 20 weeks in comparison with the placebo group [48]. These results are in contrast to the statistically significant increase in HDL concentration found by Zhang et al. in obese patients given a dose of 600 mg/day of ALA for two weeks compared with a placebo group [46]. For this reason, the effect of ALA on the lipid profile remains controversial so its indication for these purposes would not be justified.

On the other hand, ALA has been shown to have a hypoglycemic effect since it improves the uptake and utilization of glucose by fat cells and skeletal muscle by inducing the translocation of glucose transporters (GLUT 1 and GLUT 4) from the Golgi complex to the cell membrane. Likewise, ALA stimulates the activity of the insulin receptor and its substrates (IR and IRS1) as well as phosphoinositol-3-kinase (PI3K), promoting tyrosine phosphorylation in the IR and improving the glucose uptake that is dependent on PI3K. Using the above-mentioned mechanisms, the ALA is capable of attenuating the formation of advanced glycation end products by reducing the concentration of circulating glucose and preventing it from reacting with proteins with a prolonged half-life, which subsequently decreases the expression of the AGE receptor (receptor for advanced glycation end products (RAGE)) in the cell membrane [9].

In the present study, no statistically significant differences were found in HbA1c (%) after treatment in the group that consumed ALA compared to the PG and CG ($p > 0.05$), with these results being consistent with what was observed in other studies [49, 50]. However, a hypoglycemic effect has also been reported with higher doses (1200–1800 mg/day) of ALA so it has been noted that the effect on HbA1c (%) depends on the dose [37, 38]. This may explain the negative results of our study.

With respect to the antioxidant capacity of ALA, it has been pointed out that it is a powerful redox pair that is capable of neutralizing different ROS. In addition, it has the ability to restore the reduced/oxidized glutathione ratio (GSH/GSSG) by either transferring electrons directly to the GSSG for reduction or increasing the synthesis of glutathione through improving the plasma uptake of cystine to subsequently reduce it to cysteine, which is the precursor of glutathione. ALA is also able to regenerate the reduced forms of other antioxidants, such as vitamins C and E. Furthermore, ALA has the ability to chelate ionic metals and counteract their oxidizing effects, which gives it enormous antioxidant capacity [9].

Regarding the effect of ALA on the OxS markers, it has been reported that the administration of ALA at doses of 300–1200 mg/day for three to six months has a positive effect on different oxidative stress markers, such as MDA, SOD, GPx, PGF2α-isoprostane, and 8-hydroxy-2′-deoxyguanosine [37, 51]. Negative results have also been observed, as shown in the following studies: Sola et al. did not find statistically significant differences in the concentration of 8-isoprostane in adult patients with metabolic syndrome after treatment with 300 mg of ALA for 4 weeks compared with the placebo group [32]. Likewise, Khabbazi et al., in a study conducted in patients with renal failure, who were given 600 mg/day of ALA for eight weeks, did not observe statistically significant changes in MDA and total antioxidant status levels [47]; Sharman et al., in a trial conducted in healthy adults, who were given 600 mg/day of ALA for seven days, also found no changes in the levels of MDA, SOD, GPx, and catalase [52]; and Ahmadi et al. also found no changes in MDA with the administration of 600 mg/day of ALA for two months in hemodialysis patients [53]. In our study, no statistically significant differences were observed in the blood concentration of 8-isoprostane between the EG and the PG ($p > 0.05$). On the other hand, GPx, SOD, and SOD/GPx also showed no statistically significant changes in EG compared to PG after treatment. This may be due to the dose of ALA and/or the length of the follow-up of administration of the treatment, considering that ours was a population of older adults, so the degree of oxidative stress is greater due to the aging process associated to diabetes mellitus.

Regarding the anti-inflammatory properties of ALA, it has been indicated that it has the capacity to decrease the production of TNF-α, IL-1β, and IL-6 both in animal models and in humans. ALA acts at the level of phosphorylation of the factor inhibitor protein κB (IKK) and prevents the activation and release of NF-κB, which also prevents its translocation to the nucleus and the subsequent transcription of genes that direct the synthesis of proinflammatory proteins (TNF-α, IL-1β, and IL-6) [46, 47]. In this regard, a decrease in the markers of chronic inflammation has been reported in diabetic patients treated with ALA at doses of 300–600 mg/day for 3–6 months [32, 46, 47]. In contrast, we observed a significant increase ($p < 0.05$) in all proinflammatory parameters evaluated (CRP, TNF-α, IL-1β, IL-6, IL-8, and IL-10) in the GC after six months compared to the GE and GP in our study. Consistent with our findings regarding the effect of ALA on the OxS markers, our results suggest that the administration of 600 mg/day of ALA has an anti-inflammatory effect that is similar to placebo.

The multiple regression analysis allows us to demonstrate the relationship of the concentration of ALA with the markers of OxS and chronic inflammation. In this regard, although the correlation of ALA with TNF-α, IL-6, IL-1β, SOD, GPx, and 8-isoprostane was statistically significant, the effect of ALA was not sufficient to show statistically significant differences between the EG and PG in the blood concentration of these markers; therefore, our findings do not support the anti-inflammatory and antioxidant effect of ALA in older adults with type 2 diabetes mellitus with a dose of 600 mg/day of ALA for six months.

5. Limitations

It was not possible to randomize the three groups and initiate the investigation simultaneously. We did not accurately

measure some noncontrollable variables, such as the amount and type of food consumed, because although they were provided with a guide on the type and quality of food they could consume, we are not sure of the degree of compliance. In this sense, the 24-hour dietary recalls does not guarantee the reliability of the data [19]. On the other hand, although all the participants were classified as sedentary, because they did not perform periodic physical exercise, the expenditure of kilocalories for the daily activities of each participant was different, and this was not measured in the study. Another important limitation of the study was not being able to try different doses of ALA at different lengths of the follow-up of administration of the treatment.

6. Conclusions

Our findings do not support the anti-inflammatory and antioxidant effect of ALA at a dose of 600 mg/day for six months in older adults with type 2 diabetes mellitus. In this regard, the exacerbating effect of diabetes mellitus and aging on oxidative stress and inflammation should be considered [6]. For this reason, the administration of doses of 1200–1800 mg/day of ALA could be useful to mitigate the oxidative stress and inflammation as well as to avoid the production of AGEs that occurs in T2DM in older adults, although the effectiveness of such higher doses must be verified through controlled clinical trials.

Data Availability

Data on biochemical, clinical, and anthropometric values (database in Excel) used to support the findings of this study are available from the corresponding author upon request.

Conflicts of Interest

The authors declare no conflicts of interest.

Authors' Contributions

V.M.M.N. designed the study, wrote the manuscript, and analyzed the data. B.I.G.M. performed the study and analyzed the data. E.S.O., J.P.C., J.R.P., and V.J.H.A. analyzed the data. All authors reviewed the final manuscript.

Acknowledgments

This work was supported by Dirección General de Asuntos del Personal Académico, Universidad Nacional Autónoma de México (DGAPA-UNAM) (PAPIIT IN 222015); Posgrado en Ciencias Biológicas, UNAM; and Consejo Nacional de Ciencia y Tecnología (Beca de Posgrado, CVU 706595). We appreciate the support of Martha Mendieta Alcántara in the clinical evaluation and Mirna Ruiz-Ramos and Itzen Aguiñiga-Sánchez for the measurement of oxidative stress markers and inflammatory cytokines. ProductosMedix® S.A. de C.V. supplied the alpha-lipoic acid and placebo.

References

[1] T. Finkel and J. Holbrook, "Oxidants, oxidative stress and the biology of aging," *Nature*, vol. 408, no. 6809, pp. 239–247, 2000.

[2] J. A. Knight, *Free Radicals, Antioxidants, Aging, & Disease*, AACC Press, Washington, DC, 1999.

[3] R. J. Pickering, C. J. Rosado, A. Sharma, S. Buksh, M. Tate, and J. B. de Haan, "Recent novel approaches to limit oxidative stress and inflammation in diabetic complications," *Clinical and Translational Immunology*, vol. 7, no. 4, article e1016, 2018.

[4] M. F. El-Refaei, S. H. Abduljawad, and A. H. Alghamdi, "Alternative medicine in diabetes role of angiogenesis, oxidative stress, and chronic inflammation," *The Review of Diabetic Studies*, vol. 11, no. 3-4, pp. 231–244, 2014.

[5] A. Ceriello, "New insights on oxidative stress and diabetic complications may lead to a "causal" antioxidant therapy," *Diabetes Care*, vol. 26, no. 5, pp. 1589–1596, 2003.

[6] V. M. Mendoza-Núñez, J. Rosado-Pérez, E. Santiago-Osorio, R. Ortiz, M. A. Sánchez-Rodríguez, and R. E. Galván-Duarte, "Aging linked to type 2 diabetes increases oxidative stress and chronic inflammation," *Rejuvenation Research*, vol. 14, no. 1, pp. 25–31, 2011.

[7] A. Chanwitheesuk, A. Teerawutgulrag, and N. Rakariyatham, "Screening of antioxidant activity and antioxidant compounds of some edible plant of Thailand," *Food Chemistry*, vol. 92, no. 3, pp. 491–497, 2005.

[8] D. Zephy and J. Ahmad, "Type 2 diabetes mellitus: role of melatonin and oxidative stress," *Diabetes and Metabolic Syndrome: Clinical Research & Reviews*, vol. 9, no. 2, pp. 127–131, 2015.

[9] K. P. Shay, R. F. Moreau, E. J. Smith, A. R. Smith, and T. M. Hagen, "Alpha-lipoic acid as a dietary supplement: molecular mechanisms and therapeutic potential," *Biochimica et Biophysica Acta (BBA) - General Subjects*, vol. 1790, no. 10, pp. 1149–1160, 2009.

[10] I. Padmalayam, S. Hasham, U. Saxena, and S. Pillarisetti, "Lipoic acid synthase (LASY): a novel role in inflammation, mitochondrial function and insulin resistance," *Diabetes*, vol. 58, no. 3, pp. 600–608, 2009.

[11] L. J. Reed, "From lipoic acid to multi-enzyme complexes," *Protein Science*, vol. 7, no. 1, pp. 220–224, 1998.

[12] L. Packer, K. Kraemer, and G. Rimbach, "Molecular aspects of lipoic acid in the prevention of diabetes complications," *Nutrition*, vol. 17, no. 10, pp. 888–895, 2001.

[13] M. Akbari, V. Ostadmohammadi, R. Tabrizi et al., "The effects of alpha-lipoic acid supplementation on inflammatory markers among patients with metabolic syndrome and related disorders: a systematic review and meta-analysis of randomized controlled trials," *Nutrition and Metabolism*, vol. 15, no. 1, 2018.

[14] F. Moura, K. de Andrade, J. F. dos Santos, and M. F. Goulart, "Lipoic acid: its antioxidant and anti-inflammatory role and clinical applications," *Current Topics in Medicinal Chemistry*, vol. 15, no. 5, pp. 458–483, 2015.

[15] A. Gorąca, H. Huk-Kolega, A. Piechota, P. Kleniewska, E. Ciejka, and B. Skibska, "Lipoic acid - biological activity and therapeutic potential," *Pharmacological Reports*, vol. 63, no. 4, pp. 849–858, 2011.

[16] M. K. Patel, M. A. Riley, S. Hobbs, M. Cortez-Cooper, and V. J. B. Robinson, "Can α-lipoic acid mitigate progression of

aging-related decline caused by oxidative stress?," *Southern Medical Journal*, vol. 107, no. 12, pp. 780–787, 2014.

[17] V. M. Mendoza-Núñez, *Use of Alpha Lipoic Acid as a Complementary Treatment for the Control of Diabetes*, BMC, 2017, ISRCTN13159380.

[18] V. M. Mendoza-Núñez, T. L. Arista-Ugalde, J. Rosado-Pérez, M. Ruiz-Ramos, and E. Santiago-Osorio, "Hypoglycemic and antioxidant effect of Tai chi exercise training in older adults with metabolic syndrome," *Clinical Interventions in Aging*, vol. 13, pp. 523–531, 2018.

[19] G. S. Castel, L. Serra-Majem, and L. Ribas-Barba, "What and how much do we eat? 24-hour dietary recall method," *Nutrición Hospitalaria*, vol. 31, Supplement 3, pp. 46–48, 2015.

[20] Secretaría de Salud, *Norma Oficial MexicanaNOM-030-SSA-1999, para la prevención, tratamiento y control de la hipertensión arterial*, Secretaría de Salud, Mexico City, 1999.

[21] W. T. Friedewald, R. I. Levy, and D. S. Fredrickson, "Estimation of the concentration of low-density lipoprotein cholesterol in plasma, without use of the preparative ultracentrifuge," *Clinical Chemistry*, vol. 18, no. 6, pp. 499–502, 1972.

[22] N. J. Miller, "Nonvitamin plasma antioxidants," in *Free Radical and Antioxidant Protocols*, D. Armstrong, Ed., pp. 285–297, Humana Press, Totowa, New Jersey, 1998.

[23] E. B. Cook, J. L. Stahl, L. Lowe et al., "Simultaneous measurement of six cytokines in a single sample of human tears using microparticle-based flow cytometry: allergics vs. non-allergics," *Journal of Immunological Methods*, vol. 254, no. 1-2, pp. 109–118, 2001.

[24] A. Khan, Z. Iqbal, D. G. Watson et al., "Simultaneous determination of lipoic acid (LA) and dihydrolipoic acid (DHLA) in human plasma using high-performance liquid chromatography coupled with electrochemical detection," *Journal of Chromatography B Analytical Technologies in the Biomedical and Life Sciences*, vol. 879, no. 20, pp. 1725–1731, 2011.

[25] E. Park, M. Cho, and C.-S. Ki, "Correct use of repeated measures analysis of variance," *The Korean Journal of Laboratory Medicine*, vol. 29, no. 1, pp. 1–9, 2009.

[26] R. J. Parry and D. A. Trainor, "Biosynthesis of lipoic acid. 2. Stereochemistry of sulfur introduction at C-6 of octanoic acid," *Journal of the American Chemical Society*, vol. 100, no. 16, pp. 5243-5244, 1978.

[27] Y. S. Yang and P. A. Frey, "2-Ketoacid dehydrogenase complexes of *Escherichia coli*: stereospecificities of the three components for (R)-lipoate," *Archives of Biochemistry and Biophysics*, vol. 268, no. 2, pp. 465–474, 1989.

[28] J. Teichert, J. Kern, H. J. Tritschler, H. Ulrich, and R. Preiss, "Investigation on the pharmacokinetics of alpha-lipoic acid in healthy volunteers," *International Journal of Clinical Pharmacology and Therapeutics*, vol. 36, no. 12, pp. 625–628, 1998.

[29] D. A. Carlson, A. R. Smith, S. J. Fischer, K. L. Young, and L. Packer, "The plasma pharmacokinetics of R-(+)-lipoic acid administered as sodium R-(+)-lipoate to healthy human subjects," *Alternative Medicine Review*, vol. 12, no. 4, pp. 343–351, 2007.

[30] R. Uchida, H. Okamoto, N. Ikuta, K. Terao, and T. Hirota, "Enantioselective pharmacocinetics of α-lipoic acid in rats," *International Journal of Molecular Sciences*, vol. 16, no. 9, pp. 22781–22794, 2015.

[31] A. Scaramuzza, E. Giani, F. Redaelli et al., "Alpha-lipoic acid and antioxidant diet help to improve endothelial dysfunction in adolescents with type 1 diabetes: a pilot trial," *Journal of Diabetes Research*, vol. 2015, Article ID 474561, 7 pages, 2015.

[32] S. Sola, M. Q. S. Mir, F. A. Cheema et al., "Irbesartan and lipoic acid improve endothelial function and reduce markers of inflammation in the metabolic syndrome: results of the Irbesartan and Lipoic Acid in Endothelial Dysfunction (ISLAND) study," *Circulation*, vol. 111, no. 3, pp. 343–348, 2005.

[33] G. L. Mauro, P. Cataldo, G. Barbera, and A. Sanfilippo, "α-Lipoic acid and superoxide dismutase in the management of chronic neck pain: a prospective randomized study," *Drugs in R&D*, vol. 14, no. 1, pp. 1–7, 2014.

[34] H. Lin, S. Ye, J. Xu, and W. Wang, "The alpha-lipoic acid decreases urinary podocalyxin excretion in type 2 diabetics by inhibiting oxidative stress in vivo," *Journal of Diabetes and its Complications*, vol. 29, no. 1, pp. 64–67, 2015.

[35] The ALADIN Study Group, D. Ziegler, M. Hanefeld et al., "Treatment of symptomatic diabetic peripheral neuropathy with the antioxidant alpha-lipoic acid. A 3-week multicentre randomized controlled trial (ALADIN study)," *Diabetologia*, vol. 38, no. 12, pp. 1425–1433, 1995.

[36] D. Ziegler, P. A. Low, R. Freeman, H. Tritschler, and A. I. Vinik, "Predictors of improvement and progression of diabetic polyneuropathy following treatment with α-lipoic acid for 4 years in the NATHAN 1trial," *Journal of Diabetes and its Complications*, vol. 30, no. 2, pp. 350–356, 2016.

[37] S. Porasuphatana, S. Suddee, A. Nartnampong, J. Konsil, B. Harnwong, and A. Santaweesuk, "Glycemic and oxidative status of patients with type 2 diabetes mellitus following oral administration of alpha-lipoic acid: a randomized double-blinded placebo-controlled study," *Asia Pacific Journal of Clinical Nutrition*, vol. 21, no. 1, pp. 12–21, 2012.

[38] X. M. Gu, S. S. Zhang, J. C. Wu et al., "Efficacy and safety of high-dose α-lipoic acid in the treatment of diabetic polyneuropathy," *Zhonghua Yi Xue Za Zhi*, vol. 90, no. 35, pp. 2473–2476, 2010.

[39] M. Janson, "Orthomolecular medicine: the therapeutic use of dietary supplements for anti-aging," *Clinical Interventions in Aging*, vol. 1, no. 3, pp. 261–265, 2006.

[40] V. Mohammadi, S. Dehghani, and G. Askari, "Does alpha-lipoic acid supplement regulate blood pressure? A systematic review of randomized, double-blind placebo-controlled clinical trials," *International Journal of Preventive Medicine*, vol. 8, no. 1, p. 33, 2017.

[41] B. Carrier and T. Rideout, "Anti-obesity and lipid-lowering properties of alpha lipoic acid," *Journal of Human Nutrition & Food Sciences*, vol. 1, no. 1, p. 1002, 2013.

[42] S. Kucukgoncu, E. Zhou, K. B. Lucas, and C. Tek, "Alpha-lipoic acid (ALA) as a supplementation for weight loss: results from a meta-analysis of randomized controlled trials," *Obesity Reviews*, vol. 18, no. 5, pp. 594–601, 2017.

[43] N. Namazi, B. Larijani, and L. Azadbakht, "Alpha-lipoic acid supplement in obesity treatment: a systematic review and meta-analysis of clinical trials," *Clinical Nutrition*, vol. 37, no. 2, pp. 419–428, 2018.

[44] N. Li, W. Yan, X. Hu et al., "Effects of oral α-lipoic acid administration on body weight in overweight or obese subjects: a crossover randomized, double-blind, placebo-controlled trial," *Clinical Endocrinology*, vol. 86, no. 5, pp. 680–687, 2017.

[45] H. Ghelani, V. Razmovski-Naumovski, and S. Nammi, "Chronic treatment of (R)-α-lipoic acid reduces blood glucose and lipid levels in high-fat diet and low-dose streptozotocin-

induced metabolic syndrome and type 2 diabetes in Sprague-Dawley rats," *Pharmacology Research & Perspectives*, vol. 5, no. 3, article e00306, 2017.

[46] Y. Zhang, P. Han, N. Wu et al., "Amelioration of lipid abnormalities by α-lipoic acid through antioxidative and anti-inflammatory effects," *Obesity (Silver Spring)*, vol. 19, no. 8, pp. 1647–1653, 2011.

[47] T. Khabbazi, R. Mahdavi, J. Safa, and P. Pour-Abdollahi, "Effects of alpha-lipoic acid supplementation on inflammation, oxidative stress, and serum lipid profile levels in patients with end-stage renal disease on hemodialysis," *Journal of Renal Nutrition*, vol. 22, no. 2, pp. 244–250, 2012.

[48] E. H. Koh, W. J. Lee, S. A. Lee et al., "Effects of alpha-lipoic acid on body weight in obese subjects," *American Journal of Medicine*, vol. 124, no. 1, pp. 85.e1–85.e8, 2011.

[49] A. M. de Oliveira, P. H. Rondó, L. A. Luzia, F. H. D'Abronzo, and V. K. Illison, "The effects of lipoic acid and α-tocopherol supplementation on the lipid profile and insulin sensitivity of patients with type 2 diabetes mellitus: a randomized, double-blind, placebo-controlled trial," *Diabetes Research and Clinical Practice*, vol. 92, no. 2, pp. 253–260, 2011.

[50] X. H. Bao, J. Xu, Y. Chen, C. L. Yang, and S. D. Ye, "Alleviation of podocyte injury: the possible pathway implicated in anti-inflammation of alpha-lipoic acid in type 2 diabetics," *Aging Clinical and Experimental Research*, vol. 26, no. 5, pp. 483–489, 2014.

[51] G. Derosa, A. D'Angelo, D. Romano, and P. Maffioli, "A clinical trial about a food supplement containing α-lipoic acid on oxidative stress markers in type 2 diabetic patients," *International Journal of Molecular Sciences*, vol. 17, no. 11, p. 1802, 2016.

[52] J. E. Sharman, P. Gunaruwan, W. L. Knez et al., "Alpha-lipoic acid does not acutely affect resistance and conduit artery function or oxidative stress in healthy men," *British Journal of Clinical Pharmacology*, vol. 58, no. 3, pp. 243–248, 2004.

[53] A. Ahmadi, N. Mazooji, J. Roozbeh, Z. Mazloom, and J. Hasanzade, "Effect of alpha-lipoic acid and vitamin E supplementation on oxidative stress, inflammation, and malnutrition in hemodialysis patients," *Iranian Journal of Kidney Diseases*, vol. 7, no. 6, pp. 461–467, 2013.

Hindawi
Oxidative Medicine and Cellular Longevity
Volume 2019, Article ID 8745376, 11 pages
https://doi.org/10.1155/2019/8745376

Research Article

Modulation of Hippocampal Antioxidant Defense System in Chronically Stressed Rats by Lithium

Nataša Popović, Vesna Stojiljković, Snežana Pejić, Ana Todorović, Ivan Pavlović, Ljubica Gavrilović, and Snežana B. Pajović

Institute of Nuclear Sciences "Vinča", Laboratory of Molecular Biology and Endocrinology, University of Belgrade, Belgrade, Serbia

Correspondence should be addressed to Ljubica Gavrilović; gljubica@vin.bg.ac.rs

Received 17 July 2018; Revised 5 November 2018; Accepted 2 December 2018; Published 17 February 2019

Guest Editor: Luciano Saso

This study examined the effects of lithium on gene expression and activity of the antioxidant enzymes copper zinc superoxide dismutase (SOD1), manganese superoxide dismutase (SOD2), catalase (CAT), glutathione peroxidase (GPx), and glutathione reductase (GR) in the hippocampus of chronically stressed rats. In addition, we examined the effects of lithium on anxiety behaviors, hippocampal concentrations of dopamine (DA) and malondialdehyde (MDA), protein levels of brain-derived neurotrophic factor (BDNF), tyrosine hydroxylase (TH), dopamine transporter (DAT), and catechol-O-methyltransferase (COMT), as well as activity of monoamine oxidase (MAO) in chronically stressed rats. The investigated parameters were quantified by real-time RT-PCR, Western blot analyses, and assays of enzyme activities. We found that lithium did not change gene expression of SOD1, CAT, GPx, and GR but decreased gene expression of SOD2 in chronically stressed rats. A very important result in this study was that lithium treatment decreased the enzyme activities of SOD1 and SOD2 but increased the enzyme activities of GPx and GR in stress condition, which indicates the control of redox balance. The reduced concentration of MDA confirms this. In addition, we found that lithium treatment decreased high protein levels of BDNF and DAT in chronically stressed rats to the level found in unstressed animals. Also, lithium treatment increased the expression of TH but decreased the enzyme activity of MAO B, which contributed to the increase of hippocampal concentration of DA in chronically stressed rats to the level of unstressed animals. Finally, lithium treatment in animals exposed to chronic stress increased the time spent in open arms. Lithium-induced modulation of hippocampal antioxidant status and attenuation of oxidative stress stabilized behavior in animals with high anxiety index. In addition, reduced oxidative stress was followed by the changes of both turnover of DA and levels of BDNF protein in chronically stressed rats treated with lithium. These findings may be important in preclinical research of the effects of lithium on oxidative stress level in pathological conditions.

1. Introduction

Molecular interactions in the neuroendocrine system under stress condition can lead to homeostatic disorders [1, 2]. Chronic stress induces overactivation and dysfunction of stress-activated systems, resulting in further brain damage and mood disorders [3, 4]. One of the key mechanisms for the modulation of brain functions in stress conditions is monoaminergic signaling. In addition, it is known that brain-derived neurotrophic factor (BDNF) modulates the activity of monoaminergic systems in the rat brain [5]. Normal monoaminergic turnover results from balance among synthesis, degradation, release, and reuptake of monoamines. In our previous studies, we found that chronic restraint stress (CRS) induced significant decrease of both hippocampal dopamine (DA) concentration [6] and protein levels of tyrosine hydroxylase (TH), a "rate-limiting" enzyme of dopamine biosynthesis [7], which confirmed that the hippocampus was particularly sensitive to chronic stress [8, 9]. Data about the dynamics of DA transmission and degradation are very important for understanding dopaminergic turnover. The dynamics of DA transmission is regulated by reuptake through dopamine transporter (DAT). Monoamine oxidase (MAO) and catechol-O-methyltransferase (COMT) are enzymes which catalyze the oxidative deamination of monoamine neurotransmitters including DA. The byproducts of

these reactions include a number of potentially neurotoxic species, such as hydrogen peroxide and ammonia. Hydrogen peroxide can trigger the production of reactive oxygen species (ROS) and induce mitochondrial damage and neuronal apoptosis. It is known that the brain is particularly vulnerable to oxidative damage since it contains large amounts of polyunsaturated fatty acids and possesses low antioxidant capacity [10, 11]. Malondialdehyde (MDA) is the frequently used biomarker of oxidative stress in many health problems including mood disorders. The literature data have shown that there is a direct involvement of oxidative stress in anxiety-like behavior in rodents [12]. Our earlier research confirmed that chronic restraint stress (CRS) influenced anxiety-like behavior in rats [6]. In the pathophysiology of mood disorders, lithium is known as an effective drug in the long-term stabilization of moods. Also, lithium has a neurotrophic and neuroprotective function and improves total antioxidant activity [13–16]. In our earlier studies, we found that CRS induced increased activity of superoxide dismutase 1 (SOD1), superoxide dismutase 2 (SOD2), and catalase (CAT) in the hippocampus [17]. The increased activity of antioxidant enzymes may be an important adaptive phenomenon of the antioxidant defense system in chronically stressed rats [17]. It is known that treatment with antidepressants significantly decreased the activities of SOD and CAT in depressive patients [18], as well as increased DA levels in the prefrontal cortex [19]. However, very little is known about the antioxidant defense system and turnover of DA in animals with high anxiety index treated with lithium.

Because of the direct involvement of oxidative stress in anxiety-like behavior in stress conditions, detecting the changes of gene expression and activity of the antioxidant enzymes as well as monitoring the changes of dopaminergic turnover in the hippocampus in chronically stressed rats treated with lithium may be very important in the research on the role of lithium in maintaining antioxidant status in pathological conditions. Therefore, in this study we examined gene expression and activity of the antioxidant enzymes SOD, CAT, glutathione peroxidase (GPx), and glutathione reductase (GR), as well as protein levels of BDNF, TH, DAT, and COMT and activity of MAO and concentrations of DA and MDA in the hippocampus of chronically stressed rats treated with lithium. An additional aim of the study was to test anxiety in chronically stressed rats treated with lithium.

2. Materials and Methods

2.1. Animals and Stress Models. Eleven-week-old Wistar male rats (300-340 g) were maintained under standard laboratory conditions with water and food *ad libitum* and kept three to four per cage [20]. The care was taken to minimize the pain and discomfort of the animals according to the recommendations of the Ethical Committee of the Vinča Institute of Nuclear Sciences, Belgrade, Serbia, which follows the guidelines of the registered "Serbian Society for the Use of Animals in Research and Education." In accordance with our previous protocol [21], animals were divided into three groups: *CRS group* ($n = 20$) consisted of animals exposed to chronic restraint stress treatment and *CRS+Li group* ($n = 20$) consisted of animals exposed to chronic restraint stress treatment with Li given each day immediately prior to daily restraint. Restraint stress was performed by placing each animal in a 25×7 cm plastic bottle as described previously [22]. The animals in these groups were exposed to 2 h of restraint stress every day at random times during the light period of the light/dark cycle to avoid habituation during the experimental procedure of 14 days [23]. Lithium was administered intraperitoneally to the animals, once a day for 14 days as described previously [24]. The initial lithium dose was 1.5 mEq/kg for 2 days and was then increased to 2.3 mEq/kg for 7 days, followed by 3 mEq/kg for 5 days. This lithium administration protocol maintained the plasma lithium concentration above the minimal therapeutic concentration (i.e., 0.4 mM) for the treatment of bipolar disorder throughout the treatment period. Anxiety-like behaviors were assessed by elevated plus maze (EPM) test. Ten animals from each group were tested on the EPM. Animals which were used to test the behavior were not used for further analysis. In order to examine whether lithium decreased high protein levels of BDNF and DAT in chronically stressed rats to the level of unstressed animals, we introduced Control group. The *Control group* ($n = 10$) was not exposed to any treatment. To reduce variance in the physiological parameters due to daily rhythms, the remaining animals ($n = 10$ from each group) were sacrificed at the same time point in the circadian cycle, between 9:00 and 11:00 am, i.e., one day after the last treatments. Animals were sacrificed under no-stress conditions by rapid decapitation. The hippocampuses were rapidly dissected, frozen in liquid nitrogen, and stored at −70°C until analyzed.

2.2. Dopamine Measurement. Hippocampus tissues were homogenized in 0.01 N HCl in the presence of EDTA and sodium metabisulfite. Dopamine concentration in hippocampus fractions was determined using 3-CAT Research ELISA kits (Labor Diagnostika Nord, Nordhorn, Germany) according to the manufacturer's protocol. Absorbance was determined at 450 nm using a microplate reader (Stat Fax 2100). Concentrations were normalized to 1 g of tissues in homogenate. Values were expressed as ng of DA per g of *tissues* which is in accordance with our previous protocol [25].

2.3. Monoamine Oxidase Enzyme Activities. The determination of MAO B activity was performed using the Amplex Red Monoamine Oxidase Assay (A12214, Molecular Probes, USA), described by Zhou and Panchuk-Voloshina [26]. This assay is based on the detection of H_2O_2 in a horseradish peroxidase-coupled reaction using N-acetyl-3, 7-dihydroxyphenoxazine (Amplex Red), a highly sensitive and stable probe for H_2O_2. Fluorescence was measured with a fluorometer using excitation at 560 ± 10 nm and fluorescence detection at 590 ± 10 nm. Monoamine oxidase activity was expressed as U/mg of protein as previously described by Gavrilović et al. [25].

2.4. RNA Isolation, cDNA Synthesis, and Real-Time RT-PCR. Methods of RNA isolation and cDNA synthesis were described previously by Gavrilović et al. [27]. Total RNAs were isolated from the hippocampal tissue by using TRIZOL

reagent (Invitrogen, USA). Reverse transcription was performed using Ready-To-Go You-Prime First-Strand Bead (Amersham Biosciences, UK) and pd $(N)_6$ Random Hexamer (Amersham Biosciences, UK) primer according to the manufacturer's protocol, which is in accordance with the protocol of Gavrilović et al. [28]. CuZn SOD (SOD1), Mn SOD (SOD2), CAT, GPx, and GR mRNA levels were quantified by quantitative real-time RT-PCR, as described previously by Gavrilović et al. [27]. TaqMan PCR assays were carried out using Assay-on-Demand Gene Expression Products (Applied Biosystems, USA) for SOD1 (Rn00566938_m1), SOD2 (Rn00690587_g1), CAT (Rn00560930_m1), GPx (Rn00577994_g1), and GR (Rn01482159_m1). The reference gene (endogenous control) was included in each analysis to correct for the differences in the interassay amplification efficiency and all transcripts were normalized to cyclophilin A (Rn00690933_m1) expression [28]. Quantification was done using the $2^{-\Delta\Delta Ct}$ method according to Livak and Schmittgen [29]. The relative expression of the target gene was normalized to cyclophilin A and expressed in relation to the calibrator, i.e., the control sample as previously described by Gavrilović et al. [28].

2.5. Hippocampal Tissue Homogenization, Measurement of the Protein Concentration, and Western Blot Analysis. The hippocampus was homogenized in 0.05 M sodium phosphate buffer (pH 6.65). Subsequently, the protein concentration was determined using BCA method (Thermo Scientific Pierce, USA), described by Stich [30]. CuZn SOD (SOD1), Mn SOD (SOD2), CAT, GPx, GR, BDNF, TH, DAT, and COMT proteins were assayed by Western blot analysis as described previously by Gavrilović et al. [27]. Antibodies used for the quantification of specific proteins were as follows: SOD1 (SOD-101, Stressgen, USA), SOD2 (SOD-110, Stressgen, USA), CAT (Calbiochem, Germany), GPx (sc-30147 Santa Cruz Biotechnology, USA), GR (sc-32886, Santa Cruz Biotechnology, USA), BDNF (ab6201, Abcam, USA), TH (ab51191, Abcam, USA), DAT (ab18548, Abcam, USA), and β-actin (ab8227, Abcam, USA). After washing, the membranes were incubated in the secondary anti-rabbit (dilution 1 : 5000, Amersham ECL™ Western Blotting Analysis System, UK) antibodies conjugated to horseradish peroxidase. A secondary antibody was then visualized by the Western blotting-enhanced chemiluminescent detection system (ECL, Amersham Biosciences, UK). The membranes were exposed to ECL film (Amersham Biosciences, UK). The result was expressed in arbitrary units normalized in relation to β-actin, which is in accordance with our previous protocol [27].

2.6. Antioxidant Enzyme Activities. SOD, GPx, and GR activities were determined using assays for enzyme activities, as we previously described [31].

2.6.1. Assay of SOD Activity. Total SOD activity was measured using the Oxis Bioxytech® SOD-525™ Assay (Oxis International Inc., Portland, OR, USA). The method is based on the SOD-mediated increase in the rate of autoxidation of reagent 1 (5,6,6a,11b-tetrahydro-3,9,10-trihydroxybenzo[c] fluorene, R1) in aqueous alkaline solution, yielding a chromophore with maximum absorbance at 525 nm. The kinetic measurement of the change in absorbance at 525 nm was performed. One SOD-525 activity unit was defined as the activity that doubles the autoxidation rate of the control blank. CuZnSOD activity was measured as described above, after pretreating samples with ethanol-chloroform reagent (5/3 vol/vol), which inactivates MnSOD. MnSOD activity was then calculated by subtracting CuZnSOD activity from total SOD activity [17].

2.6.2. Assay of CAT Activity. CAT activity was determined by the method of Beutler [32]. The reaction is based on the rate of H_2O_2 degradation by catalase contained in the examined samples. The reaction was performed in an incubation mixture containing 1 M Tris-HCl, 5 mM EDTA, pH 8.0 and monitored spectrophotometrically at 230 nm. One unit of CAT activity was defined as 1 μmol of H_2O_2 decomposed per minute under the assay conditions [21].

2.6.3. Assay of GPx Activity. GPx activity was assessed using the Oxis Bioxytech GPx-340 Assay (Oxis International Inc., Portland, OR, USA), based on the principle that oxidized glutathione (GSSG) produced upon reduction of an organic peroxide by GPx is immediately recycled to its reduced form (GSH) with concomitant oxidation of NADPH to NADP+. The oxidation of NADPH was monitored spectrophotometrically as a decrease in absorbance at 340 nm. One GPx-340 unit was defined as 1 μmol of NADH oxidized per minute under the assay conditions [21].

2.6.4. Assay of GR Activity. Activity of GR was measured using the Oxis Bioxytech GR-340 Assay (Oxis International Inc., Portland, OR, USA). The assay is based on the oxidation of NADPH to NADP+ during the reduction of oxidized glutathione (GSSG), catalyzed by a limiting concentration of glutathione reductase. The oxidation of NADPH was monitored spectrophotometrically as a decrease in absorbance at 340 nm. One GR-340 unit was defined as 1 μmol of NADH oxidized per minute under the assay conditions [21].

2.7. Malondialdehyde Measurement. Malondialdehyde concentration in the hippocampus fractions was determined using Spectrophotometric Assay for Malondialdehyde Bioxytech® MDA-586 (OXIS Health Products Inc., USA) according to the manufacturer's protocol. The MDA-586 method is based on the reaction of a chromogenic reagent, N-methyl-2-phenylindole, with MDA at 45°C. Malondialdehyde concentration was expressed as μM/mg of protein, which is in accordance with our previous protocol [25].

2.8. Elevated Plus Maze (EPM). The EPM consisted of four elevated (50 cm) contralateral arms (50 cm long and 10 cm wide) with two opposing arms containing 40 cm high opaque walls, which is in accordance with our previous protocol [6]. On the day of EPM testing, rats were transported into the testing room one cage at a time and testing alternated between CRS animals and CRS+Li animals. Each rat was placed in a closed arm, facing the center platform and cage-mates started in the same closed arm, which was

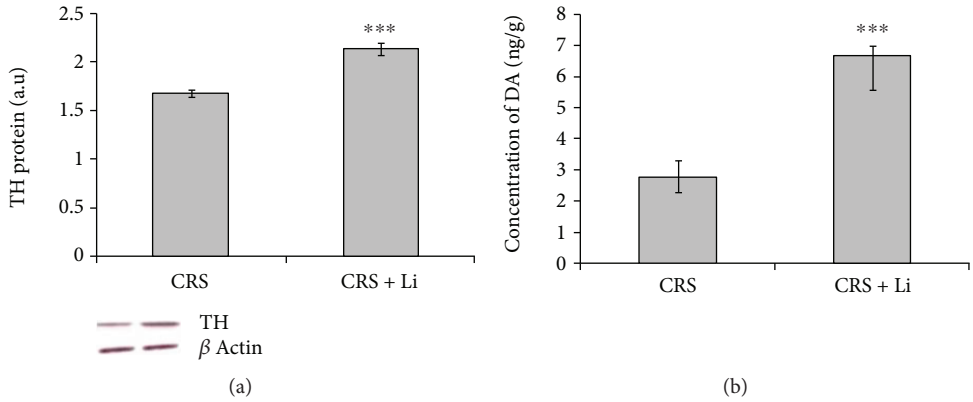

Figure 1: Effects of lithium on tyrosine hydroxylase (TH) protein levels (a) and concentration of dopamine (DA) (b) in the hippocampus of animals exposed to CRS. The values are means ± S.E.M. of 10 rats. Statistical significance: $^{***}p < 0.001$ animals exposed to CRS+Li *vs*. CRS animals (*t*-test). The level of TH protein was expressed in arbitrary units normalized in relation to β-actin, and the concentration of DA was expressed as ng per gram of tissue (ng/g).

counterbalanced across trials. Each rat was given 5 min to explore the EPM and then returned to its home cage. The EPM was cleaned thoroughly using Naturally Living Pet Odor Eliminator between each rat. EPM performance was recorded using an overhead video camera for later quantification. Open and closed arm entries were defined as the front two paws entering the arm, and open arm time began the moment the front two paws entered the open arm and ended upon exit. Rats that displayed thigmotaxis and an aversion to the open arms were considered highly anxious [33]. An added measure of anxiety was calculated for the EPM using the following equation, which unifies all EPM parameters into one unified ratio; anxiety index values range from 0 to 1, with a higher value indicating increased anxiety [34–37].

$$\text{Anxiety index} = 1 - \left[\frac{(\text{open arm time}/5\ \text{min}) + (\text{open arm entry}/\text{total entry})}{2}\right]. \quad (1)$$

2.9. Data Analysis. The data are presented as means ± S.E.M. Differences of gene expression (mRNA and protein levels) of SOD1, SOD2, CAT, GPx, GR, BDNF, TH, and DAT; activity of enzymes (MAO B, SOD1, SOD2, CAT, GPx, and GR); and concentration of DA and MDA as well as animal behavior between CRS and CRS+Li animals were analyzed by *t*-test. Statistical significance was accepted at $p < 0.05$.

3. Results

3.1. Changes of Levels of TH Protein, DA Concentrations, BDNF Protein, DAT Protein, COMT Protein, and MAO B Activity in the Hippocampus. We found that lithium treatment in animals exposed to CRS significantly increased levels of TH protein by 26% ($p < 0.001$, *t*-test, Figure 1(a)) and increased the concentration of DA by 125% ($p < 0.001$, *t*-test, Figure 1(b)) compared with CRS animals. In addition, lithium treatment decreased levels of BDNF protein by 10% ($p < 0.05$, *t*-test, Figure 2(a)) and decreased levels of DAT protein by 20% ($p < 0.01$, *t*-test, Figure 2(b)) to the level of unstressed animals. Also, the animals exposed to CRS treated with lithium showed decreased levels of MAO B activity by 43% ($p < 0.001$, *t*-test, Figure 3(a)), while levels of COMT protein remained unchanged (Figure 3(b)) compared with CRS animals.

3.2. Changes of MDA Concentrations in the Hippocampus. Lithium treatment decreased MDA concentrations by 35% ($p < 0.01$, *t*-test, Figure 4) compared with CRS animals.

3.3. Changes of SOD1 mRNA Levels, Protein Levels, and Enzyme Activity in the Hippocampus. Lithium treatment in animals exposed to CRS significantly decreased the enzyme activity of SOD1 by 25% ($p < 0.01$, *t*-test, Figure 5(a)), while levels of mRNA and protein (Figure 6(a)) remained unchanged compared with CRS animals.

3.4. Changes of SOD2 mRNA Levels, Protein Levels, and Enzyme Activity in the Hippocampus. The animals exposed to CRS treated with lithium showed decreased levels of SOD2 mRNA by 16% ($p < 0.05$, *t*-test, Figure 6(b)) and protein by 14% ($p < 0.05$, *t*-test, Figure 6(b)) and the enzyme activity by 37% ($p < 0.001$, *t*-test, Figure 5(b)) compared with CRS animals.

3.5. Changes of CAT mRNA Levels, Protein Levels, and Enzyme Activity in the Hippocampus. Lithium treatment did not change significantly gene expression and enzyme activity of CAT in animals exposed to CRS (Figures 5(c) and 6(c)).

The animals exposed to CRS treated with lithium showed a decreased ratio of SOD1/CAT and SOD2/CAT compared with CRS animals.

3.6. Changes of GPx mRNA Levels, Protein Levels, and Enzyme Activity in the Hippocampus. We found that lithium treatment in animals exposed to CRS significantly increased the enzyme activity of GPx by 23% ($p < 0.05$, *t*-test, Figure 5(d)), while levels of GPx mRNA and protein (Figure 6(d)) remained unchanged compared with CRS animals.

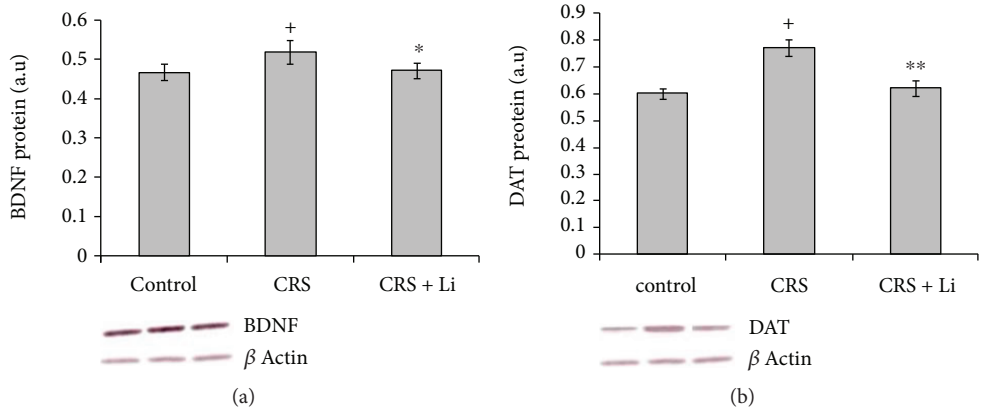

Figure 2: Effects of lithium on brain-derived neurotrophic factor (BDNF) (a) and dopamine transporter (DAT) (b) protein levels in the hippocampus of animals exposed to CRS. The values are means ± S.E.M. of 10 rats. Statistical significance: $^{*}p < 0.05$, $^{**}p < 0.01$ animals exposed to CRS+Li *vs*. CRS animals (*t*-test); $^{+}p < 0.05$ CRS animals *vs*. Control animals (*t*-test). The result was expressed in arbitrary units normalized in relation to β-actin.

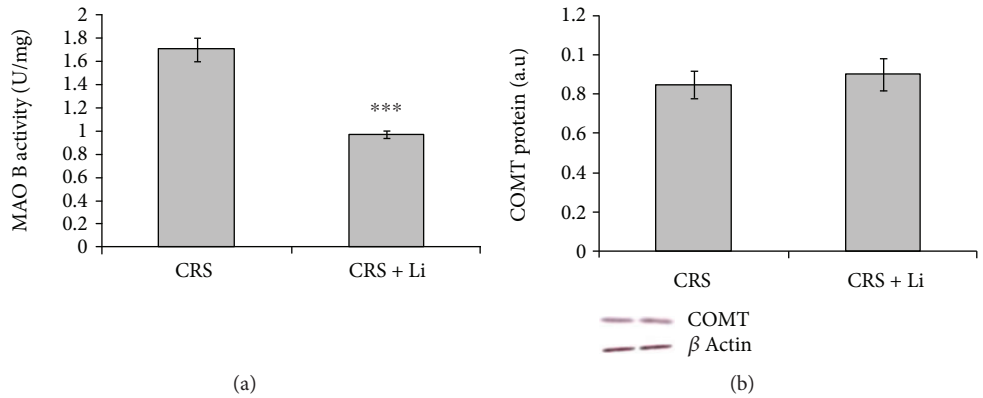

Figure 3: Effects of lithium on monoamine oxidase B (MAO B) enzyme activity (a) and catechol-O-methyltransferase (COMT) protein levels (b) in the hippocampus of animals exposed to CRS. The values are means ± S.E.M. of 10 rats. Statistical significance: $^{***}p < 0.001$ animals exposed to CRS+Li *vs*. CRS animals (*t*-test). The level of MAO B activity was expressed as units per milligram of protein (U/mg) and protein levels of COMT were expressed in arbitrary units normalized in relation to β-actin.

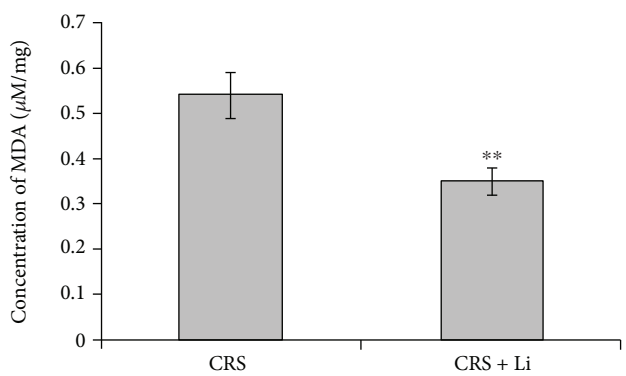

Figure 4: Effects of lithium on the concentration of malondialdehyde (MDA) in the hippocampus of animals exposed to CRS. The values are means ± S.E.M. of 10 rats. Statistical significance: $^{**}p < 0.01$ animals exposed to CRS+Li *vs*. CRS animals (*t*-test). The final result for concentration of MDA was expressed as μM/mg protein.

3.7. Changes of GR mRNA Levels, Protein Levels, and Enzyme Activity in the Hippocampus. Lithium treatment did not change the gene expression of GR enzymes (Figure 6(e)), but it significantly increased the enzyme activity of GR by 27% ($p < 0.001$, *t*-test, Figure 5(e)) in animals exposed to CRS.

3.8. Changes in Animal Behavior. The animals exposed to CRS treated with lithium showed significant increase of time spent in open arms compared to CRS rats. Based on these results, we calculated anxiety index (AI). Lithium treatment in animals exposed to CRS significantly decreased AI by 45% ($p < 0.001$, *t*-test, Figure 7), compared with CRS animals.

4. Discussion

The results of this study show that mood stabilizer lithium modulates hippocampal levels of BDNF, turnover of DA, and antioxidant defense system and stabilizes behavior in chronically stressed rats. We observed that CRS increased

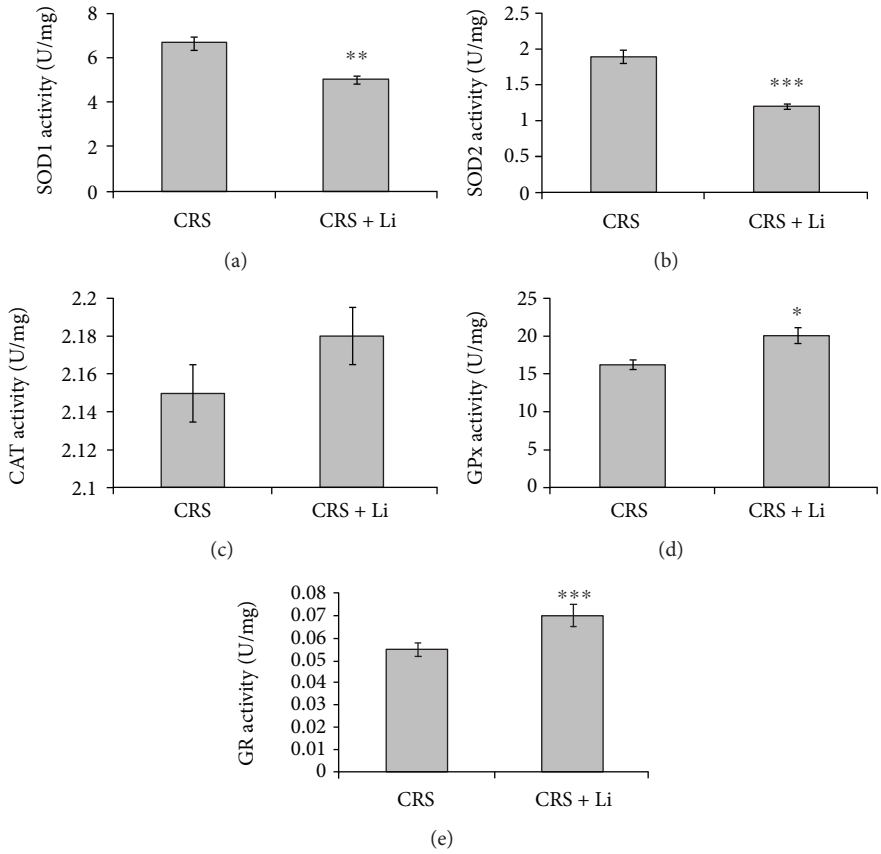

Figure 5: Effects of lithium on enzyme activity from CuZn superoxide dismutase (SOD1) (a), Mn superoxide dismutase (SOD2) (b), catalase (CAT) (c), glutathione peroxidase (GPx) (d), and glutathione reductase (GR) (e) in the hippocampus of animals exposed to CRS. The values are means ± S.E.M. of 10 rats. Statistical significance: $^{*}p < 0.05$, $^{**}p < 0.01$, and $^{***}p < 0.001$ animals exposed to CRS+Li *vs*. CRS animals (*t*-test). The final result for enzyme activity was expressed as units per milligram of protein (U/mg).

hippocampal BDNF protein, the key neurotrophic factor involved in the regulation of the release of neurotransmitters. This adaptive response is probably necessary to maintain the hippocampal BDNF capacity in conditions provoked by CRS because the hippocampus is the region that plays a crucial role in learning and memory and it is an area also particularly susceptible to chronic stress [8, 9]. However, lithium treatment decreased high protein levels of BDNF in chronically stressed rats to the level of unstressed animals. Our results show that it is possible that lithium has an effect on normalizing neuroplasticity in chronically stressed rats. In addition, in our earlier studies, we found that CRS induced a significant decrease of hippocampal DA concentration [6]. Literature data have confirmed that the decreased concentration of DA was observed in many psychiatric and neurodegenerative disorders, for example, depressive illness and Parkinson's disease [19, 38]. It is known that an increase of monoamine neurotransmitter levels is an important therapeutic strategy for several neuropsychiatric disorders [39]. In the present study, we found that lithium treatment increased both protein levels of hippocampal TH and concentration of DA in chronically stressed rats to the levels found in unstressed animals [6, 7], which indicates that lithium enabled *de novo* synthesis of hippocampal DA in chronically stressed rats. Lithium may have induced the gene expression of hippocampal TH in stress condition through the activator protein-1 (AP-1) transcription factor pathway [40]. The dynamics of DA transmission is regulated by reuptake through DAT. Dopamine transporter (DAT) is localized in the plasma membrane of axon terminals, and it reuptakes DA from the synapse [41] and controls the levels of DA in the extracellular space [42–44]. In this study, we found that CRS significantly increased protein levels of DAT. The higher protein levels of DAT suggest that DAT can be upregulated in response to a heightened demand for uptake of DA in conditions provoked by CRS. Stress-induced changes in the degradation of nonvesicular DA may play a role in the decrease of DA transmission. This is in line with the monoamine hypothesis of depression which states that depressive disorder is caused by insufficient signaling by monoamines [45]. An important result of this study is that lithium treatment in animals exposed to CRS decreased high protein levels of hippocampal DAT to the level of unstressed animals. It is possible that lithium has an effect on normalizing DA transmission in chronically stressed rats. In addition, monitoring of DA degradation is important for understanding dopaminergic turnover. The metabolism of monoamines

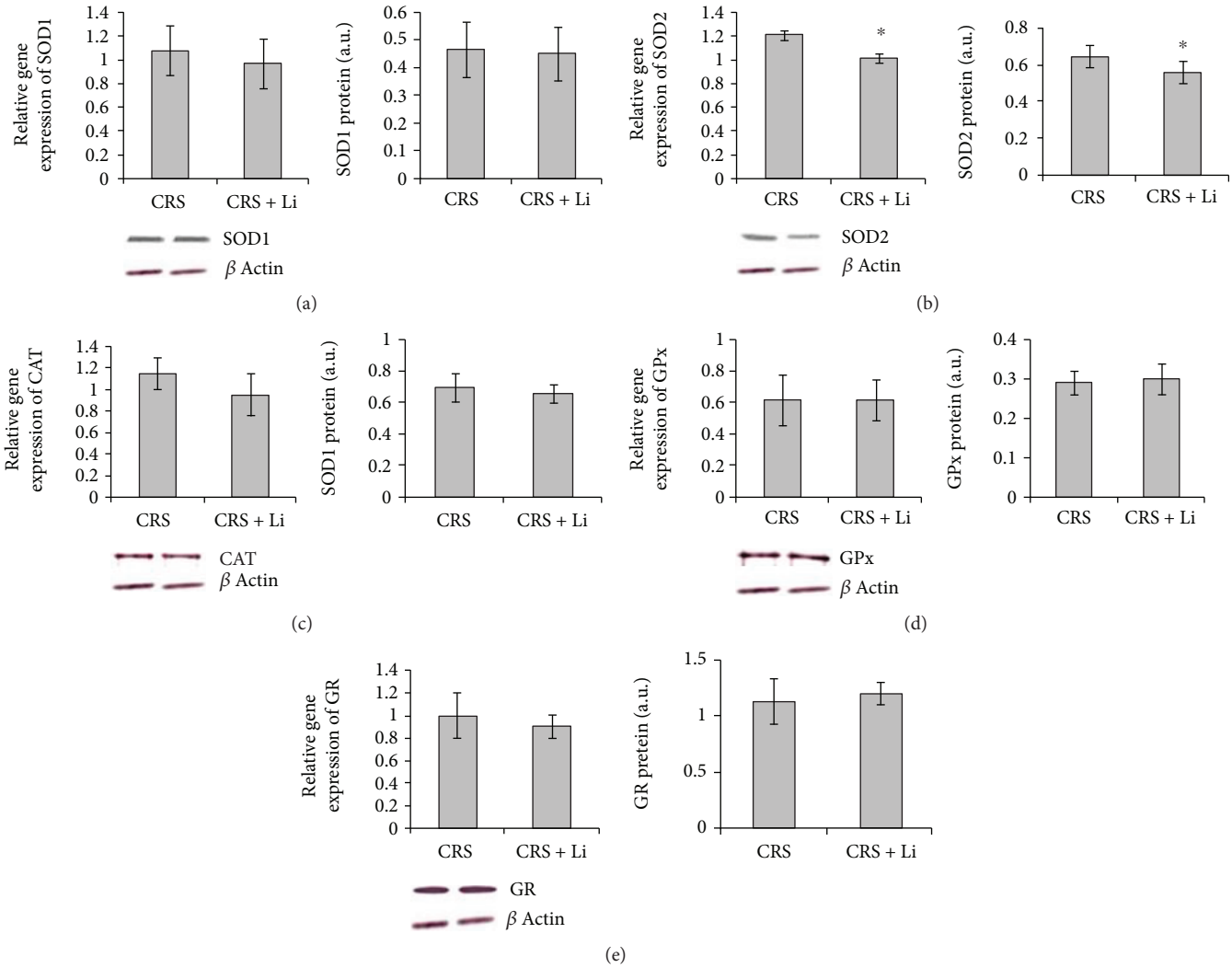

Figure 6: Effects of lithium on mRNA and protein levels from CuZn superoxide dismutase (SOD1) (a), Mn superoxide dismutase (SOD2) (b), catalase (CAT) (c), glutathione peroxidase (GPx) (d) and glutathione reductase (GR) (e) in the hippocampus of animals exposed to CRS. The values are means ± S.E.M. of 10 rats. Statistical significance: $^{*}p < 0.05$ animals exposed to CRS + Li *vs*. CRS animals (t-test). The final result was expressed as fold change relative to the calibrator and normalized to cyclophilin A and protein levels was expressed in arbitrary units normalized in relation to β-actin.

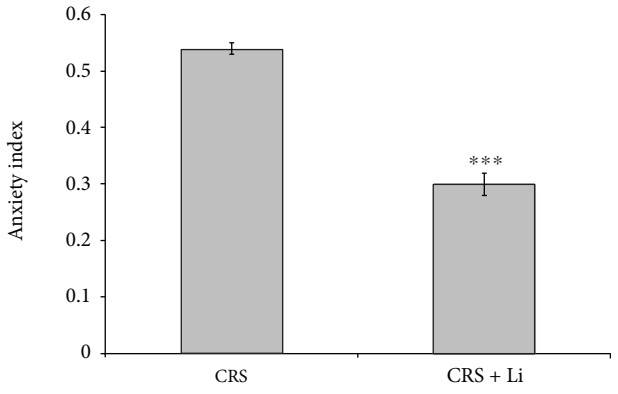

Figure 7: Effects of lithium on the anxiety index (AI) in animals exposed to CRS. The values are means ± S.E.M. of 10 rats. Statistical significance: $^{***}p < 0.001$ animals exposed to CRS + Li *vs*. CRS animals (t-test).

by MAO is the major source of hydrogen peroxide in the brain [46]. In our previous studies, we found that CRS induced significant increase of enzyme activity of MAO B, as well as levels of COMT protein in the hippocampus [7]. These findings suggest the possibility of increased degradation of monoamine in the hippocampus in chronically stressed rats [7]. Mallajosyula et al. [47] have shown that increased MAO B activity in the astrocytes causes Parkinsonian. It is known that the inhibition of MAO activity can prolong the time during which neurotransmitters are available in the synaptic cleft [48]. Therefore, the inhibition of MAO and/or increase of monoamine neurotransmitter levels are important therapeutic strategies for several neuropsychiatric disorders [39]. The literature data confirm that lithium is a very weak inhibitor of MAO. In the present study, we found that lithium treatment in animals exposed to CRS decreased hippocampal MAO B activity to the level of unstressed

animals, while levels of COMT protein remained unchanged. Decreased enzyme activity of MAO B suggests the possibility of decreased degradation of DA, which is confirmed by significantly increased concentration of DA in the hippocampus of chronically stressed rats. Our results are in accordance with the reports of Cesura and Pletscher [39] and Knoll [49] who found that the increase in DA levels was caused by MAO B inhibitors. Reduced enzymatic activity of MAO could contribute to slowing, halting, and possible reversing of neurodegeneration in dopaminergic neurons which was initiated by oxidative stress [50]. In pathological conditions, lithium treatment significantly reduces the levels of plasma lipid peroxides and improves antioxidant status [51, 52]. Decreased hippocampal MDA concentration in chronically stressed rats treated with lithium, found in this study, confirms that lithium is involved in the reduction of oxidative stress in chronic stress conditions. Based on our results, it could be speculated that decreased DA degradation via MAO may be the way by which lithium reduces oxidative stress in stress conditions. These findings suggest that further investigation of metabolites incurred from oxidative deamination of DA is needed to highlight the exact reason for reduced oxidative stress.

Modulated activities of antioxidative enzymes SOD, CAT, and GPx could be markers of oxidative stress. For example, a level of SOD is decreased when stress conditions are reduced [53]. The literature data confirm that treatment with lithium increased mRNA expression of nuclear factor (erythroid-derived 2)-like 2 (Nrf2), a signaling molecule which plays an intermediary role in defending against oxidative stress, by orchestrating the gene transcriptions of antioxidant enzymes [54–57]. In addition, nuclear factor κB (NF-κB) is regulated by redox sensitive factors. The absence of Nrf2 is associated with increased oxidative stress, leading to the amplification of cytokine production, as NF-κB is more readily activated in oxidative environments [58]. The imbalance between Nrf2 and NF-κB pathways is associated with a significant number of diseases including neurodegeneration [59]. In the present study, we observed that lithium treatment did not change the gene expression of SOD1, CAT, GPx, and GR but it decreased the gene expression of SOD2 in the hippocampus of chronically stressed rats. It is possible that the treatment with lithium is involved in maintaining a constant level of the gene expression of SOD1, CAT, GPx, and GR in chronically stressed rats for regulating the redox balance and responses to chronic stress. Furthermore, we recorded that the animals exposed to CRS treated with lithium showed a decrease of the enzyme activities of SOD1 and SOD2, while CAT activity remained unchanged. Our results are consistent with the reports of Khairova et al. [53] who also found a decrease in SOD levels, as well as unchanged CAT levels after lithium treatment. It is known that elevated SOD/CAT ratio suggests an increase in oxidative stress levels, mostly associated with the elevation in cell hydrogen peroxide concentration [60]. We recorded a reduction in SOD1/CAT ratio and SOD2/CAT ratio in animals exposed to CRS after lithium treatment, compared with CRS animals. This finding confirms that the reduction in SOD/CAT ratio may indicate lower oxidative stress, which is reflected mainly in a decrease in the concentration of cell hydrogen peroxide [60].

It is known that treatment with lithium inhibits reactive oxygen metabolite H_2O_2-induced cell death in primary cultured rat cerebral cortical cells, suggesting that lithium produces a protective effect against oxidative stress-induced cell death [61]. Glutathione (GSH) plays an important role in the cellular defense against ROS-induced oxidative damage in the brain [61]. Cui et al. [61] found that chronic treatment with lithium increased levels of GSH. The increased activity of GPx found in our study indicates the increased reduction of lipid hydroperoxides to their corresponding alcohols and free hydrogen peroxide to water in chronically stressed rats treated with lithium. It is possible that the increased activity of GPx compensated the decreased antioxidant capacity of CAT [62] in chronically stressed animals treated with lithium. Oxidized GSH can be reduced back by GR. In the present study, we found that treatment with lithium in animals exposed to CRS significantly increased the enzymatic activities of GR. Significantly increased enzymatic activities of hippocampal GR indicate increased reduction of GSH. It is known that the ratio of reduced GSH to oxidized GSH within cells is often used as a measure of cellular oxidative stress. Increased GPx and GR activities may also be the way by which lithium is involved in the reduction of oxidative damage in chronically stressed rats treated with this drug.

In addition, chronic treatment with mood stabilizing drug lithium in the animals exposed to CRS significantly increased time spent in open arms. This finding confirms that lithium stabilizes behavior in animals with anxiety-like behavior.

In summary, the modulation of hippocampal antioxidant status and reduced oxidative stress by lithium stabilized behavior in animals with high anxiety index. In addition, reduced oxidative stress was followed by the changes of both dopaminergic turnover and levels of BDNF protein in chronically stressed rats treated with lithium. These findings may be very important in the research on the effects of lithium on the modulation of antioxidant defense system in stress-induced diseases.

Data Availability

The data used to support the findings of this study have been deposited in the University Library "Svetozar Marković" (Belgrade, Serbia) repository UDC number [615.214.23: 546.34]: 616.895 (043.3).

Conflicts of Interest

The authors report no conflict of interest. The authors alone are responsible for the content and writing of the paper.

Authors' Contributions

Ljubica Gavrilović and Snežana B. Pajović equally contributed to this work.

Acknowledgments

This work was supported by the Ministry of Education, Science and Technological Development of the Republic of Serbia, Contract nos. III 41027, OI 173041, and III41022.

References

[1] D. Kanazir, R. Djordjevic-Markovic, and P. Grossarth-Maticek, "Psychosocial (emotional) stress, steriod hormones and carcinogenesis: molecular aspects, facts and speculations," in *Progress in Biorganic Chemistry and Molecular Biology*, Y. A. Ouchinnikov, Ed., pp. 509–530, Elsevier, 1984.

[2] S. Pajović, G. Nikezić, and J. V. Martinović, "Effects of ovarian hormones superoxide dismutase activity in rat brain synaptosomes," *Neuroendocrinology Letters*, vol. 16, pp. 291–296, 1994.

[3] S. F. Sorrells, J. R. Caso, C. D. Munhoz, and R. M. Sapolsky, "The stressed CNS: when glucocorticoids aggravate inflammation," *Neuron*, vol. 64, no. 1, pp. 33–39, 2009.

[4] M. Popoli, Z. Yan, B. S. McEwen, and G. Sanacora, "The stressed synapse: the impact of stress and glucocorticoids on glutamate transmission," *Nature Reviews Neuroscience*, vol. 13, no. 1, pp. 22–37, 2012.

[5] J. A. Siuciak, C. Boylan, M. Fritsche, C. A. Altar, and R. M. Lindsay, "BDNF increases monoaminergic activity in rat brain following intracerebroventricular or intraparenchymal administration," *Brain Research*, vol. 710, no. 1-2, pp. 11–20, 1996.

[6] N. Popović, S. B. Pajović, V. Stojiljković et al., "Relationship between behaviors and catecholamine content in prefrontal cortex and hippocampus of chronically stressed rats," in *RAD Conference Proceedings*, pp. 255–259, Budva, Montenegro, 2017.

[7] N. Popović, L. Gavrilović, V. Stojiljković et al., "Relationship between stress-activated dopaminergic system and glutathione antioxidant defense system in rat hippocampus," in *Seventh Congress of Serbian Neuroscience Society with International Participation, Book of Abstracts*, p. 52, Serbian Neuroscience Society, 2017.

[8] H. Eichenbaum, "Hippocampus: cognitive processes and neural representations that underlie declarative memory," *Neuron*, vol. 44, no. 1, pp. 109–120, 2004.

[9] Y. C. Tse, I. Montoya, A. S. Wong et al., "A longitudinal study of stress-induced hippocampal volume changes in mice that are susceptible or resilient to chronic social defeat," *Hippocampus*, vol. 24, no. 9, pp. 1120–1128, 2014.

[10] R. A. Floyd, "Antioxidants, oxidative stress, and degenerative neurological disorders," *Proceedings of the Society for Experimental Biology and Medicine*, vol. 222, no. 3, pp. 236–245, 1999.

[11] B. Halliwell, "Role of free radicals in the neurodegenerative diseases: therapeutic implications for antioxidant treatment," *Drugs & Aging*, vol. 18, no. 9, pp. 685–716, 2001.

[12] A. Masood, A. Nadeem, S. J. Mustafa, and J. M. O'Donnell, "Reversal of oxidative stress-induced anxiety by inhibition of phosphodiesterase-2 in mice," *The Journal of Pharmacology and Experimental Therapeutics*, vol. 326, no. 2, pp. 369–379, 2008.

[13] A. C. Andreazza, M. Kauer-Sant'Anna, B. N. Frey et al., "Effects of mood stabilizers on DNA damage in an animal model of mania," *Journal of Psychiatry & Neuroscience*, vol. 33, no. 6, pp. 516–524, 2008.

[14] L. Shao, L. T. Young, and J. F. Wang, "Chronic treatment with mood stabilizers lithium and valproate prevents excitotoxicity by inhibiting oxidative stress in rat cerebral cortical cells," *Biological Psychiatry*, vol. 58, no. 11, pp. 879–884, 2005.

[15] R. Machado-Vieira, H. K. Manji, and C. A. Zarate Jr., "The role of lithium in the treatment of bipolar disorder: convergent evidence for neurotrophic effects as a unifying hypothesis," *Bipolar Disorders*, vol. 11, pp. 92–109, 2009.

[16] M. Schafer, S. Goodenough, B. Moosmann, and C. Behl, "Inhibition of glycogen synthase kinase 3β is involved in the resistance to oxidative stress in neuronal HT22 cells," *Brain Research*, vol. 1005, no. 1-2, pp. 84–89, 2004.

[17] N. Popović, B. S. Pajović, V. Stojiljković et al., "Increased activity of hippocampal antioxidant enzymes as an important adaptive phenomenon of the antioxidant defense system in chronically stressed rats," *Acta Veterinaria*, vol. 67, no. 4, pp. 540–550, 2017.

[18] M. Bilici, H. Efe, M. A. Köroğlu, H. A. Uydu, M. Bekaroğlu, and O. Değer, "Antioxidative enzyme activities and lipid peroxidation in major depression: alterations by antidepressant treatments," *Journal of Affective Disorders*, vol. 64, no. 1, pp. 43–51, 2001.

[19] G. Tanda, E. Carboni, R. Frau, and G. Di Chiara, "Increase of extracellular dopamine in the prefrontal cortex: a trait of drugs with antidepressant potential?," *Psychopharmacology*, vol. 115, no. 1-2, pp. 285–288, 1994.

[20] L. Gavrilovic, N. Spasojevic, and S. Dronjak, "Subsequent stress increases gene expression of catecholamine synthetic enzymes in cardiac ventricles of chronic-stressed rats," *Endocrine*, vol. 37, no. 3, pp. 425–429, 2010.

[21] N. Popović, S. B. Pajović, V. Stojiljković et al., "Prefrontal catecholaminergic turnover and antioxidant defense system of chronically stressed rats," *Folia Biologica*, vol. 65, no. 1, pp. 43–54, 2017.

[22] G. D. Gamaro, M. B. Michalowski, D. H. Catelli, M. H. Xavier, and C. Dalmaz, "Effect of repeated restraint stress on memory in different tasks," *Brazilian Journal of Medical and Biological Research*, vol. 32, no. 3, pp. 341–347, 1999.

[23] K. S. Kim and P. L. Han, "Optimization of chronic stress paradigms using anxiety- and depression-like behavioral parameters," *Journal of Neuroscience Research*, vol. 83, no. 3, pp. 497–507, 2006.

[24] S. Nonaka and D. M. Chuang, "Neuroprotective effects of chronic lithium on focal cerebral ischemia in rats," *Neuroreport*, vol. 9, no. 9, pp. 2081–2084, 1998.

[25] L. Gavrilović, V. Stojiljković, N. Popović et al., "Animal models for chronic stress-induced oxidative stress in the spleen: the role of exercise and catecholaminergic system," in *Experimental Animal Models of Human Diseases - An Effective Therapeutic Strategy*, pp. 238–310, IntechOpen, Rijeka, Croatia, 2018.

[26] M. Zhou and N. Panchuk-Voloshina, "A one-step fluorometric method for the continuous measurement of monoamine oxidase activity," *Analytical Biochemistry*, vol. 253, no. 2, pp. 169–174, 1997.

[27] L. Gavrilović, V. Stojiljković, J. Kasapović, N. Popović, S. B. Pajović, and S. Dronjak, "Treadmill exercise does not change gene expression of adrenal catecholamine biosynthetic enzymes in chronically stressed rats," *Anais da Academia Brasileira de Ciências*, vol. 85, no. 3, pp. 999–1012, 2013.

[28] L. Gavrilović, V. Stojiljković, J. Kasapović et al., "Forced exercise changes catecholamine synthesis in the spleen of adult

rats," *Journal of Neuroimmunology*, vol. 251, no. 1-2, pp. 1–5, 2012.

[29] K. J. Livak and T. D. Schmittgen, "Analysis of relative gene expression data using real-time quantitative PCR and the $2^{-\Delta\Delta CT}$ method," *Methods*, vol. 25, no. 4, pp. 402–408, 2001.

[30] T. M. Stich, "Determination of protein covalently bound to agarose supports using bicinchoninic acid," *Analytical Biochemistry*, vol. 191, no. 2, pp. 343–346, 1990.

[31] V. Stojiljković, A. Todorović, S. Pejić et al., "Antioxidant status and lipid peroxidation in small intestinal mucosa of children with celiac disease," *Clinical Biochemistry*, vol. 42, no. 13-14, pp. 1431–1437, 2009.

[32] E. Beutler, "Catalase. Red cell metabolism," in *A Manual of Biochemical Methods*, Grune & Stratton, Orlando, FL, USA, 3rd edition, 1982.

[33] S. Pellow, P. Chopin, S. E. File, and M. Briley, "Validation of open : closed arm entries in an elevated plus-maze as a measure of anxiety in the rat," *Journal of Neuroscience Methods*, vol. 14, no. 3, pp. 149–167, 1985.

[34] H. Cohen, A. B. Geva, M. A. Matar, J. Zohar, and Z. Kaplan, "Post-traumatic stress behavioural responses in inbred mouse strains: can genetic predisposition explain phenotypic vulnerability?," *The International Journal of Neuropsychopharmacology*, vol. 11, no. 3, pp. 331–349, 2008.

[35] H. Cohen, M. A. Matar, D. Buskila, Z. Kaplan, and J. Zohar, "Early post-stressor intervention with high-dose corticosterone attenuates posttraumatic stress response in an animal model of posttraumatic stress disorder," *Biological Psychiatry*, vol. 64, no. 8, pp. 708–717, 2008.

[36] A. Mazor, M. A. Matar, Z. Kaplan, N. Kozlovsky, J. Zohar, and H. Cohen, "Gender-related qualitative differences in baseline and post-stress anxiety responses are not reflected in the incidence of criterion-based PTSD-like behaviour patterns," *The World Journal of Biological Psychiatry*, vol. 10, no. 4-3, pp. 856–869, 2009.

[37] T. N. Huynh, A. M. Krigbaum, J. J. Hanna, and C. D. Conrad, "Sex differences and phase of light cycle modify chronic stress effects on anxiety and depressive-like behavior," *Behavioural Brain Research*, vol. 222, no. 1, pp. 212–222, 2011.

[38] K. W. Lange, T. W. Robbins, C. D. Marsden, M. James, A. M. Owen, and G. M. Paul, "L-Dopa withdrawal in Parkinson's disease selectively impairs cognitive performance in tests sensitive to frontal lobe dysfunction," *Psychopharmacology*, vol. 107, no. 2-3, pp. 394–404, 1992.

[39] A. M. Cesura and A. Pletscher, "The new generation of monoamine oxidase inhibitors," *Progress in Drug Research*, vol. 38, pp. 171–297, 1992.

[40] G. Chen, P. X. Yuan, Y. M. Jiang, L. D. Huang, and H. K. Manji, "Lithium increases tyrosine hydroxylase levels both in vivo and in vitro," *Journal of Neurochemistry*, vol. 70, no. 4, pp. 1768–1771, 1998.

[41] B. A. Merchant and J. D. Madura, "Insights from molecular dynamics: the binding site of cocaine in the dopamine transporter and permeation pathways of substrates in the leucine and dopamine transporters," *Journal of Molecular Graphics and Modelling*, vol. 38, pp. 1–12, 2012.

[42] L. Norregaard and U. Gether, "The monoamine neurotransmitter transporters: structure, conformational changes and molecular gating," *Current Opinion in Drug Discovery & Development*, vol. 4, pp. 591–601, 2001.

[43] N. Khodayari, M. Garshasbi, F. Fadai et al., "Association of the dopamine transporter gene (DAT1) core promoter polymorphism -67T variant with schizophrenia," *American Journal of Medical Genetics*, vol. 129B, no. 1, pp. 10–12, 2004.

[44] H. Zhang, S. Li, M. Wang, B. Vukusic, Z. B. Pristupa, and F. Liu, "Regulation of dopamine transporter activity by carboxypeptidase E," *Molecular Brain*, vol. 2, no. 1, p. 10, 2009.

[45] N. R. Carlson, *Foundations of Physiological Psychology*, Allyn and Bacon, Inc., Boston, MA, USA, 1988.

[46] Z. Fisar, J. Hroudová, and J. Raboch, "Inhibition of monoamine oxidase activity by antidepressants and mood stabilizers," *Neuro Endocrinology Letters*, vol. 31, no. 5, pp. 645–656, 2010.

[47] J. K. Mallajosyula, D. Kaur, S. J. Chinta et al., "MAO-B elevation in mouse brain astrocytes results in Parkinson's pathology," *PLoS One*, vol. 3, no. 2, article e1616, 2008.

[48] A. Montoya, R. Bruins, M. Katzman, and P. Blier, "The noradrenergic paradox: implications in the management of depression and anxiety," *Neuropsychiatric Disease and Treatment*, vol. 2016, no. 12, pp. 541–557, 2016.

[49] J. Knoll, "(-)Deprenyl (selegiline): past, present and future," *Neurobiology*, vol. 8, no. 2, pp. 179–199, 2000.

[50] M. B. H. Youdim, D. Edmondson, and K. F. Tipton, "The therapeutic potential of monoamine oxidase inhibitors," *Nature Reviews Neuroscience*, vol. 7, no. 4, pp. 295–309, 2006.

[51] R. Machado-Vieira, A. C. Andreazza, C. I. Viale et al., "Oxidative stress parameters in unmedicated and treated bipolar subjects during initial manic episode: a possible role for lithium antioxidant effects," *Neuroscience Letters*, vol. 421, no. 1, pp. 33–36, 2007.

[52] A. C. Andreazza, C. Cassini, A. R. Rosa et al., "Serum S100B and antioxidant enzymes in bipolar patients," *Journal of Psychiatric Research*, vol. 41, no. 6, pp. 523–529, 2007.

[53] R. Khairova, R. Pawar, G. Salvadore et al., "Effects of lithium on oxidative stress parameters in healthy subjects," *Molecular Medicine Reports*, vol. 5, no. 3, pp. 680–682, 2012.

[54] M. Dodson, M. Redmann, N. S. Rajasekaran, V. Darley-Usmar, and J. Zhang, "KEAP1–NRF2 signalling and autophagy in protection against oxidative and reductive proteotoxicity," *Biochemical Journal*, vol. 469, no. 3, pp. 347–355, 2015.

[55] P. Milani, G. Ambrosi, O. Gammoh, F. Blandini, and C. Cereda, "SOD1 and DJ-1 converge at Nrf2 pathway: a clue for antioxidant therapeutic potential in neurodegeneration," *Oxidative Medicine and Cellular Longevity*, vol. 2013, Article ID 836760, 12 pages, 2013.

[56] L. Gan and J. A. Johnson, "Oxidative damage and the Nrf2-ARE pathway in neurodegenerative diseases," *Biochimica et Biophysica Acta (BBA) - Molecular Basis of Disease*, vol. 1842, no. 8, pp. 1208–1218, 2014.

[57] B. Alural, A. Ozerdem, J. Allmer, K. Genc, and S. Genc, "Lithium protects against paraquat neurotoxicity by NRF2 activation and miR-34a inhibition in SH-SY5Y cells," *Frontiers in Cellular Neuroscience*, vol. 9, p. 209, 2015.

[58] V. Ganesh Yerra, G. Negi, S. S. Sharma, and A. Kumar, "Potential therapeutic effects of the simultaneous targeting of the Nrf2 and NF-κB pathways in diabetic neuropathy," *Redox Biology*, vol. 1, no. 1, pp. 394–397, 2013.

[59] Y. Ben-Neriah and M. Karin, "Inflammation meets cancer, with NF-κB as the matchmaker," *Nature Immunology*, vol. 12, no. 8, pp. 715–723, 2011.

[60] W. Gsell, R. Conrad, M. Hickethier et al., "Decreased catalase activity but unchanged superoxide dismutase activity in brains of patients with dementia of Alzheimer type," *Journal of Neurochemistry*, vol. 64, no. 3, pp. 1216–1223, 1995.

[61] J. Cui, L. Shao, L. T. Young, and J. F. Wang, "Role of glutathione in neuroprotective effects of mood stabilizing drugs lithium and valproate," *Neuroscience*, vol. 144, no. 4, pp. 1447–1453, 2007.

[62] S. W. Kang, S. G. Rhee, T. S. Chang, W. Jeong, and M. H. Choi, "2-Cys peroxiredoxin function in intracellular signal transduction: therapeutic implications," *Trends in Molecular Medicine*, vol. 11, no. 12, pp. 571–578, 2005.

Hindawi
Oxidative Medicine and Cellular Longevity
Volume 2019, Article ID 2069250, 12 pages
https://doi.org/10.1155/2019/2069250

Research Article

Synthesis and Characterization of 3-(1-((3,4-Dihydroxyphenethyl) amino)ethylidene)-chroman-2,4-dione as a Potential Antitumor Agent

Dušan S. Dimić,[1] Zoran S. Marković,[2] Luciano Saso,[3] Edina H. Avdović,[4] Jelena R. Đorović,[5] Isidora P. Petrović,[6] Danijela D. Stanisavljević,[6] Milena J. Stevanović,[6,7,8] Ivan Potočňák,[9] Erika Samoľová,[9] Srećko R. Trifunović,[4] and Jasmina M. Dimitrić Marković[1]

[1]*University of Belgrade, Faculty of Physical Chemistry, Studentski trg 12-16, 11000 Belgrade, Serbia*
[2]*Department of Chemical-Technological Sciences, State University of Novi Pazar, Vuka Karadžića bb, 36300 Novi Pazar, Serbia*
[3]*Department of Physiology and Pharmacology "Vittorio Erspamer", Sapienza University of Rome, Rome, Italy*
[4]*University of Kragujevac, Faculty of Science, Radoja Domanovića 12, 34000 Kragujevac, Serbia*
[5]*BioIRC, Bioengineering R&D Center, Prvoslava Stojanovića 6, 34000 Kragujevac, Serbia*
[6]*University of Belgrade, Institute of Molecular Genetics and Genetic Engineering, Vojvode Stepe 444a, PO Box 23, 11010 Belgrade, Serbia*
[7]*University of Belgrade, Faculty of Biology, Studentski trg 16, 11000 Belgrade, Serbia*
[8]*Serbian Academy of Sciences and Art, Knez Mihajlova 35, 11000 Belgrade, Serbia*
[9]*Institute of Chemistry, P. J. Šafárik University in Košice, Moyzesova 11, 04154 Košice, Slovak Republic, Slovakia*

Correspondence should be addressed to Jasmina M. Dimitrić Marković; markovich@ffh.bg.ac.rs

Received 16 July 2018; Accepted 5 December 2018; Published 13 February 2019

Academic Editor: Daniela Giustarini

The newly synthesized coumarin derivative with dopamine, 3-(1-((3,4-dihydroxyphenethyl)amino)ethylidene)-chroman-2,4-dione, was completely structurally characterized by X-ray crystallography. It was shown that several types of hydrogen bonds are present, which additionally stabilize the structure. The compound was tested *in vitro* against different cell lines, healthy human keratinocyte HaCaT, cervical squamous cell carcinoma SiHa, breast carcinoma MCF7, and hepatocellular carcinoma HepG2. Compared to control, the new derivate showed a stronger effect on both healthy and carcinoma cell lines, with the most prominent effect on the breast carcinoma MCF7 cell line. The molecular docking study, obtained for ten different conformations of the new compound, showed its inhibitory nature against CDK_S protein. Lower inhibition constant, relative to one of 4-OH-coumarine, proved stronger and more numerous interactions with CDK_S protein. These interactions were carefully examined for both parent molecule and derivative and explained from a structural point of view.

1. Introduction

Cell structures can be significantly influenced and damaged by sustained oxidative stress which is considered to be a major cause in the pathogenesis of many, if not all, diseases. Cancer is one of the most prominent causes of death in the modern world. Cancer initiation and progression phases have been closely related to oxidative stress which increases somatic mutations, neoplastic transformation, and generally genome instability [1, 2]. In the past several years, there have been an increased number of articles that connect oxidative stress with the development of various cancers, although the actual links are a matter of dispute [1, 2].

Nowadays, there is an increased interest in new drug discovery, to adequately promote the survival rate against cancer. Presently existing anticancer drugs are insufficient due to

many side effects, nonselectivity, resistance, etc. Many of the naturally occurring molecules possessing antioxidant activity exhibit a synergistic effect when combined with other naturally occurring, or synthetic, molecules. This can lead to the creation of new types of a biological rationale for the treatment of different cancer types or their use as adjuvants with conventional therapeutic regimens. The present paper presents the design of a new coumarin/catecholamine derivative [1, 2].

Coumarins and their derivatives are widely present family of molecules in nature. They can be accumulated in fruits [3], vegetables [4, 5], trees [6], seeds [7], and vines. Coumarins have important biological activities, some of which include regulation of growth, control of respiration [8], defense against herbivores and microorganisms [9], and hormonal and signaling role [10]. The common structural elements are fused pyrone and benzene rings with a carboxyl group on the first ring. The structural diversity of coumarins allows different pharmacological properties: antibacterial, antifungal, antioxidant, and cytotoxic [11–13]. The synthetic coumarins also have great potential as drugs for the treatment of neurodegenerative [14, 15] and microbial [16, 17] diseases, HIV [18, 19], and cancer [20, 21]. They also have been used as regulators of reactive radical species [22, 23]. Several reactive derivatives of coumarin with various molecules were already synthesized, and their biological reactivity explained experimentally and theoretically [24–26].

Dopamine, on the other side, belongs to the important group of catecholamines, which function as hormones and neurotransmitters in the peripheral endocrine and central nervous system [27–30]. The other functions include control of movement, reward processing, attention, working memory, emotions, sleeping, and dreaming. Dopamine and other catecholamines, as well as their metabolites, are gaining significant attention, due to the hypothesis that the origin of some, if not all, neurodegenerative diseases lies in oxidative stress and changes at the molecular level [31–34]. More than 20% of oxygen in the body is used in the brain; therefore, a considerable amount of the present fatty acids is exposed to reactive oxygen and nitrogen species [35–38]. The low permeability of the blood-brain barrier limits the use of the external antioxidants, which increases the importance of molecules with good radical scavenging activities that are already present in the body [37]. The catechol structure, as well as various side groups, has been proven, in different experimental and theoretical studies, to enhance the antiradical potency of molecules [39–43]. Besides being good antiradical agents, catecholamines and their analogs also exhibited as potential antitumor agents [44–46]. The structure-activity studies show that catechol moiety is also the essential part of these molecules influencing their antitumor activity [45, 47, 48]. In the case of dopamine and its analogs, it has been concluded that the aminoethyl group could be replaced by methyl or aminomethyl groups without a noticeable change in activity towards P-388 leukemia cells [49]. One of the assumptions is that the formation of reactive quinone is responsible for the cytotoxic and genotoxic activity of dopamine [50].

This article presents data on the reactivity of novel coumarin/dopamine derivative towards various tumor and healthy cells lines, with special emphasis on the synergistic effect of these two molecules. The synthesis is carried out assuming that there is no formation of a quinone, which is harmful to healthy cells, and that the catechol unit is preserved and combined with the coumarin. The crystallographic structure is obtained for the synthesized derivative and explained in details. The molecular docking study is performed in order to gain better insight into the mechanism of the biological activity of new compound and possible differences in coumarin-protein and new derivative-protein interactions. The protein selected for molecular docking is cyclin-dependent kinases (CDKs), for both 4-hydroxycoumarin, as a parent molecule, and synthesized derivative. CDKs plays an important role in the control of cell division [51], and its deregulation can lead to the development of human diseases including cancer [52, 53]. Thus, the suppression of its activity could be a promising molecular route for anticancer therapy [54].

2. Materials and Methods

2.1. Substances. Dopamine hydrochloride, 4-hydroxycoumarin (4-OH-coumarin), methanol, toluene, and 96% ethanol were purchased from Sigma-Aldrich. The starting compound, 3-acetyl-4-hydroxy-coumarin, was obtained as explained in [55].

2.2. Spectral Analysis. The vibrational spectra were recorded on the Perkin-Elmer Spectrum One FT-IT spectrometer in the range between 4000 and 400 cm^{-1}. The KBr pellet technique was used. The NMR spectra (^{1}H and ^{13}C) were recorded on a Varian Gemini 200 spectrometer in $CDCl_3$ as a solvent and with TMS as an internal standard. The elemental microanalysis for C, H, and N was performed on the Vario EL III C, H, and N Elemental Analyzer. The mass spectra were obtained on a 5973 Mass spectrometer (Agilent, Santa Clara, CA) with MS quadruple, temperature 150°C, and a mass scan range of 40–600 amu at 70 eV.

2.3. Cell Culture. In this study, the following cell lines were used: healthy human keratinocyte HaCaT (AddexBio T0020001), cervical squamous cell carcinoma SiHa (ATCC®, HTB-3$5^{™}$), breast carcinoma MCF7 (ATCC® HTB-22™), and hepatocellular carcinoma HepG2 (ATCC® HB-8065™). All cell lines were grown in Dulbecco's modified Eagle's medium (DMEM) supplemented with 10% fetal bovine serum (FBS), 4500 mg/L glucose, and 1x antimycotic/antibiotic (all from Invitrogen™, USA). The cells were maintained at 37°C in 5% CO_2.

2.4. Cell Viability Assay. In order to assess whether selected compounds influence the viability of cell, the MTS Cell Proliferation Assay was applied, a colorimetric method for sensitive quantification of viable cells. The method is based on the reduction of MTS tetrazolium compound by viable cells generating a colored formazan product. This conversion is thought to be carried out by NAD(P)H-dependent dehydrogenase enzymes in metabolically active cells. The formazan dye produced by viable cells can be quantified by measuring the absorbance at 490–500 nm.

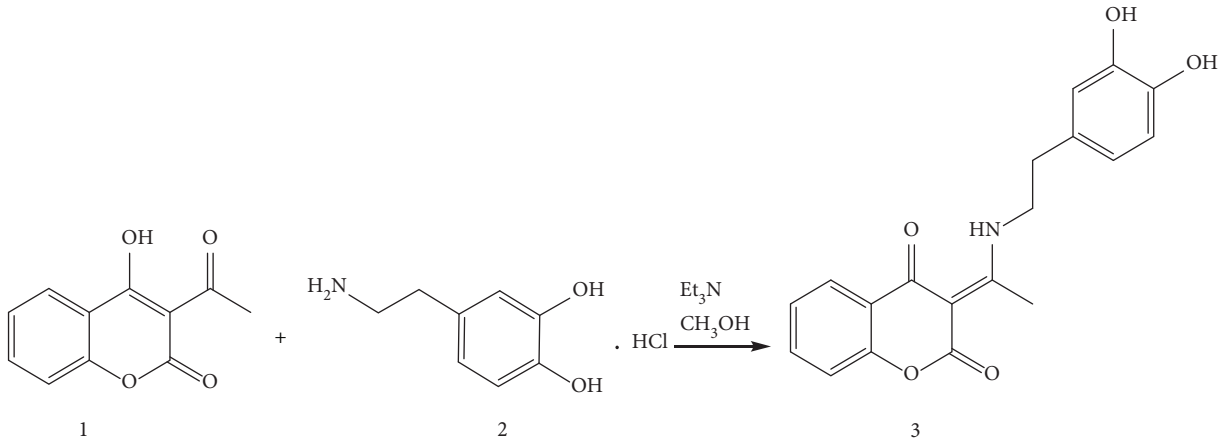

Scheme 1: Synthesis of 3-(1-((3,4-dihydroxyphenethyl)amino)ethylidene)-chroman-2,4-dione.

Cells (5×10^3 for Siha and MCF7 and 1×10^4 for HaCaT and HepG2/per well) were seeded in 96-well plates a day before treatment and then treated with various concentrations of 4-OH-coumarin or derivative **3** (100, 300, and 500 μM) for 48 hours. After 48 h, the effect of these treatments was monitored on cell's viability using MTS Cell Proliferation Assay (Promega CellTiter 96® AQueous One Solution Cell Proliferation Assay) and colorimetric quantification was done using a plate reader (Plate Reader Infinite 200 pro, Tecan).

2.5. Statistical Analyses. Statistical analyses were performed with SPSS statistical software (version 20). The data represent the means ± SEM from at least three independent experiments. Statistical analyses were performed by Student's t -test, and p value ≤ 0.05 was considered significant.

2.6. Theoretical Methods. Software package AutoDock 4.0 was used for molecular docking simulations [56]. The three-dimensional crystal structure of CDK protein was procured from the Protein Data Bank (PDB ID: 1KE9). Preparation of protein for docking simulations was done by removing the cocrystallized ligand, water molecules, and cofactors in the Discovery Studio 4.0. The calculations of Kollman charges and adding of the polar hydrogen were performed using the AutoDockTools (ADT) graphical user interface. The optimization of coumarin and coumarin derivate structures was performed at B3LYP-D3BJ/6-311++G(d,p) level of the theory [57–61] in the gas phase. For this purpose, Gaussian 09 Program package [62] was used. The structure of coumarin derivate was taken from crystallographic data. This level of theory was proven to reproduce well the crystallographic structure and experimentally obtained spectra for similar compounds [24, 25, 26]. The docking simulations were completed independently. During these simulations, the protein retained a rigid structure in the ADT, while both docked compounds possessed flexibility. All bonds of the compounds were treated as rotatable. For calculations of partial charges, the Geistenger method was selected. The Lamarckian Genetic Algorithm (LGA) method was used in all calculations for protein-ligand flexible docking simulation [63]. The grid boxes with grid center $4.0 \times 50.3 \times 11.5$ of CDK protein covered all of the protein binding sites and enabled free motion of ligands. The interactions between CDKs and the corresponding ligands were estimated and analyzed, for several most stable conformations, through the positions of the amino acids and the type of interaction that is achieved.

2.7. General Procedure for the Synthesis of 3-(1-((3,4-Dihydroxyphenethyl)amino)ethylidene)-chroman-2,4-dione. The synthesis of new coumarin derivative is presented in Scheme 1. The new compound (designated as compound **3** in Scheme 1) was obtained by refluxing and mixing of the reaction mixture (3-acetyl-4-hydroxicumarine (0.0014 mol; 0.3 g), dopamine hydrochloride (0.0014 mol; 0.23 g), and equimolar amounts of triethyl amine (0.0014 mol; 0.15 g) in 50 ml methanol for 3 h. The progress of reactions was monitored by TLC (toluene: acetone = 7: 3). When the reaction was completed, the mixture was cooled to room temperature. The obtained white crystals were filtered, air-dried, and recrystallized from methanol.

Yield, 0.321 g (64.45 %), Anal. Calcd. for $C_{19}H_{17}O_5N$ (M_r = 339.32) %: C, 67.25; H, 5.05; N, 4.12. Found: C, 67.00; H, 5.10; N, 4.16.

^{1}H NMR (DMSO, 200 MHz) δ in ppm: 2.55 (s, 3H, C2′–H), 2.80 (t, 2H, C2″–H), 3.76 (q, 2H, C1″–H), 6.5 (m, 1H, C4″–H, J=2.0 Hz), 6.67 (m, 2H, C7″–H, C8″–H), 7.25 (m, 1H, C6–H), 7.60 (dd, 2H, C5–H, C7–H), 7.91 (m, 1H, C8–H), 8.81 (s, 2H, OH), 13.66 (s, 1H, NH)

^{13}C NMR (DMSO, 50 MHz) δ in ppm: 18.35 (C2′), 34.11 (C2″), 45.71 (C1″), 96.18 (C3), 115.87 (C7″), 116.41 (C8), 119.74 (C8″), 120.41 (C10), 123.78 (C6), 125.86 (C5), 128.12 (C3″), 134.12 (C7), 144.17 (C6″), 145.46 (C5″), 153.20 (C9), 162.13 (C2), 1776.28 (C1′), 179.60 (C4).

IR (KBr, cm^{-1}): 3305 (NH and OH), 2921, 2857 (CH), 1668 (C=O), 1605, 1569, 1531, (C=C), 1118 (C–O).

2.8. X-ray Data Collection and Structure Refinement. A summary of X-ray diffraction experiment and structure refinement for **3·MeOH** is given in Table 1. The data collection was performed on an Oxford Diffraction Xcalibur Gemini ultra-diffractometer equipped with an AtlasS2 CCD

Table 1: Crystal data and structure refinement of **3·MeOH**.

Compound	**3·MeOH**	
Empirical formula	$C_{20}H_{21}NO_6$	
Formula weight	371.38	
Temperature	120(2) K	
Wavelength	1.54184 Å	
Crystal system	Triclinic	
Space group	*P*-1	
Unit cell dimensions	$a = 7.9449(3)$ Å	$\alpha = 82.538(3)^\circ$
	$b = 8.8742(3)$ Å	$\beta = 82.296(3)^\circ$
	$c = 13.1920(5)$ Å	$\gamma = 70.039(3)^\circ$
Volume	862.79(6) Å^3	
Z; density (calculated)	2; 1.430 g·cm^{-3}	
Absorption coefficient	0.883 mm^{-1}	
F(000)	392	
Crystal shape, color	Prism, white	
Crystal size	$0.311 \times 0.201 \times 0.072$ mm^3	
θ range for data collection	3.395–67.361°	
Index ranges	$-9 \le h \le 6$, $-10 \le k \le 10$, $-15 \le l \le 15$	
Reflections collected/independent	8977/3086 [R(int) = 0.0226]	
Absorption correction	Analytical	
Max. and min. transmission	0.938 and 0.841	
Data/restraints/parameters	3086/0/262	
Goodness-of-fit on F^2	1.034	
Final R indices [$I > 2\sigma(I)$]	$R1 = 0.0342$, w$R2 = 0.0876$	
R indices (all data)	$R1 = 0.0398$, w$R2 = 0.0924$	
Largest diff. peak and hole	0.226; -0.255 e.Å^{-3}	

detector using CuKα radiation. CrysAlis PRO 1.171.39.35c [64] was used for data collection, cell refinement, data reduction, and absorption correction. The structure was solved by SHELXT [65] and subsequent Fourier syntheses using SHELXL [66], implemented in WinGX program suit [67]. Anisotropic displacement parameters were refined for all nonhydrogen atoms. The hydrogen atoms bonded to nitrogen, oxygen atoms were found in the Fourier maps and refined freely, and aromatic and aliphatic carbon-bonded hydrogen atoms were placed in the calculated positions and refined riding on their parent C atoms with corresponding C–H distances and Uiso(H) = 1.2 or 1.5 Ueq(C), respectively. The analysis of bond distances and angles was performed using SHELXL and PLATON [68]. DIAMOND [69] was used for molecular graphics.

3. Results and Discussion

3.1. Chemistry. The synthesis of coumarin derivative is presented in Scheme 1. The structure of synthesized compound **3** was determined by means of elemental, spectral (IR, ^{1}H NMR, and ^{13}C NMR), and X-ray structural analysis (in the form of **3·MeOH**).

The formation of compound **3** was confirmed by IR spectra, with the presence of bands positioned at 3305 cm^{-1} assigned to NH and OH group vibrations. Also, stretching vibrations corresponding to the C=O and C–O groups from 2,4-dioxochroman moiety were identified at 1668 and 1118 cm^{-1}, respectively.

In ^{1}H NMR spectrum, the singlet positioned at 2.55 ppm was assigned to protons on C2′ atom. The resulting signals of aromatic protons of the 2,4-dioxochroman part were in the range from 7.25 to 7.91 ppm. Aromatic protons belonging to the phenyl group of dopamine part were detected in the range from 6.5 to 6.67 ppm. The protons of the methylene C2″–H and C1″–H groups were identified as triplets at 2.80 and 3.6 ppm. Signals of protons of the phenyl OH and enamine NH group were identified as broadened singlets at 8.81 and 13.66 ppm.

The ^{13}C NMR spectra of compound **3** indicated the presence of aromatic carbon atoms of the dopamine part in the range from 115.87 to 145.46 ppm. The signals of carbon atoms of coumarine moiety were identified in the range from 96.18 to 179.60 ppm. The carbons of lactone (C–2) and ketone (C–4) showed resonances at 162.13 and 179.60 ppm. Signals at 18.35, 34.11, and 45.71 ppm were assigned to C2′, C1″, and C2″ carbons, respectively.

3.2. Crystallographic Structure. X-ray structure analysis revealed that **3** crystallizes in the triclinic *P*-1 space group. Its molecular structure is formed by the molecule of **3**,

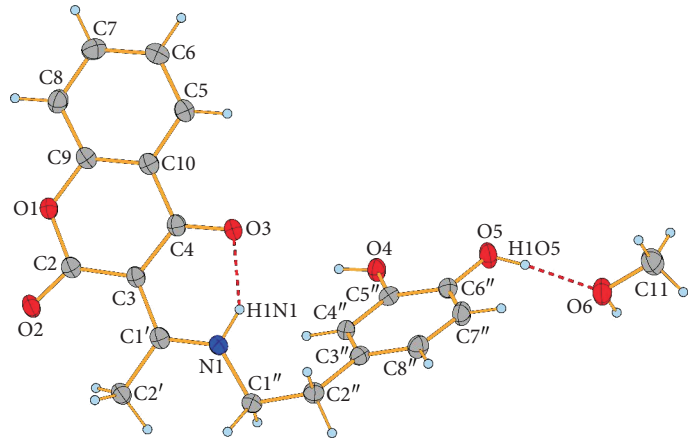

Figure 1: Molecular structure with an atom numbering scheme of **3·MeOH**. Displacement ellipsoids are drawn at 50% probability; hydrogen bonds are shown as red dashed lines.

Table 2: Hydrogen bonds for **3·MeOH** [Å and °].

D–H···A	*d*(D–H)	*d*(H···A)	*d*(D···A)	<(DHA)
N1–H1N1···O3	0.91 (2)	1.76 (2)	2.550 (1)	143.7 (16)
O5–H1O5···O6	0.87 (2)	1.80 (2)	2.661 (1)	169.2 (18)
O4–H1O4···O2^{i}	0.84 (2)	1.88 (2)	2.700 (1)	167.5 (18)
O6–H1O6···O4^{ii}	0.88 (2)	1.92 (2)	2.786 (1)	167.0 (19)
C4″–H4″···O1^{i}	0.95	2.57	3.417 (2)	148.6

Symmetry transformations used to generate equivalent atoms: $-x+2, -y+1, -z+1$; (ii): $-x+2, -y+2, -z+2$.

consisting of bicyclic coumarine and 3,4-dihydroxyphenethyl fragments joined by aminoethylidine chain, and by a solvated molecule of methanol tied with the mentioned molecule by a hydrogen bond (Figure 1). Within the molecule, the dihedral angle between the planes of coumarin fragment and the 3,4-dihydroxyphenyl ring is 61.46(3)°.

A typical structural feature of that type of compounds is an intramolecular N – H···O hydrogen bond which forms a six-membered ring with S(6) graph-set motif [70] and thus the molecule occurs in a ketoamine tautomeric form. Considering the O3=C4–C3=C1′–N1–H1N1-conjugated bond ring system created, owing to the intramolecular hydrogen bond formation, the equalization of the C3–C4 and C3=C1′ (both 1.442(2) Å) bond lengths (Table S1) is observed although the bonds are formally single and double, respectively. This can be explained by the π-electron delocalization within the system, and thus, we may conclude that the above hydrogen bond can be classified as a resonance-assisted hydrogen bond [71]. Interestingly, in the related 3-(1-((m-toluidine)amino)ethylidene)-chroman-2,4-dione and in 3-(1-(2-hydroxyethylamino)ethylidene)-chroman-2,4-dione [72] compounds, C3–C4 bond (1.434(2) and 1.430(3) Å, respectively) is even slightly shorter than C3=C1′ bond (1.436(2) and 1.437(3) Å, respectively). The elongation of C4=O3 (1.248(2) Å) bond, which is markedly longer than C2=O2 (1.223(2) Å) bond not involved in a strong hydrogen bond, and shortening of C1′–N1 (1.309(2) Å) bond in **3** can also be observed. Very similar bond lengths were observed in related compounds, like 3-(1-((o-toluidine)amino)ethylidene)-chroman-2,4-dione [72], 3-(1-(phenylamino)ethylidene)-chroman-2,4-dione [24], 3-(1-(3-hydroxypropylamino)propylidene) chroman-2,4-dione [73], 2-(1-(2,4-dioxochroman-3-ylidene) ethylamino)-3-methylbutanoate [74], 3-[(1-benzylamino) ethylidene]-2*H*-chromene-2,4(3*H*)-dione [75], or 3-[1-((2-hydroxyphenyl)amino)ethylidene]-2*H*-chromene-2,4(3*H*)-dione compound [76]. All other bond lengths and angles (Table S1) in the molecule of **3** are within normal ranges [77].

Except for above discussed N1–H1N1···O3 intramolecular hydrogen bond, due to which the exocyclic C3=C1′ double bond has an *E* geometry, the molecules of **3** are stabilized in the solid state by intermolecular O–H···O and C–H···O hydrogen bonds. Further stabilization of the solid state structure occurs when molecule of methanol occupies empty space between molecules of **3** and is tied with the molecules by a pair of O–H···O hydrogen bonds (Table 2). Due to these bonds, the molecules of **3** and methanol are tied to form chains parallel with the [011] direction (Figure S2). These chains are further connected by π-π interactions between pyran-2,4-dione (py) and phenyl (ph) rings of coumarin moieties in adjacent chains into a 2D structure parallel with (011) (Figure 2). These π-π interactions are characterized by $Cg_{py}\cdots Cg_{py}^{iii}$ and $Cg_{py}\cdots Cg_{ph}^{iii}$ centroid-centroid distances of 3.6479(1) and 3.7569(1) Å, respectively (iii = $1-x, 1-y, 1-z$).

3.3. Antitumor Activity. The effect of both 4-OH coumarin and its derivate **3** on selected cell lines was monitored and compared to the effect of DMSO that was used as a control

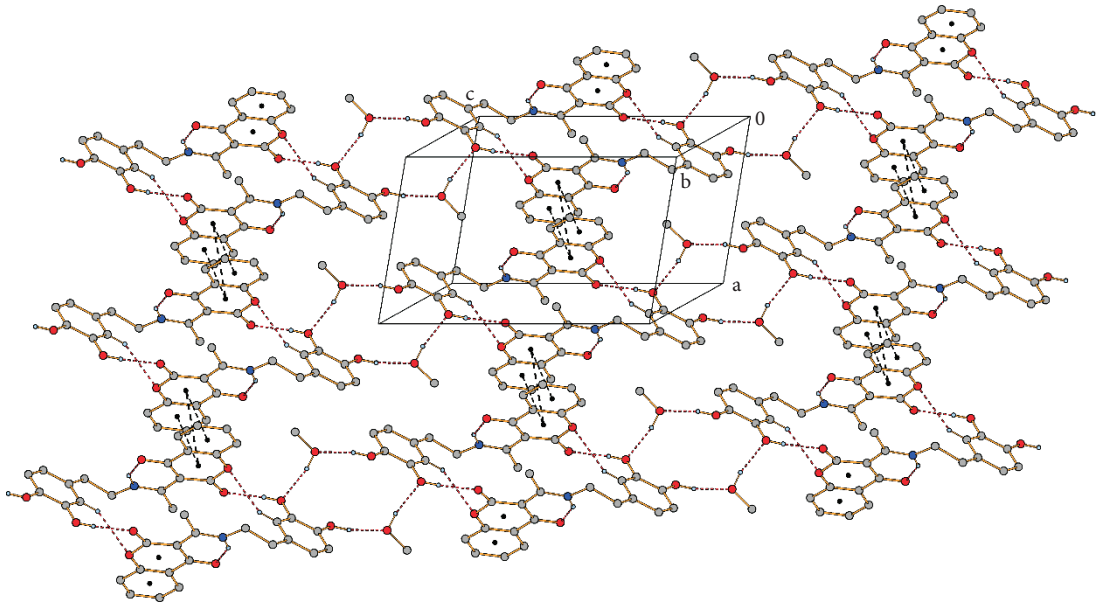

Figure 2: Molecular packing of **3·MeOH** showing π-π interactions (black dashed lines) between neighboring chains formed by hydrogen bonds (red dashed lines). Hydrogen atoms not involved in hydrogen bonds are omitted for clarity.

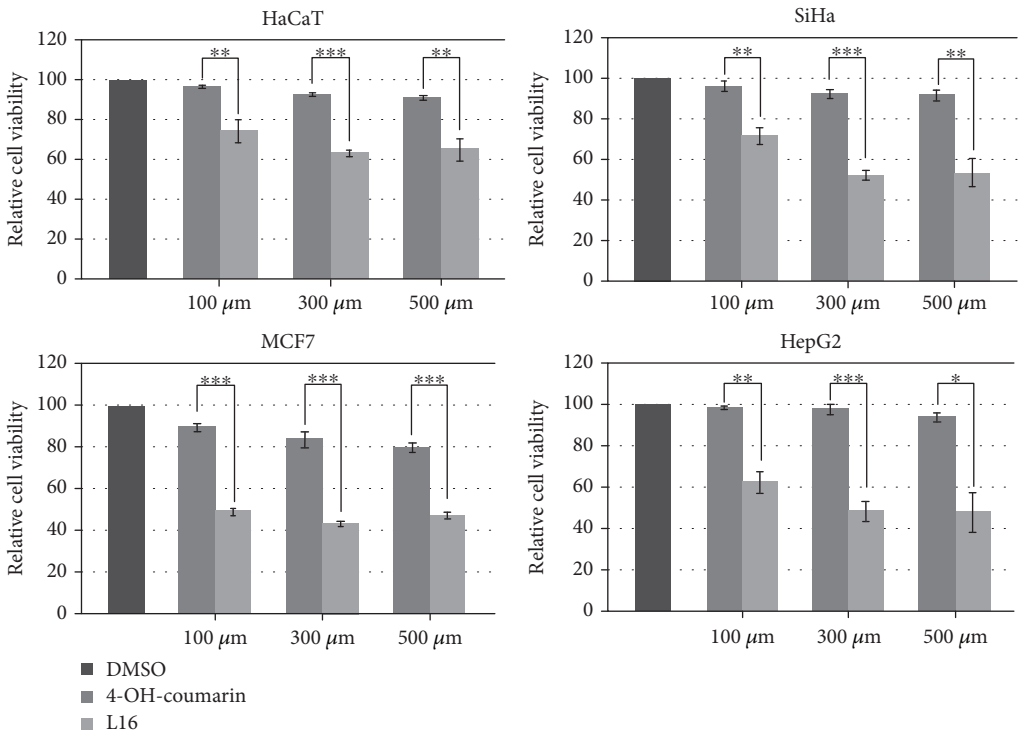

Figure 3: Cell viability assay (MTS assay) on HaCaT, SiHa, MCF7, and HepG2 cells performed 48 h after treatment with either 4-OH-coumarin or compound **3**. Relative cell viability of cells treated with selected compounds was calculated as a percentage of DMSO-treated cell viability that was set as 100%. Data are presented as the means ± S.E.M. (standard error mean) of at least three independent experiments performed in triplicate for each concentration. Mean values of relative cell viability were compared with Student's t-test, and p values are presented as $^{*}p \leq 0.05$, $^{**}p \leq 0.01$, and $^{***}p \leq 0.001$. Each color corresponds to a bar presented on the histogram.)

(vehicle). As presented in Figure 3, 4-OH-coumarin exhibited a mild effect on cell's viability in all tested cell types with the maximal effect on breast carcinoma cell line MCF7, inducing 20% reduction in viability of these cells 48 h after treatment at 500 μM concentration ($p = 0{,}023$). On the other hand, its derivate **3** had, in comparison with the control sample, a significantly stronger effect on both healthy and carcinoma cell lines with the most prominent effect on the

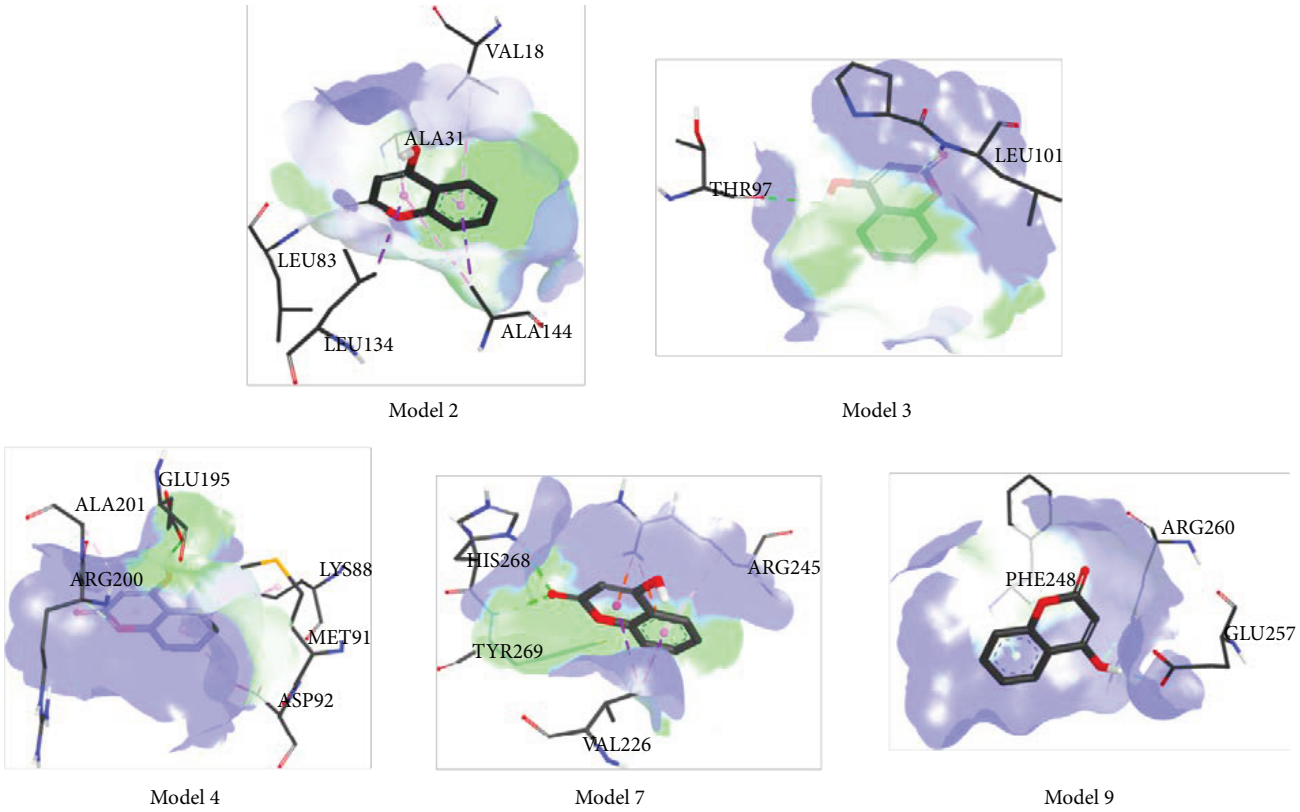

Figure 4: Docking positions of 4-OH-coumarin.

MCF7 cell line. In particular, 100 μM concentration of derivative **3** led to the reduction of cell's viability to approximately 75% in HaCat cells ($p = 0{,}023$), 72% in SiHa cells ($p = 0{,}008$), 49% in MCF7 cells ($p = 0{,}008$), and 62% in HepG2 cells ($p = 0{,}005$). The reduction effect increased with the concentration of the derivative **3** and had the greatest effect on the MCF7 cells, with a reduction percentage of 43% at the concentration of 300 μM ($p = 0.001$). The statistical significance is also observed when the effect of **3** is compared with the effect of 4-OH–coumarin (Figure 3, p values are indicated as asterisks). Taken together, the higher cytotoxic effect of derivate **3** is observed, both for healthy and for carcinoma cells, compared to 4-OH-coumarin, where the effect on the carcinoma cells was somewhat stronger.

It is clearly demonstrated that coumarin derivate **3** exhibits a cytotoxic activity against all analyzed cell types *in vitro*. The observed effect is somewhat stronger against carcinoma cell lines compared to healthy keratinocytes, with the most prominent effect on breast carcinoma cell line MCF7. Antitumor activity of natural and synthetic coumarin derivatives has been previously reported by various authors including high cytotoxicity against ovarian cancer cells, lung carcinoma cells, pancreatic carcinoma, hepatocarcinoma, and breast and colon carcinoma [78–82]. Depending on their structures, coumarins can act on various tumor cells by different mechanisms such as inhibition of the telomerase and protein kinase activities, downregulation of oncogene expression or induction of the caspase-9-mediated apoptosis, and suppression of cancer cell proliferation [82]. A further work is needed to elucidate the mechanism of action for this newly synthesized derivate **3**.

3.4. Molecular Docking. The molecular docking studies were performed for the evaluation of the inhibitory nature of examined compounds against CDK_S protein. These simulations gave the predicted protein-ligand binding energies and identified the potential ligand binding sites. The structure of the newly synthesized compound was optimized at the B3LYP-D3BJ/6-311++G(d,p) level of theory, based on the crystallographic positions of atoms (Tables S3 and S4). Ten different conformations were analyzed for both investigated compounds. Tables S5 and S6 give values of the estimated free energy of binding and inhibition constant values (K_i), the distance between respective active sites of ligand and amino acids, and pairwise interaction energies (E_i), as well as types of interactions for the investigated models with the lowest docked conformation energies. The most stable conformations are presented in Figures 4 and 5.

The parent compound contains several polar groups, namely, a hydroxy group in position 4, a carbonyl group, and an oxygen atom in the pyrone ring. Since the rest of the structure makes the benzene ring, therefore, the most of interactions, presented in Table S5, include π-alkyl and π-σ hydrophobic interactions with leucine, valine, alanine, arginine, and phenylalanine in various positions [83–85]. These interactions are characterized by low pairwise interaction energy and large atomic distances (≥2.5 Å). Due

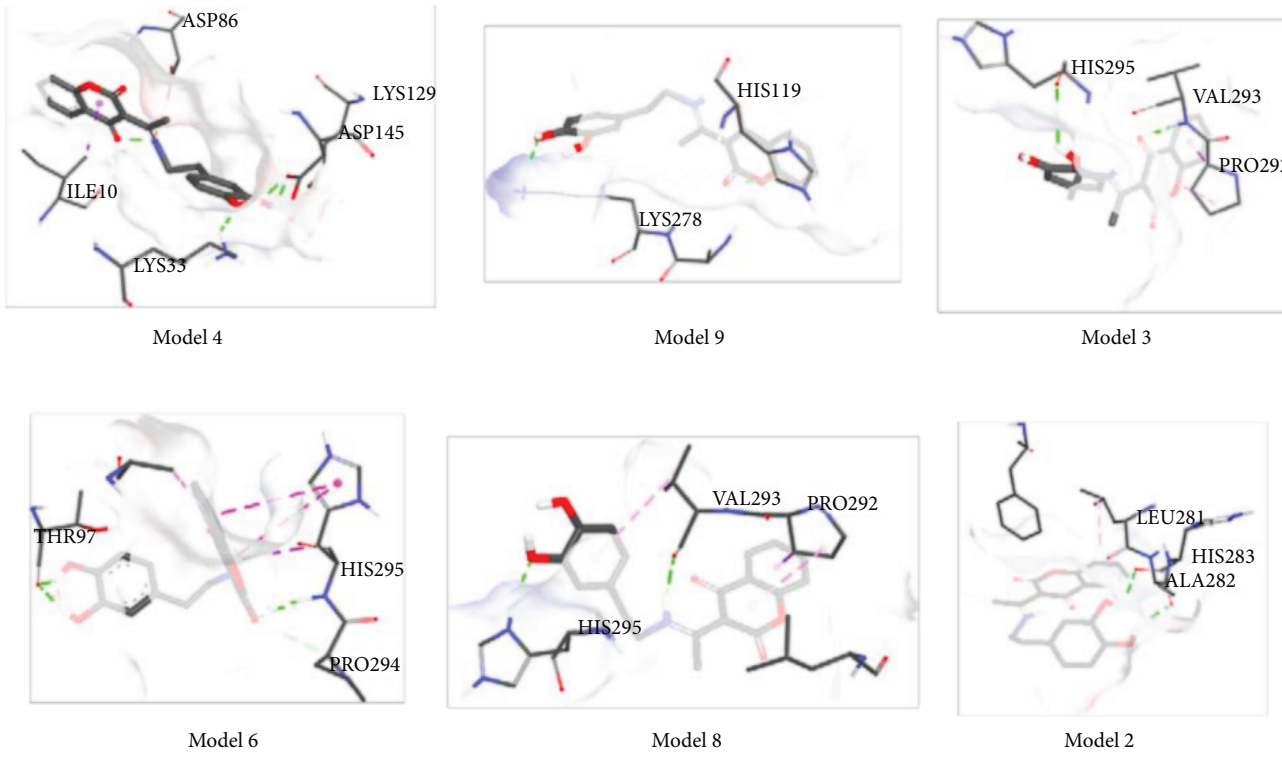

Figure 5: Docking positions of coumarin derivate.

to a large number of weak noncovalent interactions, all of the models obtained for 4-OH-coumarin have very low binding energy and high value of inhibition constant, which is in accordance with the obtained experimental result.

It is also evident that two types of hydrogen bonds are formed in given models. The first type is the conventional hydrogen bond. Only two bonds of this type, with significant values of pairwise interaction energy, have atomic distances lower than 2 Å. These bonds are formed upon the interaction between CDKs and LEU83 and GLU257. It should be pointed out that in models 3 and 4 there are two more bonds which deserve attention, THR97 and GLU195, respectively. It should be pointed out that the hydroxy group of 4-OH-coumarine behaves as the hydrogen atom donor in the interaction with THR97 (model 2), GLU195 (model 3), and GLU257 (model 9). There are more interactions in which the parent molecule behaves as the hydrogen atom acceptor. Other conventional hydrogen bonds are weak, due to high atomic distances and low pairwise interaction energy. These interactions are established with positively charged amino acids, lysine, histidine, and arginine. The second type of hydrogen bonds is the carbon-hydrogen bond. Predicted values of the interaction energy for this bond type are very low, and the atomic distances much larger (≥3 Å). These bonds are formed between donating groups of HIS268 and ARG260 and hydrogen-acceptor groups of the CDKs.

Table S6 presents molecular docking results for compound **3**. When the structures of two investigated compounds are compared, it is notable that only compound **3** possesses a catechol moiety and longer aliphatic chain with a nitrogen atom. This increases the number of possible interactions with amino acids. If results from Tables S5 and S6 are compared, it is obvious that the relative abundance of hydrogen bonds increases with respect to other noncovalent interactions. There are also still hydrophobic π-σ (ILE10 in model 4 and PRO292 in model 8) and hydrophobic $\pi\rightarrow$alkyl (in models 2, 3, 8, and 9) interactions. All these interactions have very low pairwise interaction energies. When these interactions are formed, atomic distances fall into the very wide range of values (3.5-4.40 Å). In spite the fact that these interactions are very weak, they additionally stabilize the structures.

When hydrogen bonds are concerned, there are also two types of bonds, the conventional and carbon-hydrogen bonds. Compound **3** behaves as the hydrogen atom donor with ASP in positions 145 and 86 (model 4), THR97 (model 6), VAL293 (model 8), ALA282, and HIS293 (model 2). It is important to point out that the number of possible hydrogen atom accepting amino acids increases, due to the fact that compound **3** has additional polar groups. The strength of formed conventional hydrogen bonds and interatomic distances are in the same range as in 4-OH-coumarine. Therefore, it can be concluded that the reactivity of coumarin part is conserved and that the additional groups contribute to the increasing number of interactions.

It should be emphasized that both values, the binding energy and inhibition constant, of the compound **3** are lower in comparison with the parent molecule. Moreover, it should be pointed out that the value of inhibition constant for compound **3** is more than six times lower than the one of 4-OH-coumarine. This indicates that compound **3** interacts

better with CDK_S protein. Obviously, the additional hydroxy groups and an aromatic ring, with an aliphatic chain containing a nitrogen atom, allow new interactions which inhibit the reactivity of the protein. This could be one of the reasons for the increased reactivity of compound **3** towards tumor cells.

4. Conclusion

The coumarin and dopamine derivative, 3-(1-((3,4-dihydroxyphenethyl)amino)-ethylidene)-chroman-2,4-dione, was synthesized under mild conditions. The new compound was analyzed by NMR, IR, microanalysis, and X-ray crystallography. The X-ray analysis showed that the similar structural motifs are present, as with other previously obtained derivatives with aminophenols. Several types of hydrogen bonds, both intramolecular and intermolecular, stabilize the structure within the crystal. The molecule is not planar, but there is the dihedral angle between the planes of coumarin fragment and 3,4-dihydroxyphenyl ring of 61.46(3)°. There are also $\pi \rightarrow \pi$ and stacking interactions within the crystal structure.

The antitumor activity was investigated against healthy and tumor cell lines both for 4-OH-coumarin and its derivative. Compared to 4-OH coumarin, new derivative showed a significantly stronger effect on both healthy and carcinoma cell lines. When treated with 100 μM solution of compound **3**, the reduction of cell's viability was approximately 75% in HaCat cells, 72% in SiHa cells, 49% in MCF7 cells, and 62% in HepG2. The most prominent effect was observed on the breast carcinoma MCF7 cell line.

The molecular docking study was performed in order to better understand the difference in binding between the two investigated molecules and CDK protein. Different interactions are possible due to the presence of polar groups in the coumarin structure. The hydrogen bonds are the strongest interactions observed, in which 4-OH-coumarin can act as the hydrogen atom acceptor and hydrogen atom donor. The most numerous are $\pi \rightarrow$alkyl interactions with various amino acids. The strength of interactions, given as the pairwise interaction energy, is preserved in coumarin derivative. New interactions are established as a result of the presence of additional polar groups: catechol moiety and alkyl chain. The obtained result implies that a number of interactions determine the activity towards investigated protein.

In the end, it can be concluded that the presented results are promising. Future experiments, which would include new cell lines and new coumarin-neurotransmitter derivatives, in addition to all the above levels of testing, will be also supplemented with classical MD calculations in order to better explain the mechanisms of action.

Data Availability

The X-ray structure analysis and molecular docking data used to support the findings of this study are included within the supplementary information file.

Conflicts of Interest

The authors declare that there is no conflict of interest regarding the publication of this paper.

Acknowledgments

This research was funded by the Ministry of Education, Science and Technological Development of the Republic of Serbia through Grant nos. OI172040, OI172015, OI173051, OI172016, and OI174028. The instruments used for crystallographic measurements are from the ASTRA lab established within the Operation Program Prague Competitiveness (project CZ.2.16/3.1.00/24510).

Supplementary Materials

The Supplementary information file contains additional information on crystallographic data of the newly synthesized molecule, along with selected bond lengths and angles, as well as results of docking analysis with CDKs (type of interaction, atom distances, bonding energy, estimated free energy of binding, and inhibition constants). *(Supplementary Materials)*

References

[1] B. Halliwell, "Oxidative stress and cancer: have we moved forward?," *The Biochemical Journal*, vol. 401, no. 1, pp. 1–11, 2007.

[2] S. Reuter, S. C. Gupta, M. M. Chaturvedi, and B. B. Aggarwal, "Oxidative stress, inflammation, and cancer: how are they linked?," *Free Radical Biology & Medicine*, vol. 49, no. 11, pp. 1603–1616, 2010.

[3] J. A. R. Mead, J. N. Smith, and R. T. Williams, "Studies in detoxication. 72. The metabolism of coumarin and of *o*-coumaric acid," *Biochemical Journal*, vol. 68, no. 1, pp. 67–74, 1958.

[4] S. Rosselli, A. M. Maggio, N. Faraone et al., "The cytotoxic properties of natural coumarins isolated from roots of Ferulago campestris (Apiaceae) and of synthetic ester derivatives of aegelinol," *Natural Product Communications*, vol. 4, no. 12, pp. 1701–1706, 2009.

[5] Atta-ur-Rahman, M. Shabbir, S. Ziauddin Sultani, A. Jabbar, and M. Iqbal Choudhary, "Cinnamates and coumarins from the leaves of *Murraya paniculata*," *Phytochemistry*, vol. 44, no. 4, pp. 683–685, 1997.

[6] R. W. Fuller, H. R. Bokesch, K. R. Gustafson et al., "HIV-inhibitory coumarins from latex of the tropical rainforest tree *Calophyllum teysmannii* var. *inophylloide*," *Bioorganic & Medicinal Chemistry Letters*, vol. 4, no. 16, pp. 1961–1964, 1994.

[7] C. Spino, M. Dodier, and S. Sotheeswaran, "Anti-HIV coumarins from calophyllum seed oil," *Bioorganic & Medicinal Chemistry Letters*, vol. 8, no. 24, pp. 3475–3478, 1998.

[8] T. Hatano, T. Yasuhara, T. Fukuda, T. Noro, and T. Okuda, "Phenolic constituents of licorice. II. Structures of licopyranocoumarin, licoarylcoumarin and glisoflavone, and inhibitory effects of licorice phenolics on xanthine oxidase," *Chemical & Pharmaceutical Bulletin*, vol. 37, no. 11, pp. 3005–3009, 1989.

[9] J. B. Harborne, "Classes and functions of secondary products from plants," in *Chemicals from Plants: Perspectives on Plant Secondary Products*, N. J. Walton and D. E. Brown, Eds., Imperial College Press, London, 1999.

[10] F. Bourgaud, A. Hehn, R. Larbat et al., "Biosynthesis of coumarins in plants: a major pathway still to be unravelled for cytochrome P450 enzymes," *Phytochemistry Reviews*, vol. 5, no. 2-3, pp. 293–308, 2006.

[11] T. Ojala, S. Remes, P. Haansuu et al., "Antimicrobial activity of some coumarin containing herbal plants growing in Finland," *Journal of Ethnopharmacology*, vol. 73, no. 1-2, pp. 299–305, 2000.

[12] F. Cottigli, G. Loy, D. Garau et al., "Antimicrobial evaluation of coumarins and flavonoids from the stems of *Daphne gnidium* L," *Phytomedicine*, vol. 8, no. 4, pp. 302–305, 2001.

[13] A. Basile, S. Sorbo, V. Spadaro et al., "Antimicrobial and antioxidant activities of coumarins from the roots of Ferulago campestris (Apiaceae)," *Molecules*, vol. 14, no. 3, pp. 939–952, 2009.

[14] P. O. Patil, S. B. Bari, S. D. Firke, P. K. Deshmukh, S. T. Donda, and D. A. Patil, "A comprehensive review on synthesis and designing aspects of coumarin derivatives as monoamine oxidase inhibitors for depression and Alzheimer's disease," *Bioorganic & Medicinal Chemistry*, vol. 21, no. 9, pp. 2434–2450, 2013.

[15] X. Zhou, X.-B. Wang, T. Wang, and L.-Y. Kong, "Design, synthesis, and acetylcholinesterase inhibitory activity of novel coumarin analogues," *Bioorganic & Medicinal Chemistry*, vol. 16, no. 17, pp. 8011–8021, 2008.

[16] S. A. Patil, S. N. Unki, and P. S. Badami, "In vitro antibacterial, antifungal, and DNA cleavage studies of coumarin Schiff bases and their metal complexes: synthesis and spectral characterization," *Medicinal Chemistry Research*, vol. 21, no. 12, pp. 4017–4027, 2012.

[17] M. S. Refat, I. M. El-Deen, Z. M. Anwer, and S. El-Ghol, "Bivalent transition metal complexes of coumarin-3-yl thiosemicarbazone derivatives: spectroscopic, antibacterial activity and thermogravimetric studies," *Journal of Molecular Structure*, vol. 920, no. 1-3, pp. 149–162, 2009.

[18] D. Bhavsar, J. Trivedi, S. Parekh et al., "Synthesis and in vitro anti-HIV activity of N-1,3-benzo[d]thiazol-2-yl-2-(2-oxo-2H-chromen-4-yl)acetamide derivatives using MTT method," *Bioorganic & Medicinal Chemistry Letters*, vol. 21, no. 11, pp. 3443–3446, 2011.

[19] I. Kostova, "Coumarins as inhibitors of HIV reverse transcriptase," *Current HIV Research*, vol. 4, no. 3, pp. 347–363, 2006.

[20] Y. Chen, H.-R. Liu, H.-S. Liu et al., "Antitumor agents 292. Design, synthesis and pharmacological study of S- and O-substituted 7-mercapto- or hydroxy-coumarins and chromones as potent cytotoxic agents," *European Journal of Medicinal Chemistry*, vol. 49, pp. 74–85, 2012.

[21] A. Thakur, R. Singla, and V. Jaitak, "Coumarins as anticancer agents: a review on synthetic strategies, mechanism of action and SAR studies," *European Journal of Medicinal Chemistry*, vol. 101, pp. 476–495, 2015.

[22] C. Kontogiorgis and D. Hadjipavlou-Litina, "Biological evaluation of several coumarin derivatives designed as possible anti-inflammatory/antioxidant agents," *Journal of Enzyme Inhibition and Medicinal Chemistry*, vol. 18, no. 1, pp. 63–69, 2003.

[23] C. A. Kontogiorgis and D. J. Hadjipavlou-Litina, "Synthesis and antiinflammatory activity of coumarin derivatives," *Journal of Medicinal Chemistry*, vol. 48, no. 20, pp. 6400–6408, 2005.

[24] E. H. Avdović, D. Milenković, J. M. Dimitrić Marković et al., "Synthesis, spectroscopic characterization (FT-IR, FT-Raman, and NMR), quantum chemical studies and molecular docking of 3-(1-(phenylamino)ethylidene)-chroman-2,4-dione," *Spectrochimica Acta Part A: Molecular and Biomolecular Spectroscopy*, vol. 195, pp. 31–40, 2018.

[25] E. H. Avdović, D. Milenković, J. M. Dimitrić-Marković, N. Vuković, S. R. Trifunović, and Z. Marković, "Structural, spectral and NBO analysis of 3-(1-(3-hydroxypropylamino)ethylidene)chroman-2,4-dione," *Journal of Molecular Structure*, vol. 1147, pp. 69–75, 2017.

[26] D. Milenković, E. H. Avdović, D. Dimić et al., "Reactivity of the coumarine derivative towards cartilage proteins: combined NBO, QTAIM, and molecular docking study," *Monatshefte für Chemie - Chemical Monthly*, vol. 149, no. 1, pp. 159–166, 2018.

[27] O. Hornykiewicz, "Dopamine miracle: from brain homogenate to dopamine replacement," *Movement Disorders*, vol. 17, no. 3, pp. 501–508, 2002.

[28] R. M. Berman, M. Narasimhan, H. L. Miller et al., "Transient depressive relapse induced by catecholamine depletion: potential phenotypic vulnerability marker?," *Archives of General Psychiatry*, vol. 56, no. 5, pp. 395–403, 1999.

[29] H. M. Kravitz, H. C. Sabelli, and J. Fawcett, "Dietary supplements of phenylalanine and other amino acid precursors of brain neuroamines in the treatment of depressive disorders," *The Journal of the American Osteopathic Association*, vol. 84, 1 Supplement, pp. 119–123, 1984.

[30] L. Pauling, "Orthomolecular psychiatry. Varying the concentrations of substances normally present in the human body may control mental disease," *Science*, vol. 160, no. 3825, pp. 265–271, 1968.

[31] L. Lyras, N. J. Cairns, A. Jenner, P. Jenner, and B. Halliwell, "An assessment of oxidative damage to proteins, lipids, and DNA in brain from patients with Alzheimer's disease," *Journal of Neurochemistry*, vol. 68, no. 5, pp. 2061–2069, 1997.

[32] L. M. Sayre, M. A. Smith, and G. Perry, "Chemistry and biochemistry of oxidative stress in neurodegenerative disease," *Current Medicinal Chemistry*, vol. 8, no. 7, pp. 721–738, 2001.

[33] P. K. Toshniwal and E. J. Zarling, "Evidence for increased lipid peroxidation in multiple sclerosis," *Neurochemical Research*, vol. 17, no. 2, pp. 205–207, 1992.

[34] J. Emerit, M. Edeas, and F. Bricaire, "Neurodegenerative diseases and oxidative stress," *Biomedicine & Pharmacotherapy*, vol. 58, no. 1, pp. 39–46, 2004.

[35] T. L. Lemke, D. A. Williams, W. O. Foye, and S. W. Zito, *Foye's Principles of Medicinal Chemistry*, Wolters Kluwer Health/Lippincott Williams & Wilkins, 2013.

[36] J. Smythies, "Redox aspects of signaling by catecholamines and their metabolites," *Antioxidants & Redox Signaling*, vol. 2, no. 3, pp. 575–583, 2000.

[37] Y. Gilgun-Sherki, E. Melamed, and D. Offen, "Oxidative stress induced-neurodegenerative diseases: the need for antioxidants that penetrate the blood brain barrier," *Neuropharmacology*, vol. 40, no. 8, pp. 959–975, 2001.

[38] J. K. Andersen, "Oxidative stress in neurodegeneration: cause or consequence?," *Nature Reviews Neuroscience*, vol. 10, no. 7, pp. S18–S25, 2004.

[39] T. Shimizu, Y. Nakanishi, M. Nakahara et al., "Structure effect on antioxidant activity of catecholamines toward singlet oxygen and other reactive oxygen species in vitro," *Journal of Clinical Biochemistry and Nutrition*, vol. 47, no. 3, pp. 181–190, 2010.

[40] C. Sârbu and D. Casoni, "Comprehensive evaluation of biogenic amines and related drugs' antiradical activity using reactive 2,2-diphenyl-1-picrylhydrazyl (DPPH) radical," *Open Chemistry*, vol. 11, no. 5, pp. 679–688, 2013.

[41] A. Kładna, P. Berczyński, I. Kruk, T. Michalska, and H. Y. Aboul-Enein, "Superoxide anion radical scavenging property of catecholamines," *Luminescence*, vol. 28, no. 4, pp. 450–455, 2013.

[42] D. Dimić, D. Milenković, J. Dimitrić Marković, and Z. Marković, "Antiradical activity of catecholamines and metabolites of dopamine: theoretical and experimental study," *Physical Chemistry Chemical Physics*, vol. 19, no. 20, pp. 12970–12980, 2017.

[43] D. S. Dimić, D. A. Milenković, J. M. D. Marković, and Z. S. Marković, "Thermodynamic and kinetic analysis of the reaction between biological catecholamines and chlorinated methylperoxy radicals," *Molecular Physics*, vol. 116, no. 9, pp. 1166–1178, 2018.

[44] K. Yamafuji, H. Murakami, and M. Shinozuka, "Antitumour activity of dopa, dopamine, noradrenalin or adrenalin and their reaction with nucleic acids," *Zeitschrift für Krebsforschung*, vol. 73, no. 3, pp. 195–203, 1970.

[45] M. M. Wick, "Levodopa and dopamine analogs: melanin precursors as antitumor agents in experimental human and murine leukemia," *Cancer Treatment Reports*, vol. 63, no. 6, pp. 991–997, 1979.

[46] P. S. Dasgupta and T. Lahiri, "Antitumor effect of i.p. dopamine in mice bearing Ehrlich ascites carcinoma," *Journal of Cancer Research and Clinical Oncology*, vol. 113, no. 4, pp. 363–368, 1987.

[47] M. M. Wick, "Levodopa and dopamine analogs: dihydroxy and trihydroxybenzylamines as novel quinol antitumor agents in experimental leukemia in vivo," *Cancer Treatment Reports*, vol. 65, no. 9-10, pp. 861–867, 1981.

[48] M. M. Wick, "Levodopa and dopamine analogs as DNA polymerase inhibitors and antitumor agents in human melanoma," *Cancer Research*, vol. 40, no. 5, pp. 1414–1418, 1980.

[49] J. S. Driscoll, "Catecholamine analogs as potential antitumor agents," *Journal of Pharmaceutical Sciences*, vol. 68, no. 12, pp. 1519–1521, 1979.

[50] A. H. Stokes, T. G. Hastings, and K. E. Vrana, "Cytotoxic and genotoxic potential of dopamine," *Journal of Neuroscience Research*, vol. 55, no. 6, pp. 659–665, 1999.

[51] N. A. Abdel Latif, R. Z. Batran, M. A. Khedr, and M. M. Abdalla, "3-Substituted-4-hydroxycoumarin as a new scaffold with potent CDK inhibition and promising anticancer effect: synthesis, molecular modeling and QSAR studies," *Bioorganic Chemistry*, vol. 67, pp. 116–129, 2016.

[52] D. O. Morgan, "Cyclin-dependent kinases: engines, clocks, and microprocessors," *Annual Review of Cell and Developmental Biology*, vol. 13, no. 1, pp. 261–291, 1997.

[53] L. Meijer, S. Leclerc, and M. Leost, "Properties and potential applications of chemical inhibitors of cyclin-dependent kinases," *Pharmacology & Therapeutics*, vol. 82, no. 2-3, pp. 279–284, 1999.

[54] S. A. Morsy, A. A. Farahat, M. N. A. Nasr, and A. S. Tantawy, "Synthesis, molecular modeling and anticancer activity of new coumarin containing compounds," *Saudi Pharmaceutical Journal*, vol. 25, no. 6, pp. 873–883, 2017.

[55] S. Sukdolak, S. Solujić, N. Manojlović, N. Vuković, and L. J. Krstić, "Hantzsch reaction of 3-(2-bromoacetyl)-4-hydroxy--chromen-2-one. Synthesis of 3-(thiazol-4-yl)-4-hydroxy coumarines," *Journal of Heterocyclic Chemistry*, vol. 41, no. 4, pp. 593–596, 2004.

[56] G. M. Morris, R. Huey, W. Lindstrom et al., "AutoDock4 and AutoDockTools4: automated docking with selective receptor flexibility," *Journal of Computational Chemistry*, vol. 30, no. 16, pp. 2785–2791, 2009.

[57] T. H. Dunning Jr, "Gaussian basis sets for use in correlated molecular calculations. I. The atoms boron through neon and hydrogen," *The Journal of Chemical Physics*, vol. 90, no. 2, pp. 1007–1023, 1989.

[58] A. D. Becke and E. R. Johnson, "A density-functional model of the dispersion interaction," *The Journal of Chemical Physics*, vol. 123, no. 15, article 154101, 2005.

[59] A. D. Becke, "Density-functional thermochemistry. III. The role of exact exchange," *The Journal of Chemical Physics*, vol. 98, no. 7, pp. 5648–5652, 1993.

[60] A. D. Becke, "Density-functional exchange-energy approximation with correct asymptotic behavior," *Physical Review A*, vol. 38, no. 6, pp. 3098–3100, 1988.

[61] S. Grimme, S. Ehrlich, and L. Goerigk, "Effect of the damping function in dispersion corrected density functional theory," *Journal of Computational Chemistry*, vol. 32, no. 7, pp. 1456–1465, 2011.

[62] M. J. Frisch, G. W. Trucks, H. B. Schlegel et al., *Gaussian 09, revision C.01*, Gaussian Inc., Wallingford, 2009, http://www.gaussian.com.

[63] J. Fuhrmann, A. Rurainski, H. P. Lenhof, and D. Neumann, "A new Lamarckian genetic algorithm for flexible ligand-receptor docking," *Journal of Computational Chemistry*, vol. 31, no. 9, pp. 1911–1918, 2010.

[64] Rigaku Oxford Diffraction, *Crysalis Pro*, Rigaku Oxford Diffraction, Yarnton, England, 2017.

[65] G. M. Sheldrick, "*SHELXT* – integrated space-group and crystal-structure determination," *Acta Crystallographica Section A Foundations and Advances*, vol. 71, no. 1, pp. 3–8, 2015.

[66] G. M. Sheldrick, "Crystal structure refinement with *SHELXL*," *Acta Crystallographica Section C Structural Chemistry*, vol. 71, no. 1, pp. 3–8, 2015.

[67] L. J. Farrugia, "*WinGX* suite for small-molecule single-crystal crystallography," *Journal of Applied Crystallography*, vol. 32, no. 4, pp. 837-838, 1999.

[68] A. L. Spek, "Structure validation in chemical crystallography," *Acta Crystallographica Section D Biological Crystallography*, vol. 65, no. 2, pp. 148–155, 2009.

[69] K. Brandenburg, *Diamond (Version 3.2k)*, Crystal Impact GbR, Bonn, Germany, 2012.

[70] J. Bernstein, R. E. Davis, L. Shimoni, and N. L. Chang, "Patterns in hydrogen bonding: functionality and graph set analysis in crystals," *Angewandte Chemie International Edition in English*, vol. 34, no. 15, pp. 1555–1573, 1995.

[71] G. Gilli, F. Bellucci, V. Ferretti, and V. Bertolasi, "Evidence for resonance-assisted hydrogen bonding from crystal-structure

correlations on the enol form of the .beta.-diketone fragment," *Journal of the American Chemical Society*, vol. 111, no. 3, pp. 1023–1028, 1989.

[72] M. Małecka, S. J. Grabowski, and E. Budzisz, "Crystal and molecular structures of 3-[1-(2-hydroxyethylamino)-ethylidene]-chroman-2,4-dione and 2-methoxy-3-[1-(benzylamino)-ethylidene]-2,3-dihydro-2,4-dioxo-2λ5-benzo[e][1,2]oxaphosphinane and DFT study of intramolecular H-bonds of related compounds," *Chemical Physics*, vol. 297, no. 1-3, pp. 235–244, 2004.

[73] E. H. Avdović, D. L. J. Stojković, V. V. Jevtić et al., "Synthesis, characterization and cytotoxicity of a new palladium(II) complex with a coumarin-derived ligand 3-(1-(3-hydroxypropylamino)ethylidene)chroman-2,4-dione. Crystal structure of the 3-(1-(3-hydroxypropylamino)ethylidene)-chroman-2,4-dione," *Inorganica Chimica Acta*, vol. 466, pp. 188–196, 2017.

[74] D. L. Stojković, V. V. Jevtić, N. Vuković et al., "Crystal and molecular structure of a new palladium(II) complex with a coumarin-valine derivate," *Journal of Structural Chemistry*, vol. 58, no. 3, pp. 550–557, 2017.

[75] M. Małecka and E. Budzisz, "3-[(1-Benzylamino)ethylidene]-2*H*-chromene-2,4(3*H*)-dione," *Acta Crystallographica Section E Structure Reports Online*, vol. 62, no. 11, pp. o5058–o5060, 2006.

[76] A. Brahmia, T. Ben Ayed, and R. Ben Hassen, "3-[1-(2-Hydroxyanilino)ethylidene]-3*H*-chromen-2,4-dione," *Acta Crystallographica Section E Structure Reports Online*, vol. 69, no. 8, pp. o1296–o1296, 2013.

[77] C. R. Groom, I. J. Bruno, M. P. Lightfoot, and S. C. Ward, "The Cambridge Structural Database," *Acta Crystallographica Section B Structural Science, Crystal Engineering and Materials*, vol. 72, no. 2, pp. 171–179, 2016.

[78] R. K. Singh, T. S. Lange, K. K. Kim, and L. Brard, "A coumarin derivative (RKS262) inhibits cell-cycle progression, causes pro-apoptotic signaling and cytotoxicity in ovarian cancer cells," *Investigational New Drugs*, vol. 29, no. 1, pp. 63–72, 2011.

[79] N. Khaghanzadeh, Z. Mojtahedi, M. Ramezani, N. Erfani, and A. Ghaderi, "Umbelliprenin is cytotoxic against QU-DB large cell lung cancer cell line but anti-proliferative against A549 adenocarcinoma cells," *DARU Journal of Pharmaceutical Sciences*, vol. 20, no. 1, p. 69, 2012.

[80] M. A. Musa, M. Y. Joseph, L. M. Latinwo, V. Badisa, and J. S. Cooperwood, "In vitro evaluation of 3-arylcoumarin derivatives in A549 cell line," *Anticancer Research*, vol. 35, no. 2, pp. 653–659, 2015.

[81] T. Nasr, S. Bondock, and M. Youns, "Anticancer activity of new coumarin substituted hydrazide–hydrazone derivatives," *European Journal of Medicinal Chemistry*, vol. 76, pp. 539–548, 2014.

[82] K. M. Amin, A. A. M. Eissa, S. M. Abou-Seri, F. M. Awadallah, and G. S. Hassan, "Synthesis and biological evaluation of novel coumarin–pyrazoline hybrids endowed with phenylsulfonyl moiety as antitumor agents," *European Journal of Medicinal Chemistry*, vol. 60, pp. 187–198, 2013.

[83] D. B. Ninković, D. Z. Vojislavljević-Vasilev, V. B. Medaković, M. B. Hall, E. N. Brothers, and S. D. Zarić, "Aliphatic–aromatic stacking interactions in cyclohexane–benzene are stronger than aromatic–aromatic interaction in the benzene dimer," *Physical Chemistry Chemical Physics*, vol. 18, no. 37, pp. 25791–25795, 2016.

[84] D. B. Ninković, J. M. Andrić, S. N. Malkov, and S. D. Zarić, "What are the preferred horizontal displacements of aromatic–aromatic interactions in proteins? Comparison with the calculated benzene–benzene potential energy surface," *Physical Chemistry Chemical Physics*, vol. 16, no. 23, pp. 11173–11177, 2014.

[85] A. A. M. Kamal, L. Petrera, J. Eberhard, and R. W. Hartmann, "Structure–functionality relationship and pharmacological profiles of Pseudomonas aeruginosa alkylquinolone quorum sensing modulators," *Organic & Biomolecular Chemistry*, vol. 15, no. 21, pp. 4620–4630, 2017.

Hindawi
Oxidative Medicine and Cellular Longevity
Volume 2019, Article ID 6452390, 14 pages
https://doi.org/10.1155/2019/6452390

Research Article

Counteraction of HCV-Induced Oxidative Stress Concurs to Establish Chronic Infection in Liver Cell Cultures

Simona Anticoli,[1,2] **Donatella Amatore**,[2] **Paola Matarrese**,[1] **Marta De Angelis**,[2] **Anna Teresa Palamara**,[2,3] **Lucia Nencioni**,[2] **and Anna Ruggieri**[1]

[1]*Istituto Superiore di Sanità, Center for Gender-Specific Medicine, Rome, Italy*
[2]*Department of Public Health and Infectious Diseases, Istituto Pasteur Italia-Fondazione Cenci-Bolognetti, Sapienza University of Rome, Italy*
[3]*IRCSS San Raffaele Pisana, Department of Human Sciences and Promotion of the Quality of the Life, San Raffaele Open University, Rome, Italy*

Correspondence should be addressed to Anna Teresa Palamara; annateresa.palamara@uniroma1.it
and Anna Ruggieri; anna.ruggieri@iss.it

Received 2 August 2018; Revised 2 November 2018; Accepted 2 December 2018; Published 13 February 2019

Academic Editor: Pablo Muriel

Hepatitis C virus (HCV) is a blood-borne pathogen causing acute and chronic hepatitis. A significant number of people chronically infected with HCV develop cirrhosis and/or liver cancer. The pathophysiologic mechanisms of hepatocyte damage associated with chronic HCV infection are not fully understood yet, mainly due to the lack of an *in vitro* system able to recapitulate the stages of infection *in vivo*. Several studies underline that HCV virus replication depends on redox-sensitive cellular pathways; in addition, it is known that virus itself induces alterations of the cellular redox state. However, the exact interplay between HCV replication and oxidative stress has not been elucidated. In particular, the role of reduced glutathione (GSH) in HCV replication and infection is still not clear. We set up an *in vitro* system, based on low m.o.i. of Huh7.5 cell line with a HCV infectious clone (J6/JFH1), that reproduced the acute and persistent phases of HCV infection up to 76 days of culture. We demonstrated that the acute phase of HCV infection is characterized by the elevated levels of reactive oxygen species (ROS) associated in part with an increase of NADPH-oxidase transcripts and activity and a depletion of GSH accompanied by high rates of viral replication and apoptotic cell death. Conversely, the chronic phase is characterized by a reestablishment of reduced environment due to a decreased ROS production and increased GSH content in infected cells that might concur to the establishment of viral persistence. Treatment with the prooxidant auranofin of the persistently infected cultures induced the increase of viral RNA titer, suggesting that a prooxidant state could favor the reactivation of HCV viral replication that in turn caused cell damage and death. Our results suggest that targeting the redox-sensitive host-cells pathways essential for viral replication and/or persistence may represent a promising option for contrasting HCV infection.

1. Introduction

Hepatitis C virus (HCV), an RNA virus belonging to the *Flaviviridae* family, represents a major worldwide concern causing about 400,000 deaths worldwide every year [1]. HCV replication cycle takes place into the cytoplasmic compartment of hepatocyte, and it causes acute or chronic hepatitis. The persistent HCV infection is clinically characterized by lifelong low-level virus production, and it is accompanied by the development of chronic liver infection (in about 80% of infected patients) that can evolve to steatosis, fibrosis, cirrhosis, and in a small percentage (about 20%) of chronically infected patients it can develop to the end-stage hepatocellular carcinoma [2].

Although the exact molecular mechanisms underlying the HCV-related liver injury are not fully understood, redox alterations of hepatocytes have been extensively described in several chronic liver diseases [3, 4]. Oxidative stress, an imbalance between the reactive oxygen species (ROS) production and their clearance by scavenging molecules, has

been recognized as a leading factor in inducing hepatocyte death, inflammation, and fibrogenesis, which are responsible for induction and perpetuation of liver damage [5]. Several authors report a rise of ROS levels during HCV infection [6–13], and various viral proteins are known to induce and/or augment the ROS production, including HCV core, E1, E2, nonstructural (NS) 3, NS4B, and NS5A [11, 14–17]. Moreover, the simultaneous induction of several ROS-producing pathways and enzymes, such as the endoplasmic reticulum (ER) oxidoreductases [15, 18] and NADPH (nicotinamide adenine dinucleotide phosphate) oxidases (NOXs) [15, 16, 19], also contributes to HCV-induced oxidative stress. On the contrary, other studies report an increase in the antioxidant defenses, such as superoxide dismutase (SOD), peroxiredoxin (PRDX), glutathione S-transferase (GST) enzyme activity, and GSH levels [14, 20–23]. Glutathione is an important radical scavenger that directly and indirectly neutralizes a variety of reactive molecules, such as superoxide anions ($O_2^{\cdot-}$), hydroxyl radicals, and hydrogen peroxide (H_2O_2) [24]. The ratio between reduced (GSH) and oxidized (GSSG) form of GSH is considered an important indicator of the antioxidant capacity of the cell. Conflicting results are shown about the effect of HCV on intracellular GSH metabolism [17, 19, 23, 25–27]. Indeed, Roe and collaborators [27] report a significant raise of GSSG in HCV-infected cells, while increased GSH concentration has been demonstrated by de Mochel et al. [19] using the same *in vitro* infection system. Interestingly, Abdalla et al. [20] describe the different effects of two viral proteins on cell antioxidant defenses. In fact, hepatocytes overexpressing HCV core protein have reduced GSH levels and increased the oxidation of thioredoxin (Trx), while the overexpression of viral NS5A protein (known for its ability to cause oxidative stress) [16] increases antioxidant enzymes (MnSOD and catalase), heme oxygenase-1 (HO-1), and GSH content. Finally, patients with chronic hepatitis C show a depletion of GSH content, which increases after antioxidant treatment [28]. However, different genotypes of HCV exhibit different abilities to induce oxidative stress [29]. In fact, in patients chronically infected with genotype 1a/b, a sharp decrease of reduced GSH level has been observed with respect to the other genotypes, suggesting the more serious disease associated with this genotype [29].

Interestingly, the de novo synthesis of GSH is controlled by the transcription factor Nrf2 (NF-E2-related factor 2), which regulates the expression of cytoprotective genes. Some studies demonstrate that acute HCV infection is associated with an early induction of proteins functioning in cellular stress responses, including the Nrf2-mediated oxidative stress response [23, 25]. On the other hand, HCV core impairs the Nrf2/ARE signaling pathway by inducing the translocation of sMaf proteins in the cytoplasm, where they bind to NS3 as part of the replication complex. As a result, Nrf2 is trapped in the cytoplasm and is unable to function as transcription factor [26, 30].

On the basis of the conflicting results reported in the literature about the relationship between redox balance and HCV infection, the goal of this study was to clarify whether the virus is able to condition the redox environment of infected cells in order to induce acute infection or to establish its persistence into the cells. For this reason, we set up an *in vitro* system that mimics as closely as possible the acute and chronic HCV infection.

Here, we demonstrate that during the acute phase of infection HCV replicates with a high rate, thus inducing intense apoptosis in infected cells; in this phase, a marked oxidative stress was registered mainly due to NOX4 activity and to a decrease of GSH and consequently of GSH/GSSG ratio. Conversely, during the chronic phase of infection, low level of both HCV replication and apoptosis was observed, ROS production returned to basal level, GSH content was reestablished, and the GSH/GSSG ratio shifted versus the reduced form of GSH. Moreover, the treatment of HCV-chronically infected cells with a prooxidant drug, auranofin, was able to reactivate viral replication.

2. Materials and Methods

2.1. Cell Lines. Huh-7.5 human hepatoma cells were generously provided by Dr. Charles M. Rice [31]. Cells were grown in high-glucose Dulbecco's modified Eagle's medium (DMEM) (Sigma) supplemented with 100 U/ml of penicillin, 100 μg/ml of streptomycin, nonessential amino acids, and 10% fetal bovine serum (FBS) (Invitrogen) at 37°C in 5% CO_2.

2.2. Virus. The virus stock used in this study was prepared as described below. The FL-J6/JFH1-5'C19RLuc 2Ubi plasmid, encoding the entire viral genome of a chimeric strain of HCV genotype 2a, J6/JFH1 [32], was kindly provided by C. M. Rice. The plasmid was linearized by XbaI digestion and treated with mung bean nuclease to remove 5′ end overhangs. The linearized DNA templates were first purified by phenol:chloroform extraction and ethanol precipitation and then transcribed with T7 RNA polymerase using a MEGAscript™ T7 kit (Ambion, Austin, TX) according to the manufacturer's protocol. For electroporation, Huh-7.5 cells were grown to 60–80% confluence, trypsinized, washed twice in cold PBS, and resuspended in cold PBS at a concentration of 2×10^7 cells/ml. 0.4 ml aliquots were mixed with 10 μg of *in vitro* transcribed RNA and dispensed into 0.4 cm Gene Pulser cuvettes (Bio-Rad). Samples were pulsed using a Gene Pulser apparatus (Bio-Rad, Hercules, CA) with a single pulse at 0.27 kV and 960 mF. Cells were resuspended in 20 ml of complete growth medium, plated and incubated at 37°C, 5% CO_2, and 100% relative humidity. Cells were splitted every 3 days, and virus infectivity was measured by immunofluorescence assay as described below and expressed as $TCDI_{50}$/ml. The culture supernatant from the 4th passage was used to infect naïve Huh-7.5 cells at a multiplicity of infection (m.o.i.) of 0.2 in serum-free high-glucose DMEM. After 2 hours at 37°C, the medium was removed and replaced with complete medium. After 7 days and 2 passages, the supernatants were collected, centrifuged at 1200 rpm for 10 min at 4°C, cleared of debris through filtration on 0.45 μm pore size filters, and stored at -80°C as virus stocks.

2.3. Cell Infection and Viral Titer Assays. Huh7.5 cells were plated, grown for 24 h, and then challenged with virus stock in serum-free medium at 0.01 m.o.i. Culture supernatants of uninfected cells served as a control (mock preparation). Cells were incubated in the presence of the virus for 6 h at 37°C. After the viral challenge, mock-infected and virus-infected cells were washed with PBS and then cultured with fresh medium containing 10% FBS.

The titer of infectious HCV was determined by the 50% tissue culture infective dose ($TCID_{50}$) assay. Cell supernatants were serially diluted 10-fold in complete DMEM and used to infect 1×10^4/well naïve Huh-7.5 cells in 96-well plates (8 wells per dilution). The level of HCV infection was determined three days postinfection by immunofluorescence staining for HCV core protein. The wells showing positive staining for HCV core protein were counted, and the $TCID_{50}$ titer was interpolated using the Reed-Muench method [33].

2.4. Cell Treatments. Auranofin was obtained from Sigma-Aldrich (Heidelberg, Germany). The compound was dissolved in dimethylsulfoxide (DMSO) and applied to the cells at a final concentration of 200 nM that is the concentration at which no toxic effects were observed. The highest DMSO concentration present in the culture medium was 0.05%. Control cells were treated with an equivalent concentration of vehicle.

2.5. Cytotoxicity Assay. Cytotoxicity of auranofin was determined by cell count, and cell viability was assessed by trypan blue dye exclusion test.

2.6. Immunofluorescence Assay. Cells were fixed in methanol : acetone (50 : 50, *V*/*V*) for 20 min at -20°C. After blocking with PBS containing 1% bovine serum albumin (BSA) for at least 30 min, cells were incubated with mouse monoclonal antihepatitis C virus core 1b antibody (Abcam, AB 58713); bound antibodies were revealed with mouse anti-human IgG conjugated with Alexa Fluor 488 (Life Technologies, Z25102). After washing, the nuclei were stained with 1 μg/ml 4,6-diamidino-2-phenylindole (DAPI; Molecular Probes) in PBS for 15 min at room temperature. Fluorescent images were acquired on an Olympus IX70 microscope equipped with Nanomover and softWoRx DeltaVision image acquisition software (Applied Precision, WA, USA) and a U-PLAN-APO 40× objective. Images were captured under constant exposure time, gain, and offset.

2.7. Western Blotting. Cells were detached, washed with cold PBS, and centrifuged at 700 g for 10 min. The pellet was lysed in cold RIPA lysis buffer (20 mM TRIS pH 8, 150 mM NaCl, 1% Triton-X 100, 0.1% SDS, 1% sodium deoxycholate) containing protease and phosphatase inhibitors for 30 min on ice. Lysates were centrifuged at 10 000 g for 30 min at 4°C to remove debris.

Protein concentration of cell extracts was determined by the Bradford method (Bio-Rad, 5000006). Lysates were resolved by SDS-PAGE and blotted onto nitrocellulose membranes. The membranes were blocked with 10% nonfat dry milk in Tris-buffered saline containing 0.01% Tween-100 for 1 h at room temperature (RT) and then incubated with specific primary antibodies used at final concentration of 1 μg/ml. The antibodies used are as follows: rabbit polyclonal anti-NOX4 (Santa Cruz Biotechnology, sc-30141), rabbit polyclonal anti-NOX1 (Abcam, ab55831), rabbit monoclonal anti-Nrf2 (D1Z9C) (Cell Signaling Technology, Euroclone, Pero (MI) Italy, 12721S), mouse monoclonal antitubulin (Sigma-Aldrich, T5168), and mouse monoclonal anti-Lamin A/C (Sigma-Aldrich, L1293). Immunocomplexes were detected through peroxidase-coupled secondary antibodies (Jackson), followed by enhanced chemiluminescence (GE Healthcare Life Sciences). Densitometry was done using Quantity One 1-D Analysis software (Bio-Rad).

2.8. Glutathione Assay. The measurement of total intracellular glutathione (tGSH) (including the reduced and oxidized forms, GSH and GSSG, respectively) and GSSG was performed by means of Cayman's GSH assay kit (Cayman Chemical Co., 703002) according to the manufacturer's instructions. Briefly, the confluent control and infected Huh7.5 cells were washed twice with PBS, harvested using a rubber policeman, and were homogenized by a freeze-thaw method in 1 ml of 50 mM MES buffer pH 6 containing 1 mM EDTA. After centrifugation, a small amount of the supernatant was used for the protein assay (Bio-Rad protein assay). The residual supernatant was deproteinated by adding an equal amount of 5% *w*/*v* of metaphosphoric acid. After centrifugation (at 3000 ×g for 5 min), the supernatant was neutralized with 50 μL of triethanolamine per ml of sample. The tGSH level was then determined by the endpoint method reading absorbance at 405 nm after 25 min, according to the procedures recommended by the manufacturer. In another experiment, GSH was masked by 2-vinylpyridine for 1 h before the assay to determine the GSSG levels in the samples. The tGSH and GSSG were determined by comparison with standards, normalized to protein content, and expressed as nmol/mg protein. The GSH content was obtained by subtracting the GSSG from the tGSH.

2.9. Cell Death Determination. The quantitative evaluation of apoptosis was performed by a double-staining flow cytometry method using fluorescein isothiocyanate- (FITC-) conjugated annexin V(AV)/propidium iodide (PI) apoptosis detection kit (Marine Biological Laboratory, MBL, Woods Hole, MA, USA), according to the manufacturer's protocol, which allows discrimination among early apoptotic, late apoptotic, and necrotic cells.

2.10. ROS Assay. ROS production was determined by means of the CellROX deep red reagent (Thermo Fisher, C10491), which is a fluorogenic probe, as described in the manufacturer's instructions. CellROX (5 μM) was added to cell cultures and incubated at 37°C for 30 minutes. Then cells were fixed with paraformaldehyde (4%), and samples were immediately analyzed with an LRS II cytometer (Becton Dickinson, San Jose, CA, USA) equipped with a 488 argon laser and a UVB laser. The data obtained were analyzed by DIVA software (B&D). The median values of fluorescence intensity histograms were used to provide a semiquantitative

assessment of ROS production. Samples were acquired with a FACScalibur cytometer (BD Biosciences) equipped with a 488 argon laser and with a 635 red diode laser. At least 20,000 events were acquired. Data were recorded and statistically analyzed by a Macintosh computer using CellQuest software (BD Biosciences). The median values of fluorescence intensity histograms were used to provide a semiquantitative assessment of ROS production.

2.11. Real-Time RT-PCR Analysis. Total RNA was isolated from control and HCV-infected cells, harvested at the indicated times p.i., with the RNeasy kit (Qiagen, 74104) according to the manufacturer's instructions. Isolated RNA (1 μg) was reverse transcribed to cDNA using iScript™ cDNA Synthesis Kit (Bio-Rad, 1708890). A comparative real-time PCR analysis of gene expression was performed with the iQ™ SYBR Green Supermix (Bio-Rad, 170-8880) and analyzed on LightCycler iQ™ 5 (Bio-Rad). The following forward and reverse primers were used: NOX4 (5′-CAGGAGAAC CAGGAGATTGTTG-3′ forward; 5′-GAAGTTGAGGGCA TTCACCAGATG-3′ reverse), GR (5′-TTCAGTTGGCATG TCATC-3′ forward; 5′-CCGTGGATAATTTCTATGTGA-3′ reverse), GS (5′-GTGCTACTGATTGCTCAA-3′ forward; 5′-ACATGGATCTTCCTGTCT-3′ reverse), GCL (5′-AAGT CCCTCTTCTTTCCA-3′ forward; 5′-CCTTGAATATTGG CACATTG reverse), and GAPDH (5′-TGCGACTTCAA CAGCAACTC-3′ forward; 5′-ATGTAGGCCATGAGGT CCAC-3′ reverse).

The housekeeping glyceraldehyde-3-phosphate dehydrogenase (GAPDH) was used for normalization. Relative quantitative evaluation was performed by the comparative ΔΔCt method. The results are presented as fold increase relative to control cells. Dissociation curves were generated to ensure a single amplicon had been produced.

The production of intracellular viral RNA was assessed by quantitative one-step RT-PCR carried out using an ABI 7000 Real-Time PCR System (Applied Biosystems). 5 μl of total RNA was mixed with 2x TaqMan One-Step RT-PCR Master Mix (ABI) and 1 μM forward (TCCCGGGAGAG CCATAGT), 1 μM reverse primers (CCCAGTCTTCCCGG CAATT), and 200 nM probe (FAM- CACCGGTTCCG CAGACC -TAMRA). *In vitro* transcribed genotype 2a RNA was used as a standard to quantify the copy numbers of viral RNA.

2.12. Data Analysis and Statistics. A statistical significance was evaluated using GraphPad Prism™ (San Diego, CA, USA) software version 6.0. All data reported were verified in at least 3 independent experiments and are reported as means ± standard deviation (SD). Test details of each experiment are described in the figure legends. P values < 0.05 were considered significant.

3. Results

3.1. Generation of an In Vitro Model of Acute and Chronic HCV Infection. In the attempt to set up an HCV infectious cell culture system that mimics acute and chronic HCV infection, human hepatocellular carcinoma cell line (Huh7.5) was infected with HCV at low (0.01) m.o.i. to allow a multiple-cycle replication, as described in Materials and Methods, and cultured up to 76 days.

After viral adsorption, cell culture viability was monitored at different time points, and viral replication was evaluated by both real-time RT-PCR and immunofluorescence assay for HCV core protein.

The number of viral core positive cells was estimated by immunofluorescence to evaluate the extension of HCV-infected cells. During the first two passages (8 days postinfection), about 80% of the cells were stained for HCV core protein, thus indicating a high rate of HCV replication corresponding to the "acute" phase of infection (Figure 1(a) left side). On the contrary, in the late stage of infection (76 days postinfection p.i.), here referred as the "chronic" phase, only about 15% of the cells expressed the core protein (Figure 1(a) right side). Similarly, the HCV RNA in intracellular compartment reached the highest titer ($3.59 \times 10^7 \pm 1.3 \times 10^6$ copies/μg total RNA $^{***}P < 0.001$ vs. p0) 8 days p.i., and it decreased after the recovery phase of the cell culture and during the chronic phase ($2.09 \times 10^6 \pm 1.2 \times 10^6$/$\mu$g total RNA at 44 days p.i and $6 \times 10^5 \pm 9 \times 10^2$ copies/μg total RNA at 76 days p.i.) (Figure 1(b)) that is consistent with a persistently infected cell culture. Furthermore, in correspondence with the maximum titer of HCV RNA, the number of HCV-infected cells was significantly reduced compared to uninfected ones (Figure 1(c)). In fact, trypan blue dye exclusion assay showed a significant decrease of alive cells during the so-called "crisis" phase that lasted about two weeks during which the infected cultures were not splitted. Particularly, on days 8 and 14 most of the cells became rounded, detached from the plate, and floated in the culture medium (data not shown). Furthermore, FACS analysis of annexin V/PI double staining of cells showed that infected cells underwent apoptotic death only during the crisis phase. In fact, as shown in Figure 1(d) (right panel), the percentage of double-stained PI+/AV+ cells increased with respect to uninfected cells (CTR) at passage 2 (p2). The 5-fold increase in percentage of apoptotic cells (obtained as mean from 4 independent experiments) was detected in infected cultures at 14 days p.i., compared to the uninfected ones (Figure 1(d), right panel). Interestingly, apoptotic death in infected cell cultures coincided with the highest intracellular viral RNA titer (Figure 1(b)), thus suggesting a causative link between the rate of HCV replication and cell death. Subsequently to the crisis phase, cells started a recovery phase at the end of which the number of live cells, in HCV-infected cultures, was comparable to that of control cells (Figure 1(c); see value at p4). Accordingly, FACS analysis demonstrated that from 37 days p.i. up to 76 days p.i., the percentage of apoptotic cells returned to control values upon recovery of the cultures (Figure 1(d) right panel; see values at p4, p6, p13, and p18). Moreover, from this time point up to 76 days p.i. (chronic phase), the percentage of HCV core-positive cells decreased to 15% (Figure 1(a) right panel) vs. 80% of the acute phase, thus mirroring viral titer trend (see Figure 1(b)). These results strongly suggested a steady state level of HCV replication.

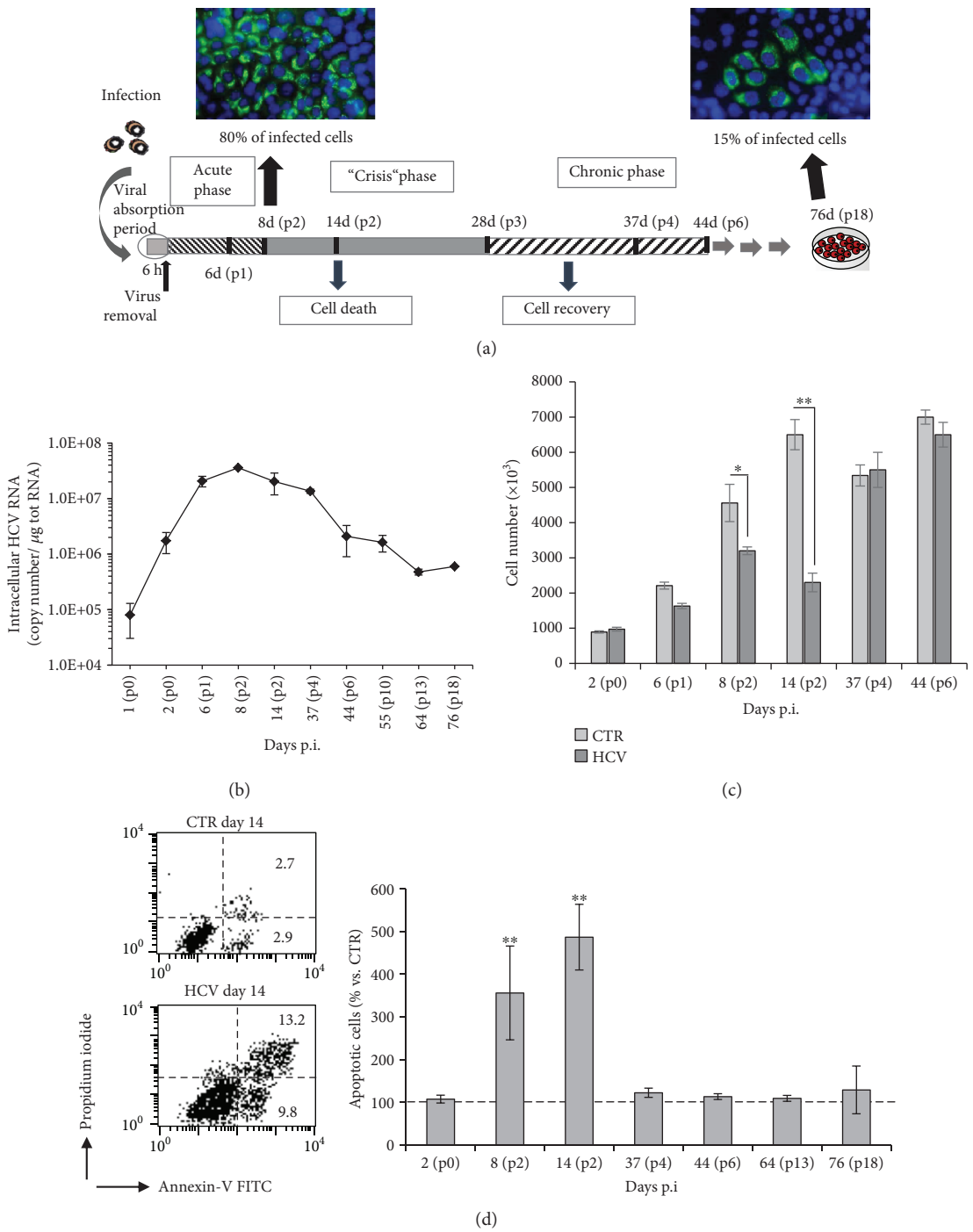

Figure 1: Generation of an *in vitro* model of acute and chronic HCV infection. (a) Schematic representation of the strategy to obtain long-term infected culture (LTIC). The fluorescence microscopy pictures were obtained from one representative experiment out of three performed. Cells were labelled with anti-hepatitis C virus core 1b protein followed by Alexa Fluor 488-conjugated secondary antibody (green); the nuclei were stained with DAPI (blue), 40× objective; (b) virus titration by qRT-PCR at different times of infection. (c) Trypan blue dye exclusion analysis of cell viability in uninfected (CTR) and HCV-infected Huh7.5 cells at different days postinfection. Means ± SD from three independent experiments are shown. $^{*}P < 0.05$; $^{**}P < 0.01$. (d) Biparametric flow cytometry analysis of apoptosis at different time points after HCV infection. In the left panel, a representative dot blot of apoptosis detection is shown relative to the samples obtained from 14 days p.i. Numbers represent the percentage of apoptotic cells either annexin V/PI double-positive (upper right quadrant) or annexin V single-positive (low right quadrant). In the right panel, the bar graphs show the mean ± SD of the percentage of annexin V/PI-positive cells expressed as percentage of variation vs. control uninfected cells. The mean values were obtained from four independent experiments. $^{**}P < 0.01$ vs. CTR uninfected cells.

Collectively, the results demonstrate that initial infection of Huh7.5 cells with low m.o.i. leads to obtain an acute *in vitro* infection featured by apoptotic death of infected cells, here named "acute phase". This latter is followed by the recovery of the infected cell cultures characterized by lower virus replication and subsequently by the establishment of a persistent infection, here named "chronic phase". All these characteristics indicated that an *in vitro* model of persistent infection with Jc1-HCV was set up.

3.2. HCV Infection Increases ROS Production through NOX4 and NOX1 Activity. Redox changes, in particular increased ROS levels, had been associated with HCV infection [34, 35]. Nevertheless, the impact of intracellular HCV replication on cellular redox environment is so far contradictory. To this aim, confluent monolayers of Huh7.5 cells were infected with HCV, and at different time points after viral adsorption, ROS production was measured through FACS using the ROS-sensitive probe CellROX. As shown in Figure 2(a), a significant increase in intracellular ROS levels (more than 3 times higher compared to control) was detected in infected cells 8 days p.i. (p2), when HCV RNA reached the maximum value, and was maintained at high levels during all the apoptotic crisis period. After cell cultures recovery from 37 up to 76 days p.i., the ROS levels in infected cells returned to control values (Figure 2(a) right panel). These results suggest that intracellular ROS-mediated oxidative stress was induced by HCV replication, and it was simultaneously accompanied by the apoptotic phase.

Next, we investigated whether in our model the increase of ROS levels was associated with NOXs activity, particularly with two isoforms, NOX1 and NOX4, involved in the severity of HCV infection [19, 36]. To this aim, Huh7.5 cells were infected with HCV and assayed for NOX4 mRNA by RT-PCR during the different phases of HCV infection. The results demonstrated that the NOX4 mRNA levels doubled 6 days p.i. (p1) in infected cells with respect to uninfected control cells; then the NOX4 mRNA levels decreased and returned to physiological level (Figure 2(b)). Consistently, NOX4 protein expression was upregulated in infected cells during the acute phase, while it was decreased during the chronic phase (Figure 2(c)). Similar results were obtained for NOX1 enzyme, although its decrease began earlier (p3) than NOX4.

Collectively, these data suggest NOX enzymes as one possible player in HCV-induced ROS production.

3.3. HCV Alters the GSH Redox Homeostasis. To test whether Huh7.5 cells activated GSH antioxidant system in response to HCV-induced oxidative stress, the intracellular content of both reduced (GSH) and oxidized (GSSG) forms of glutathione was measured at different times after HCV infection by using a colorimetric assay. As shown in Figure 3(a), in the early steps of acute phase of infection GSH content diminished of about 40% ($^{*}P < 0.05$, $^{**}P < 0.01$ at 2 (p0) and 6 (p1) days p.i, respectively) compared to uninfected cells. In contrast, the GSH levels in infected cells were significantly higher (about 70%) during cell recovery (p3) compared to the control cells and were maintained at higher levels during the chronic phase (p4, p5, and p10). More interestingly, by comparing the acute and chronic phases, a significant rise trend of GSH content in infected cells was detected in the latter phases (p3, p4, and p5 vs. p0). Conversely, as shown in Figure 3(b), the GSSG levels increased during the acute phase, in particular the content was doubled 8 days p.i. (p2). Interestingly, as shown in Figure 3(c), the GSH/GSSG ratio that under physiological conditions is maintained >1 [37] was shifted toward the oxidized form and was <1 (p1 and p2), just when viral replication reached the peak (Figure 1(b)), while during the chronic phase the ratio was >1, indicating a restore of physiological redox environment.

Intracellular GSH is regenerated from the oxidized form by glutathione reductase (GR) or synthesized *ex novo* by the consecutive actions of glutamate cysteine ligase (GCL) and GSH synthase (GS) [38]. Therefore, we evaluated the transcriptional expression of these 3 enzymes both during the acute and chronic phase of infection. As shown in Figure 4(a), the mRNA levels of GR were strongly upregulated during the early steps of infection (p1 and p2), when the GSSG levels were high, while GCL and GS enzyme expression increased starting from the end of acute phase until the recovery period and when the peak of GSH content (p3) was detected. Interestingly, these enzymes were still activated during the chronic phase (p4), suggesting the necessity to maintain a reduced environment in long-term cultures.

Finally, we decided to evaluate whether these enzymes were under the control of Nrf2 pathway. Therefore, we analyzed Nrf2 protein expression during both the acute and chronic phases. As shown in Figure 4(b), Nrf2 seemed to be downregulated by the virus in the early phases of infection, while it was more expressed late in infection, at p4 and p10 when the chronic phase was well-established.

All these results suggest that oxidative stress during the acute phase is useful for promoting viral replication, while the reducing conditions observed in the chronic phase probably favor viral persistence into the cells.

3.4. Auranofin-Induced Oxidative Stress Leads to Increased Levels of HCV RNA Copies. Since the intracellular redox conditions seem to play a key role in the establishment of the chronic phase of HCV infection, we decided to evaluate whether the oxidative stress could reactivate HCV replication in chronically infected cells. For this reason, a chemical treatment with auranofin (Au), a well-known prooxidant drug [39] that induces ROS production in infected cells [40, 41], was used. In our experimental model, treatment with Au (200 nM) for 48 hrs was able to induce an increment of intracellular ROS levels by twofold, either in uninfected (CTR) or in HCV-infected cells (Figure 5(a)). In parallel, the number of intracellular HCV RNA copies in Au-treated cultures was about 40% greater than that of untreated infected cells (Figure 5(b)). Interestingly, in this condition, only HCV-infected cell cultures underwent apoptosis (Figure 5(c)), suggesting that oxidative stress induction could favor viral replication that in turn caused cell damage and death.

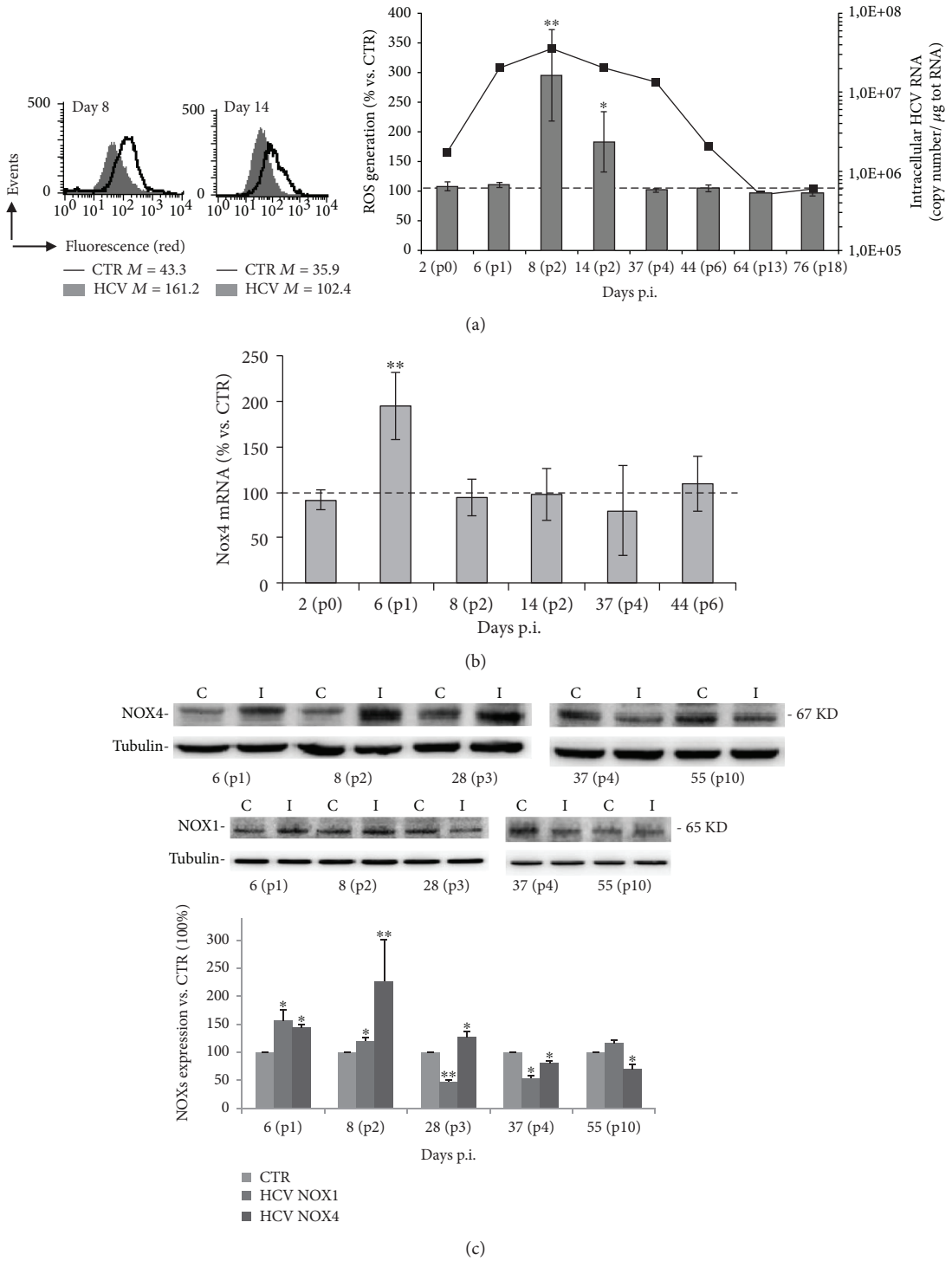

Figure 2: HCV infection increases ROS production through the activity of NOX4. (a) Quantitative cytofluorimetric analysis of intracellular ROS production at different time points after HCV infection in cells stained with CellROX deep red. In the left panel, data obtained from the samples relative to 8 and 14 days p.i. are shown as one representative experiment out of three performed. Numbers represent the median fluorescence intensity. In the right panel, mean ± SD of the results obtained from three different experiments are reported; the results are expressed as percentage of variation vs. CTR uninfected cells considered as 100, as indicated by the dashed line. $^{*}P < 0.05$ and $^{**}P < 0.01$ vs. CTR uninfected cells. The dark line refers to the intracellular HCV genome copy number. (b) Real-time PCR assay of NOX4 isoform levels in HCV-infected Huh7.5 cells, normalized to levels in uninfected cells (CTR), indicated with the horizontal dashed line. Data shown are the means ± SD of three performed experiments $^{**}P < 0.01$. (c) Western blot of uninfected (C) and HCV-infected (I) Huh7.5 cells at different times from infection, using anti-NOX4 and anti-NOX1 antibodies. Tubulin was used as a loading control. Blot is one representative experiment out of three performed. Densitometric analysis of the blots is shown. Data represent the mean ± SD of six different technical replicates; unpaired t test: $^{*}P < 0.05$ and $^{**}P < 0.01$ vs. CTR (considered as 100%).

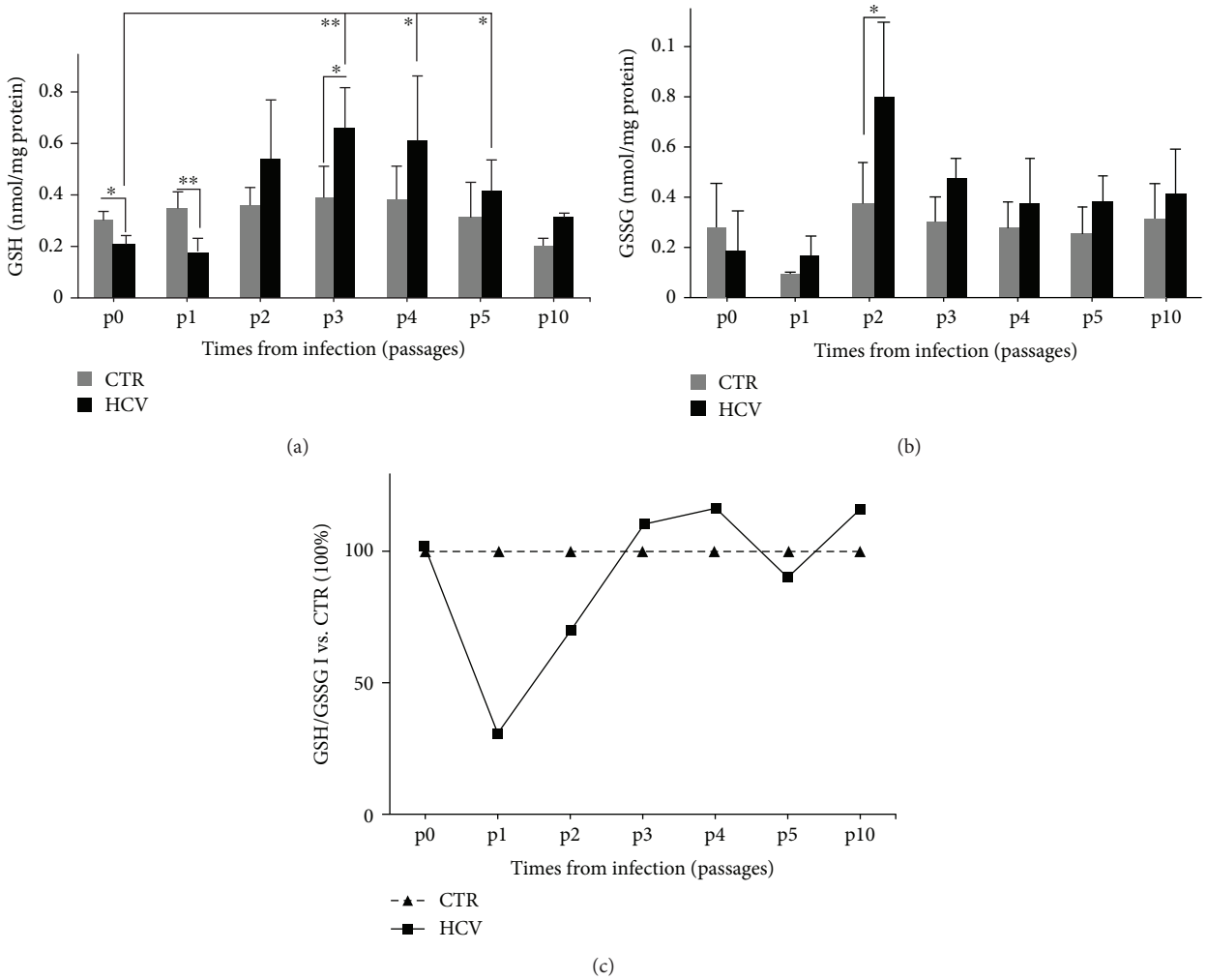

Figure 3: HCV alters the GSH redox homeostasis. Intracellular levels of GSH (a) and GSSG (b) in uninfected (CTR) and HCV-infected (HCV) Huh7.5 cells at different passages of infection. Data are expressed as mean ± SD of three experiments each done in duplicate ($n = 6$). 2way ANOVA followed by Sidak's multiple comparisons test: $^{*}P < 0.05$ and $^{**}P < 0.01$ I vs. CTR; $^{*}P < 0.05$ I (p4 and p5) vs. I (p0, 2 days); $^{**}P < 0.01$ I (p3) vs. I (p0, 2 days). (b) $^{*}P < 0.05$ I vs. CTR; (c) ratio of reduced glutathione (GSH) versus oxidized glutathione (GSSG). The graph represents the ratio GSH/GSSG in infected cells (I) vs. CTR cells (considered as 100%).

4. Discussion

Oxidative stress has emerged as a key contributor to the development and progression of HCV-induced pathogenesis of liver [34, 35, 42] and the associated development of hepatocellular carcinoma [43]. The lack of an *in vitro* system that recapitulates the different stages of HCV chronic infection has hampered the disclosure of the exact mechanisms and the mutual effect of HCV infection and oxidative stress pathways on the host cells. In this study, we were able to set up the HCV infectious system in Huh7.5 cells, which are permissive to the JFH1 infectious clone [31]. Particularly, infection of cell monolayers with low m.o.i. of HCV allowed to obtain first an acute infection and subsequently the establishment of a persistent infection. We demonstrated that, during the acute phase, high percentage of infected cells underwent apoptosis and viral titer peaked, whereas during the chronic phase viral replication was reduced and consequently the percentage of apoptotic-infected cells. This model called "long-term infected cultures" (LTIC) could mimic the same stages of a natural HCV infection. It is interesting that HCV has long been believed noncytopathic virus, and the hepatocyte damage during infection was considered to be mediated by the immune system. However, consistent with previously reported results [44], we could demonstrate that HCV induces cell death during *in vitro* infection of Huh7.5 cells in the absence of RIG-I-mediated innate immune response. The presence of low number of core expressing cells, during the here called "chronic phase", paralleled by the low level viral RNA titer, indicated the ability of the JFH1 clone of HCV to persistently infect susceptible cell cultures. With regard to the mechanisms involved in establishing *in vitro* persistence, there could be a close virus-host cell interaction, and as reported by Zhong et al. [44], in Huh7.5 cells long-term infected by HCV, some cells resistant to reinfection, due to the loss of HCV receptor CD81, can be selected during the chronic phase. From the virus side, HCV is known to exist as quasispecies in patients *in vivo*, and

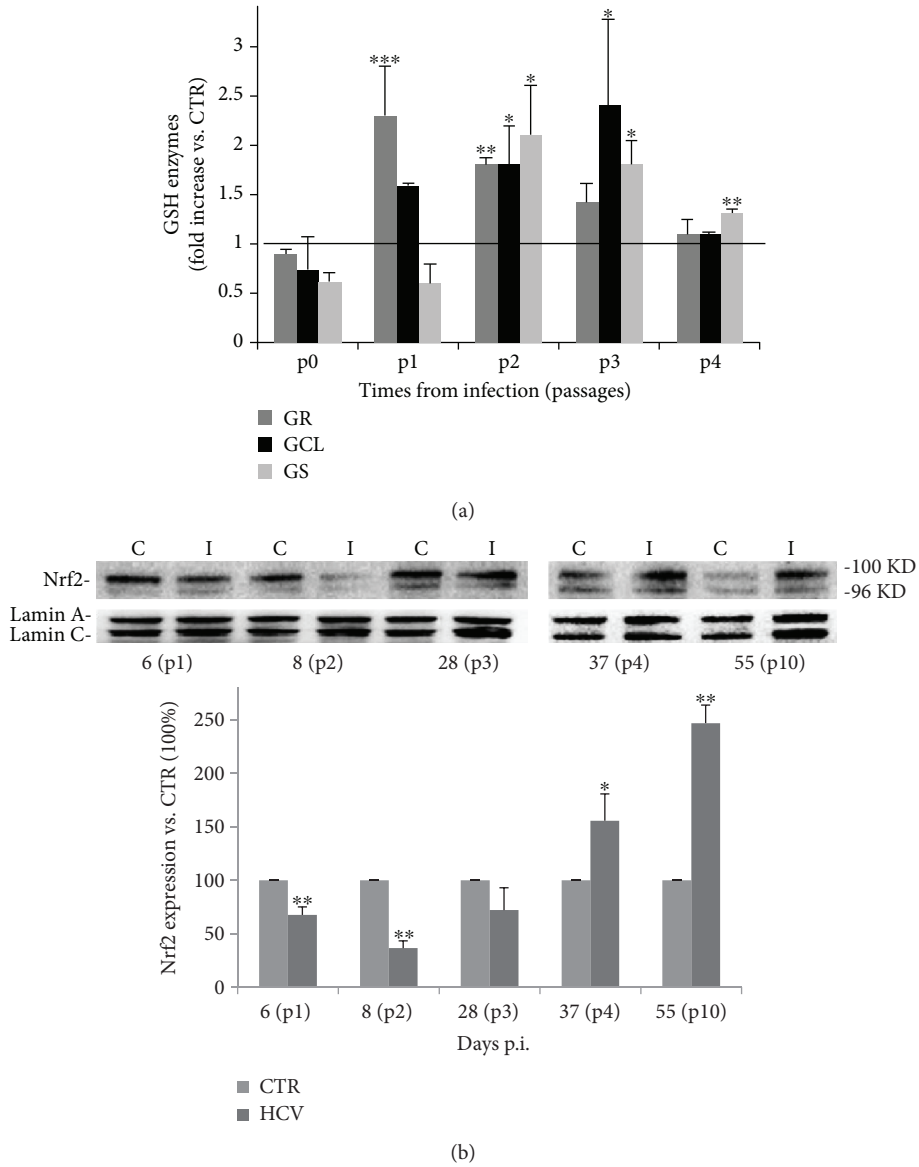

Figure 4: Nrf2 protein and enzymes responsible for recycling and de novo biosynthesis of GSH are differently activated during HCV infection. (a) RT-PCR quantification of enzymes responsible for recycling (GR) and biosynthesis of GSH (GCL and GS). Gene expression was measured in uninfected (CTR) and HCV-infected cells at different passages of infection. The graph represents the fold increases relative to CTR. Unpaired t test: $^{*}P < 0.05$, $^{**}P < 0.01$, and $^{***}P < 0.001$ vs. CTR, represented by the horizontal line. (b) Western blot of uninfected (C) and HCV-infected (I) Huh7.5 cells at different times of infection, using anti-Nrf2 antibody. Lamin A/C was used as a loading control. Densitometric analysis of the blot is shown. Data shown are the mean ± SD of four different technical replicates; unpaired t test: $^{*}P < 0.05$ and $^{**}P < 0.01$ vs. CTR (considered as 100%).

during persistent infection *in vitro*, some virus variants can arise that are more adapted in cultures and able to persist without killing the host cells or having reduced infectivity [44]. These points will deserve deeper investigation in the future.

Furthermore, during HCV acute infection, a ROS overproduction, mainly mediated by NADPH-oxidase NOX4, was registered in infected cells. NOXs are a family of seven enzymes, generating $O_2^{\cdot -}$ or H_2O_2 from molecular oxygen [45]. Accumulating evidence indicates that NOX-mediated ROS production has a critical role in hepatic fibrosis [46, 47], and in particular, NOX4 is involved in the severity of HCV-associated liver disease [19, 36], as well as in the regulation of viral replication of different viruses [48–50]. Here, we found that NOX4 and NOX1 rise mirrored the trend of ROS production and that of viral replication; in fact, their expression was increased during the acute phase of infection, while it decreased late in infection, thus suggesting a critical role for NOXs also in regulating HCV replication cycle. The reason why both NOX enzymes were downmodulated in infected cells during the chronic phase is still unclear, but we hypothesize that it could be a further mechanism induced by the virus to maintain reducing environment into host cell for the establishment of its persistence. Indeed, other

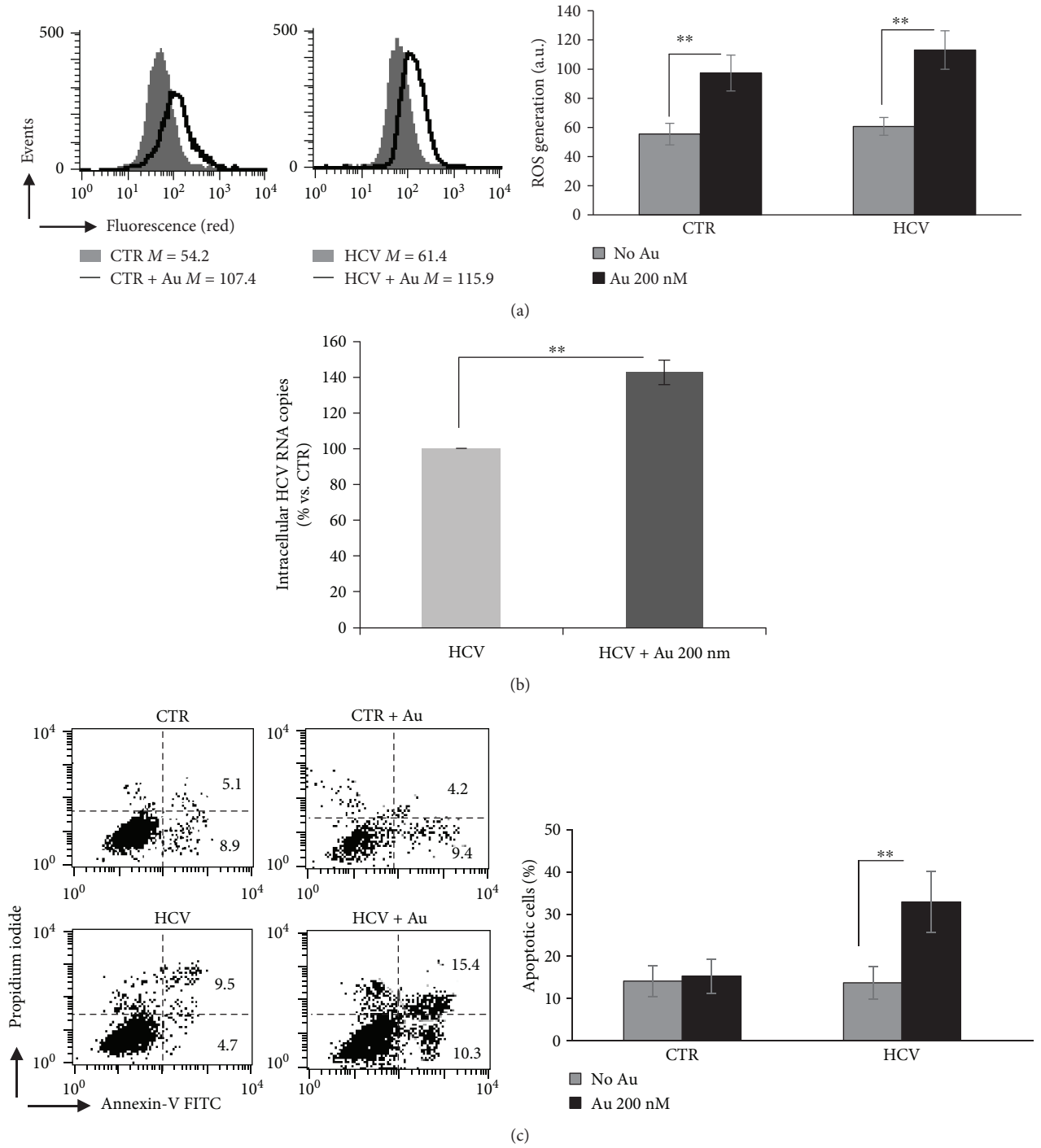

Figure 5: HCV induction by auranofin treatment. (a) Quantitative cytofluorimetric analysis of intracellular ROS production during the chronic phase of infection in cells treated or untreated with auranofin (Au) 200 nM and then stained with CellROX deep red. Left panel: results from one representative experiment out of three performed, are shown. Numbers represent the median fluorescence intensity. Right panel: mean ± SD of the results obtained from three independent experiments. In ordinate, median fluorescence intensity. $^{**}P < 0.01$ vs. CTR uninfected cells. (b) RT-PCR analysis of HCV viral titer in the absence or presence of Au. $^{**}P < 0.01$ vs. untreated infected cells. (c) Left panel: flow cytometry analysis after double staining of cells with annexin V-FITC/propidium iodide. Results from one representative experiment out of three performed, are shown. Right panel: percentage of apoptotic cells in uninfected (CTR) and HCV-infected Huh7.5 cells in the presence or absence of Au. Data are the mean ± SD of three independent experiments. $^{**}P < 0.01$ vs. untreated infected cells.

viruses are able at the same time to positively and negatively modulate NOX isoforms to their advantage [48–50]. Further studies will be needed to clarify this aspect.

It is noteworthy that NOX4 is mainly localized in the nuclei and ER and that during HCV infection the amount of NOX4 in the nucleus increases [19], which seems to be

one of the mechanisms underlying HCV pathogenesis. Therefore, it is also possible to speculate that nuclear NOX4 may increase during the acute phase of HCV infection in our experimental system, thus promoting the DNA damage and apoptosis of infected cells. Apoptotic death might favor virus spread throughout the cell culture. Further studies are in progress to deepen this aspect.

It is important to note, however, that NOXs are not the only source of ROS production in HCV-infected cells [51]. In fact, some viral proteins, i.e., core, NS3/NS4A, and NS5A, have been shown to increase ROS levels [7, 9, 52–54] through direct or indirect interaction with mitochondria. Therefore, we cannot rule out that ROS increase in HCV-infected cells might be in part produced by mitochondrial compartment, other than NOXs.

Because of high chemical reactivity of ROS, cells possess antioxidant defense mechanisms for maintaining redox homeostasis [55], whose principal component is GSH, the main abundant intracellular antioxidant. It plays a crucial role in sustaining redox balance, and the ratio of GSH to GSSG is considered as a good indicator of the redox environment. To date, there is a great debate on the induction and modulation of oxidative stress by HCV and its relationship with acute or chronic phase of infection.

Hepatocytes are the major source of GSH in the body, and the GSH antioxidant system plays an important role against oxidative stress in these cells [56]. Interestingly, reduced GSH levels were found in the serum and liver of chronically HCV-infected patients [28, 57]. Here, we found that intracellular GSH levels were significantly decreased in infected cells during the acute phase, while those of GSSG were increased, and, consequently, the ratio GSH/GSSG shifted toward GSSG, thus reflecting an impaired antioxidant potential. The oxidized environment seems to be necessary for HCV to replicate as demonstrated by viral titer peak in the acute phase. These data are in line with different *in vitro* studies on viruses responsible for acute infection, demonstrating the role of virus-induced oxidative stress in promoting viral replication [48, 50, 58–60]. On the contrary, during the chronic phase, reducing redox environment was restored by increased GSH content in infected cells that might be useful for the establishment of viral persistence. Indeed, treatment of persistently HCV-infected cells with the prooxidant drug auranofin caused the reactivation of HCV replication. The mechanisms through which HCV manipulates redox environment to its advantage are not fully clarified yet.

It is known that GSH de novo synthesis is driven by Nrf2 (nuclear factor erythroid 2-related factor), one of the major cellular defense mechanisms against oxidative stress and a master regulator of different cytoprotective genes including those involved in the antioxidant GSH pathway [61]. It has been recently demonstrated that higher expression of nuclear Nrf2 contributes to persistent HCV infection and that knockdown of Nrf2 suppresses its persistent infection [62]. The authors suggest that the nuclear translocation of p-Nrf2 might play an important role in the expression of the genes which contribute to regulate apoptosis and HCV persistence [25, 26, 30, 62]. Accordingly, we found higher mRNA levels of GCL and GS enzymes during the recovery period; at the same time, Nrf2 protein content was highly expressed during the chronic phase. On the basis of these evidences, we suggest that the high GSH levels registered in chronically infected cells compared to those measured during the acute phase of infection might be partly related to the activation of Nrf2 pathway.

There is a great debate regarding the supplementation of antioxidants in combination with antiviral drugs. In fact several clinical trials reported that antioxidant therapy decreases viral load and ameliorates hepatic damage [63]. However, other studies reported that supplementation with vitamin C, E, and selenium increased the antioxidant status but had no effects on viral load or oxidative markers [64]. All these conflicting results highlight the "dark side" of some antioxidants. Therefore, on the basis of our evidences and on the literature available, we suggest to carefully consider the use of antioxidants in chronically HCV-infected patients, since, although they could limit liver tissue injury, they would contribute to establish virus persistence that, in turn, can contribute to the development of hepatocellular carcinoma.

The lack of HCV vaccine and the emergence of viral strains resistant to antiviral therapy underline our limits in the current weapons used to fight the infection. In the recent years, new drugs acting specifically on HCV viral proteins (DAA) have been developed among which are the inhibitors of protease (telaprevir, boceprevir, and simeprevir) and the last approved RNA polymerase inhibitor, sofosbuvir [65]. Since the emergence of drug-resistant HCV variants has been recently described [66], there is an urgent need to identify novel targets for the design of new effective therapeutic strategies. In this context, targeting of redox-sensitive host-cells pathways essential for viral replication and/or persistence may represent a promising option for contrasting HCV infection.

5. Conclusions

In conclusion, we demonstrate that the acute phase of HCV infection is characterized by a marked oxidative stress that, similarly to other viruses, is useful for viral replication. On the contrary, the restoration of reducing redox conditions that characterize the chronic phase of infection might play a key role in decreasing viral replication and apoptotic death. Overall, our data indicate that redox sensitive pathways control the different phases of HCV infection and suggest a particular wariness in the supplementation of exogenous antioxidants in chronically HCV-infected patients for their potential role in favoring viral persistence.

Data Availability

The data used to support the findings of this study are available from the corresponding author upon request.

Conflicts of Interest

The authors declare that there is no conflict of interests.

Authors' Contributions

S. Anticoli and D. Amatore equally contributed to the execution of the experiments and drafted the paper; A.Ruggieri and L. Nencioni conceived the idea, designed the study, participated to the analysis and interpretation of data, and supervised the manuscript; M. De Angelis was in charge of western blotting experiments; P. Matarrese was in charge of the flow cytometry experimental analysis and interpretation of the resulting data; AT Palamara was the overall supervisor.

Acknowledgments

The authors are grateful to Prof. C. Rice for kindly providing the Jc1 infectious clone, FL-J6/JFH1-5′C19RLuc 2Ubi plasmid. The research was supported in part by a research grant to SA provided by Prof. AT Palamara. The research was further supported in part by the Italian Ministry of Education, University and Research - MIUR PRIN (ATP), Ateneo (LN, ATP) grants, Istituto Superiore di Sanità intramural funds (AR), Italian Association for Cancer Research (N.18526 2016 to PM), Arcobaleno Onlus (PM), and the Italian INAIL-BRIC (ID50 2016 to AR).

References

[1] WHO, "Global hepatitis report," 2017, https://www.who.int/hepatitis/publications/global-hepatitis-report2017/en/.

[2] R. H. Westbrook and G. Dusheiko, "Natural history of hepatitis C," *Journal of Hepatology*, vol. 61, no. 1, pp. S58–S68, 2014.

[3] S. Clément, S. Pascarella, and F. Negro, "Hepatitis C Virus infection: molecular pathways to steatosis, insulin resistance and oxidative stress," *Viruses*, vol. 1, no. 2, pp. 126–143, 2009.

[4] K. Tanikawa and T. Torimura, "Studies on oxidative stress in liver diseases: important future trends in liver research," *Medical Molecular Morphology*, vol. 39, no. 1, pp. 22–27, 2006.

[5] K. de Andrade, F. Moura, J. dos Santos, O. de Araújo, J. de Farias Santos, and M. Goulart, "Oxidative stress and inflammation in hepatic diseases: therapeutic possibilities of N-acetylcysteine," *International Journal of Molecular Sciences*, vol. 16, no. 12, pp. 30269–30308, 2015.

[6] C. Bureau, J. Bernad, N. Chaouche et al., "Nonstructural 3 protein of hepatitis C virus triggers an oxidative burst in human monocytes via activation of NADPH oxidase," *The Journal of Biological Chemistry*, vol. 276, no. 25, pp. 23077–23083, 2001.

[7] G. Gong, G. Waris, R. Tanveer, and A. Siddiqui, "Human hepatitis C virus NS5A protein alters intracellular calcium levels, induces oxidative stress, and activates STAT-3 and NF-κB," *Proceedings of the National Academy of Sciences of the United States of America*, vol. 98, no. 17, pp. 9599–9604, 2001.

[8] N. Fu, H. Yao, Y. Nan, and L. Qiao, "Role of oxidative stress in hepatitis C virus induced hepatocellular carcinoma," *Current Cancer Drug Targets*, vol. 17, no. 6, pp. 498–504, 2017.

[9] M. Okuda, K. Li, M. R. Beard et al., "Mitochondrial injury, oxidative stress, and antioxidant gene expression are induced by hepatitis C virus core protein," *Gastroenterology*, vol. 122, no. 2, pp. 366–375, 2002.

[10] G. Waris, J. Turkson, T. Hassanein, and A. Siddiqui, "Hepatitis C virus (HCV) constitutively activates STAT-3 via oxidative stress: role of STAT-3 in HCV replication," *Journal of Virology*, vol. 79, no. 3, pp. 1569–1580, 2005.

[11] S. Pal, S. J. Polyak, N. Bano et al., "Hepatitis C virus induces oxidative stress, DNA damage and modulates the DNA repair enzyme NEIL1," *Journal of Gastroenterology and Hepatology*, vol. 25, no. 3, pp. 627–634, 2010.

[12] S. Blackham, A. Baillie, F. al-Hababi et al., "Gene expression profiling indicates the roles of host oxidative stress, apoptosis, lipid metabolism, and intracellular transport genes in the replication of hepatitis C virus," *Journal of Virology*, vol. 84, no. 10, pp. 5404–5414, 2010.

[13] R. Medvedev, D. Ploen, and E. Hildt, "HCV and oxidative stress: implications for HCV life cycle and HCV-associated pathogenesis," *Oxidative Medicine and Cellular Longevity*, vol. 2016, Article ID 9012580, 13 pages, 2016.

[14] A. V. Ivanov, V. T. Valuev-Elliston, D. A. Tyurina et al., "Oxidative stress, a trigger of hepatitis C and B virus-induced liver carcinogenesis," *Oncotarget*, vol. 8, no. 3, pp. 3895–3932, 2017.

[15] A. Ivanov, O. Smirnova, I. Petrushanko et al., "HCV core protein uses multiple mechanisms to induce oxidative stress in human hepatoma Huh7 cells," *Viruses*, vol. 7, no. 6, pp. 2745–2770, 2015.

[16] O. A. Smirnova, O. N. Ivanova, B. Bartosch et al., "Hepatitis C virus NS5A protein triggers oxidative stress by inducing NADPH oxidases 1 and 4 and cytochrome P450 2E1," *Oxidative Medicine and Cellular Longevity*, vol. 2016, Article ID 8341937, 10 pages, 2016.

[17] A. V. Ivanov, O. A. Smirnova, O. N. Ivanova, O. V. Masalova, S. N. Kochetkov, and M. G. Isaguliants, "Hepatitis C virus proteins activate NRF2/ARE pathway by distinct ROS-dependent and independent mechanisms in HUH7 cells," *PLoS One*, vol. 6, no. 9, article e24957, 2011.

[18] C. X. C. Santos, L. Y. Tanaka, J. Wosniak Jr, and F. R. M. Laurindo, "Mechanisms and implications of reactive oxygen species generation during the unfolded protein response: roles of endoplasmic reticulum oxidoreductases, mitochondrial electron transport, and NADPH oxidase," *Antioxidants & Redox Signaling*, vol. 11, no. 10, pp. 2409–2427, 2009.

[19] N. S. R. de Mochel, S. Seronello, S. H. Wang et al., "Hepatocyte NAD(P)H oxidases as an endogenous source of reactive oxygen species during hepatitis C virus infection," *Hepatology*, vol. 52, no. 1, pp. 47–59, 2010.

[20] M. Y. Abdalla, I. M. Ahmad, D. R. Spitz, W. N. Schmidt, and B. E. Britigan, "Hepatitis C virus-core and non structural proteins lead to different effects on cellular antioxidant defenses," *Journal of Medical Virology*, vol. 76, no. 4, pp. 489–497, 2005.

[21] C. Brault, P. Lévy, S. Duponchel et al., "Glutathione peroxidase 4 is reversibly induced by HCV to control lipid peroxidation and to increase virion infectivity," *Gut*, vol. 65, no. 1, pp. 144–154, 2016.

[22] A. Kasprzak and A. Adamek, "Role of hepatitis C virus proteins (C, NS3, NS5A) in hepatic oncogenesis," *Hepatology Research*, vol. 38, no. 1, pp. 1–26, 2008.

[23] D. L. Diamond, A. J. Syder, J. M. Jacobs et al., "Temporal proteome and lipidome profiles reveal hepatitis C virus-associated reprogramming of hepatocellular metabolism and bioenergetics," *PLoS Pathogens*, vol. 6, no. 1, article e1000719, 2010.

[24] H. J. Forman and D. A. Dickinson, "Oxidative signaling and glutathione synthesis," *BioFactors*, vol. 17, no. 1-4, pp. 1–12, 2003.

[25] D. Burdette, M. Olivarez, and G. Waris, "Activation of transcription factor Nrf2 by hepatitis C virus induces the

cell-survival pathway," *The Journal of General Virology*, vol. 91, no. 3, pp. 681–690, 2010.

[26] M. Carvajal-Yepes, K. Himmelsbach, S. Schaedler et al., "Hepatitis C virus impairs the induction of cytoprotective Nrf2 target genes by delocalization of small Maf proteins," *The Journal of Biological Chemistry*, vol. 286, no. 11, pp. 8941–8951, 2011.

[27] B. Roe, E. Kensicki, R. Mohney, and W. W. Hall, "Metabolomic profile of hepatitis C virus-infected hepatocytes," *PLoS One*, vol. 6, no. 8, article e23641, 2011.

[28] M. S. Farias, P. Budni, C. M. Ribeiro et al., "Antioxidant supplementation attenuates oxidative stress in chronic hepatitis C patients," *Gastroenterología y Hepatología*, vol. 35, no. 6, pp. 386–394, 2012.

[29] M. H. Khadem Ansari, M. D. Omrani, and F. Kheradmand, "Oxidative stress response in patients infected by diverse hepatitis C virus genotypes," *Hepatitis Monthly*, vol. 15, no. 2, article e22069, 2015.

[30] R. Medvedev, D. Ploen, C. Spengler et al., "HCV-induced oxidative stress by inhibition of Nrf2 triggers autophagy and favors release of viral particles," *Free Radical Biology & Medicine*, vol. 110, pp. 300–315, 2017.

[31] K. J. Blight, J. A. McKeating, and C. M. Rice, "Highly permissive cell lines for subgenomic and genomic hepatitis C virus RNA replication," *Journal of Virology*, vol. 76, no. 24, pp. 13001–13014, 2002.

[32] B. D. Lindenbach, M. J. Evans, A. J. Syder et al., "Complete replication of hepatitis C virus in cell culture," *Science*, vol. 309, no. 5734, pp. 623–626, 2005.

[33] L. J. Reed and H. Muench, "A simple method of estimating fifty per cent endpoints," *American Journal of Epidemiology*, vol. 27, no. 3, pp. 493–497, 1938.

[34] J. Choi, N. L. B. Corder, B. Koduru, and Y. Wang, "Oxidative stress and hepatic Nox proteins in chronic hepatitis C and hepatocellular carcinoma," *Free Radical Biology & Medicine*, vol. 72, pp. 267–284, 2014.

[35] A. Ruggieri, S. Anticoli, L. Nencioni, R. Sgarbanti, E. Garaci, and A. Palamara, "Interplay between hepatitis C virus and redox cell signaling," *International Journal of Molecular Sciences*, vol. 14, no. 3, pp. 4705–4721, 2013.

[36] H. E. Boudreau, S. U. Emerson, A. Korzeniowska, M. A. Jendrysik, and T. L. Leto, "Hepatitis C virus (HCV) proteins induce NADPH oxidase 4 expression in a transforming growth factor β-dependent manner: a new contributor to HCV-induced oxidative stress," *Journal of Virology*, vol. 83, no. 24, pp. 12934–12946, 2009.

[37] A. Meister and M. E. Anderson, "Glutathione," *Annual Review of Biochemistry*, vol. 52, no. 1, pp. 711–760, 1983.

[38] A. Meister and S. S. Tate, "Glutathione and related γ-glutamyl compounds: biosynthesis and utilization," *Annual Review of Biochemistry*, vol. 45, no. 1, pp. 559–604, 1976.

[39] V. Gandin and A. Fernandes, "Metal- and semimetal-containing inhibitors of thioredoxin reductase as anticancer agents," *Molecules*, vol. 20, no. 7, pp. 12732–12756, 2015.

[40] M. G. Lewis, S. DaFonseca, N. Chomont et al., "Gold drug auranofin restricts the viral reservoir in the monkey AIDS model and induces containment of viral load following ART suspension," *AIDS*, vol. 25, no. 11, pp. 1347–1356, 2011.

[41] J. M. Madeira, S. M. Schindler, and A. Klegeris, "A new look at auranofin, dextromethorphan and rosiglitazone for reduction of glia-mediated inflammation in neurodegenerative diseases," *Neural Regeneration Research*, vol. 10, no. 3, pp. 391–393, 2015.

[42] K. D. Tardif, G. Waris, and A. Siddiqui, "Hepatitis C virus, ER stress, and oxidative stress," *Trends in Microbiology*, vol. 13, no. 4, pp. 159–163, 2005.

[43] K. Moriya, K. Nakagawa, T. Santa et al., "Oxidative stress in the absence of inflammation in a mouse model for hepatitis C virus-associated hepatocarcinogenesis," *Cancer Research*, vol. 61, no. 11, pp. 4365–4370, 2001.

[44] J. Zhong, P. Gastaminza, J. Chung et al., "Persistent hepatitis C virus infection in vitro: coevolution of virus and host," *Journal of Virology*, vol. 80, no. 22, pp. 11082–11093, 2006.

[45] K. Bedard and K. H. Krause, "The NOX family of ROS-generating NADPH oxidases: physiology and pathophysiology," *Physiological Reviews*, vol. 87, no. 1, pp. 245–313, 2007.

[46] T. Luangmonkong, S. Suriguga, H. A. M. Mutsaers, G. M. M. Groothuis, P. Olinga, and M. Boersema, "Targeting oxidative stress for the treatment of liver fibrosis," *Reviews of Physiology, Biochemistry and Pharmacology*, vol. 175, pp. 71–102, 2018.

[47] S. Liang, T. Kisseleva, and D. A. Brenner, "The role of NADPH oxidases (NOXs) in liver fibrosis and the activation of myofibroblasts," *Frontiers in Physiology*, vol. 7, p. 17, 2016.

[48] D. Amatore, R. Sgarbanti, K. Aquilano et al., "Influenza virus replication in lung epithelial cells depends on redox-sensitive pathways activated by NOX4-derived ROS," *Cellular Microbiology*, vol. 17, no. 1, pp. 131–145, 2015.

[49] R. Vlahos, J. Stambas, S. Bozinovski, B. R. S. Broughton, G. R. Drummond, and S. Selemidis, "Inhibition of Nox2 oxidase activity ameliorates influenza A virus-induced lung inflammation," *PLoS Pathogens*, vol. 7, no. 2, article e1001271, 2011.

[50] I. Celestino, P. Checconi, D. Amatore et al., "Differential redox state contributes to sex disparities in the response to influenza virus infection in male and female mice," *Frontiers in Immunology*, vol. 9, p. 1747, 2018.

[51] T. Wang and S. A. Weinman, "Interactions between hepatitis C virus and mitochondria: impact on pathogenesis and innate immunity," *Current Pathobiology Reports*, vol. 1, no. 3, pp. 179–187, 2013.

[52] M. V. García-Mediavilla, S. Sánchez-Campos, P. González-Pérez et al., "Differential contribution of hepatitis C virus NS5A and core proteins to the induction of oxidative and nitrosative stress in human hepatocyte-derived cells," *Journal of Hepatology*, vol. 43, no. 4, pp. 606–613, 2005.

[53] K. Machida, K. T.-H. Cheng, C.-K. Lai, K.-S. Jeng, V. M.-H. Sung, and M. M. C. Lai, "Hepatitis C virus triggers mitochondrial permeability transition with production of reactive oxygen species, leading to DNA damage and STAT3 activation," *Journal of Virology*, vol. 80, no. 14, pp. 7199–7207, 2006.

[54] L. C. Robinson and J. S. Marchant, "Enhanced Ca2+ leak from ER Ca2+ stores induced by hepatitis C NS5A protein," *Biochemical and Biophysical Research Communications*, vol. 368, no. 3, pp. 593–599, 2008.

[55] M. Valko, D. Leibfritz, J. Moncol, M. T. D. Cronin, M. Mazur, and J. Telser, "Free radicals and antioxidants in normal physiological functions and human disease," *The International Journal of Biochemistry & Cell Biology*, vol. 39, no. 1, pp. 44–84, 2007.

[56] M. Marí, A. Morales, A. Colell, C. García-Ruiz, and J. C. Fernández-Checa, "Mitochondrial glutathione, a key survival

antioxidant," *Antioxidants & Redox Signaling*, vol. 11, no. 11, pp. 2685–2700, 2009.

[57] C. Espinosa-Diez, V. Miguel, D. Mennerich et al., "Antioxidant responses and cellular adjustments to oxidative stress," *Redox Biology*, vol. 6, pp. 183–197, 2015.

[58] L. Nencioni, R. Sgarbanti, D. Amatore et al., "Intracellular redox signaling as therapeutic target for novel antiviral strategy," *Current Pharmaceutical Design*, vol. 17, no. 35, pp. 3898–3904, 2011.

[59] R. C. Gullberg, J. Jordan Steel, S. L. Moon, E. Soltani, and B. J. Geiss, "Oxidative stress influences positive strand RNA virus genome synthesis and capping," *Virology*, vol. 475, pp. 219–229, 2015.

[60] Y.-. H. Wu, C.-P. Tseng, M.-L. Cheng, H.-Y. Ho, S.-R. Shih, and D. T.-Y. Chiu, "Glucose-6-phosphate dehydrogenase deficiency enhances human coronavirus 229E infection," *The Journal of Infectious Diseases*, vol. 197, no. 6, pp. 812–816, 2008.

[61] S. Vomund, A. Schäfer, M. Parnham, B. Brüne, and A. von Knethen, "Nrf2, the master regulator of anti-oxidative responses," *International Journal of Molecular Sciences*, vol. 18, no. 12, p. 2772, 2017.

[62] K. Sugiyama, H. Ebinuma, N. Nakamoto et al., "Prominent steatosis with hypermetabolism of the cell line permissive for years of infection with hepatitis C virus," *PLoS One*, vol. 9, no. 4, article e94460, 2014.

[63] S. A. Lozano-Sepulveda, O. L. Bryan-Marrugo, C. Cordova-Fletes, M. C. Gutierrez-Ruiz, and A. M. Rivas-Estilla, "Oxidative stress modulation in hepatitis C virus infected cells," *World Journal of Hepatology*, vol. 7, no. 29, pp. 2880–2889, 2015.

[64] K. Groenbaek, H. Friis, M. Hansen, H. Ring-Larsen, and H. B. Krarup, "The effect of antioxidant supplementation on hepatitis C viral load, transaminases and oxidative status: a randomized trial among chronic hepatitis C virus-infected patients," *European Journal of Gastroenterology & Hepatology*, vol. 18, no. 9, pp. 985–989, 2006.

[65] J. Vermehren, J. S. Park, I. M. Jacobson, and S. Zeuzem, "Challenges and perspectives of direct antivirals for the treatment of hepatitis C virus infection," *Journal of Hepatology*, vol. 69, no. 5, pp. 1178–1187, 2018.

[66] S. Bagaglio, C. Uberti-Foppa, and G. Morsica, "Resistance mechanisms in hepatitis C virus: implications for direct-acting antiviral use," *Drugs*, vol. 77, no. 10, pp. 1043–1055, 2017.

Hindawi
Oxidative Medicine and Cellular Longevity
Volume 2019, Article ID 6026902, 12 pages
https://doi.org/10.1155/2019/6026902

Research Article

Isolated Silymarin Flavonoids Increase Systemic and Hepatic Bilirubin Concentrations and Lower Lipoperoxidation in Mice

Jakub Šuk,[1] Jana Jašprová,[1] David Biedermann,[2] Lucie Petrásková,[2] Kateřina Valentová,[2] Vladimír Křen,[2] Lucie Muchová,[1] and Libor Vítek[1,3]

[1]*Institute of Medical Biochemistry and Laboratory Diagnostics, 1st Faculty of Medicine, Charles University, Kateřinská 32, Praha 2 12000, Czech Republic*
[2]*Laboratory of Biotransformation, Institute of Microbiology of the Czech Academy of Sciences, Vídeňská 1082, Praha 4 14000, Czech Republic*
[3]*4th Department of Internal Medicine, 1st Faculty of Medicine, Charles University, Kateřinská 32, Praha 2 12000, Czech Republic*

Correspondence should be addressed to Libor Vítek; vitek@cesnet.cz

Received 20 July 2018; Revised 25 October 2018; Accepted 25 November 2018; Published 12 February 2019

Guest Editor: Luciano Saso

Bilirubin is considered to be one of the most potent endogenous antioxidants in humans. Its serum concentrations are predominantly affected by the activity of hepatic bilirubin UDP-glucuronosyl transferase (UGT1A1). Our objective was to analyze the potential bilirubin-modulating effects of natural polyphenols from milk thistle (*Silybum marianum*), a hepatoprotective herb. Human hepatoblastoma HepG2 cells were exposed to major polyphenolic compounds isolated from milk thistle. Based on *in vitro* studies, 2,3-dehydrosilybins A and B were selected as the most efficient compounds and applied either intraperitoneally or orally for seven days to C57BL/6 mice. After, *UGT1A1* mRNA expression, serum, intrahepatic bilirubin concentrations, and lipoperoxidation in the liver tissue were analyzed. All natural polyphenols used increased intracellular concentration of bilirubin in HepG2 cells to a similar extent as atazanavir, a known bilirubinemia-enhancing agent. Intraperitoneal application of 2,3-dehydrosilybins A and B (the most efficient flavonoids from *in vitro* studies) to mice (50 mg/kg) led to a significant downregulation of *UGT1A1* mRNA expression ($46 \pm 3\%$ of controls, $p < 0.005$) in the liver and also to a significant increase of the intracellular bilirubin concentration (0.98 ± 0.03 *vs.* 1.21 ± 0.02 nmol/mg, $p < 0.05$). Simultaneously, a significant decrease of lipoperoxidation ($61 \pm 2\%$ of controls, $p < 0.005$) was detected in the liver tissue of treated animals, and similar results were also observed after oral treatment. Importantly, both application routes also led to a significant elevation of serum bilirubin concentrations ($125 \pm 3\%$ and $160 \pm 22\%$ of the controls after intraperitoneal and oral administration, respectively, $p < 0.005$ in both cases). In conclusion, polyphenolic compounds contained in silymarin, in particular 2,3-dehydrosilybins A and B, affect hepatic and serum bilirubin concentrations, as well as lipoperoxidation in the liver. This phenomenon might contribute to the hepatoprotective effects of silymarin.

1. Introduction

Bilirubin, the end product of heme catabolism in the systemic circulation, is a potent antioxidant substance [1]. Despite the fact that for decades bilirubin has been considered a toxic catabolic waste product and an ominous sign of liver dysfunction, its role as a powerful protective molecule has increasingly been recognized [2]. *In vitro* and *in vivo* studies have shown that bilirubin may suppress the oxidation of lipids [1] and has anti-inflammatory [3], antiproliferative [4], antigenotoxic [5], antimutagenic [6], or even anti-aging properties [7]. Interestingly, bilirubin has been reported as a potent peroxisome proliferator-activated receptor-α (PPARα) agonist, thus acting as a real endocrine molecule, with all potential clinical consequences [8]. The clinical evidence is even more important. Bilirubin, when only mildly elevated, has been demonstrated to protect from a wide array of oxidative stress-related diseases, including cardiovascular diseases, certain cancers, and autoimmune or neurodegenerative diseases [2, 9]. In fact, substantial protective effects of

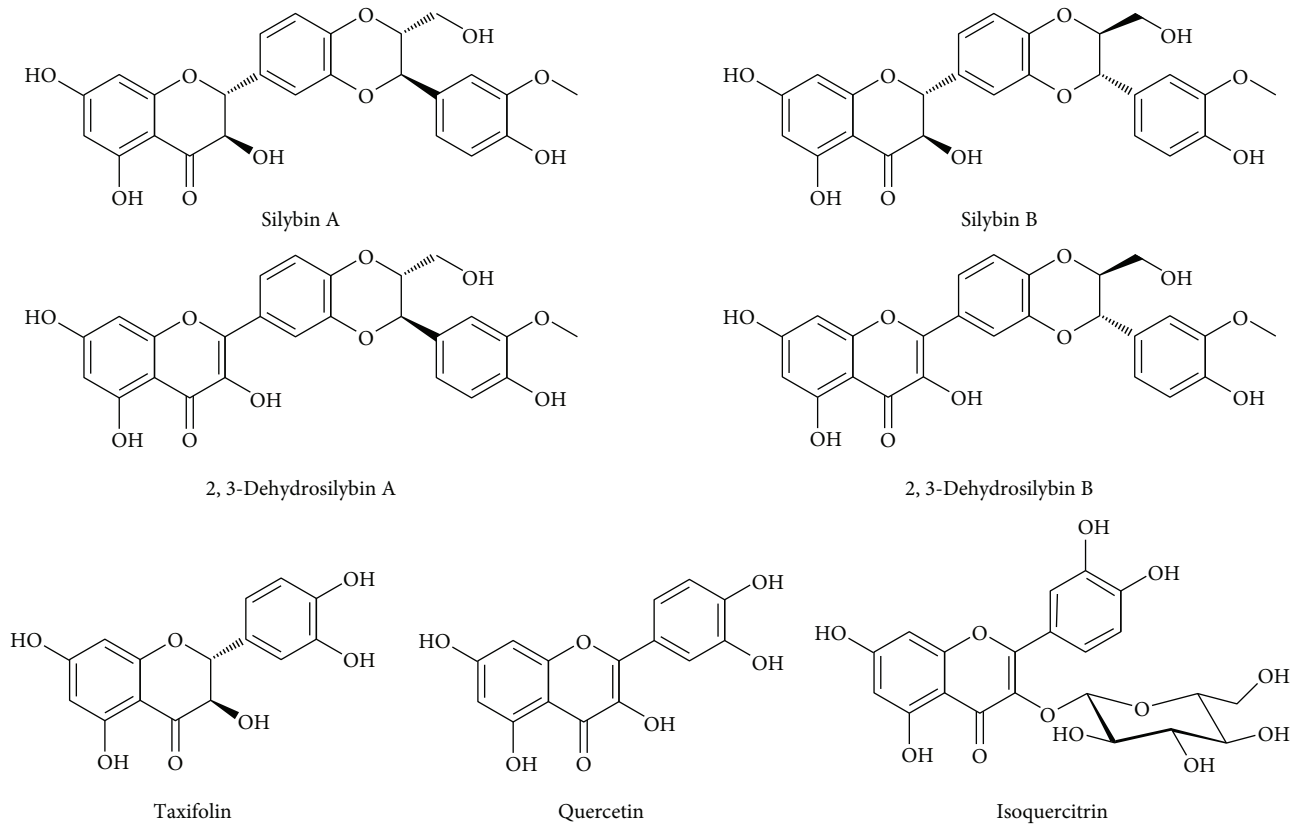

Figure 1: Structures of flavonolignans of the silymarin complex and related flavonols.

mild unconjugated hyperbilirubinemia, as seen in subjects with Gilbert syndrome (benign hyperbilirubinemia), have been reported for atherosclerotic diseases in particular [10].

Bilirubin production is dependent on heme oxygenase (HMOX) activity, but systemic bilirubin concentrations are predominantly affected by hepatic bilirubin UDP-glucuronosyl transferase (UGT1A1), its biotransforming enzyme [11]. Partial inhibition of bilirubin glucuronosylation was proposed as a wise strategy used to induce "iatrogenic" Gilbert syndrome [12]. This indeed was demonstrated as a "side effect" of several drugs used in various indications, typically for atazanavir, whose administration is often associated with mildly elevated concentrations of unconjugated bilirubin. Surprisingly, hyperbilirubinemia induced by atazanavir was reported to decrease markers of oxidative stress [13] and cardiometabolic risk factors [14], as well as endothelial functions [15], but safer approaches are certainly needed.

Since xenobiotics used in clinical medicine are often associated with potentially severe side effects, natural compounds interfering with the UGT1A1 hepatic biotransformation system seem a better strategy to induce mild hyperbilirubinemia. Based on the scarce data reported in the literature (mainly as the result of investigating potential nutraceuticals/herb-drug interactions), it seems that flavonoids from silymarin might modulate this enzyme. This assumption is based on the fact that many herbal extracts including silymarin, a seed extract of milk thistle (*Silybum marianum* (L.) Gaertn.), are rich in phenolic phytochemicals that are substrates for UGT1A1 or even exhibit UGT1A1-inhibiting activities [16–18]. Indeed, therapy for prostate cancer patients with high doses of silybin (silibinin) has been associated with unconjugated hyperbilirubinemia, which was considered by the authors as an adverse effect of such treatment [19]. Similar findings were also reported in hepatitis C patients receiving silybin therapy [20–23]. Although most of the experimental reports as well as some clinical data suggest its beneficial role, silymarin is generally considered to have a negligible importance clinically [24]. There are many possible reasons: one of them being the poorly defined content of the active ingredients and also the improperly characterized biological properties of individual pure flavonoids in the silymarin complex [25, 26]. Silymarin is a mixture of 5 major flavonolignans (silybins A and B, isosilybin A, silychristin A, and silydianin) plus their precursor taxifolin, as well as other minor polyphenolic compounds (Figure 1) [27]. Among them, the 2,3-dehydroflavonolignans such as 2,3-dehydrosilybins A and B possess potent biological activities [28–32].

Thus, the aim of our study was to investigate the potential bilirubin-modulating effects of natural polyphenols present in milk thistle and related compounds.

2. Materials and Methods

2.1. Chemicals. Silymarin (containing 13.0% of silybin A, 17.9% silybin B, 14.7% silychristin A, 9.3% silychristin B +silydianin, 8.9% isosilybin A, 6.8% isosilybin B, 3.0%

taxifolin, 1.9% 2,3-dehydrosilybin, 0.5% 2,3-dehydrosilychristin, 6.5% of other nonidentified 2,3-dehydroflavonolignans, plus 17.5% of yet other substances (probably polymers, for details of the analysis, see the Supplementary Data and Supplementary Figures 1–3), silybin AB (approximately an equimolar mixture of silybin A and silybin B), quercetin, and rutin (quercetin-3-*O*-β-rutinoside)) was all purchased from Sigma-Aldrich (St. Louis, MO, USA); atazanavir was obtained from Santa Cruz (Santa Cruz Biotechnology, Dallas, TX, USA). Silybin A and silybin B were isolated from silymarin (purchased from Liaoning Senrong Pharmaceutical, Panjin, China; batch no. 120501), as described in [33]. 2,3-Dehydrosilybin, 2,3-dehydrosilybin A, and 2,3-dehydrosilybin B were prepared by oxidation of silybin, silybin A, and silybin B, respectively [34]. Taxifolin hydrate (92%) was purchased from Amagro (Prague, CZ), and isoquercitrin (quercetin-3-*O*-glucoside, 97%) was prepared from rutin (Sigma-Aldrich) using thermophilic α-L-rhamnosidase from *Aspergillus terreus* heterologously expressed in *Pichia pastoris* [35]. The deconjugation enzymes β-glucuronidase and sulfatase from *Helix pomatia* were obtained from Sigma-Aldrich.

2.2. Cell Cultures. The HepG2 human hepatoblastoma cell line was used for the *in vitro* studies (ATCC, Manassas, VA, USA). Cells were cultured in MEM Eagle medium, containing 10% of fetal bovine serum, in 75 cm^2 culture flasks, at 37°C, in a 5% CO_2 atmosphere. For an estimation of the intracellular bilirubin concentration, the cells were plated in 10 cm Petri dishes and treated with natural polyphenols dissolved in DMSO (vehicle; 0.66%, *v*/*v*) for 24 h. For qPCR measurement, the cells were cultured in 24-well plates and treated with natural flavonoids dissolved in DMSO (vehicle; 0.66%, *v*/*v*) for 4 h.

The cell lines were authenticated at ATCC by STR profiling before distribution and also reauthenticated at the end of the study by an external laboratory (Generi Biotech, Hradec Králové, Czech Republic).

2.3. MTT Cytotoxicity Assays. The MTT (3-(4,5-dimethylthiazol-2-yl)-2,5-diphenyltetrazolium bromide) reduction assay in a 96-well format was used for the determination of the cytotoxicity of the compounds tested. HepG2 cells were seeded into a 96-well plate at a density of 1×10^5 cells/well. Following 24 h incubation, the cells were treated for 24 h with natural flavonoids at concentrations of 0.1-200 μM dissolved in DMSO (vehicle; 0.66%, *v*/*v*). MTT assay was measured spectrophotometrically at 540 nm (TECAN, Schoeller Instruments s.r.o., Prague, Czech Republic).

2.4. RNA Isolation and Real-Time PCR. Total mRNA was isolated using a 5 Prime PerfectPure RNA Cultured Cell Kit and a 5 Prime PerfectPure RNA Tissue Kit (Eppendorf, Germany); and cDNA was generated using a High Capacity RNA-to-cDNA Master Mix (Life Technologies, Carlsbad, CA, USA) according to the manufacturer's instructions. qPCR for the cell culture was performed using the SYBR™ Select Master Mix (Life Technologies). For each reaction, the final 20 μL volume was comprised of 10 μL of SYBR Green PCR Mix, 2 μL of each primer (Supplementary Table 1), and 6 μL of a 1/5 dilution of the RT products. qPCR for the liver tissue was performed using a TaqMan® Gene Expression Assay Kit (Life Technologies). Threshold cycle (Ct) values were analyzed using the comparative Ct ($\Delta\Delta$Ct) method as recommended by the manufacturer (Applied Biosystems, Foster City, CA, USA). The data were normalized to the expression of hypoxantin phosphoribosyl transferase (*HPRT*) and expressed as the multiplicity change from the control levels.

2.5. Serum Markers of Liver Damage. Hepatic enzyme (alanine aminotransferase (ALT), aspartate aminotransferase (AST), and alkaline phosphatase (ALP)) activities were determined on an automatic analyzer (Modular Analyzer, Roche Diagnostics GmbH, Germany) using standard assays.

2.6. Determination of Bilirubin. For the determination of bilirubin in HepG2 cells and liver tissue, the biological materials were sonicated on ice and then extracted with methanol/chloroform/hexane 10/5/1 (*v*/*v*/*v*) against PBS buffer (pH 6.2). The lower organic phase was subsequently extracted into 50 μL of carbonate buffer (pH 10) in hexane. The resulting polar droplet was loaded onto a C-8 reverse phase column (Luna 3 μm, 150 × 4.6 mm, Phenomenex, Torrance, CA, USA), and bilirubin was determined using an HPLC Agilent 1200 with a diode array detector (Agilent, Santa Clara, CA, USA) as described earlier [36, 37]. The concentration of bilirubin was calculated in nmol/g of wet tissue or pmol/mg of protein for tissue samples or cell cultures, respectively.

For determination of bilirubin in serum, the LC-MS/MS method was used. Ten μL of serum was mixed with 2.5 μL of internal standard (mesobilirubin, $c = 20$ μmol/L) and deproteinized by 50 μL of 1% BHT in methanol, 50 μL of 0.4% ascorbic acid in methanol, and 200 μL of methanol (pH 11). Five μL of the resulting supernatant was loaded on a Poroshell 120 EC-C18 2.1 μm 3.0 × 50 mm column (Agilent), with a gradient of 1 mM NH_4F in water (A) and methanol (B) as follows: 60% of B was changed in 5 minutes to 100% of B, with a flow rate of 0.4 mL/min and was kept at 100% of B for 3 minutes, with the gradient of flow rate at 0.5 mL/min. The flow was then maintained at 0.5 mL/min until the end of the gradient program. Phase B was changed back to 60% in 0.1 minutes and was kept at 60% until the end of the program at 10 minutes. The mass spectra were recorded on an Agilent 6470 LC/QQQ (Agilent) LC-MS/MS device with electrospray ionization and multiple reaction monitoring in a positive mode. Conditions of the electrospray ionization source, gas flows, and potentials of the mass spectrometer were manually tuned for high sensitivity and a low signal-to-noise ratio of the analytes: ion spray voltage, 3000 V; source temperature, 250°C; heater gas, 8 L/min; nebulizer, 300 psi; sheath gas temperature, 400°C; sheath gas flow, 12 L/min; and nozzle voltage, 500 V. Within the total scan time of 10 min, m/z 585.3 → 299.1, 16 eV collision energy (CE) at 5.96 min was monitored for bilirubin and m/z 589.3 → 301.2, 20 eV CE at 6.084 min for mesobilirubin.

2.7. HMOX Activity Assay. Twenty μL of liver sonicate (10%) was incubated for 15 min at 37°C in CO-free septum-sealed vials containing 20 μL of 150 μM heme and 20 μL of 4.5 mM NADPH, as previously described [38]. Blank reaction vials contained potassium phosphate buffer in place of NADPH. The amount of CO generated by the reaction and released into the vial headspace was quantified by gas chromatography (GC) with a reduction gas analyzer (Peak Laboratories, Mountain View, CA, USA). HMOX activity was calculated as pmol CO/h/mg fresh weight and expressed as percentage of the control.

2.8. UGT1A1 Inhibition Assay. The UGT activity in the microsomal samples was determined by a UGT-Glo™ assay kit according to the manufacturer's instructions (Promega, Madison, WI, USA). Briefly, microsomes with recombinant UGT1A1 (0.0125 mg/mL) were incubated with 16 mM UDPGA and 20 μM multienzyme substrate with increasing concentrations of 2,3-dehydrosilybins A and B at 37°C for 30 min. Then, 40 μL of reconstituted luciferin detection reagent containing D-cysteine was added, and the luminescent signal was allowed to stabilize for 20 min at room temperature. Luminescence was read on a Synergy II plate reader (BioTek, VT, USA). The data were analyzed using the curve fitting method with GraphPad Prism (GraphPad Software, San Diego, CA).

2.9. Malondialdehyde Determination. Malondialdehyde (MDA) in the tissue homogenates was measured according to the method described by Wills [39], with some modifications. A 200 μL aliquot of 10% tissue homogenate was mixed with 2 mL of the thiobarbituric acid-trichloroacetic acid reagent (0.375 and 15%, respectively). The mixture was heated on a water bath at 95°C for 20 min. The solution was then cooled to room temperature. The reaction product (thiobarbituric acid-MDA complex) was extracted by adding 3 mL of *n*-butanol to the above solution. The absorbance of the pink-colored extract in *n*-butanol was measured at 532 nm using a spectrophotometer (Sunrise, Tecan, USA). The amount of MDA was calculated using the molar extinction coefficient of $1.56 \times 10^5\ M^{-1} \times cm^{-1}$ and expressed as a percentage of the control.

2.10. 2,3-Dehydrosilybin Determination in Sera. 2,3-Dehydrosilybin concentrations in serum samples were determined after deconjugation of phase II conjugates (sulfates and glucuronide). The activity of the deconjugation enzymes (β-glucuronidase and sulfatase) was checked on the selected glucuronides and sulfates prior to analysis. All the samples were measured in duplicate.

The conjugates in serum samples were deconjugated in acetate buffer (50 mM, pH 5.0) by adding β-glucuronidase (440 U) with sulfatase (35 U), incubated for 2 h at 37°C and 600 rpm. The reaction mixture was then freeze-dried, and an internal standard (2,3-dehydrosilychristin, 4.8 μg/mL, 150 μL, in acetonitrile/DMSO 1 : 1) was added. Samples were incubated (1 h, 37°C, 600 rpm) and centrifuged (15 min), and the supernatant was injected into a LC-MS (injection volume 25 μL).

2.10.1. LC-MS Conditions. LC-MS chromatograms and mass spectra were obtained using the Shimadzu Prominence system consisting of a DGU-20A3 mobile phase degasser, two LC-20AD solvent delivery units, a SIL-20AC cooling autosampler, a CTO-10AS column oven with the SPD-M20A diode array detector, plus a LCMS-2020 mass detector with a single quadrupole, equipped with an electrospray ion source (Shimadzu, Kyoto, Japan).

The LC-MS of the serum samples and standard solutions of 2,3-dehydrosilybin were measured on a Chromolith RP-18e (100 × 3 mm) column (Merck) and Chromolith RP-18e (5 × 4.6 mm) precolumn (Merck) (mobile phase: A = 5% acetonitrile, 0.1% HCOOH; B = 80% acetonitrile, 0.1% HCOOH; gradient: 0 min 20% B, 5 min 90% B, 6 min 90% B, and 8-10 min 20% B; flow rate: 0.4 mL/min, 25°C). The concentration of 2,3-dehydrosilybin in the serum was calculated using a calibration curve. The MS parameters were as follows: ESI interface voltage, 4.5 kV; detector voltage, 1.15 kV; nebulizing gas flow, 1.5 mL·min^{-1}; drying gas flow, 15 mL·min^{-1}; heat block temperature, 200°C; DL temperature, 250°C; negative scan mode, 478.8-481.0 *m*/*z*; and software, LabSolutions ver. 5.75 SP2 (Shimadzu, Kyoto, Japan).

2.11. Animal Studies. Female C57BL/6 mice (n = at least 6 in each group, 8 w old) obtained from Velaz (Prague, Czech Republic) had access to both water and a standard diet *ad libitum*. An equimolar mixture of dehydrosilybins A and B dissolved in DMSO (vehicle; 5%, *v*/*v*) was applied intraperitoneally, and individual dehydrosilybins were applied orally for seven days at a dose of 50 mg/kg b.wt. After 24 h of the last application, the mice were sacrificed and blood from their *superior vena cava* was collected for further analyses. The livers were cleaned and stored as pieces in nitrogen until used. For RNA analysis, 100 mg of each tissue was immediately placed in 1.5 mL microfuge tubes containing RNAlater and stored following the manufacturer's protocol until the RNA isolation was performed.

All animal studies met the criteria for the care and use of animals in experiments and were approved by the Animal Research Committee of the 1st Faculty of Medicine, Charles University, Prague.

2.12. Statistical Analyses. All data are expressed as mean ± SEM. Depending on their normality, the data were analyzed either by the Student t-test or the Mann–Whitney rank sum test and Kruskal-Wallis ANOVA with Dunn's correction. Differences were considered statistically significant when P values were less than 0.05.

3. Results

3.1. The Effect of Silymarin Flavonoids and Related Compounds on HMOX and UGT1A1 Expressions and Activities in HepG2 Cells. In our *in vitro* screening studies, focused on evaluation of the possible modulating effect of silymarin flavonoids and related compounds on *HMOX1* and *UGT1A1* expressions, a wide array of compounds were used (Figure 1). Based on the MTT assays (Table 1), *HMOX1* and *UGT1A* mRNA expression analyses were performed

Table 1: Inhibitory concentrations of individual silymarin flavonoids and related compounds.

Compound	IC_{50} (μM)
Silybin A	>200
Silybin B	>200
Silybin AB	>200
Isosilybin A	148 ± 3
Isosilybin B	185 ± 4
2,3-Dehydrosilybin A	>200
2,3-Dehydrosilybin B	>200
Silychristin	>200
2,3-Dehydrosilychristin	>200
Silydianin	>200
2,3-Dehydrosilydianin	>200
Isoquercitrin	115 ± 4
Quercetin	105 ± 3
Taxifolin	>200

HepG2 cells were treated for 24 h with natural flavonoids in concentrations of 0.1-200 μM. IC: inhibitory concentration, measured by the MTT test.

with the nontoxic plus 1/2 of nontoxic concentrations for HepG2 cells.

Significant *HMOX1* mRNA overexpression was observed for quercetin and isoquercitrin; on the other hand, *HMOX1* mRNA downregulation was present after exposure to 2,3-dehydrosilybins A and B (Figure 2). More importantly, the activity of HMOX was upregulated not only by quercetin and isoquercitrin but also after exposure to the silymarin complex *per se*, as well as silybins A and B. Downregulation of *HMOX1* mRNA expression by 2,3-dehydrosilybins A and B (Figure 2) was also reflected by decreased HMOX activity (Figure 3(a)).

Significant underexpression of *UGT1A1* mRNA was noted after exposure of HepG2 cells to the equimolar mixture of silybins A and B, to quercetin, isoquercitrin, taxifolin, and 2,3-dehydrosilybins A and B (Figure 2). These results were reflected by the inhibition of UGT1A1 activity, as determined for 2,3-dehydrosilybins A and B (IC_{50} values of 2.1 ± 0.2 and 4.1 ± 0.2 μmol/L, respectively; Figure 3(b)).

3.2. The Effect of Silymarin Flavonoids and Related Compounds on Intracellular Concentrations of Bilirubin in HepG2 Cells. To investigate whether the effects of silymarin flavonoids and related compounds on HMOX and UGT1A1 are translated into phenotypic changes, we analyzed bilirubin concentrations within the HepG2 cells after 24 h exposure to individual compounds.

Most of silymarin flavonoids and related compounds significantly elevated intracellular bilirubin (Figure 4) in a dose-dependent manner (data not shown). Interestingly, the increase of intracellular bilirubin concentrations caused by exposure of both 2,3-dehydrosilybins A and B was even higher than that caused by atazanavir, a known inhibitor of UGT1A1 [40] (Figure 4).

Based on these *in vitro* results, 2,3-dehydrosilybins A and B were selected for the *in vivo* studies.

3.3. The Effect of 2,3-Dehydrosilybins A and B on Bilirubin Metabolism in Mice

3.3.1. Concentrations of 2,3-Dehydrosilybins in Sera. Since 2,3-dehydrosilybins have a low solubility in water and the poor oral bioavailability might contribute to the low clinical efficiency of silymarin in humans, we first measured concentrations of 2,3-dehydrosilybins in sera to verify whether they pass into the systemic circulation. Use of both application routes (*i.e.*, intraperitoneal as well as oral administration of 2,3-dehydrosilybins (50 mg/kg b.wt.)), after 24 h, resulted in a substantial appearance in the systemic blood, reaching serum concentrations up to 300 ng/mL (0.62 μmol/L) (Figure 5).

3.3.2. Hepatic HMOX1 and UGT1A1 mRNA Expressions. Then we analyzed the effect of 2,3-dehydrosilybin administration on *HMOX1* and *UGT1A1* mRNA expressions in the livers of treated mice. Treatment with an equimolar mixture of 2,3-dehydrosilybins A and B (50 mg/kg b.wt.) administered intraperitoneally for 7 days led to a significant downregulation of *UGT1A1* mRNA expression in the liver (57 ± 19% of the controls) with no change in *HMOX1* expression (Figure 6(a)). Similar results were observed for oral treatment with 2,3-dehydrosilybin A (downregulation of *UGT1A1* mRNA expression to 55 ± 26% of the control, Figure 6(b)); while no effect was demonstrated for 2,3-dehydrosilybin B. None of the individual dehydrosilybins had any effect on *HMOX1* expression (Figure 6(b)).

3.3.3. Intracellular and Systemic Bilirubin Concentrations. Intraperitoneal application of 2,3-dehydrosilybins A and B mixture significantly increased intracellular concentrations of bilirubin in the liver tissue (to 149 ± 24%, $p < 0.05$, Figure 6(c)). An even higher increase was observed after oral treatment of 2,3-dehydrosilybin A (to 236 ± 28%, $p < 0.05$; Figure 6(d)), whereas treatment with 2,3-dehydrosilybin B only led to a moderate but not significant elevation (Figure 6(d)).

Neither intraperitoneal nor oral administration of 2,3-dehydrosilybins caused any increase in markers of liver damage (ALT, AST, and ALP activities; data not shown).

Consistent with the results of intrahepatic bilirubin concentrations, intraperitoneal administration of the 2,3-dehydrosilybins A and B mixture also significantly elevated serum bilirubin concentrations (by 27%; 0.96 ± 0.09 vs. 1.22 ± 0.35 μM; Figure 6(e)). Even a more pronounced elevation of serum bilirubin concentrations was observed after oral treatment with 2,3-dehydrosilybin A (by 44%; 0.96 ± 0.18 vs. 1.38 ± 0.29 μM; Figure 6(f)). Treatment with 2,3-dehydrosilybin B did not cause any changes in serum bilirubin concentrations (Figure 6(f)).

3.3.4. Hepatic Lipoperoxidation. Treatment of mice with 2,3-dehydrosilybins had consistent inhibitory effects on lipid peroxidation in the liver tissue. MDA concentrations in the liver tissue were significantly reduced after intraperitoneal

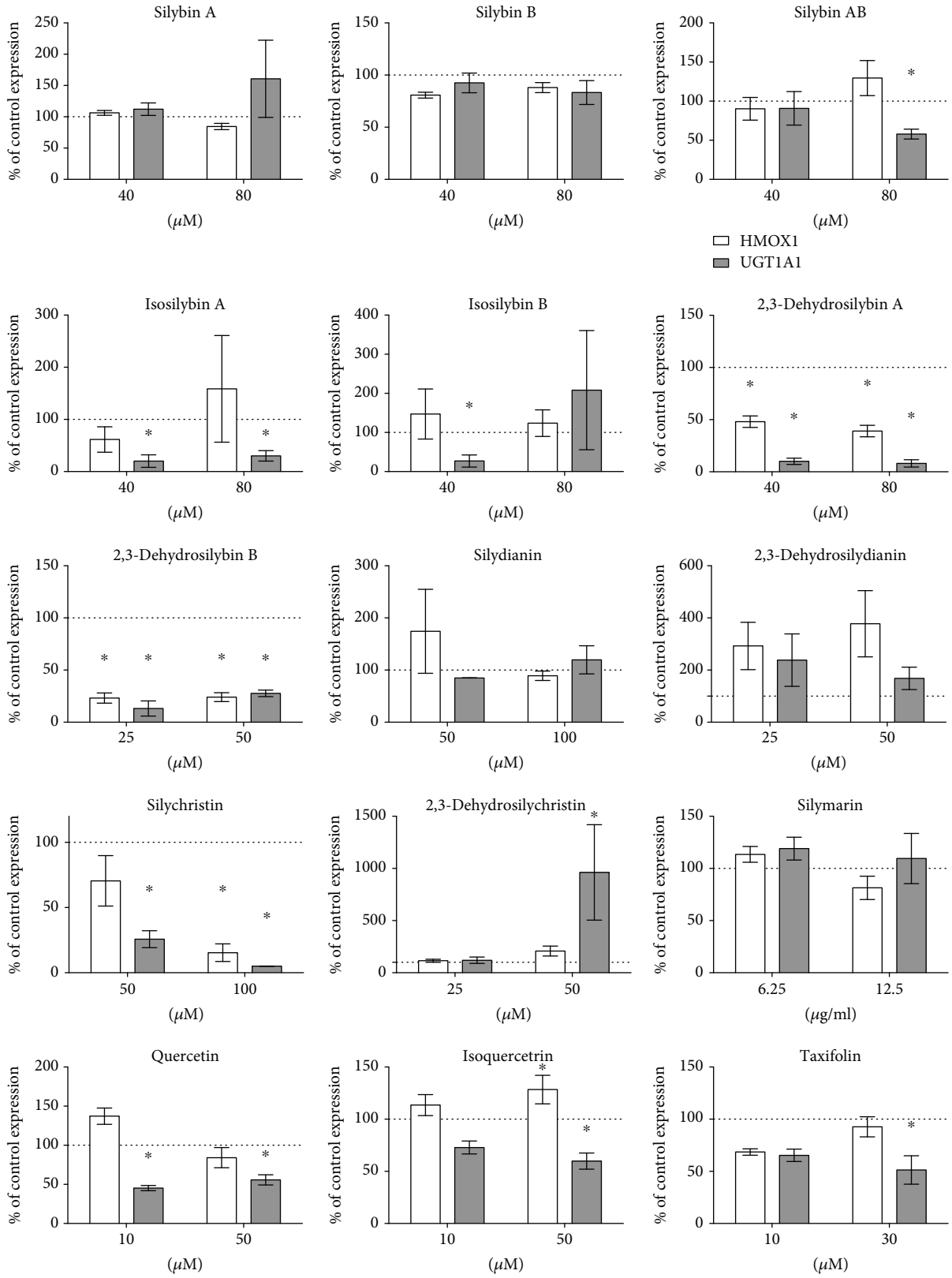

Figure 2: The effect of silymarin flavonoids and related compounds on *HMOX1* and *UGT1A1* expressions in HepG2 cells. mRNA expressions were analyzed after 4 h exposure of HepG2 cells to individual flavonolignans (in corresponding nontoxic concentrations). Data are expressed as percentage of control values. $^{*}P < 0.05$.

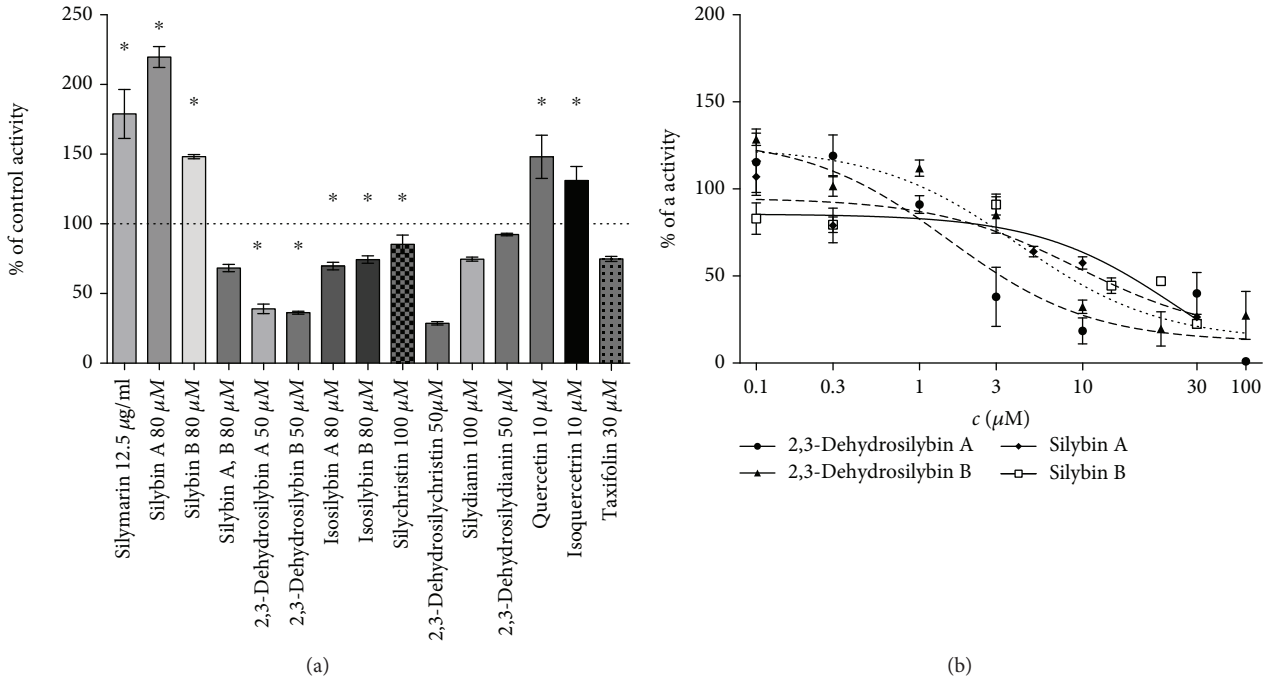

Figure 3: The effect of silymarin flavonoids and related compounds on (a) HMOX and (b) UGT1A1 activities in HepG2 cells. HMOX and UGT1A1 activities were analyzed after 24 h exposure of HepG2 cells to individual flavonolignans. HMOX activity was calculated as pmol CO/h/mg fresh weight and expressed as a percentage of the control values. UGT1A1 enzyme activity was based on relative light unit values and expressed as a percentage of the remaining activity. $^{*}P < 0.05$.

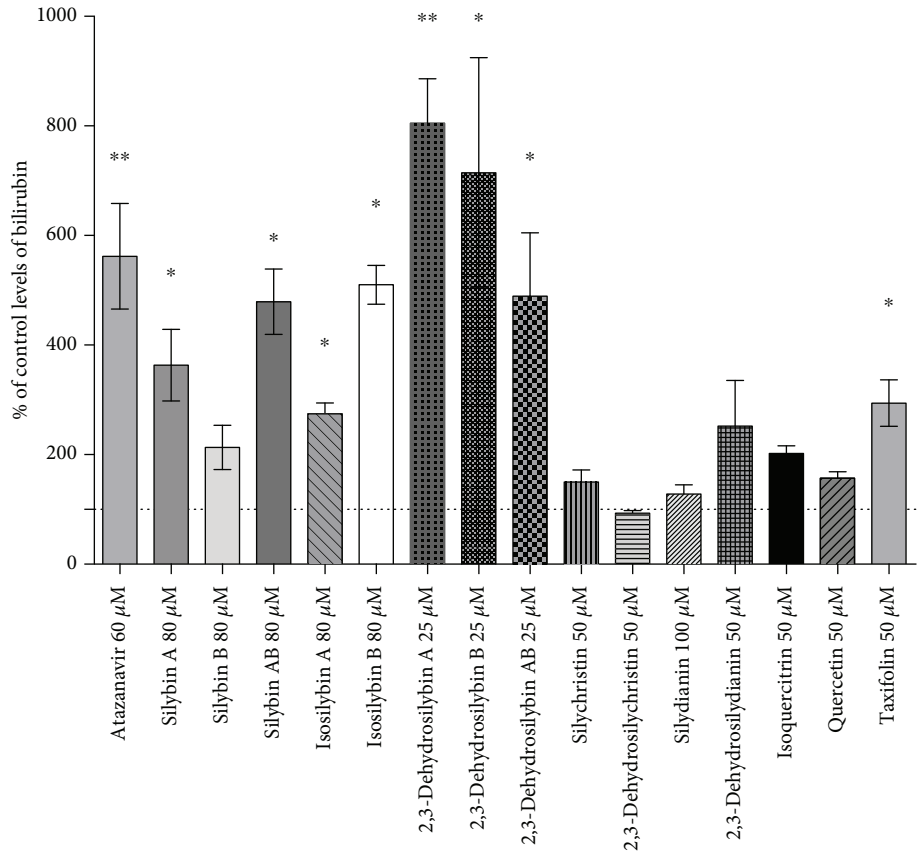

Figure 4: The effect of silymarin flavonoids and related compounds on intracellular concentrations of bilirubin in HepG2 cells. Control values are expressed as 100% and correspond to 2 pmol of bilirubin per mg of protein. $^{*}P < 0.05$; $^{**}P < 0.005$.

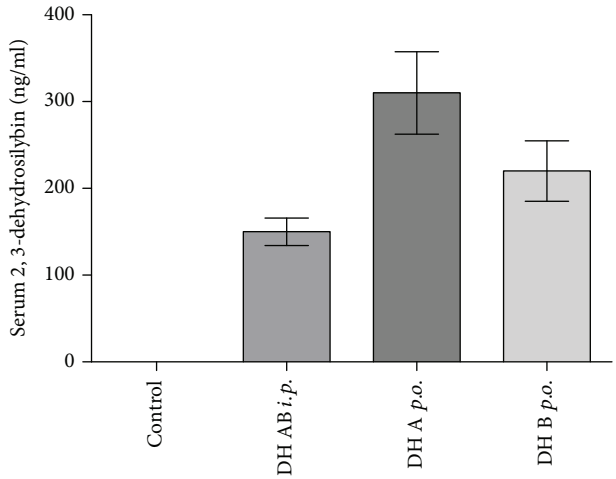

Figure 5: Serum concentrations of 2,3-dehydrosilybins after intraperitoneal and oral administration. 2,3-Dehydrosilybins (DH) were administered at a dose of 50 mg/kg b.wt. *i.p.*: intraperitoneal; *p.o.*: oral; b.wt.: body weight.

application of the mixture of 2,3-dehydrosilybins (to 70 ± 7% of the control; Figure 7(a)), and the same effect was also observed after oral administration of both 2,3-dehydrosilybins A and B (61 ± 15% and 64 ± 13% of the control, respectively; Figure 7(b)).

4. Discussion

Bilirubin, a bile pigment, for decades considered only an ominous sign of liver diseases, has been revisited as a potent antioxidant, immunosuppressive, and cytoprotective agent [2, 9, 10, 41]. Even single micromolar elevations of systemic concentrations of bilirubin, still within the physiological range, are associated with a substantial decreases of the risks of cardiovascular, cancer, and inflammatory diseases [42–44], and this association is clearly evident in subjects with Gilbert syndrome, characterized with mild systemic elevations of unconjugated bilirubin [9, 45]. This led to the suggestion to induce Gilbert syndrome iatrogenically in order to suppress the development of oxidative stress-related diseases [12].

As reported in our recent study, due to a dynamic equilibrium, a correlation between systemic and intracellular concentrations of bilirubin exists in the liver (and also probably in other organs and tissues) [37]. Thus, it is important to monitor intrahepatic concentrations of bilirubin when assessing potential hepatoprotective effects, in particular when considering the fact that hepatic UGT1A1 is the major enzyme affecting systemic concentrations of bilirubin [11]. Hepatic UGT1A1 is a biotransforming enzyme important not only for bilirubin but also for a variety of other endogenous substances as well as xenobiotics, including natural agents often used as nutraceuticals, including the flavonolignans and flavonols of the silymarin complex. In fact, inhibitory effects towards UGT1A1 were reported for silybin, a major flavonoid constituent of milk thistle extract [46]; indeed, the therapy with this substance has also been associated with marked unconjugated hyperbilirubinemia [19]. A significant increase in serum bilirubin levels was also reported in other human studies on patients with chronic hepatitis C receiving silybin therapy [20–23]. These clinical data are consistent with our findings, *i.e.*, increased intracellular as well as systemic concentrations of bilirubin upon exposure to silymarin flavonoids. It is important to emphasize that these effects differed substantially among individual flavonoids—dehydrosilybins A and B being the most efficient.

Despite generally low bioavailability of silymarin flavonoids, effective serum concentrations of both 2,3-dehydrosilybins A and B were detected in our study (up to 300 ng/mL (Figure 5), corresponding to concentrations of 0.62 μmol/L). This value entirely fits to the mean peak plasma concentration of silybin, reached after oral administration of a 700 mg dose of silymarin (containing approximately 250 mg of silybin), which was 0.6 μmol/L [46]. Very similar plasma silybin concentrations were reported in another human study (0.4, 1.4, and 4 μmol/L after 360, 720, or 1440 mg of silybin administered daily for 7 days), with corresponding concentrations in the liver tissue [47], as well as in the studies by Barzaghi et al. (silybin plasma levels of 0.38 μmol/L after administration of 240 mg of silybin given daily for 7 consecutive days) [48] and Wen et al. (plasma concentrations of 0.8 μmol/L after oral administration of 600 mg of silymarin) [49].

In addition, silybin was demonstrated to potently inhibit UGT1A1, with the IC_{50} value correlating with the clinically relevant plasma concentrations [46]. Similar inhibitory concentrations were also reported by others for other silymarin flavonoids, although 2,3-dehydrosilybins were not tested in these studies [50]. These data are consistent with our findings, with the UGT1A1 IC_{50} value for 2,3-dehydrosilybin A = 2.1 μmol/L and the mean serum concentration of 0.62 μmol/L. Importantly, we found the UGT1A1 IC_{50} value for 2,3-dehydrosilybin A even lower than that reported for atazanavir (2.3 μmol/L), the well-known hyperbilirubinemia-inducing drug [40] indicating the high bilirubinemia-enhancing potential of this flavonolignan.

Although the UGT1A1 IC_{50} values of 2,3-dehydrosilybin A are slightly higher than those reported for silybin, 2,3-dehydrosilybin A most efficiently increased both the hepatic intracellular and systemic concentrations of bilirubin. The reason for this might be that 2,3-dehydrosilybin A also affects other mechanisms implicated in hepatic bilirubin metabolism. Such an example may include the modulation of the basolateral bilirubin organic anion-transporting proteins OATP1B1/3, which are also inhibited by silymarin flavonoids [51].

2,3-Dehydrosilybins, together with other 2,3-dehydroflavonolignans, belong to the minor flavonoids of the silymarin complex, usually accounting for 1-2% of all flavonolignans (1.8% in the preparation used in the present work; Supplementary Figure 3). Their biological effects, however, might be of real clinical importance [28]. This is supported by a recent observation that 2,3-dehydrosilybins A/B significantly suppressed oxidative stress in *C. elegans*

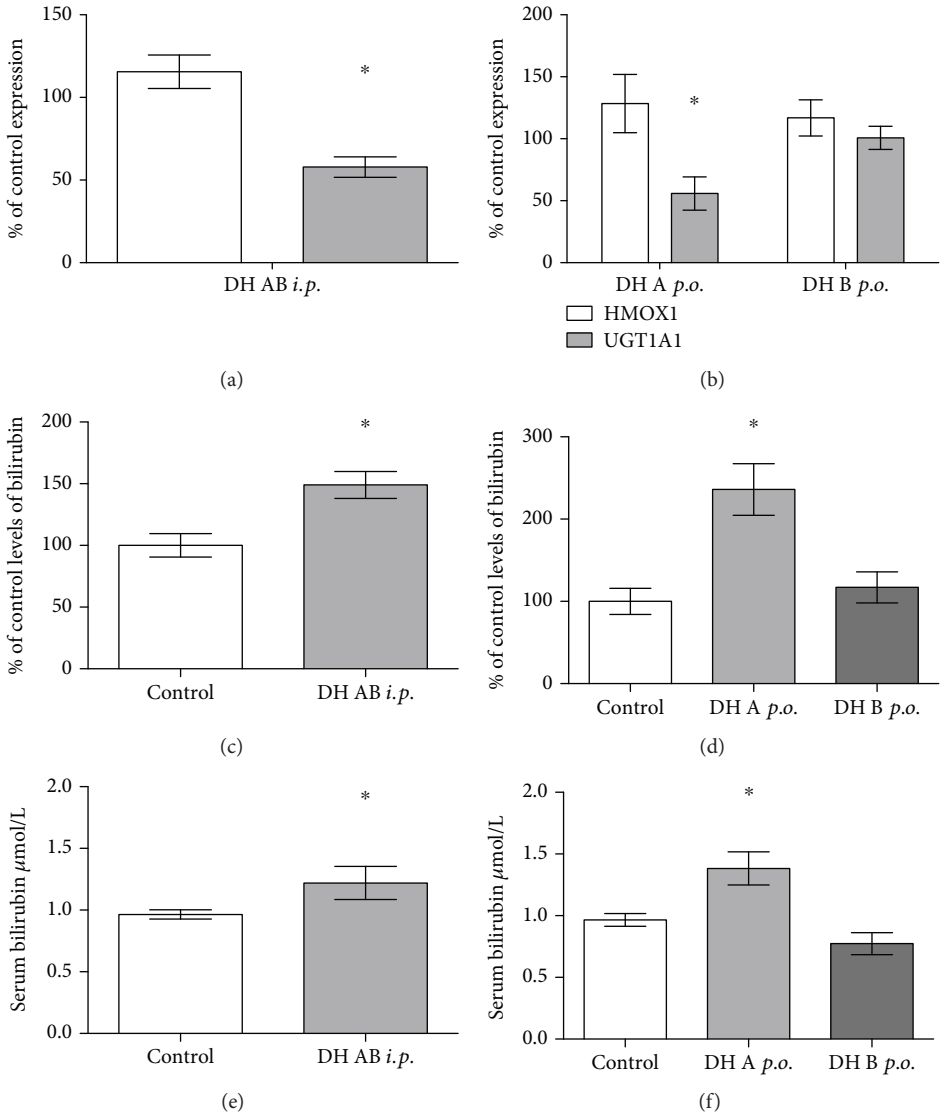

Figure 6: The effect of 2,3-dehydrosilybins on hepatic *HMOX1* and *UGT1A1* mRNA expressions and intrahepatic and systemic bilirubin concentrations. (a) *HMOX1* and *UGT1A1* mRNA expressions in mouse livers after intraperitoneal administration of a mixture of 2,3-dehydrosilybins A and B (50 mg/kg b.wt. for 7 days). (b) *HMOX1* and *UGT1A1* mRNA expressions in mouse livers after oral administration of either 2,3-dehydrosilybin A or B (50 mg/kg b.wt. for 7 days). (c) Intrahepatic bilirubin concentrations after intraperitoneal administration of a mixture of 2,3-dehydrosilybins A and B (50 mg/kg b.wt. for 7 days). (d) Intrahepatic bilirubin concentrations after oral administration of either 2,3-dehydrosilybin A or B (50 mg/kg b.wt. for 7 days). (e) Systemic bilirubin concentrations after intraperitoneal administration of a mixture of 2,3-dehydrosilybins A and B (50 mg/kg b.wt. for 7 days). (f) Systemic bilirubin concentrations after oral administration of either 2,3-dehydrosilybin A or B (50 mg/kg b.wt. for 7 days). $^*P < 0.05$. b.wt.: body weight.

resulting in lifespan extension [32]. Although the effect on bilirubin metabolism was not investigated in this study, it is important to note that the antiaging effects of bilirubin have been demonstrated in another of our studies [7]. In this respect, it is also important to emphasize the antioxidant effects of 2,3-dehydrosilybins observed in our study. Indeed, decreased MDA concentrations in the livers of mice treated with 2,3-dehydrosilybins might have been mediated, at least partially, *via* increased intracellular bilirubin concentrations. It is thus likely that these antioxidant effects are not directly related to antioxidant activities of the flavonolignans per se, but rather parahormetic action is more important [52].

5. Conclusions

Natural silymarin flavonolignans contained in milk thistle and related flavonols, in particular 2,3-dehydrosilybins A and B, affect hepatic and serum bilirubin concentrations, as well as lipoperoxidation in the liver. This phenomenon might contribute to the hepatoprotective effects of silymarin observed in many, although not all clinical studies.

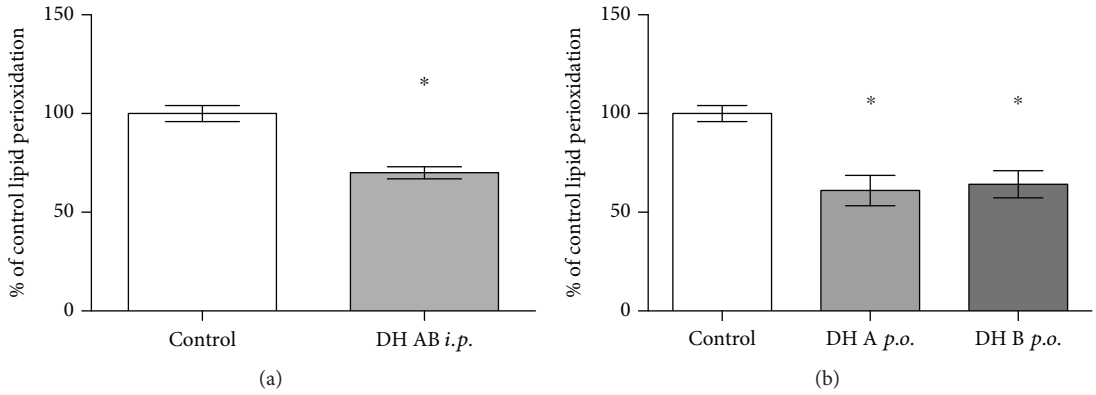

Figure 7: The effect of intraperitoneal and oral administration of 2,3-dehydrosilybins on lipoperoxidation in the liver tissue. (a) MDA concentrations in the mouse liver tissue after intraperitoneal administration of a mixture of 2,3-dehydrosilybins A and B (50 mg/kg b.wt. for 7 days). (b) MDA concentrations in the mouse liver tissue after oral administration of either 2,3-dehydrosilybin A or B (50 mg/kg b.wt. for 7 days). Data are expressed as a percentage of the control values. $^*P < 0.05$. b.wt.: body weight.

Modulation of bilirubin metabolism by well-defined natural polyphenols can represent a safe chemopreventive approach against oxidative stress-mediated diseases including atherosclerosis, cancer, diabetes, or inflammatory diseases.

Abbreviations

UGT1A1: UDP-glucuronosyl transferase
HMOX: Heme oxygenase
HPRT: Hypoxantin phosphoribosyl transferase
ALT: Alanine aminotransferase
AST: Aspartate aminotransferase
ALP: Alkaline phosphatase
MDA: Malondialdehyde
IC: Inhibitory concentration.

Data Availability

The data used to support the findings of this study are available from the corresponding author upon request.

Disclosure

Part of the study has been presented at the 68th Annual Meeting of the American Association for the Study of Liver Diseases: The Liver Meeting, Washington, USA. The funding bodies had no role in the design of the study or collection, analysis, and interpretation of the data, or in writing of the manuscript.

Conflicts of Interest

The authors declare that they have no financial or commercial conflicts of interest.

Authors' Contributions

All authors contributed to the data analysis and interpretation and have read and approved the final manuscript.

Acknowledgments

This work was supported by grants GAUK 337815, SVV 260370/2018, and PROGRES Q25/LF1 from Charles University, Prague, Czech Republic; AZV 16-27317A and RVO-VFN64165/2018 from the Czech Ministry of Health; and grant 16-06008S from the Czech Science Foundation.

Supplementary Materials

Supplementary Material: a detailed analytical HPLC-MS method for the determination of silymarin flavonolignans together with obtained data from the analyses, i.e., detailed composition of silymarin complex used in the study. Supplementary Table 1: primers used for gene expression studies. *(Supplementary Materials)*

References

[1] R. Stocker, Y. Yamamoto, A. F. McDonagh, A. N. Glazer, and B. N. Ames, "Bilirubin is an antioxidant of possible physiological importance," *Science*, vol. 235, no. 4792, pp. 1043–1046, 1987.

[2] S. Gazzin, L. Vitek, J. Watchko, S. M. Shapiro, and C. Tiribelli, "A novel perspective on the biology of bilirubin in health and disease," *Trends in Molecular Medicine*, vol. 22, no. 9, pp. 758–768, 2016.

[3] S. Jangi, L. Otterbein, and S. Robson, "The molecular basis for the immunomodulatory activities of unconjugated bilirubin," *The International Journal of Biochemistry & Cell Biology*, vol. 45, no. 12, pp. 2843–2851, 2013.

[4] R. Ollinger, P. Kogler, J. Troppmair et al., "Bilirubin inhibits tumor cell growth via activation of ERK," *Cell Cycle*, vol. 6, no. 24, pp. 3078–3085, 2007.

[5] C. Molzer, H. Huber, A. Steyrer et al., "Interaction between TNFone and tetrapyrroles may account for their anti-genotoxic effects — a novel mechanism for DNA-protection," *Journal of Porphyrins and Phthalocyanines*, vol. 17, no. 12, pp. 1157–1166, 2013.

[6] A. C. Bulmer, K. Ried, J. T. Blanchfield, and K. H. Wagner, "The anti-mutagenic properties of bile pigments," *Mutation Research*, vol. 658, no. 1-2, pp. 28–41, 2008.

[7] J. Zelenka, A. Dvorak, L. Alan, M. Zadinova, M. Haluzik, and L. Vitek, "Hyperbilirubinemia protects against aging-associated inflammation and metabolic deterioration," *Oxidative Medicine and Cellular Longevity*, vol. 2016, Article ID 6190609, 10 pages, 2016.

[8] D. E. Stec, K. John, C. J. Trabbic et al., "Bilirubin binding to PPARα inhibits lipid accumulation," *PLoS One*, vol. 11, no. 4, article e0153427, 2016.

[9] K. H. Wagner, M. Wallner, C. Molzer et al., "Looking to the horizon: the role of bilirubin in the development and prevention of age-related chronic diseases," *Clinical Science*, vol. 129, no. 1, pp. 1–25, 2015.

[10] L. Vitek, "Bilirubin and atherosclerotic diseases," *Physiological Research*, vol. 66, Supplement 1, pp. S11–S20, 2017.

[11] J. P. Lin, L. Vitek, and H. A. Schwertner, "Serum bilirubin and genes controlling bilirubin concentrations as biomarkers for cardiovascular disease," *Clinical Chemistry*, vol. 56, no. 10, pp. 1535–1543, 2010.

[12] M. F. McCarty, ""Iatrogenic Gilbert syndrome" - a strategy for reducing vascular and cancer risk by increasing plasma unconjugated bilirubin," *Medical Hypotheses*, vol. 69, no. 5, pp. 974–994, 2007.

[13] V. Estrada, S. Monge, D. Gomez-Garre et al., "Comparison of oxidative stress markers in HIV-infected patients on efavirenz or atazanavir/ritonavir-based therapy," *Journal of the International AIDS Society*, vol. 17, no. 4, article 19544, Supplement 3, 2014.

[14] J. Milian, A. B. Goldfine, J. P. Zuflacht, C. Parmer, and J. A. Beckman, "Atazanavir improves cardiometabolic measures but not vascular function in patients with long-standing type 1 diabetes mellitus," *Acta Diabetologica*, vol. 52, no. 4, pp. 709–715, 2015.

[15] D. Dekker, M. J. Dorresteijn, M. Pijnenburg et al., "The bilirubin-increasing drug atazanavir improves endothelial function in patients with type 2 diabetes mellitus," *Arteriosclerosis, Thrombosis, and Vascular Biology*, vol. 31, no. 2, pp. 458–463, 2011.

[16] M. E. Mohamed and R. F. Frye, "Effects of herbal supplements on drug glucuronidation. Review of clinical, animal, and *in vitro* studies," *Planta Medica*, vol. 77, no. 4, pp. 311–321, 2011.

[17] M. F. Mohamed, T. Tseng, and R. F. Frye, "Inhibitory effects of commonly used herbal extracts on UGT1A1 enzyme activity," *Xenobiotica*, vol. 40, no. 10, pp. 663–669, 2010.

[18] V. D'Andrea, L. M. Perez, and E. J. Sanchez Pozzi, "Inhibition of rat liver UDP-glucuronosyltransferase by silymarin and the metabolite silibinin-glucuronide," *Life Sciences*, vol. 77, no. 6, pp. 683–692, 2005.

[19] T. W. Flaig, D. L. Gustafson, L. J. Su et al., "A phase I and pharmacokinetic study of silybin-phytosome in prostate cancer patients," *Investigational New Drugs*, vol. 25, no. 2, pp. 139–146, 2007.

[20] K. Rutter, T. M. Scherzer, S. Beinhardt et al., "Intravenous silibinin as 'rescue treatment' for on-treatment non-responders to pegylated interferon/ribavirin combination therapy," *Antiviral Therapy*, vol. 16, no. 8, pp. 1327–1333, 2011.

[21] Z. Marino, G. Crespo, M. D'Amato et al., "Intravenous silibinin monotherapy shows significant antiviral activity in HCV-infected patients in the peri-transplantation period," *Journal of Hepatology*, vol. 58, no. 3, pp. 415–420, 2013.

[22] S. Beinhardt, S. Rasoul-Rockenschaub, T. M. Scherzer, and P. Ferenci, "Silibinin monotherapy prevents graft infection after orthotopic liver transplantation in a patient with chronic hepatitis C," *Journal of Hepatology*, vol. 54, no. 3, pp. 591-592, 2011.

[23] U. P. Neumann, M. Biermer, D. Eurich, P. Neuhaus, and T. Berg, "Successful prevention of hepatitis C virus (HCV) liver graft reinfection by silibinin mono-therapy," *Journal of Hepatology*, vol. 52, no. 6, pp. 951-952, 2010.

[24] C. R. de Avelar, E. M. Pereira, P. R. de Farias Costa, R. P. de Jesus, and L. P. M. de Oliveira, "Effect of silymarin on biochemical indicators in patients with liver disease: systematic review with meta-analysis," *World Journal of Gastroenterology*, vol. 23, no. 27, pp. 5004–5017, 2017.

[25] V. Simanek, V. Kren, J. Ulrichova, J. Vicar, and L. Cvak, "Silymarin: what is in the name…? An appeal for a change of editorial policy," *Hepatology*, vol. 32, no. 2, pp. 442–444, 2000.

[26] C. S. Chambers, V. Holeckova, L. Petraskova et al., "The silymarin composition… and why does it matter???," *Food Research International*, vol. 100, Part 3, pp. 339–353, 2017.

[27] N. C. Kim, T. N. Graf, C. M. Sparacino, M. C. Wani, and M. E. Wall, "Complete isolation and characterization of silybins and isosilybins from milk thistle (*Silybum marianum*)," *Organic & Biomolecular Chemistry*, vol. 1, no. 10, pp. 1684–1689, 2003.

[28] V. Kren and D. Walterova, "Silybin and silymarin - new effects and applications," *Biomed Papers*, vol. 149, no. 1, pp. 29–41, 2005.

[29] M. Pyszkova, M. Biler, D. Biedermann et al., "Flavonolignan 2,3-dehydroderivatives: preparation, antiradical and cytoprotective activity," *Free Radical Biology and Medicine*, vol. 90, pp. 114–125, 2016.

[30] D. Karas, R. Gazak, K. Valentova et al., "Effects of 2,3-dehydrosilybin and its galloyl ester and methyl ether derivatives on human umbilical vein endothelial cells," *Journal of Natural Products*, vol. 79, no. 4, pp. 812–820, 2016.

[31] D. Biedermann, M. Buchta, V. Holeckova et al., "Silychristin: skeletal alterations and biological activities," *Journal of Natural Products*, vol. 79, no. 12, pp. 3086–3092, 2016.

[32] K. Filippopoulou, N. Papaevgeniou, M. Lefaki et al., "2,3-Dehydrosilybin A/B as a pro-longevity and anti-aggregation compound," *Free Radical Biology and Medicine*, vol. 103, pp. 256–267, 2017.

[33] R. Gazak, P. Marhol, K. Purchartova et al., "Large-scale separation of silybin diastereoisomers using lipases," *Process Biochemistry*, vol. 45, no. 10, pp. 1657–1663, 2010.

[34] R. Gazak, P. Trouillas, D. Biedermann et al., "Base-catalyzed oxidation of silybin and isosilybin into 2,3-dehydroderivatives," *Tetrahedron Letters*, vol. 54, no. 4, pp. 315–317, 2013.

[35] D. Gerstorferova, B. Fliedrova, P. Halada, P. Marhol, V. Kren, and L. Weignerova, "Recombinant α-L-rhamnosidase from *Aspergillus terreus* in selective trimming of rutin," *Process Biochemistry*, vol. 47, no. 5, pp. 828–835, 2012.

[36] J. Zelenka, M. Lenicek, L. Muchova et al., "Highly sensitive method for quantitative determination of bilirubin in biological fluids and tissues," *Journal of Chromatography B*, vol. 867, no. 1, pp. 37–42, 2008.

[37] J. Zelenka, L. Muchova, M. Zelenkova et al., "Intracellular accumulation of bilirubin as a defense mechanism against

increased oxidative stress," *Biochimie*, vol. 94, no. 8, pp. 1821–1827, 2012.

[38] H. J. Vreman and D. K. Stevenson, "Heme oxygenase activity as measured by carbon monoxide production," *Analytical Biochemistry*, vol. 168, no. 1, pp. 31–38, 1988.

[39] E. D. Wills, "Mechanisms of lipid peroxide formation in animal tissues," *The Biochemical Journal*, vol. 99, no. 3, pp. 667–676, 1966.

[40] D. Zhang, T. J. Chando, D. W. Everett, C. J. Patten, S. S. Dehal, and W. G. Humphreys, "In vitro inhibition of UDP glucuronosyltransferases by atazanavir and other HIV protease inhibitors and the relationship of this property to in vivo bilirubin glucuronidation," *Drug Metabolism and Disposition*, vol. 33, no. 11, pp. 1729–1739, 2005.

[41] S. Gazzin, F. Masutti, L. Vitek, and C. Tiribelli, "The molecular basis of jaundice: an old symptom revisited," *Liver International*, vol. 37, no. 8, pp. 1094–1102, 2017.

[42] L. Novotny and L. Vitek, "Inverse relationship between serum bilirubin and atherosclerosis in men: a meta-analysis of published studies," *Experimental Biology and Medicine*, vol. 228, no. 5, pp. 568–571, 2003.

[43] A. Jiraskova, J. Novotny, L. Novotny et al., "Association of serum bilirubin and promoter variations in HMOX1 and UGT1A1 genes with sporadic colorectal cancer," *International Journal of Cancer*, vol. 131, no. 7, pp. 1549–1555, 2012.

[44] M. Lenicek, D. Duricova, O. Hradsky et al., "The relationship between serum bilirubin and Crohn's disease," *Inflammatory Bowel Diseases*, vol. 20, no. 3, pp. 481–487, 2014.

[45] L. Vitek, M. Jirsa, M. Brodanova et al., "Gilbert syndrome and ischemic heart disease: a protective effect of elevated bilirubin levels," *Atherosclerosis*, vol. 160, no. 2, pp. 449–456, 2002.

[46] C. Sridar, T. C. Goosen, U. M. Kent, J. A. Williams, and P. F. Hollenberg, "Silybin inactivates cytochromes P450 3A4 and 2C9 and inhibits major hepatic glucuronosyltransferases," *Drug Metabolism and Disposition*, vol. 32, no. 6, pp. 587–594, 2004.

[47] C. Hoh, D. Boocock, T. Marczylo et al., "Pilot study of oral silibinin, a putative chemopreventive agent, in colorectal cancer patients: silibinin levels in plasma, colorectum, and liver and their pharmacodynamic consequences," *Clinical Cancer Research*, vol. 12, no. 9, pp. 2944–2950, 2006.

[48] N. Barzaghi, F. Crema, G. Gatti, G. Pifferi, and E. Perucca, "Pharmacokinetic studies on IdB 1016, a silybin-phosphatidylcholine complex, in healthy human subjects," *European Journal of Drug Metabolism and Pharmacokinetics*, vol. 15, no. 4, pp. 333–338, 1990.

[49] Z. Wen, T. E. Dumas, S. J. Schrieber, R. L. Hawke, M. W. Fried, and P. C. Smith, "Pharmacokinetics and metabolic profile of free, conjugated, and total silymarin flavonolignans in human plasma after oral administration of milk thistle extract," *Drug Metabolism and Disposition*, vol. 36, no. 1, pp. 65–72, 2008.

[50] B. T. Gufford, G. Chen, P. Lazarus, T. N. Graf, N. H. Oberlies, and M. F. Paine, "Identification of diet-derived constituents as potent inhibitors of intestinal glucuronidation," *Drug Metabolism and Disposition*, vol. 42, no. 10, pp. 1675–1683, 2014.

[51] K. Wlcek, F. Koller, P. Ferenci, and B. Stieger, "Hepatocellular organic anion-transporting polypeptides (OATPs) and multidrug resistance-associated protein 2 (MRP2) are inhibited by silibinin," *Drug Metabolism and Disposition*, vol. 41, no. 8, pp. 1522–1528, 2013.

[52] H. J. Forman, K. J. Davies, and F. Ursini, "How do nutritional antioxidants really work: nucleophilic tone and para-hormesis versus free radical scavenging *in vivo*," *Free Radical Biology and Medicine*, vol. 66, pp. 24–35, 2014.

Hindawi
Oxidative Medicine and Cellular Longevity
Volume 2019, Article ID 7090534, 17 pages
https://doi.org/10.1155/2019/7090534

Review Article

Role of Nrf2 and Its Activators in Respiratory Diseases

Qinmei Liu,[1] Yun Gao,[2] and Xinxin Ci[1]

[1]*Institute of Translational Medicine, The First Hospital of Jilin University, Changchun 130001, China*
[2]*Department of Respiratory Medicine, The First Hospital of Jilin University, Changchun 130001, China*

Correspondence should be addressed to Xinxin Ci; cixinxin@jlu.edu.cn

Received 26 July 2018; Revised 22 November 2018; Accepted 3 December 2018; Published 8 January 2019

Guest Editor: Luciano Saso

Transcription factor nuclear factor erythroid 2-related factor 2 (Nrf2) is a major regulator of antioxidant response element- (ARE-) driven cytoprotective protein expression. The activation of Nrf2 signaling plays an essential role in preventing cells and tissues from injury induced by oxidative stress. Under the unstressed conditions, natural inhibitor of Nrf2, Kelch-like ECH-associated protein 1 (Keap1), traps Nrf2 in the cytoplasm and promotes the degradation of Nrf2 by the 26S proteasome. Nevertheless, stresses including highly oxidative microenvironments, impair the ability of Keap1 to target Nrf2 for ubiquitination and degradation, and induce newly synthesized Nrf2 to translocate to the nucleus to bind with ARE. Due to constant exposure to external environments, including diverse pollutants and other oxidants, the redox balance maintained by Nrf2 is fairly important to the airways. To date, researchers have discovered that Nrf2 deletion results in high susceptibility and severity of insults in various models of respiratory diseases, including bronchopulmonary dysplasia (BPD), respiratory infections, acute respiratory distress syndrome (ARDS), chronic obstructive pulmonary disease (COPD), asthma, idiopathic pulmonary fibrosis (IPF), and lung cancer. Conversely, Nrf2 activation confers protective effects on these lung disorders. In the present review, we summarize Nrf2 involvement in the pathogenesis of the above respiratory diseases that have been identified by experimental models and human studies and describe the protective effects of Nrf2 inducers on these diseases.

1. Oxidative Stress and Antioxidant Responses in Respiratory Diseases

In the past few decades, environmental issues due to man-made and natural factors have sharply increased the incidence of malignant and nonmalignant respiratory diseases. Therefore, the reason underlying why the respiratory system is so easily affected by environmental problems and the pathogenesis of respiratory diseases has attracted increasing attention.

As the location of gas exchange, the airways with large surface area constantly interface with the external environment and are exposed to various airborne toxicants especially inhaled oxidants (e.g., environmental ozone, particles, and cigarette smoke) [1]. Due to the special characteristics of anatomy and physiology, the airways are placed in highly oxidative microenvironments. Therefore, redox homeostasis in the airways can be easily disturbed, which is referred to as oxidative stress [2]. Oxidative stress is a common status defined as the imbalance between reactive oxygen species (ROS) production and antioxidant capacity in cells under temporary or constant stimulation of the abundant oxidant stressors [3]. Recently, oxidative stress has been proven to be associated with the pathogenesis of diverse acute and chronic respiratory diseases, including respiratory infections, acute respiratory distress syndrome (ARDS), chronic obstructive pulmonary disease (COPD), asthma, idiopathic pulmonary fibrosis (IPF), and lung cancer [4–6]. In the lungs of individuals with these diseases, the disruption of redox balance is always observed and may be represented by increased biomarkers of oxidative stress.

Nevertheless, during the long journey of life evolution, the organism has developed a series of antioxidant responses to counteract the toxicity of oxidative stress. The antioxidant system in cellular response includes either proteins (e.g., enzymes) or small molecules (e.g., vitamins C and E). As enzymes have been proven to play a significant role in life cycles, their effects on antioxidant defense have been investigated extensively. Direct antioxidant enzymes refer to classical enzymes including superoxide dismutases (SODs),

catalase, and glutathione peroxidase (GPx), while indirect antioxidant enzymes mainly refer to phase 2 detoxifying enzymes such as glutathione-S-transferase (GST) isozymes, catalytic and modifier subunits of γ-glutamyl cysteine ligase (GCLC, GCLM), and NADP(H):quinone oxidoreductase (NQO1). Moreover, the stress response protein heme oxygenase (HO-1) is reported to be a particularly potent antioxidant protein [7–9]. Antioxidant substances are present in relative abundance in both epithelial lining fluid (ELF) and lung tissues, as airways are places where detoxification reactions routinely occur, and protect the lungs from oxidative insults in healthy individuals [2]. Unfortunately, in susceptible individuals, the depletion of GSH and other antioxidants can occur, and these individuals are prone to developing oxidative respiratory diseases. Moreover, the protective role of the antioxidant system in the prevention of these respiratory diseases may also be proven by several therapies aimed at defending against oxidative stress that have already been applied in BPD, COPD, and IPF, such as treatment with vitamins C and E or N-acetylcysteine (NAC, a GSH precursor) or treatment with polyethylene glycol-conjugated SOD and catalase.

2. Nrf2-Mediated Antioxidant Pathway and Respiratory Diseases

Although the functional mechanisms are diverse in the antioxidant system, a large number of typical phase 2 detoxifying enzymes and the stress response protein HO-1 are regulated by the transcription factor nuclear factor erythroid 2-related factor 2 (Nrf2), which indicates that this transcription factor is a possible and imperative upstream regulator of antioxidative responses that maintains cellular redox homeostasis and reduces severe oxidative damage [10–13].

Nrf2, which belongs to the cap "n" collar (CNC) family of transcription factors, is a major transcription factor that counteracts oxidative stress and inflammation through the coordinated induction of antioxidant response element- (ARE-) driven cytoprotective gene transcription [14, 15]. The classical mechanisms of Nrf2 activation include oxidative modification and conformational changes in its major repressor protein Kelch-like ECH associated protein 1 (Keap1), followed by Nrf2 stabilization due to escape from ubiquitination by Cul3-Rbx1. This molecular model is proven by the constitutive accumulation of Nrf2 in the nuclei of Keap1-knockout mice [16]. In fact, Nrf2 consists of six functional domains recognized as Nrf2-ECH homologies 1–6 (Neh1–6), including the Keap1 binding domain (Neh2) and the leucine zipper domain (Neh1), through which Nrf2 can heterodimerize with small Maf or Jun proteins and then bind to ARE [17]. The Nrf2 repressor keap1 is a cytoplasmic and cysteine-rich protein whose N-terminal BTB domain binds to Cullin 3- (Cul3-) Rbx1, while the C-terminal DGR domain binds to Nrf2. Keap1 represses Nrf2 by serving as a substrate adaptor for the Cul3-containing E3 ubiquitin ligase complex. Under physiological conditions, Keap1 holds Nrf2 in the cytoplasm and ubiquitinates Nrf2 to facilitate its degradation by the 26S proteasome. However, when oxidative stimuli exist, the cysteine residues of Keap1 can be modified, leading to Nrf2 stabilization and accumulation in the nucleus [18]. Several mechanisms for the activation of Nrf2 by Keap1 have been proposed as the following up to now [17, 19, 20]. (1) Keap1 dissociation: the modification of a cysteine in Keap1 makes Nrf2 dissociate from Keap1. (2) Keap1 hinge and latch: as a more extensively accepted model, Nrf2 binds with the Keap1 homodimer through a high-affinity ETGE motif as the "hinge" and a low-affinity DLG motif as the "latch." The modification of cysteine in Keap1 leads to a conformational change but does not trigger the dissociation of Nrf2, which may inhibit ubiquitin binding onto Nrf2 by disrupting the weak latch binding site. (3) Keap1 ubiquitination: the modification of a cysteine in Keap1 moves the ubiquitin conjugation from Nrf2 to itself. Nevertheless, the precise molecular mechanisms behind how Nrf2 bypasses the Keap1 gate under stressed conditions still remain to be elucidated. Several studies in recent years have proposed fairly intriguing theories. For example, Cys-151 in the BTB domain of Keap1 is likely to play an important role in response to Nrf2 activators, and this action may be associated with its destructive effect on the interaction of Keap1 with Cul3 [21]. Diverse Nrf2 activators activate Nrf2 signaling through this canonical mechanism, and the mutation of cysteine 151 to serine (Keap1-C151S) in Keap1 completely abolishes the Nrf2 upregulation [22, 23]. Other studies indicate that Cys-273 and Cys-288 in Keap1 may also contribute to the structural integrity and activity of Keap1 for maintaining ubiquitin ligase activity [24]. In addition, there are also Keap1-independent pathways for Nrf2 activation, among which protein kinases play an essential role. A previous study showed that phosphorylation at a specific amino acid residue of Nrf2 can increase its stability and transactivation activity [8]. Typical protein kinase pathways include phosphatidylinositol 3-kinase (PI3K), MAPKs, PKC, and glycogen synthase kinase-3 (GSK-3). The phosphorylation of Nrf2 by PI3K, PKC, c-Jun, N-terminal kinase (JNK) and extracellular signal-regulated protein kinase (ERK) confers positive regulation, whereas p38 MAPK regulates the Nrf2 pathway both positively and negatively [19, 25–29]. Recently, a noncanonical pathway of Nrf2 activation involving autophagy has attracted increasing attention due to its double effect. This pathway is closely associated with the autophagy substrate protein sequestosome 1 (SQSTM1 or p62). p62 can compete with Nrf2 for Keap1 binding, sequester Keap1 into the autophagosome, and allow Nrf2 stabilization and accumulation [30]. However, autophagy-mediated Nrf2 activation has both positive and negative effects: induction of autophagy leads to sequestration of Keap1-p62 complexes into autophagosomes and lysosomal-mediated degradation of Keap1, resulting in controlled Nrf2 activation, and exerts protective effects, while autophagy dysregulation results in prolonged Nrf2 activation in a pathological state and exerts detrimental effects.

Moreover, recent studies have shown that in addition to Keap1, other pathways involving cullin adaptor proteins also direct the ubiquitination of Nrf2. For instance, the phosphorylation of Nrf2 at specific serine residues in the Neh6 domain by GSK-3 forms a degradation part for

recognition by the ubiquitin ligase adapter Skp1-Cul1-F-box protein (SCF)/β-TrCP (β-transducin repeat-containing protein) and proteasome degradation by the Cullin1/Rbx1 complex [31, 32]. Similarly, WDR23, a substrate receptor for the Cullin4- (CUL4-) DDB1 (damaged DNA-binding protein 1) E3-ubiquitin ligase, binds with the Neh2 domain of Nrf2 and negatively regulates the level and activity of Nrf2 [33].

The functional process occurs when de novo synthesized Nrf2 translocates to the nucleus, after which Nrf2 heterodimerizes with small Maf or Jun proteins and then binds to ARE in the regulatory regions of Nrf2 target genes and either upregulates or inhibits target genes. Previous studies have shown that in the protection of the respiratory system by Nrf2, Nrf2-targeted genes are essential effectors that are identified by microarray analyses and bioinformatic studies. The Nrf2/ARE pathway regulates more than 500 genes, including genes that regulate oxidative stress (HO-1, GCLM, and GCLC), inflammation (TGF-β and NF-κB), xenobiotic metabolism and excretion (NQO1, AKR1C1, and MRP1), apoptosis (Bcl-2 and BclxL), and autophagy (p62) [12, 23]. Therefore, Nrf2-downstream target genes have diverse functions, including antioxidation, anti-inflammation, xenobiotic metabolism, detoxification, and cell growth regulation [25, 34, 35]. In particular, cytoprotective proteins such as HO-1, GCLM, GCLC, and NQO1 catalyze diverse detoxification reactions, converting harmful substances to hydrophilic metabolites, and are not consumed during their actions [36] (Figure 1). Moreover, the protective effects of Nrf2 are more likely to be exerted when its activation is tightly controlled. A recent study showed that once the redox homeostasis is restored or the compounds are metabolized and eliminated, signal termination will occur, and Keap1 enters the nucleus, binds to Nrf2, and then brings it back to the cytosol for degradation [37].

Accordingly, previous studies have shown that in tissues where routine antioxidation and detoxification processes occur, such as the lungs, liver, and kidneys, Nrf2 is relatively abundant. The expression level of Nrf2 is highly correlated with the susceptibility, severity, and recovery of airway disorders. Data from Nrf2-knockout mice identify the protective effects of Nrf2 on airway disorders: compared to wild-type mice, Nrf2-knockout mice have enhanced lung inflammation, epithelial cell injury, and increased sensitivity to cigarette smoke, elastase, ovalbumin, bleomycin, and other stimuli [38–41]. These findings motivate researchers to discover potential Nrf2 activators.

3. Protective Role of Nrf2 and Its Activators in Respiratory Diseases

As described above, the respiratory system is directly exposed to inhaled oxidants, and this oxidative burden makes this system more vulnerable to oxidant stress, which has proven to be associated with the pathogenesis of diverse respiratory diseases. Currently, the protective roles of Nrf2 signaling in respiratory disorders have been identified with the application of Nrf2 knockout mice, including three different genetic backgrounds (ICR, C57BL/6J, and Balbc/J) and lung-specific conditional knockout mice [1]. For instance, the deletion of Nrf2 is associated with more severe insults that are caused by oxidative, inflammatory, or carcinogenesis factors such as infection, hyperoxia, cigarette, ovalbumin, bleomycin, butylated hydroxytoluene, and diesel exhaust particles. Conversely, the activation of Nrf2 exerts protective effects on these lung disorders. Therefore, many studies focus on the benefits of Nrf2 inducers, including natural products, in the therapeutic intervention for oxidant-associated lung diseases [42]. In the present review, we discuss the involvement of Nrf2 in the pathogenesis of airway disorders and the protective role of diverse Nrf2 inducers in different airway disorders. Furthermore, the effects of major Nrf2 activators on different respiratory diseases are summarized in form of table (Table 1).

3.1. Bronchopulmonary Dysplasia (BPD). Bronchopulmonary dysplasia (BPD) is a chronic respiratory disease that usually occurs in premature infants with very low birth weight. BPD is mainly characterized by a failure in alveolarization, which results in impaired alveolar growth and vascular development, pulmonary inflammation, and abnormal lung function [43, 44]. Furthermore, BPD not only results in significant mortality in the perinatal period but also contributes to long-term sequelae in adolescents or early adulthood with clinically significant respiratory symptoms [45].

Although the pathogenesis of BPD has not been fully understood, the lung injury in BPD can be divided into two groups described as "new" BPD and "old" BPD. The former refers to early developmental arrest by prenatal exposure or genetic factors, while the latter develops into surfactant-deficient premature infants who receive respiratory support. Further studies elucidate that important trigger events for BPD may include oxidative damage and inflammation. Particularly, as human infants undergo critical postnatal alveolar growth, therapeutically administered oxygen to improve the oxygenation of premature infants is a major risk factor, which may be associated with the induction of p21 and p53 cell cycle regulatory genes [46]. For oxidative disorders in adults, Nrf2 activation has been extensively proven to be beneficial; however, the investigation of its effects on neonatal diseases is still a novel area. As evidenced by recent studies, during the process of saccular lung maturation, Nrf2 may modulate diverse genes implicated in maintaining redox balance, organ development and lung morphogenesis, and cell growth and death as well as immunity. Indeed, previous studies indicate the effects of Nrf2 on molecular processes of alveolarization and lung diseases of premature births: deficiency in Nrf2 and exposure to hyperoxia in newborn mice increases mortality and the severity of alveolar growth inhibition, and transcriptome analysis of immature lung tissue suggests that the protection against O_2 toxicity of Nrf2 may be mediated by its regulation of the cell cycle, metabolism processes, cell–cell interactions, and redox homeostasis [47, 48].

These findings may elucidate a possible beneficial role for Nrf2 activators in the BPD of preterm infants with respect to both lung development and hyperoxia-mediated lung injury, and several studies have attempted to unveil such potential. For instance, aurothioglucose (ATG), a TrxR1 inhibitor,

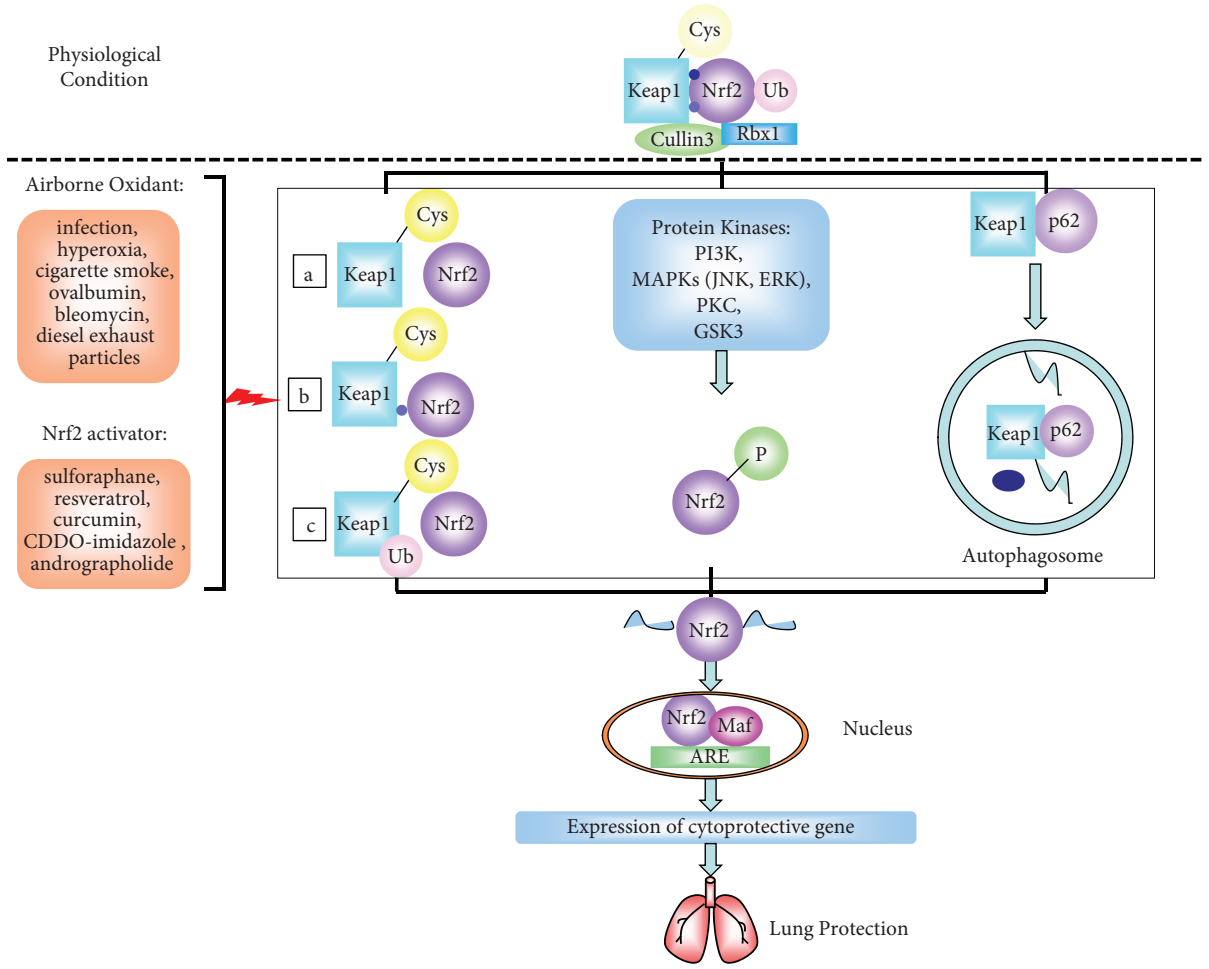

Figure 1: The mechanism of Nrf2 activation and Nrf2-mediated antioxidant responses in the lungs. Under unstressed conditions, Keap1 protein traps Nrf2 in the cytoplasm and targets this protein for the Cul3-Rbx1 ubiquitination system, which promotes the proteolysis of Nrf2 by the 26S proteasome. Diverse oxidative insults or pharmacological Nrf2 activators impair the ability of Keap1 to target Nrf2 for ubiquitination and degradation, promote newly synthesized Nrf2 to translocate to nucleus, and induce ARE-driven cytoprotective gene expression. Several accepted mechanisms include the modification of cysteine in Keap1: (a) Keap1 dissociation, (b) Keap1 hinge and latch, and (c) Keap1 ubiquitination. (2) There are also Keap1-independent pathways, among which protein kinases including PI3K, MAPKs, PKC, and GSK-3 play an essential role in phosphorylation of Nrf2 to increase its stability and transactivation activity. (3) Moreover, a noncanonical pathway induces Nrf2 activation by autophagy, which declares that p62 competes with Nrf2 for Keap1 binding, sequesters Keap1 into the autophagosome, and promotes its degradation. After de novo synthesized Nrf2 translocates to the nucleus, it heterodimerizes with small Maf then binds to ARE in the regulatory regions of Nrf2 target genes to induce their expression, which confer protective effects to various pulmonary diseases including BPD, respiratory infection, ARDS, COPD, asthma, IPF, and lung cancer.

inhibits thioredoxin reductase-1 (TrxR1) activity and activates the Nrf2 pathway in the lungs of newborn C3H/HeN mice exposed to hyperoxia, attenuating the decrease in body weight and alterations in alveolar development. However, the effects on alveolarization and sustained Nrf2 activation are not observed in the lungs of newborn C57BL/6 mice under the same conditions [49, 50]. In a newborn rat model of BPD, the Nrf2 activator curcumin can attenuate hyperoxic lung injury, and the protective role is considered to be at least partially related to the activation of Nrf2; unfortunately, whether the Nrf2 pathway is activated was not studied [51, 52]. Another study shows that the in utero administration of a well-recognized Nrf2 inducer, sulforaphane, can inhibit hyperoxia-induced lung inflammation in neonatal mice, but the inhibition of alveolar growth is not improved in this model of BPD [53]. Such results are provoking, and whether Nrf2 induction is beneficial under the current conditions in BPD may be controversial, and studies on the long-term effects of in utero Nrf2 inducers on alveolar growth, inflammation, and survival are needed. In consideration of these discoveries, Nrf2 activation may be a novel strategy in preventing or modulating the severity of BPD, as well as helping to improve the outcomes of the disease. However, caution should be taken when evaluating the effects of Nrf2 inducers in BPD before clinical use because the results from previous studies are still limited and controversial in some respects, such as the mode of administration, the delivery time, and even the species.

Table 1: The effects of major Nrf2 activators on different respiratory diseases.

Nrf2 activator	Respiratory disease	Effects	Ref.
Curcumin	BPD	Attenuates hyperoxic lung injury in newborn rats	[46, 47]
	IAV infection	Inactivates IAV and inhibits IAV-induced oxidative stress, inflammation, and IAV replication	[71]
	Lung cancer	Exerts anti-initiating effects in B(a)P-treated mice	[167]
Derivative BHBA	Lung cancer	Counteracts As(III)-induced cytoxicity in lung epithelial cells and inhibits tumor formation in vinyl carbamate-induced lung cancer	[169]
Sulforaphane	BPD	Inhibits hyperoxia-induced lung inflammation in neonatal mice	[48]
	RSV infection	Limits lung RSV replication and acute inflammation	[57]
	IAV infection	Inhibits oxidative stress and viral replication	[68]
	ARDS	Exerts protective effects on LPS and oleic acid-induced ARDS murine model	[95, 96]
	COPD	Counteracts CSE-induced oxidative injury in alveolar epithelial cells and augments bacteria phagocytosis by alveolar macrophages	[112, 113]
	Asthma	Inhibits DEPs-stimulated inflammation in airway epithelial cells, suppresses ovalbumin and Cl2-induced allergic airway inflammation in mice, and improves bronchoprotective response against MCh in asthmatics	[128–131]
	IPF	Provides antifibrosis effects in IPF fibroblasts even under TGF-β stimulation	[144]
	Lung cancer	Exerts suppressive effects on B(a)P-initiated lung carcinogenesis in mice and inhibits ROS production and malignant cell transformation in untransformed BEAS-2BR cells, but alleviates apoptosis resistance in cadmium-transformed BEAS-2BR cells	[164, 165]
tBHQ	RSV infection	Rescues decrease in Nrf2 activation induced by RSV	[56]
	ARDS	Protects against LPS-induced lung injury via regulating polarization of macrophages and balance of pro- or anti-inflammatory factors	[91]
Resveratrol	Pneumococcal infection	Ameliorates pneumococcal-induced oxidative stress in the airway epithelium	[75]
	ARDS	Protects against LPS-induced ARDS	[97]
	COPD	Protects against CS-induced lung injury	[118]
CDDO-Im	ARDS	Inhibits lung injury in hyperoxia and aspiration-induced ARDS	[92]
	COPD	Mitigates CS-induced lung oxidative stress, tissue destruction, emphysema development, and even pulmonary hypertension in mice	[110]
	Lung cancer	Reduces number, size, and severity of tumors in vinyl carbamate-induced lung carcinogenesis	[170]
Analogue CDDO-Me	Lung cancer	Reduces number, size, and severity of tumors more potently in vinyl carbamate-induced lung carcinogenesis	[170]
Andrographolide	COPD	Protects lung from CS-induced oxidative injury and suppresses NTHi-increased inflammatory and oxidative lung injury in a CS-predisposed mouse model that imitates COPD exacerbation	[115, 116]
Vitamin E	Asthma	Protects against IgE-induced asthma and alleviates asthma exacerbation stimulated by ozone in the OVA-induced murine model	[134, 135]
Isoform γ-tocotrienol	COPD	Protects against lung injury induced by CS	[120]
Emodin	IAV infection	Inhibits IAV-induced oxidative stress/inflammation and viral replication	[72]
	IPF	Suppresses BLM-induced fibrotic lung injuries in rats and reverses recombinant TGF-β1-stimulated EMT-like shifts in alveolar epithelial cultured cells	[145]
Quercetin	IPF	Induces antioxidant defense and suppresses inflammation in bleomycin-challenged BEAS-2B cells and inhibits TGF-β-induced fibrosis in fibroblasts	[146, 147]

3.2. Respiratory Infections. As the respiratory tract directly contacts various pathogens from internal and external environments, the associated infections are highly prevalent and variable. Thus, there is still an unmet need for new therapeutic methods for these diseases, especially for infections with viruses. Recent studies indicate that during the process of respiratory infections, the excessive ROS produced by phagocytic cells usually causes an imbalance between oxidants and antioxidants, which may contribute to the pathogenesis of infection-related respiratory diseases. As an essential fighter

against oxidative stress, Nrf2 is also considered to play a protective role in antiviral and antibacterial processes in several common infections of the respiratory tract.

3.2.1. Respiratory Syncytial Virus (RSV) Infection. Respiratory syncytial virus (RSV) is not only a leading cause of acute respiratory tract infections in infants and children but also an essential factor for substantial respiratory morbidity and mortality in the elderly [54, 55]. However, the details regarding the pathogenesis of RSV infection have not been clarified, and effective vaccines or treatments are still not available. In recent studies, researchers have discovered that rapidly generated ROS during RSV infection are involved in lung inflammatory and oxidative damage in this clinical disease [56]. Accordingly, treatment with antioxidants can ameliorate RSV-induced pulmonary inflammation in a mouse model of RSV infection [57]. While examining the antioxidant activity of Nrf2 signaling, researchers have also detected the activation of Nrf2 during RSV infection. These results show that RSV infection induces a clear decrease in Nrf2 levels and airway antioxidant enzymes in mouse lungs as well as in child nasopharyngeal secretions, which may be due to RSV-induced Nrf2 degradation [58–61]. RSV infection promotes Nrf2 ubiquitination and degradation via the proteasomal pathway, which may be plausible because the proteasomal inhibitors MG132 and lactacystin can restore RSV-reduced Nrf2 activity. More importantly, phenotypes of RSV infection are more severe in Nrf2-deficient mice than in wild-type mice, which are reflected in more severe bronchopulmonary inflammation and epithelial injury, as well as attenuated viral clearance [62]. Studies show that the more severe airway inflammation in $Nrf2^{-/-}$ mice induced by RSV is likely due to the enhanced concurrent activation of AP-1 and NF-κB. Additionally, Nrf2 deficiency makes mice more "Th1-like" with lower GSH and IFN-γ levels, which may impair virus clearance. Therefore, the Nrf2 pathway may be targeted for protection against RSV-induced lung injury.

In recent years, several Nrf2 inducers have been found to display beneficial effects on RSV infection. The potent Nrf2 inducer sulforaphane pretreatment significantly limits lung RSV replication and acute inflammation in wild-type but not Nrf2-deficient mice [62]. Butylated hydroxyanisole (BHA), a compound that is also known to induce the Nrf2 pathway, can accelerate viral clearance and ameliorate RSV-induced lung inflammation in mice, which indicates that the anti-RSV activity of BHA may be derived from Nrf2 activation [57, 63]. Furthermore, a phosphodiesterase 4 (PDE4) inhibitor, roflumilast N-oxide (RNO), can reverse RSV-induced Nrf2 loss, and such effects may be associated with its inhibition of cilia activity, mucin production, and inflammatory mediators in RSV infection in well-differentiated normal human bronchial epithelial cells (WD-HBE) [64]. Similarly, the Nrf2 inducer tert-butylhydroquinone (tBHQ) can also rescue the decrease in Nrf2 activation induced by RSV [61].

3.2.2. Influenza A Virus (IAV) Infection. Influenza A virus (IAV) infection ranging from upper respiratory infection to pneumonia has troubled individuals for a long time [65, 66]. Although some antiviral drugs, such as neuraminidase (NA) inhibitors, have been developed and applied, IAV infection is still a substantial threat to human health with significant morbidity and mortality due to its virus variability and resistant viral strains, including H1N1, H5N1, and H7N9 [67–69]. Thus, it is still a critical challenge to develop novel anti-influenza drugs to control influenza epidemics and pandemics in the future. In recent decades, studies have revealed that influenza viruses can induce oxidative stress, cytotoxicity, apoptosis, and inflammation in the respiratory system [70, 71]. Consistently, antioxidant compounds protect against injury induced by IAV via inhibiting virus replication and immune clearance and diminishing inflammatory mediator production [72]. Furthermore, the antioxidant pathway controlled by Nrf2 has been proven to be central in lung antioxidant defense against inflammation and injury induced by influenza virus both in human nasal epithelial cells and in mice [73, 74]. Studies have also shown that during IAV infection, Nrf2 protects human alveolar epithelial cells from the cytopathic effects induced by oxidative stress in an interferon-independent manner. The knockdown of Nrf2 makes ATI-like cells and ATII cells more vulnerable to injury, while the overexpression of Nrf2 decreases virus replication and related nucleoprotein expression [75]. However, cells from other vulnerable populations, including smokers and patients with COPD, will be needed in future studies.

To date, several Nrf2 inducers have been examined for their protective role in IAV infection. It has been recently reported that the Nrf2 inducer epigallocatechin gallate decreases influenza A/Bangkok/1/79 virus entry and replication in nasal epithelial cells; however, the inhibitory effect on replication is blocked when Nrf2 is knocked down [73], while curcumin, a classical Nrf2 inducer, not only inactivates IAV and suppresses IAV adsorption directly but also induces Nrf2 activation and inhibits IAV-induced oxidative stress, inflammation, and even IAV replication [76]. Similarly, the Nrf2 inducer sulforaphane and emodin can also lead to the significant inhibition of IAV-induced oxidative stress/inflammation and viral replication [73, 77]. Other reported compounds that may exert anti-influenza effects through the activation of Nrf2 also include bakuchiol and the rupestonic acid derivative, YZH-106 [67, 78].

3.2.3. Bacterial Infections. Recently, Nrf2 has been reported to have a beneficial role in infection with diverse bacteria, and the application of Nrf2 inducers may represent a novel treatment for respiratory tract bacterial infections, although related studies are limited.

Streptococcus is an important bacterium that colonizes the upper respiratory airways. This bacterium is not only the most common cause of community-acquired pneumonia but also an essential risk factor for several life-threatening diseases, including sepsis [79]. Previous studies have shown that *S. pneumoniae* can release several bacterial components to cause an enhanced oxidant burden on the lung epithelial surface, while the specific Nrf2 inducer resveratrol can ameliorate pneumococcal-induced oxidative stress in the airway

epithelium [80]. Similarly, Nrf2 can also effectively attenuate mouse lung injury and the mortality rate induced by *Staphylococcus aureus* and lung inflammation in *Haemophilus influenzae* infections [81, 82]. Furthermore, the preactivation of Nrf2 by high mobility group nucleosomal binding protein 2 (HMGN2) can attenuate the oxidative stress induced by *Pseudomonas aeruginosa* (PA) infection and inhibit the internalization of the bacteria in A549 cells [83]. Regrettably, there still lacks evidence for the application of Nrf2 activators in these infections.

Moreover, tuberculosis (TB) is a typical example of a specific infection and the top infectious disease killer worldwide. TB mainly refers to infections with *Mycobacterium tuberculosis*, especially in the respiratory tract [84, 85]. Recently, the role of oxidative stress and Nrf2 in TB infection has gained increasing attention. Oxidative stress has been proven to exist in the guinea pig model of tuberculosis along with the loss of Nrf2 activation, and the administration of NAC, an ROS scavenger and Nrf2 activator, significantly decreases bacterial burden and lung injury in TB infection, indicating a possible protective role for Nrf2 [86].

3.3. Acute Respiratory Distress Syndrome (ARDS). Acute respiratory distress syndrome (ARDS) refers to the severe clinical condition of dyspnea, refractory hypoxemia, and noncardiogenic pulmonary edema and affects millions of people throughout the world. According to existing statistics, the etiology of ARDS is fairly complex, varying from severe pneumonia, sepsis, and major trauma to massive transfusion, and severe pneumonia or sepsis may be the major cause [87]. Nevertheless, the typical pathological changes in ARDS still have similar characteristics, including acute diffuse lung inflammation and the disruption of the epithelial-vascular barrier caused by the damage of epithelial and endothelial integrity [88]. These changes cooperatively result in the destruction of lung structure and function, mainly shown as impaired lung compliance and gas exchange [89]. In spite of the improvement in supportive care today, unfortunately, ARDS is still responsible for significant morbidity and mortality, owing to its elusive therapeutic methods.

Although the mechanisms responsible for the pathogenesis of ARDS have not been fully understood, there is already evidence indicating the involvement of two essential and interactional factors, oxidative stress and inflammation. The overproduction of ROS or RNS, infiltration of inflammatory cells, and synthesis of inflammatory mediators have been proven to inflict severe lung damage. Recently, increasing evidence has demonstrated the importance of Nrf2 activation in coping with oxidative stress and inflammation in ARDS. A previous study showed that Nrf2 may act as a candidate gene of ARDS susceptibility for humans, as over 500 single-nucleotide polymorphisms (SNPs) of Nrf2 have been identified to date, and the risk of ARDS after severe trauma has increased in people with a functional NRF2 SNP in European and African American individuals [90]. For experiments conducted with animals, hyperoxia or LPS-induced ARDS are perhaps two of the most well-studied models that benefit from Nrf2 activation, and Nrf2-deficient mice are extensively used in studies focused on the beneficial role of Nrf2 in ARDS. In the hyperoxia-induced rodent model of ARDS, Nrf2 is supposed to be a susceptibility gene because functional SNPs have been found in hyperoxia-susceptible C57BL/6J (B6) and hyperoxia-resistant C3H/HeJ (C3) mice, and the B6C3F2 progeny is reported to have a hyperoxia-susceptibility promoter SNP [91, 92]. Furthermore, compared to wild-type mice, Nrf2-deficient mice are more likely to develop ARDS with enhanced lung hyperpermeability, epithelium injury, and inflammation under the stimulation of hyperoxia and butylated hydroxytoluene [93, 94]. A recent study also showed that the specific deletion of Nrf2 in the airway epithelium (Clara cell) in a hyperoxia-induced ARDS model is sufficient to promote the full development of acute lung injury and delays the subsequent resolution of inappropriate lung inflammation and epithelial sloughing [95]. For the LPS-induced ARDS model, in addition to increasing susceptibility and severity in Nrf2-deficient mice, it is also intriguing to find that Nrf2 may provide protective effects on LPS-induced ARDS via its promotion of M2 polarization in macrophages in a recent study adopting the Nrf2 activator tert-butylhydroquinone (tBHQ) and Nrf2 siRNA [96].

Therefore, in recent years, numerous investigations have focused on the protection against ARDS by Nrf2 activators, especially in hyperoxia- or LPS-induced ARDS models. The oleanane triterpenoid CDDO-imidazole (CDDO-Im) is reported to activate Nrf2/ARE signaling by breaking the interactions between Keap1 and Nrf2 in the cytosol and confer protective effects such as the inhibition of pulmonary hemorrhage, proteinaceous edema, and inflammatory cell infiltration on hyperoxia-induced ARDS. However, these protective effects are almost abolished in Nrf2-deficient mice [97]. Moreover, this compound also dampened aspiration-induced ARDS in another experiment. Importantly, its analogs, CDDO-methyl esters, have already been used in clinical trials for cancer treatment (http://clinicaltrials.gov), which brings the hope of the clinical application of CDDO-Im. Similarly, vitexin and aucubin both mitigate inflammatory and oxidative injury along with the suppression of inflammatory signaling, such as NLRP3/NF-κB, and the induction of Nrf2 in the LPS-induced ARDS model in wild-type but not Nrf2 knockdown mice/macrophages [98, 99]. The most well-recognized Nrf2 inducer, sulforaphane, also exerts protective effects on an ARDS murine model induced by LPS via inhibiting the increase of NF-κB and activating the Nrf2 pathway and is also reported to alleviate lung injury in another oleic acid-induced ARDS model [100, 101]. Indeed, a large number of compounds have been reported to act in a similar manner that activates Nrf2 signaling in an LPS-challenged ARDS model, such as resveratrol, alpha-lipoic acid, ethyl gallate, cordycepin, and syringin [102–107]. More intriguingly, another potent Nrf2 activator, tBHQ, protects against LPS-induced lung injury in an ARDS mouse model by promoting the polarization of M2 macrophages, suppressing the polarization of M1 macrophages and modulating the balance between proinflammatory and anti-inflammatory factors [96]. Furthermore, the transfection of Nrf2 is also able to reinforce the efficacy of human amniotic mesenchymal stem cells (hAMSCs) to inhibit inflammation, fibrosis, and lung injury

and promote hAMSCs to differentiate into type II alveolar epithelial (AT II) cells with enhanced activity of Nrf2 in an LPS-induced mouse ARDS model [108].

3.4. Chronic Obstructive Pulmonary Disease (COPD). Chronic obstructive pulmonary disease (COPD), a common chronic pulmonary disease characterized by irreversible airflow limitation, is projected to emerge as the third most prevalent cause of death by 2020 [109]. The pathological basis of COPD is associated with small airway obstruction and tissue remodeling, which may result from abnormal inflammation and lung parenchyma destruction in response to diverse stimuli, including genetic/environmental risk factors and their complicated interactions [110, 111]. Moreover, in recent decades, oxidative stress has also been recognized as an important predisposing factor that accounts for the pathogenesis of COPD, and cigarette smoking (CS) containing rich oxidants and other detrimental substances has long been regarded as a dominant environmental risk factor for COPD [112].

Exposure to cigarette smoke can lead to obvious oxidative stress, inflammation, and alveolar cell apoptosis. In healthy smokers, to cope with such high oxidant burden, there is a significant increase in numerous antioxidant defenses, among which Nrf2 is largely relied on. This reliance may be evidenced by the transient Nrf2 expression induced by CS in human airway cells. However, decreased levels of Nrf2 and its stabilizer DJ1 (PARK7) in lung tissues of COPD patients have been observed, and multiple human studies have demonstrated that the NRF2–KEAP1–BACH1 equilibrium in lung and alveolar macrophages is lowered in the population of aged smokers and COPD patients. Moreover, a cohort study on the relationship between polymorphisms of the Nrf2 gene and limitations of airflow in smokers also indicates that impaired Nrf2 may contribute to the development of COPD owing to excessive oxidant burden and apoptosis in the lungs [113]. The severity of COPD and the occurrence of respiratory failure may also be associated with the haplotype of the Nrf2 gene promoter, which affects its activity [114]. Consistent with these findings, Nrf2-deficient mice are more susceptible to cigarette smoke exposure and develop more severe lung emphysema and apoptosis, and the activity of antioxidant enzymes is repressed [40]. Additionally, the relationship between Nrf2 and COPD has also been addressed in vitro: Nrf2 knockdown increases 10% cigarette smoke exposure- (CSE-) induced apoptosis, while Nrf2 overexpression protects cells from apoptosis induced by CSE. Notably, the deletion of Keap1 and subsequent activation of Nrf2 signaling in Clara cells not only protects cells against oxidative stress ex vivo and in human epithelial cells but also suppresses oxidative stress and CS-induced inflammation in vivo [115]. Furthermore, Nrf2 has an influence on the infection-related acute exacerbations and therapeutic responses to corticosteroids in COPD. During COPD, oxidative stress has been reported to disrupt innate immune defenses and amplify inflammation. On the one hand, Nrf2 deletion impairs the clearance of respiratory infections via its effects on scavenger receptor macrophage receptor with collagenous structure (MARCO). On the other hand, a reduction in HDAC2 activity may lead to increased inflammation and corticosteroid resistance. A recent study has already shown that CS-exposed and LPS-induced $Nrf2^{-/-}$ mice display augmented lung inflammation that cannot be alleviated by steroids and revealed that deficits in Nrf2 may play an essential role in steroid resistance via HDAC2 repression: the recruitment of HDAC2 is important in mediating the anti-inflammatory activities of glucocorticoids by its interaction with promoters of proinflammatory genes, while Nrf2 deficiency may significantly reduce histone deacetylase 2 (HDAC2) level and deacetylase activity [116].

Therefore, novel therapies, such as Nrf2 activators, may show promise for therapy in COPD patients. Several Nrf2 activators have the potential to protect against exposure to cigarette smoke. For example, upon chronic CS exposure, CDDO-Im induces a more significant upregulation of Nrf2 and its target genes, mitigating CS-induced lung oxidative stress, tissue destruction, and even pulmonary hypertension in wild-type mice; however, these protective effects are not obviously observed in Nrf2-deficient mice. Additionally, it is interesting that CDDO-Im shows no inhibitory effect on CS-induced inflammation, despite its prevention of emphysema development, which may suggest that the inhibition of oxidative stress is enough to interrupt the development of emphysema [117]. Similarly, the WNT activator LiCl suppresses emphysematous changes and the lung inflammation induced by elastase or CSE, respectively, in WT mice along with the upregulation of Nrf2 signaling; however, such protective effects are almost abolished in elastase-challenged Nrf2-deficient mice. Additionally, the protective effects of the AMPK activator metformin on CSE-stimulated increases in inflammatory markers in Nrf2-deficient NHBE cells are not obviously observed [118]. Moreover, two well-known Nrf2 activators, sulforaphane and andrographolide, not only protect against CS/CSE-induced injury but also act in controlling infections that exacerbate COPD. In a recent study, sulforaphane was reported to counteract the oxidative injury induced by CSE with the activation of Nrf2 signaling in a rat alveolar epithelial cell line [119]. Furthermore, sulforaphane can augment the phagocytosis of bacteria (such as PA and NTHI isolated from COPD patients) by alveolar macrophages from COPD patients, but the ability is absent in Nrf2 siRNA-transfected macrophages, and similar results are obtained in wild-type and Nrf2 knockout mice. The study further shows that the Nrf2-dependent bacterial clearance by sulforaphane may be associated with Nrf2-mediated regulation of scavenger receptor MARCO but not dependent on the antioxidant glutathione [120]. However, although these findings suggest that sulforaphane protects against COPD and COPD exacerbation, the administration of sulforaphane to COPD patients unfortunately failed to induce Nrf2 target gene expression or affect the levels of other antioxidants or inflammation markers in a randomized, double-blind, placebo controlled trial in the US [121]. Another typical compound for COPD treatment, andrographolide, is a kind of lactone extracted from *Andrographis paniculata*. Recent studies reveal that andrographolide has the ability to protect the lungs from oxidative injury caused by cigarette smoke and suppress nontypeable *Haemophilus influenza*- (NTHi-)

increased inflammatory and oxidative lung injury in a CS-predisposed mouse model that imitates COPD exacerbation, while the mechanism of action may be attained by the induction of Nrf2-mediated cytoprotective responses [122, 123]. Intriguingly, this compound has already been applied as a drug component in some areas of China. In addition, influenza virus (FluV) is important in the acute exacerbations of COPD, and a recent study found that CS-exposed $Nrf2^{-/-}$ mice showed increased mortality and lung damage of increased severity after FluV infection [74]. Therefore, Nrf2 inducers that are effective in FluV infection, such as curcumin, may also provide protection to certain acute exacerbations of COPD. Indeed, there are many other compounds that have been reported to protect against lung tissue or epithelial injury induced by CS/CSE via the modulation of Nrf2, such as resveratrol, ursolic acid, the vitamin E isoform γ-tocotrienol, and aspirin-triggered resolvin D1 (AT-RvD1) [124–127].

3.5. Asthma. Asthma is a complex respiratory disorder characterized by chronic airway inflammation, airway hyperreactivity (AHR), and extensive and polytropic reversible airway obstruction [128]. Supported by previous studies, oxidative stress is highly involved in the pathogenesis of human asthma, and the oxidant burden plays a pivotal role in airway inflammation, AHR, and even insensitivity to steroids [129, 130]. As reported, patients with asthma may have more problems coping with oxidant burden than healthy people, which may be intimately related to impaired Nrf2 activity. Recent studies have also shown that Nrf2-driven GST is a possible marker for asthma susceptibility in humans: the homozygous GSTM1-null genotype increases the risk for asthma, but homozygous GSTP1 expression can protect against asthma [131, 132]. In mice, it has also been reported that Nrf2 deficiency significantly enhances ovalbumin or diesel exhaust particle- (DEP-) driven oxidative stress, airway inflammation, and AHR in an asthma model [41, 133]. In the OVA-challenged asthma model, the disruption of Nrf2 not only leads to increased levels of eosinophils, particularly in BALF and lung tissues, in $Nrf2^{-/-}$ mice but also causes higher levels of neutrophils, which may be responsible for airway remodeling in severe asthma. In turn, eosinophils and neutrophils generate more ROS to cause damage to the lung. In addition, the disruption of Nrf2 may also be associated with more obvious AHR, goblet cell hyperplasia, epithelial cell apoptosis, and an elevated level of Th2 cytokines in this model. In the DEP-challenged asthma model, $Nrf2^{-/-}$ mice also display increased eosinophils, AHR, IL-12, IL-13, and thymus and activation-regulated chemokines (TARC) in BALF. Moreover, when dendritic cells (DCs) from both Nrf2-deficient and wild-type cells were exposed to particulate matter (PM), Nrf2 successfully restrains the production of a proallergic phenotype via the inhibition of oxidative stress and Th2-directed proallergic immunity regulated by DCs [134]. During this process, the constitutive immune-polarizing cytokine milieu due to Nrf2 deficiency in DC plays an essential role in the augmenting promoting effect of PM on allergic sensitization. Taken together, Nrf2-mediated antioxidant responses can serve as an important determinant of susceptibility to asthma.

In recent decades, the protective role of Nrf2 inducers in asthma has been extensively investigated, and ovalbumin is used as a classical asthma inducer. Until recently, different studies have examined the protection of sulforaphane against asthma. Sulforaphane administration can suppress ovalbumin-induced allergic airway inflammation in mice, and a recent study further investigated the protective effects of sulforaphane in asthmatics. The results reveal that Nrf2 signaling may play an essential role in individuals whose bronchoprotective responses against methacholine (MCh) are improved by sulforaphane [135, 136]. Moreover, in a Cl_2-induced murine asthma model defined as irritant-induced asthma (IIA) and DEP-stimulated airway epithelial cells, sulforaphane administration with augmented Nrf2 activity inhibited airway inflammation [137, 138]. Notably, sulforaphane administration in healthy human subjects fails to increase Nrf2 and its target antioxidant gene expression but protects against neutrophilic airway inflammation induced by ozone [139]. Therefore, whether sulforaphane can be used clinically still needs more evidence from studies on different populations and allergens. Similarly, another Nrf2 inducer, sappanone A (SA), can protect against allergic airway inflammation induced by OVA, inhibiting the increase of inflammatory cells, cytokines, and OVA-specific IgE in BALF and restoring the level of IFN-γ, and the mechanism of action may derive from Nrf2-regulated Th1/Th2 balance [140]. The well-known antioxidant vitamin E (α-tocopherol) is also reported to protect against IgE-induced asthma by reversing the impairment of Nrf2 activity in alveolar macrophages in vivo and alleviating asthma exacerbation stimulated by ozone in the OVA-induced murine model via the Nrf2 pathway, although its effect is absent on OVA-induced asthma symptoms [141, 142]. Moreover, compounds such as vitamin D3, forsythiaside A (FSA), and mainstream anti-malarial drug artesunate all have similar effects on the amelioration of airway inflammation and AHR in OVA-induced asthma through activating the Nrf2/HO-1 signaling pathway [143–145].

3.6. Idiopathic Pulmonary Fibrosis (IPF). Idiopathic pulmonary fibrosis (IPF), an important representative of interstitial lung disease, is described as a chronic progressive lung disease with fibroproliferation and excessive extracellular matrix (ECM) deposition, which ultimately results in irreversible lung interstitial fibrosis and respiratory failure [146]. Although great efforts have been made to combat this disease, unfortunately, no treatment is reported to have actual benefits to improve the survival rate. Like many other chronic diseases, the pathogenesis of IPF is still unknown; however, oxidative stress is closely implicated according to previous studies, in which increased oxidative burden has already been observed in IPF patients [147, 148]. Oxidative stress-driven insults of lung tissue may come from different dimensions. For example, excessive ROS results in DNA damage and apoptosis in lung epithelial cells and drives IPF progression via triggering the activation and release of TGF-β1, which can accelerate ROS generation, existing

inflammation, and lung scarring as well as suppress antioxidant gene expression by mediating the interaction of Smad3-ATF3 with Nrf2. Moreover, ROS play an essential role in myofibroblastic differentiation, which is intimately involved in the pathogenesis of IPF. Therefore, it is not surprising that the dysregulation of Nrf2, a master regulator of oxidative stress, is reported to contribute greatly to pulmonary fibrosis [149]. In previous studies, Nrf2-deficient mice are more susceptible to the inducer of IPF-like lung fibrosis and bleomycin than wild-type mice, and these deficient mice more obviously display lung inflammation and fibrogenesis, along with increased fibrosis indices and decreased antioxidant response [38]. In vitro, Nrf2 siRNA leads to not only augmented oxidant burden but also increased myofibroblastic differentiation, whereas the knockdown of Keap1 induces the opposite effects. Nevertheless, evidence in humans for similar conclusions still remains to be explored, although augmented Nrf2 expression accompanied by oxidant markers is found in lung tissues from IPF patients, especially when the major inflammatory response and the oxidant nature in the common model induced by bleomycin still contrast with the histological features of human IPF.

Several Nrf2 activators have been studied to protect against pulmonary fibrosis. Pirfenidone (PFD) is a current approved drug for the therapy of IPF, and its antifibrosis activity in transforming growth factor-β- (TGF-β-) stimulated fibroblasts and bleomycin-challenged murine models is associated with the restoration of Nrf2/Bach1 equilibrium through Bach1 inhibition and Nrf2 activation [150]. The classical Nrf2 activator sulforaphane also shows antifibrosis effects on IPF fibroblasts in vitro by reversing the hallmarks of myofibroblastic differentiation (such as the increase of α-SMA, collagen I, fibroblast proliferation, migration, and contraction), even under TGF-β stimulation, and the antifibrosis activity is dependent on the restoration of redox balance by Nrf2 activation. However, studies have reported that sulforaphane cannot protect against bleomycin-induced lung fibrosis in mice, which may be related to the fact that this model does not address the effects of Nrf2 activators in lung fibrosis due to the absence of Nrf2 activation in mouse lung fibroblasts [151]. Another Nrf2 inducer, emodin, similarly suppressed BLM-induced fibrotic lung injuries in rats via the inhibition of collagen overproduction, epithelial-mesenchymal transition (EMT), and TGF-β and p-Smad expression. In addition, emodin can reverse recombinant TGF-β1-stimulated EMT-like shifts in alveolar epithelial-cultured cells [152]. Additionally, quercetin significantly induces antioxidant defense via Nrf2 activation and suppresses inflammation in bleomycin-challenged BEAS-2B cells, and its inhibitory effect on TGF-β-induced fibrosis in fibroblasts is also at least partly mediated by HO-1, a main downstream target of Nrf2 [153, 154]. Apart from the above compounds, the antifibrotic effects of berberine and epigallocatechin-3-gallate (EGCG) on bleomycin-induced pulmonary fibrosis in a murine model may also be at least partly mediated by the activation of Nrf2 signaling, accompanied by the inhibition of inflammation and other biological events [149, 155].

3.7. Lung Cancer. Lung cancer is reported to be the leading cause of cancer-related mortality worldwide [156]. In all types of lung cancer, non-small-cell lung carcinoma (NSCLC) is the most common and has been extensively studied on its different subtypes, while small-cell lung carcinoma (SCLC) only accounts for approximately 20% of lung cancer [157, 158]. As this disease is prone to be diagnosed late and the response to existing drugs is poor, patients with lung cancer always have poor prognoses. Therefore, novel possible drugs to prevent this disease and improve the outcomes are still in urgent need.

To decrease the incidence of cancer, people attempt to apply chemicals to detoxify or remove carcinogens [159]. Among these potential chemicals, Nrf2 inducers have been proven to have special advantages as chemopreventive agents [160]. However, the effects of Nrf2 on cancer pathogenesis are still controversial in the lungs [161]. In addition to cytoprotective functions, Nrf2 and its targeted genes also take part in several oncogenic signaling pathways, such as PI3K and K-ras, and connect with other transcription factors, structural proteins and epigenetic enzymes involved in the pathogenesis of cancer [162]. Nrf2 indeed displays opposing biological activities during carcinogenesis. Therefore, numerous studies have attempted to reveal the precise role of Nrf2 in lung cancer and have gained certain possible points. In a vinyl carbamate/urethane-induced and $Kras^{G12D}$-driven genetic lung cancer mouse model, Nrf2 is able to inhibit lung cancer initiation in a vinyl carbamate/urethane-induced model but promotes existing tumor progression in either model [163, 164]. Another study showed abnormal immunity associated with impaired Nrf2 in vinyl carbamate-induced lung cancer. Upon vinyl carbamate challenge, the lungs and tumors in Nrf2-deficient mice display the increased infiltration of immune cells that promote the development of tumors and upregulated gene expression that responds to the immune response. Data in patients with lung cancer also provide support for the importance of such findings [165]. The possible protective effects of Nrf2 on certain stages of lung cancer have also been observed in several other studies. For instance, coal tar pitch- (CTP-) induced malignant BEAS-2B cell transformation is accelerated when Nrf2 expression is knocked down [166]. In the Lewis lung carcinoma metastasis model of mice, Nrf2 is reported to prevent carcinoma metastasis because Nrf2-deficient mice have more metastatic nodules than wild-type mice [167]. These findings indicate that determining whether Nrf2 activation is protective may depend on the stage of lung cancer. Nevertheless, although Nrf2 exerts a chemopreventive effect on certain lung cancer mouse models, related clinical evidence is still lacking. In contrast, some clinical evidence indicates that the constitutive upregulation of Nrf2 is related not only to cancer progression but also to resistance to traditional therapy and worse outcomes in NSCLC [164, 168]. According to an investigation conducted by The Cancer Genome Atlas (TCGA), changes in the Keap1/Nrf2/Cullin3 pathway exist in a third of squamous cell lung cancer, while the rate may be variable due to the number of study subjects and cancer subtypes in different studies [169]. Keap1 dysfunction due to somatic mutation/methylation and abnormal Nrf2

activation in NSCLC patients may be related to worse progress-free and overall survival. Conversely, silencing Nrf2 by siRNA in cells inhibits tumor growth and reverses chemotherapeutic resistance. Similarly, Nrf2 activation induced by mutant p53 in NSCLC mediates the resistance of cisplatin-based chemotherapy and leads to poor prognosis [170].

Considering the double effect of Nrf2 on lung cancer, the application of the Nrf2 activator in the early stages of carcinogenesis to prevent cancer may be more promising. Indeed, several well-known Nrf2 inducers have been studied in this respect. One of the most potent activators of Nrf2, sulforaphane, activates Nrf2 signaling via its impact on Keap1 and exerts suppressive effects on benzo(a)pyrene- (B(a)P-) initiated lung carcinogenesis in mice [171]. Intriguingly, another study revealed that in untransformed BEAS-2BR cells, sulforaphane activates the Nrf2 pathway and inhibits ROS production, ultimately repressing malignant cell transformation. However, in cadmium-transformed BEAS-2BR cells, sulforaphane suppresses the constitutive activation of Nrf2 and alleviates apoptosis resistance. The dual effects of sulforaphane make this compound a possible ideal agent for protection against cadmium-induced carcinogenesis, including lung carcinogenesis [172]. Curcumin, another classical Nrf2 activator, is reported to have chemopreventive efficacy in different models and be a radiotherapy/chemotherapy sensitizer or protector [173]. A recent study revealed that curcumin exerts anti-initiating effects via reducing phase I and inducing phase II enzymes in B[a]P-treated mice [174]. However, curcumin displayed limited effects in clinical trials due to its poor bioavailability [175]. To overcome such disadvantages, researchers have studied its derivatives with better bioavailability. Intriguingly, one of its major derivatives, bis[2-hydroxybenzylidene]acetone (BHBA), also significantly upregulates Nrf2 signaling, counteracts sodium arsenite- [As(III)-] induced cytotoxicity in a lung epithelial cell line and inhibits tumor formation in a vinyl carbamate-induced lung adenocarcinoma model of A/J mice [176]. Moreover, CDDO-methyl ester (CDDO-Me), a synthetic oleanolic triterpenoid similar to CDDO-Im, has been reported to significantly activate the Nrf2 pathway and reduce the number, size, and severity of tumors in vinyl carbamate-induced lung carcinogenesis in A/J mice. Additionally, CDDO-Im has semblable activity, although it seems less potent [177]. In addition, the inhalation of the Nrf2 inducer oltipraz can also suppress B(a)P-initiated lung adenocarcinoma in A/J mice [178].

4. Concluding Remarks

Oxidative stress has been reported to participate in the occurrence and development of various respiratory diseases, including BPD, respiratory infection, ARDS, COPD, asthma, IPF, and lung cancer. Thus, the master antioxidant transcription factor Nrf2, which is abundant in the lungs, drives diverse cellular defense pathways to counteract detrimental stimuli that are involved in the pathogenesis of these pulmonary disorders, including oxidative stress, inflammation, apoptosis, and carcinogenesis. Currently, Nrf2-deficient mice have provided an effective tool for investigating Nrf2 function in oxidative pulmonary disease models and have led to a better understanding of Nrf2 function in the pathogenesis of related pulmonary diseases. In fact, researchers have adopted three different genetic backgrounds (ICR, C57BL/6J, and Balbc/J) and lung-specific conditional knockout mice to conduct experiments to obtain insight into the protective roles of Nrf2. Therefore, in recent decades, a large number of studies have focused on the protective effects of Nrf2 activators on the above pulmonary diseases and found that certain compounds may provide new strategies to intervene or prevent oxidative airway diseases via Nrf2 induction.

Disclosure

The authors alone are responsible for the content of this manuscript.

Conflicts of Interest

The authors report no conflicts of interest.

Acknowledgments

This work was in part supported by the National Natural Science Foundation of China (Grant No. 81603174) and the General Financial Grant from the China Postdoctoral Science Foundation (Grant No. 168847).

References

[1] H. Y. Cho and S. R. Kleeberger, "Noblesse oblige: Nrf2 functions in the airways," *American Journal of Respiratory Cell and Molecular Biology*, vol. 50, no. 5, pp. 844–847, 2014.

[2] H. Y. Cho and S. R. Kleeberger, "Nrf2 protects against airway disorders," *Toxicology and Applied Pharmacology*, vol. 244, no. 1, pp. 43–56, 2010.

[3] H. Kumar, H. W. Lim, S. V. More et al., "The role of free radicals in the aging brain and Parkinson's disease: convergence and parallelism," *International Journal of Molecular Sciences*, vol. 13, no. 8, pp. 10478–10504, 2012.

[4] I. Fridovich, "Oxygen toxicity: a radical explanation," *The Journal of Experimental Biology*, vol. 201, Part 8, pp. 1203–1209, 1998.

[5] B. Halliwell, J. M. Gutteridge, and C. E. Cross, "Free radicals, antioxidants, and human disease: where are we now?," *The Journal of Laboratory and Clinical Medicine*, vol. 119, no. 6, pp. 598–620, 1992.

[6] O. D. Saugstad, "Bronchopulmonary dysplasia-oxidative stress and antioxidants," *Seminars in Neonatology*, vol. 8, no. 1, pp. 39–49, 2003.

[7] A. Giudice and M. Montella, "Activation of the Nrf2-are signaling pathway: a promising strategy in cancer prevention," *BioEssays*, vol. 28, no. 2, pp. 169–181, 2006.

[8] T. Nguyen, P. J. Sherratt, H. C. Huang, C. S. Yang, and C. B. Pickett, "Increased protein stability as a mechanism that enhances Nrf2-mediated transcriptional activation of the antioxidant response element. Degradation of Nrf2 by the 26 s proteasome," *The Journal of Biological Chemistry*, vol. 278, no. 7, pp. 4536–4541, 2003.

[9] Y. Zhang and G. B. Gordon, "A strategy for cancer prevention: stimulation of the Nrf2-are signaling pathway," *Molecular Cancer Therapeutics*, vol. 3, no. 7, pp. 885–893, 2004.

[10] K. Itoh, N. Wakabayashi, Y. Katoh et al., "Keap1 represses nuclear activation of antioxidant responsive elements by Nrf2 through binding to the amino-terminal Neh2 domain," *Genes & Development*, vol. 13, no. 1, pp. 76–86, 1999.

[11] A. K. Jaiswal, "Nrf2 signaling in coordinated activation of antioxidant gene expression," *Free Radical Biology & Medicine*, vol. 36, no. 10, pp. 1199–1207, 2004.

[12] T. W. Kensler, N. Wakabayashi, and S. Biswal, "Cell survival responses to environmental stresses via the Keap1-Nrf2-ARE pathway," *Annual Review of Pharmacology and Toxicology*, vol. 47, no. 1, pp. 89–116, 2007.

[13] A. Kobayashi, M. I. Kang, H. Okawa et al., "Oxidative stress sensor Keap1 functions as an adaptor for Cul3-based E3 ligase to regulate proteasomal degradation of Nrf2," *Molecular and Cellular Biology*, vol. 24, no. 16, pp. 7130–7139, 2004.

[14] J. W. Kaspar, S. K. Niture, and A. K. Jaiswal, "Nrf2:INrf2 (keap1) signaling in oxidative stress," *Free Radical Biology & Medicine*, vol. 47, no. 9, pp. 1304–1309, 2009.

[15] D. D. Zhang, "Mechanistic studies of the Nrf2-Keap1 signaling pathway," *Drug Metabolism Reviews*, vol. 38, no. 4, pp. 769–789, 2008.

[16] H. Okawa, H. Motohashi, A. Kobayashi, H. Aburatani, T. W. Kensler, and M. Yamamoto, "Hepatocyte-specific deletion of the keap1 gene activates Nrf2 and confers potent resistance against acute drug toxicity," *Biochemical and Biophysical Research Communications*, vol. 339, no. 1, pp. 79–88, 2006.

[17] L. Baird and A. T. Dinkova-Kostova, "The cytoprotective role of the Keap1-Nrf2 pathway," *Archives of Toxicology*, vol. 85, no. 4, pp. 241–272, 2011.

[18] T. Suzuki and M. Yamamoto, "Molecular basis of the Keap1-Nrf2 system," *Free Radical Biology and Medicine*, vol. 88, no. Part B, pp. 93–100, 2015.

[19] K. I. Tong, Y. Katoh, H. Kusunoki, K. Itoh, T. Tanaka, and M. Yamamoto, "Keap1 recruits Neh2 through binding to ETGE and DLG motifs: characterization of the two-site molecular recognition model," *Molecular and Cellular Biology*, vol. 26, no. 8, pp. 2887–2900, 2006.

[20] A. T. Dinkova-Kostova, M. A. Massiah, R. E. Bozak, R. J. Hicks, and P. Talalay, "Potency of Michael reaction acceptors as inducers of enzymes that protect against carcinogenesis depends on their reactivity with sulfhydryl groups," *Proceedings of the National Academy of Sciences of the United States of America*, vol. 98, no. 6, pp. 3404–3409, 2001.

[21] T. Suzuki and M. Yamamoto, "Stress-sensing mechanisms and the physiological roles of the Keap1-Nrf2 system during cellular stress," *The Journal of Biological Chemistry*, vol. 292, no. 41, pp. 16817–16824, 2017.

[22] M. Kobayashi, L. Li, N. Iwamoto et al., "The antioxidant defense system Keap1-Nrf2 comprises a multiple sensing mechanism for responding to a wide range of chemical compounds," *Molecular and Cellular Biology*, vol. 29, no. 2, pp. 493–502, 2008.

[23] M. C. Jaramillo and D. D. Zhang, "The emerging role of the Nrf2-Keap1 signaling pathway in cancer," *Genes & Development*, vol. 27, no. 20, pp. 2179–2191, 2013.

[24] A. Kobayashi, M. I. Kang, Y. Watai et al., "Oxidative and electrophilic stresses activate Nrf2 through inhibition of ubiquitination activity of Keap1," *Molecular and Cellular Biology*, vol. 26, no. 1, pp. 221–229, 2005.

[25] A. I. Rojo, M. R. de Sagarra, and A. Cuadrado, "GSK-3β down-regulates the transcription factor Nrf2 after oxidant damage: relevance to exposure of neuronal cells to oxidative stress," *Journal of Neurochemistry*, vol. 105, no. 1, pp. 192–202, 2008.

[26] M. Kobayashi and M. Yamamoto, "Nrf2-keap1 regulation of cellular defense mechanisms against electrophiles and reactive oxygen species," *Advances in Enzyme Regulation*, vol. 46, no. 1, pp. 113–140, 2006.

[27] R. Yu, S. Mandlekar, W. Lei, W. E. Fahl, T. H. Tan, and A. N. T. Kong, "P38 mitogen-activated protein kinase negatively regulates the induction of phase ii drug-metabolizing enzymes that detoxify carcinogens," *The Journal of Biological Chemistry*, vol. 275, no. 4, pp. 2322–2327, 2000.

[28] H. C. Huang, T. Nguyen, and C. B. Pickett, "Phosphorylation of Nrf2 at Ser-40 by protein kinase C regulates antioxidant response element-mediated transcription," *The Journal of Biological Chemistry*, vol. 277, no. 45, pp. 42769–42774, 2002.

[29] R. Yu, W. Lei, S. Mandlekar et al., "Role of a mitogen-activated protein kinase pathway in the induction of phase ii detoxifying enzymes by chemicals," *The Journal of Biological Chemistry*, vol. 274, no. 39, pp. 27545–27552, 1999.

[30] T. Jiang, B. Harder, M. Rojo de la Vega, P. K. Wong, E. Chapman, and D. D. Zhang, "P62 links autophagy and Nrf2 signaling," *Free Radical Biology and Medicine*, vol. 88, no. Part B, pp. 199–204, 2015.

[31] P. Rada, A. I. Rojo, S. Chowdhry, M. McMahon, J. D. Hayes, and A. Cuadrado, "Scf/{beta}-TrCP promotes glycogen synthase kinase 3-dependent degradation of the Nrf2 transcription factor in a keap1-independent manner," *Molecular and Cellular Biology*, vol. 31, no. 6, pp. 1121–1133, 2011.

[32] A. Cuadrado, "Structural and functional characterization of Nrf2 degradation by glycogen synthase kinase 3/β-TrCP," *Free Radical Biology and Medicine*, vol. 88, no. Part B, pp. 147–157, 2015.

[33] J. Y. Lo, B. N. Spatola, and S. P. Curran, "WDR23 regulates NRF2 independently of KEAP1," *PLoS Genetics*, vol. 13, no. 4, article e1006762, 2017.

[34] R. K. Thimmulappa, K. H. Mai, S. Srisuma, T. W. Kensler, M. Yamamoto, and S. Biswal, "Identification of Nrf2-regulated genes induced by the chemopreventive agent sulforaphane by oligonucleotide microarray," *Cancer Research*, vol. 62, no. 18, pp. 5196–5203, 2002.

[35] J. M. Lee, M. J. Calkins, K. Chan, Y. W. Kan, and J. A. Johnson, "Identification of the NF-E2-related factor-2-dependent genes conferring protection against oxidative stress in primary cortical astrocytes using oligonucleotide microarray analysis," *The Journal of Biological Chemistry*, vol. 278, no. 14, pp. 12029–12038, 2003.

[36] P. Talalay, A. T. Dinkova-Kostova, and W. D. Holtzclaw, "Importance of phase 2 gene regulation in protection against electrophile and reactive oxygen toxicity and carcinogenesis," *Advances in Enzyme Regulation*, vol. 43, no. 1, pp. 121–134, 2003.

[37] Z. Sun, T. Wu, F. Zhao, A. Lau, C. M. Birch, and D. D. Zhang, "KPNA6 (importin {alpha}7)-mediated nuclear import of Keap1 represses the Nrf2-dependent antioxidant response," *Molecular and Cellular Biology*, vol. 31, no. 9, pp. 1800–1811, 2011.

[38] H.-Y. Cho, S. P. M. Reddy, M. Yamamoto, and S. R. Kleeberger, "The transcription factor Nrf2 protects against pulmonary fibrosis," *The FASEB Journal*, vol. 18, no. 11, pp. 1258–1260, 2004.

[39] Y. Ishii, K. Itoh, Y. Morishima et al., "Transcription factor Nrf2 plays a pivotal role in protection against elastase-induced pulmonary inflammation and emphysema," *Journal of Immunology*, vol. 175, no. 10, pp. 6968–6975, 2005.

[40] T. Rangasamy, C. Y. Cho, R. K. Thimmulappa et al., "Genetic ablation of Nrf2 enhances susceptibility to cigarette smoke-induced emphysema in mice," *The Journal of Clinical Investigation*, vol. 114, no. 9, pp. 1248–1259, 2004.

[41] T. Rangasamy, J. Guo, W. A. Mitzner et al., "Disruption of Nrf2 enhances susceptibility to severe airway inflammation and asthma in mice," *The Journal of Experimental Medicine*, vol. 202, no. 1, pp. 47–59, 2005.

[42] I. Rahman, S. K. Biswas, and P. A. Kirkham, "Regulation of inflammation and redox signaling by dietary polyphenols," *Biochemical Pharmacology*, vol. 72, no. 11, pp. 1439–1452, 2006.

[43] A. H. Jobe and E. Bancalari, "Bronchopulmonary dysplasia," *American Journal of Respiratory and Critical Care Medicine*, vol. 163, no. 7, pp. 1723–1729, 2001.

[44] E. Baraldi and M. Filippone, "Chronic lung disease after premature birth," *The New England Journal of Medicine*, vol. 357, no. 19, pp. 1946–1955, 2007.

[45] W. H. Northway Jr., R. B. Moss, K. B. Carlisle et al., "Late pulmonary sequelae of bronchopulmonary dysplasia," *The New England Journal of Medicine*, vol. 323, no. 26, pp. 1793–1799, 1990.

[46] A. H. Jobe and M. Ikegami, "Mechanisms initiating lung injury in the preterm," *Early Human Development*, vol. 53, no. 1, pp. 81–94, 1998.

[47] S. McGrath-Morrow, T. Lauer, M. Yee et al., "Nrf2 increases survival and attenuates alveolar growth inhibition in neonatal mice exposed to hyperoxia," *American Journal of Physiology-Lung Cellular and Molecular Physiology*, vol. 296, no. 4, pp. L565–L573, 2009.

[48] H. Y. Cho, B. van Houten, X. Wang et al., "Targeted deletion of Nrf2 impairs lung development and oxidant injury in neonatal mice," *Antioxidants & Redox Signaling*, vol. 17, no. 8, pp. 1066–1082, 2012.

[49] Q. Li, R. Li, S. B. Wall et al., "Aurothioglucose does not improve alveolarization or elicit sustained Nrf2 activation in C57BL/6 models of bronchopulmonary dysplasia," *American Journal of Physiology-Lung Cellular and Molecular Physiology*, vol. 314, no. 5, pp. L736–L742, 2018.

[50] Q. Li, S. B. Wall, C. Ren et al., "Thioredoxin reductase inhibition attenuates neonatal hyperoxic lung injury and enhances nuclear factor E2-related factor 2 activation," *American Journal of Respiratory Cell and Molecular Biology*, vol. 55, no. 3, pp. 419–428, 2016.

[51] R. Sakurai, Y. Li, J. S. Torday, and V. K. Rehan, "Curcumin augments lung maturation, preventing neonatal lung injury by inhibiting TGF-β signaling," *American Journal of Physiology-Lung Cellular and Molecular Physiology*, vol. 301, no. 5, pp. L721–L730, 2011.

[52] R. Sakurai, P. Villarreal, S. Husain et al., "Curcumin protects the developing lung against long-term hyperoxic injury," *American Journal of Physiology-Lung Cellular and Molecular Physiology*, vol. 305, no. 4, pp. L301–L311, 2013.

[53] S. A. McGrath-Morrow, T. Lauer, J. M. Collaco et al., "Transcriptional responses of neonatal mouse lung to hyperoxia by Nrf2 status," *Cytokine*, vol. 65, no. 1, pp. 4–9, 2014.

[54] C. B. Hall, G. A. Weinberg, M. K. Iwane et al., "The burden of respiratory syncytial virus infection in young children," *The New England Journal of Medicine*, vol. 360, no. 6, pp. 588–598, 2009.

[55] C. B. Hall, "Respiratory syncytial virus and parainfluenza virus," *The New England Journal of Medicine*, vol. 344, no. 25, pp. 1917–1928, 2001.

[56] A. Casola, N. Burger, T. Liu, M. Jamaluddin, A. R. Brasier, and R. P. Garofalo, "Oxidant tone regulates RANTES gene expression in airway epithelial cells infected with respiratory syncytial virus. Role in viral-induced interferon regulatory factor activation," *The Journal of Biological Chemistry*, vol. 276, no. 23, pp. 19715–19722, 2001.

[57] S. M. Castro, A. Guerrero-Plata, G. Suarez-Real et al., "Antioxidant treatment ameliorates respiratory syncytial virus-induced disease and lung inflammation," *American Journal of Respiratory and Critical Care Medicine*, vol. 174, no. 12, pp. 1361–1369, 2006.

[58] T. Ivanciuc, E. Sbrana, A. Casola, and R. P. Garofalo, "Protective role of nuclear factor erythroid 2-related factor 2 against respiratory syncytial virus and human metapneumovirus infections," *Frontiers in Immunology*, vol. 9, no. 854, 2018.

[59] Y. M. Hosakote, T. Liu, S. M. Castro, R. P. Garofalo, and A. Casola, "Respiratory syncytial virus induces oxidative stress by modulating antioxidant enzymes," *American Journal of Respiratory Cell and Molecular Biology*, vol. 41, no. 3, pp. 348–357, 2009.

[60] N. Komaravelli, B. Tian, T. Ivanciuc et al., "Respiratory syncytial virus infection down-regulates antioxidant enzyme expression by triggering deacetylation-proteasomal degradation of Nrf2," *Free Radical Biology and Medicine*, vol. 88, no. Part B, pp. 391–403, 2015.

[61] Y. M. Hosakote, P. D. Jantzi, D. L. Esham et al., "Viral-mediated inhibition of antioxidant enzymes contributes to the pathogenesis of severe respiratory syncytial virus bronchiolitis," *American Journal of Respiratory and Critical Care Medicine*, vol. 183, no. 11, pp. 1550–1560, 2011.

[62] H. Y. Cho, F. Imani, L. Miller-DeGraff et al., "Antiviral activity of Nrf2 in a murine model of respiratory syncytial virus disease," *American Journal of Respiratory and Critical Care Medicine*, vol. 179, no. 2, pp. 138–150, 2009.

[63] C. Xu, C. Y.-T. Li, and A.-N. T. Kong, "Induction of phase I, II and III drug metabolism/transport by xenobiotics," *Archives of Pharmacal Research*, vol. 28, no. 3, pp. 249–268, 2005.

[64] M. Mata, I. Martinez, J. A. Melero, H. Tenor, and J. Cortijo, "Roflumilast inhibits respiratory syncytial virus infection in human differentiated bronchial epithelial cells," *PLoS One*, vol. 8, no. 7, article e69670, 2013.

[65] H. Guo, P. Kumar, T. M. Moran, A. Garcia-Sastre, Y. Zhou, and S. Malarkannan, "The functional impairment of natural killer cells during influenza virus infection," *Immunology and Cell Biology*, vol. 87, no. 8, pp. 579–589, 2009.

[66] M. D. Tate, H. C. Schilter, A. G. Brooks, and P. C. Reading, "Responses of mouse airway epithelial cells and alveolar macrophages to virulent and avirulent strains of influenza a virus," *Viral Immunology*, vol. 24, no. 2, pp. 77–88, 2011.

[67] M. Shoji, Y. Arakaki, T. Esumi et al., "Bakuchiol is a phenolic isoprenoid with novel enantiomer-selective anti-influenza A virus activity involving Nrf2 activation," *The Journal of Biological Chemistry*, vol. 290, no. 46, pp. 28001–28017, 2015.

[68] P. A. Reece, "Neuraminidase inhibitor resistance in influenza viruses," *Journal of Medical Virology*, vol. 79, no. 10, pp. 1577–1586, 2007.

[69] F. G. Hayden, R. L. Atmar, M. Schilling et al., "Use of the selective oral neuraminidase inhibitor oseltamivir to prevent influenza," *The New England Journal of Medicine*, vol. 341, no. 18, pp. 1336–1343, 1999.

[70] M. Phillips, R. N. Cataneo, A. Chaturvedi et al., "Effect of influenza vaccination on oxidative stress products in breath," *Journal of Breath Research*, vol. 4, no. 2, article 026001, 2010.

[71] S. Fukuyama and Y. Kawaoka, "The pathogenesis of influenza virus infections: the contributions of virus and host factors," *Current Opinion in Immunology*, vol. 23, no. 4, pp. 481–486, 2011.

[72] M. Mata, E. Morcillo, C. Gimeno, and J. Cortijo, "N-Acetyl-l-cysteine (NAC) inhibit mucin synthesis and pro-inflammatory mediators in alveolar type ii epithelial cells infected with influenza virus a and b and with respiratory syncytial virus (RSV)," *Biochemical Pharmacology*, vol. 82, no. 5, pp. 548–555, 2011.

[73] M. J. Kesic, S. O. Simmons, R. Bauer, and I. Jaspers, "Nrf2 expression modifies influenza A entry and replication in nasal epithelial cells," *Free Radical Biology & Medicine*, vol. 51, no. 2, pp. 444–453, 2011.

[74] Y. Yageta, Y. Ishii, Y. Morishima et al., "Role of nrf2 in host defense against influenza virus in cigarette smoke-exposed mice," *Journal of Virology*, vol. 85, no. 10, pp. 4679–4690, 2011.

[75] B. Kosmider, E. M. Messier, W. J. Janssen et al., "Nrf2 protects human alveolar epithelial cells against injury induced by influenza a virus," *Respiratory Research*, vol. 13, no. 1, p. 43, 2012.

[76] J. Dai, L. Gu, Y. Su et al., "Inhibition of curcumin on influenza A virus infection and influenzal pneumonia via oxidative stress, TLR2/4, p38/JNK MAPK and NF-κB pathways," *International Immunopharmacology*, vol. 54, pp. 177–187, 2018.

[77] J. P. Dai, Q. W. Wang, Y. Su et al., "Emodin inhibition of influenza a virus replication and influenza viral pneumonia via the Nrf2, TLR4, p38/JNK and NF-kappaB pathways," *Molecules*, vol. 22, no. 10, 2017.

[78] L. L. Ma, H. Q. Wang, P. Wu et al., "Rupestonic acid derivative YZH-106 suppresses influenza virus replication by activation of heme oxygenase-1-mediated interferon response," *Free Radical Biology and Medicine*, vol. 96, pp. 347–361, 2016.

[79] T. van der Poll and S. M. Opal, "Pathogenesis, treatment, and prevention of pneumococcal pneumonia," *The Lancet*, vol. 374, no. 9700, pp. 1543–1556, 2009.

[80] J. Zahlten, Y. J. Kim, J. M. Doehn et al., "Streptococcus pneumoniae-induced oxidative stress in lung epithelial cells depends on pneumococcal autolysis and is reversible by resveratrol," *The Journal of Infectious Diseases*, vol. 211, no. 11, pp. 1822–1830, 2015.

[81] N. C. MacGarvey, H. B. Suliman, R. R. Bartz et al., "Activation of mitochondrial biogenesis by heme oxygenase-1-mediated NF-E2-related factor-2 induction rescues mice from lethal Staphylococcus aureus sepsis," *American Journal of Respiratory and Critical Care Medicine*, vol. 185, no. 8, pp. 851–861, 2012.

[82] A. A. Lugade, R. R. Vethanayagam, M. Nasirikenari, P. N. Bogner, B. H. Segal, and Y. Thanavala, "Nrf2 regulates chronic lung inflammation and b-cell responses to nontypeable haemophilus influenzae," *American Journal of Respiratory Cell and Molecular Biology*, vol. 45, no. 3, pp. 557–565, 2011.

[83] K. Liu, X. Wang, K. Sha et al., "Nuclear protein HMGN2 attenuates pyocyanin-induced oxidative stress via Nrf2 signaling and inhibits pseudomonas aeruginosa internalization in A549 cells," *Free Radical Biology and Medicine*, vol. 108, pp. 404–417, 2017.

[84] C. Chen, D. Pung, V. Leong et al., "Induction of detoxifying enzymes by garlic organosulfur compounds through transcription factor Nrf2: effect of chemical structure and stress signals," *Free Radical Biology & Medicine*, vol. 37, no. 10, pp. 1578–1590, 2004.

[85] T. R. Frieden, T. R. Sterling, S. S. Munsiff, C. J. Watt, and C. Dye, "Tuberculosis," *The Lancet*, vol. 362, no. 9387, pp. 887–899, 2003.

[86] G. S. Palanisamy, N. M. Kirk, D. F. Ackart, C. A. Shanley, I. M. Orme, and R. J. Basaraba, "Evidence for oxidative stress and defective antioxidant response in guinea pigs with tuberculosis," *PLoS One*, vol. 6, no. 10, article e26254, 2011.

[87] E. L. Costa, I. A. Schettino, and G. P. Schettino, "The lung in sepsis: guilty or innocent?," *Endocrine, Metabolic & Immune Disorders Drug Targets*, vol. 6, no. 2, pp. 213–216, 2006.

[88] E. R. Johnson and M. A. Matthay, "Acute lung injury: epidemiology, pathogenesis, and treatment," *Journal of Aerosol Medicine and Pulmonary Drug Delivery*, vol. 23, no. 4, pp. 243–252, 2010.

[89] L. B. Ware and M. A. Matthay, "The acute respiratory distress syndrome," *The New England Journal of Medicine*, vol. 342, no. 18, pp. 1334–1349, 2000.

[90] J. M. Marzec, J. D. Christie, S. P. Reddy et al., "Functional polymorphisms in the transcription factor Nrf2 in humans increase the risk of acute lung injury," *The FASEB Journal*, vol. 21, no. 9, pp. 2237–2246, 2007.

[91] H. Y. Cho, "Genomic structure and variation of nuclear factor (erythroid-derived 2)-like 2," *Oxidative Medicine and Cellular Longevity*, vol. 2013, Article ID 286524, 24 pages, 2013.

[92] H.-Y. Cho, A. E. Jedlicka, S. P. M. Reddy, L.-Y. Zhang, T. W. Kensler, and S. R. Kleeberger, "Linkage analysis of susceptibility to hyperoxia. Nrf2 is a candidate gene," *American Journal of Respiratory Cell and Molecular Biology*, vol. 26, no. 1, pp. 42–51, 2002.

[93] K. Chan and Y. W. Kan, "Nrf2 is essential for protection against acute pulmonary injury in mice," *Proceedings of the National Academy of Sciences of the United States of America*, vol. 96, no. 22, pp. 12731–12736, 1999.

[94] H.-Y. Cho, A. E. Jedlicka, S. P. M. Reddy et al., "Role of Nrf2 in protection against hyperoxic lung injury in mice," *American Journal of Respiratory Cell and Molecular Biology*, vol. 26, no. 2, pp. 175–182, 2002.

[95] N. M. Reddy, H. R. Potteti, T. J. Mariani, S. Biswal, and S. P. Reddy, "Conditional deletion of Nrf2 in airway epithelium exacerbates acute lung injury and impairs the resolution of inflammation," *American Journal of Respiratory Cell and Molecular Biology*, vol. 45, no. 6, pp. 1161–1168, 2011.

[96] J. Wei, G. Chen, X. Shi et al., "Nrf2 activation protects against intratracheal LPS induced mouse/murine acute respiratory distress syndrome by regulating macrophage polarization," *Biochemical and Biophysical Research Communications*, vol. 500, no. 3, pp. 790–796, 2018.

[97] N. M. Reddy, V. Suryanaraya, M. S. Yates et al., "The triterpenoid CDDO-imidazolide confers potent protection against hyperoxic acute lung injury in mice," *American Journal of Respiratory and Critical Care Medicine*, vol. 180, no. 9, pp. 867–874, 2009.

[98] Y. L. Qiu, X. N. Cheng, F. Bai, L. Y. Fang, H. Z. Hu, and D. Q. Sun, "Aucubin protects against lipopolysaccharide-induced acute pulmonary injury through regulating Nrf2 and AMPK pathways," *Biomedicine & Pharmacotherapy*, vol. 106, pp. 192–199, 2018.

[99] Y. Lu, T. Yu, J. Liu, and L. Gu, "Vitexin attenuates lipopolysaccharide-induced acute lung injury by controlling the Nrf2 pathway," *PLoS One*, vol. 13, no. 4, article e0196405, 2018.

[100] Z. Sun, Z. Niu, S. Wu, and S. Shan, "Protective mechanism of sulforaphane in Nrf2 and anti-lung injury in ARDS rabbits," *Experimental and Therapeutic Medicine*, vol. 15, no. 6, pp. 4911–4915, 2018.

[101] T. Qi, F. Xu, X. Yan, S. Li, and H. Li, "Sulforaphane exerts anti-inflammatory effects against lipopolysaccharide-induced acute lung injury in mice through the Nrf2/ARE pathway," *International Journal of Molecular Medicine*, vol. 37, no. 1, pp. 182–188, 2016.

[102] Y. Wang, X. Wang, L. Zhang, and R. Zhang, "Alleviation of acute lung injury in rats with sepsis by resveratrol via the phosphatidylinositol 3-kinase/nuclear factor-erythroid 2 related factor 2/heme oxygenase-1 (PI3K/Nrf2/HO-1) pathway," *Medical Science Monitor*, vol. 24, pp. 3604–3611, 2018.

[103] R. Qing, Z. Huang, Y. Tang, Q. Xiang, and F. Yang, "Cordycepin alleviates lipopolysaccharide-induced acute lung injury via Nrf2/HO-1 pathway," *International Immunopharmacology*, vol. 60, pp. 18–25, 2018.

[104] J. Lei, Y. Wei, P. Song et al., "Cordycepin inhibits LPS-induced acute lung injury by inhibiting inflammation and oxidative stress," *European Journal of Pharmacology*, vol. 818, pp. 110–114, 2018.

[105] K. Mehla, S. Balwani, A. Agrawal, and B. Ghosh, "Ethyl gallate attenuates acute lung injury through Nrf2 signaling," *Biochimie*, vol. 95, no. 12, pp. 2404–2414, 2013.

[106] Y. C. Lin, Y. S. Lai, and T. C. Chou, "The protective effect of alpha-lipoic acid in lipopolysaccharide-induced acute lung injury is mediated by heme oxygenase-1," *Evidence-Based Complementary and Alternative Medicine*, vol. 2013, Article ID 590363, 12 pages, 2013.

[107] A. Zhang, Z. Liu, L. Sheng, and H. Wu, "Protective effects of syringin against lipopolysaccharide-induced acute lung injury in mice," *Journal of Surgical Research*, vol. 209, pp. 252–257, 2017.

[108] S. Zhang, W. Jiang, L. Ma, Y. Liu, X. Zhang, and S. Wang, "Nrf2 transfection enhances the efficacy of human amniotic mesenchymal stem cells to repair lung injury induced by lipopolysaccharide," *Journal of Cellular Biochemistry*, vol. 119, no. 2, pp. 1627–1636, 2018.

[109] K. F. Rabe, S. Hurd, A. Anzueto et al., "Global strategy for the diagnosis, management, and prevention of chronic obstructive pulmonary disease: gold executive summary," *American Journal of Respiratory and Critical Care Medicine*, vol. 176, no. 6, pp. 532–555, 2007.

[110] M. G. Cosio, M. Saetta, and A. Agusti, "Immunologic aspects of chronic obstructive pulmonary disease," *The New England Journal of Medicine*, vol. 360, no. 23, pp. 2445–2454, 2009.

[111] G. G. Brusselle, G. F. Joos, and K. R. Bracke, "New insights into the immunology of chronic obstructive pulmonary disease," *The Lancet*, vol. 378, no. 9795, pp. 1015–1026, 2011.

[112] A. M. Cantin, "Cellular response to cigarette smoke and oxidants: adapting to survive," *Proceedings of the American Thoracic Society*, vol. 7, no. 6, pp. 368–375, 2010.

[113] D. Malhotra, R. Thimmulappa, A. Navas-Acien et al., "Decline in NRF2-regulated antioxidants in chronic obstructive pulmonary disease lungs due to loss of its positive regulator, DJ-1," *American Journal of Respiratory and Critical Care Medicine*, vol. 178, no. 6, pp. 592–604, 2008.

[114] C. C. Hua, L. C. Chang, J. C. Tseng, C. M. Chu, Y. C. Liu, and W. B. Shieh, "Functional haplotypes in the promoter region of transcription factor Nrf2 in chronic obstructive pulmonary disease," *Disease Markers*, vol. 28, no. 3, 193 pages, 2010.

[115] D. J. Blake, A. Singh, P. Kombairaju et al., "Deletion of Keap1 in the lung attenuates acute cigarette smoke-induced oxidative stress and inflammation," *American Journal of Respiratory Cell and Molecular Biology*, vol. 42, no. 5, pp. 524–536, 2010.

[116] D. Adenuga, S. Caito, H. Yao et al., "Nrf2 deficiency influences susceptibility to steroid resistance via HDAC2 reduction," *Biochemical and Biophysical Research Communications*, vol. 403, no. 3-4, pp. 452–456, 2010.

[117] T. E. Sussan, T. Rangasamy, D. J. Blake et al., "Targeting Nrf2 with the triterpenoid CDDO-imidazolide attenuates cigarette smoke-induced emphysema and cardiac dysfunction in mice," *Proceedings of the National Academy of Sciences of the United States of America*, vol. 106, no. 1, pp. 250–255, 2009.

[118] W. Cui, Z. Zhang, P. Zhang et al., "Nrf2 attenuates inflammatory response in COPD/emphysema: crosstalk with Wnt3a/β-catenin and AMPK pathways," *Journal of Cellular and Molecular Medicine*, vol. 22, no. 7, pp. 3514–3525, 2018.

[119] Z. Jiao, J. Chang, J. Li, D. Nie, H. Cui, and D. Guo, "Sulforaphane increases Nrf2 expression and protects alveolar epithelial cells against injury caused by cigarette smoke extract," *Molecular Medicine Reports*, vol. 16, no. 2, pp. 1241–1247, 2017.

[120] C. J. Harvey, R. K. Thimmulappa, S. Sethi et al., "Targeting Nrf2 signaling improves bacterial clearance by alveolar macrophages in patients with copd and in a mouse model," *Science Translational Medicine*, vol. 3, no. 78, article 78ra32, 2011.

[121] R. A. Wise, J. T. Holbrook, G. Criner et al., "Lack of effect of oral sulforaphane administration on Nrf2 expression in COPD: a randomized, double-blind, placebo controlled trial," *PLoS One*, vol. 11, no. 11, article e0163716, 2016.

[122] S. P. Guan, W. Tee, D. S. Ng et al., "Andrographolide protects against cigarette smoke-induced oxidative lung injury via augmentation of Nrf2 activity," *British Journal of Pharmacology*, vol. 168, no. 7, pp. 1707–1718, 2013.

[123] W. S. Daniel Tan, H. Y. Peh, W. Liao et al., "Cigarette smoke-induced lung disease predisposes to more severe infection with nontypeable Haemophilus influenzae: protective effects of andrographolide," *Journal of Natural Products*, vol. 79, no. 5, pp. 1308–1315, 2016.

[124] S. V. Posso, N. Quesnot, J. A. Moraes et al., "At-RVD1 repairs mouse lung after cigarette smoke-induced emphysema via downregulation of oxidative stress by NRF2/KEAP1 pathway," *International Immunopharmacology*, vol. 56, pp. 330–338, 2018.

[125] A. Kode, S. Rajendrasozhan, S. Caito, S. R. Yang, I. L. Megson, and I. Rahman, "Resveratrol induces glutathione synthesis by activation of Nrf2 and protects against cigarette smoke-mediated oxidative stress in human lung epithelial cells," *American Journal of Physiology-Lung Cellular and Molecular Physiology*, vol. 294, no. 3, pp. L478–L488, 2008.

[126] L. Lin, Y. Yin, G. Hou, D. Han, J. Kang, and Q. Wang, "Ursolic acid attenuates cigarette smoke-induced emphysema in rats by regulating perk and Nrf2 pathways," *Pulmonary Pharmacology & Therapeutics*, vol. 44, pp. 111–121, 2017.

[127] H. Y. Peh, W. S. D. Tan, T. K. Chan, C. W. Pow, P. S. Foster, and W. S. F. Wong, "Vitamin E isoform γ-tocotrienol protects against emphysema in cigarette smoke-induced COPD," *Free Radical Biology and Medicine*, vol. 110, pp. 332–344, 2017.

[128] J. A. Elias, C. G. Lee, T. Zheng, B. Ma, R. J. Homer, and Z. Zhu, "New insights into the pathogenesis of asthma," *The Journal of Clinical Investigation*, vol. 111, no. 3, pp. 291–297, 2003.

[129] A. Andreadis, S. Hazen, S. Comhair, and S. Erzurum, "Oxidative and nitrosative events in asthma," *Free Radical Biology & Medicine*, vol. 35, no. 3, pp. 213–225, 2003.

[130] P. A. J. Henricks and F. P. Nijkamp, "Reactive oxygen species as mediators in asthma," *Pulmonary Pharmacology & Therapeutics*, vol. 14, no. 6, pp. 409–421, 2001.

[131] C. E. Mapp, A. A. Fryer, N. De Marzo et al., "Glutathione s-transferase GSTP1 is a susceptibility gene for occupational asthma induced by isocyanates," *The Journal of Allergy and Clinical Immunology*, vol. 109, no. 5, pp. 867–872, 2002.

[132] M. A. Spiteri, A. Bianco, R. C. Strange, and A. A. Fryer, "Polymorphisms at the glutathione s-transferase, GSTP1 locus: a novel mechanism for susceptibility and development of atopic airway inflammation," *Allergy*, vol. 55, Supplement 61, pp. 15–20, 2000.

[133] Y. J. Li, H. Takizawa, A. Azuma et al., "Disruption of NRF2 enhances susceptibility to airway inflammatory responses induced by low-dose diesel exhaust particles in mice," *Clinical Immunology*, vol. 128, no. 3, pp. 366–373, 2008.

[134] M. A. Williams, T. Rangasamy, S. M. Bauer et al., "Disruption of the transcription factor Nrf2 promotes pro-oxidative dendritic cells that stimulate Th2-like immunoresponsiveness upon activation by ambient particulate matter," *Journal of Immunology*, vol. 181, no. 7, pp. 4545–4559, 2008.

[135] R. H. Brown, C. Reynolds, A. Brooker, P. Talalay, and J. W. Fahey, "Sulforaphane improves the bronchoprotective response in asthmatics through Nrf2-mediated gene pathways," *Respiratory Research*, vol. 16, no. 1, p. 106, 2015.

[136] J. H. Park, J. W. Kim, C. M. Lee et al., "Sulforaphane inhibits the Th2 immune response in ovalbumin-induced asthma," *BMB Reports*, vol. 45, no. 5, pp. 311–316, 2012.

[137] S. Ano, A. Panariti, B. Allard et al., "Inflammation and airway hyperresponsiveness after chlorine exposure are prolonged by Nrf2 deficiency in mice," *Free Radical Biology and Medicine*, vol. 102, pp. 1–15, 2017.

[138] S. A. Ritz, J. Wan, and D. Diaz-Sanchez, "Sulforaphane-stimulated phase II enzyme induction inhibits cytokine production by airway epithelial cells stimulated with diesel extract," *American Journal of Physiology-Lung Cellular and Molecular Physiology*, vol. 292, no. 1, pp. L33–L39, 2007.

[139] C. G. Duran, A. J. Burbank, K. H. Mills et al., "A proof-of-concept clinical study examining the Nrf2 activator sulforaphane against neutrophilic airway inflammation," *Respiratory Research*, vol. 17, no. 1, p. 89, 2016.

[140] X. Liu, D. Yu, and T. Wang, "Sappanone a attenuates allergic airway inflammation in ovalbumin-induced asthma," *International Archives of Allergy and Immunology*, vol. 170, no. 3, pp. 180–186, 2016.

[141] L. Duan, J. Li, P. Ma, X. Yang, and S. Xu, "Vitamin e antagonizes ozone-induced asthma exacerbation in Balb/c mice through the Nrf2 pathway," *Food and Chemical Toxicology*, vol. 107, no. Part A, pp. 47–56, 2017.

[142] R. Dworski, W. Han, T. S. Blackwell, A. Hoskins, and M. L. Freeman, "Vitamin E prevents NRF2 suppression by allergens in asthmatic alveolar macrophages in vivo," *Free Radical Biology & Medicine*, vol. 51, no. 2, pp. 516–521, 2011.

[143] W. E. Ho, C. Cheng, H. Y. Peh et al., "Anti-malarial drug artesunate ameliorates oxidative lung damage in experimental allergic asthma," *Free Radical Biology & Medicine*, vol. 53, no. 3, pp. 498–507, 2012.

[144] J. Qian, X. Ma, Y. Xun, and L. Pan, "Protective effect of forsythiaside a on ova-induced asthma in mice," *European Journal of Pharmacology*, vol. 812, pp. 250–255, 2017.

[145] Z. Wang, H. Zhang, X. Sun, and L. Ren, "The protective role of vitamin D3 in a murine model of asthma via the suppression of TGF-β/Smad signaling and activation of the Nrf2/HO-1 pathway," *Molecular Medicine Reports*, vol. 14, no. 3, pp. 2389–2396, 2016.

[146] G. Raghu, H. R. Collard, J. J. Egan et al., "An official ATS/ERS/JRS/ALAT statement: idiopathic pulmonary fibrosis: evidence-based guidelines for diagnosis and management," *American Journal of Respiratory and Critical Care Medicine*, vol. 183, no. 6, pp. 788–824, 2011.

[147] K. M. Beeh, J. Beier, I. C. Haas, O. Kornmann, P. Micke, and R. Buhl, "Glutathione deficiency of the lower respiratory tract in patients with idiopathic pulmonary fibrosis," *The European Respiratory Journal*, vol. 19, no. 6, pp. 1119–1123, 2002.

[148] A. M. Cantin, S. L. North, G. A. Fells, R. C. Hubbard, and R. G. Crystal, "Oxidant-mediated epithelial cell injury in idiopathic pulmonary fibrosis," *The Journal of Clinical Investigation*, vol. 79, no. 6, pp. 1665–1673, 1987.

[149] P. Chitra, G. Saiprasad, R. Manikandan, and G. Sudhandiran, "Berberine attenuates bleomycin induced pulmonary toxicity and fibrosis via suppressing NF-κB dependant TGF-β activation: a biphasic experimental study," *Toxicology Letters*, vol. 219, no. 2, pp. 178–193, 2013.

[150] Y. Liu, F. Lu, L. Kang, Z. Wang, and Y. Wang, "Pirfenidone attenuates bleomycin-induced pulmonary fibrosis in mice by regulating Nrf2/Bach1 equilibrium," *BMC Pulmonary Medicine*, vol. 17, no. 1, p. 63, 2017.

[151] E. Artaud-Macari, D. Goven, S. Brayer et al., "Nuclear factor erythroid 2-related factor 2 nuclear translocation induces myofibroblastic dedifferentiation in idiopathic pulmonary fibrosis," *Antioxidants & Redox Signaling*, vol. 18, no. 1, pp. 66–79, 2013.

[152] S. L. Tian, Y. Yang, X. L. Liu, and Q. B. Xu, "Emodin attenuates bleomycin-induced pulmonary fibrosis via anti-inflammatory

and anti-oxidative activities in rats," *Medical Science Monitor*, vol. 24, pp. 1–10, 2018.

[153] T. Nakamura, M. Matsushima, Y. Hayashi et al., "Attenuation of transforming growth factor–β–stimulated collagen production in fibroblasts by quercetin-induced heme oxygenase–1," *American Journal of Respiratory Cell and Molecular Biology*, vol. 44, no. 5, pp. 614–620, 2011.

[154] C. Veith, M. Drent, A. Bast, F. J. van Schooten, and A. W. Boots, "The disturbed redox-balance in pulmonary fibrosis is modulated by the plant flavonoid quercetin," *Toxicology and Applied Pharmacology*, vol. 336, pp. 40–48, 2017.

[155] N. Sriram, S. Kalayarasan, and G. Sudhandiran, "Epigallocatechin-3-gallate augments antioxidant activities and inhibits inflammation during bleomycin-induced experimental pulmonary fibrosis through Nrf2-keap1 signaling," *Pulmonary Pharmacology & Therapeutics*, vol. 22, no. 3, pp. 221–236, 2009.

[156] A. Jemal, F. Bray, M. M. Center, J. Ferlay, E. Ward, and D. Forman, "Global cancer statistics," *CA: A Cancer Journal for Clinicians*, vol. 61, no. 2, pp. 69–90, 2011.

[157] A. Jemal, R. Siegel, E. Ward et al., "Cancer statistics, 2008," *CA: A Cancer Journal for Clinicians*, vol. 58, no. 2, pp. 71–96, 2008.

[158] C. S. Dela Cruz, L. T. Tanoue, and R. A. Matthay, "Lung cancer: epidemiology, etiology, and prevention," *Clinics in Chest Medicine*, vol. 32, no. 4, pp. 605–644, 2011.

[159] R. G. Mehta, G. Murillo, R. Naithani, and X. Peng, "Cancer chemoprevention by natural products: how far have we come?," *Pharmaceutical Research*, vol. 27, no. 6, pp. 950–961, 2010.

[160] X. Yu and T. Kensler, "Nrf2 as a target for cancer chemoprevention," *Mutation Research*, vol. 591, no. 1-2, pp. 93–102, 2005.

[161] M. B. Sporn and K. T. Liby, "Nrf2 and cancer: the good, the bad and the importance of context," *Nature Reviews Cancer*, vol. 12, no. 8, pp. 564–571, 2012.

[162] A. Sparaneo, F. P. Fabrizio, and L. A. Muscarella, "Nrf2 and notch signaling in lung cancer: near the crossroad," *Oxidative Medicine and Cellular Longevity*, vol. 2016, Article ID 7316492, 17 pages, 2016.

[163] S. Tao, M. Rojo de la Vega, E. Chapman, A. Ooi, and D. D. Zhang, "The effects of nrf2 modulation on the initiation and progression of chemically and genetically induced lung cancer," *Molecular Carcinogenesis*, vol. 57, no. 2, pp. 182–192, 2018.

[164] H. Satoh, T. Moriguchi, J. Takai, M. Ebina, and M. Yamamoto, "Nrf2 prevents initiation but accelerates progression through the Kras signaling pathway during lung carcinogenesis," *Cancer Research*, vol. 73, no. 13, pp. 4158–4168, 2013.

[165] D. Zhang, J. Rennhack, E. R. Andrechek, C. E. Rockwell, and K. T. Liby, "Identification of an unfavorable immune signature in advanced lung tumors from Nrf2-deficient mice," *Antioxidants & Redox Signaling*, vol. 29, no. 16, pp. 1535–1552, 2018.

[166] S. Yu, Z. Yan, F. Feng et al., "NF-E2-related factor 2 serves a key function in resistance to malignant transformation of BEAS-2B cells induced by coal tar pitch," *Oncology Letters*, vol. 15, no. 4, pp. 5143–5148, 2018.

[167] H. Satoh, T. Moriguchi, K. Taguchi et al., "Nrf2-deficiency creates a responsive microenvironment for metastasis to the lung," *Carcinogenesis*, vol. 31, no. 10, pp. 1833–1843, 2010.

[168] H. M. Leinonen, E. Kansanen, P. Pölönen, M. Heinäniemi, and A.-L. Levonen, "Dysregulation of the Keap1-Nrf2 pathway in cancer," *Biochemical Society Transactions*, vol. 43, no. 4, pp. 645–649, 2015.

[169] The Cancer Genome Atlas Research Network, "Comprehensive genomic characterization of squamous cell lung cancers," *Nature*, vol. 489, no. 7417, pp. 519–525, 2012.

[170] M. C. Tung, P. L. Lin, Y. C. Wang et al., "Mutant p53 confers chemoresistance in non-small cell lung cancer by upregulating Nrf2," *Oncotarget*, vol. 6, no. 39, pp. 41692–41705, 2015.

[171] D. Kalpana Deepa Priya, R. Gayathri, and D. Sakthisekaran, "Role of sulforaphane in the anti-initiating mechanism of lung carcinogenesis in vivo by modulating the metabolic activation and detoxification of benzo(a)pyrene," *Biomedicine & Pharmacotherapy*, vol. 65, no. 1, pp. 9–16, 2011.

[172] Y. Wang, A. K. Mandal, Y.-O. K. Son et al., "Roles of ROS, NRF2, and autophagy in cadmium-carcinogenesis and its prevention by sulforaphane," *Toxicology and Applied Pharmacology*, vol. 353, pp. 23–30, 2018.

[173] Y. Tian, Q. Liu, X. He et al., "Emerging roles of NRF2 signal in non-small cell lung cancer," *Journal of Hematology & Oncology*, vol. 9, no. 1, p. 14, 2016.

[174] R. Garg, S. Gupta, and G. B. Maru, "Dietary curcumin modulates transcriptional regulators of phase I and phase II enzymes in benzo[a]pyrene-treated mice: mechanism of its anti-initiating action," *Carcinogenesis*, vol. 29, no. 5, pp. 1022–1032, 2008.

[175] P. Anand, A. B. Kunnumakkara, R. A. Newman, and B. B. Aggarwal, "Bioavailability of curcumin: problems and promises," *Molecular Pharmaceutics*, vol. 4, no. 6, pp. 807–818, 2007.

[176] T. Shen, T. Jiang, M. Long et al., "A curcumin derivative that inhibits vinyl carbamate-induced lung carcinogenesis via activation of the Nrf2 protective response," *Antioxidants & Redox Signaling*, vol. 23, no. 8, pp. 651–664, 2015.

[177] C. To, C. S. Ringelberg, D. B. Royce et al., "Dimethyl fumarate and the oleanane triterpenoids, CDDO-imidazolide and CDDO-methyl ester, both activate the Nrf2 pathway but have opposite effects in the a/j model of lung carcinogenesis," *Carcinogenesis*, vol. 36, no. 7, pp. 769–781, 2015.

[178] S. Sharma, P. Gao, and V. E. Steele, "The chemopreventive efficacy of inhaled oltipraz particulates in the b[a]p-induced a/j mouse lung adenoma model," *Carcinogenesis*, vol. 27, no. 8, pp. 1721–1727, 2006.

Hindawi
Oxidative Medicine and Cellular Longevity
Volume 2018, Article ID 6069150, 10 pages
https://doi.org/10.1155/2018/6069150

Research Article

Uric Acid Protects against Focal Cerebral Ischemia/Reperfusion-Induced Oxidative Stress via Activating Nrf2 and Regulating Neurotrophic Factor Expression

Bai-liu Ya,[1] **Qian Liu**,[2] **Hong-fang Li**,[3] **Hong-ju Cheng**,[1] **Ting Yu**,[1] **Lin Chen**,[4] **You Wang**,[4] **Li-li Yuan**,[4] **Wen-juan Li**,[5] **Wen-yan Liu**,[1] **and Bo Bai**[1]

[1]*Department of Physiology, Jining Medical University, Shandong 272067, China*
[2]*School of Clinical Medicine, Jining Medical University, Shandong 272067, China*
[3]*Department of Neurology, Affiliated Hospital of Jining Medical University, Shandong 272067, China*
[4]*School of Basic Medicine, Jining Medical University, Shandong 272067, China*
[5]*School of Forensic and Laboratory Medicine, Jining Medical University, Shandong 272067, China*

Correspondence should be addressed to Bai-liu Ya; yabailiu@126.com

Received 18 July 2018; Revised 5 October 2018; Accepted 16 October 2018; Published 18 November 2018

Guest Editor: Luciano Saso

The aim of this study was to investigate whether uric acid (UA) might exert neuroprotection via activating the nuclear factor erythroid 2-related factor 2 (Nrf2) pathway and regulating neurotrophic factors in the cerebral cortices after transient focal cerebral ischemia/reperfusion (FCI/R) in rats. UA was intravenously injected through the tail vein (16 mg/kg) 30 min after the onset of reperfusion in rats subjected to middle cerebral artery occlusion for 2 h. Neurological deficit score was performed to analyze neurological function at 24 h after reperfusion. Terminal deoxynucleotidyl transferase-mediated dNTP nick end labeling (TUNEL) staining and hematoxylin and eosin (HE) staining were used to detect histological injury of the cerebral cortex. Malondialdehyde (MDA), the carbonyl groups, and 8-hydroxyl-2′-deoxyguanosine (8-OHdG) levels were employed to evaluate oxidative stress. Nrf2 and its downstream antioxidant protein, heme oxygenase- (HO-) 1,were detected by western blot. Nrf2 DNA-binding activity was observed using an ELISA-based measurement. Expressions of BDNF and NGF were analyzed by immunohistochemistry. Our results showed that UA treatment significantly suppressed FCI/R-induced oxidative stress, accompanied by attenuating neuronal damage, which subsequently decreased the infarct volume and neurological deficit. Further, the treatment of UA activated Nrf2 signaling pathway and upregulated BDNF and NGF expression levels. Interestingly, the aforementioned effects of UA were markedly inhibited by administration of brusatol, an inhibitor of Nrf2. Taken together, the antioxidant and neuroprotective effects afforded by UA treatment involved the modulation of Nrf2-mediated oxidative stress and regulation of BDNF and NGF expression levels. Thus, UA treatment could be of interest to prevent FCI/R injury.

1. Introduction

The principal therapy for cerebral ischemia is the restoration of cerebral blood flow as early as possible. Early recanalization with recombinant tissue plasminogen activator (rt-PA) has been developed to treat acute ischemic stroke. However, reperfusion after cerebral ischemia may be injurious and increase the risk of brain hemorrhage, promote the development of cerebral edema, and cause more serious damage to the blood-brain barrier. The potential mechanisms responsible for the additional injuries in the ischemic brain caused by reperfusion itself remain unclear [1]. Acute cerebral ischemia starts with cerebral blood flow interruption that causes severely limited oxygen and glucose supply, eliciting a cascade of pathological events such as excitotoxicity, calcium dysregulation, oxidative stress, and inflammatory that could ultimately result in tissue death. Oxidative stress is linked with a progressive increase in reactive oxygen species (ROS), and it affects the pathogenesis of cerebral ischemia/reperfusion (I/R) injury seriously [2–4]. Oxidative

insult after I/R injury increases pathological alteration of lipids, proteins, and DNA, thereby damaging function of the cell, which lastly causes the cell death. Enhanced ROS production after reperfusion increases hemorrhagic infarction, brain edema, and infarction size. So the intervention of oxidative damage using safe and effective therapeutic agents with antioxidant properties provides an encouraging therapeutic strategy.

Phase 2 enzymes have been implicated to be the important means by which neurons protect themselves against intense oxidative stress. The expression of phase 2 enzymes, including heme oxygenase (HO)-1, is regulated by nuclear factor E2-related factor 2 (Nrf2) [5]. Considerable efforts have been made to develop effective strategies and drugs to relieve or prevent cerebral I/R injury. Extensive research has confirmed that Nrf2 activation during I/R is becoming a promising therapeutic target for neuroprotection [6, 7]. We also have recently indicated a key role of Nrf2 activation in prevention of ischemic cerebrovascular disease in our previous studies [8].

Neurotrophic factors are essential regulators in post-stroke recovery [9–11]. Both brain-derived neurotrophic factor (BDNF) and nerve growth factor (NGF) have been reported to be neuroprotective in the middle cerebral artery occlusion (MCAO) rat model of ischemia [12, 13]. Previous experimental studies have demonstrated that these neurotrophic factors confer neuroprotective effects as important candidates for prevention of oxidative stress and subsequent neurotoxicity [14, 15]. The expression levels of neurotrophic factors such as BDNF and NGF, which are causally related to oxidative stress, exert key effects in keeping the balance between oxidation and antioxidation mechanisms. Both BDNF and NGF are Nrf2-target genes [16]. In addition, it has been demonstrated that neurotrophins can activate Nrf2 [17–19]. So our choice of regulator molecules, BDNF and NGF, and the transcription factor, Nrf2, which participate in multiple steps of the active process of oxidative stress, is justified because dysfunction of any of these proteins causes a redox imbalance that leads to oxidative damage.

Uric acid (UA) is a major antioxidant in the blood in humans and is responsible for almost two-thirds of all free radical scavenging capacity with a concentration that surpasses other antioxidants by as much as tenfold in plasma [20]. Since UA has a wide variety of profound antioxidant properties, including quenching superoxide and hydroxyl and peroxynitrite radicals, and may have beneficial effects via reducing lipid peroxidation [21, 22]; it should have protective effects against ischemic brain damage. Actually, there are several animal experimental data in which the neuroprotective property of exogenous administration of uric acid is demonstrated [23–27]. Evidence has been presented that UA can exert much of its neuroprotective effect by astrocytic Nrf2/antioxidant response element (ARE) pathway activation indirectly causing increased levels of glutathione concentration [28], which implies that Nrf2 pathway may participate in the neuroprotection of UA. However, it remains unknown whether the Nrf2 pathway activation is involved in the UA-induced neuroprotection against the cerebral I/R injury via neuronal antioxidation approach and whether neurotrophic factors are involved in the UA's neuroprotection against oxidative damage after stroke. Therefore, we employed the MCAO-induced focal cerebral I/R (FCI/R) rat model to test the hypothesis that UA protects against FCI/R-induced oxidative stress injury by activating Nrf2 pathway and targeting BDNF and NGF expression. Furthermore, this study may help understanding the relationship between Nrf2 signaling activation and the roles of BDNF and NGF in the pathogenesis of the ischemic brain in the neuroprotection induced by UA.

2. Materials and Methods

2.1. FCI/R Rat Model. Male Sprague–Dawley (SD) rats (280–300 g) from Pengyue Experimental Animal Breeding Institute of Jinan, China, were maintained in a room (23-24°C, 50-60% humidity) under 12 h light–dark cycle with free access to water and food. All experimental protocols were conducted according to ARRIVE (Animal Research: Reporting In Vivo Experiments) guidelines. Every effort was made to minimize animal suffering and the number of animals used. The Ethics Committee of Jining Medical University approved all the experimental protocols. All sample analysis was conducted under a strictly blinded manner. 193 rats were used, of which 11 died after transient FCI/R insult and 2 died after left lateral ventricle puncture, and consequently a total of 180 rats were separated randomly into 4 groups which included the sham group ($n = 45$), vehicle-treated I/R group ($n = 45$), 16 mg/kg UA-treated I/R group (UA group, $n = 45$), and UA plus brusatol-treated I/R group (UA + Bru, a specific inhibitor of Nrf2, $n = 45$).

The procedure for transient FCI/R has been described previously [29]. For MCAO, a 4-0 nylon thread with a rounded tip was inserted into the left external carotid artery (CA) and subsequently went into the internal CA approximately 20–21 mm from the carotid bifurcation. Then, the thread was withdrawn to initiate reperfusion after 2 h ischemia. The left CA was isolated with no thread inserted in the sham group. Rectal temperature was monitored and maintained between 37.0 and 37.5°C with a heating pad throughout surgery.

2.2. Drug Treatment and Experimental Design. UA diluted with Locke's buffer (vehicle) was injected intravenously through the tail vein (16 mg/kg) 30 min after reperfusion. An equal volume of vehicle was given to sham and model rats. Rats in the UA + Bru group were treated with UA plus brusatol. The dose of UA was chosen based on previous reports of UA treatment in rats induced by transient FCI/R [24–26]. Left lateral ventricle puncture (anteroposterior, −0.9 mm; lateral, 1.5 mm; depth, 3.6 mm; from bregma) was performed before MCAO. In the UA + Bru group, rats were infused intracerebroventricularly with Nrf2 inhibitor brusatol 30 min prior to ischemia (1 mg/kg, dissolved in 5 μl 1% DMSO) [30]. The other three groups also received equal volume vehicle injection after surgery. After animals underwent neurological evaluation at 24 h of reperfusion, their brains were harvested for the experiments described below.

2.3. Measurement of Cerebral Infarct Area. 2,3,5-Triphenyltetrazolium chloride (TTC) staining technique was employed to test the cerebral infarct volume. TTC stains the noninfarcted region with a deep red pigment, while the infarcted brain area appears white. Infarct volume was calculated with correction of edema in the ischemic hemisphere as previously described [29].

2.4. Evaluation of Neurological Deficits. A blinded observer evaluated the neurological status 24 h after FCI/R. A 5-point scale was used as follows [31, 32]: 0, no neurological deficits; 1, failure to fully extend the right forepaw; 2, decreased resistance to a lateral push toward the left side and failure to fully extend the right forepaw; 3, decreased resistance to a lateral push toward the left side, failure to fully extend the right forepaw, and circling to the left side; and 4, inability to walk spontaneously and lack of response to stimulation.

2.5. Determination of Brain Edema. The brains were carefully removed after decapitation. The wet weight was obtained immediately by weighing the ischemic hemispheres. The dry weight was obtained by weighing the samples dried at 60°C for 72 h. The percentage tissue water content was determined as previously described [8].

2.6. Histology and Immunochemistry Analysis. Rats were transcardially perfused with PBS and 4% paraformaldehyde 24 h after transient FCI/R ($n = 3$/group). The brain coronal sections from bregma at 0.3 to −1.8 mm were cut at 20 μm thickness. The sections were stained for hematoxylin and eosin (HE), terminal deoxynucleotidyl transferase- (TdT-) mediated dNTP nick end labeling (TUNEL), the expression of BDNF and NGF, and 8-hydroxy-deoxyguanosine (8-OHdG). Sections were incubated with primary antibody (anti-BDNF, Santa Cruz, USA; anti-NGF, Abcam Inc., Cambridge, MA; anti-8-OHdG, JaICa, Shizuoka, Japan) and then with the biotinylated secondary antibody. Negative controls performed the same staining procedure with the omission of primary antibody. HE staining was performed according to the standard procedure. TUNEL labeling assay kit (Roche Company, Switzerland) was used to measure DNA fragmentation. The number of HE-, TUNEL-, BDNF-, NGF-, and 8-OHdG-positive cells in the penumbra of ischemic ipsilateral parietal cortex in the ischemic area was quantified under a 400x magnification by a blinded investigator.

2.7. Western Blot. The ischemic side cerebral cortex (left side, $n = 4$/group) was dissected to extract total protein using a total protein extraction kit (Applygen Technologies Inc., Beijing). A nuclear-cytosol extraction kit (Applygen Technologies Inc., Beijing) was used to isolate the nuclear and cytosol fractions. We examined the expression levels of Nrf2 in the cytoplasm and nucleus and HO-1 in the cytoplasm. Each sample contained 50 μg protein. The primary antibodies were anti-HO-1 polyclonal antibody (Santa Cruz, USA) and anti-Nrf2 polyclonal antibody (Abcam Inc., Cambridge, MA). Each protein blot was normalized to histone H3 or β-actin to obtain the final result expressed as intensity ratio (% sham-operated control).

2.8. DNA-Binding Activity Assay of Nrf2. A commercially available Active Motif's (Carlsbad, CA, USA) ELISA-based TransAM® Nrf2 kit was used to analyze Nrf2 DNA-binding activity [8]. 10 μg nuclear protein was assayed per the manufacturer's protocol.

2.9. Determination of Protein Oxidation and Lipid Peroxidation. A commercial OxyBlot kit (#S7150; Millipore) was employed to determine the extent of protein oxidation [8]. The protein carbonyl content was used as an index for oxidative protein damage [33]. The cytoplasmic supernatant fluids of tissue samples were reacted with 2,4-dinitrophenylhydrazone (DNP) to get the DNP derivatized carbonyl groups. Then western blotting was used to test the DNP-derivatized protein with an anti-DNP antibody.

We analyzed total malondialdehyde (MDA) levels as the indicators of lipid peroxidation with the MDA detection kit (Nanjing Jiancheng, China) [8]. The absorption of the thiobarbituric acid (TBA) reactive substances which were produced by the reaction of TBA with MDA was measured at 532 nm to determine the extent of MDA. Results were presented as nmol/mg protein of wet tissue.

2.10. Statistical Analysis. Neurological deficits were analyzed using the Kruskal-Wallis test followed by Dunn's test, and results are expressed as median ± interquartile range. One-way analysis of variance (ANOVA) with subsequent Duncan's test as post hoc analysis was used for statistical analysis of all the other data, and results are reported as mean ± standard error (SE). A P value < 0.05 was considered to indicate statistical significance.

3. Results

3.1. UA Decreases Cerebral Infarct Size and Improves Neurological Functional Outcome. The infarct size induced by MCAO was determined using TTC staining (Figure 1(a)). No infarct tissue was detected in the sham group, while in the vehicle group, large volumes of infarct tissue were developed. Sections from rats treated with UA had significantly decreased infarct volumes (22.93% ± 3.04%) compared to the vehicle-treated I/R group (40.18% ± 2.30%, $P < 0.01$). In order to evaluate the role of Nrf2 pathway in UA-induced neuroprotection, the effect of brusatol on cerebral infarct volume was also detected. As observed in the UA + Bru group, a larger cerebral infarct volume was presented compared with the UA-treated I/R group (Figures 1(a) and 1(b)). Neurological deficit scores are presented in Figure 1(c). For vehicle-treated I/R animals, the median score was 3.25 (interquartile range (IQR): 2.88 to 3.50), indicative of severe neurological injury. When compared to the vehicle-treated I/R group, treatment with 16 mg/kg UA (median score: 2, IQR: 2 to 2.50) decreased the neurological deficit score significantly. The brain water content decreased significantly in UA-treated rats compared with model rats (83.0 + 1.8% vs. 88.5 + 1.5%, $P < 0.05$), whereas brusatol attenuated the decrease (87.7 + 1.6%, $P < 0.05$, Figure 1(d)).

3.2. UA Attenuated Neuronal Injury. HE staining was an effective way to evaluate neuronal cell death. In the sham

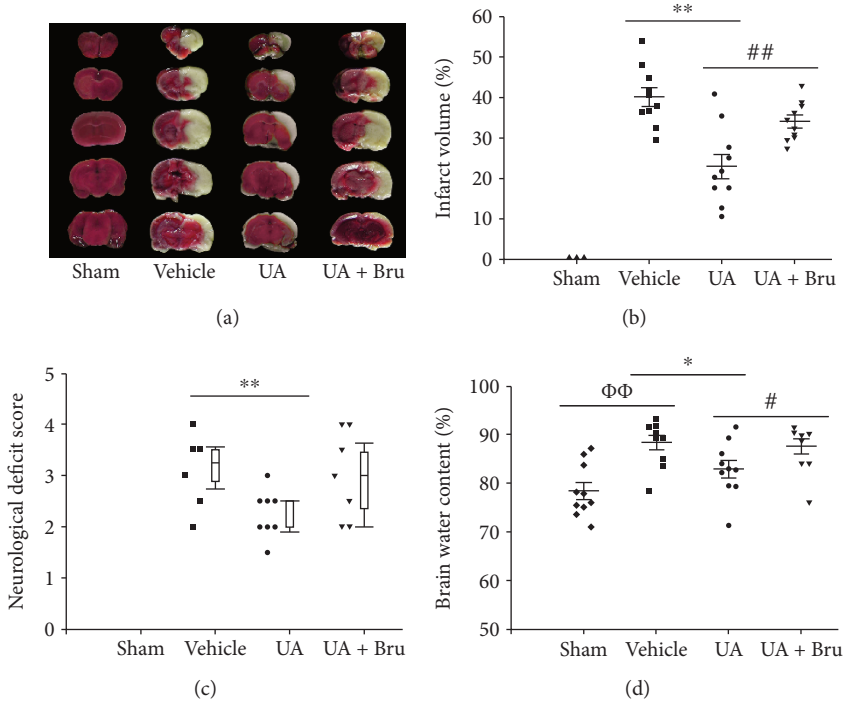

Figure 1: Effect of UA on the infarct volume, neurological deficit, and brain water content in rats. (a) Representative TTC-stained coronal sections. (b) Quantification of infarct volume; data are means ± SE ($n = 10$). (c) Neurological deficit scores; data are medians ± interquartile range ($n = 10$). Box plots show the interquartile range (25% to 75%) as the box, median as the horizontal line in the box, and the 95% range as the whiskers. (d) Brain water content; data are means ± SE ($n = 12$). $\Phi\Phi P < 0.01$ vs. the sham group; $^{*}P < 0.05$, $^{**}P < 0.01$ vs. the vehicle-treated I/R group; $^{\#}P < 0.05$, $^{\#\#}P < 0.01$ vs. the UA-treated I/R group.

group, no significant neuronal damage or neuronal loss was observed. A significant loss of neuronal cell was observed in model rats compared with sham rats (1150 ± 130 cells/mm^2 vs. 110 ± 23 cells/mm^2, $P < 0.01$). More intact cells in UA-treated rats were observed in comparison with model rats owing to the neuroprotection of UA (890 ± 120 cells/mm^2, $P < 0.01$, Figures 2(a) and 2(b)). Pretreatment with brusatol markedly abolished the protection of UA.

Apoptotic cells were identified by TUNEL staining. The apoptotic cell had round and shrunken shapes and the nuclei were darkly stained. Only few TUNEL-positive cells were observed in sham rats. TUNEL-positive cells increased significantly in model rats compared with sham rats (510 ± 80 cells/mm^2 vs. 60 ± 10 cells/mm^2, $P < 0.01$). TUNEL-positive cells were markedly reduced by UA administration (150 ± 29 cells/mm^2, $P < 0.01$). However, a marked increase of TUNEL-positive cells was observed in the UA + Bru group (390 ± 38 cells/mm^2, $P < 0.01$), suggesting brusatol pretreatment attenuated neuroprotection of UA (Figures 2(c) and 2(d)).

3.3. UA Alleviated Oxidative Injury. We examined the role of UA in postischemic lipid peroxidation injury by determining the concentration of MDA in ischemic side cerebral cortex. The extent of MDA increased 1.2-fold compared with the sham group. With UA administration, the MDA levels significantly decreased compared with the model group. However, the decrease was ablated by brusatol pretreatment (Figure 3(a)).

The extent of protein oxidation was measured by the levels of protein carbonylation. The protein carbonylation levels of the model rats significantly increased compared to those of the sham rats, while UA treatment decreased them compared with the model rats ($p < 0.01$, Figures 3(b) and 3(c)). The improving effect of UA on protein carbonylation levels was diminished in the ischemic cortex via pretreatment with brusatol.

Few 8-OHdG-positive cells were observed in sham rats, while a significant amount of 8-OHdG-positive cells was presented in the vehicle group (580 ± 120 cells/mm^2 vs. 240 ± 45 cells/mm^2, $P < 0.01$, Figures 3(d) and 3(e)). UA treatment significantly decreased the amount of 8-OHdG-positive cells. However, preadministration of brusatol significantly increased the levels of 8-OHdG immunoactivity compared with that in the UA-treated group (410 ± 67 cells/mm^2 vs. 240 ± 45 cells/mm^2, $p < 0.01$, Figures 3(d) and 3(e)).

3.4. UA Activated the Nrf2 Pathway. To find out whether the Nrf2 pathway was involved in the neuroprotection of UA, we detected the expression levels of proteins related to Nrf2 pathway carefully in the cerebral cortices of variously treated animals in the presence of brusatol. UA treatment significantly increased Nrf2 levels in the nucleus, with a corresponding decrease in the cytoplasm, compared with the vehicle group. Further studies showed that cotreatment with

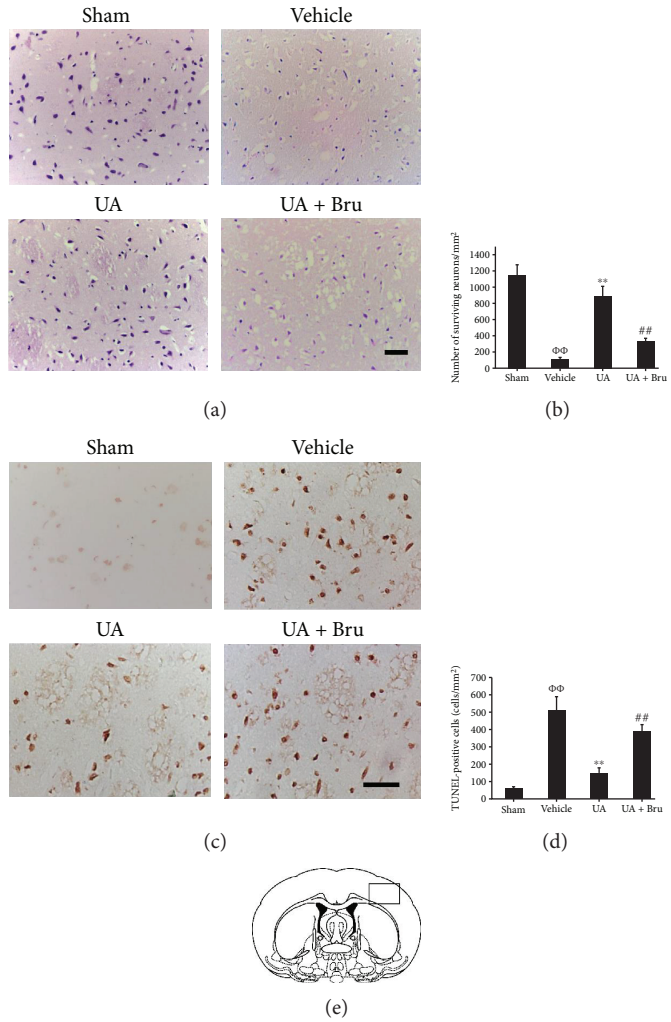

Figure 2: Effect of UA on neuronal injury in cerebral cortices in rats. (a) Representative photomicrographs of HE staining. Scale bar in all panels = 50 μm. (b) Quantification of surviving neuronal cells. (c) Representative photomicrographs of TUNEL staining. Scale bar in all panels = 50 μm. (d) Quantification of apoptotic cells. (e) Schematic diagram of coronal brain section. Black rectangle in the ischemic ipsilateral parietal cortex of penumbra represents the region selected for histology. Data are means ± SE ($n = 3$). $\Phi\Phi P < 0.01$ vs. the sham group; $^{**}P < 0.01$ vs. the vehicle-treated I/R group; $^{\#\#}P < 0.01$ vs. the UA-treated I/R group.

UA and brusatol significantly attenuated the nuclear translocation of Nrf2 ($P < 0.05$ or $P < 0.01$, Figure 4).

We next examined whether the expression of HO-1 was induced by UA. HO-1 levels were obviously increased by UA treatment, as compared to the vehicle group, an effect that was reversed by pretreatment with brusatol ($P < 0.05$ or $P < 0.01$, Figures 4(c) and 4(e)).

Furthermore, DNA-binding activity of Nrf2 was also analyzed. UA treatment enhanced Nrf2 transcriptional activity; however, brusatol blocked the increased Nrf2 DNA-binding activity of UA significantly ($P < 0.01$, Figure 4(f)).

3.5. UA Upregulated Expression of BDNF and NGF in Ischemic Rat Brain. We examined whether UA had any effect on BDNF and NGF protein expressions using immunohistochemistry. The numbers of BDNF-immunopositive cells and NGF-immunopositive cells significantly decreased in vehicle animals; however, UA treatment successfully restored BDNF and NGF expressions, as indicated by an elevated number of BDNF-immunopositive cells and NGF-immunopositive cells ($P < 0.01$). In addition, cotreatment with UA and brusatol decreased BDNF and NGF expressions comparable to the UA-treated group ($P < 0.05$, Figure 5).

4. Discussion

In this study, where SD rats were exposed to FCI/R, we found that UA treatment (16 mg/kg, i.v.) decreased cerebral infarct volume, neurological deficit core, and degree of brain edema, consistent with the previous studies [23–25]. The neuroprotective properties of UA are related closely to the reduction of oxidative stress known to occur during cerebral I/R. The most novel finding of our study is that UA promoted nuclear translocation of Nrf2 and increased the expression of HO-1, as well as neurotrophic factors such as BDNF and NGF. Furthermore, the neuroprotective effects induced by UA were

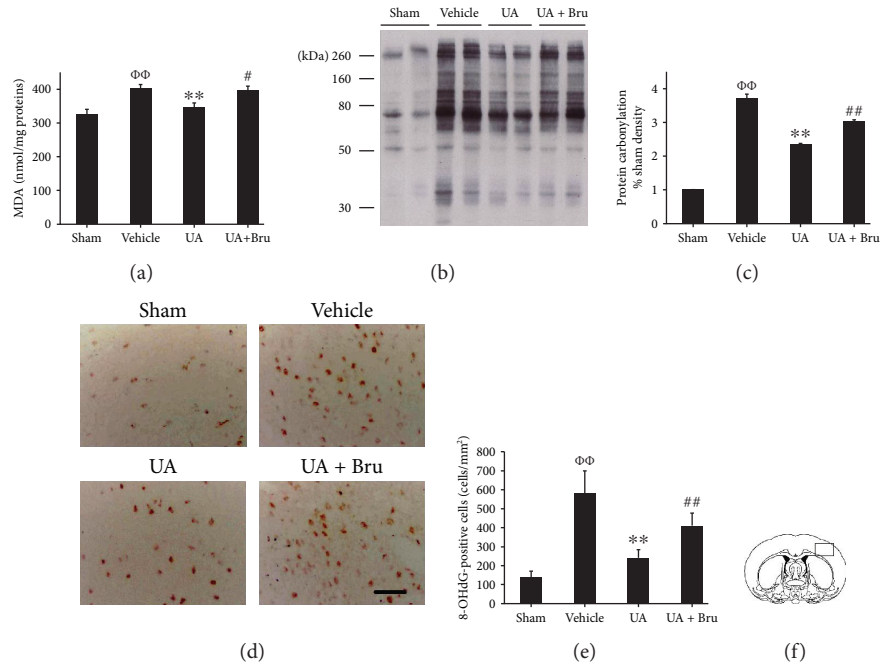

Figure 3: Effect of UA on oxidative injury in cerebral cortices in rats. (a) Quantification of MDA; data are means ± SE ($n = 12$). (b, c) Representative blot of protein oxidation. Quantification of carbonyl group bands; data are means ± SE ($n = 4$). (d) Representative photomicrographs of 8-OHdG immunostaining. Scale bar in all panels = 50 μm. (e) Quantification of 8-OHdG-positive cells; data are means ± SE ($n = 3$). (f) Schematic diagram of coronal brain section. The black rectangle in the ischemic ipsilateral parietal cortex of the penumbra represents the region selected for histology. $\Phi\Phi P < 0.01$ vs. the sham group; $^{**}P < 0.01$ vs. the vehicle-treated I/R group; $^{\#}P < 0.05$, $^{\#\#}P < 0.01$ vs. the UA-treated I/R group.

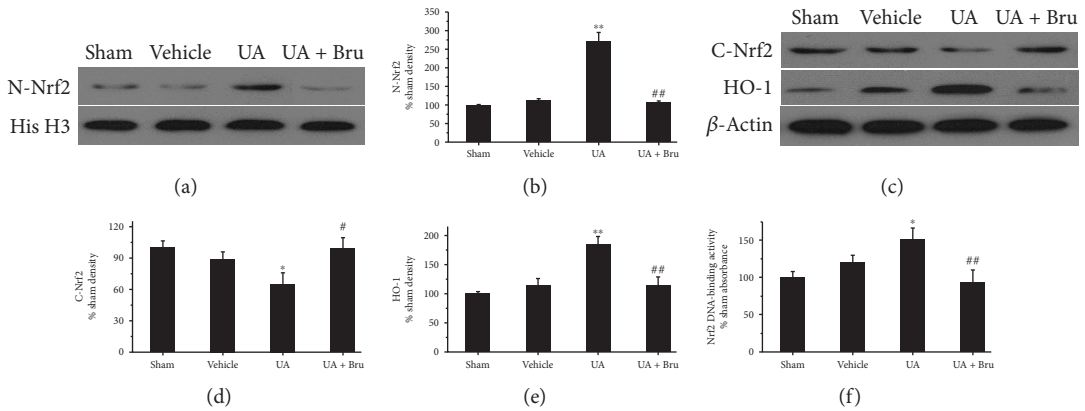

Figure 4: Effect of UA on Nrf2 protein distribution, HO-1 protein expression, and Nrf2 DNA-binding activity in cerebral cortices in rats. (a, b) Representative western blot of nuclear Nrf2. Quantification of nuclear Nrf2 normalized with histone H3. (c, d) Representative western blot of cytosolic Nrf2 and HO-1. Quantification of cytosolic Nrf2 and HO-1 normalized with β-actin. (e) Nuclear Nrf2 DNA-binding activity. Data are means ± SE ($n = 4$). $^{*}P < 0.05$, $^{**}P < 0.01$ vs. the vehicle-treated I/R group; $^{\#}P < 0.05$, $^{\#\#}P < 0.01$ vs. the UA-treated I/R group.

prevented by treatment with brusatol, an inhibitor of Nrf2. These results demonstrated that UA protected the brain from I/R injury potently and Nrf2 pathway activation as well as the upregulation of BDNF and NGF expression levels might be involved in this brain protection.

The cellular injury and downstream pathway activation caused by oxidative stress may exacerbate the postischemic brain damage [2]. MDA, protein carbonyls, and 8-OHdG, which are oxidized products of lipid, protein, and DNA, respectively, are the major oxidative stress biomarkers. We observed a significant amount of MDA, protein carbonyls, and 8-OHdG in I/R rats. UA is a powerful natural antioxidant and radical scavenger that has cytoprotective effects against oxidative stress by scavenging ROS and suppressing lipid peroxidation in cultured hippocampal neurons after exposure to glutamate or cyanide [25]. In addition, UA protects the brain via reducing oxidative/nitrative stress following I/R in rats [24]. In the current study, the concentrations

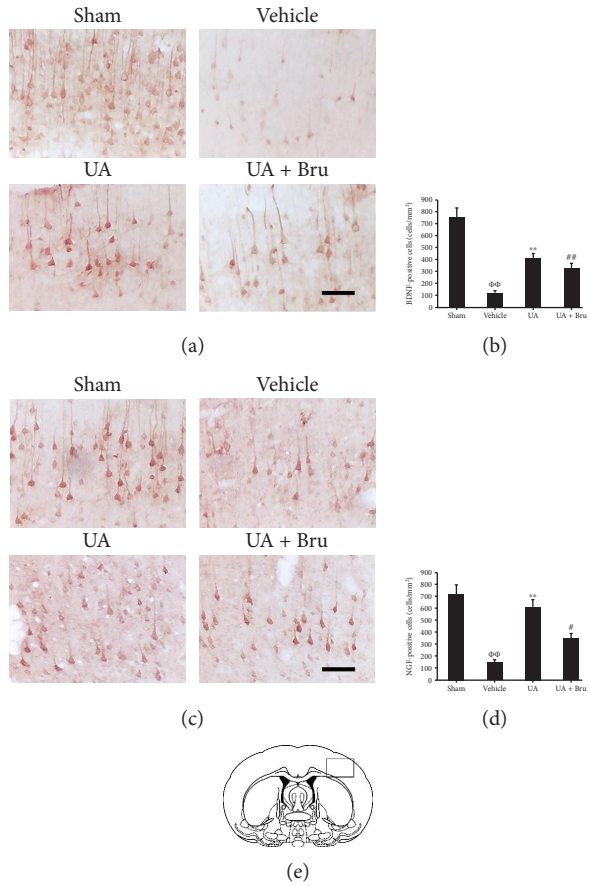

Figure 5: Effect of UA on the expression of BDNF and NGF in cerebral cortices in rats. (a) Representative photomicrographs of BDNF immunostaining. Scale bar in all panels = 50 μm. (b) Quantification of BDNF positive cells. (c) Representative photomicrographs of NGF immunostaining. Scale bar in all panels = 50 μm. (d) Quantification of NGF positive cells. (e) Schematic diagram of coronal brain section. The black rectangle in the ischemic ipsilateral parietal cortex of the penumbra represents the region selected for histology. Data are means ± SE ($n = 3$). $\Phi\Phi P < 0.01$ vs. the sham group; $^{**}P < 0.01$ vs. the vehicle-treated I/R group; $^{\#}P < 0.05$ vs. the UA-treated I/R group.

of MDA, protein carbonyls, and 8-OHDG were markedly decreased in rats with administration of UA. However, these changes could be largely blocked by the function of brusatol. Our results also showed that neuronal cells largely decreased with damaged morphology and the apoptotic cell death increased in the TUNEL assay in model rats. UA administration was able to improve histology changes and also attenuate TUNEL-positive cells. All these data support the view that UA treatment alleviates brain damage through reducing lipid, protein, and DNA peroxidation in cortical cells, subsequently reducing brain infarction.

Little is known about the mechanisms on how UA treatment protects neurons against oxidative stress. Evidences demonstrated that Nrf2 is a master regulator of the antioxidative defense responses [34]. Under basal conditions, Nrf2 largely localizes in the cytoplasm in an inactive form to maintain the expression of Nrf2-regulated genes in a low basal level. Under stressful conditions, Nrf2 translocates from the cytoplasm to the nucleus to bind ARE, which results in activation of transcription of multiple antioxidant and detoxifying genes [35, 36]. Our group and others have evidenced the Nrf2 pathway as therapeutic target of ischemic stroke [8, 37, 38]. Therefore, this study further detected whether UA could activate the Nrf2 pathway. UA stimulation elevated Nrf2 protein expression in the nucleus and the binding activity of Nrf2 to AREs, with a corresponding decrease in the cytoplasm, suggesting that UA treatment induced nuclear translocation of Nrf2. The structure-activity relationship may account for one of the mechanisms that urate activates Nrf2. Structurally, UA displays ketoenol tautomeric forms and can react with cysteine residues in Kelch-like ECH-associated protein 1 (Keap1), which principally regulates the protein stability and transcriptional activity of Nrf2, through adduct formation and redox modifications as an electrophilic compound, triggering Nrf2 nuclear translocation. Simultaneously, UA promoted HO-1 expression. HO-1, which is regulated by Nrf2, has been recently considered to be important against ischemic brain injury [39]. It directly affects the antioxidative balance in the body, and it has antiapoptotic activities as well [40]. Importantly, the ability to promote Nrf2/HO-1 protein expression and Nrf2 nuclear translocation of UA was significantly blocked after preadministration of brusatol, suggesting that UA may regulate ARE-related gene expression through promoting Nrf2 activation to play antioxidative effects after FCI/R. In addition, brusatol treatment suppressed the antioxidative stress activities of UA

and aggravated neuronal injury after FCI/R. These data strongly demonstrated that UA activated Nrf2 signaling pathway to perform its antioxidative and antiapoptotic activities as well as neuroprotective effects. However, while we have evidenced that the protein expression of HO-1 increased via UA treatment in this study, it is noteworthy that it does not implicate that HO-1 is the only factor involved in the protective effects of UA. An in vitro study proved that UA treatment increased mRNA levels of the modifier subunit of the γ-glutamyl cysteine ligase (GCL) and NAD(P)H:quinone oxidoreductase 1 (NQO1) and protein levels of GCLM in astrocyte cultures, whose inductions are governed by Nrf2, suggesting other antioxidants induced by Nrf2, may also contribute to the protective effects of UA [28]. Thus, the neuroprotective actions of UA may also be due to a wide spectrum of other Nrf2-regulated antioxidant genes potentially.

In addition, our study demonstrated that UA significantly increases the endogenous BDNF and NGF expressions. Several studies indicate that increased levels of neurotrophins have a protective role in experimental stroke studies [10]. The family of neurotrophins includes BDNF and NGF. Both animal and clinical studies have shown that BDNF has an effect to improve neurological recovery, prevent neuronal death, and support the survival of many types of neurons after cerebral ischemia [12, 13, 41]. NGF is also critical for neuronal survival, proliferation, and differentiation, and it has been reported that NGF is essential to improve neurological function after cerebral ischemia [12, 42]. By binding to tropomyosin receptor kinase (Trk) receptors, BDNF and NGF activate the downstream signaling pathways such as phosphatidylinositol 3-kinase (PI3K)/protein kinase B (Akt) pathways and the mitogen-activated protein kinase (MAPK)/extracellular signal-regulated kinase (ERK) [43, 44]. Several lines of evidence reported that Nrf2 activation can be regulated via PI3K/Akt and MAPK/ERK pathways and thereby affects redox homeostasis [17, 19, 45–47]. Some studies suggested that BDNF can active antioxidant mechanisms constantly by inducing Nrf2 nuclear translocation [18]. Neurotrophic signaling pathway may be an upstream mechanism of the Nrf2 activation. Other studies have demonstrated that Nrf2 played a physiological role in the neuroprotective response to regulate BDNF and NGF expressions in a Nrf2-dependent manner which may confer neuroprotection by attenuating oxidative stress [48–50]. It is still difficult to propose the precise mechanisms that control Nrf2 translocation and how the Nrf2 antioxidant system talks to the neurotrophic signaling pathway. In the present study, the upregulation of BDNF and NGF expressions by UA was partially depressed by brusatol, suggesting that UA stimulates BDNF and NGF expressions through a Nrf2-mediated pathway. Although the precise mechanism of Nrf2-mediated induction of the BDNF and NGF expressions is still unclear, these findings implicate that augmenting the levels of neurotrophins via pharmacological strategies may be one of the factors contributing to the beneficial effects of UA, which may offer a powerful therapeutic target of oxidative damage. However, the exact events in the upregulation of neurotrophin expression by UA in the I/R rat brain need further exploration.

Our study has several limitations. First, it has been demonstrated that hyperemia at reperfusion can be a sign of worse I/R injury [51, 52]. Prior study has shown that the neuroprotective effect of UA is more marked in the rats that develop a hyperperfusion state after reperfusion [26]. However, the state of brain blood perfusion at early reperfusion was not detected in the current study. Second, sample sizes as 3-4 per group for immunochemistry and western blot detection methods are fairly small. The relatively small number of the samples often causes low statistical power, which is one of the factors related to low reproducibility of results from preclinical animal research. So sample sizes should be enlarged in the future investigation to validate our findings. And last, in the current study, 24 hours after transient FCI was chosen as the endpoint based on previous literature data as many studies reported neuroprotective effects of UA at this time point [23, 26]. The present study strengthens the concept that UA exhibits short-term antioxidant and neuroprotective effects. Further studies are essential to extend observation periods after transient FCI to detect the longer therapeutic effect of UA.

5. Conclusions

For the first time, this study demonstrates that UA confers neuroprotection against FCI/R-induced oxidative stress via Nrf2 pathway activation as well as BDNF and NGF expression upregulation. The protective effect of UA was blocked by Nrf2 inhibitor brusatol. Nonetheless, further study deserves to be done in the future to investigate whether other pathways or mechanisms participated in the neuroprotective effects of UA.

Data Availability

The data used to support the findings of this study are included within the article.

Conflicts of Interest

The authors have no conflicts of interest related to this research.

Authors' Contributions

Bai-liu Ya and Qian Liu contributed equally to this work.

Acknowledgments

This work was supported by the National Natural Science Foundation of China (nos. 81703490 and 81870948), the Natural Science Foundation of Shandong Province (nos. ZR2015HQ019 and ZR2017HQ056), the National Undergraduates Innovation Training Program (no. 201610443001), the Undergraduates Innovation Training Program and the Undergraduates Scientific Research Programs of Jining Medical University (nos. cx2016001, cx2017029, 2015, JYXS2017KJ011), the Jining Science and Technology Boost New Energy Conversion Plan (no. 2017SMNS004), the Teacher Scientific Research Support Fund of Jining Medical University (JY2017KJ021),

and the International Cooperation Training Program of Outstanding Young Teachers of Shandong Province (2013).

References

[1] M. A. Moskowitz, E. H. Lo, and C. Iadecola, "The science of stroke: mechanisms in search of treatments," *Neuron*, vol. 67, no. 2, pp. 181–198, 2010.

[2] H. Chen, H. Yoshioka, G. S. Kim et al., "Oxidative stress in ischemic brain damage: mechanisms of cell death and potential molecular targets for neuroprotection," *Antioxidants & Redox Signaling*, vol. 14, no. 8, pp. 1505–1517, 2011.

[3] A. Janyou, P. Wicha, J. Jittiwat, A. Suksamrarn, C. Tocharus, and J. Tocharus, "Dihydrocapsaicin attenuates blood brain barrier and cerebral damage in focal cerebral ischemia/reperfusion via oxidative stress and inflammatory," *Scientific Reports*, vol. 7, no. 1, article 10556, 2017.

[4] S. Pundik, K. Xu, and S. Sundararajan, "Reperfusion brain injury: focus on cellular bioenergetics," *Neurology*, vol. 79, 13, Supplement 1, pp. S44–S51, 2012.

[5] T. Suzuki and M. Yamamoto, "Molecular basis of the Keap1–Nrf2 system," *Free Radical Biology & Medicine*, vol. 88, Part B, pp. 93–100, 2015.

[6] R. Zhang, M. Xu, Y. Wang, F. Xie, G. Zhang, and X. Qin, "Nrf2—a promising therapeutic target for defensing against oxidative stress in stroke," *Molecular Neurobiology*, vol. 54, no. 8, pp. 6006–6017, 2017.

[7] Y. Ding, M. Chen, M. Wang, Y. Li, and A. Wen, "Posttreatment with 11-keto-β-boswellic acid ameliorates cerebral ischemia–reperfusion injury: Nrf2/HO-1 pathway as a potential mechanism," *Molecular Neurobiology*, vol. 52, no. 3, pp. 1430–1439, 2015.

[8] B. Ya, H. Li, H. Wang et al., "5-HMF attenuates striatum oxidative damage via Nrf2/ARE signaling pathway following transient global cerebral ischemia," *Cell Stress and Chaperones*, vol. 22, no. 1, pp. 55–65, 2017.

[9] S. Otsuka, H. Sakakima, M. Sumizono, S. Takada, T. Terashi, and Y. Yoshida, "The neuroprotective effects of preconditioning exercise on brain damage and neurotrophic factors after focal brain ischemia in rats," *Behavioural Brain Research*, vol. 303, pp. 9–18, 2016.

[10] S. Lanfranconi, F. Locatelli, S. Corti et al., "Growth factors in ischemic stroke," *Journal of Cellular and Molecular Medicine*, vol. 15, no. 8, pp. 1645–1687, 2011.

[11] E. J. Huang and L. F. Reichardt, "Trk receptors: roles in neuronal signal transduction," *Annual Review of Biochemistry*, vol. 72, no. 1, pp. 609–642, 2003.

[12] Z. Kokaia, Q. Zhao, M. Kokaia et al., "Regulation of brain-derived neurotrophic factor gene expression after transient middle cerebral artery occlusion with and without brain damage," *Experimental Neurology*, vol. 136, no. 1, pp. 73–88, 1995.

[13] W. R. Schabitz, S. Schwab, M. Spranger, and W. Hacke, "Intraventricular brain-derived neurotrophic factor reduces infarct size after focal cerebral ischemia in rats," *Journal of Cerebral Blood Flow & Metabolism*, vol. 17, no. 5, pp. 500–506, 1997.

[14] M. P. Mattson, M. A. Lovell, K. Furukawa, and W. R. Markesbery, "Neurotrophic factors attenuate glutamate-induced accumulation of peroxides, elevation of intracellular Ca^{2+} concentration, and neurotoxicity and increase antioxidant enzyme activities in hippocampal neurons," *Journal of Neurochemistry*, vol. 65, no. 4, pp. 1740–1751, 1995.

[15] X. Y. Mao, H. H. Zhou, X. Li, and Z. Q. Liu, "Huperzine a alleviates oxidative glutamate toxicity in hippocampal HT22 cells via activating BDNF/TrkB-dependent PI3K/Akt/mTOR signaling pathway," *Cellular and Molecular Neurobiology*, vol. 36, no. 6, pp. 915–925, 2016.

[16] K. U. Tufekci, E. Civi Bayin, S. Genc, and K. Genc, "The Nrf2/ARE pathway: a promising target to counteract mitochondrial dysfunction in Parkinson's disease," *Parkinson's Disease*, vol. 2011, article 314082, 14 pages, 2011.

[17] T. Ishii, E. Warabi, and G. E. Mann, "Circadian control of BDNF-mediated Nrf2 activation in astrocytes protects dopaminergic neurons from ferroptosis," *Free Radical Biology & Medicine*, 2018.

[18] E. Bouvier, F. Brouillard, J. Molet et al., "Nrf2-dependent persistent oxidative stress results in stress-induced vulnerability to depression," *Molecular Psychiatry*, vol. 22, no. 12, p. 1795, 2017.

[19] O. Firuzi, F. Moosavi, R. Hosseini, and L. Saso, "Modulation of neurotrophic signaling pathways by polyphenols," *Drug Design, Development and Therapy*, vol. 10, pp. 23–42, 2015.

[20] B. F. Becker, "Towards the physiological function of uric acid," *Free Radical Biology and Medicine*, vol. 14, no. 6, pp. 615–631, 1993.

[21] G. L. Squadrito, R. Cueto, A. E. Splenser et al., "Reaction of uric acid with peroxynitrite and implications for the mechanism of neuroprotection by uric acid," *Archives of Biochemistry and Biophysics*, vol. 376, no. 2, pp. 333–337, 2000.

[22] G. R. Buettner, "The pecking order of free radicals and antioxidants: lipid peroxidation, α-tocopherol, and ascorbate," *Archives of Biochemistry and Biophysics*, vol. 300, no. 2, pp. 535–543, 1993.

[23] Y. H. Ma, N. Su, X. D. Chao et al., "Thioredoxin-1 attenuates post-ischemic neuronal apoptosis via reducing oxidative/nitrative stress," *Neurochemistry International*, vol. 60, no. 5, pp. 475–483, 2012.

[24] E. Romanos, A. M. Planas, S. Amaro, and A. Chamorro, "Uric acid reduces brain damage and improves the benefits of rt-PA in a rat model of thromboembolic stroke," *Journal of Cerebral Blood Flow & Metabolism*, vol. 27, no. 1, pp. 14–20, 2007.

[25] Z. F. Yu, A. J. Bruce-Keller, Y. Goodman, and M. P. Mattson, "Uric acid protects neurons against excitotoxic and metabolic insults in cell culture, and against focal ischemic brain injury in vivo," *Journal of Neuroscience Research*, vol. 53, no. 5, pp. 613–625, 1998.

[26] Y. Onetti, A. P. Dantas, B. Perez et al., "Middle cerebral artery remodeling following transient brain ischemia is linked to early postischemic hyperemia: a target of uric acid treatment," *American Journal of Physiology-Heart and Circulatory Physiology*, vol. 308, no. 8, pp. H862–H874, 2015.

[27] C. Justicia, A. Salas-Perdomo, I. Pérez-de-Puig et al., "Uric acid is protective after cerebral ischemia/reperfusion in hyperglycemic mice," *Translational Stroke Research*, vol. 8, no. 3, pp. 294–305, 2017.

[28] R. Bakshi, H. Zhang, R. Logan et al., "Neuroprotective effects of urate are mediated by augmenting astrocytic glutathione synthesis and release," *Neurobiology of Disease*, vol. 82, pp. 574–579, 2015.

[29] B. Ya, C. Li, L. Zhang, W. Wang, and L. Li, "Cornel iridoid glycoside inhibits inflammation and apoptosis in brains of rats with focal cerebral ischemia," *Neurochemical Research*, vol. 35, no. 5, pp. 773–781, 2010.

[30] B. Chen, H. Cao, L. Chen et al., "Rifampicin attenuated global cerebral ischemia injury via activating the nuclear factor erythroid 2-related factor pathway," *Frontiers in Cellular Neuroscience*, vol. 10, p. 273, 2016.

[31] L. Belayev, O. F. Alonso, R. Busto, W. Zhao, and M. D. Ginsberg, "Middle cerebral artery occlusion in the rat by intraluminal suture. Neurological and pathological evaluation of an improved model," *Stroke*, vol. 27, no. 9, pp. 1616–1623, 1996, discussion 1623.

[32] T. Mokudai, I. A. Ayoub, Y. Sakakibara, E. J. Lee, C. S. Ogilvy, and K. I. Maynard, "Delayed treatment with nicotinamide (vitamin B_3) improves neurological outcome and reduces infarct volume after transient focal cerebral ischemia in Wistar rats," *Stroke*, vol. 31, no. 7, pp. 1679–1685, 2000.

[33] K. A. Conlon, D. O. Zharkov, and M. Berrios, "Immunofluorescent localization of the murine 8-oxoguanine DNA glycosylase (mOGG1) in cells growing under normal and nutrient deprivation conditions," *DNA Repair*, vol. 2, no. 12, pp. 1337–1352, 2003.

[34] J. W. Thompson, S. V. Narayanan, K. B. Koronowski, K. Morris-Blanco, K. R. Dave, and M. A. Perez-Pinzon, "Signaling pathways leading to ischemic mitochondrial neuroprotection," *Journal of Bioenergetics and Biomembranes*, vol. 47, no. 1-2, pp. 101–110, 2015.

[35] K. M. Kanninen, Y. Pomeshchik, H. Leinonen, T. Malm, J. Koistinaho, and A. L. Levonen, "Applications of the Keap1-Nrf2 system for gene and cell therapy," *Free Radical Biology & Medicine*, vol. 88, Part B, pp. 350–361, 2015.

[36] V. P. Nakka, P. Prakash-Babu, and R. Vemuganti, "Crosstalk between endoplasmic reticulum stress, oxidative stress, and autophagy: potential therapeutic targets for acute CNS injuries," *Molecular Neurobiology*, vol. 53, no. 1, pp. 532–544, 2016.

[37] Z. A. Shah, R. C. Li, A. S. Ahmad et al., "The flavanol (−)-epicatechin prevents stroke damage through the Nrf2/HO1 pathway," *Journal of Cerebral Blood Flow & Metabolism*, vol. 30, no. 12, pp. 1951–1961, 2010.

[38] A. Alfieri, S. Srivastava, R. C. M. Siow et al., "Sulforaphane preconditioning of the Nrf2/HO-1 defense pathway protects the cerebral vasculature against blood-brain barrier disruption and neurological deficits in stroke," *Free Radical Biology & Medicine*, vol. 65, pp. 1012–1022, 2013.

[39] Y. M. Kim, H. O. Pae, J. E. Park et al., "Heme oxygenase in the regulation of vascular biology: from molecular mechanisms to therapeutic opportunities," *Antioxidants & Redox Signaling*, vol. 14, no. 1, pp. 137–167, 2011.

[40] X. Fan and L. Mu, "The role of heme oxygenase-1 (HO-1) in the regulation of inflammatory reaction, neuronal cell proliferation and apoptosis in rats after intracerebral hemorrhage (ICH)," *Neuropsychiatric Disease and Treatment*, vol. 13, pp. 77–85, 2017.

[41] M. Ploughman, V. Windle, C. L. MacLellan, N. White, J. J. Dore, and D. Corbett, "Brain-derived neurotrophic factor contributes to recovery of skilled reaching after focal ischemia in rats," *Stroke*, vol. 40, no. 4, pp. 1490–1495, 2009.

[42] D. M. Holtzman, R. A. Sheldon, W. Jaffe, Y. Cheng, and D. M. Ferriero, "Nerve growth factor protects the neonatal brain against hypoxic-ischemic injury," *Annals of Neurology*, vol. 39, no. 1, pp. 114–122, 1996.

[43] A. Brunet, S. R. Datta, and M. E. Greenberg, "Transcription-dependent and -independent control of neuronal survival by the PI3K–Akt signaling pathway," *Current Opinion in Neurobiology*, vol. 11, no. 3, pp. 297–305, 2001.

[44] A. Bonni, A. Brunet, A. E. West, S. R. Datta, M. A. Takasu, and M. E. Greenberg, "Cell survival promoted by the Ras-MAPK signaling pathway by transcription-dependent and -independent mechanisms," *Science*, vol. 286, no. 5443, pp. 1358–1362, 1999.

[45] T. Chen, Y. Wu, Y. Wang et al., "Brain-derived neurotrophic factor increases synaptic protein levels via the MAPK/Erk signaling pathway and Nrf2/Trx Axis following the transplantation of neural stem cells in a rat model of traumatic brain injury," *Neurochemical Research*, vol. 42, no. 11, pp. 3073–3083, 2017.

[46] M. Chen, L. H. Dai, A. Fei, S. M. Pan, and H. R. Wang, "Isoquercetin activates the ERK1/2-Nrf2 pathway and protects against cerebral ischemia-reperfusion injury in vivo and in vitro," *Experimental and Therapeutic Medicine*, vol. 13, no. 4, pp. 1353–1359, 2017.

[47] B. Li, J. Sun, G. Lv et al., "Sevoflurane postconditioning attenuates cerebral ischemia-reperfusion injury via protein kinase B/nuclear factor-erythroid 2-related factor 2 pathway activation," *International Journal of Developmental Neuroscience*, vol. 38, pp. 79–86, 2014.

[48] J. Mimura, K. Kosaka, A. Maruyama et al., "Nrf2 regulates NGF mRNA induction by carnosic acid in T98G glioblastoma cells and normal human astrocytes," *The Journal of Biochemistry*, vol. 150, no. 2, pp. 209–217, 2011.

[49] Y. Y. Hsu, Y. T. Tseng, and Y. C. Lo, "Berberine, a natural antidiabetes drug, attenuates glucose neurotoxicity and promotes Nrf2-related neurite outgrowth," *Toxicology and Applied Pharmacology*, vol. 272, no. 3, pp. 787–796, 2013.

[50] A. Shi, J. Xiang, F. He et al., "The phenolic components of *Gastrodia elata* improve prognosis in rats after cerebral ischemia/reperfusion by enhancing the endogenous antioxidant mechanisms," *Oxidative Medicine and Cellular Longevity*, vol. 2018, Article ID 7642158, 16 pages, 2018.

[51] F. J. Pérez-Asensio, X. de la Rosa, F. Jiménez-Altayó et al., "Antioxidant CR-6 protects against reperfusion injury after a transient episode of focal brain ischemia in rats," *Journal of Cerebral Blood Flow & Metabolism*, vol. 30, no. 3, pp. 638–652, 2010.

[52] A. Tamura, T. Asano, and K. Sano, "Correlation between rCBF and histological changes following temporary middle cerebral artery occlusion," *Stroke*, vol. 11, no. 5, pp. 487–493, 1980.

Hindawi
Oxidative Medicine and Cellular Longevity
Volume 2018, Article ID 2518676, 17 pages
https://doi.org/10.1155/2018/2518676

Research Article

C_{60} Fullerene Prevents Restraint Stress-Induced Oxidative Disorders in Rat Tissues: Possible Involvement of the Nrf2/ARE-Antioxidant Pathway

Olga O. Gonchar,[1] **Andriy V. Maznychenko**,[1] **Nataliya V. Bulgakova**,[1] **Inna V. Vereshchaka**,[2] **Tomasz Tomiak**,[2] **Uwe Ritter**,[3] **Yuriy I. Prylutskyy**,[4] **Iryna M. Mankovska**,[1] **and Alexander I. Kostyukov**[1]

[1]*Bogomoletz Institute of Physiology, Bogomoletz Str. 4, Kyiv 01024, Ukraine*
[2]*Gdansk University of Physical Education and Sport, Kazimierza Gorskiego Str. 1, 80-336 Gdansk, Poland*
[3]*Institute of Chemistry and Biotechnology, Technical University of Ilmenau, Weimarer Str. 25, Ilmenau 98693, Germany*
[4]*Taras Shevchenko National University of Kyiv, ESC "Institute of Biology and Medicine", Volodymyrska Str. 64, Kyiv 01601, Ukraine*

Correspondence should be addressed to Olga O. Gonchar; olga.gonchar@i.ua

Received 11 July 2018; Accepted 9 October 2018; Published 13 November 2018

Guest Editor: Luciano Saso

The effects of C_{60}FAS (50 and 500 μg/kg) supplementation, in a normal physiological state and after restraint stress exposure, on prooxidant/antioxidant balance in rat tissues were explored and compared with the effects of the known exogenous antioxidant N-acetylcysteine. Oxidative stress biomarkers (ROS, $O_2\cdot^-$, H_2O_2, and lipid peroxidation) and indices of antioxidant status (MnSOD, catalase, GPx, GST, γ-GCL, GR activities, and GSH level) were measured in the brain and the heart. In addition, protein expression of Nrf2 in the nuclear and cytosol fractions as well as the protein level of antiradical enzyme MnSOD and GSH-related enzymes γ-GCLC, GPx, and GSTP as downstream targets of Nrf2 was evaluated by western blot analysis. Under a stress condition, C_{60}FAS attenuates ROS generation and $O_2\cdot^-$ and H_2O_2 releases and thus decreases lipid peroxidation as well as increases rat tissue antioxidant capacity. We have shown that C_{60}FAS supplementation has dose-dependent and tissue-specific effects. C_{60}FAS strengthened the antiradical defense through the upregulation of MnSOD in brain cells and maintained MnSOD protein content at the control level in the myocardium. Moreover, C_{60}FAS enhanced the GSH level and the activity/protein expression of GSH-related enzymes. Correlation of these changes with Nrf2 protein content suggests that under stress exposure, along with other mechanisms, the Nrf2/ARE-antioxidant pathway may be involved in regulation of glutathione homeostasis. In our study, in an *in vivo* model, when C_{60}FAS (50 and 500 μg/kg) was applied alone, no significant changes in Nrf2 protein expression as well as in activity/protein levels of MnSOD and GSH-related enzymes in both tissues types were observed. All these facts allow us to assume that in the *in vivo* model, C_{60}FAS affects on the brain and heart endogenous antioxidative statuses only during the oxidative stress condition.

1. Introduction

Today, everybody of the living organism is exposed to stress of various origins. Numerous researches indicate that the most harmful effects to an organism result from social and psychological factors [1, 2]. Emotional overstrain as one of the types of stress states is constantly encountered not only in daily life but also as an imperative component of such human activities as sports, military, and aerospace. Acute stress of sufficient strength threatens body homeostasis, which results in biochemical and physiological disturbances leading to serious health risks [2–4]. Exposure to a stressful situation is well known to stimulate various damaging pathways, causing overproduction of free radicals such as superoxide anion ($O_2\cdot^-$), hydroxyl radical (OH·), and nonradical hydrogen peroxide (H_2O_2), leading to lipid peroxidation,

protein oxidation, DNA damage, and cell death [5]. In response to oxidative attack, cells have developed an antioxidant defense system to maintain cellular redox homeostasis and to protect cells from injury [6, 7]. Classical antioxidant enzymes including superoxide dismutase (SOD), catalase, and glutathione peroxidase (GPx) as well as small thiol-containing compound glutathione (GSH) may directly inactivate ROS and prevent ROS-initiated reactions [8]. Intracellular glutathione is the most abundant nonprotein thiol with several vital functions such as direct scavenging of free radicals, detoxification of electrophilic compounds, and modulation of cellular redox status and thiol-disulphide status of proteins, as well as regulation of cell signaling and repair pathways [9]. GSH homeostasis is modulated by self-adjusting the balance among GSH synthesis, utilization, and recycling, and the disturbances of these processes may cause an oxidant/antioxidant imbalance. Antioxidants of indirect action include so-called phase II detoxifying enzymes, which contribute to biosynthesis/recycling of thiols and facilitate excretion of oxidized, reactive secondary metabolites (e.g., quinones, epoxides, aldehydes, and peroxides) through reduction/conjugation reactions. They are represented by glutathione-S-transferase (GST) isozymes, NADPH: quinone oxidoreductase (NQO1), heavy (catalytic) and light (modifier) subunits of γ-glutamate-cysteine ligase (γ-GCL), glutathione peroxidase (GPx), and glutathione reductase (GR) and stress response proteins such as heme oxygenase- (HO-) 1 and heavy (FTH) and light (FTL) chains of ferritin [10].

Restraint is the one specific and classic method to simultaneously induce emotional and physiological stresses. Therefore, restraint is widely used for modulation of oxidative stress-induced pathological states [11]. Studies from several laboratories have demonstrated that acute restraint stress significantly elevated oxidative status and lipid peroxidation through downregulation of antioxidative enzymes, with glutathione depletion that disrupted the cellular redox state [12–15]. Restraint stress can affect central nervous system functions by producing neurochemical and hormonal disorders associated with imbalance in a prooxidant/antioxidant system [16, 17].

Numerous reports have shown that negative consequences of stress are amenable to improvement by exogenous antioxidant acting through various pathways to enhance resistance to stress exposure [10, 12, 18]. Indeed, pharmacological interventions targeting cellular endogenous antioxidants may be a promising stress management strategy for protecting against oxidative stress-induced cell damage. Fullerene (C_{60}) is known as a spherical carbon molecule with a unique cage structure and is characterized as a strong radical sponge [19]. The antioxidant level of C_{60} has been reported to be several hundredfold higher than the level of other antioxidants [20, 21]. A great deal of information has accumulated concerning the beneficial effects of fullerene and its water-soluble derivatives, which include neuroprotection, radioprotection, antiproliferative, antitumor, and anti-inflammatory activities [22–25], but little is known of C_{60} protective effects and mechanisms of action in rat tissues under restraint stress condition.

Fullerene pretreatment has been known to prevent oxidative stress deleterious effects by direct ROS scavenging and/or increasing the antioxidant enzyme activities [20, 26, 27]. However, the mechanism involved in the cell protective actions of C_{60} is still open for discussion. Recently, polyhydroxylated derivatives of fullerene were demonstrated to induce endogenous phase II antioxidant enzymes via Nrf2/ARE-dependent mechanisms and attenuate oxidative stress-mediated cell death, thus providing new insights into the mechanisms of the antioxidant properties of fullerene [28, 29]. NF-E2-related factor 2 (Nrf2) is a member of the cap'n'collar family of bZIP transcription factors that bind to the antioxidant response element (ARE) and thereby regulate the induction of genes encoding antioxidant proteins and phase II detoxifying enzymes. Nrf2 activation in response to oxidative injury has been shown to protect cells and tissues from oxidative stress [30]. Under normal conditions, Nrf2 is localized in the cytoplasm where it binds with the Keap1, which functions as an adaptor for Cul3-based E3 ligase to regulate the proteasomal degradation of Nrf2. However, after direct attack by ROS or resulting indirect actions such as phosphorylation, Nrf2 dissociates from Keap1 and thereby translocates into the nucleus and transactivates its target genes through ARE [31]. The coordinated transcriptional activation of the Nrf2-mediated antioxidant and prosurvival enzymes is a potential mechanism to maintain redox homeostasis and to abolish the deleterious effects of oxidative stress [32].

Therefore, our aim was to examine the effects of C_{60}FAS in comparison with the actions of the known exogenous antioxidant N-acetylcysteine [33] on prooxidant/antioxidant homeostasis in rats in a normal physiological state and following restraint stress exposure. Many studies have shown that restraint stress exerts a profound impact on organs with a high metabolic level and the highest mass-specific oxygen consumption rates in the body such as the brain and the heart. Since the association of restraint stress with several neurodegenerative and cardiovascular diseases is well-documented [1–3], we investigated restraint stress-induced oxidative damage in the brain as well as in the heart as an important stress-sensitive peripheral organ.

Nrf2 is known to control both the basal and inducible expressions of genes encoding the heavy and light chains of γ-GCL, one of the important enzymes in GSH biosynthesis, and thereby takes part in the regulation of GSH recycling [10, 34]. However, whether and how Nrf2 modulates GSH homeostasis in rat tissues after C_{60}FAS supplementation and following restraint stress exposure are poorly understood.

To further investigate the potential mechanisms of C_{60}FAS-mediated protection against oxidative stress induced by restraint exposure, we examined protein expression of Nrf2 in the nuclear and cytosol fractions. In addition, the protein level of the antiradical enzyme MnSOD and GSH-related enzymes as downstream targets of Nrf2 was evaluated by western blot analysis.

2. Materials and Methods

2.1. Material Preparation and Characterization. A highly stable pristine C_{60} fullerene aqueous colloid solution (C_{60}FAS)

with purity of more than 99.96% has been prepared and characterized [27, 35]. This method is based on transferring fullerene from organic solution into the aqueous phase by ultrasonic treatment. The purity of the prepared C_{60}FAS (i.e., the presence/absence of any residual impurities such as carbon black, toluene phase) was determined by HPLC analysis. The state of C_{60} fullerene in aqueous solution was monitored using atomic force microscopy. Small-angle neutron scattering measurements were carried out at the YuMO small-angle diffractometer at the IBR-2 pulsed reactor in the time-of-flight mode with a two-detector setup. The maximal concentration of C_{60} fullerenes in water obtained by this method was 0.15 mg/ml. Concentrated C_{60}FAS contains both single C_{60} and its labile nanoassociates with sizes of 3–70 nm.

2.2. Experimental Design and Sample Collection. Male Wistar rats weighing 220–260 g were used in the study. The rats were housed in Plexiglas cages (4 rats per cage) and maintained in an air-filtered and temperature-controlled (20–22°C) room. Rats received a standard pellet diet and water ad libitum. The use of the animals was approved by the Ethics Committee of the Institute, and the study was performed in accordance with the European Communities Council Directive of 24 November 1986 (86/609/EEC). All chemicals were purchased from Sigma, Fluka, and Merck and were of the highest purity.

The study was performed in two phases. Phase I aimed at investigating the effect of C_{60}FAS at various doses and N-acetylcysteine (NAC) as a positive control on markers of prooxidant/antioxidant balance in the whole brain and heart tissues. Rats were divided into four groups ($n = 8$/group) based on treatment: control/vehicle (C), fullerene-treated at a dose of 50 μg/kg (F1), fullerene-treated at a dose of 500 μg/kg (F2), and NAC-treated at a dose of 100 mg/kg in physiological saline (NAC). Animals were treated with F1, F2, or NAC intraperitoneally (i.p.) once daily for 1 week. The controls/vehicles were administrated i.p. with an equal volume of physiological saline during the same time period. The NAC was used according to previous study [36] that described the effective dose in similar experiments with animals. The C_{60}FAS dosage was based on previous studies where the safety profile was checked and found to be nonlethal. No toxic effects or death has been fixed under the action of C_{60}FAS after their oral administration to rats in the total dosage of 2 mg/kg for 5 days [21] and i.p. injection in the dose of 0.15 mg/kg [27].

Phase II was an acute restraint stress model alone and after pretreatment with the above-mentioned drugs. The experimental groups were as follows: group 1 received vehicle (physiological saline) and served as a control (1); group 2 was exposed to restraint for 6 h, representing an acute stressor (AS); group 3 was exposed to AS and received C_{60}FAS (50 μg/kg) (AS + F1); group 4 was subjected to AS and received C_{60}FAS (500 μg/kg) (AS + F2); group 5 was subjected to AS and received NAC (100 mg/kg) (AS + NAC). Drugs were administered i.p. between 9:00 a.m. and 10:00 a.m. once a day for 1 week prior to the restraint exposure. To habituate the rats to i.p. injection, all rats in groups 1 and 2 were administered physiological saline (1 ml/kg) daily for 1 week before the impact. The restraint was performed using a plastic rodent restrainer that allowed for a close fit to the rats. Experiments with the acute stressor were performed between 8:00 and 10:00 a.m. to minimize possible hormonal interference by circadian rhythms. During restraint stress, animals were not physically compressed, but food and water were deprived. Animals were decapitated immediately after the restraint sessions. At the time of sacrifice, the animals were lightly anesthetized with ether.

The brain and heart were rapidly removed, washed in ice-cold sterile physiological saline (0.9%), and a 10% homogenate (50 mM sodium phosphate buffer with 2 mM EDTA, pH 7.4) was prepared. Cellular debris was removed by centrifugation at 15,000g (4°C, 15 min), and supernatants were stored at −70°C. The protein concentration was estimated using the Bradford method with bovine serum albumin as a standard.

2.3. Evaluation of Oxidative Stress Markers

2.3.1. Corticosterone Analysis. Whole blood, removed under ether anesthesia, was collected into heparin-coated test tubes, centrifuged at 1500g for 10 min at 4°C to separate plasma from erythrocytes and kept at −70°C until assayed. Plasma corticosterone was quantified using a commercial Demeditec Corticosterone rat/mouse ELISA kit (DEV9922, version 7-06/17, Demeditec Diagnostics, Germany) according to the manufacturer's instructions. The resulting concentration of plasma corticosterone was expressed as ng/ml using a corticosterone standard curve.

2.3.2. Measurement of Reactive Oxygen Species (ROS) Formation. The data on ROS formation were obtained from dichlorofluorescein (DCF) fluorescence [37]. The tissue homogenates were loaded for 20 min at 37°C with a nonfluorescent probe (2′,7′-dichlorodihydrofluorescein diacetate, DCFH-DA) which is known to be decomposed in cells to give dichlorofluorescein upon oxidation by ROS, primarily hydroperoxide and superoxide anion. The final concentration of DCFH-DA was 5 mM. DCF formation was followed at the excitation wavelength of 488 nm and emission wavelength of 525 nm for 30 min by using a Hitachi F-2000 fluorescence spectrometer. The rate of DCFH-DA conversion to DCF was linear for at least 60 min, corrected with the autooxidation rate of DCFH-DA without protein. All assays were carried out in duplicate. Fluorescence was expressed as arbitrary fluorescence units.

2.3.3. Measurement of Superoxide Radical Production. Tissue superoxide production was measured by superoxide dismutase-sensitive ferricytochrome *c* reduction assays, as described previously [38]. Briefly, equal portions of tissue homogenate (0.5 mg of protein) were incubated with 50 μM acetylated ferricytochrome *c* in the presence or absence of superoxide dismutase (400 U/ml). To further ensure that any reduced ferricytochrome *c* is not reoxidized, catalase (125 U/ml) was added to the reaction, which removes any H_2O_2 formed. After incubation at 37°C for 15 min, reactions were terminated by adding 1 mM N-ethylmaleimide. Reduction of ferricytochrome *c* was measured by reading

absorbance at 550 nm in a spectrophotometer. The amount of $O_2{\cdot}^-$ release was calculated by dividing the difference in absorbance of the samples with and without superoxide dismutase by the extinction coefficient for the change from ferricytochrome c to ferrocytochrome c ($\varepsilon = 24\,mM^{-1}\,cm^{-1}$), and the results are expressed as nmol/min/mg protein.

2.3.4. Measurement of Hydroperoxide. The H_2O_2 concentration in the tissue homogenates was measured using the FOX method, which is based on the peroxide-mediated oxidation of Fe^{2+}, followed by the reaction of Fe^{3+} with xylenol orange (*o*-cresolsulphonephthalein 3′,3″-bis [methylimino] diacetic acid, sodium salt). This method is extremely sensitive and is used to measure low levels of water-soluble hydroperoxide present in the aqueous phase. To determine the H_2O_2 concentration, 500 μl of the incubation medium was added to 500 μl of the assay reagent (500 μM ammonium ferrous sulphate, 50 mM H_2SO_4, 200 μM xylenol orange, and 200 mM sorbitol). The absorbance of the Fe^{3+}-xylenol orange complex (A560) was detected after 45 min. Standard curves of H_2O_2 were obtained for each independent experiment by adding variable amounts of H_2O_2 to 500 μl of basal medium mixed with 500 μl of the assay reagent. The data were normalized and are expressed as μM H_2O_2 per mg of protein [39].

2.3.5. Lipid Peroxidation Assay. Lipid peroxidation was measured from the formation of thiobarbituric acid-reactive substances (TBARS) using the method of Buege and Aust [40]. TBARS were isolated by boiling tissue homogenates for 15 min at 100°C with the thiobarbituric acid reagent (0.5% 2-thiobarbituric acid/10% trichloroacetic acid/0.63 mM hydrochloric acid) and measuring the absorbance at 532 nm. The results are expressed as nM/mg of protein using $\varepsilon = 1.56 \times 10^5\,mM^{-1}\,cm^{-1}$.

2.4. Evaluation of Biochemical Parameters

2.4.1. Enzyme Activity Assay. Manganese superoxide dismutase (MnSOD) activity was measured by the method of Misra and Fridovich [41], based on the inhibition of autooxidation of adrenaline to adrenochrome by SOD contained in the examined samples. The samples were preincubated at 0°C for 60 min with 6 mM KCN, which produces total inhibition of Cu, Zn-SOD activity. The results are expressed as specific activity of the enzyme in units per mg protein. One unit of SOD activity was defined as the amount of protein causing 50% inhibition of the conversion rate of adrenaline to adrenochrome under specified conditions.

Catalase activity was measured by the decomposition of hydrogen peroxide, determined by a decrease in the absorbance at 240 nm [42].

γ-Glutamylcysteinyl ligase (γ-GCL) activity was determined following the method described by Seelig and Meister [43]. Briefly, enzyme activity was assayed at 37°C in reaction mixtures containing 0.1 M Tris-HCl buffer (pH 8.2), 0.15 M KCl, 5 mM ATP, 2 mM phosphoenolpyruvate, 10 mM glutamate, 10 mM γ-aminobutyrate, 20 mM $MgCl_2$, 2 mM EDTA, 0.2 mM NADH, 17 mg pyruvate kinase, and 17 mg lactate dehydrogenase. The reaction was initiated by adding the sample, and the rate of decrease in absorbance at 340 nm was monitored. Enzyme-specific activity was measured as μM of NADH oxidized per minute per milligram protein.

Activity of selenium-dependent glutathione peroxidase (GPx) was determined according to the method of Flohé and Gunzler [44]. Briefly, the reaction mixtures consisted of 50 mM KPO_4 (pH 7.0), 1 mM EDTA, 1 mM NaN_3, 0.2 mM NADPH, 1 mM GSH, 0.25 mM H_2O_2, and 226 U/ml glutathione reductase, and rates of NADPH oxidation followed at 340 nm.

The glutathione reductase (GR) reaction mixture contained phosphate buffer (0.2 M) pH 7.0, EDTA (2 mM), NADPH (2 mM), and GSSG (20 mM). The reaction is initiated by the addition of the sample, and the decrease in absorbance at 340 nm is followed at 30°C [45].

Glutathione-S-transferase (GST) activity was determined by assaying 1-chloro-2, 4-dinitrobenzene (CDNB) conjugation with GSH, as described by Warholm et al. [46]. The working solution contained 20 mM CDNB, 20 mM GSH, and 1 mM EDTA in 200 mM phosphate buffer. The conjugated product was recorded at 340 nm continuously for 5 min at 30°C ($\varepsilon = 9.6 \times 10^3\,M^{-1}\,cm^{-1}$).

2.4.2. Measurement of the Reduced Glutathione Level. The reduced glutathione (GSH) was determined as described [47]. The tissue sample was mixed with sulphosalicylic acid (4%) and incubated at 4°C for 30 min. Thereafter, the mixture was centrifuged at 1200g for 15 min at 4°C, and 0.1 ml of this supernatant was added to phosphate buffer (0.1 M, pH 7.4) containing DTNB in abs. ethanol. The yellow color that developed was read immediately at 412 nm. The GSH content was calculated as nM GSH/mg of protein ($\varepsilon = 13.6 \times 10^3\,M^{-1}\,cm^{-1}$).

2.5. Western Blot Analysis. For immunoblotting analysis, cytosolic and nuclear proteins were extracted from the blood-free (heparin was injected, and buffer was perfused in situ) heart and brain as was described previously [48]. Briefly, the tissues were homogenized in ice-cold lysis buffer containing 10 mM HEPES (pH 7.9), 1.5 mM $MgCl_2$, 10 mM KCl, 1 mM dithiothreitol, 0.1 mM EDTA, and 0.2 mM phenylmethylsulphonyl fluoride (PMSF) plus 1 μg/ml Halt™ Protease and Phosphatase Inhibitor Cocktail (78440, Thermo Scientific Inc., USA). This suspension was incubated on ice for 15 min. Then, 12.5 μl of 10% Nonidet P-40 was added, and the mixture was vigorously vortexed for 15 s. The cytoplasmic and nuclear fractions were separated by centrifugation at 15,000g at 4°C for 2 min. Equal amounts of protein were mixed with Laemmli buffer (S3401, Sigma), heated (99°C, 5 min), and then loaded onto 10–12% SDS polyacrylamide gels. Separated proteins were transferred onto polyvinylidene difluoride (PVDF) membranes, which were blocked in 5% nonfat milk in Tris-buffered saline-Tween (TBS-T) for 1 h at room temperature. Primary antibodies were applied overnight at 4°C. After washing in 1% nonfat milk in TBS-T, membranes were incubated with a secondary antibody conjugated to horseradish peroxidase (HRP) for 1 h at room temperature. Each antigen-antibody complex was visualized by the amino-ethylcarbazole

reaction. The relative expression of the proteins was quantified using densitometric scanning and analyzed by ImageJ and is expressed as a percent of controls. All samples were analyzed at least twice, and the average value was calculated for each sample. β-Actin and Lamin B1 were used as loading controls. Antibodies and dilutions were as follow: Nrf2 1 : 1000 (Sigma-Aldrich Co.), MnSOD 1 : 500 (Sigma-Aldrich Co.), GPx 1/2 (B-6) 1 : 500 (Santa Cruz Biotechnology Inc.), GSTP 1 : 500 (Santa Cruz Biotechnology Inc.), GCLC 1 : 500 (Sigma-Aldrich Co.), β-actin 1 : 1000 (Santa Cruz Biotechnology Inc.), Lamin B1 1 : 1000 (Santa Cruz Biotechnology Inc.), anti-mouse IgG HRP 1 : 1000 (Sigma-Aldrich Co.), and anti-rabbit IgG HRP 1 : 1000 (Sigma-Aldrich Co.).

2.6. Statistical Analysis. Data are expressed as the mean ± standard deviation for each group. The differences among multiple experimental groups were detected by one-way Analysis of Variance (ANOVA) followed by Bonferroni's multiple comparison test. A P value of less than 0.05 was considered as significant.

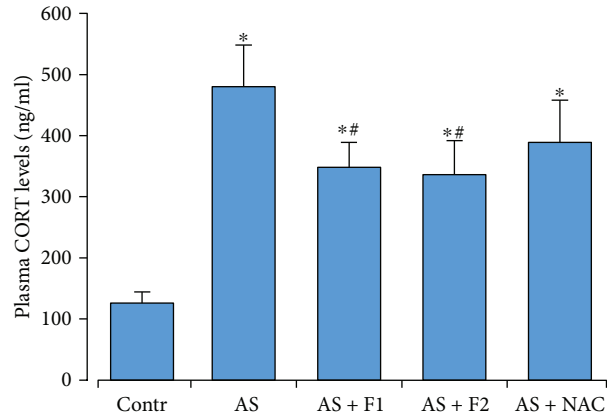

Figure 1: Effect of C_{60}FAS (50 μg/kg (F1) and 500 μg/kg (F2)) and NAC on plasma corticosterone levels after acute restraint stress exposure (AS). Values are means ± SD ($n = 8$). The data were analyzed for statistical significance using ANOVA followed by the Bonferroni post hoc test. $^{*}P < 0.05$ vs. the control group; $^{\#}P < 0.05$ vs. the stress group (AS).

3. Results

3.1. Plasma Corticosterone Level. The results of plasma corticosterone levels determined in controls and all stressed rat groups are presented in Figure 1. Monitoring changes in the corticosterone level may serve as an indicator of stress response [4, 16]. Acute stress caused a remarkable increase in the plasma corticosterone level (approximately 3–8-fold higher than the level control group, $P < 0.05$), whereas pretreatment with C_{60}FAS (50 and 500 μg/kg) significantly decreased the release of plasma corticosterone (by 28 and 32%, respectively) compared to the AS groups alone ($P < 0.05$). NAC administration showed a reduction in the corticosterone level of 19% in comparison with the AS group ($P > 0.05$). There were no significant differences in corticosterone concentration between the controls and any drug treatment alone groups (data not shown).

3.2. Oxidative Status of the Brain Tissue after Drug Supplementation and Acute Stress Exposure. Exposure to acute restraint stress significantly elevated the level of ROS generation and $O_2\cdot^-$ and H_2O_2 productions by 45, 25, and 60%, respectively ($P < 0.05$) as well as the TBARS accumulation (by 71%), which are the secondary products of lipid peroxidation in comparison with the control rats ($P < 0.05$) (Figure 2). These changes were accompanied by a significant increase in MnSOD and catalase activities by ~37–38% ($P < 0.05$). At the same time, activity levels of GSH-related enzymes (GPx, GR, γ-GCL, and GST) were lower by 20–24% ($P < 0.05$) than those in the control rats ($P < 0.05$). Because of the above events, the level of reduced glutathione was diminished (by 19%, $P < 0.05$) (Figure 3). Supplementation of C_{60}FAS and NAC before acute stress exposure significantly reduced the free radical level (ROS and $O_2\cdot^-$ generation), H_2O_2 concentration, and the intensity of lipid peroxidation as well as increased GSH content compared to the AS alone group as shown in Figures 2 and 3. We have found that C_{60}FAS, in both applied doses, prevented the superoxide anion production to a great extent and was more efficient for correction of lipid peroxidation in brain tissue in comparison with NAC ($P < 0.05$). Pretreatment with C_{60}FAS (in both concentrations) as well as NAC diminished stress-induced overactivation of MnSOD. All drugs caused significant induction in GSH content and activity of GSH-related enzymes, and these effects were similar. For GR activity, C_{60}FAS (500 μg/kg) and NAC administration significantly increased the activity of this enzyme in comparison with C_{60}FAS (50 μg/kg). NAC application decreased MnSOD activity to the control level and was more effective than C_{60}FAS (in both doses) pretreatment.

3.3. Oxidative Status of the Heart Tissue after Drug Supplementation and Acute Stress Exposure. Acute restraint stress stimulated ROS and $O_2\cdot^-$ productions (by 55 and 53%, respectively) and increased H_2O_2 and TBARS levels (by 54 and 62%, respectively) in relation to the control rats ($P < 0.05$) (Figure 4). In turn, in the heart tissue in response to these changes, there was a significant decrease in the activity and content of endogenous antioxidants, including GPx (by 22%), γ-GCL (by 38%), GST (by 27%), and GSH (by 23%) with concomitant increase in MnSOD activities (by 60%) compared to the control groups ($P < 0.05$). No significant changes in GR or catalase activities were observed (Figure 5).

Pretreatment with C_{60}FAS (50 and 500 μg/kg) and NAC before stress exposure induced the reduction of the lipid peroxidation because of the inhibition of ROS generation and superoxide anion and H_2O_2 releases which we registered in cardiomyocytes. As shown in Figure 4, C_{60}FAS (50 and 500 μg/kg) decreased ROS formation (by 22 and 32%), $O_2\cdot^-$ production (by 43 and 35%), H_2O_2 concentration (by 15 and 27%), and TBARS content (by 23 and 32%), respectively, compared with the AS alone group ($P < 0.05$). A similar dynamic has been revealed in changes in the above

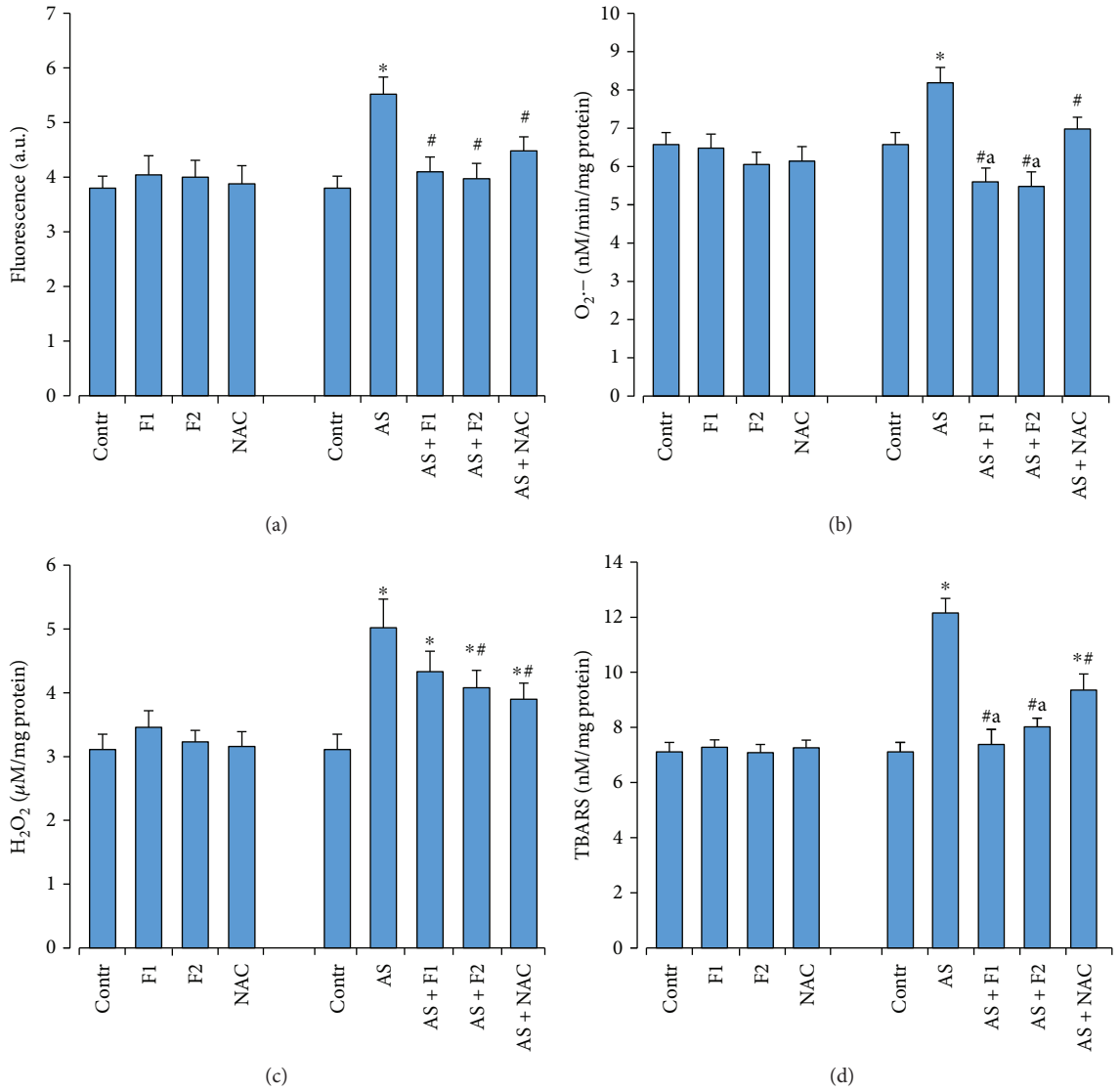

Figure 2: Effect of C_{60}FAS (50 μg/kg (F1) and 500 μg/kg (F2)) and NAC on oxidative stress markers: ROS formation (a), $O_2\cdot^-$ (b), H_2O_2 (c), and TBARS (d) production in brain tissue after alone administration and after acute restraint stress exposure (AS). Values are means ± SD ($n = 8$). The data were analyzed for statistical significance using ANOVA followed by the Bonferroni post hoc test. $^*P < 0.05$ vs. control group; $^\#P < 0.05$ vs. acute stress group; $^aP < 0.05$ vs. AS + NAC group.

parameters in the NAC treatment group. However, the degree of their inhibition was less than that in the group with C_{60}FAS administration, especially after C_{60}FAS (500 μg/kg) injection. Applications of C_{60}FAS (in both doses) and NAC elevated GSH content ($P < 0.05$) and activities of GPx, GST, and γ-GCL ($P < 0.05$) in comparison with the AS rats, reversed the MnSOD overactivation ($P < 0.05$), and maintained GR and catalase activities on the optimal control level (Figure 5).

Interestingly, C_{60}FAS (500 μg/kg) was more successful in preventing oxidative stress in heart tissue than administration of C_{60}FAS at a lower concentration and NAC. This applied dose of C_{60}FAS decreased TBARS, $O_2\cdot^-$, and H_2O_2 levels as well as enhanced GSH content and reduced overactivation of MnSOD to a greater extent than did C_{60}FAS (50 μg/kg) and NAC ($P < 0.05$).

3.4. Effect of C_{60}FAS Supplementation and Acute Stress Exposure on Protein Expression of Nrf2, MnSOD, and GSH-Related Enzymes in Brain and Heart Tissues. Nrf2 is a critical transcription factor that tightly controls cellular defense to oxidative stress [34]. Therefore, we first attempted to examine the effects of C_{60}FAS supplementation alone and after acute restraint stress on Nrf2 protein content in the nuclear and cytosolic fractions of different rat tissues. Because the nuclear Nrf2 level, specifically, is a direct reflection of ARE-mediated transcriptional activity [32], we examined the cytosolic protein expression of crucial downstream genes such as MnSOD, GPx, GSTP, and GCLC regulated by Nrf2.

Restraint exposure results in decrease (by 22%) in Nrf2 nuclear protein levels in the brain, with a concomitant increase in cytosolic Nrf2 protein levels ($P < 0.05$). In contrast, in the heart, no significant changes in these indices

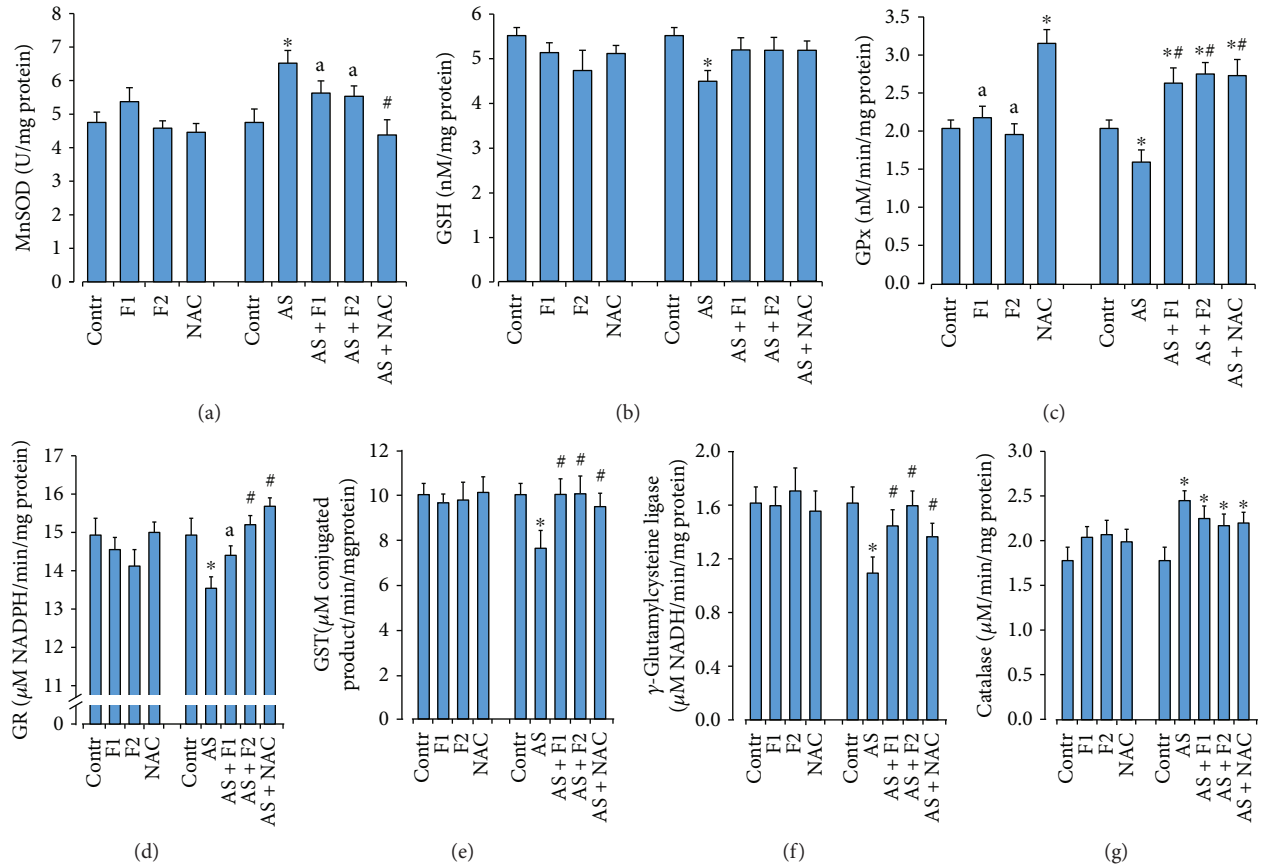

FIGURE 3: Effect of C_{60}FAS (50 μg/kg (F1) and 500 μg/kg (F2)) and NAC on MnSOD activity (a), GSH content (b), and activity of GSH-related enzymes GPx (c), GR (d), GST (e), γ-GCL (f), and catalase (g) in the cytosol fraction of brain tissue after alone administration and after acute restraint stress exposure (AS). Values are means ± SD ($n = 8$). The data were analyzed for statistical significance using ANOVA followed by the Bonferroni post hoc test. $^{*}P < 0.05$ vs. control group; $^{\#}P < 0.05$ vs. acute stress group; $^{a}P < 0.05$ vs. AS + NAC group.

were observed (Figure 6). As shown in Figure 7, in the brain, acute stress triggered a decrease in the protein content of GCLC and GSTP by 30 and 20%, respectively, ($P < 0.05$). The GPx protein content has only the tendency to decrease, but the MnSOD protein level was significantly enhanced (by 26%, $P < 0.05$) in comparison with the control group. These findings correlate with the reduction in GSH content (Figure 3), suggesting that the Nrf2 pathway takes part in GSH synthesis in the brain tissues under AS conditions. At the same time, the heart protein expression of MnSOD and GSH-related enzymes did not show significant changes in comparison with the control group. We found that C_{60}FAS (50 μg/kg and 500 μg/kg) administration before AS caused a significant elevation in the Nrf2 protein level in both the brain and heart nuclear extracts in comparison with the control and AS alone groups ($P < 0.05$), which was accompanied by decreases in the Nrf2 cytosolic protein expression ($P < 0.05$) indicating translocation of Nrf2 from cytosol to the nucleus. Together with the increase in nuclear Nrf2 levels, we registered a statistically significant increase in the protein expression of MnSOD, GPx, GSTP, and GCLC in the brain as well as in the heart cytosolic fractions relative to the AS alone and control groups ($P < 0.05$). The above indices are expressed to a greater degree after supplementation of C_{60}FAS at a higher dose.

3.5. Effect of Drug Administration on Prooxidant/Antioxidant Balance and Protein Expression in Rat Tissues in a Normal Physiological State. When the investigated drugs were applied alone in the brain and heart tissues, there were no changes in oxidative stress markers or indices of antioxidant defense systems except GPx activity, which in the brain tissue after NAC administration was significantly raised in comparison with the control and C_{60}FAS-treated rats ($P < 0.05$) (Figures 2–5). The effect of C_{60}FAS administration alone on the Nrf2 protein expression is depicted in Figure 8. In both tissues, the protein level of Nrf2 in the nuclear level was close to the control level ($P > 0.05$) as well as in cytosol (data not shown). Protein content of MnSOD and GSH-related enzymes in both tissues tended to increase, but this effect had no statistical significance (Figure 9).

4. Discussion

Although several previous studies have shown that C_{60} can protect cells against oxidative stress-induced cell death by activating the Nrf2/ARE pathway in vitro on cell cultures [28, 29], it remains unclear whether C_{60} could have the same effect on oxidative stress in vivo in animal models. In this study, as the first step towards understanding the protective role of Nrf2 activation, we studied the effect of C_{60}FAS in

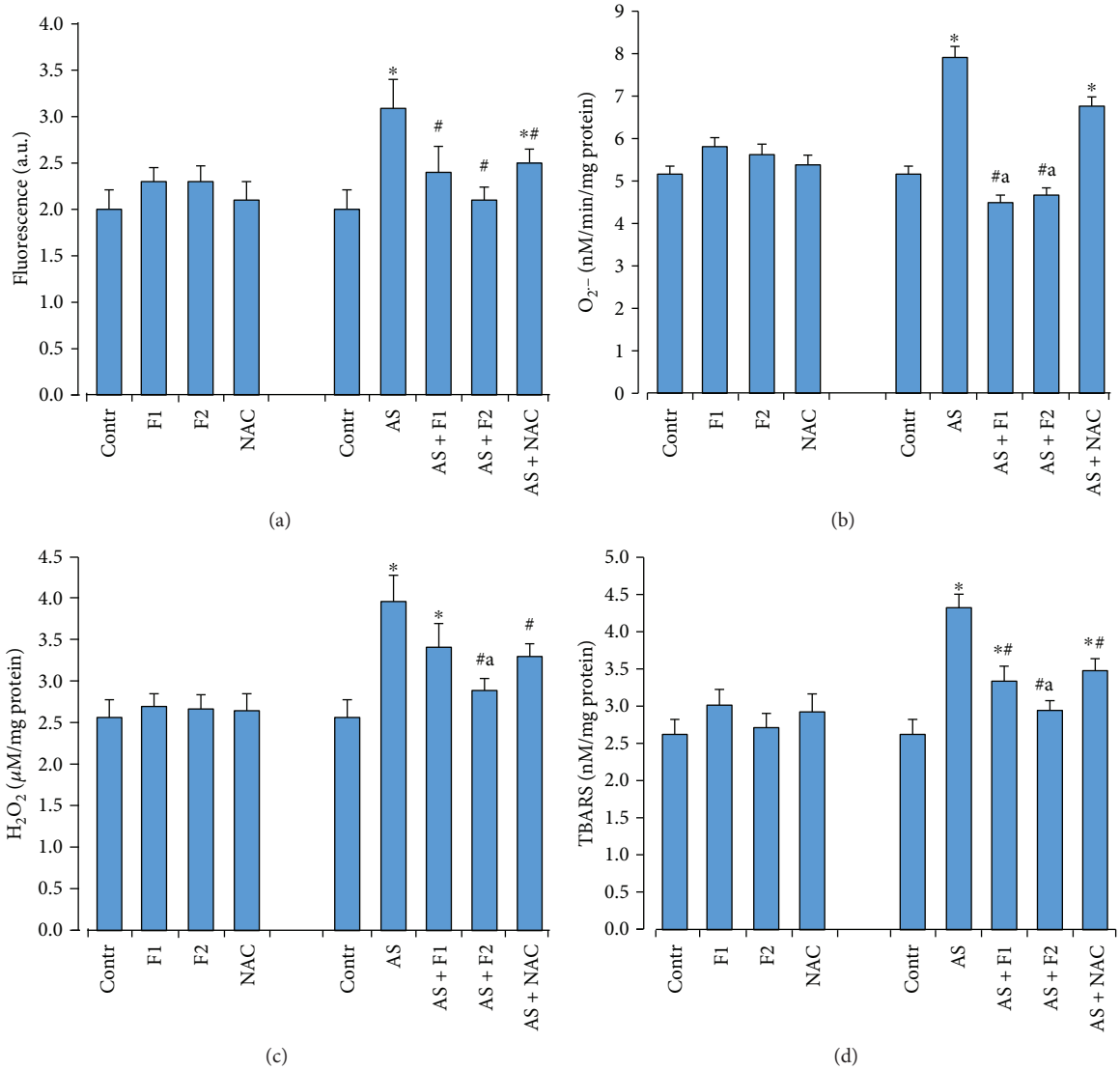

Figure 4: Effect of C_{60}FAS (50 μg/kg (F1) and 500 μg/kg (F2)) and NAC on oxidative stress markers: ROS formation (a), $O_2{\cdot}^-$ (b), H_2O_2 (c), and TBARS (d) production in heart tissue after alone administration and after acute restraint stress exposure (AS). Values are means ± SD ($n = 8$). The data were analyzed for statistical significance using ANOVA followed by the Bonferroni post hoc test. $^{*}P < 0.05$ vs. control group; $^{\#}P < 0.05$ vs. acute stress group; $^{a}P < 0.05$ vs. AS + NAC group.

two doses and NAC as the positive control, on prooxidant/antioxidant homeostasis in rats that were subjected to acute restraint stress.

In the present study, 6 h of restraint stress markedly increases ROS, $O_2{\cdot}^-$, and H_2O_2 productions and the consequent LPO intensification that induces disorders in antioxidant status of the brain and the heart tissues, in accordance with many studies showing that restraint stress significantly elevates oxidative status and increases or decreases antioxidant enzyme activities in different rat tissues, depending on the severity and duration of the restraint stress protocol [12, 13, 15]. Indeed, previous studies have already shown that immobilization stress targets the brain for lipid peroxidation, as the levels were found to be highest in this tissue [14, 49].

We found that AS significantly altered activity of SOD and GPx, two of the key enzymes that are a first line of antioxidant defense and function in concert to prevent ROS reactions in response to oxidative stress. Overactivation of MnSOD without a concomitant increase in GPx activity, which we demonstrated in our study, results in the accumulation of H_2O_2 that not only changes the cellular redox status but also participates in the Fenton reaction, leading to production of noxious hydroxyl radicals [5]. A significant diminution in GSH content and GSH-related enzymes denotes disorders in GSH biosynthesis because of the absence of an adequate antioxidative defense in rat tissues after restraint exposure [8, 9]. In our study, together with intensification of the oxidative process, we registered a significantly elevated level of plasma corticosterone, which is an important indicator of the stress condition. Stress is known to activate the hypothalamic–pituitary–adrenal axis, which results in an increased secretion of glucocorticoids that affect not only the brain but also the peripheral organs [16]. A high level of glucocorticoids may affect the redox status of tissues

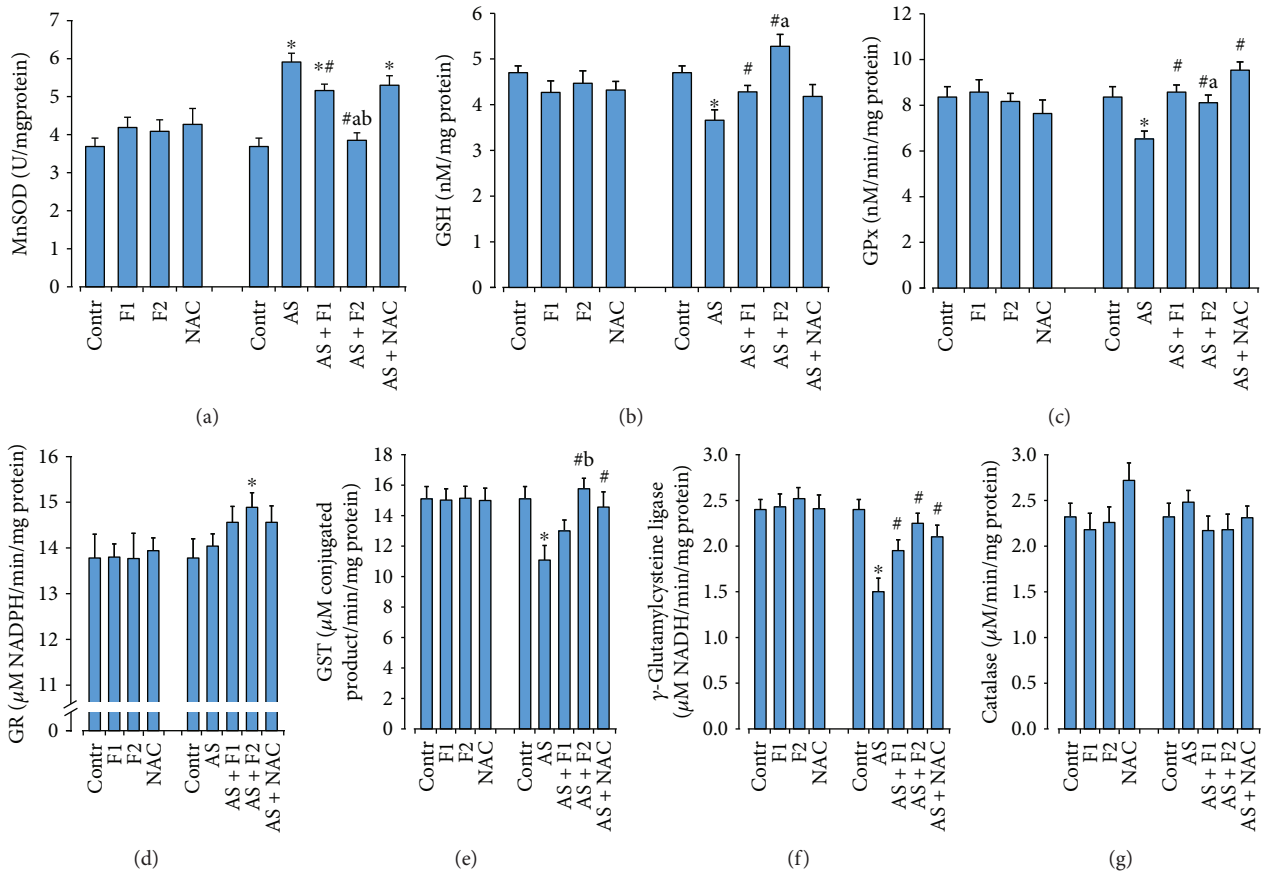

FIGURE 5: Effect of C_{60}FAS (50 μg/kg (F1) and 500 μg/kg (F2)) and NAC on MnSOD activity (a), GSH content (b), and activity of GSH-related enzymes GPx (c), GR (d), GST (e), γ-GCL (f), and catalase (g) in the cytosol fraction of heart tissue after alone administration and after acute restraint stress exposure (AS). Values are means ± SD ($n = 8$). The data were analyzed for statistical significance using ANOVA followed by the Bonferroni post hoc test. $^{*}P < 0.05$ vs. control group; $^{\#}P < 0.05$ vs. acute stress group; $^{a}P < 0.05$ vs. AS + NAC group; $^{b}P < 0.05$ vs. AS + F1 group.

via different mechanisms, including an increase in superoxide cell production and the impairment of tissue antioxidant capacity [49]. Previous reports show that high levels of corticosterone decrease the activity of the key antioxidant enzyme glutathione peroxidase, directly reducing the total glutathione pool as well as the NADPH levels, required for regeneration of GSH from oxidized glutathione [17, 50]. The increase in the levels of circulating corticosterone after acute immobilization was demonstrated to be directly proportional to the increase in oxidative mediators as well as injuring neuro- and cardiosystems [51]. All these findings permit us to suggest that the increased corticosterone level during our stress model may in addition affect the antioxidant capacity in both rat tissues that were investigated.

Under these circumstances, the use of different antioxidants and agents with free radical scavenging properties to counteract the noxious events elicited by acute stress represents an effective therapeutic strategy mostly employed to handle oxidative damage [52]. Among these strategies, carbon nanoparticles with intrinsic ROS scavenging and antioxidant properties exhibit superior pharmacological features due to enhanced absorption and bioavailability [53].

We have shown that 1 week of treatment with C_{60}FAS (50 and 500 μg/kg) before restraint stress exposure induces the reduction of the lipid peroxidation intensity because of the inhibition of ROS production, namely, superoxide anion release and H_2O_2 generation, which we registered in cardiomyocytes and brain cells. The mitochondrial respiratory chain and enzymatic reactions by NADPH oxidase, xanthine oxidase, cyclooxygenases, and lipoxygenase are known to be an important endogenous source of ROS under stress conditions [7]. Superoxide anion is a common precursor of ROS that is quickly involved in two metabolic pathways: rapid conversion into hydrogen peroxide and oxygen by superoxide dismutase and generation of highly toxic peroxynitrite via reaction with nitric oxide [5]. We observed that C_{60}FAS application (in both doses investigated) drops the hyperactivity of MnSOD and therefore the production of superoxide anion, which serves as the substrate for this enzyme and designate of MnSOD activity. The consequence of this activity was a decrease in the level of peroxide in the brain cells and cardiomyocytes. Although MnSOD is a mitochondrial enzyme, we detected the MnSOD protein in the cytosolic fraction. Since MnSOD is encoded in the nucleus,

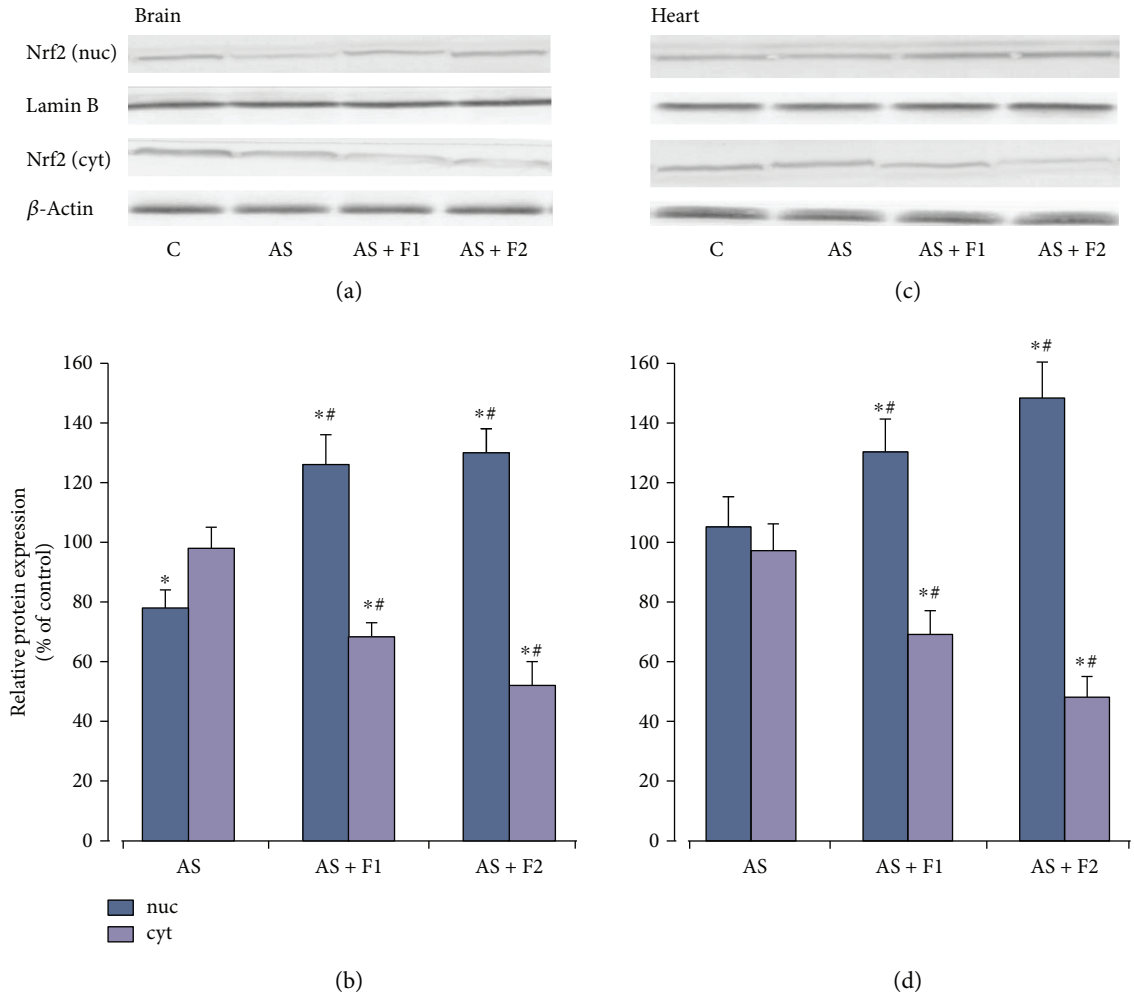

Figure 6: Changes in the nuclear and cytosolic Nrf2 protein expressions in brain and heart tissues after pretreatment of C_{60}FAS (50 μg/kg (F1) and 500 μg/kg (F2)) and acute restraint stress exposure (AS). (a and c) Representative western blot and (b and d) densitometric analysis of Nrf2 protein content. Protein extracts were separated by performing SDS PAGE and subsequently electroblotted onto PVDF membranes. The values of the nuclear and cytosolic Nrf2 proteins were normalized to Lamin B and β-actin, respectively. Final western blot figured as the histogram is expressed as mean percentages (±SD) over control values from two independent experiments. The control values are taken as 100%. Statistically significant differences are indicated as $^{*}P < 0.05$ vs. control; $^{\#}P < 0.05$ vs. AS.

synthesized as a precursor in the cytoplasm, and transported to the mitochondria through a mitochondrial targeting sequence, the measured cytosolic MnSOD level may illustrate its transit to the mitochondria after nuclear synthesis [54]. Thus, an increased cytosolic MnSOD protein level could be derived from mitochondrial MnSOD and/or inappropriate transport of newly synthesized MnSOD into mitochondria. In any case, the appearance of MnSOD in the cytosolic fraction clearly indicates a loss of brain and heart mitochondrial membrane integrity under the stress condition. Our findings that C_{60}FAS affects the MnSOD activity suggest that C_{60}FAS has an unlimited ability to penetrate biological barriers with subsequent easy access to subcellular compartments, as was reported earlier [55].

Fullerene and its derivatives are a powerful antioxidant due to the delocalization of the $\eth$-electrons over the carbon cage, which can readily react with ROS, in particular superoxide anion, hydroxyl, and lipid radicals. Numerous studies have demonstrated the free radical scavenging capabilities to such a degree that fullerenes have been described as "free radical sponges" [19, 26, 28]. Fullerene is postulated to act as a peculiar antioxidant that does not only react directly with free radicals but also initiate and catalyse the reaction of ROS recombination (dismutation) occurring in ordered interfacial water shells near the fullerene's surface. This assumption could explain why fullerene exhibits prolonged bioactive effects, including antioxidant capacity, even in small and supersmall concentrations [20].

GSH homeostasis is known to be regulated by the following three aspects: (a) GSH is synthesized from glutamate, glycine, and cysteine by glutathione synthetase and γ-glutamylcysteine ligase; (b) GSH is oxidized to GSSG by the activity of GPx, thus regulating and maintaining the cell redox status; (c) GSSG is reduced to GSH with the mediation of GR, by which is a substantial part of the intracellular GSH recycling [9]. GSH-related enzymes such as GPx, GR,

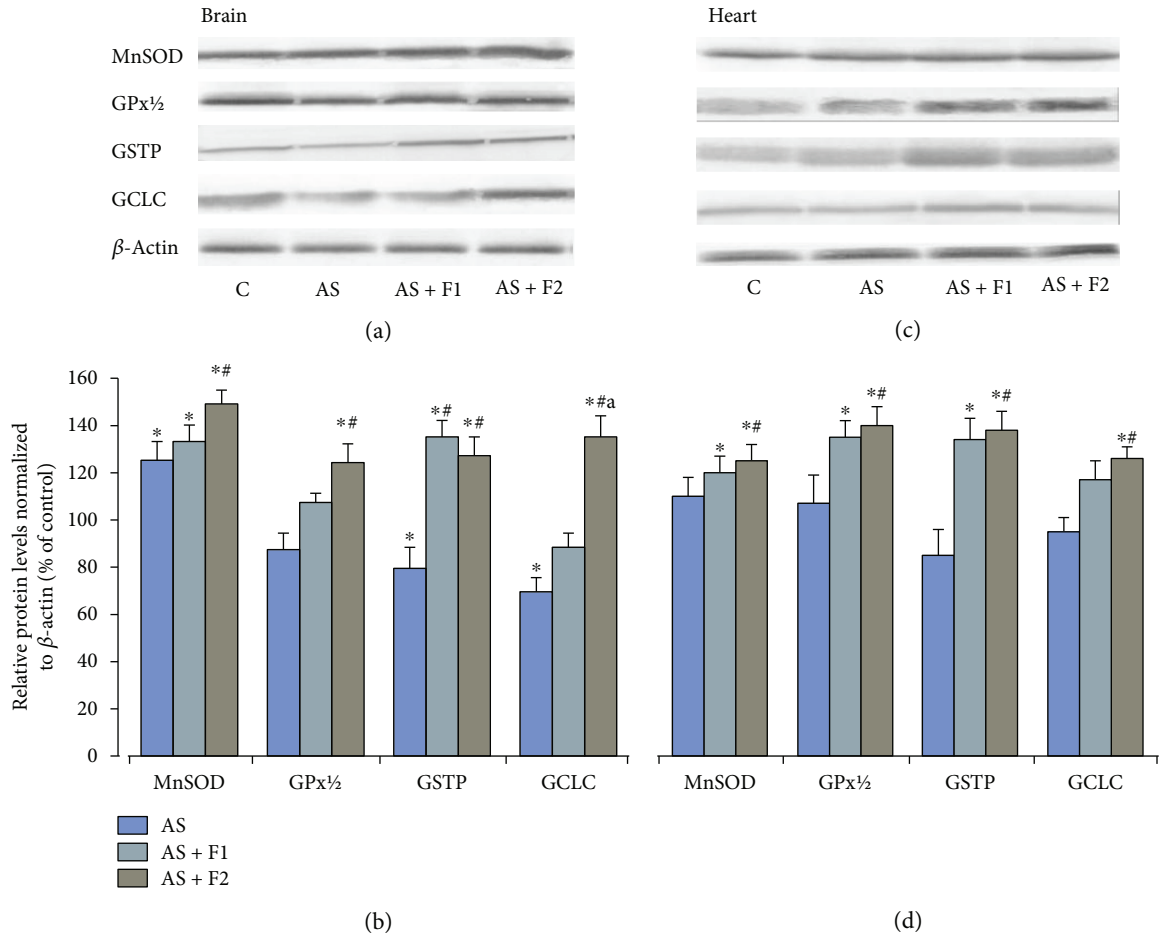

Figure 7: Changes in the MnSOD, GPx 1/2, GSTP, and GCLC protein expressions in brain and heart tissues after pretreatment of C_{60}FAS (50 μg/kg (F1) and 500 μg/kg (F2)) and acute restraint stress exposure (AS). (a and c) Representative western blot and (b and d) densitometric analysis of protein levels. Protein extracts were separated by performing SDS PAGE and subsequently electroblotted onto PVDF membranes. Final western blot figured as the histogram is expressed as mean percentages (±SD) over control values from three independent experiments. The control values are taken as 100%. Statistically significant differences are indicated as $^{*}P < 0.05$ vs. control; $^{\#}P < 0.05$ vs. AS; $^{a}P < 0.05$ vs. AS + F1.

GST, and γ-GCL are pivotal enzymes in the regulation of intracellular redox status through modulation of glutathione homeostasis and upregulation through the Nrf2-Keap1-ARE pathway [8, 52].

We found that 6 h restraint caused a decrease in the GSH level and GCL activity in brain cells that indicates disorders in the GSH-biosynthetic cycle. The decreased activity in glutathione reductase induces the accumulation of oxidized glutathione in the brain, which is indicative of the severity of the oxidative stress [8]. In addition to peroxide-mediated inactivation of GPx, superoxide anion and peroxynitrite overproductions can inhibit GPx activity [56] as was obtained in our study. A previous study by Atif et al. [15] demonstrated that the activity of both GR and GPx enzymes is decreased in the hippocampus following similar stress durations. In the heart, we demonstrated decrease in γ-GCL and GPx activities without changes in GR activity. In both tissues, we registered decrease in GST activity, which correlated with GST protein content. At the same time, the activity of CAT, the main scavenger of H_2O_2 in the neurons, was increased in the brain and had a tendency to increase in the heart that agreed with early reports [57]. GSTs are ubiquitous, multifunctional enzymes that detoxify endogenous and exogenous electrophiles, including epoxides, aldehydes, and peroxides [58]. Therefore, the decrease in GST that was observed after acute stress in rat tissues may induce additional intoxication by harmful LPO byproducts.

Various tissues are known to have different sensitivities to oxidative stress challenges depending on several factors such as oxygen consumption, metabolic rates, susceptibility to oxidants, and antioxidant levels. In the present study, after analysis of the oxidative stress markers, we established that the brain, in contrast to the heart, was more vulnerable to oxidative stress in our experimental model.

C_{60}FAS supplementation showed the increase in GSH content as well as GPx, GST, and GR activities in both tissues investigated in comparison with the AS alone group promoted coordinated action GSH redox-cycle enzymes and involvement of GSH in the metabolism of toxic aldehydes and peroxides with a decrease in cell injuries. The increased

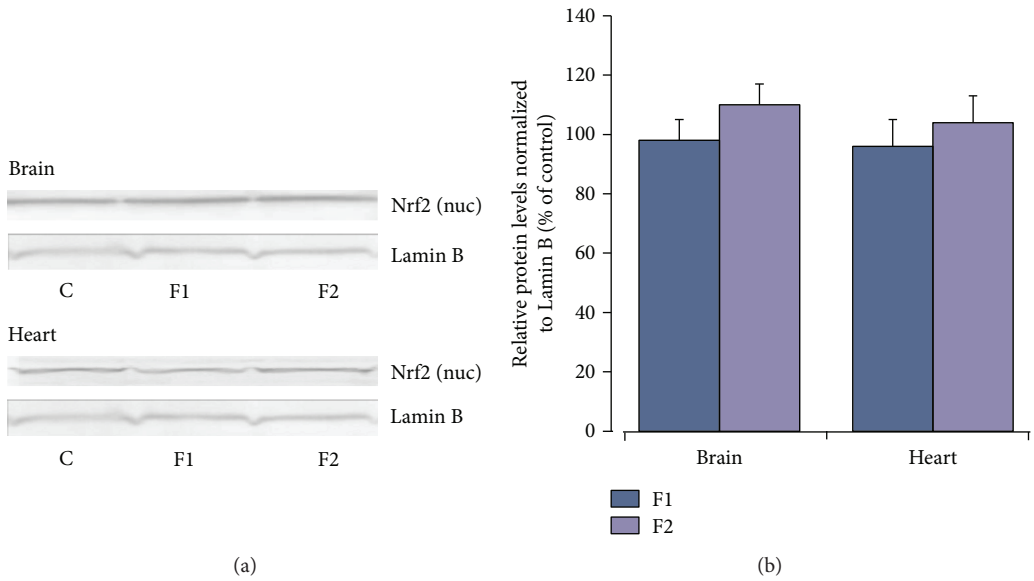

Figure 8: Changes in the nuclear Nrf2 protein expression in brain and heart tissues after pretreatment of C_{60}FAS (50 μg/kg (F1) and 500 μg/kg (F2)). (a) Representative western blot and (b) densitometric analysis of Nrf2 protein content. Protein extracts were separated by performing SDS PAGE and subsequently electroblotted onto PVDF membranes. Final western blot figured as the histogram is expressed as mean percentages (±SD) over control values from two independent experiments. The control values are taken as 100%.

GCL activity suggests the involvement of C_{60} in modulating glutathione biosynthesis under AS condition. C_{60}FAS administration induced some decrease in CAT activity in both tissues compared with the AS alone group with normalization of GPx activity indicating the decrease in the intensity of peroxidation processes. Similar reports on several other stresses such as doxorubicin intoxication and irradiation showed that fullerene administration reduces ROS generation and lipid peroxidation and increases the GSH level and activity of GSH-related enzymes [23, 24]. In our study, we used NAC as a positive control during the investigation of cell prooxidant/antioxidant homeostasis because this drug is an antioxidant that potentially reduces the damaging effect of oxidative stress [36]. NAC exerts its effect both as a source of sulphhydryl groups (preventing GSH depletion) and as a free radical scavenging agent through a direct reaction with highly oxidizing radicals such as ·OH, $\cdot NO_2$, and $CO_3\cdot^-$ [33]. Treatment with NAC inhibited lipid peroxidation, increased catalytic activity of glutathione peroxidase, glutathione reductase, and superoxide dismutase, and replenished GSH levels in animal tissues under different pathological conditions [59, 60].

We observed that C_{60}FAS pretreatment provided sufficiently strong antioxidant defense with a kind of effect like the effect of NAC. The C_{60}FAS (500 μg/kg) was more effective in preventing oxidative stress disorders than NAC and C_{60}FAS at the concentration of 50 μg/kg.

Neuro- and cardioprotective actions of C_{60}FAS under restraint stress were also confirmed by a significant decrease in corticosterone concentration, as demonstrated in our study. The reduction markers of oxidative stress and normalization antioxidant activity suggest that C_{60}FAS may induce heart and brain tissues to maintain sufficient antioxidant capacity against ongoing oxidative stress.

Free radical metabolites generated during extreme influence are known to function as signaling molecules activating transcription factors and specific genes that result in de novo protein synthesis, including antioxidant enzymes. These molecular mechanisms might be substantial for triggering of adaptive reactions and forming protective mechanisms against oxidative stress [32].

To further investigate the potential mechanisms of C_{60}FAS-mediated protection against oxidative stress, we examined the protein expression of Nrf2, which has demonstrated a pivotal role in cell protection by the coordinate transcription of ARE-regulated antioxidant genes, including GPx2, GST, γ-GCLC, GR, and SOD [52].

In the present study, exposure to AS induced some decrease in the Nrf2 nuclear protein content in the brain with concomitant increase in the cytosol fraction. Our results agreed with previous findings showing significant decrease in Nrf2 nuclear protein in the whole brain tissue after 6 h of restraint stress [12, 18], in the rat hippocampus, without changes in the prefrontal cortex after acute immobilization for 30 min [61]. Spiers et al. [14] reported a transiently decreased nuclear Nrf2 that coincided with increased expression of 11β-HSD1-corticosterone regenerating enzyme in the hippocampus of rats subjected to 4 h restraint stress.

Numerous factors are involved in Nrf2 regulation at both transcriptional and posttranscriptional levels and affect its distribution in cell compartments [30]. On the one hand, Nrf2 belongs to the stress-responsive transcription factors that are largely controlled at the level of protein stability. Nrf2 has been found to be an unstable protein, due to the proteolytic degradation through the ubiquitin-dependent pathway. Under basal conditions, Keap1 continuously drives the regulation of Nrf2 maintaining low cellular levels of the protein. However, under oxidative stress, the regulation of

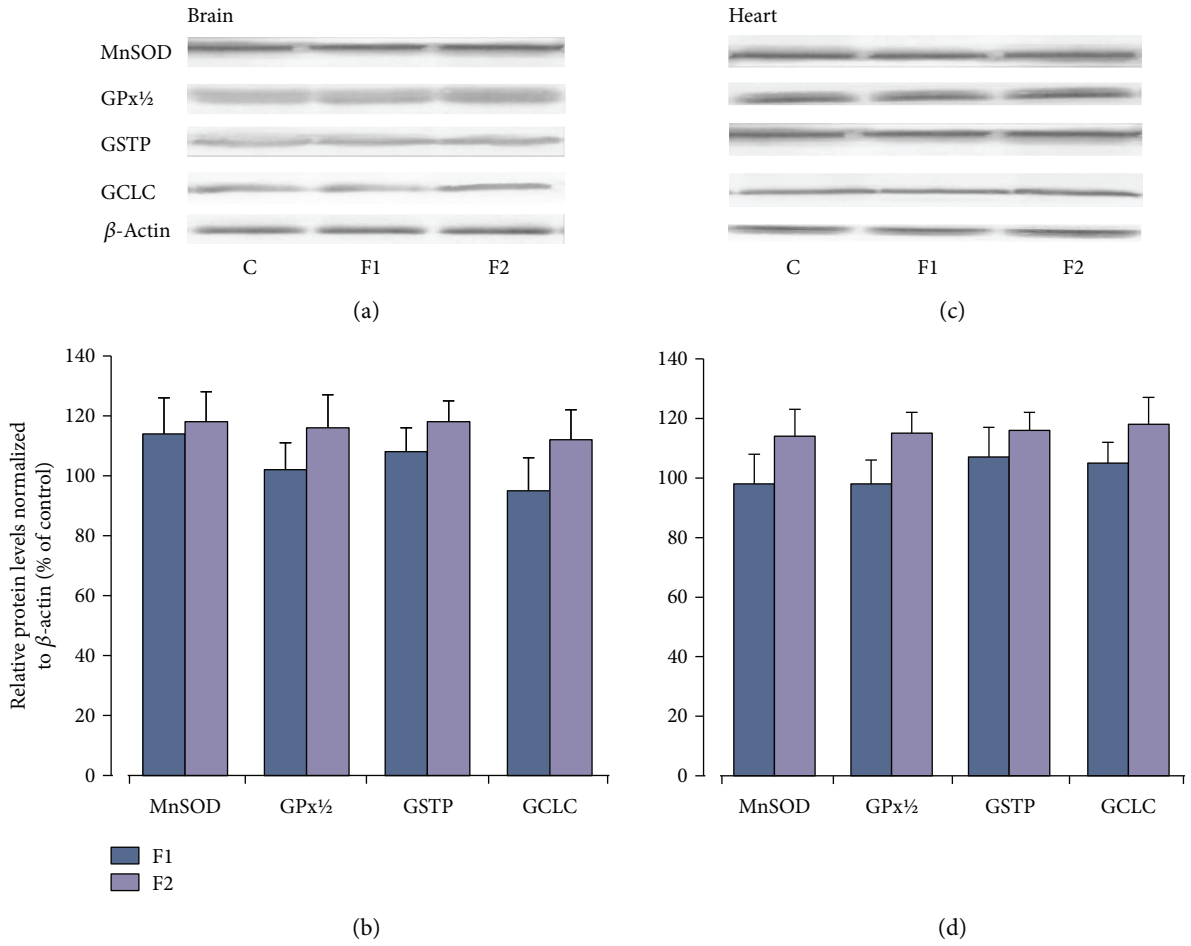

Figure 9: Changes in the MnSOD, GPx 1/2, GSTP, and GCLC protein expressions in brain and heart tissues after pretreatment of C_{60}FAS (50 μg/kg (F1) and 500 μg/kg (F2)). (a and c) Representative western blot and (b and d) densitometric analysis of protein levels. Protein extracts were separated by performing SDS PAGE and subsequently electroblotted onto PVDF membranes. Final western blot figured as the histogram is expressed as mean percentages (±SD) over control values from two independent experiments. The control values are taken as 100%.

Nrf2 becomes complex, involving both Keap1-dependent and -independent mechanisms [31]. On the other hand, there are alternative mechanisms of Nrf2 regulation, including phosphorylation of Nrf2 by various protein kinases (PKC, PI3K/Akt, GSK-3b, and JNK), interaction with other protein partners (p21 and caveolin-1), and epigenetic factors (micro-RNAs-144, -28, and -200a and promoter methylation) [30]. Thus, Keum et al. demonstrated that p38 phosphorylates Nrf2 and promotes its association with Keap1, thereby preventing its nuclear translocation. Besides, prolonged inflammation induces activation of specific kinases and epigenetic modification, which blocks the Nrf2 and contribute to neurological injury [62]. In addition, Ki et al. [63] showed that the activated glucocorticoid receptor modulates Nrf2 signaling and alters Nrf2 target gene expression in the brain through binding of the glucocorticoid receptor to its glucocorticoid response element. Under stress conditions, glucocorticoids can suppress cellular antioxidant defense capacity by impairing Nrf2-dependent antioxidant response [17]. Furthermore, NF-κB is a negative regulator of NRF2 by binding to response elements in the NRF2 gene promoter [64]. As was shown, the p65 subunit can block NRF2 binding to CREB protein and recruit histone deacetylase 3, a corepressor of ARE [65]. These pathways can be regulated by acute stress and could be implicated, at least in part, in the effects reported here.

In parallel with loss in Nrf2 protein content in the brain nuclear fraction, we observed some decease in the protein level of GCLC ($P < 0.05$), GPx ($P > 0.05$), and GSTP ($P < 0.05$) after acute stress exposure. Although MnSOD is a target of Nrf2 activation, poor Nrf2 function did not correspond to MnSOD protein expression in our study where we found significant enhancement in MnSOD protein content ($P < 0.05$). Such a difference could be due to alternative signaling pathways operating in the brain that upregulated MnSOD. MnSOD is known to be an NF-κB-related protein, and under stress conditions, NF-κB is actively involved in the expression of MnSOD [66]. In addition, a high level of H_2O_2 generation as product of MnSOD catalytic activity, which we observed in our study after stress exposure, may act as a signaling molecule in the NF-κB activation [67].

No statistically significant changes were observed in nuclear and cytosol Nrf2 protein accumulations as well as in protein expression of Nrf2-target genes MnSOD, GPx, and GCL except GST in the myocardium of rats that were subjected to restraint stress.

The present study showed that C_{60}FAS administration induced significant enhancement of nuclear Nrf2 protein in the brain and the myocardium of rats subjected to restraint stress for 6 h with concomitant decrease in the cytosol fraction. The levels of protein expression of GSH-related enzymes positively correlated with Nrf2, suggesting that the upregulation of GCLC, GST, and GPx may depend on the Nrf2/ARE pathway. We assume that C_{60}FAS effects on GSH recycle via induction of γ-GCL as well as GPx and GST protein expressions, and this is necessary and sufficient to reestablish GSH system homeostasis.

In the brain, the MnSOD protein level continued to increase in comparison with AS. In contrast, in the heart, this index remains at the level of the control and AS alone groups. These findings confirm that the effect of C_{60}FAS application for MnSOD was a tissue specific. Significant modulation of the antioxidative enzymatic system at the protein level that was observed in our study showed a complex network of transcriptional and translational events modified by C_{60}FAS during the cellular response to restraint stress.

Recently, Ye et al. [29] have shown that in the *in vitro* model, polyhydroxylated derivatives of fullerene after administration alone enhanced Nrf2 nuclear protein translocation and upregulated mRNA and protein expression of phase II antioxidant enzymes, including HO-1, NADPH: quinine oxidoreductase 1, and γ-glutamate cysteine ligase, in 549 cells. By analogy, pretreatment with $C_{60}(OH)_{24}$ showed significant protective effects in the 1-methyl-4-phenylpyridinium- (MPP+-) induced acute cellular Parkinson disease model in human neuroblastoma cells through increase in expression of Nrf2 and expression and activity of γ-glutamyl cysteine ligase and the level of glutathione [28]. In contrast, in our study, in the *in vivo* model when C_{60}FAS (50 and 500 μg/kg) was applied in a normal physiological state, the western blot analysis showed only a tendency to increase without statistically significant changes in protein expression of MnSOD and GSH-related enzymes of both tissues that correlated with Nrf2 protein content in the nuclear and cytosol fractions. Similarly, C_{60}FAS (50 and 500 μg/kg) applied alone did not induce any changes in investigated oxidative stress markers and antioxidant enzyme activity in the brain and the heart tissues. All these facts allow us to assume that *in vivo*, C_{60}FAS did not affect the endogenous antioxidant status of the rat tissues in the absence of any stress conditions.

5. Conclusions

In conclusion, our results suggest that the neuro- and cardioprotection of C_{60}FAS are mediated, on the one hand, by direct removal of ROS, namely, superoxide anion and hydrogen peroxide, and thus decrease lipid peroxidation, on the other hand, by the effect on rat tissue antioxidant capacity. Under stress condition, C_{60}FAS administration promotes Nrf2 nuclear accumulation and triggers the protein expression of a panel of antioxidant and phase II enzymes, at least partially, through the Nrf2/ARE signaling pathway. We suggest that C_{60}FAS affects endogenous glutathione homeostasis by modulation of glutathione biosynthesis as well as antiperoxide defense via upregulation of activity and protein expression of GSH-related enzymes γ-GCL, GPx, and GST. Under stress exposure, C_{60}FAS strengthens antiradical defense through upregulation of MnSOD in brain cells and maintains MnSOD protein content at the control level in the myocardium. C_{60}FAS supplementation has dose-dependent and tissue-specific effects. These results suggest that the use of C_{60}FAS may be of interest as a potential therapeutic strategy in correction of oxidative stress-based stress conditions.

Abbreviations

C_{60}FAS: Pristine C_{60} fullerene aqueous colloid solution
ROS: Reactive oxygen species
$O_2\cdot^-$: Superoxide anion
H_2O_2: Hydrogen peroxide
GST: Glutathione-S-transferase
GPx: Glutathione peroxidase
γ-GCL: γ-Glutamate-cysteine ligase
GR: Glutathione reductase
GSH: Reduced glutathione
MnSOD: Manganese superoxide dismutase
Nrf2/ARE: NF-E2-related factor 2/antioxidant response element.

Data Availability

The biochemical data used to support the findings of this study are available from the corresponding author upon request.

Conflicts of Interest

The authors declare no conflicts of interest.

Authors' Contributions

OOG originated the study idea and designed and conducted this analysis. AVM and NVB assisted in the design of this study. IVV and TT helped with preparation of the manuscript and provided funding support. UR and YIP were responsible for C_{60}FAS synthesis and characterization. IMM and AIK provided supervision and guidance throughout this work. All authors revised the manuscript for important intellectual content and approved the final version of the article.

Acknowledgments

This work was supported by a Statutory Research of Physical Education Department ((DS_WF) January 16, 2017), Gdansk University Physical Education and Sport, Poland.

References

[1] S. J. Lupien, B. S. Mcewen, M. R. Gunnar, and C. Heim, "Effects of stress throughout the lifespan on the brain, behaviour and cognition," *Nature Reviews Neuroscience*, vol. 10, no. 6, pp. 434–445, 2009.

[2] P. H. Black and L. D. Garbutt, "Stress, inflammation and cardiovascular disease," *Journal of Psychosomatic Research*, vol. 52, no. 1, pp. 1–23, 2002.

[3] C. M. Mazure, "Life stressors as risk factors in depression," *Clinical Psychology: Science and Practice*, vol. 5, no. 3, pp. 291–313, 1998.

[4] H. Shoji and K. Mizoguchi, "Acute and repeated stress differentially regulates behavioral, endocrine, neural parameters relevant to emotional and stress response in young and aged rats," *Behavioural Brain Research*, vol. 211, no. 2, pp. 169–177, 2010.

[5] D. P. Jones, "Radical-free biology of oxidative stress," *American Journal of Physiology-Cell Physiology*, vol. 295, no. 4, pp. C849–C868, 2008.

[6] H. Sies, "Oxidative stress: a concept in redox biology and medicine," *Redox Biology*, vol. 4, pp. 180–183, 2015.

[7] B. Halliwell, "Oxidative stress and neurodegeneration: where are we now?," *Journal of Neurochemistry*, vol. 97, no. 6, pp. 1634–1658, 2006.

[8] J. D. Hayes and L. I. McLellan, "Glutathione and glutathione-dependent enzymes represent a co-ordinately regulated defence against oxidative stress," *Free Radical Research*, vol. 31, no. 4, pp. 273–300, 2009.

[9] S. C. Lu, "Regulation of glutathione synthesis," *Molecular Aspects of Medicine*, vol. 30, no. 1-2, pp. 42–59, 2009.

[10] L. E. Tebay, H. Robertson, S. T. Durant et al., "Mechanisms of activation of the transcription factor Nrf 2 by redox stressors, nutrient cues, and energy status and the pathways through which it attenuates degenerative disease," *Free Radical Biology and Medicine*, vol. 88, Part B, pp. 108–146, 2015.

[11] G. B. Glavin, W. P. Paré, T. Sandbak, H.-K. Bakke, and R. Murison, "Restraint stress in biomedical research: an update," *Neuroscience & Biobehavioral Reviews*, vol. 18, no. 2, pp. 223–249, 1994.

[12] H. I. Choi, H. W. Lee, T. M. Eom et al., "A traditional Korean multiple herbal formulae (Yuk-Mi-Jihwang-Tang) attenuates acute restraint stress-induced brain tissue oxidation," *Drug and Chemical Toxicology*, vol. 40, no. 2, pp. 125–133, 2017.

[13] A. E. Freitas, L. E. B. Bettio, V. B. Neis et al., "Agmatine abolishes restraint stress-induced depressive-like behavior and hippocampal antioxidant imbalance in mice," *Progress in Neuro-Psychopharmacology & Biological Psychiatry*, vol. 50, pp. 143–150, 2014.

[14] J. G. Spiers, H. J. C. Chen, J. S. M. Cuffe, C. Sernia, and N. A. Lavidis, "Acute restraint stress induces rapid changes in central redox status and protective antioxidant genes in rats," *Psychoneuroendocrinology*, vol. 67, pp. 104–112, 2016.

[15] F. Atif, S. Yousuf, and S. K. Agrawal, "Restraint stress-induced oxidative damage and its amelioration with selenium," *European Journal of Pharmacology*, vol. 600, no. 1–3, pp. 59–63, 2008.

[16] N. D. Goncharova, Marenin VIu, T. E. Oganian et al., "Stress, aging, hypothalamic-pituitary-adrenal axis and reliability of antioxidant enzyme defence," *Advances in Gerontology*, vol. 21, no. 4, pp. 548–554, 2008.

[17] D. V. Kratschmar, D. Calabrese, J. Walsh et al., "Suppression of the Nrf2-dependent antioxidant response by glucocorticoids and 11β-HSD1-mediated glucocorticoid activation in hepatic cells," *PLoS One*, vol. 7, no. 5, article e36774, 2012.

[18] K. S. MacDowell, J. R. Caso, D. Martín-Hernández et al., "The atypical antipsychotic paliperidone regulates endogenous antioxidant/anti-inflammatory pathways in rat models of acute and chronic restraint stress," *Neurotherapeutics*, vol. 13, no. 4, pp. 833–843, 2016.

[19] Z. Markovic and V. Trajkovic, "Biomedical potential of the reactive oxygen species generation and quenching by fullerenes (C60)," *Biomaterials*, vol. 29, no. 26, pp. 3561–3573, 2008.

[20] G. V. Andrievsky, V. I. Bruskov, A. A. Tykhomyrov, and S. V. Gudkov, "Peculiarities of the antioxidant and radioprotective effects of hydrated C60 fullerene nanostuctures in vitro and in vivo," *Free Radical Biology and Medicine*, vol. 47, no. 6, pp. 786–793, 2009.

[21] I. V. Vereshchaka, N. V. Bulgakova, A. V. Maznychenko et al., "C_{60} fullerenes diminish muscle fatigue in rats comparable to N-acetylcysteine or β-alanine," *Frontiers in Physiology*, vol. 9, p. 517, 2018.

[22] J. Grebowski, P. Kazmierska, and A. Krokosz, "Fullerenols as a new therapeutic approach in nanomedicine," *BioMed Research International*, vol. 2013, Article ID 751913, 9 pages, 2013.

[23] V. M. Torres, B. Srdjenovic, V. Jacevic, V. Dragojevic Simic, A. Djordjevic, and A. L. Simplício, "Fullerenol C60 (OH)24 prevents doxorubicin-induced acute cardiotoxicity in rats," *Pharmacological Reports*, vol. 62, no. 4, pp. 707–718, 2010.

[24] K. Stankov, I. Borisev, V. Kojic, L. Rutonjski, G. Bogdanovic, and A. Djordjevic, "Modification of antioxidative and antiapoptotic genes expression in irradiated K562 cells upon fullerenol C60 (OH)624 nanoparticle treatment," *Journal of Nanoscience and Nanotechnology*, vol. 13, no. 1, pp. 105–113, 2013.

[25] F. Jiao, Y. Liu, Y. Qu et al., "Studies on anti-tumor and antimetastatic activities of fullerenol in a mouse breast cancer model," *Carbon*, vol. 48, no. 8, pp. 2231–2243, 2010.

[26] J.-J. Yin, F. Lao, P. P. Fu et al., "The scavenging of reactive oxygen species and the potential for cell protection by functionalized fullerene materials," *Biomaterials*, vol. 30, no. 4, pp. 611–621, 2009.

[27] Y. I. Prylutskyy, I. V. Vereshchaka, A. V. Maznychenko et al., "C_{60} fullerene as promising therapeutic agent for correcting and preventing skeletal muscle fatigue," *Journal of Nanobiotechnology*, vol. 15, no. 1, p. 8, 2017.

[28] X. Cai, H. Jia, Z. Liu et al., "Polyhydroxylated fullerene derivative C60(OH)24prevents mitochondrial dysfunction and oxidative damage in an MPP+-induced cellular model of Parkinson's disease," *Journal of Neuroscience Research*, vol. 86, no. 16, pp. 3622–3634, 2008.

[29] S. Ye, M. Chen, Y. Jiang et al., "Polyhydroxylated fullerene attenuates oxidative stress-induced apoptosis via a fortifying Nrf2-regulated cellular antioxidant defence system," *International Journal of Nanomedicine*, vol. 9, pp. 2073–2087, 2014.

[30] H. K. Bryan, A. Olayanju, C. E. Goldring, and B. K. Park, "The Nrf2 cell defence pathway: Keap1-dependent and -independent mechanisms of regulation," *Biochemical Pharmacology*, vol. 85, no. 6, pp. 705–717, 2013.

[31] A. Kobayashi, M. I. Kang, H. Okawa et al., "Oxidative stress sensor Keap1 functions as an adaptor for Cul3-based E3 ligase

to regulate proteasomal degradation of Nrf2," *Molecular and Cellular Biology*, vol. 24, no. 16, pp. 7130–7139, 2004.

[32] Q. Ma, "Transcriptional responses to oxidative stress: pathological and toxicological implications," *Pharmacology and Therapeutics*, vol. 125, no. 3, pp. 376–393, 2010.

[33] Y. Samuni, S. Goldstein, O. M. Dean, and M. Berk, "The chemistry and biological activities of N-acetylcysteine," *Biochimica et Biophysica Acta (BBA) - General Subjects*, vol. 1830, no. 8, pp. 4117–4129, 2013.

[34] W. Miao, L. Hu, P. J. Scrivens, and G. Batist, "Transcriptional regulation of NF-E2 p45-related factor (NRF2) expression by the aryl hydrocarbon receptor-xenobiotic response element signaling pathway," *Journal of Biological Chemistry*, vol. 280, no. 21, pp. 20340–20348, 2005.

[35] U. Ritter, Y. I. Prylutskyy, M. P. Evstigneev et al., "Structural features of highly stable reproducible C60 fullerene aqueous colloid solution probed by various techniques," *Fullerenes, Nanotubes, and Carbon Nanostructures*, vol. 23, no. 6, pp. 530–534, 2014.

[36] A. M. Sadowska, B. Manuel-y-Keenoy, and W. A. de Backer, "Antioxidant and anti-inflammatory efficacy of NAC in the treatment of COPD: discordant in vitro and in vivo dose-effects: a review," *Pulmonary Pharmacology & Therapeutics*, vol. 20, no. 1, pp. 9–22, 2007.

[37] M. J. Reiniers, R. F. van Golen, S. Bonnet et al., "Preparation and practical applications of 2′,7′-dichlorodihydrofluorescein in redox assays," *Analytical Chemistry*, vol. 89, no. 7, pp. 3853–−3857, 2017.

[38] A. Boveris, "Determination of the production of superoxide radicals and hydrogen peroxide in mitochondria," *Methods in Enzymology*, vol. 105, pp. 429–435, 1984.

[39] S. P. Wolff, "Ferrous ion oxidation in presence of ferric ion indicator xylenol orange for measurement of hydroperoxides," *Methods in Enzymology*, vol. 233, pp. 182–189, 1994.

[40] J. A. Buege and S. D. Aust, "Microsomal lipid peroxidation," *Methods in Enzymology*, vol. 52, pp. 302–310, 1978.

[41] H. Misra and I. Fridovich, "The role of superoxide anion in the autoxidation of epinephrine and a simple assay for superoxide dismutase," *Journal of Biological Chemistry*, vol. 247, no. 10, pp. 3170–3175, 1972.

[42] H. Aebi, "Catalase in vitro," *Methods in Enzymology*, vol. 105, pp. 121–126, 1984.

[43] G. F. Seelig and A. Meister, "Gamma-glutamylcysteine synthetase. Interactions of an essential sulfhydryl group," *Journal of Biological Chemistry*, vol. 259, no. 6, pp. 3534–3538, 1984.

[44] L. Flohé and W. A. Gunzler, "Assays of glutathione peroxidase," *Methods in Enzymology*, vol. 105, pp. 114–120, 1984.

[45] I. Carlberg and B. Mannervik, "Glutathione reductase," *Methods in Enzymology*, vol. 113, pp. 484–490, 1985.

[46] M. Warholm, C. Guthenberg, C. von Bahr, and B. Mannervik, "Glutathione transferases from human liver," *Methods in Enzymology*, vol. 113, pp. 499–504, 1985.

[47] J. Sedlak and R. H. Lindsay, "Estimation of total, protein-bound, and nonprotein sulfhydryl groups in tissue with Ellman's reagent," *Analytical Biochemistry*, vol. 25, no. 1, pp. 192–205, 1968.

[48] O. Gonchar and I. Mankovska, "Hypoxia/reoxygenation modulates oxidative stress level and antioxidative potential in lung mitochondria: possible participation of P 53 and NF-κB target proteins," *Archives of Pulmonology and Respiratory Care*, vol. 3, no. 2, pp. 35–43, 2015.

[49] J. Liu, X. Wang, M. K. Shigenaga, H. C. Yeo, A. Mori, and B. N. Ames, "Immobilization stress causes oxidative damage to lipid, protein, and DNA in the brain of rats," *The FASEB Journal*, vol. 10, no. 13, pp. 1532–1538, 1996.

[50] A. Zafir and N. Banu, "Modulation of in vivo oxidative status by exogenous corticosterone and restraint stress in rats," *Stress*, vol. 12, no. 2, pp. 167–177, 2009.

[51] B. G. Pérez-Nievas, B. García-Bueno, J. R. Caso, L. Menchén, and J. C. Leza, "Corticosterone as a marker of susceptibility to oxidative/nitrosative cerebral damage after stress exposure in rats," *Psychoneuroendocrinology*, vol. 32, no. 6, pp. 703–711, 2007.

[52] A. T. Dinkova-Kostova and P. Talalay, "Direct and indirect antioxidant properties of inducers of cytoprotective proteins," *Molecular Nutrition & Food Research*, vol. 52, pp. S28–38, 2008.

[53] N. Gharbi, M. Pressac, M. Hadchouel, H. Szwarc, S. R. Wilson, and F. Moussa, "Fullerene is a powerful antioxidant in vivo with no acute or subacute toxicity," *Nano Letters*, vol. 5, no. 12, pp. 2578–2585, 2005.

[54] D. Candas and J. J. Li, "MnSOD in oxidative stress response-potential regulation via mitochondrial protein influx," *Antioxidants and Redox Signaling*, vol. 20, no. 10, pp. 1599–1617, 2014.

[55] S. Foley, C. Crowley, M. Smaihi et al., "Cellular localisation of a water-soluble fullerene derivative," *Biochemical and Biophysical Research Communications*, vol. 294, no. 1, pp. 116–119, 2002.

[56] E. Lubos, J. Loscalzo, and D. E. Handy, "Glutathione peroxidase-1 in health and disease: from molecular mechanisms to therapeutic opportunities," *Antioxidants and Redox Signaling*, vol. 15, no. 7, pp. 1957–1997, 2011.

[57] J. Djordjevic, A. Djordjevic, M. Adzic, and M. B. Radojcic, "Chronic social isolation compromises the activity of both glutathione peroxidase and catalase in hippocampus of male Wistar rats," *Cellular and Molecular Neurobiology*, vol. 30, no. 5, pp. 693–700, 2010.

[58] J. D. Hayes, J. U. Flanagan, and I. R. Jowsey, "Glutathione transferases," *Annual Review of Pharmacology and Toxicology*, vol. 45, no. 1, pp. 51–88, 2005.

[59] I. Smaga, B. Pomierny, W. Krzyżanowska et al., "N-Acetylcysteine possesses antidepressant-like activity through reduction of oxidative stress: behavioral and biochemical analyses in rats," *Progress in Neuro-Psychopharmacology & Biological Psychiatry*, vol. 39, no. 2, pp. 280–287, 2012.

[60] K. Nagata, Y. Iwasaki, T. Yamada et al., "Overexpression of manganese superoxide dismutase by N-acetylcysteine in hyperoxic lung injury," *Respiratory Medicine*, vol. 101, no. 4, pp. 800–807, 2007.

[61] J. Djordjevic, A. Djordjevic, M. Adzic, M. Mitic, I. Lukic, and M. B. Radojcic, "Alterations in the Nrf 2–Keap 1 signaling pathway and its downstream target genes in rat brain under stress," *Brain Research*, vol. 1602, pp. 20–31, 2015.

[62] Y.-S. Keum, S. Yu, P. P.-J. Chang et al., "Mechanism of action of sulforaphane: inhibition of p38 mitogen-activated protein kinase isoforms contributing to the induction of antioxidant response element–mediated heme oxygenase-1 in human hepatoma HepG2 cells," *Cancer Research*, vol. 66, no. 17, pp. 8804–8813, 2006.

[63] S. H. Ki, I. J. Cho, D. W. Choi, and S. G. Kim, "Glucocorticoid receptor (GR)-associated SMRT binding to C/EBPbeta TAD

and Nrf 2 Neh 4/5: role of SMRT recruited to GR in GSTA2 gene repression," *Molecular and Cellular Biology*, vol. 25, no. 10, pp. 4150–4165, 2005.

[64] S. Nair, S. T. Doh, J. Y. Chan, A. N. Kong, and L. Cai, "Regulatory potential for concerted modulation of Nrf2- and Nfkb1-mediated gene expression in inflammation and carcinogenesis," *British Journal of Cancer*, vol. 99, no. 12, pp. 2070–2082, 2008.

[65] G. H. Liu, J. Qu, and X. Shen, "NF-κB/p65 antagonizes Nrf2-ARE pathway by depriving CBP from Nrf2 and facilitating recruitment of HDAC3 to MafK," *Biochimica et Biophysica Acta (BBA) - Molecular Cell Research*, vol. 1783, no. 5, pp. 713–727, 2008.

[66] F. Yamakura and H. Kawasaki, "Post-translational modifications of superoxide dismutase," *Biochimica et Biophysica Acta*, vol. 1804, no. 2, pp. 318–325, 2010.

[67] V. Oliveira-Marques, H. S. Marinho, L. Cyrne, and F. Antunes, "Role of hydrogen peroxide in NF-κB activation: from inducer to modulator," *Antioxidants and Redox Signaling*, vol. 11, no. 9, pp. 2223–2243, 2009.

Hindawi
Oxidative Medicine and Cellular Longevity
Volume 2018, Article ID 6430601, 11 pages
https://doi.org/10.1155/2018/6430601

Research Article

Oxidative Stress in Autistic Children Alters Erythrocyte Shape in the Absence of Quantitative Protein Alterations and of Loss of Membrane Phospholipid Asymmetry

Alessandra Bolotta,[1,2] **Michela Battistelli**,[3] **Elisabetta Falcieri**,[3] **Alessandro Ghezzo**,[1] **Maria Cristina Manara**,[4] **Stefano Manfredini**,[5] **Marina Marini**,[1,2] **Annio Posar**,[6,7] **Paola Visconti**,[7] **and Provvidenza Maria Abruzzo**[1,2]

[1]*Department of Experimental, Diagnostic and Specialty Medicine, Bologna University, Via Belmeloro 8, 40126 Bologna, Italy*
[2]*IRCCS Fondazione Don Carlo Gnocchi, Via A. Capecelatro 66, 20148 Milan, Italy*
[3]*Department of Biomolecular Sciences, Urbino University, Via A. Saffi 2, 61029 Urbino, Italy*
[4]*CRS Development of Biomolecular Therapies, Experimental Oncology Laboratory, Istituto Ortopedico Rizzoli, Via di Barbiano 1/10, 40136 Bologna, Italy*
[5]*Department of Life Sciences and Biotechnologies, Ferrara University, Via G. Savonarola 9, 44121 Ferrara, Italy*
[6]*Department of Biomedical and Neuromotor Sciences, Bologna University, Via U. Foscolo 7, 40123 Bologna, Italy*
[7]*Child Neurology and Psychiatry Unit, IRCCS Istituto delle Scienze Neurologiche di Bologna, Via Altura 3, 40139 Bologna, Italy*

Correspondence should be addressed to Marina Marini; marina.marini@unibo.it

Received 18 July 2018; Accepted 20 September 2018; Published 11 November 2018

Academic Editor: Tomris Ozben

Red blood cells (RBCs) from people affected by autism spectrum disorders (ASDs) are a target of oxidative stress. By scanning electron microscopy, we analyzed RBC morphology from 22 ASD children and show here that only 47.5 ± 3.33% of RBC displayed the typical biconcave shape, as opposed to 87.5 ± 1.3% (mean ± SD) of RBC from 21 sex- and age-matched healthy typically developing (TD) controls. Codocytes and star-shaped cells accounted for about 30% of all abnormally shaped ASD erythrocytes. RBC shape alterations were independent of the anticoagulant used (Na_2-EDTA or heparin) and of different handling procedures preceding glutaraldehyde fixation, thus suggesting that they were not artefactual. Incubation for 24 h in the presence of antioxidants restored normal morphology in most erythrocytes from ASD patients. By Coomassie staining, as well as Western blotting analysis of relevant proteins playing a key role in the membrane-cytoskeleton organization, we were unable to find differences in RBC ghost composition between ASD and normal subjects. Phosphatidylserine (PS) exposure towards the extracellular membrane domain was examined in both basal and erythroptosis-inducing conditions. No differences were found between ASD and TD samples except when the aminophospholipid translocase was blocked by N-ethylmaleimide, upon which an increased amount of PS was found to face the outer membrane in RBC from ASD. These complex data are discussed in the light of the current understanding of the mode by which oxidative stress might affect erythrocyte shape in ASD and in other pathological conditions.

1. Introduction

The erythrocyte plasma membrane has unique properties, which allow the cell to provide an extended surface for gaseous exchanges and to undergo large passive deformations while the erythrocyte squeezes itself through narrow capillaries, some of them with cross sections one-third its own diameter. These unusual properties are due to the complexity of the structural network supporting the plasma membrane, where the phospholipid bilayer is anchored to a two-dimensional spectrin hexagonal lattice via protein junctional complexes centered on band 3, the anion-exchange

channel. Two major complexes connect band 3 with the cytoskeletal spectrin network, the ankyrin complex and the actin complex, but, according to a recent review [1], the composition of these band 3-associated protein complexes is not constant. On the overall, the red cell membrane contains about 20 major proteins and at least 850 minor ones [1]. A recent paper [2] pointed out the role of nonmuscle myosin IIA in maintaining erythrocyte shape by interacting with the actin network associated with band 3 complexes.

The membrane structure, which assures both shape resiliency and a marked physiological deformability, also allows RBC to undergo unique and reversible shape changes, from discocytes to spherical globes (spherocytes), or to concave (stomatocytes), or to crenated (echinocytes) shapes. These changes are triggered by a variety of chemical and physical agents (including pH and ATP concentration) and, in certain conditions, can even occur cyclically in sequence [3]. In his paper, Rudenko [3] extensively discusses RBC shape transitions, pointing out that two main theories have been advanced to explain them: (i) one based on the bilayer couple of biological membranes, which suggests that any effect that expands the outer leaflet relative to the inner one produces a tendency to form convex structures on the cell surface (e.g., echinocytic spicules), whereas an expansion of the inner leaflet relative to the outer one favors concavities (e.g., stomatocytic shapes) [4, 5]; (ii) the other based on changes in band 3 conformation, leading to altered ionic composition within the cell [6, 7]. However, recent research [8] challenged the current theories linking in a straightforward way RBC shape alterations to disturbances of the membrane-cytoskeleton network.

A number of pathological conditions are associated with characteristic RBC shape alterations, which, at variance with Rudenko's transitions, tend to be stable over time [9]. For instance, typical thorny red cells (acanthocytes) are prevalent in neuroacanthocytosis, a group of rare genetic diseases [10]; hereditary spherocytosis, elliptocytosis, and stomatocytosis are RBC disorders resulting from mutations in genes encoding various membrane and skeletal proteins [11]; codocytes are a common occurrence in beta-thalassemia [12], which is also characterized by oxidative stress [13]. Leptocytes and other abnormal erythrocyte shapes were found in Rett patients [14], a genetic neurodevelopmental disorder accompanied by oxidative stress and hypoxia. A marked beta-actin deficiency was afterwards described in RBC from these patients [15]. The same team also described the presence of abnormal RBC shapes and, in a less convincing way, of decreased beta-actin expression in "classical" (i.e., nonsyndromic) autistic patients [16]. "Classical" autism is the most common of the neurodevelopmental disorders characterized by social and behavioral impairments and collectively named autism spectrum disorders (ASDs). ASD has a prevalent genetic etiology; however, epigenetically acting environmental factors (e.g., immune dysregulation, pollutants) seem to have a key role in the development of the disease [17]. Oxidative stress is a distinctive feature of ASD [18, 19] and deeply affects RBC membrane, impairing its fluidity, altering its lipid composition, and affecting the activity on Na^+/K^+-ATPase [18, 20].

In patients with chronic obstructive pulmonary disease, chronic oxidative stress alters RBC shape, but normal shape is reestablished following appropriate antioxidant medication [21]. Similarly, RBC storage in blood banks leads to the build-up of reactive oxygen species (ROS) and of oxidation products such as malondialdehyde. The ensuing oxidative stress leads to the formation of spiculated cells (echinocytes), to the budding of micro- and nanovesicles from the spiculae [22], and eventually to hemolysis; all of which may be prevented by supplementation with antioxidants [23]. Moreover, oxidative stress triggers PS externalization [24], but with modalities still not clarified.

Understanding how oxidative stress alters RBC morphology—and possibly function—requires the evaluation of how it affects the band 3-centered cytoskeletal network. It has been shown that oxidative stress, as well as other stimuli, increases phosphorylation of band 3 on tyrosine residues, thus markedly reducing band 3 affinity for ankyrin, leading to the disruption of the membrane skeletal architecture and favoring progressive plasma membrane vesiculation [25]. However, in the presence of oxidative stress, the antioxidant enzyme peroxiredoxin-2 (Prx2) progressively migrates to the RBC plasma membrane, where it associates with the amino domain of band 3 [26, 27]. The band 3 amino domain is also the regulatory site where glucose metabolism is addressed towards the glycolytic ATP production or, conversely, towards the production of molecules offering antioxidant protection—NADPH and GSH [28]. Thus, PRX2 binding to the band 3 sites allows at the same time ATP production and its own antioxidant protection to the membrane site.

This work is aimed at understanding the extent of RBC shape alteration in ASD, its molecular base(s), and how it may affect RBC functions. As we recently demonstrated [20] that the amount of beta-actin in RBC from ASD children did not differ from that of TD controls, we turned our attention to the quantification of band 3 and stomatin. These proteins were chosen because band 3 has a pivotal role in cytoskeletal organization, while stomatin was among the few RBC membrane proteins found to be differentially expressed in ASD leukocytes [29].

2. Materials and Methods

2.1. Subjects. Twenty-two children diagnosed with nonsyndromic ASD (17 males and 5 females, age (mean ± SD) 7.75 ± 1.87 years, age range 5.25–11.08 years) and 21 typically developing children (14 males and 7 females, age (mean ± SD) 9.44 ± 1.96 years, age range 5.25–11.83 years) were recruited by the Child Neuropsychiatry Unit of the Bellaria Hospital (IRCCS, Bologna) within a larger study approved by Local Ethical Committee (Azienda USL Bologna, Imola, Ferrara, CE 13062, 23/07/2013; Prot. N.1198/CE). The study was conducted according to the Declaration of Helsinki guidelines. Written consent was obtained from parents as well as from children through pictures and simplified information. The patients were affected by nonsyndromic autism, according to a complete clinical diagnostic assessment (ADOS, DSM-5) and a comprehensive neurological

workup, detailed in a previous manuscript by our group [30]. Moreover, patients were subjected to a complete pediatric assessment, including the evaluation of hematological parameters and of electrolytes, which ruled out the presence of iron deficiency (occasionally reported to occur in ASD children [31]), hemolysis, and splenomegaly. Control typically developing (TD) children were recruited in the same local community and were free of cognitive, learning, and psychiatric problems. Subjects did not take any dietary supplement or medication in the 4 months preceding the evaluation and were on a typical Mediterranean diet. Demographic and clinical data are shown in Tables 1(a) and 1(b).

2.2. Materials. Unless otherwise specified, chemicals were analytical grade and purchased from Sigma-Aldrich, St. Louis, MO.

2.3. RBC Preparation and Morphological Evaluation. From each subject, two blood samples (1 mL) were collected, one in Na_2-EDTA and the other in sodium heparin vacutainers. For morphological evaluation with scanning electron microscopy, we always treated the samples within 1 h from collection. We compared two preparation protocols. In the first protocol, aimed at limiting mechanical stress to the cells, 30 μL of whole blood was transferred to an Eppendorf 1.5 mL tube, centrifuged (5 min at 100 ×g) in order to separate plasma, which was gently removed with a micropipette. Cells were fixed in suspension with 2.5% glutaraldehyde in cold 0.1 M phosphate buffer pH 7.2 for 2 h at room temperature. During this step, RBC underwent spontaneous sedimentation. The supernatant was then gently removed with a micropipette, phosphate buffer was added, and the sample was maintained at 4°C till successive steps. In the "rougher" protocol, 30 μL of RBC suspension was obtained after Ficoll density gradient and three washing steps in phosphate-buffered saline. The RBC suspension was then fixed in 2.5% glutaraldehyde in 0.1 M phosphate buffer pH 7.2 as described for the more gentle protocol. Cells were quickly washed in 0.15 M phosphate buffer at pH 7.2, and then drops of the suspension were deposited on poly-L-lysine-coated coverslips [32]. The adhesion was carried out overnight in a moist and sealed chamber at 4°C. Afterwards, the slides were washed and postfixed with 1% OsO_4 in the same buffer for 1 h. A gentle progressive alcohol dehydration was performed, and specimens were critical point-dried. After mounting on conventional SEM stubs by means of silver glue, specimens were gold sputtered, by a sputtering device [33] and finally observed with a Philips 515 scanning electron microscopy. The morphological alterations were evaluated by two different observers, in separate observation sessions. The entire slide was evaluated, and then twenty microscope fields, for each sample, were photographed at the same magnification (1770x magnitude). The images were used for the classification of erythrocytes according to their morphology.

2.4. Antioxidant In Vitro Treatment. This study was carried out in a subgroup of subjects, 6 ASD and 8 TD. RBC suspensions obtained from Ficoll gradient and washed three times in phosphate-buffered saline were used. RBC suspensions were diluted in 2 mL SAGM storage medium (NaCl 8.77 g/L; adenine 0.169 g/L; dextrose 9 g/L; mannitol 5.25 g/L) at the concentration of 250 μL RBC/mL. Three parallel samples, 2.5 mL each, were seeded in 6-well culture plates (9.6 cm^2/well surface area). The RBC suspension was (i) treated with an antioxidant mix containing 8 μM (final dilution) tocotrienol (Carlo Sessa SpA, Milan, Italy) dissolved at 1000x concentration in dimethyl sulphoxide (DMSO) and 0.7 μM (final dilution) Q10 (ACEF SpA, Fiorenzuola D'Arda, Italy) dissolved 1000x in N,N-dimethylformamide (DMF); (ii) untreated; and (iii) additioned with DMSO plus DMF alone. The cell suspensions were incubated 24 h at 37°C in 5% CO_2 atmosphere. 40 μL was then collected from each well, centrifuged (5 min at 100 ×g) to remove the SAGM solution, and fixed in 2.5% glutaraldehyde solution for scanning electron microscopy as described above.

Ghost suspension was prepared as previously described [20].

SDS-polyacrylamide gel electrophoresis (SDS-PAGE) was carried out with ghost suspensions; gels were loaded semiquantitatively (equal volume of packed ghosts/lane), as described [34]. Precast gradient gels (Mini-PROTEAN TGX Stain-Free Protein Gel, 4–15% polyacrylamide, Bio-Rad Laboratories, Hercules, CA) were used. Some gels were stained with Coomassie Brilliant Blue-R250 (Bio-Rad, Hercules, CA).

Western blotting was performed following SDS-PAGE and transferred to nitrocellulose membranes [20]. The following primary antibodies were used: mouse monoclonal anti-beta-actin (C4) (Santa Cruz Biotechnology, Dallas, Texas) at 1 : 1000 dilution; mouse monoclonal anti-stomatin (E-5) (Santa Cruz Biotechnology, Dallas, Texas) at 1 : 1000 dilution; and mouse monoclonal SLC4A1, antianion exchanger 1 or band 3 (IVF12) (DSHB Hybridoma Product IVF12, deposited to the DSHB by Jennings M.L. at 1 : 30000 dilution). Secondary antibody was ImmunoPure® Goat Anti-Mouse IgG, (H + L), peroxidase conjugated (Thermo Scientific, Waltham, Massachusetts), and was used at the following dilutions: 1 : 5000, 1 : 15000, and 1 : 20000, respectively. ECL: Western Bright™ ECL (Advansta, Menlo Park, CA) was used for detection. Specific protein band density was quantified by means of Bio-Rad GelDoc 2000 with reference to the actin band.

2.5. Evaluation of Phosphatidylserine Exposure. This study was carried out in a subgroup of subjects, 11 ASD and 10 TD. Phosphatidylserine (PS) exposure was evaluated by flow cytometry. The procedure outlined by Kuypers et al. [35] was followed, with small modifications. RBCs from a Ficoll gradient suspension were initially diluted with Hanks' balanced salt solution (HBSS) and distributed into 6 tubes which were examined in the following conditions: (1) basal, untreated; (2) N-ethylmaleimide (NEM); (3) osmotic shock (OS); (4) OS + NEM; (5) Ca^{2+} ionophore A23187; and (6) ionophore A23187 + NEM. For samples (2), (4), and (6), RBCs (30% hematocrit) were incubated with 10 mM NEM for 30 min at 37°. After incubation, the samples were washed in HBSS and then diluted at 16% hematocrit before the evaluation or the successive treatments. OS was performed at 16% hematocrit 10 min at room temperature with

Table 1

(a) Demographic and clinical features of the ASD children

No.	Gender	Age (months)	Onset pattern: 1 (early); 2 (regressive); 3 (mixed)	Brief nonverbal IQ*	ADOS score**	CARS total score	CARS activity level item score	CARS body use (stereotypies) item score	CARS verbal communication item score	CARS nonverbal communication item score	CARS total number of items whose score was ≥3
1	M	68	1	48	20	41.5	2.5	3	3	3	11
2	M	94	1	52	21	46	3.5	4	4	4	11
3	F	68	3	71	20	43.5	2.5	3	3.5	3	10
4	M	93	2	45	20	48.5	3	4	3.5	3	12
5	M	82	2	55	19	42	3	3	3	3	9
6	M	115	1	52	19	39.5	3	3	3	3	7
7	M	74	3	68	19	41	2.5	3	3	3	9
8	M	99	1	56	16	35	2.5	2	3	3	3
9	M	85	1	62	22	41	2.5	2	3	3	7
10	F	74	1	47	17	38	2	2.5	3	3	7
11	F	124	3	87	21	33.5	2	2	2.5	2.5	4
12	M	129	1	68	19	39	2	2.5	3	3	7
13	M	78	3	82	17	39	3	2.5	3	3	6
14	M	96	1	67	22	44	2.5	3	3	3	11
15	M	84	1	95	18	39.5	2.5	3	3	3	8
16	M	114	1	45	21	47	3	3.5	3.5	3	13
17	M	103	3	47	16	41.5	4	2	3	3	10
18	M	131	1	96	18	35	2	3	2.5	2.5	3
19	F	64	1	75	17	39.5	2.5	2.5	3.0	3.0	6.0
20	F	64	1	74	17	41.0	2.5	2.5	3.0	3.0	7.0
21	M	98	1	49	20	41	2	3.5	2.5	2	9
22	M	133	3	80	13	34	2	1.5	3	2.5	2

*Cognitive level: ≥70, normal; 50–69, mild cognitive impairment; 35–49, moderate cognitive impairment; and <35, severe cognitive impairment. (ICD-10 classification of mental and behavioural disorders, WHO, 1992). **ADOS modules 1 or 2 (total score autism cutoff = 12).

(b) Demographic features of the typically developing children

No.	Gender	Age (months)
1	F	140
2	F	74
3	F	97
4	F	93

Table 1: Continued.

No.	Gender	Age (months)
5	M	142
6	M	127
7	M	116
8	M	142
9	M	135
10	M	63
11	F	125
12	M	115
13	M	115
14	M	125
15	F	102
16	F	120
17	M	101
18	M	130
19	M	123
20	M	136
21	M	65

9 g/100 mL NaCl. For the treatment with Ca^{2+} ionophore 23187, RBCs at 16% hematocrit were previously loaded with 1 mM $CaCl_2$ for 3 min in incubator, and then the ionophore was added at 4 μM final concentration; the samples were incubated at 37°C for 20 min, and then the reaction was stopped with 2.5 mM Na_2-EDTA. Cells were then washed 3 times with HBSS buffer +1% BSA. Before loading the samples to the cytometer, the samples were diluted in 10 mL phosphate-buffered saline, and then 1 mL was centrifuged (5 min at 400 ×g) and the pellet was incubated with FITC-labelled annexin V using the annexin V-FLUOS Staining Kit (Roche, Basel, Switzerland) according to the manufacturer's instructions. Samples were acquired using a FACSCalibur instrument and analyzed with the CellQuest Software (Becton Dickinson, Italy).

2.6. Statistical Analysis. Data were tested for normality using GraphPad Prism7, which employed the D'Agostino-Pearson test, following which appropriate parametric tests (Student's t for independent data) or the nonparametric equivalent (Mann-Whitney) was used. Differences were considered significant at $p < 0.05$.

3. Results

3.1. Scanning Electron Microscopy Reveals Altered Erythrocyte Shape in RBC from ASD Subjects. Figure 1 shows the distribution of RBC by morphology in TD and in ASD children. Most RBC (87.5 ± 1.3%, mean ± SD) from TD children displayed the typical normal biconcave shape, which characterized only 47.5 ± 3.33% (mean ± SD) of RBC from ASD children. The difference was highly significant ($p = 3 * e^{-13}$). The extremely low variability among the samples makes impossible to correlate morphological shapes to clinical features, which display a much higher variability. Among abnormally shaped RBC, codocytes and star-shaped cells were the most represented ones, whereas echinocytes were relatively few. Abnormal morphologies were not peculiar of RBC from ASD subjects, rather ASD subjects displayed abnormal RBC shapes in a higher percentage of erythrocytes with respect to healthy subjects. Representative images of microscopic fields form one TD and from one ASD subject, as well as a gallery of abnormal morphologies are shown in Figure 2.

Notably, no difference was found with respect to the anticoagulant used or the prefixation procedures.

3.2. Incubation with Antioxidants Restores Normal Morphology to RBC from ASD Subjects. In vitro treatment with the antioxidant mix brought the percentage of discocytes from 47.5 to 82%, thus substantially restoring the normal morphology to control levels. A representative image is shown in Figure 3. Incubation in SAGM alone or additioned with the DMSO + DMF vehicle did not alter the original RBC morphology.

3.3. Qualitative and Semiquantitative Evaluations of Ghost Proteins Do Not Show Appreciable Differences between ASD and TD Subjects. Ghost extracts were run in SDS-polyacrylamide gradient gels and stained with Coomassie

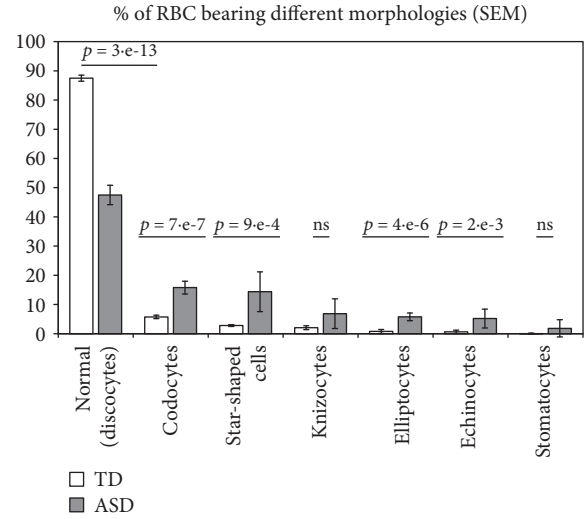

Figure 1: RBC bearing different morphologies, as percent of total RBC. Open columns: RBC from typically developing children. Dark columns: RBC from children affected by autistic spectrum disorder. Mean ± SD. Numbers over the columns indicate whether the difference was statistically significant ($p < 0.05$ by Student t-test).

Blue in order to allow an overview of the protein composition of the extracts. As shown in Figure 4, no difference could be appreciated at a qualitative level. In particular, bands 4.1 and 4.2, which were reported to be differentially expressed in ASD leukocytes [29], display the same staining intensity in TD and ASD samples.

We recently reported that TD- and ASD-derived RBC did not vary in beta-actin amount, as evaluated by Western blotting performed according to the most rigorous standards [20]. This result allowed us to use beta-actin as reference protein to quantitate other proteins by Western blotting. We chose to evaluate band 3 and stomatin, basing the choice on the motivations mentioned in Introduction. Figure 5 reports representative WB results for the two proteins. Band intensity of the two examined proteins, as quantified relative to beta-actin, was the same in TD- and ASD-derived ghost samples.

3.4. Phosphatidylserine Exposure Does Not Seem to Differ in Erythrocytes between TD and ASD Children, but Addition of N-Ethylmaleimide Suggests That ASD RBC Undergo an Increased PS Flip-Flop Cycling in Basal Conditions. The localization of PS on the outer side of the lipid bilayer was assessed in order to evaluate the tendency of RBC from ASD children to undergo erythroptosis, as a consequence of oxidative stress and as a result of morphological anomalies, both in basal conditions (i.e., without any treatment) and when exposed to either osmotic stress or calcium overload. Results, reported in Figure 6, show that no difference in PS exposure is present in basal conditions. However, when the aminophospholipid translocase was blocked by NEM, a significant ($p = 0.03$) increase in PS exposure could be appreciated in ASD RBC, suggesting that in basal conditions, PS flippase was actively engaged in reimporting PS from the outer bilayer. The addition of NEM to osmotic stressed or to calcium overloaded

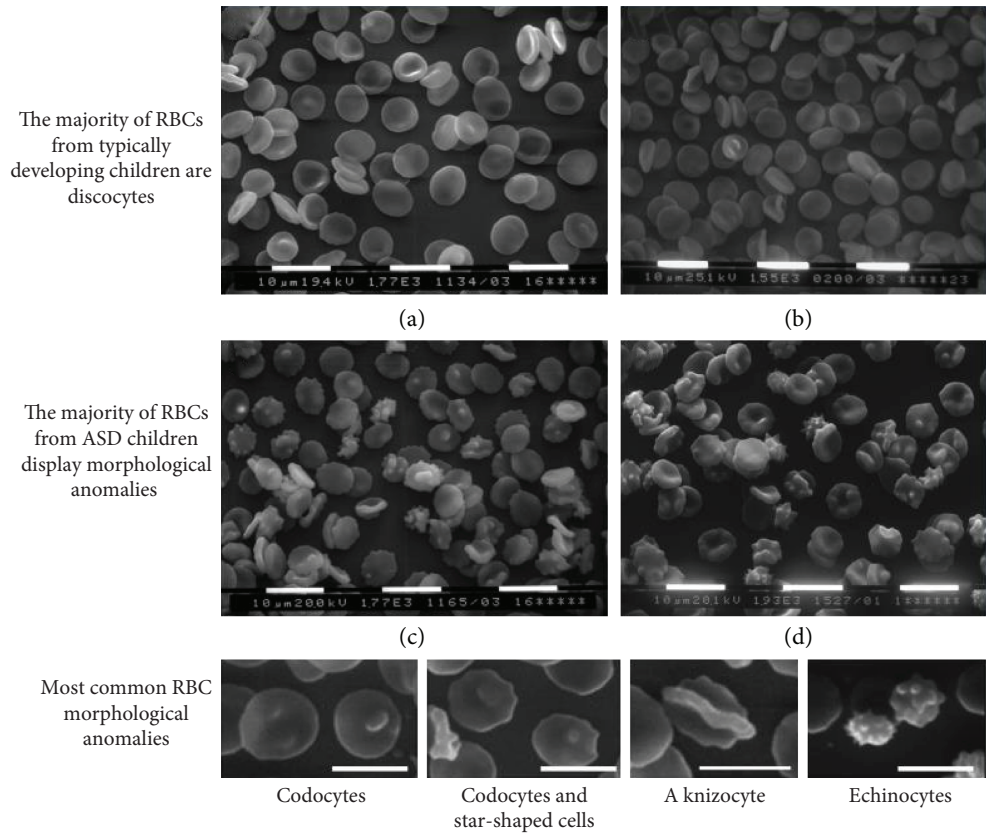

Figure 2: RBC morphology at scanning electron microscopy. (a, b) Normal RBC morphology (discocytes) found in typically developing children. (c, d) A variety of RBC abnormal morphologies found in children affected by autistic spectrum disorder. Bottom panel: a gallery of abnormal RBC morphologies.

RBC was not able to unveil any difference between RBCs from TD and ASD subjects, although one should remark the rather high variability in percent PS exposure following OS and the maximal PS exposure as a response to calcium overload, both situations where a ≈50% increase of PS exposure could have gone unnoticed.

4. Discussion

In the present work, we addressed the question of how oxidative stress, which affects ASD subjects altering in multiple ways RBC and their plasma membrane [18–20, 30], impinges on RBC shape, composition of the plasma membrane-cytoskeletal network and propensity to undergo erythroptosis. Although the group of Ciccoli et al. had reported multiple shape anomalies and a decrease in β-actin in RBC from "classical autistic" subjects [16], our experience with hyperspectral microscopy [30] was not confirming the presence of shape alterations at a large extent; moreover, our accurate evaluation of β-actin content had not revealed differences between RBCs from TD and ASD children [20]. By studying the extensive literature on the determinants of erythrocyte shape alterations, we understood that the apparent lack of morphological alterations found with hyperspectral microscopy was probably to be ascribed to the so-called "glass effect," as described by Wong [6] that likely cancels the difference between TD and ASD RBC morphology. In fact, when RBC shape changes are "fixed" by abnormal aggregation or clusterization of RBC proteins, as in beta-thalassemia or in sickle cell anemia, the "glass effect" does not take place; on the other hand, the contact with the glass slide in isosmotic unbuffered medium favors ionic concentration adjustments and makes very hard to distinguish the difference between TD and ASD RBC morphology in both fresh blood samples and standard Giemsa-stained slides. Thus, scanning electron microscopy is better suited for the morphological analysis of RBC shape alterations, as those described by the group of Ciccoli et al. By a careful study, which took into consideration some of the possible artifacts that could affect erythrocyte shape, and in particular by comparing with the same modalities ASD and TD RBC, we confirmed the findings of Ciccoli et al. group about shape anomalies in more than half of the RBC from autistic children. Remarkably, these abnormal morphologies were (i) independent of the anticoagulant used, confirming that only a long conservation in Na_2-EDTA may affect RBC shape [36], and (ii) unaffected by repeated preparative centrifugations, carried out in buffered saline. Of note, RBC from ASD did not display bizarre or unique morphologies; rather they had a higher percentage of altered morphologies found in lesser amounts in RBC from TD subjects. In particular, one would expect to find a prevalence of echinocytes, since there are numerous reported instances where discocytes exposed to oxidative stress turned into echinocytes [25, 26].

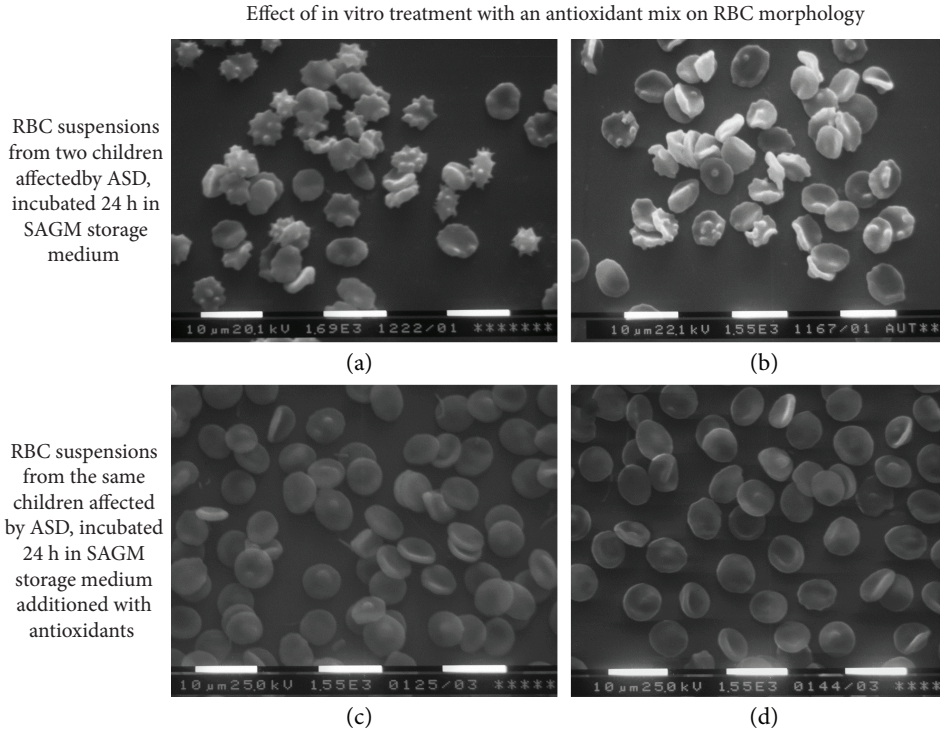

Figure 3: Effect of antioxidant treatment on the morphology of RBC from children affected by autistic spectrum disorder. (a, b) Before the in vitro 24 h treatment. (c, d) After the treatment with tocotrienol and Q10. The percentage of abnormally shaped erythrocytes is clearly decreased.

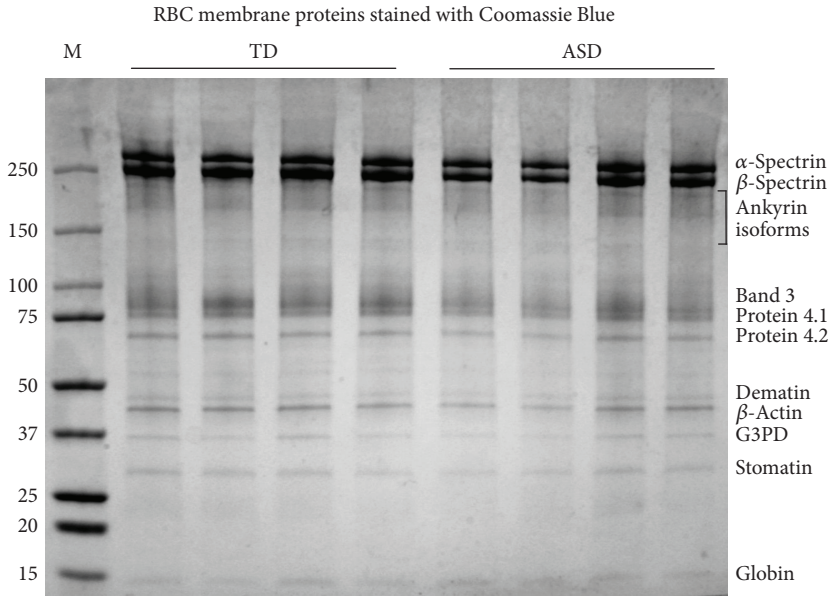

Figure 4: A representative SDS-PAGE stained with Coomassie Blue. The gel was a precast 4–15% polyacrylamide gel. M: markers; TD: RBC samples from typically developing children; ASD: RBC samples from children affected by autistic spectrum disorder. On the left side: MW of the markers. On the right side: bands presumably corresponding to major RBC proteins.

This however was not the case with ASD RBC, although their exposure to ROS is indisputable. It is our opinion that ASD RBC do not assume the echinocyte shape because they *do not* loose ATP, at least at the extent lost by RBC in the abovementioned models of oxidative stress.

An eye evaluation of ghost proteins separated by SDS-PAGE and stained by Coomassie Blue does not suggest the occurrence of major differences in the protein set between TD and ASD subjects. This has been demonstrated by us for β-actin [20] and for band 3 and stomatin in the present

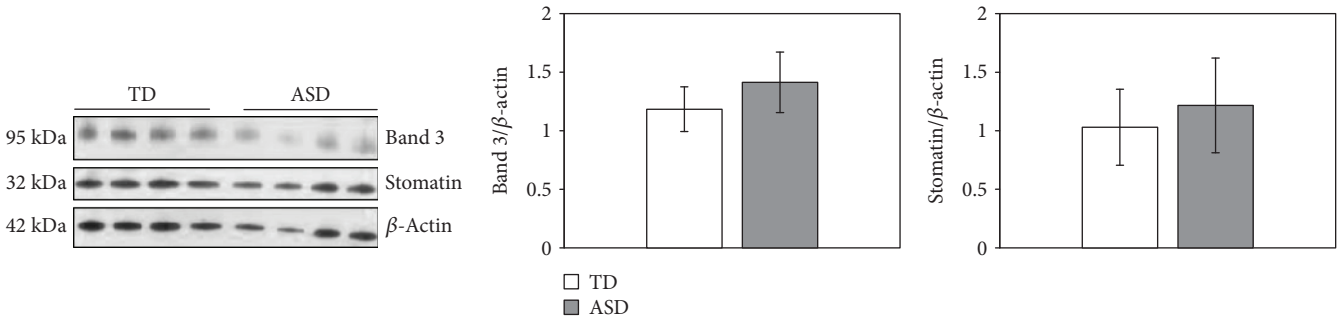

(a) Western blot of RBC membrane proteins

(b) Band 3 and stomatin protein expression

Figure 5: (a) A representative Western blot where anti-band 3 and anti-stomatin antibodies were used to quantitate specific proteins separated by SDS-PAGE; β-actin was used as loading control. The gel was a precast 4–15% polyacrylamide gel. TD: four RBC samples from typically developing children; ASD: four RBC samples from children affected by autistic spectrum disorder. (b) Densitometry showing the intensity of specific protein bands relative to the corresponding β-actin band. Ghost samples from all patients and controls were examined. Differences between TD and ASD RBC were not statistically significant.

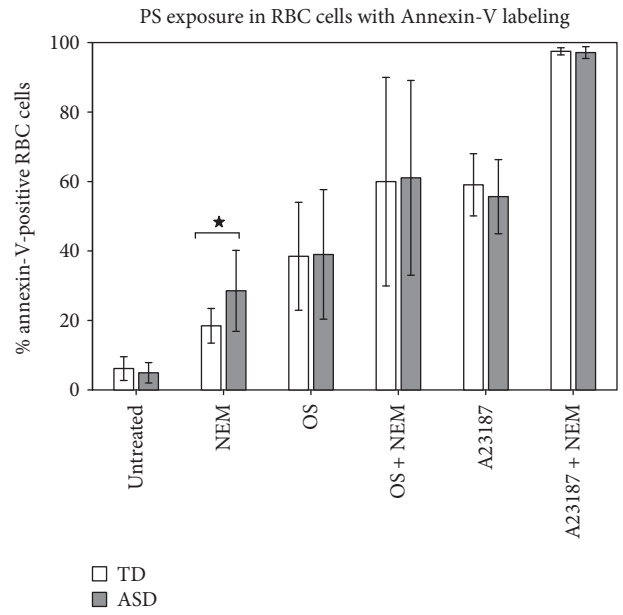

Figure 6: Percent of annexin V (+) RBC in typically developing children (TD, open columns) or in children affected by autistic spectrum disorder (ASD, dark columns). Treatments are shown under the columns: NEM: N-ethylmaleimide; OS: osmotic shock; A23187: calcium ionophore. Mean ± SD. Star: difference was statistically significant ($p = 0.03$ by Student t-test).

work. However, in order to study the ≈870 different proteins located at the erythrocyte plasma membrane and to find possible expression differences between TD and ASD subjects, one should use an -omic approach; proteomics allowed Mohanty et al. [37] to find many differentially expressed proteins in RBC from Alzheimer patients and healthy individuals. On the other hand, using a transcriptomic approach, Glatt et al. [29] found a relevant number of differentially expressed genes in leukocytes from ASD patients. Nevertheless, the fact that incubation with an antioxidant mix was able to almost completely restore the normal morphology in ASD RBC points to oxidative stress-induced modifications of the protein-to-protein associations or of membrane proteins themselves rather than to major quantitative differences.

The most obvious culprit of the morphological anomalies would be band 3 protein, which, as discussed above, undergoes multiple phosphorylations in an oxidative environment, thus altering its interaction with the other proteins of the junctional complexes [25]. However, other proteins are likely to be involved as well; for instance, it may be worth investigating whether the newly found actin-myosin IIA interaction [2] is affected by oxidative stress. Advanced glycation end products are found in the plasma of ASD children [19], but the presence of glycated proteins in ASD erythrocytes has not been evaluated. For instance, spectrin is easily glycated [38] and its glycation would be a normal occurrence in steady-state conditions, due to the high-glucose concentration and the rich-oxygen milieu of the erythrocyte. Spectrin glycation occurs at sites of PS binding; thus, translocation of PS from the inner to the outer lipid monolayer not only provides the basis for erythroptosis but also contributes to alteration of the spectrin-based membrane skeleton, to shape modification and to decreased deformability of the cell. Such events do not occur in steady-state conditions since an ATP-powdered aminophospholipid translocase is continuously relocating PS to the inner membrane side [39]. In a murine model of β-thalassemia [13], oxidative stress leads to massive PS externalization and to erythrocyte loss. Indeed, our cytometric data strongly suggest not only an increased PS externalization in ASD RBC but also its efficient contrast by the activity of aminophospholipid translocases.

5. Conclusions

As far as we know so far, oxidative stress in ASD children is not generated within the erythrocyte and might be a consequence of chronic low-level (neuro)inflammation. Despite the extensive shape anomalies, the enhanced bilayer stiffness, the reduced activity of its Na^+/K^+-ATPase, and the increased needs to replenish the ATP supply required to maintain an accelerated activity of aminophospholipid translocases, it is

amazing that oxidative stress at the erythrocyte level seems to be limited in consequences, as suggested by the fact that no clinical sign of reduced erythrocyte activity (e.g., impaired peripheral tissue oxygenation) has been so far described in ASD patients.

At a mere speculative level, we advance the hypothesis that a key role may be played by the interplay of PRX2 with the N-terminal domain of band 3. As oxidative stress promotes the migration of PRX2 to the membrane and its binding to the N-terminal domain of band 3, glucose metabolism is addressed towards the glycolytic ATP production for a longer fraction of time or in more numerous membrane locations, thus supplying the energy required for maintaining membrane phospholipid symmetry. Moreover, RBC antioxidant defenses are so abundant that RBCs are able to cope with many threats brought by exogenous ROS.

Data Availability

The data used to support the findings of this study are available from the corresponding author upon request.

Disclosure

The funders had no role in the study design, data collection and analysis, decision to publish, or preparation of the manuscript.

Conflicts of Interest

The authors declare the absence of conflicts of interest.

Acknowledgments

The authors are grateful to the children who contributed a blood sample and to their families. The present work was exclusively supported by the ANGSA (Associazione Nazionale Genitori Soggetti Autistici).

References

[1] S. E. Lux IV, "Anatomy of the red cell membrane skeleton: unanswered questions," *Blood*, vol. 127, no. 2, pp. 187–199, 2016.

[2] A. S. Smith, R. B. Nowak, S. Zhou et al., "Myosin IIA interacts with the spectrin-actin membrane skeleton to control red blood cell membrane curvature and deformability," *Proceedings of the National Academy of Sciences of the United States of America*, vol. 115, no. 19, pp. E4377–E4385, 2018.

[3] S. V. Rudenko, "Erythrocyte morphological states, phases, transitions and trajectories," *Biochimica et Biophysica Acta (BBA) - Biomembranes*, vol. 1798, no. 9, pp. 1767–1778, 2010.

[4] J. F. Hoffman, "Quantitative study of factors which control shape transformations of human red blood cells of constant volume," *Nouvelle Revue Française d'Hématologie*, vol. 12, no. 6, pp. 771–774, 1972.

[5] M. P. Sheetz and S. J. Singer, "Biological membranes as bilayer couples. A molecular mechanism of drug-erythrocyte interactions," *Proceedings of the National Academy of Sciences of the United States of America*, vol. 71, no. 11, pp. 4457–4461, 1974.

[6] P. Wong, "A basis of echinocytosis and stomatocytosis in the disc-sphere transformations of the erythrocyte," *Journal of Theoretical Biology*, vol. 196, no. 3, pp. 343–361, 1999.

[7] J. Gimsa and C. Ried, "Do band 3 protein conformational changes mediate shape changes of human erythrocytes?," *Molecular Membrane Biology*, vol. 12, no. 3, pp. 247–254, 1995.

[8] J. C. A. Cluitmans, F. Gevi, A. Siciliano et al., "Red blood cell homeostasis: pharmacological interventions to explore biochemical, morphological and mechanical properties," *Frontiers in Molecular Biosciences*, vol. 3, p. 10, 2016.

[9] J. Ford, "Red blood cell morphology," *International Journal of Laboratory Hematology*, vol. 35, no. 3, pp. 351–357, 2013.

[10] J. C. A. Cluitmans, C. Tomelleri, Z. Yapici et al., "Abnormal red cell structure and function in neuroacanthocytosis," *PLoS One*, vol. 10, no. 5, article e0125580, 2015.

[11] L. Da Costa, J. Galimand, O. Fenneteau, and N. Mohandas, "Hereditary spherocytosis, elliptocytosis, and other red cell membrane disorders," *Blood Reviews*, vol. 27, no. 4, pp. 167–178, 2013.

[12] A. Bunyaratvej, S. Sahaphong, N. Bhamarapravati, and P. Wasi, "Quantitative changes of red blood cell shapes in relation to clinical features in beta-thalassemia/HbE disease," *American Journal of Clinical Pathology*, vol. 83, no. 5, pp. 555–559, 1985.

[13] L. De Franceschi, F. Turrini, M. Honczarenko et al., "In vivo reduction of erythrocyte oxidant stress in a murine model of β-thalassemia," *Haematologica*, vol. 89, no. 11, pp. 1287–1298, 2004.

[14] L. Ciccoli, C. De Felice, E. Paccagnini et al., "Morphological changes and oxidative damage in Rett syndrome erythrocytes," *Biochimica et Biophysica Acta (BBA) - General Subjects*, vol. 1820, no. 4, pp. 511–520, 2012.

[15] A. Cortelazzo, C. De Felice, A. Pecorelli et al., "Beta-actin deficiency with oxidative posttranslational modifications in Rett syndrome erythrocytes: insights into an altered cytoskeletal organization," *PLoS One*, vol. 9, no. 3, article e93181, 2014.

[16] L. Ciccoli, C. De Felice, E. Paccagnini et al., "Erythrocyte shape abnormalities, membrane oxidative damage, and β-actin alterations: an unrecognized triad in classical autism," *Mediators of Inflammation*, vol. 2013, Article ID 432616, 11 pages, 2013.

[17] Y. J. Loke, A. J. Hannan, and J. M. Craig, "The role of epigenetic change in autism spectrum disorders," *Frontiers in Neurology*, vol. 6, p. 107, 2015.

[18] A. Ghezzo, P. Visconti, P. M. Abruzzo et al., "Oxidative stress and erythrocyte membrane alterations in children with autism: correlation with clinical features," *PLoS One*, vol. 8, no. 6, article e66418, 2013.

[19] A. Anwar, P. M. Abruzzo, S. Pasha et al., "Advanced glycation endproducts, dityrosine and arginine transporter dysfunction in autism - a source of biomarkers for clinical diagnosis," *Molecular Autism*, vol. 9, no. 1, p. 3, 2018.

[20] A. Bolotta, P. Visconti, G. Fedrizzi et al., "Na^+, K^+-ATPase activity in children with autism spectrum disorder: searching for the reason(s) of its decrease in blood cells," *Autism Research*, vol. 11, no. 10, pp. 1388–1403, 2018.

[21] G. Lucantoni, D. Pietraforte, P. Matarrese et al., "The red blood cell as a biosensor for monitoring oxidative imbalance in chronic obstructive pulmonary disease: an ex vivo and in vitro study," *Antioxidants & Redox Signaling*, vol. 8, no. 7-8, pp. 1171–1182, 2006.

[22] T. J. Greenwalt, "The how and why of exocytic vesicles," *Transfusion*, vol. 46, no. 1, pp. 143–152, 2006.

[23] V. Pallotta, F. Naro, F. Gevi, A. D'Alessandro, and L. Zolla, "Supplementation of anti-oxidants in leucofiltered erythrocyte concentrates: assessment of morphological changes through scanning electron microscopy," *Blood Transfusion*, vol. 12, no. 3, pp. 421–424, 2014.

[24] I. Freikman, J. Amer, J. S. Cohen, I. Ringel, and E. Fibach, "Oxidative stress causes membrane phospholipid rearrangement and shedding from RBC membranes—an NMR study," *Biochimica et Biophysica Acta (BBA) - Biomembranes*, vol. 1778, no. 10, pp. 2388–2394, 2008.

[25] E. Ferru, K. Giger, A. Pantaleo et al., "Regulation of membrane-cytoskeletal interactions by tyrosine phosphorylation of erythrocyte band 3," *Blood*, vol. 117, no. 22, pp. 5998–6006, 2011.

[26] S. Rinalducci, G. M. D'Amici, B. Blasi, S. Vaglio, G. Grazzini, and L. Zolla, "Peroxiredoxin-2 as a candidate biomarker to test oxidative stress levels of stored red blood cells under blood bank conditions," *Transfusion*, vol. 51, no. 7, pp. 1439–1449, 2011.

[27] A. Matte, M. Bertoldi, N. Mohandas et al., "Membrane association of peroxiredoxin-2 in red cells is mediated by the N-terminal cytoplasmic domain of band 3," *Free Radical Biology & Medicine*, vol. 55, pp. 27–35, 2013.

[28] W. H. Dzik, "The air we breathe: three vital respiratory gases and the red blood cell: oxygen, nitric oxide, and carbon dioxide," *Transfusion*, vol. 51, no. 4, pp. 676–685, 2011.

[29] S. J. Glatt, M. T. Tsuang, M. Winn et al., "Blood-based gene expression signatures of infants and toddlers with autism," *Journal of the American Academy of Child & Adolescent Psychiatry*, vol. 51, no. 9, pp. 934–944.e2, 2012.

[30] G. Giacometti, C. Ferreri, A. Sansone et al., "High predictive values of RBC membrane-based diagnostics by biophotonics in an integrated approach for autism spectrum disorders," *Scientific Reports*, vol. 7, no. 1, p. 9854, 2017.

[31] S. Gunes, O. Ekinci, and T. Celik, "Iron deficiency parameters in autism spectrum disorder: clinical correlates and associated factors," *Italian Journal of Pediatrics*, vol. 43, no. 1, p. 86, 2017.

[32] M. Battistelli, R. De Sanctis, R. De Bellis, L. Cucchiarini, M. Dachà, and P. Gobbi, "Rhodiola rosea as antioxidant in red blood cells: ultrastructural and hemolytic behaviour," *European Journal of Histochemistry*, vol. 49, no. 3, pp. 243–254, 2005.

[33] S. Salucci, S. Burattini, F. Buontempo, A. M. Martelli, E. Falcieri, and M. Battistelli, "Protective effect of different antioxidant agents in UVB-irradiated keratinocytes," *European Journal of Histochemistry*, vol. 61, no. 3, p. 2784, 2017.

[34] R. F. Robledo, S. L. Ciciotte, B. Gwynn et al., "Targeted deletion of α-adducin results in absent β- and γ-adducin, compensated hemolytic anemia, and lethal hydrocephalus in mice," *Blood*, vol. 112, no. 10, pp. 4298–4307, 2008.

[35] F. A. Kuypers, R. A. Lewis, M. Hua et al., "Detection of altered membrane phospholipid asymmetry in subpopulations of human red blood cells using fluorescently labeled annexin V," *Blood*, vol. 87, no. 3, pp. 1179–1187, 1996.

[36] L. O. Simpson, "Red cell shape in different anticoagulants," *British Journal of Haematology*, vol. 79, no. 1, pp. 136-137, 1991.

[37] J. G. Mohanty, H. D. Shukla, J. D. Williamson, L. J. Launer, S. Saxena, and J. M. Rifkind, "Alterations in the red blood cell membrane proteome in Alzheimer's subjects reflect disease-related changes and provide insight into altered cell morphology," *Proteome Science*, vol. 8, no. 1, p. 11, 2010.

[38] Y. S. Mahindrakar, A. N. Suryakar, R. D. Ankush, R. V. Katkam, and K. M. Kumbhar, "Comparison between erythrocyte hemoglobin and spectrin glycosylation and role of oxidative stress in type-2 diabetes mellitus," *Indian Journal of Clinical Biochemistry*, vol. 22, no. 1, pp. 91–94, 2007.

[39] S. Manno, N. Mohandas, and Y. Takakuwa, "ATP-dependent mechanism protects spectrin against glycation in human erythrocytes," *The Journal of Biological Chemistry*, vol. 285, no. 44, pp. 33923–33929, 2010.

Hindawi
Oxidative Medicine and Cellular Longevity
Volume 2018, Article ID 8087598, 15 pages
https://doi.org/10.1155/2018/8087598

Review Article

The Possible Pathophysiological Outcomes and Mechanisms of Tourniquet-Induced Ischemia-Reperfusion Injury during Total Knee Arthroplasty

Prangmalee Leurcharusmee,[1,2,3] Passakorn Sawaddiruk,[1,2,3] Yodying Punjasawadwong,[2] Nipon Chattipakorn,[1,3] and Siriporn C. Chattipakorn[1,3,4]

[1]*Neurophysiology Unit, Cardiac Electrophysiology Research and Training Center, Faculty of Medicine, Chiang Mai University, Chiang Mai, Thailand*
[2]*Department of Anesthesiology, Faculty of Medicine, Chiang Mai University, Chiang Mai, Thailand*
[3]*Center of Excellence in Cardiac Electrophysiology Research, Chiang Mai University, Chiang Mai, Thailand*
[4]*Department of Oral Biology and Diagnostic Sciences, Faculty of Dentistry, Chiang Mai University, Chiang Mai, Thailand*

Correspondence should be addressed to Siriporn C. Chattipakorn; scchattipakorn@gmail.com

Received 15 August 2018; Accepted 4 October 2018; Published 5 November 2018

Guest Editor: Luciano Saso

Ischemia and reperfusion (I/R) injury induced by tourniquet (TQ) application leads to the release of both oxygen free radicals and inflammatory cytokines. The skeletal muscle I/R may contribute to local skeletal muscle and remote organ damage affecting outcomes after total knee arthroplasty (TKA). The aim of the study is to summarize the current findings associated with I/R injury following TKA using a thigh TQ, which include cellular alterations and protective therapeutic interventions. The PubMed database was searched using the keywords "ischemia reperfusion injury," "oxidative stress," "tourniquet," and "knee arthroplasty." The search was limited to research articles published in the English language. Twenty-eight clinical studies were included in this qualitative review. Skeletal muscle I/R reduces protein synthesis, increases protein degradation, and upregulates genes in cell stress pathways. The I/R of the lower extremity elevates local and systemic oxidative stress as well as inflammatory reactions and impairs renal function. Propofol reduces oxidative injury in this I/R model. Ischemic preconditioning (IPC) and vitamin C may prevent oxygen free radical production. However, a high dose of *N*-acetylcysteine possibly induces kidney injury. In summary, TQ-related I/R during TKA leads to muscle protein metabolism alteration, endothelial dysfunction, oxidative stress, inflammatory response, and renal function disturbance. Propofol, IPC, and vitamin C show protective effects on oxidative and inflammatory markers. However, a relationship between biochemical parameters and postoperative clinical outcomes has not been validated.

1. Introduction

Total knee arthroplasty (TKA) is a surgical treatment aiming at improving the mobility and quality of life of patients suffering from advanced knee osteoarthritis. The prevalence of this procedure has substantially increased in the past decade and is expected to continue [1, 2]. A hallmark of the clinical success of TKA is postoperative quadriceps muscle function. Muscle atrophy following a use of intraoperative thigh tourniquet (TQ) results in early postoperative deficits in quadriceps strength and subsequently impaired TKA rehabilitation. The majority of TKA patients are in the elderly population [1] whose TQ-induced muscle loss is likely permanent and may increase risk for falls as well as loss of independence [3].

A TQ is routinely used in extremity surgery to produce a bloodless surgical field. However, TQ application alters normal physiology and is associated with several complications [4]. Locally, a circumferential inflatable cuff compresses the structures beneath the cuff and

can possibly cause mechanical and ischemic injuries to localized muscles and nerves. Skeletal muscles distal to the TQ are also affected at a molecular level by prolonged inadequate blood flow and subsequent restoration of circulation. Systemically, limb exsanguination followed by TQ inflation transiently increases central blood volume and systemic vascular resistance, induces a hypercoagulable state, and activates fibrinolytic activity. Clinically, the use of a TQ is considered a risk factor for thromboembolism [5]. However, the incidence of deep vein thrombosis and pulmonary thromboembolism after TKA was found to be similar regardless of the use of the TQ [6].

TQ inflation induces ischemia to an extremity, and its release may lead to an ischemia and reperfusion (I/R) injury to not only localized skeletal muscle but also systemic circulation and vital distant organs including the brain, heart, lungs, and kidneys. The restoration of blood flow following an ischemic period is essential to preventing irreversible cellular injury; however, the reperfusion can augment secondary damage to ischemia. During oxygen deprivation, intracellular ionic and metabolic changes including ATP depletion, intracellular acidosis, and cytosolic calcium overload occur and cause damage to cells [7]. In addition, ischemia can exacerbate reactive oxygen species (ROS) production and promote a proinflammatory state, which subsequently increases tissue vulnerability to further injury during reperfusion. Upon the reintroduction of oxygen, excessive production of ROS disproportionate to the antioxidant capacity results in cell injury through the oxidation of proteins, lipids, and DNA.

Several treatment strategies have been proposed to prevent or attenuate the effects of I/R injury following TQ use in cases of orthopedic surgery [8]. Studies into the use of ischemic preconditioning (IPC) and antioxidants have generated inconclusive results depending on the administration techniques. Of the anesthetic agents, propofol is the best medication producing both antioxidative and anti-inflammatory effects. However, the correlation between the benefits of these interventional and pharmacologic strategies with the postoperative clinical outcomes has not been drawn.

Therefore, the aim of this review is to summarize current findings relating to the effects of TQ-induced I/R injury on localized skeletal muscles, local and systemic circulation, and remote organs in TKA surgery and therapeutic interventions in clinical study. Furthermore, the controversial reports regarding these issues are included and discussed.

2. Effects of TQ-Induced I/R Injury on Localized Skeletal Muscles

TQ application during TKA has been shown to produce I/R injury in human skeletal muscle by triggering cascades of cellular events resulting in a reduction in protein synthesis [9], an increase in protein degradation [10, 11], and an upregulation of the genes in cell stress pathways [12]. Alterations in the protein metabolism as a result of I/R injury lead to the mobilization of free amino acids [11] which subsequently contribute to quadriceps muscle atrophy [3]. Cap-dependent translation initiation and elongation in the protein synthesis pathway were inhibited during ischemia and in early reperfusion phases causing downregulation of protein synthesis and a 12% loss of mid-thigh quadriceps volume as measured by magnetic resonance imaging (MRI) at two weeks after surgery [9]. The ubiquitin (Ub) proteasome system, the main pathway of skeletal muscle proteolysis, was upregulated at 60 minutes of ischemia suggesting an increase in muscle protein breakdown [10]. Regarding the analysis of gene expression profiles following TKA, 72 genes in skeletal muscle cells were significantly upregulated at two hours after TQ release [12]. The genes related to the cell stress pathways were altered and potentially induced apoptosis, cell cycle regulation, and complement activation.

Other mechanisms of skeletal muscle I/R injury have been investigated [13, 14]. Many studies [15–17] have reported that endothelial dysfunction resulting from an imbalance of vasoactive substances, including endothelin 1 (ET-1), as well as neuronal and endothelial nitric oxide synthases (nNOS and eNOS) plays a role in the pathophysiology of several ischemic conditions. Concordantly, ET-1, nNOS, and eNOS are involved in skeletal muscle I/R. The rise in ET-1 tissue protein levels occurred during the periods of I/R and was attributed to an increase in the release of stored peptides or the conversion of precursor peptides to ET-1 [13]. Furthermore, the upregulation of NOSs occurred in postischemic skeletal muscle. The increased protein expression of nNOS was controlled at the mRNA level, whereas the upregulation of the eNOS protein was regulated by posttranscriptional processes [14]. All these findings suggest that agents modulating the ET-1 and NO pathways such as an ET antagonist may have therapeutic benefits in this condition.

The cellular bioenergetics and mitochondria are preserved during skeletal muscle I/R in the TKA setting [11, 18, 19]. For example, (1) adenosine triphosphate (ATP) concentrations and mitochondrial enzymes were maintained during 60–90 minutes of ischemic time and at 24 hours after reperfusion [11, 18], despite significant metabolic changes which suggested ischemic injury to the skeletal muscle cell at approximately 75 minutes of ischemia [20], and (2) a previous human study [19] showed mitochondria to have normal appearance when viewed under an electron microscope after 15 minutes of ischemia. However, in cases of myocardial I/R condition, mitochondrial respiratory chain activity was reduced after 30 minutes of ischemia and restored upon reperfusion as a biphasic process [21, 22]. All those findings suggest that alterations in mitochondrial function induced by I/R injury are tissue-specific and the severity of the cellular damage depends on the duration of ischemia. However, the actual period of total ischemia which results in mitochondrial damage and the reversal time of mitochondrial dysfunction have not yet been validated. Therefore, the ischemic time inducing skeletal muscle mitochondrial impairment should be further defined and therapeutic strategies to address the prevention and modulation of mitochondrial injury should

be studied. A comprehensive summary of those findings is shown in Table 1.

3. Effects of TQ-Induced I/R Injury on Local and Systemic Circulation

TQ use can lead to a production of oxygen free radicals and stimulation of inflammatory processes in the ischemic skeletal muscle cells and endothelium. Upon TQ release, activated endothelial cells generate more oxygen free radicals and release inflammatory mediators [23]. The elevated oxidative stress levels and the inflammatory reaction in both the local and systemic circulation after TQ deflation were demonstrated in the TKA-related I/R models [24–26]. Interestingly, the changes were observed earlier and more intensely in the blood from the reperfused area than from the systemic circulation. The rise in systemic prooxidant and hypoxanthine levels as well as in xanthine oxidase activity is probably explained by a dispersal of these molecules from the injured area into the systemic circulation because hypoxanthine accumulates in hypoxic conditions [25]. On the other hand, the circulatory increase in pro- and anti-inflammatory cytokines can be explained by systemically induced stress responses secondary to tissue trauma. The number and type of lymphocytes can be used to monitor the systemic effect of the stress response, and the application of a TQ has been shown to induce genotoxic and cytotoxic effects on peripheral leukocytes during the reperfusion period with possible irreversible damage [27]. Despite these acknowledged deleterious effects of use of a TQ, the surgical trauma per se generates surgical stress which is characterized by neuroendocrine, immunological, and hematological changes. When compared to the procedure without TQ application, the increase in plasma interleukin-6 (IL-6), C-reactive protein (CRP), creatine phosphokinase (CPK) and white blood cell counts at 24 hours and seven days after surgery were not different and improvement of knee function at one year after operation was comparable [28]. It is possible that these long-term systemic responses originated from the surgical injury. Further studies focusing on differentiation between responses from surgical stress and those from I/R injury in this setting should be investigated. A comprehensive summary of those findings is shown in Table 2.

4. Effects of TQ-Induced I/R Injury on Remote Organs

The I/R of the lower extremity affects not only the local structures but also distant organs. The remote response to I/R is associated with microvascular dysfunction [23]. Activated endothelial cells produce excessive ROS at the initiation of reperfusion and lead to an imbalance between superoxide and nitric oxide in all segments of the microcirculation, which subsequently induce a systemic inflammatory response and cause multiple organ damage. A previous study [29] reported hepatic and renal dysfunction as well as pulmonary damage in animals subjected to three hours of bilateral hind limb ischemia, followed by three hours of reperfusion. In relation to TQ-induced I/R in the clinical setting, remote kidney damage was suggested by the elevation of two sensitive indicators of proximal tubular function [30]. However, no significant myocardial, cerebral, or lung injury was demonstrated after unilateral TKA surgery [31–33]. It is likely that the severity of distant organ injury is related to the degree of local tissue injury and systemic inflammatory activation. This supposition is supported by higher postoperative complications affecting multiple organ systems among bilateral TKA patients compared to those undergoing a unilateral TKA [34]. A comprehensive summary of these findings is shown in Table 3.

5. Effects of Ischemic Conditioning on TQ-Induced I/R Injury in TKA

Ischemic preconditioning (IPC) is an exposure of tissues to one or more brief periods of I/R which generates small amounts of free radicals resulting in an adaptive response to subsequent prolonged ischemic stress and reperfusion injury [35]. The IPC results in protection, consisting of two phases, an early phase and a late phase [23, 36]. The early phase affects ion channel permeability, posttranslational modification of proteins, and release of autocoids such as adenosine, bradykinin, and nitric oxide. The later phase is dependent on the gene expression and de novo protein synthesis involved in endothelial function, an inflammatory response, and hemostasis. During the conditioning, the released autocoids bind to G-protein-coupled receptors (GPCRs) which subsequently activate growth factor receptors (GFRs) and in addition stimulate intracellular kinase pathways. These processes result in an increase in antiapoptotic proteins, inhibition of proapoptotic proteins, translocation of transcription factors, opening of ATP-sensitive potassium channels (K_{ATP}), and inhibition of the mitochondrial permeability transition pores (mPTPs). The IPC of the lower extremity in unilateral TKA patients showed protective genomic responses, which resulted in an upregulated expression of immediate early response genes, oxidative stress defense genes and prosurvival genes, and regulation of neuron apoptosis [37, 38]. However, the systemic inflammatory signals were not suppressed by IPC performed with one to three cycles of five-minute ischemia and five-minute reperfusion [33, 37, 39]. A comprehensive summary of these findings is shown in Table 4.

Remote ischemic preconditioning (rIPC) is the conditioning applied to distant tissues or organs in order to render tissues with a subsequent sustained ischemic episode resistant to I/R injury. The potential mechanisms of rIPC consist of two components which are humoral and neural [40, 41]. The two hypotheses involve production of endogenous substrates, such as adenosine, bradykinin, and calcitonin gene-related peptides (CGRP) in the remote ischemic tissues. These endogenous mediators enter the bloodstream and initiate protective effects *via* their respective receptors in other tissues. In a different way, these substrates stimulate afferent nerve fibers and transmit protection to distant organs through efferent nerve fibers.

Table 1: Effects of TQ-induced I/R injury on localized skeletal muscles.

Study model/specimen/ sample size/age	TQ pressure/ ischemia time	Major findings (compared to baseline level)			Interpretation	References
		Clinical outcome	Mechanism			
			Ischemia phase	Reperfusion phase		
Cross-sectional study/vastus lateralis muscle biopsy/n = 13 /62–76 yr	≥300 mmHg, 32–52 min	↓ 12% of quadriceps muscle volume at 2 weeks after surgery	↔ eIF4G gene expression ↓ phosphorylation of Akt at Ser^{473} and 4E-BP1 ↑ phosphorylation of eEF2	↑ eIF4G gene expression ↓ phosphorylation of Akt at Ser^{473} and 4E-BP1 ↑ phosphorylation of eEF2	Cap-dependent translation initiation and elongation may be inhibited during skeletal muscle I/R	[9]
Randomized controlled trial/ vastus medialis muscle biopsy/n = 34/55–85 yr	380 mmHg, 60 min	N/A	↔ free, conjugated Ub ↔ total Ub-protein ligase activity ↑ proteasome-dependent and -independent peptidase activities	N/A	Upregulated proteasome-dependent and -independent peptidase activities suggested an increase in protein degradation at 60-minute ischemia time	[10]
Randomized controlled trial/ vastus lateralis muscle biopsy/ n = 15/63–76 yr	Double SBP mmHg, 56–92 min	N/A	↑ all muscle-free amino acids, except glutamate ↔ mitochondrial enzymes	↓ all muscle-free amino acids ↔ mitochondrial enzymes	Degradation of free amino acids was more than synthesis during skeletal muscle ischemia No mitochondrial dysfunction occurred at maximum ischemia and at 24 hours after reperfusion	[11]
Cross-sectional study/vastus lateralis muscle biopsy/n = 13 /60–78 yr	≥300 mmHg, 33–50 min	N/A	N/A	Upregulation of 72 genes including JAK-STAT, p53, JNK, NFκB, Akt, and MAPK	Genes related to cell stress pathways involved in reperfusion injury	[12]
Cross-sectional study/ quadriceps muscle biopsy, venous blood/n = 13/64–89 yr	300 mmHg	N/A	↑ positive ET-1-immunostaining cells ↔ ET-1 mRNA expression ↔ plasma ET-1	↑ positive ET-1-immunostaining cells ↔ ET-1 mRNA expression ↔ plasma ET-1	ET-1 is involved in skeletal muscle I/R	[13]
Cross-sectional study/ quadriceps muscle biopsy/n = 12 /64–89 yr	300 mmHg	N/A	↔ nNOS, iNOS, and eNOS immunostaining in muscle fibers ↑ nNOS mRNA expression	↑ nNOS and eNOS immunostaining in muscle fibers ↑ nNOS mRNA expression	nNOS and eNOS were upregulated in postischemic muscle, but their activities were not altered	[14]

Table 1: Continued.

Study model/specimen/ sample size/age	TQ pressure/ ischemia time	Major findings (compared to baseline level)			Interpretation	References
		Clinical outcome	Mechanism			
			Ischemia phase	Reperfusion phase		
			↔ nNOS and eNOS protein expression ↔ NOS activity	↑ nNOS and eNOS protein expression ↔ NOS activity		
Randomized controlled trial/ interstitial space fluid at gastrocnemius muscle/$n = 31/68 \pm 8$ yr	250 mmHg, 74 ± 4 min	N/A	↓ glucose ↓ pyruvate ↑ lactate ↑ L/P ratio ↑ glycerol	↓ glucose ↑ pyruvate ↑ lactate ↔ L/P ratio ↑ glycerol	Changes in the level of metabolic markers in the extracellular space suggested ischemic injury and persisted for up to 180 minutes after reperfusion	[20]
Randomized controlled trial/ vastus medialis muscle biopsy/$n = 10/74 \pm 3$ yr	380 mmHg, 60 min	N/A	↔ mitochondrial enzymes	N/A	No effects on amount and function of mitochondria at 60-minute ischemia time	[18]

4E-BP1: eukaryotic initiation factor 4E-binding protein; eEF2: eukaryotic elongation factor 2; eIF4G: eukaryotic translation initiation factor 4 gamma; ET-1: endothelin 1; I/R: ischemia and reperfusion; JAK-STAT: Janus kinase/signal transducer and activator of transcription; JNK: c-Jun N-terminal kinase; L/P: lactate/pyruvate; MAPK: mitogen-activated protein kinase; mRNA: messenger ribonucleic acid; N/A: not available; NFκB: nuclear factor kappa-light-chain-enhancer of activated B cells; NOS: nitric oxide synthase; SBP: systolic blood pressure; TQ: tourniquet; Ub: ubiquitin.

Table 2: Effects of TQ-induced I/R injury on local and systemic circulation.

Study model/specimen/ sample size/age	TQ pressure/ischemia time	Main findings (compared to baseline level)			Interpretation	References
		Clinical outcome	Mechanism			
			Local circulation	Systemic circulation		
Randomized controlled trial/antecubital venous blood/n = 15/blood from surgical drain/n = 17 /approx. 70 ± 7 yr	250 mmHg, approx. 90 ± 15 min	N/A	Surgical drainage tube ↓↓ GSH ↑↑ GSSG ↑↑ MDA	Antecubital vein ↓ GSH ↑ GSSG ↑ MDA	Changes in glutathione oxidation and lipid peroxidation happened earlier and more intensely in the blood from the reperfused area than from the systemic circulation	[24]
Cross-sectional study/ antecubital and femoral venous blood/n = 10/69 ± 2 yr	Double SBP mmHg, 85 ± 8 min	N/A	Femoral vein of operated leg ↑↑ hypoxanthine, XO activity, and xanthine ↑ GSSG/GSH	Antecubital vein ↑ hypoxanthine, XO activity, and xanthine ↔ GSSG/GSH	Higher increase in prooxidants and oxidative stress in the blood from the reperfused area compared to the systemic circulation	[25]
Cross-sectional study/great saphenous venous blood of both legs, blood from surgical drain/ n = 9/57–71 yr	250–300 mmHg, 78–125 min	N/A	Surgical drainage tube ↑↑ IL-6 ↑ IL-10	Great saphenous vein of nonoperated leg ↑ IL-6 ↔ IL-10	Higher increase in pro- and anti-inflammatory cytokines in the blood from the reperfused area compared to the systemic circulation	[26]
Cross-sectional study/ peripheral blood lymphocytes/ n = 11/60–75 yr	100–120 min	N/A	N/A	↑ genotoxicity index ↑ cytotoxicity index ↔ cytostaticity index	Genotoxic and cytotoxic effects on peripheral lymphocytes were most pronounced at onset of reperfusion and remained so 1 hour afterward	[27]
Case-control study/ venous blood/n = 20 /74 ± 7 yr	250–300 mmHg, 80 ± 20 min	↑ knee function scores No surgical site infection at 1 yr	N/A	↑ IL-6, CPR, CPK, and white cell count	Oxidative stress after TKA surgery primarily originated from surgical stress only	[28]

CPK: creatine phosphokinase; CRP: c-reactive protein; GSH: reduced glutathione; GSSG: oxidized glutathione; IL: interleukin; I/R: ischemia and reperfusion; MDA: malondialdehyde; N/A: not available; SBP: systolic blood pressure; TKA: total knee arthroplasty; TQ: tourniquet; XO: xanthine oxidase.

Table 3: Effects of TQ-induced I/R injury on remote organs.

Sample size/age	TQ pressure/ischemia time	Main findings (compared to baseline level)		Interpretation	References
		Outcomes on remote organ	Systemic effects		
$n = 16/70 \pm 4$ yr	91 ± 11 min, N/A	Heart: ↔ CPK-MB ↔ Troponin I	↑ serum MDA	No cardiac muscle injury after TKA with TQ	[31]
$n = 36/71 \pm 7$ yr	N/A	Brain: ↔ $rScO_2$ No POCD at 1 week Lungs: ↔ PF ratio Kidney: ↔ serum Cr	↑ plasma lactate ↑ serum CPK ↔ serum LDH, AST ↔ serum IL-6, TNF-α, IL-10 ↓ serum TNF-β	No adverse effects on regional cerebral oxygenation, pulmonary oxygenation, and renal function after TKA with TQ	[32]
$n = 17/67 \pm 10$ yr	250 mmHg, 52 ± 11 min	Lungs: ↔ urine desmosine /Cr ratio	↑ serum IL-6, TNF-α, CRP, and WBC count	No lung injury occurred as indicated by the unaltered marker of elastin breakdown after TKA with TQ	[33]
$n = 15/64$–73 yr	300–350 mmHg, 83–121 min	Kidney: ↑ urine α-1-microglobulin/Cr ratio ↑ urine GST-α/Cr ratio ↔ urine NAG/Cr ratio ↓ serum cystatin C ↓ serum Cr and urea	↑ plasma lactate ↑ serum myoglobin ↑ serum lactoferrin	Possible proximal tubular injury after TKA with TQ	[30]

AST: aspartate aminotransferase; CPK: creatinine phosphokinase; CRP: c-reactive protein; Cr: creatinine; GST-α: glutathione-S-transferase-α; IL: interleukin; LDH: lactate dehydrogenase; MDA: malondialdehyde; N/A: not available; NAG: *N*-acetyl-β-D-glucosaminidase; PF ratio: ratio of arterial oxygen partial pressure to fractional inspired oxygen; POCD: postoperative cognitive dysfunction; $rScO_2$: regional cerebral oxygen saturation; TKA: total knee arthroplasty; TNF: tumor necrosis factor; TQ: tourniquet; WBC: white blood cell.

Thus, an intact neural pathway is required for the complete signaling of remote preconditioning. The skeletal muscle ischemia resulting from use of a TQ on a nonoperated thigh has been investigated in the TKA setting. This rIPC with three cycles of five-minute ischemia improved regional cerebral and pulmonary oxygenation during the early reperfusion period in the patients undergoing unilateral TKA under general anesthesia [32]. However, in cases of bilateral TKA, application of a thigh TQ in the first-operated knee may prevent I/R injury from occurring during the subsequent ischemic surgical procedure on the other knee [31, 42, 43]. Nonetheless, the conditioning stimulus of rIPC in these previous studies was unclear. The ischemic times of the preconditioning, of approximately 60–90 minutes, were longer than a typical ischemic stimulus of IPC. It is uncertain whether a longer conditioning time is more effective than a conventional time [44]. It is noteworthy that the anesthesia technique should be focused because spinal anesthesia can block neural impulses at spinal nerve roots and may interfere with the neural pathway of rIPC. A comprehensive summary of these findings is shown in Table 4.

6. Effects of Anesthetic Agents on TQ-Induced I/R Injury in TKA

Anesthetic intervention to reduce TQ-related I/R injury in cases of orthopedic surgery has been systematically reviewed [8]. Anesthetic agents with proven antioxidative effects include propofol, dexmedetomidine, and ketamine. Intravenous propofol (2,6-diisopropylphenol) is a common choice as an anesthetic agent for sedation and maintenance of anesthesia. Its antioxidative properties arise from its chemical structure which is similar to the endogenous antioxidant α-tocopherol and phenol-based free radical scavengers [45]. The cardioprotective effect of propofol in cases of cardiac I/R is dose-dependent and mediated by the activation of mitochondrial respiratory chain complexes [46, 47]. However, in skeletal muscle I/R, the small or sedation dose of propofol (2 mg/kg/h)

Table 4: Effects of ischemic preconditioning (IPC) and remote IPC (rIPC) on TQ-induced I/R injury in TKA.

Study model/specimen/ TQ pressure	IPC protocol/TQ ischemia time/sample size/age Intervention	Control	Main findings (compared to control) Clinical outcome	Mechanism	Interpretation	References
RCT/antecubital venous blood, quadriceps muscle biopsy, SBP + 100 mmHg	3 cycles of 5 min ischemia and 5 min reperfusion at operated thigh, 68–87 min, $n = 10$	no IPC, 68–87 min, $n = 10$	N/A	↑ gene expression (i) immediate early response genes (ii) oxidative stress defense genes (iii) mitochondrial genes (iv) prosurvival genes ↓ gene expression (i) proapoptotic genes ↔ serum IL-6, CRP, ESR, and WBC count	IPC induced a protective genomic response IPC did not prevent systemic inflammatory response	[37]
Case-control study/ quadriceps muscle biopsy	N/A, $n = 4$	No IPC, $n = 4$	N/A	Altered expression of genes involved in neurological system process and regulation of neuron apoptosis	IPC induced a protective genomic response	[38]
RCT/venous blood, urine/ 250 mmHg	1 cycle of 5 min ischemia and 5 min reperfusion at operated thigh, 58 ± 11 min, $n = 17$, 67 ± 11 yr	no IPC, 52 ± 11 min, $n = 17$, 67 ± 10 yr	↓ median pain scores within 48 h after surgery ↔ postoperative analgesic consumption ↓ length of hospital stay	↔ serum IL-6, TNF-α, CRP, and WBC count ↔ urine desmosine/ Cr ratio	IPC did not prevent systemic inflammatory response or the level of lung injury IPC may improve postoperative pain control	[33]
RCT/venous blood, blood from surgical drain/ 250 mmHg	1 cycle of 5 min ischemia and 5 min reperfusion at operated thigh, 48 min (IQR 13), $n = 30$, 67 yr (IQR 10.8)	no IPC, 54 min (IQR 18), $n = 30$, 72.5 yr (IQR 13)	↓ pain scores within 48 h after surgery ↔ postoperative analgesic consumption ↔ physical therapy parameters ↔ length of hospital stay	↔ intraarticular IL-6, TNF-α ↔ systemic prothrombotic levels	IPC may improve postoperative pain control Hypercoagulative state occurred after TKA surgery using TQ application	[39]
RCT/arterial blood, venous blood/double SBP mmHg	3 cycles of 5 min ischemia at nonoperated thigh, $n = 36$, 69 ± 7 yr	No IPC, $n = 36$, 71 ± 7 yr	Brain: ↑ $rScO_2$ ↔ POCD at 1 week Lungs: ↑ PF ratio	↓ serum LDH ↔ serum CPK and AST ↔ serum IL-6, TNF-α, IL-10, and TNF-β	Remote IPC improved regional cerebral and pulmonary oxygenation possibly via a decrease in tissue damage	[32]
			N/A			[42]

Table 4: Continued.

Study model/specimen/ TQ pressure	IPC protocol/TQ ischemia time/sample size/age Intervention	Control	Main findings (compared to control) Clinical outcome	Mechanism	Interpretation	References
Cross-sectional study/ venous blood/double SBP mmHg	Approx. 60 min ischemia at previously operated thigh, 62 ± 19 min, $n = 12$, 67 ± 5 yr	First-operated knee, 63 ± 14 min, $n = 12$, 67 ± 5 yr		Tend to ↓ whole blood ROS production ↔ plasma PCOOH	Remote IPC may occur during bilateral TKA with sequential application of TQ	
Cross-sectional study/ venous blood	Approx. 90 min ischemia at previously operated thigh, 89 ± 9 min, $n = 16$, 70 ± 4 yr	First-operated knee, 91 ± 11 min, $n = 16$, 70 ± 4 yr	N/A	Tend to ↓ serum MDA	Remote IPC may occur during bilateral TKA with sequential application of TQ	[31]
Cross-sectional study/ venous blood (dorsum of each foot)/double SBP mmHg	Approx. 60 min ischemia at previously operated thigh with 20 min reperfusion, 62 ± 19 min, $n = 30$, 64 ± 5 yr	First-operated knee (right), 61 ± 5 min, $n = 30$, 64 ± 5 yr	Muscle: ↔ WOMAC scores (assessment of joint pain, stiffness, and function) at 1 month	↔ serum MDA ↔ serum LDH	Sequential ischemic surgical procedure did not reduce oxidative injury after reperfusion	[43]

AST: aspartate aminotransferase; CPK: creatinine phosphokinase; CRP: c-reactive protein; Cr: creatinine; IL: interleukin; ESR: erythrocyte sedimentation rate; IPC: ischemic preconditioning; I/R: ischemia and reperfusion; IQR: interquantile range; LDH: lactate dehydrogenase; MDA: malondialdehyde; N/A: not available; PCOOH: phosphatidylcholine hydroperoxide; PF ratio: ratio of arterial oxygen partial pressure to fractional inspired oxygen; POCD: postoperative cognitive dysfunction; RCT: randomized controlled trial; ROS: reactive oxygen species; $rScO_2$: regional cerebral oxygen saturation; SBP: systolic blood pressure; TKA: total knee arthroplasty; TNF: tumor necrosis factor; TQ: tourniquet; WBC: white blood cell; WOMAC: Western Ontario and McMaster University Osteoarthritis Index.

Table 5: Effects of anesthetic agents on TQ-induced I/R injury in TKA.

Study model/specimen/TQ pressure	Anesthetic agent/dose/TQ ischemia time/sample size/age		Main findings (compared between groups)		Interpretation	References
	Intervention	Control	Clinical outcome	Mechanism		
RCT/venous blood/350 mmHg	Propofol, 2 mg/kg/h, 90 ± 7 min, $n = 18$, 66 ± 7 yr	Normal saline, 0.2 ml/kg/h, 93 ± 10 min, $n = 17$, 69 ± 10 yr	Sedation effect Propofol > control	Plasma SOD, TCA Propofol > control Serum MDA, hsCRP, and blood neutrophil count Propofol < control	Sedation dose of propofol has antioxidative and anti-inflammatory properties	[48]
RCT/arterial blood/double SBP mmHg	Propofol, 0.2 mg/kg then 2 mg/kg/h, 72 ± 18 min, $n = 11$, 67 ± 5 yr	Midazolam, 5 mg, 69 ± 14 min, $n = 11$, 63 ± 7 yr	N/A	Whole blood ROS production Propofol < midazolam	Sedation dose of propofol attenuates ROS production compared to midazolam	[49]
RCT/venous blood	Propofol, 2–2.5 mg/kg then 6–10 mg/kg/h, 79 ± 13 min, $n = 10$, 70 ± 6 yr	Sevoflurane, 1.5–2%, 83 ± 15 min, $n = 10$, 69 ± 5 yr	N/A	Serum MDA Propofol < sevoflurane	Propofol reduces oxidative injury in the TQ-induced I/R model	[51]
RCT/arterial blood, venous blood/350–400 mmHg	Propofol, 2 mg/kg then 4–8 mg/kg/h, 114 ± 19 min, $n = 15$, 69 ± 6 yr	Halothane, 0.7–1%, 116 ± 25 min, $n = 15$, 66 ± 5 yr	MAP, pH, PaO_2, $PaCO_2$ Propofol ↔ halothane	Serum MDA Propofol < halothane	Propofol reduces oxidative injury in the TQ-induced I/R model	[52]

hsCRP: high-sensitivity C-reactive protein; I/R: ischemia and reperfusion; MAP: mean arterial pressure; MDA: malondialdehyde; N/A: not available; $PaCO_2$: arterial carbon dioxide partial pressure; PaO_2: arterial oxygen tension; RCT: randomized controlled trial; ROS: reactive oxygen species; SBP: systolic blood pressure; SOD: superoxide dismutase; TAC: total antioxidative capacity; TQ: tourniquet.

Table 6: Effects of pharmacological intervention on TQ-induced I/R injury in TKA.

Study model/specimen/ TQ pressure	Drug/dose/TQ ischemia time/sample size/age Intervention	Control	Main findings (compared between groups)	Interpretation	References
RCT/venous blood	Vitamin C, 0.03 g/kg during ischemia then 0.01 g/kg after reperfusion, 91 ± 11 min, $n = 16$, 71 ± 4 yr	Normal saline, 91 ± 14 min, $n = 16$, 70 ± 4 yr	Serum MDA Serum troponin I Vitamin C group < control	High-dose vitamin C prevents oxygen free radical production and may have myocardial protection properties	[31]
RCT/vastus lateralis muscle biopsy/double SBP mmHg	Mannitol, 930 mosmol/kg, 12.5 mL/kg/day, 75–93 min, $n = 8$, 64–74 yr	5% glucose, 18.75 mL/kg/day, 50–88 min, $n = 7$, 62–79 yr	Muscle GSH, tGSH Muscle amino acid Mannitol group ↔ control	No positive effects of mannitol in this TQ-induced I/R model	[11]
RCT/venous blood, quadriceps femoris muscle biopsy/ 300 mmHg	iNO, 80 ppm entire operation, 101 ± 20 min, $n = 15$, 63 ± 14 yr Partial iNO, 80 ppm during operation except ischemia period, 103 ± 19 min, $n = 15$, 65 ± 9 yr	Nitrogen, 95 ± 19 min, $n = 15$, 64 ± 9 yr	Plasma ICAM, VCAM Plasma P-selectin, E-selectin $CD68^+$ macrophage expression Expression of ICAM, VCAM, P-selectin iNO, partial iNO groups ↔ control	No beneficial effects of iNO in this TQ-induced I/R model	[55]
RCT/antecubital venous blood/ 200 mmHg	Lower O_2 tension, $FiO_2 = 0.4$, 61–110 min, $n = 19$, 66–77 yr	Higher O_2 tension, $FiO_2 = 0.5$, 86–107 min, $n = 20$, 62–74 yr	Plasma isofurans Lower FiO_2 < higher FiO_2	Elevated O_2 tension during general anesthesia reflects increased oxidative stress	[53]
RCT/venous blood, urine/ 300–350 mmHg	NAC, 150 mg/kg before ischemia then 6.25 mg/kg/h during ischemia, 77–113 min, $n = 15$, 62–77 yr	5% glucose, 83–121 min, $n = 15$, 64–73 yr	Urine α-1-microglobulin/Cr ratio Urine NAG/Cr ratio Urine myoglobin NAC group > control	High-dose NAC may aggravate proximal tubular injury	[30]

Cr: creatinine; FiO_2: fraction of inspired oxygen; GSH: reduced glutathione; ICAM: intercellular adhesion molecule; iNO: inhaled nitric oxide; I/R: ischemia and reperfusion; MDA: malondialdehyde; NAC: *N*-acetylcysteine; NAG: *N*-acetyl-β-D-glucosaminidase; RCT: randomized controlled trial; tGSH: total glutathione; TQ: tourniquet; VCAM: vascular adhesion molecule.

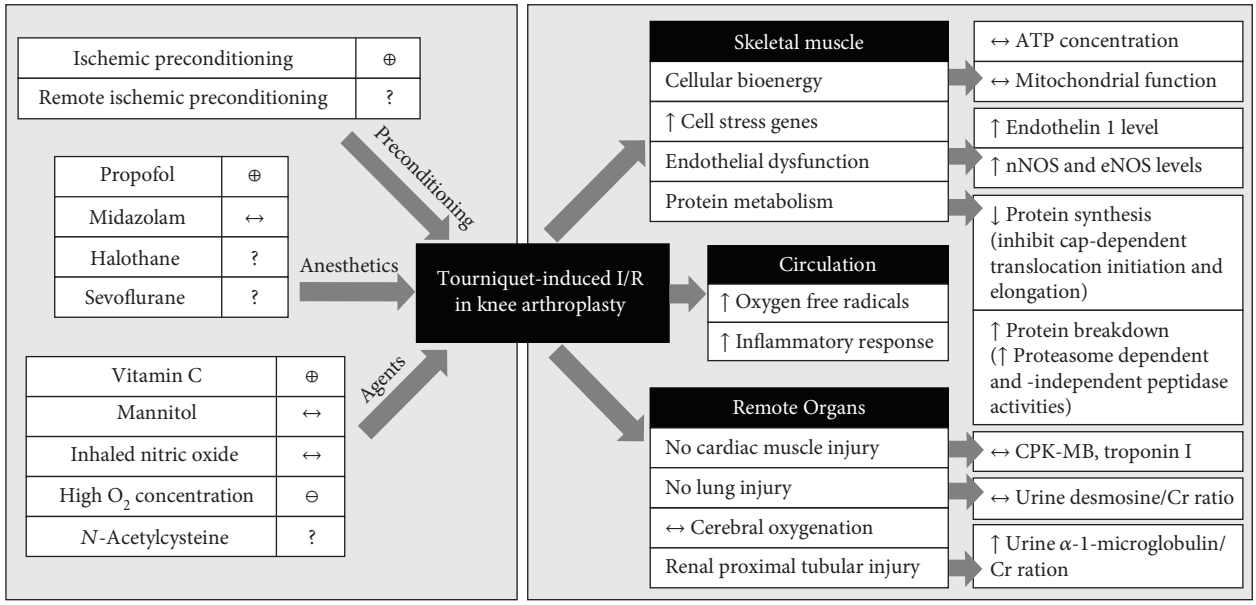

Figure 1: Effects of tourniquet- (TQ-) induced I/R injury on localized skeletal muscle, circulation, and remote organs and the effects of therapeutic interventions on the skeletal muscle I/R in cases of surgery for knee arthroplasty (TKA). The skeletal muscle I/R condition results in (1) preserved cellular bioenergy and mitochondrial function, (2) upregulation of genes related to cell stress pathways, (3) endothelial dysfunction as indicated by an increase in endothelin 1 and NOS levels, (4) alteration in protein metabolism, (4) increased oxidative stress and inflammatory responses, and (5) injury to distant organs including the kidney. Ischemic preconditioning (IPC), propofol, and vitamin C demonstrated positive or protective effects in the cases of I/R injury in this setting, while elevated O_2 tension aggravated the injury and *N*-acetylcysteine may have dose-dependent responses. Other interventions including remote ischemic preconditioning (rIPC), volatile anesthetic agents, mannitol, and nitric oxide possibly produce positive outcomes, and additional studies in this I/R condition should be investigated. ⊕: positive effect; ⊖: negative effect; ?: inadequate evidence; ↑: increase; ↓: decrease; ↔: no change; ATP: adenosine triphosphate; CPK-MB: creatinine phosphokinase-MB; Cr: creatinine; eNOS: endothelial nitric oxide synthase; nNOS: neuronal nitric oxide synthase; O_2: oxygen.

infused throughout the operation demonstrated antioxidant and anti-inflammatory properties [48, 49]. Sevoflurane and other halogenated volatile anesthetics have shown protective effects on the myocardium after cardiac I/R [50]. However, the antioxidative effect of sevoflurane and halothane were less than intravenous propofol in this skeletal muscle I/R setting [51, 52]. Therefore, a reasoned anesthetic technique for TKA with TQ is a combined spinal anesthesia with small-dose propofol infusion [48, 49, 51–53]. A role of peripheral nerve blockade for post-TKA pain control has received increasing attention, but its effects on oxidative stress and inflammatory responses have not been investigated. A comprehensive summary of these findings is shown in Table 5.

7. Effects of Pharmacological Intervention on TQ-Induced I/R Injury in TKA

ROS from the TQ-related I/R can be modulated by antioxidants. The antioxidants may reduce the cellular level of oxygen free radicals either by inhibiting ROS production, enhancing antioxidant enzymes, or reacting with the free radical intermediates in chain reactions [54]. Besides the antioxidants, interventions preventing mitochondrial dysfunction and local and systemic inflammation processes possibly play an important role in skeletal muscle I/R protection.

Previous studies [11, 30, 31, 53, 55] concerning the preventive effects of vitamin C, mannitol, *N*-acetylcysteine (NAC), inhaled nitric oxide (iNO) and a low concentration of oxygen on I/R injury following TKA have been investigated. Vitamin E and vitamin C are natural nonenzymatic antioxidants that effectively scavenge lipid peroxyl radicals and terminate the lipid peroxidase chain reaction [56]. Administrated intravenously for ten minutes before TQ deflation and 20 minutes after reperfusion, high-dose vitamin C significantly reduced serum malondialdehyde (MDA) levels, a toxic metabolite of lipid peroxidation. Furthermore, vitamin C showed protective effects on the myocardium by significantly reducing troponin I levels at eight hours after the operation compared to the level observed in the controls [31]. Mannitol, a scavenger of hydroxyl free radicals, did not decrease the effects of reperfusion injury on skeletal muscle [11] although a dose-dependent attenuation of oxidative stress induced lung injury following liver I/R has been reported [57]. The exogenous administration of NO lessened the reperfusion inflammatory response in knee surgery patients having general anesthesia [58]. However, with the spinal anesthesia technique, neither local nor systemic signs of endothelial cell activation or inflammatory response were detected at two hours after TQ release. Therefore, the presence of intraoperative iNO did not have a positive effect in this setting [55]. A lower oxygen tension during spinal anesthesia may be an explanation

because the formation of isofurans, a free radical mediated peroxidation of arachidonic acid, increased concomitantly with elevated O_2 concentrations occurring during general anesthesia [53]. Regarding NAC, it is a direct precursor to glutathione (GSH) which directly scavenges ROS and indirectly supports GSH peroxidase [59]. The beneficial effect of NAC on TQ-related I/R injury has been reported [60, 61]. However, a high dose of NAC significantly increased urine markers indicating renal tubular damage [30]. Therefore, techniques of administration including optimal dose, route, and timing of pharmacological interventions should be carefully validated in the skeletal muscle I/R model. A comprehensive summary of these findings is shown in Table 6.

8. Conclusions

Use of a TQ during TKA resulted in skeletal muscle I/R injury to localized skeletal muscle, systemic circulation, and distant organs. In the skeletal muscle, changes in protein metabolism suggest inhibition of protein synthesis and enhancement of protein breakdown. During I/R, genes related to the cell stress pathways are upregulated in skeletal muscle cells without evidence of mitochondrial dysfunction. In terms of circulation, oxidative injuries and inflammatory responses are more intense in the reperfused area than in the systemic circulation. As regards remote organs, no significant myocardial, cerebral, or lung injuries were reported but the renal proximal tubular function was impaired.

Several studies investigated the protective effects of IPC, anesthetic agents, and other pharmacological interventions. Sedative doses of propofol have antioxidative and anti-inflammatory properties. However, biochemical outcomes of the use of IPC and other medication to prevent I/R damage were diversified depending on the technique of administration. The optimal technique of therapeutic interventions and the biochemical results thereof should be further verified and correlated to clinical outcomes after TKA.

The effects of TQ-induced I/R injury on localized skeletal muscle, circulation, and remote organs and the effects of therapeutic interventions on the skeletal muscle I/R in TKA are summarized in Figure 1.

Conflicts of Interest

All authors declare no conflict of interest.

Acknowledgments

This work was supported by the Thailand Research Fund (TRF) Senior Research scholar (SCC) (RTA 6080003), a NSTDA Research Chair Grant from the National Science and Technology Development Agency Thailand (NC), and a Chiang Mai University Center of Excellence Award (NC). The authors would like to thank Ms. Dalila Monica Moisescu for her editorial assistance.

References

[1] H. Maradit Kremers, D. R. Larson, C. S. Crowson et al., "Prevalence of total hip and knee replacement in the United States," *The Journal of Bone and Joint Surgery. American Volume*, vol. 97, no. 17, pp. 1386–1397, 2015.

[2] S. M. Kurtz, K. L. Ong, E. Lau et al., "International survey of primary and revision total knee replacement," *International Orthopaedics*, vol. 35, no. 12, pp. 1783–1789, 2011.

[3] H. C. Dreyer, "Tourniquet use during knee replacement surgery may contribute to muscle atrophy in older adults," *Exercise and Sport Sciences Reviews*, vol. 44, no. 2, pp. 61–70, 2016.

[4] K. Kumar, C. Railton, and Q. Tawfic, "Tourniquet application during anesthesia: "what we need to know?"," *Journal of Anaesthesiology Clinical Pharmacology*, vol. 32, no. 4, pp. 424–430, 2016.

[5] T. O. Smith and C. B. Hing, "Is a tourniquet beneficial in total knee replacement surgery? A meta-analysis and systematic review," *Knee*, vol. 17, no. 2, pp. 141–147, 2010.

[6] I. Alcelik, R. D. Pollock, M. Sukeik, J. Bettany-Saltikov, P. M. Armstrong, and P. Fismer, "A comparison of outcomes with and without a tourniquet in total knee arthroplasty: a systematic review and meta-analysis of randomized controlled trials," *The Journal of Arthroplasty*, vol. 27, no. 3, pp. 331–340, 2012.

[7] S. Paradis, A. L. Charles, A. Meyer et al., "Chronology of mitochondrial and cellular events during skeletal muscle ischemia-reperfusion," *American Journal of Physiology. Cell Physiology*, vol. 310, no. 11, pp. C968–C982, 2016.

[8] N. L. Halladin, F. V. Zahle, J. Rosenberg, and I. Gogenur, "Interventions to reduce tourniquet-related ischaemic damage in orthopaedic surgery: a qualitative systematic review of randomised trials," *Anaesthesia*, vol. 69, no. 9, pp. 1033–1050, 2014.

[9] S. M. Ratchford, A. N. Bailey, H. A. Senesac et al., "Proteins regulating cap-dependent translation are downregulated during total knee arthroplasty," *American Journal of Physiology. Regulatory, Integrative and Comparative Physiology*, vol. 302, no. 6, pp. R702–R711, 2012.

[10] A. Jawhar, S. Hermanns, N. Ponelies, U. Obertacke, and H. Roehl, "Tourniquet-induced ischaemia during total knee arthroplasty results in higher proteolytic activities within vastus medialis cells: a randomized clinical trial," *Knee Surgery, Sports Traumatology, Arthroscopy*, vol. 24, no. 10, pp. 3313–3321, 2016.

[11] B. Westman, L. Weidenhielm, O. Rooyackers, K. Fredriksson, J. Wernerman, and F. Hammarqvist, "Knee replacement surgery as a human clinical model of the effects of ischaemia/reperfusion upon skeletal muscle," *Clinical Science*, vol. 113, no. 7, pp. 313–318, 2007.

[12] J. B. Muyskens, A. D. Hocker, D. W. Turnbull et al., "Transcriptional profiling and muscle cross-section analysis reveal signs of ischemia reperfusion injury following total knee arthroplasty with tourniquet," *Physiological Reports*, vol. 4, no. 1, article e12671, 2016.

[13] J. C. S. Tsui, D. M. Baker, E. Biecker, S. Shaw, and M. R. Dashwood, "Altered endothelin-1 levels in acute lower limb ischemia and reperfusion," *Angiology*, vol. 55, no. 5, pp. 533–539, 2016.

[14] J. C. S. Tsui, D. M. Baker, S. G. Shaw, and M. R. Dashwood, "Alterations in nitric oxide synthase isoforms in acute lower

limb ischemia and reperfusion," *Angiology*, vol. 58, no. 5, pp. 586–592, 2007.

[15] Q. Yang, G. W. He, M. J. Underwood, and C. M. Yu, "Cellular and molecular mechanisms of endothelial ischemia/reperfusion injury: perspectives and implications for postischemic myocardial protection," *American Journal of Translational Research*, vol. 8, no. 2, pp. 765–777, 2016.

[16] N. Abu-Saleh, E. Ovcharenko, H. Awad et al., "Involvement of the endothelin and nitric oxide systems in the pathogenesis of renal ischemic damage in an experimental diabetic model," *Life Sciences*, vol. 91, no. 13-14, pp. 669–675, 2012.

[17] J. A. Madden, "Role of the vascular endothelium and plaque in acute ischemic stroke," *Neurology*, vol. 79, 13, Supplement 1, pp. S58–S62, 2012.

[18] A. Jawhar, N. Ponelies, and L. Schild, "Effect of limited ischemia time on the amount and function of mitochondria within human skeletal muscle cells," *European Journal of Trauma and Emergency Surgery*, vol. 42, no. 6, pp. 767–773, 2016.

[19] H.-J. Appell, S. Glöser, J. A. R. Duarte, A. Zellner, and J. M. C. Soares, "Skeletal muscle damage during tourniquet-induced ischaemia. The initial step towards atrophy after orthopaedic surgery?," *European Journal of Applied Physiology and Occupational Physiology*, vol. 67, no. 4, pp. 342–347, 1993.

[20] A. Ejaz, A. C. Laursen, A. Kappel, T. Jakobsen, P. T. Nielsen, and S. Rasmussen, "Tourniquet induced ischemia and changes in metabolism during TKA: a randomized study using microdialysis," *BMC Musculoskeletal Disorders*, vol. 16, no. 1, article 326, 2015.

[21] H. L. Lee, C. L. Chen, S. T. Yeh, J. L. Zweier, and Y. R. Chen, "Biphasic modulation of the mitochondrial electron transport chain in myocardial ischemia and reperfusion," *American Journal of Physiology. Heart and Circulatory Physiology*, vol. 302, no. 7, pp. H1410–H1422, 2012.

[22] G. Paradies, G. Petrosillo, M. Pistolese, N. Di Venosa, A. Federici, and F. M. Ruggiero, "Decrease in mitochondrial complex I activity in ischemic/reperfused rat heart: involvement of reactive oxygen species and cardiolipin," *Circulation Research*, vol. 94, no. 1, pp. 53–59, 2004.

[23] D. L. Carden and D. N. Granger, "Pathophysiology of ischaemia-reperfusion injury," *The Journal of Pathology*, vol. 190, no. 3, pp. 255–266, 2000.

[24] J. Garcia-de-la-Asuncion, A. Perez-Solaz, M. Carrau, F. J. Belda, J. Perez-Griera, and B. Garriges, "Different oxidative stress marker levels in blood from the operated knee or the antecubital vein in patients undergoing knee surgery: a tourniquet-induced ischemia-reperfusion model," *Redox Report*, vol. 17, no. 5, pp. 194–199, 2013.

[25] E. Karg, I. Nemeth, G. Virag, T. Meszaros, D. Boda, and S. Pinter, "Oxidative stress induced by bloodless limb surgery on humans," *European Journal of Clinical Investigation*, vol. 27, no. 12, pp. 984–991, 1997.

[26] T. Clementsen and O. Reikeras, "Cytokine patterns after tourniquet-induced skeletal muscle ischaemia reperfusion in total knee replacement," *Scandinavian Journal of Clinical and Laboratory Investigation*, vol. 68, no. 2, pp. 154–159, 2009.

[27] T. Lialiaris, A. Kouskoukis, E. Tiaka et al., "Cytogenetic damage after ischemia and reperfusion," *Genetic Testing and Molecular Biomarkers*, vol. 14, no. 4, pp. 471–475, 2010.

[28] K. Tsunoda, M. Sonohata, H. Kugisaki et al., "The effect of air tourniquet on interleukin-6 levels in total knee arthroplasty," *The Open Orthopaedics Journal*, vol. 11, no. 1, pp. 20–28, 2017.

[29] M. M. Yassin, D. W. Harkin, B. D'Sa AA, M. I. Halliday, and B. J. Rowlands, "Lower limb ischemia-reperfusion injury triggers a systemic inflammatory response and multiple organ dysfunction," *World Journal of Surgery*, vol. 26, no. 1, pp. 115–121, 2002.

[30] M. Laisalmi-Kokki, E. Pesonen, H. Kokki et al., "Potentially detrimental effects of N-acetylcysteine on renal function in knee arthroplasty," *Free Radical Research*, vol. 43, no. 7, pp. 691–696, 2009.

[31] J. Y. Lee, C. J. Kim, and M. Y. Chung, "Effect of high-dose vitamin C on oxygen free radical production and myocardial enzyme after tourniquet ischaemia-reperfusion injury during bilateral total knee replacement," *The Journal of International Medical Research*, vol. 38, no. 4, pp. 1519–1529, 2010.

[32] C. S. Oh, S. H. Kim, J. Lee, and K. Y. Rhee, "Impact of remote ischaemic preconditioning on cerebral oxygenation during total knee arthroplasty," *International Journal of Medical Sciences*, vol. 14, no. 2, pp. 115–122, 2017.

[33] S. G. Memtsoudis, A. G. Della Valle, K. Jules-Elysse et al., "Perioperative inflammatory response in total knee arthroplasty patients: impact of limb preconditioning," *Regional Anesthesia and Pain Medicine*, vol. 35, no. 5, pp. 412–416, 2010.

[34] S. G. Memtsoudis, A. Gonzalez Della Valle, M. C. Besculides, L. Gaber, and T. P. Sculco, "In-hospital complications and mortality of unilateral, bilateral, and revision TKA: based on an estimate of 4,159,661 discharges," *Clinical Orthopaedics and Related Research*, vol. 466, no. 11, pp. 2617–2627, 2008.

[35] C. E. Murry, R. B. Jennings, and K. A. Reimer, "Preconditioning with ischemia: a delay of lethal cell injury in ischemic myocardium," *Circulation*, vol. 74, no. 5, pp. 1124–1136, 1986.

[36] C. K. Pac-Soo, H. Mathew, and D. Ma, "Ischaemic conditioning strategies reduce ischaemia/reperfusion-induced organ injury," *British Journal of Anaesthesia*, vol. 114, no. 2, pp. 204–216, 2015.

[37] T. Murphy, P. M. Walsh, P. P. Doran, and K. J. Mulhall, "Transcriptional responses in the adaptation to ischaemia-reperfusion injury: a study of the effect of ischaemic preconditioning in total knee arthroplasty patients," *Journal of Translational Medicine*, vol. 8, no. 1, p. 46, 2010.

[38] Y. Sha, Y. Q. Xu, W. Q. Zhao et al., "Protective effect of ischaemic preconditioning in total knee arthroplasty," *European Review for Medical and Pharmacological Sciences*, vol. 18, no. 10, pp. 1559–1566, 2014.

[39] S. G. Memtsoudis, O. Stundner, D. Yoo et al., "Does limb preconditioning reduce pain after total knee arthroplasty? A randomized, double-blind study," *Clinical Orthopaedics and Related Research*, vol. 472, no. 5, pp. 1467–1474, 2014.

[40] D. J. Hausenloy and D. M. Yellon, "Ischaemic conditioning and reperfusion injury," *Nature Reviews. Cardiology*, vol. 13, no. 4, pp. 193–209, 2016.

[41] R. Gill, R. Kuriakose, Z. M. Gertz, F. N. Salloum, L. Xi, and R. C. Kukreja, "Remote ischemic preconditioning for myocardial protection: update on mechanisms and clinical relevance," *Molecular and Cellular Biochemistry*, vol. 402, no. 1-2, pp. 41–49, 2015.

[42] Y. J. Cheng, C. T. Chien, and C. F. Chen, "Oxidative stress in bilateral total knee replacement, under ischaemic tourniquet," *Journal of Bone and Joint Surgery. British Volume*, vol. 85-B, no. 5, pp. 679–682, 2003.

[43] E. Aktas, C. Atay, M. A. Deveci, M. Arikan, G. Togral, and A. Yildirim, "Impact of oxidative stress on early postoperative knee function and muscle injury biochemical markers: is it possible to create an ischemic preconditioning effect in sequential ischemic surgical procedures?," *Acta Orthopaedica et Traumatologica Turcica*, vol. 49, no. 4, pp. 387–393, 2015.

[44] S. Koch, D. Della-Morte, K. R. Dave, R. L. Sacco, and M. A. Perez-Pinzon, "Biomarkers for ischemic preconditioning: finding the responders," *Journal of Cerebral Blood Flow and Metabolism*, vol. 34, no. 6, pp. 933–941, 2014.

[45] P. G. Murphy, D. S. Myers, M. J. Davies, N. R. Webster, and J. G. Jones, "The antioxidant potential of propofol (2,6-diisopropylphenol)," *British Journal of Anaesthesia*, vol. 68, no. 6, pp. 613–618, 1992.

[46] S. Lemoine, L. Zhu, S. Gress, J. L. Gerard, S. Allouche, and J. L. Hanouz, "Mitochondrial involvement in propofol-induced cardioprotection: an *in vitro* study in human myocardium," *Experimental Biology and Medicine*, vol. 241, no. 5, pp. 527–538, 2015.

[47] H. Shao, J. Li, Y. Zhou et al., "Dose-dependent protective effect of propofol against mitochondrial dysfunction in ischaemic/reperfused rat heart: role of cardiolipin," *British Journal of Pharmacology*, vol. 153, no. 8, pp. 1641–1649, 2008.

[48] D. Ozkan, T. Akkaya, A. Yalcindag et al., "Propofol sedation in total knee replacement: effects on oxidative stress and ischemia-reperfusion damage," *Anaesthesist*, vol. 62, no. 7, pp. 537–542, 2013.

[49] Y. J. Cheng, Y. P. Wang, C. T. Chien, and C. F. Chen, "Small-dose propofol sedation attenuates the formation of reactive oxygen species in tourniquet-induced ischemia-reperfusion injury under spinal anesthesia," *Anesthesia and Analgesia*, vol. 94, no. 6, pp. 1617–1620, 2002.

[50] B. Agarwal, D. F. Stowe, R. K. Dash, Z. J. Bosnjak, and A. K. S. Camara, "Mitochondrial targets for volatile anesthetics against cardiac ischemia-reperfusion injury," *Frontiers in Physiology*, vol. 5, article 341, 2014.

[51] H. Arnaoutoglou, G. Vretzakis, D. Souliotis, M. Cambili, D. Galaris, and G. Papadopoulos, "The effects of propofol or sevoflurane on free radical production after tourniquet induced ischaemia-reperfusion injury during knee arthroplasty," *Acta Anaesthesiologica Belgica*, vol. 58, no. 1, pp. 3–6, 2007.

[52] O. Aldemir, H. Celebi, C. Cevik, and E. Duzgun, "The effects of propofol or halothane on free radical production after tourniquet induced ischaemia-reperfusion injury during knee arthroplasty," *Acta Anaesthesiologica Scandinavica*, vol. 45, no. 10, pp. 1221–1225, 2001.

[53] E. Mas, A. E. Barden, T. B. Corcoran, M. Phillips, L. J. Roberts II, and T. A. Mori, "Effects of spinal or general anesthesia on F_2-isoprostanes and isofurans during ischemia/reperfusion of the leg in patients undergoing knee replacement surgery," *Free Radical Biology & Medicine*, vol. 50, no. 9, pp. 1171–1176, 2011.

[54] J. M. Lu, P. H. Lin, Q. Yao, and C. Chen, "Chemical and molecular mechanisms of antioxidants: experimental approaches and model systems," *Journal of Cellular and Molecular Medicine*, vol. 14, no. 4, pp. 840–860, 2010.

[55] L. Hallstrom, C. Frostell, A. Herrlin, E. Lindroos, I. Lundberg, and A. Soop, "No signs of inflammation during knee surgery with ischemia: a study involving inhaled nitric oxide," *Mediators of Inflammation*, vol. 2014, Article ID 620281, 8 pages, 2014.

[56] S. B. Nimse and D. Pal, "Free radicals, natural antioxidants, and their reaction mechanisms," *RSC Advances*, vol. 5, no. 35, pp. 27986–28006, 2015.

[57] A. A. Weinbroum, I. Shapira, R. B. Abraham, and A. Szold, "Mannitol dose-dependently attenuates lung reperfusion injury following liver ischemia reperfusion: a dose-response study in an isolated perfused double-organ model," *Lung*, vol. 180, no. 6, pp. 327–338, 2002.

[58] M. Mathru, R. Huda, D. R. Solanki, S. Hays, and J. D. Lang, "Inhaled nitric oxide attenuates reperfusion inflammatory responses in humans," *Anesthesiology*, vol. 106, no. 2, pp. 275–282, 2007.

[59] G. F. Rushworth and I. L. Megson, "Existing and potential therapeutic uses for N-acetylcysteine: the need for conversion to intracellular glutathione for antioxidant benefits," *Pharmacology & Therapeutics*, vol. 141, no. 2, pp. 150–159, 2014.

[60] F. Saricaoglu, D. Dal, A. E. Salman et al., "Effect of low-dose N-acetyl-cysteine infusion on tourniquet-induced ischaemia-reperfusion injury in arthroscopic knee surgery," *Acta Anaesthesiologica Scandinavica*, vol. 49, no. 6, pp. 847–851, 2005.

[61] M. H. Mohamed and T. Y. Hamawy, "Comparative evaluation between ascorbic acid and N-acetyl cysteine for preventing tourniquet induced ischaemic reperfusion injury during lower limb surgery, a randomized controlled trial," *Egyptian Journal of Anaesthesia*, vol. 32, no. 1, pp. 103–109, 2016.

Hindawi
Oxidative Medicine and Cellular Longevity
Volume 2018, Article ID 4081890, 13 pages
https://doi.org/10.1155/2018/4081890

Review Article

Pharmacological Regulation of Oxidative Stress in Stem Cells

Jungwoon Lee,[1] Yee Sook Cho,[1,2] Haiyoung Jung,[1,3] and Inpyo Choi[1,3]

[1]*Immunotherapy Convergence Research Center, Korea Research Institute of Bioscience and Biotechnology (KRIBB), 125 Gwahak-ro, Yuseong-gu, Daejeon 34141, Republic of Korea*
[2]*Department of Bioscience, University of Science and Technology (UST), 113 Gwahak-ro, Yuseong-gu, Daejeon 34113, Republic of Korea*
[3]*Department of Functional Genomics, University of Science and Technology (UST), 113 Gwahak-ro, Yuseong-gu, Daejeon 34113, Republic of Korea*

Correspondence should be addressed to Haiyoung Jung; haiyoung@kribb.re.kr and Inpyo Choi; ipchoi@kribb.re.kr

Received 20 July 2018; Accepted 6 September 2018; Published 30 September 2018

Guest Editor: Luciano Saso

Oxidative stress results from an imbalance between reactive oxygen species (ROS) production and antioxidant defense mechanisms. The regulation of stem cell self-renewal and differentiation is crucial for early development and tissue homeostasis. Recent reports have suggested that the balance between self-renewal and differentiation is regulated by the cellular oxidation-reduction (redox) state; therefore, the study of ROS regulation in regenerative medicine has emerged to develop protocols for regulating appropriate stem cell differentiation and maintenance for clinical applications. In this review, we introduce the defined roles of oxidative stress in pluripotent stem cells (PSCs) and hematopoietic stem cells (HSCs) and discuss the potential applications of pharmacological approaches for regulating oxidative stress in regenerative medicine.

1. Introduction

Reactive oxygen species (ROS) are originally thought to be a harmful byproduct that is produced intracellularly through aerobic metabolism in the mitochondria [1, 2]. However, recent studies have suggested that ROS regulate physiological and biological functions in cellular processes [3]. ROS are tightly regulated by antioxidant enzymes and modulators under normal physiological conditions. Excessive ROS accumulation occurs in certain conditions and thus makes detoxification beyond the capacity of the antioxidant cellular defense system difficult [4, 5]. Oxidative stress resulting from excessive ROS production and impaired antioxidant systems can affect proliferation, differentiation, genomic mutations, aging, and stem cell death [3, 6–8]. The balance between stem cell self-renewal and differentiation is critical for tissue homeostasis throughout an organism's lifespan, and recent embryonic and adult stem cell reports have shown that this balance is regulated by ROS [2]. Thus, the regulation of the redox state is important for maintaining the function of stem cells and is critical for the fate decision of stem cells (Figure 1).

In regenerative medicine, stem cells are developed to replace damaged tissues; therefore, the appropriate differentiation and maintenance of stem cells are crucial processes for clinical applications. The regulatory mechanisms of oxidative stress and the redox state should be fully defined before stem cells are used in clinical trials. To regulate oxidative stress in stem cells, many research groups have found critical signaling pathways and have suggested their own pharmacologic approaches for mediating them. Therefore, we will review the function, critical signaling pathways, and pharmacological regulation of oxidative stress in pluripotent stem cells (PSCs) and hematopoietic stem cells (HSCs).

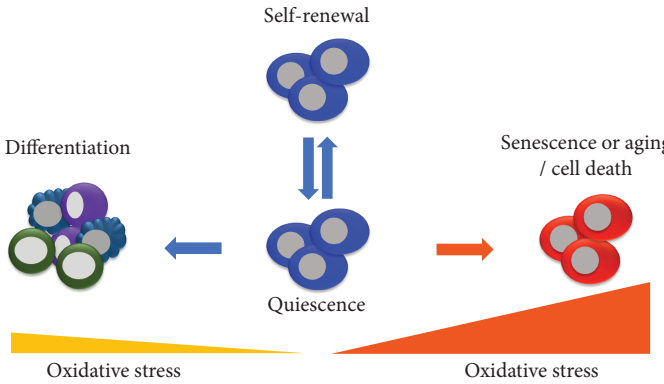

Figure 1: The impact of oxidative stress on stem cells. Quiescent and self-renewing stem cells maintain low ROS level and reside in hypoxic environment. Mild increase of ROS in stem cells causes lineage differentiation; however, acute or excessive ROS cause stem cell senescence or aging and cell death.

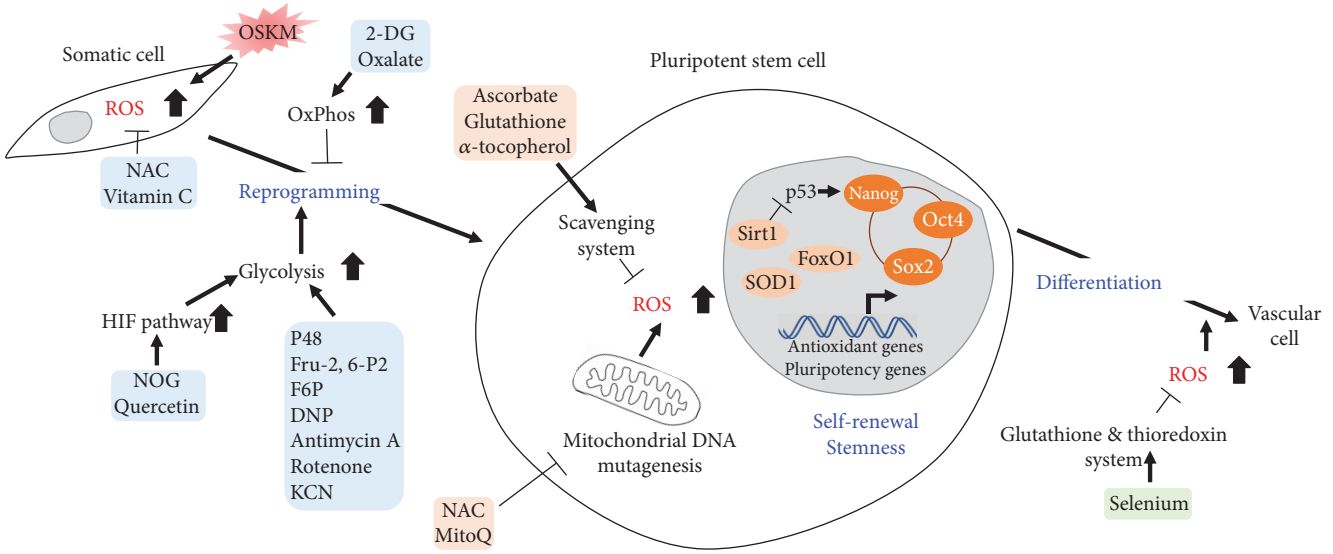

Figure 2: Pharmacological regulation of oxidative stress in PSCs. Forced transduction of OSKM reprogramming factors increases ROS levels which causes DNA damage and inhibits somatic cellular reprogramming into iPSCs. Antioxidants are able to improve reprogramming efficiency and genome stability by quenching ROS levels. During somatic cellular reprogramming, metabolic shift from OxPhos to glycolysis can be modified by different antioxidants, thereby affects the efficient iPSC generation. PSCs are highly sensitive to oxidative stress and affected by the fine control of antioxidants for the maintenance and enhancement of PSC functions as well as the differentiation toward vascular lineage. Oct4, Sox2, Klf4, and c-Myc (OSKM); N-acetyl-L-cysteine (NAC); 2-deoxyglucose (2-DG); fructose 2,6-bisphosphate (Fru-2,6-P_2); fructose 6-phosphate (F6P); 2,4-dinitrophenol (DNP); N-oxaloylglycine (NOG); mitochondria-targeted ubiquinone (MitoQ).

2. Oxidative Stress in Pluripotent Stem Cells

PSCs, including embryonic stem cells (ESCs) and induced pluripotent stem cells (iPSCs), have the unique properties of undergoing infinite self-renewal and retaining pluripotency to differentiate into every cell type in the body; thus, PSCs represent a valuable source of cells for applications in regenerative medicine [9]. The balance between stem cell self-renewal and differentiation is critical for the developmental process and tissue homeostasis [4]. Recent studies have shown that this manipulation of stem cell fate is partially regulated by ROS, which mediate the oxidation-reduction (redox) state of cells as a secondary messenger [2, 4]. Low ROS levels are necessary for the maintenance of PSCs, whereas oxidative stress due to increased ROS production and damaged ROS scavenging systems can lead to genomic instability, differentiation, death, and/or PSC aging [2]. Here, we introduce the signaling pathways, significant roles and functions of ROS, and the pharmacological regulation of oxidative stress in PSC stemness, pluripotency, and reprogramming (Figure 2).

2.1. Oxidative Stress in Stemness. At the early embryo developmental stages, ESCs reside in a hypoxic microenvironment, where the cells use glycolysis to quickly produce very low levels of ATP; however, during the differentiation process, ATP production increases via oxidative phosphorylation (OxPhos), which in turn generates ROS [10]. Thus, it is

not surprising that PSCs have the unique features of only a few mitochondria with immature morphology, low oxygen consumption, upregulated glycolytic or antioxidant enzymes, and a shortened G1 cell cycle phase [2, 5], which allow for rapid proliferation, DNA replication, and biomass reproduction compared with typically quiescent differentiated cells [11].

PSCs are sensitive to H_2O_2-induced senescence, and they enter a transient G2/M cell cycle arrest state with self-renewal capacity [12]. In addition, PSCs sustain clonal recovery, genomic integrity [13], and pluripotency [14] when cultured in hypoxic conditions. Stemness feature of PSCs is especially sensitive to subtle changes in ROS signaling, originating from mitochondrial DNA (mtDNA) mutagenesis which is associated with an increase in mitochondrial H_2O_2. Two different antioxidants, N-acetyl-L-cysteine (NAC) and mitochondria-targeted ubiquinone (MitoQ), efficiently rescue and improve PSC stemness, indicating that PSC functions are modulated by mitochondrial ROS levels [15, 16]. Interestingly, the low-dose components of an antioxidant cocktail (ascorbate, glutathione, and α-tocopherol) also affect the free-radical scavenging activity and in turn improve the quality and stability of PSCs; however, high-dose antioxidants which result in an extreme suppression of ROS level downregulate the DNA repair-related kinases and conversely cause the genomic instability of PSCs [17] (Figure 2). Therefore, PSCs are highly sensitive to oxidative stress and affected by the fine control of antioxidants.

2.2. Oxidative Stress in Pluripotency. The metabolic shifts between glycolysis and OxPhos are accompanied by the differentiation of PSCs [4]. The enhancement of glycolysis via hypoxia and the suppression of OxPhos, which lead to concomitantly decreased ROS levels, promote the maintenance and proliferation of PSCs, thereby repressing differentiation [14, 18]. Endogenous ROS levels are increased by the sirtuin 1- (SIRT1-) mediated inhibition of p53's antioxidant function. SIRT1, a longevity-promoting NAD^+-dependent class III histone deacetylase, is also involved in PSC functions by regulating the p53-dependent expression of the pluripotency marker Nanog [19]. SIRT1 is suppressed precisely during human PSC differentiation, resulting in the reactivation of developmental genes, such as the neuroretinal morphogenesis regulators DLL4, TBX3, and PAX6 [20]. Another cellular antioxidant regulator, forkhead box O 1 (FoxO1), is essential for maintaining human ESC pluripotency mediated by the direct activation of octamer-binding transcription factor 4 (Oct4) and sex-determining region Y-box 2 (Sox2), which regulate the circuit of pluripotency [21]. Similarly, superoxide dismutase 1 (Sod1) is also modulated by Oct4, Sox2, and Nanog, suggesting a core relationship between redox homeostasis and pluripotency in PSCs [22].

Conversely, the forced activation of OxPhos led to the loss of stem cell properties and increased differentiation changes. For example, uncoupling protein 2 (UCP2), which is a gatekeeper for the oxidation of carbon substrates, plays an important role in regulating PSC metabolism and differentiation [23]. To achieve differentiation into functional cardiomyocytes, PSCs must be converted to preferentially use the more efficient mitochondrial-mediated oxidative metabolism. In particular, mitochondrial-dependent energetic circuits are key regulators of cardiogenesis and heart regeneration [4, 24]. These marked metabolic differences between PSCs and cardiomyocytes facilitate the large-scale purification of cardiomyocytes from PSCs because culture with glucose-depleted medium containing abundant lactate results in only cardiomyocyte survival [25]. In addition, PSC differentiation toward vascular smooth muscle cells (VSMCs) has been shown to be dependent on the H_2O_2 signaling induced by the upregulation of NADPH oxidase 4 (Nox4), which contributes to the production of ROS [26]. The redox function of apurinic/apyrimidinic (AP) endonuclease 1/redox factor 1 (Ape/Ref1) is also critical for mouse ESC differentiation towards the hematopoietic lineage [27], and thioredoxin (Trx) is involved in the regulation of Oct4 activity [28]. Selenium, which enhances antioxidant activities of the glutathione and Trx systems, is able to reduce increased ROS production by Nox4 moderately, thereby promoting the vascular differentiation of human ESCs [29] (Figure 2). Taken together, the decision of PSC fate may be regulated directly by the cellular redox state, which is influenced by PSC metabolic shifts.

2.3. Oxidative Stress in Somatic Reprogramming. Somatic cellular reprogramming into iPSCs by the forced transduction of a combination of defined reprogramming factors, namely, Oct4, Sox2, kruppel-like factor 4 (Klf4), and c-Myc (OSKM, named as the "Yamanaka factors"), is a major technological breakthrough in stem cell biology and regenerative medicine; this breakthrough provides a way to produce patient-specific personalized PSCs [30, 31]. However, concerns remain regarding technical issues, including the low efficiency and safety of iPSC generation for their application for therapeutic use.

Similar to the early embryogenesis that occurs in hypoxic niches, hypoxic conditions, which increase glycolysis, play an important role in somatic cellular reprogramming. In this way, the efficiency of mouse and human iPSC generation is higher in hypoxic conditions (1% and 5% O_2) than in normoxic (21% O_2) conditions. Moreover, iPSC generation is achieved with only two of the four factors (Oct4 and Klf4) when cultured in hypoxic conditions [5, 32]. Hypoxia-inducible factors (HIFs) regulate not only glycolysis-related genes, such as pyruvate dehydrogenase kinase-1 (PDK1), lactate dehydrogenase (LDH), and glycogen phosphorylase liver (PYGL) [33], but also transcriptional networks that control stemness, such as Oct4, Sox2, and Nanog, which all are associated with somatic cellular reprogramming [5]. In particular, HIF-2α, but not HIF-1α, binds directly to predicted hypoxic response elements (HREs) in the proximal promoters of Oct4, Sox2, and Nanog in human PSCs under only hypoxia (5% O_2) conditions; in this way, HIF-2α helps regulate the function of PSCs [34, 35]. These findings suggest that hypoxic conditions enhance induced pluripotency, consistent with the responses observed for PSC phenotypes.

During somatic cellular reprogramming, OSKM reprogramming factor-transduced cells have substantially elevated

ROS and oxidative stress levels both *in vitro* [36, 37] and *in vivo* [38, 39]. ROS are also produced by metabolic stress and increased ROS levels then lead to cell damage, senescence, and apoptosis. The survival rate of reprogrammed cells may be decreased by increased ROS levels, as suggested by the abovementioned observations of enhanced iPSC generation under hypoxic conditions. In addition, oxidative stress suppresses the ability to generate or maintain PSCs [40, 41], suggesting that ROS production induced by the reprogramming factors is unfavorable for iPSC generation. Supplementation with antioxidants, such as N-acetylcysteine (NAC) or vitamin C (Vc), prevents this damage, and iPSC generation is enhanced with significantly fewer de novo copy number variations (CNVs) [42] (Figure 2). Paradoxically, the depletion of ROS levels by antioxidants or Nox inhibitors in early reprogramming decreases the efficiency of iPSC generation substantially. However, excessive ROS production can also impair the efficiency of iPSC generation, and antioxidant enzyme levels are elevated in late reprogramming [43]. These data indicate that optimal ROS levels are necessary to initiate and maintain the process of efficient *in vitro* somatic cell reprogramming to pluripotency.

Interestingly, OSKM induces two different cellular fates *in vivo*: reprogramming in a subset of cells and senescence in many other neighboring cells [38, 44]. Senescent cells release paracrine factors such as interleukin-6 (IL6) to surrounding cells that promote the reprogramming and dedifferentiation [38, 39]. Thus, biological conditions associated to cellular senescence such as tissue damage and aging positively contribute to a permissive microenvironment for *in vivo* reprogramming [38, 39, 44], which seems to be contradictory to *in vitro* reprogramming. IL6 has been shown to induce ROS production in cells such as neuron, monocyte, and neutrophil, inducing a prooxidant environment [45, 46]. Paradoxically, IL6 can also induce an adaptive response to oxidative stress in normal tissues of the injury models [47, 48]. Therefore, *in vivo* OSKM-induced senescence enhances cellular plasticity, which is linked to tissue regeneration and organismal rejuvenation, although further studies are needed [49, 50].

The metabolic shift from OxPhos to glycolysis is also critical for somatic cellular reprogramming. As mentioned above, reprogrammed iPSCs have an increased dependence on glycolysis under aerobic metabolism conditions, with deliberate OxPhos suppression, similar to the Warburg effect in cancer cells. Induced pluripotency and tumorigenesis are stepwise processes that share many similarities to the immortal transformation of somatic cells [51]. Indeed, the accumulation of glycolytic intermediates is essential for rapid proliferation and minimizes ROS-induced damage in both PSCs and cancer cells [52]. Significantly, the known reprogramming factors possess oncogenic potential; for example, Oct4/Sox2 are correlated to carcinomas, and Klf4/c-Myc are well-known oncogenes [53, 54]. It has also been reported that c-Myc increases glycolysis and inhibits OxPhos, and Lin28, which is also associated with tumorigenesis and reprogramming, promotes glucose metabolism [55, 56]. In addition, the inhibition of the p53 tumor suppressor gene, which increases glycolysis as mentioned above, also enhances somatic cellular reprogramming. Similarly, PS48, which is a potent activator of PDK1; fructose 2,6-bisphosphate (Fru-2,6-P_2); fructose 6-phosphate (F6P); 2,4-dinitrophenol (DNP); N-oxaloylglycine (NOG); quercetin; and mitochondrial inhibitors (e.g., antimycin A, rotenone, and KCN), which are involved in the metabolic transition from OxPhos to glycolysis, facilitate somatic cellular reprogramming [57–60], whereas small molecules, such as 2-deoxyglucose (2-DG), 3-bromopyruvic acid (BrPA), 6-aminonicotinamide (6-AN), oxalate, and dichloroacetate (DCA), which are associated with OxPhos, decrease the efficiency of iPSC generation [57, 60, 61] (Figure 2). These data suggest that a metabolic shift from oxidative catabolism to anaerobic glycolysis is crucial for efficient iPSC generation.

Human and mouse iPSCs are reprogrammed by the forced transduction of the same Yamanaka factors, but the cell status of iPSCs is distinctive between humans and mice. Human iPSCs are reprogrammed to a primed state similar to human ESCs, whereas mouse iPSCs are reprogrammed to a naïve state similar to mouse ESCs. Key differences between primed and naïve PSCs are in their derivation of germline competency, epigenetic states, expression patterns for pluripotency and lineage-specific genes, signaling requirements for self-renewal, and central carbon metabolism [52, 62]. In particular, naïve PSCs utilize OxPhos more than primed PSCs, which are dependent almost entirely on glycolysis [62, 63]. It remains unclear whether this difference is similar to *in vivo* situations in which embryos first use mitochondrial OxPhos but then switch to anaerobic glycolysis after implantation [52]. Current studies suggest that the metabolic shift in PSCs relies on the culture conditions [64] or the pluripotency factors that are involved in regulating the epigenetic machinery to modulate the naïve and primed pluripotency states [65, 66]. Thus, metabolic reprogramming to the pluripotent substates of PSCs may require a fine balance between the extrinsic environment containing nutrients and/or oxygen levels and the intrinsic needs mediated by the pluripotency factors [52]; however, the mechanism underlying PSC metabolic reprogramming remains largely unknown.

3. Oxidative Stress in HSCs

HSCs are a type of adult stem cells that undergo hematopoiesis to replenish mature blood lineages throughout an organism's lifetime [67]. For many decades, HSCs were used for treating hematological and immune diseases. However, their limited number prevents the more reliable and broader application of HSC-based therapies, and many attempts to propagate HSCs *in vitro* have failed, primarily because self-renewal and *in vivo* regenerative capacity are lost rapidly in culture [68]. Thus, genetic analyses using mutant animal model have identified essential regulators, and transcriptome, epigenome, and proteome studies have provided important insights into HSC biology [69, 70].

HSCs reside in hypoxic niches in the bone marrow (BM), and this hypoxic environment presumably ensures that HSCs are protected from much of the oxidative stress and can maintain their self-renewal ability [71–73]. HSCs need to be

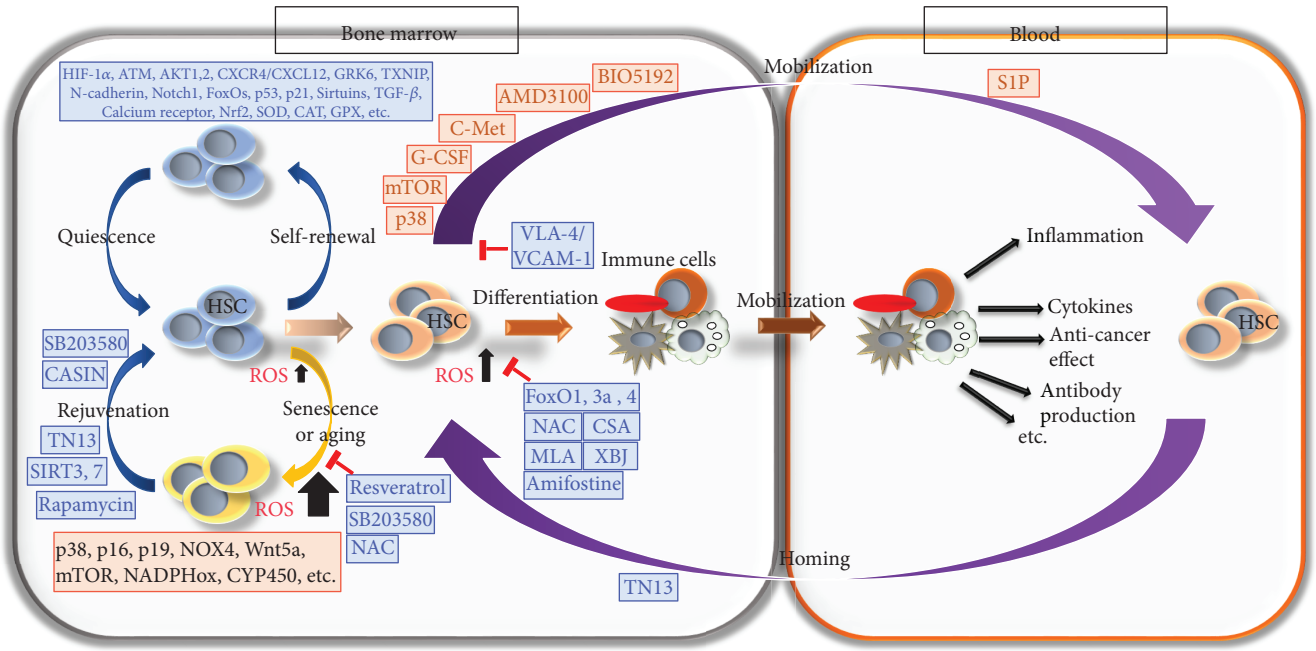

FIGURE 3: Critical regulators and pharmacological regulation of oxidative stress in HSCs. Schematic diagram illustrating the functional role of signaling proteins and pharmacological agents in the regulation of ROS in HSCs. Blue-colored proteins or agents generally reduce ROS level in HSCs or microenvironment; therefore, they help HSCs to maintain the balance between HSC self-renewal and differentiation, which is critical for tissue homeostasis. But orange-colored proteins and agents induce ROS level and result in cellular senescence or aging, differentiation, and mobilization in HSCs. Interestingly, SB203580, CASIN, TN13, and rapamycin rejuvenate aged HSCs.

protected from high ROS levels to avoid stem cell exhaustion; however, continuous low ROS production will lead to the lack of stem cell function. Ultimately, balanced ROS levels are crucial for maintaining the stem cell pool and host immunity during conditions of both homeostasis and stress [74]. Recent reports have suggested the crucial role of ROS in the regulation of differentiation, self-renewal, migration, and quiescence and proliferation balance in HSCs [74, 75]. Here, we introduce ROS as emerging regulators of HSC fate decision, motility, and aging and also describe the pharmacologic approaches in ROS regulation of HSCs (Figure 3).

3.1. Oxidative Stress in HSC Fate Decisions. Quiescent HSCs rely primarily on glycolysis for energy production, and compared with mitochondrial oxidative phosphorylation, glycolysis is much less efficient for energy production but is good for maintaining low levels of ROS in HSCs [76, 77]. Oxidative stress regulators are highly enriched in HSCs, and they activate robust oxidative stress responses to scavenge ROS [6]. Recently, many stem cell research groups have reported extensive interactions between HSCs and their niche via a variety of soluble factors, such as Wnt, BMP, TPO, IL-3, and IL-6; various adhesion molecules, including CXCL12-CXCR4 and N-cadherin; and different signaling pathways, including SCF/c-Kit, Jagged/Notch, and angiopoietin-1/Tie2 (Ang-1/Tie2); these interactions provide a special environment that supports the self-renewal and survival of HSCs and help them be quiescent [78, 79].

In the hematopoietic system, cellular ROS levels are considerably lower in HSCs than in differentiated lineage cells, and HSCs mostly remain in a quiescent state [6, 80]. Quiescent, long-term repopulating HSCs are characterized by low levels of ROS. Increased ROS levels enhance the cycling of HSCs and promote the exhaustion of the stem cell pool [81, 82]. Quiescent HSCs exhibit low metabolic rates and presumably produce less ROS, which are capable of causing oxidative damage. Hypoxia-inducible factor-1 α (HIF-1 α) is activated in HSCs and shifts cellular metabolism from mitochondrial respiration to glycolysis, thus limiting ROS production; without HIF-1 α, HSCs lose their ROS regulation ability and long-term repopulation capacity [74, 83]. The presence of the ataxia telangiectasia mutated (ATM) protein is required for HSC self-renewal and quiescence because it limits ROS levels. ATM-deficient mice showed a defect in HSC function that was associated with elevated ROS levels, and the repopulating capacity of $Atm^{-/-}$ HSCs was rescued by N-acetyl-L-cysteine (NAC) treatment [81]. $Foxo3a^{-/-}$ HSCs showed increased ROS levels and p38 MAPK activity and had defective quiescence maintenance; $Foxo3a^{-/-}$ mice were sensitive to 5-FU-induced myelotoxic injury [84].

One research group has proven the relationship between ROS and hematopoietic differentiation. The critical role of ROS in the lineage decision of myeloid progenitors was proven, and high intracellular ROS levels were observed in granulocyte-monocyte progenitor cells. The authors also showed that intracellular ROS levels in common myeloid progenitors (CMPs) were inversely correlated with their MEP differentiation potential [85]. AKT 1 and AKT 2 double-deficient long-term HSCs (LT-HSCs) showed defects in repopulation capacity and ROS regulation. Double-deficient cells were sensitive to pharmacologic increases in

ROS and showed increased differentiation capacity with BSO treatment [86]. In response to increasing levels of ROS, p38 MAPK limits the lifespan of HSCs *in vivo*, and the inhibition of p38 MAPK by SB203580 treatment rescued ROS-induced defects in the HSC repopulating capacity and HSC quiescence maintenance [82]. Disrupting the CXCR4 receptor in mice led to ROS production, p38 MAPK activation, DNA double-strand break induction, and apoptosis in HSCs. Increased ROS levels are directly responsible for the exhaustion of the HSC pool and repopulating capacity [64]. G protein-coupled receptor kinases (GRKs) are critically involved in immune responses through regulating cytokine receptors in mature leukocytes. $GRK6^{-/-}$ mice exhibit lymphocytopenia, HSC loss, and multiple progenitor populations, thus leading to compromised lymphoid differentiation largely due to impaired HSC self-renewal. GRK6 is involved in ROS signaling, and ROS scavenger α-lipoic acid treatment partially rescued HSC loss [87]. Granulocyte colony-stimulating factor (G-CSF) is used to treat leukopenia induced by radiotherapy or chemotherapy in patients and can cause sustained low white blood cell counts in PB. This adverse effect is caused by G-CSF-induced HSC proliferation and differentiation, which impair HSC self-renewal and may exhaust the BM's capacity to exacerbate IR-induced LT-BM injury. Increased HSC damage was associated with increased ROS production, p38 MAPK activation, and senescence induction in HSCs [88].

Many of radioprotective drugs have been developed to protect hematopoietic injury from irradiation stress. Melatonin (N-acetyl-5-methoxytryptamine, MLT) and α-lipoic acid (LA) conjugated 5-methoxytryptamine-α-lipoic acid (MLA) decreased the levels of ROS in hematopoietic cells by inhibiting NOX4 expression under total body irradiation condition. MLA remarkably prevents radiation-induced hematopoietic syndrome [89]. Amifostine is a ROS scavenger and radioprotective drug that has been approved by the US Food and Drug Administration (FDA) and protects primitive hematopoietic progenitors against chemotherapy cytotoxicity [90, 91]. Xuebijing injection (XBJ) was a traditional Chinese medicine and also protected hematopoietic injury by decreasing ROS production via increasing glutathione (GSH) and superoxide dismutase (SOD) levels in serum [92].

Exposure to air during collection limited the yield of HSCs from BM and cord blood (CB). HSCs lost their long-term repopulating capacity, and progenitor cells were increased in BM and CB cells under nonphysiologic ambient air. To limit ROS production and HSC differentiation, they collected and handled HSCs under hypoxia (3% O_2) condition and compared to air-harvested HSCs. Up to 5-fold greater number of HSCs were recovered by hypoxic harvest than air harvest. This phenomenon was mediated by ROS production linked to cyclophilin D (CypD), p53, and the mitochondrial permeability transition pore (MPTP). Interestingly, inhibition of CypD using cyclosporine A (CSA), a small molecule inhibitor of CypD, antagonized MPTP induction, reduced ROS, and enhanced the yield of HSCs and the efficacy of their transplantation [93].

Recently, many reports have suggested that the function of neighboring cells was crucial for ROS regulation of HSCs in BM niches. In particular, endothelial cells (ECs) are components of blood vessels and regulate trafficking and maintenance of HSCs in BM. One group has reported that arterial blood vessels were less permeable and maintained HSCs in a low ROS state, whereas the more permeable sinusoids promoted hematopoietic stem and progenitor cell (HSPC) activation and were used for leukocyte trafficking site. Increased permeability of blood vessels could increase ROS levels, migration, and differentiation of HSPCs by penetrating plasma, carrying ROS-inducing factors [94]. Most HSCs are present in perivascular locations in close contact with either sinusoids or arterioles [95]. Arterial ECs in the BM (aBMECs) created an endosteal vascular niche for nonactive quiescent HSCs, while sinusoidal ECs (sBMECs) constitute a leukocyte trafficking site or HSPC activation site. aBMECs showed lower ROS levels and higher glucose uptake and have different anatomical structure and metabolic signature as compared to sBMECs [94, 96]. ECs are exposed to oxygen in the blood and have developed to scavenge excessive ROS and rely mainly on glycolysis to avoid ROS production via oxidative phosphorylation [94, 97, 98]. Glycolysis in ECs may enable them to regulate ROS levels in cells and their surroundings and contribute to serve an ideal site for HSC maintenance in BM. Another neighboring cells including megakaryocytes (MKs) and nonmyelinating Schwann cells secrete transforming growth factor β (TGF-β), which is known as a niche factor to regulate HSC dormancy in BM niche [99, 100].

Overall, the importance of ROS as a critical regulator of HSC quiescence and differentiation was revealed by *in vitro* and *in vivo* signaling pathway studies and pharmacological challenges (Figure 3).

3.2. Oxidative Stress in HSC Motility. HSCs reside in the BM and can migrate out of the BM to the peripheral blood (PB) under stress conditions as a part of the host defense and repair mechanisms [68, 74]. HSC movement from the osteoblastic niche to the vascular niche or PB is regulated by the ROS levels in HSCs. One research group divided HSCs into ROS^{low} and ROS^{high} populations and then analyzed their functional differences. The ROS^{low} population showed higher quiescence, self-renewal potential, and calcium receptor, N-cadherin, Notch1, and p21 levels and resided in the low-oxygen osteoblastic niche; however, the ROS^{high} population showed significant HSC exhaustion after serial transplantation and p38 MAPK and mammalian target of rapamycin (mTOR) activation and resided in the high-oxygenic vascular niche. Pharmacologic inhibition of the p38 and mTOR pathways by SB203580 and rapamycin restored the functions of ROS^{high} HSCs [72].

G-CSF could mobilize hematopoietic cells in large numbers from the marrow into the circulation, with increased progenitor cells of all lineages detected in the spleens of G-CSF-treated mice [101]. Animal studies indicated that hematopoietic progenitors lacking G-CSFR were mobilized with an efficiency equivalent to those expressing the receptor. However, in the mice in which all hematopoietic cells lacked G-CSFR, these cells completely failed to mobilize. The response of hematopoietic cells to G-CSF is essential

for HSC mobilization and is indirect; moreover, a specific response of individual HSCs to G-CSF is not required [101, 102]. One group has reported that G-CSF induces c-Met expression and mobilization of hematopoietic progenitor cells. G-CSF administration causes transient upregulation of stromal cell-derived factor-1 (SDF-1) and subsequently activates CXC chemokine receptor-4 (CXCR4) signaling for hepatocyte growth factor (HGF) production. HGF binds to c-Met and thus activates c-Met signaling to regulate mTOR/FOXO3a signaling pathway. Ultimately, this signaling causes ROS production and promotes hematopoietic stem and progenitor cell egress out of the BM [103].

CXCL12 is a cytokine secreted by osteoblasts, endothelial cells, and reticular mesenchymal stem and progenitor cells; in addition, CXCL12 induces active stem and progenitor cell migration and mobilization that is increased by ROS, JNK, and MMP9. However, cell surface, membrane-bound CXCL12 is essential for stem cell quiescence, retention, and self-renewal when presented by the BM stroma [104]. Elevated ROS levels promote CXCL12 secretion and then induce HSC mobilization [74]. CXCR4 is a major receptor of CXCL12 and is also regulated by oxidative stress. ROS regulate nuclear factor- (erythroid-derived 2-) related factor 2 (Nrf2) activity, and Nrf2 induces CXCR4 expression by acting directly on the CXCR4 promoter [105]. Steady-state CXCL12-CXCR4 interactions are essential for maintaining the stem cells in a quiescent nonmotile, ROS^{low} mode, suggesting that CXCL12 signaling can limit ROS levels [74]. The CXCR4 antagonist AMD3100 was first approved in 2008 by the US Food and Drug Administration (FDA) for use in combination with G-CSF to mobilize HSCs; now, AMD3100 is commonly used worldwide for this purpose. CXCR4 antagonists mobilize HSCs by blocking the retentive activity of CXCL12 [101].

Vascular cell adhesion molecule 1 (VCAM-1) binds to integrin alpha-4 (VLA-4), which is expressed by osteoblasts, and VCAM-1 binds to VLA-4 on endothelial cells. ROS are involved in modulating endothelial cell function to promote VCAM-1-dependent lymphocyte migration [106]. The VLA-4/VCAM1 adhesive interaction is disrupted during G-CSF-induced HSC mobilization [101]. A small molecule inhibitor of VLA-4 binding, BIO5192, has been developed and, as anticipated, increases the degree of mobilization induced by G-CSF in mice [107].

The bioactive lipid sphingosine 1-phosphate (S1P) is a chemo-attractant for hematopoietic cells, including HSCs, and this activity is mediated by a series of G-protein-coupled receptors, S1P1–S1P5, with S1P1 being the principal receptor on HSCs [108]. S1P is present at high concentrations in plasma and low concentrations in tissues, including the bone marrow, providing an appropriately directed gradient. Amplifying the S1P gradient between the blood and the BM provides a potential mechanism to increase HSC trafficking into the peripheral blood [101, 109]. Altogether, HSC motility is regulated by the ROS levels in HSCs or the BM microenvironment (Figure 3).

3.3. Oxidative Stress in HSC Aging. Organ aging is linked to the aging-associated decline in somatic stem cell function in various animal model systems. HSC aging is driven by intrinsic and extrinsic factors linked to the impaired self-renewal and regeneration of lineage cells. Defining the mechanisms regulating the process of aging is important for understanding aging-associated disease and promoting a longer and healthier lifespan [110–112]. Recent advances in HSC aging studies have reached a consensus in the phenotypes of aged HSCs. The number of HSCs increases in both mice and humans, and there are two- to tenfold more HSCs present in aged BM than in young BM [113, 114]. In serial transplantation assays, aged HSCs exhibit decreased repopulation capacity as a consequence of lower long-term self-renewal capacity and heightened replicative stress on cell cycling and decreased ribosomal biogenesis [115]. Additionally, aged HSCs lose their homing ability to the BM, and young and aged HSCs occupy distinct niches within the BM. Aged HSCs exhibit impaired adhesion to stromal cells and can then better mobilize into the PB [114, 116]. Myeloid genes are upregulated in aged HSCs, which is consistent with their myeloid bias [114]. Recently, numerous studies have aimed to prove the causal roles of ROS in HSC aging in various model systems. HSCs are relatively sensitive to oxidative stress because they reside in a hypoxic niche and are maintained in a quiescent state. A moderate increase in ROS levels can induce self-renewal and differentiation defects in HSCs via inducing HSC senescence, which causes premature HSC aging [117]. Therefore, the induction of HSC senescence resulting from increased ROS production has been implicated in the pathogenesis of BM suppression under various pathological conditions [79, 118].

In particular, DNA damage responses and increased ROS levels have been causatively attributed to HSC aging [110]. DNA damage constantly arises from DNA replication errors, spontaneous chemical reactions, and assaults from external or metabolism-derived agents. Endogenous sources of DNA damage include replication and recombination errors, spontaneous hydrolysis, and reactive metabolites, such as ROS, created as by-products of cellular metabolism [81, 114]. ATM is involved in a DNA damage checkpoint and regulates HSC self-renewal. ATM-deficient mice showed bone marrow failure after 24 weeks of age due to a functional decrease in HSCs resulting from increased ROS levels. The increase in ROS levels led to the activation of p38 mitogen-activated protein kinase (MAPK), which in turn caused the upregulation of the cyclin-dependent kinase (CDK) inhibitors p16Ink4a and p19Arf. NAC treatment restored the repopulation capacity of $Atm^{-/-}$ HSCs, resulting in the prevention of bone marrow failure. Inducing p16INK4a and p19Arf in response to increased ROS levels might lead to cellular senescence in $Atm^{-/-}$ HSCs. The self-renewal capacity and cellular senescence of HSCs may depend on the ATM-mediated inhibition of oxidative stress [81, 119].

Mice with conditional Foxo1, Foxo3a, and Foxo4 knockout showed myeloid lineage expansion and lymphoid developmental abnormalities, as well as a marked decrease in the lineage-negative $Sca\text{-}1^{+}$, $c\text{-}Kit^{+}$ (LSK) compartment, and defective long-term repopulating activity that correlated with increased cell cycling and apoptosis in HSCs. FoxO-deficient HSCs also showed a marked increase in ROS levels compared

with wild-type HSCs. *In vivo* treatment with NAC resulted in the reversion of the FoxO-deficient HSC phenotypes [120]. Total body irradiation (TBI) induces long-term BM suppression in part by inducing HSC senescence through NADPH oxidase 4- (NOX4-) derived ROS. Treatment with 3,5,4′-trihydroxy-trans-stilbene (resveratrol), a potent antioxidant and putative activator of SIRT1, significantly inhibited the TBI-induced increase in ROS production in HSCs and ameliorated TBI-induced long-term BM injury by inhibiting radiation-induced chronic oxidative stress and senescence in HSCs [118]. SIRT3 is a mammalian sirtuin that regulates the global acetylation of mitochondrial proteins and reduces oxidative stress. SIRT3 is highly enriched in HSCs and is suppressed in differentiated hematopoietic cells. SIRT3 is dispensable for HSC maintenance and tissue homeostasis at a young age and under homeostatic conditions, but it is essential under stress and at an old age. Upregulating SIRT3 improves the regenerative capacity of aged HSCs. It has been suggested that SIRT3 regulates mitochondrial metabolic homeostasis and reduces ROS in HSCs; additionally, aging-associated degeneration can be reversed by sirtuins [121].

Aged HSCs showed an increase in intracellular superoxide anion (1.4-fold), hydrogen peroxide (2-fold), nitric oxide (1.6-fold), and peroxynitrite/hidroxil (2.6-fold) levels compared with young cells. Mitochondria and NADPHox were the major sources of ROS production. CYP450 contributed in middle and aged mice, and only xanthine oxidase contributed in aged mice; DNA damage and apoptosis were increased in the middle (4.2- and 2-fold, respectively) and aged (6- and 4-fold, respectively) mice, and aged mice exhibited significantly shorter telomere lengths [122]. We have found that thioredoxin-interacting protein (TXNIP) regulates intracellular ROS in HSCs by regulating p53 activity via direct interaction. TXNIP-deficient old mice exhibited elevated ROS levels in HSCs and showed a reduction in the hematopoietic cell population. TXNIP-deficient mice were more sensitive to oxidative stress. TXNIP interacted with the p53 protein and induced p53 transcriptional activity to upregulate antioxidant genes. Transducing TXNIP or p53 into $Txnip^{-/-}$ bone marrow cells rescued the HSC frequency and greatly increased survival in mice following oxidative stress [123].

Recently, HSC aging studies have reported the concept of rejuvenation in animal models. One report has shown that prolonged fasting regulates IGF-1/PKA signaling and rejuvenates the aging-associated phenotypes including myeloid bias, reducing long-term repopulation capacity of aged HSCs [110, 124]. Mammalian target of rapamycin (mTOR) activity is increased in aged HSCs. To induce mTOR signaling, they deleted Tsc1, which encodes tuberous sclerosis complex (TSC) protein 1, leading to constitutive activation of mTOR in HSCs. $TSC^{-/-}$ HSCs showed higher expression of aging-associated genes including p16, p19, and p21 and the reductions in hematopoiesis and in lymphopoiesis. Inhibition of mTOR activity by rapamycin enhances the lifespan of aged mice and the repopulation capacity of aged HSCs [125]. Mohrin et al. have reported the interaction between sirtuin 7 (SIRT7) and nuclear respiratory factor 1 (NRF1). NRF1 recruited SIRT7 to the proximal promoters of genes encoding mitochondrial ribosomal proteins (mRPs) and mitochondrial translation factors (mTFs). SIRT7 repressed the expression of mRPs and mTFs. $SIRT7^{-/-}$ HSCs showed an increase in proliferation and displayed a 40% reduction in their ability to reconstitute the hematopoietic system of recipient mice and showed myeloid-biased differentiation. SIRT7 upregulation improved the regenerative capacity of aged HSCs [126]. Another groups have reported that aged HSCs showed higher expression of Wnt5a and they have showed the rejuvenation of aged HSCs by inhibiting Cdc42 activity using a specific inhibitor of Cdc42 (CASIN) [127].

Recently, we have found that TXNIP regulates the aging of HSCs by inhibiting p38 MAPK activity via direct interaction. In addition, a TXNIP-derived peptide inhibits p38 MAPK activity and rejuvenates aged HSCs by reducing ROS levels. The TXNIP/p38 MAPK axis regulated the aging of HSCs by causing a higher frequency of long-term HSCs, lineage skewing, a decrease in engraftment, an increase in ROS levels, and a loss of Cdc42 polarity. A cell-penetrating peptide- (CPP-) conjugated peptide (TN13) derived from the TXNIP-p38 interaction motif inhibited p38 activity in HSCs *in vitro* and *in vivo*, rescued homing ability, and rejuvenated aged HSCs. We have suggested that the TXNIP-p38 axis regulates HSC aging and have proven the pharmacologic potential of TN13 to rejuvenate aged HSCs [128].

From HSC aging studies, we could find that the increased ROS levels induced HSC aging; however, it could be reversible by reducing ROS using rejuvenating agents (Figure 3).

4. Conclusion

Here, we have introduced that oxidative stress plays a critical role as a regulator of stem cell fate decision and have described the defined mechanisms of oxidative stress regulation in stem cells. ROS regulate physiological and biological functions in cellular processes and are tightly regulated by antioxidant enzymes and modulators under normal physiological conditions. These reports have shown that the balance between stem cell self-renewal and differentiation is critical for tissue homeostasis throughout an organism's lifespan, and this balance is regulated by ROS in embryonic and adult stem cells. Oxidative stress is regulated by intrinsic or extrinsic pathways and regulates proliferation, differentiation, genomic mutation, aging, and apoptosis of stem cells. Interestingly, many of the dysregulated functions of stem cells under oxidative stress were reversible or rescued by targeting critical signaling pathways using pharmacological approaches or overexpression of specific genes. In this review, we have discussed the sources and regulation mechanisms of oxidative stress and have suggested the possibility or impact of pharmacological regulation of ROS in stem cells for regenerative medicine or clinical trials. However, stem cell research is faced with ethical and political controversies and limitations for human or animal model studies. Therefore, we need to develop new model systems to replace animal models or human primary cells. Recently, iPSCs and organoid-based three dimensional (3D) cell culture and ESC-derived HSCs are developed to replace animals or

primary cells. In the future, stem cell research will be replaced by these kinds of model systems.

Abbreviations

ATM: Ataxia telangiectasia mutated
CXCR4: CXC chemokine receptor-4
ESC: Embryonic stem cell
FoxO1: Forkhead box O 1
G-CSF: Granulocyte colony-stimulating factor
HGF: Hepatocyte growth factor
HIF-1α: Hypoxia-inducible factor-1α
HSC: Hematopoietic stem cell
iPSCs: Induced pluripotent stem cells
Klf4: Kruppel-like factor 4
mTOR: Mammalian target of rapamycin
NAC: N-acetyl-L-cysteine
Nox4: NADPH oxidase 4
Oct4: Octamer-binding transcription factor-4
OxPhos: Oxidative phosphorylation
PSCs: Pluripotent stem cells
ROS: Reactive oxygen species
SDF-1: Stromal cell-derived factor-1
SIRT1: Sirtuin 1
Sox2: Sex-determining region Y-box 2
TRX: Thioredoxin
UCP2: Uncoupling protein 2
VSMCs: Vascular smooth muscle cells.

Conflicts of Interest

The authors declare no potential conflicts of interest.

Acknowledgments

This work was supported in part by the National Research Council of Science & Technology (NST) grant (no. CRC-15-02-KRIBB) and the KRIBB Research Initiative Program from the Korea government (MSIP).

References

[1] S. Qi, Z. Fang, D. Wang, P. Menendez, K. Yao, and J. Ji, "Concise review: induced pluripotency by defined factors: prey of oxidative stress," *Stem Cells*, vol. 33, no. 5, pp. 1371–1376, 2015.

[2] A. Cieślar-Pobuda, J. Yue, H. C. Lee, M. Skonieczna, and Y. H. Wei, "ROS and oxidative stress in stem cells," *Oxidative Medicine and Cellular Longevity*, vol. 2017, Article ID 5047168, 2 pages, 2017.

[3] C. R. Reczek and N. S. Chandel, "ROS-dependent signal transduction," *Current Opinion in Cell Biology*, vol. 33, pp. 8–13, 2015.

[4] C. L. Bigarella, R. Liang, and S. Ghaffari, "Stem cells and the impact of ROS signaling," *Development*, vol. 141, no. 22, pp. 4206–4218, 2014.

[5] A. Mohyeldin, T. Garzón-Muvdi, and A. Quiñones-Hinojosa, "Oxygen in stem cell biology: a critical component of the stem cell niche," *Cell Stem Cell*, vol. 7, no. 2, pp. 150–161, 2010.

[6] H. Luo, H. H. Chiang, M. Louw, A. Susanto, and D. Chen, "Nutrient sensing and the oxidative stress response," *Trends in Endocrinology and Metabolism*, vol. 28, no. 6, pp. 449–460, 2017.

[7] R. S. Balaban, S. Nemoto, and T. Finkel, "Mitochondria, oxidants, and aging," *Cell*, vol. 120, no. 4, pp. 483–495, 2005.

[8] D. Hernández-García, C. D. Wood, S. Castro-Obregón, and L. Covarrubias, "Reactive oxygen species: a radical role in development?," *Free Radical Biology & Medicine*, vol. 49, no. 2, pp. 130–143, 2010.

[9] X. Fu and Y. Xu, "Self-renewal and scalability of human embryonic stem cells for human therapy," *Regenerative Medicine*, vol. 6, no. 3, pp. 327–334, 2011.

[10] Y. M. Cho, S. Kwon, Y. K. Pak et al., "Dynamic changes in mitochondrial biogenesis and antioxidant enzymes during the spontaneous differentiation of human embryonic stem cells," *Biochemical and Biophysical Research Communications*, vol. 348, no. 4, pp. 1472–1478, 2006.

[11] J. Zhang, E. Nuebel, G. Q. Daley, C. M. Koehler, and M. A. Teitell, "Metabolic regulation in pluripotent stem cells during reprogramming and self-renewal," *Cell Stem Cell*, vol. 11, no. 5, pp. 589–595, 2012.

[12] Y.-L. Guo, S. Chakraborty, S. S. Rajan, R. Wang, and F. Huang, "Effects of oxidative stress on mouse embryonic stem cell proliferation, apoptosis, senescence, and self-renewal," *Stem Cells and Development*, vol. 19, no. 9, pp. 1321–1331, 2010.

[13] N. R. Forsyth, A. Musio, P. Vezzoni, A. H. R. W. Simpson, B. S. Noble, and J. McWhir, "Physiologic oxygen enhances human embryonic stem cell clonal recovery and reduces chromosomal abnormalities," *Cloning and Stem Cells*, vol. 8, no. 1, pp. 16–23, 2006.

[14] T. Ezashi, P. Das, and R. M. Roberts, "Low O_2 tensions and the prevention of differentiation of hES cells," *Proceedings of the National Academy of Sciences of the United State of America*, vol. 102, no. 13, pp. 4783–4788, 2005.

[15] S. Shaban, M. W. A. el-Husseny, A. I. Abushouk, A. M. A. Salem, M. Mamdouh, and M. M. Abdel-Daim, "Effects of antioxidant supplements on the survival and differentiation of stem cells," *Oxidative Medicine and Cellular Longevity*, vol. 2017, Article ID 5032102, 16 pages, 2017.

[16] R. H. Hämäläinen, K. J. Ahlqvist, P. Ellonen et al., "mtDNA mutagenesis disrupts pluripotent stem cell function by altering redox signaling," *Cell Reports*, vol. 11, no. 10, pp. 1614–1624, 2015.

[17] L. Luo, M. Kawakatsu, C. W. Guo et al., "Effects of antioxidants on the quality and genomic stability of induced pluripotent stem cells," *Scientific Reports*, vol. 4, no. 1, article 3779, 2014.

[18] S. Mandal, A. G. Lindgren, A. S. Srivastava, A. T. Clark, and U. Banerjee, "Mitochondrial function controls proliferation and early differentiation potential of embryonic stem cells," *Stem Cells*, vol. 29, no. 3, pp. 486–495, 2011.

[19] M.-K. Han, E. K. Song, Y. Guo, X. Ou, C. Mantel, and H. E. Broxmeyer, "SIRT1 regulates apoptosis and *Nanog* expression in mouse embryonic stem cells by controlling p53 subcellular localization," *Cell Stem Cell*, vol. 2, no. 3, pp. 241–251, 2008.

[20] V. Calvanese, E. Lara, B. Suarez-Alvarez et al., "Sirtuin 1 regulation of developmental genes during differentiation of stem cells," *Proceedings of the National Academy of Sciences*, vol. 107, no. 31, pp. 13736–13741, 2010.

[21] X. Zhang, S. Yalcin, D. F. Lee et al., "FOXO1 is an essential regulator of pluripotency in human embryonic stem cells," *Nature Cell Biology*, vol. 13, no. 9, pp. 1092–1099, 2011.

[22] C. Solari, M. V. Petrone, C. Vazquez Echegaray et al., "Superoxide dismutase 1 expression is modulated by the core pluripotency transcription factors Oct4, Sox2 and Nanog in embryonic stem cells," *Mechanisms of Development*, 2018.

[23] J. Zhang, I. Khvorostov, J. S. Hong et al., "UCP2 regulates energy metabolism and differentiation potential of human pluripotent stem cells," *The EMBO Journal*, vol. 30, no. 24, pp. 4860–4873, 2011.

[24] S. Chung, P. P. Dzeja, R. S. Faustino, C. Perez-Terzic, A. Behfar, and A. Terzic, "Mitochondrial oxidative metabolism is required for the cardiac differentiation of stem cells," *Nature Clinical Practice Cardiovascular Medicine*, vol. 4, Supplement 1, pp. S60–S67, 2007.

[25] S. Tohyama, F. Hattori, M. Sano et al., "Distinct metabolic flow enables large-scale purification of mouse and human pluripotent stem cell-derived cardiomyocytes," *Cell Stem Cell*, vol. 12, no. 1, pp. 127–137, 2013.

[26] Q. Xiao, Z. Luo, A. E. Pepe, A. Margariti, L. Zeng, and Q. Xu, "Embryonic stem cell differentiation into smooth muscle cells is mediated by Nox4-produced H_2O_2," *American Journal of Physiology-Cell Physiology*, vol. 296, no. 4, pp. C711–C723, 2009.

[27] G.-M. Zou, M. H. Luo, A. Reed, M. R. Kelley, and M. C. Yoder, "Ape1 regulates hematopoietic differentiation of embryonic stem cells through its redox functional domain," *Blood*, vol. 109, no. 5, pp. 1917–1922, 2007.

[28] Y. Guo, L. Einhorn, M. Kelley et al., "Redox regulation of the embryonic stem cell transcription factor oct-4 by thioredoxin," *Stem Cells*, vol. 22, no. 3, pp. 259–264, 2004.

[29] S. H. Song, K. Kim, J. J. Park, K. H. Min, and W. Suh, "Reactive oxygen species regulate the quiescence of CD34-positive cells derived from human embryonic stem cells," *Cardiovascular Research*, vol. 103, no. 1, pp. 147–155, 2014.

[30] K. Takahashi and S. Yamanaka, "Induction of pluripotent stem cells from mouse embryonic and adult fibroblast cultures by defined factors," *Cell*, vol. 126, no. 4, pp. 663–676, 2006.

[31] K. Takahashi, K. Tanabe, M. Ohnuki et al., "Induction of pluripotent stem cells from adult human fibroblasts by defined factors," *Cell*, vol. 131, no. 5, pp. 861–872, 2007.

[32] Y. Yoshida, K. Takahashi, K. Okita, T. Ichisaka, and S. Yamanaka, "Hypoxia enhances the generation of induced pluripotent stem cells," *Cell Stem Cell*, vol. 5, no. 3, pp. 237–241, 2009.

[33] K. L. Eales, K. E. R. Hollinshead, and D. A. Tennant, "Hypoxia and metabolic adaptation of cancer cells," *Oncogene*, vol. 5, no. 1, article e190, 2016.

[34] K. L. Covello, J. Kehler, H. Yu et al., "HIF-2α regulates Oct-4: effects of hypoxia on stem cell function, embryonic development, and tumor growth," *Genes & Development*, vol. 20, no. 5, pp. 557–570, 2006.

[35] R. Petruzzelli, D. R. Christensen, K. L. Parry, T. Sanchez-Elsner, and F. D. Houghton, "HIF-2α regulates NANOG expression in human embryonic stem cells following hypoxia and reoxygenation through the interaction with an Oct-Sox cis regulatory element," *PLoS One*, vol. 9, no. 10, article e108309, 2014.

[36] A. Banito, S. T. Rashid, J. C. Acosta et al., "Senescence impairs successful reprogramming to pluripotent stem cells," *Genes & Development*, vol. 23, no. 18, pp. 2134–2139, 2009.

[37] M. A. Esteban, T. Wang, B. Qin et al., "Vitamin C enhances the generation of mouse and human induced pluripotent stem cells," *Cell Stem Cell*, vol. 6, no. 1, pp. 71–79, 2010.

[38] L. Mosteiro, C. Pantoja, N. Alcazar et al., "Tissue damage and senescence provide critical signals for cellular reprogramming in vivo," *Science*, vol. 354, no. 6315, article aaf4445, 2016.

[39] L. Mosteiro, C. Pantoja, A. de Martino, and M. Serrano, "Senescence promotes in vivo reprogramming through $p16^{INK4a}$ and IL-6," *Aging Cell*, vol. 17, no. 2, article e12711, 2018.

[40] N. Mah, Y. Wang, M. C. Liao et al., "Molecular insights into reprogramming-initiation events mediated by the OSKM gene regulatory network," *PLoS One*, vol. 6, no. 8, article e24351, 2011.

[41] S.-S. Chiou, S. Wang, D. C. Wu et al., "Control of oxidative stress and generation of induced pluripotent stem cell-like cells by Jun dimerization protein 2," *Cancers*, vol. 5, no. 4, pp. 959–984, 2013.

[42] J. Ji, V. Sharma, S. Qi et al., "Antioxidant supplementation reduces genomic aberrations in human induced pluripotent stem cells," *Stem Cell Reports*, vol. 2, no. 1, pp. 44–51, 2014.

[43] G. Zhou, S. Meng, Y. Li, Y. T. Ghebre, and J. P. Cooke, "Optimal ROS signaling is critical for nuclear reprogramming," *Cell Reports*, vol. 15, no. 5, pp. 919–925, 2016.

[44] A. Chiche, I. le Roux, M. von Joest et al., "Injury-induced senescence enables in vivo reprogramming in skeletal muscle," *Cell Stem Cell*, vol. 20, no. 3, pp. 407–414.e4, 2017, e4.

[45] M. M. Behrens, S. S. Ali, and L. L. Dugan, "Interleukin-6 mediates the increase in NADPH-oxidase in the ketamine model of schizophrenia," *The Journal of Neuroscience*, vol. 28, no. 51, pp. 13957–13966, 2008.

[46] A. Kharazmi, H. Nielsen, C. Rechnitzer, and K. Bendtzen, "Interleukin 6 primes human neutrophil and monocyte oxidative burst response," *Immunology Letters*, vol. 21, no. 2, pp. 177–184, 1989.

[47] N. S. Ward, A. B. Waxman, R. J. Homer et al., "Interleukin-6-induced protection in hyperoxic acute lung injury," *American Journal of Respiratory Cell and Molecular Biology*, vol. 22, no. 5, pp. 535–542, 2000.

[48] Z. Sun, A. S. Klein, S. Radaeva et al., "In vitro interleukin-6 treatment prevents mortality associated with fatty liver transplants in rats," *Gastroenterology*, vol. 125, no. 1, pp. 202–215, 2003.

[49] J. Taguchi and Y. Yamada, "*In vivo* reprogramming for tissue regeneration and organismal rejuvenation," *Current Opinion in Genetics & Development*, vol. 46, pp. 132–140, 2017.

[50] J. Taguchi and Y. Yamada, "Unveiling the role of senescence-induced cellular plasticity," *Cell Stem Cell*, vol. 20, no. 3, pp. 293-294, 2017.

[51] V. Ramos-Mejia, M. F. Fraga, and P. Menendez, "iPSCs from cancer cells: challenges and opportunities," *Trends in Molecular Medicine*, vol. 18, no. 5, pp. 245–247, 2012.

[52] N. Shyh-Chang and H.-H. Ng, "The metabolic programming of stem cells," *Genes & Development*, vol. 31, no. 4, pp. 336–346, 2017.

[53] S. Boumahdi, G. Driessens, G. Lapouge et al., "Sox2 controls tumour initiation and cancer stem-cell functions in

squamous-cell carcinoma," *Nature*, vol. 511, no. 7508, pp. 246–250, 2014.

[54] I. K. Rony, A. Baten, J. A. Bloomfield, M. E. Islam, M. M. Billah, and K. D. Islam, "Inducing pluripotency in vitro: recent advances and highlights in induced pluripotent stem cells generation and pluripotency reprogramming," *Cell Proliferation*, vol. 48, no. 2, pp. 140–156, 2015.

[55] H. Zhu, N. Shyh-Chang, A. V. Segrè et al., "The Lin28/let-7 axis regulates glucose metabolism," *Cell*, vol. 147, no. 1, pp. 81–94, 2011.

[56] N. Shyh-Chang, H. Zhu, T. Yvanka de Soysa et al., "*Lin28* enhances tissue repair by reprogramming cellular metabolism," *Cell*, vol. 155, no. 4, pp. 778–792, 2013.

[57] C. D. L. Folmes, T. J. Nelson, A. Martinez-Fernandez et al., "Somatic oxidative bioenergetics transitions into pluripotency-dependent glycolysis to facilitate nuclear reprogramming," *Cell Metabolism*, vol. 14, no. 2, pp. 264–271, 2011.

[58] S. Zhu, W. Li, H. Zhou et al., "Reprogramming of human primary somatic cells by OCT4 and chemical compounds," *Cell Stem Cell*, vol. 7, no. 6, pp. 651–655, 2010.

[59] J. Wu, A. Ocampo, and J. C. I. Belmonte, "Cellular metabolism and induced pluripotency," *Cell*, vol. 166, no. 6, pp. 1371–1385, 2016.

[60] M. Baranek, A. Belter, M. Z. Naskręt-Barciszewska, M. Stobiecki, W. T. Markiewicz, and J. Barciszewski, "Effect of small molecules on cell reprogramming," *Molecular BioSystems*, vol. 13, no. 2, pp. 277–313, 2017.

[61] C. D. Folmes, T. J. Nelson, and A. Terzic, "Energy metabolism in nuclear reprogramming," *Biomarkers in Medicine*, vol. 5, no. 6, pp. 715–729, 2011.

[62] K. C. Davidson, E. A. Mason, and M. F. Pera, "The pluripotent state in mouse and human," *Development*, vol. 142, no. 18, pp. 3090–3099, 2015.

[63] H. Sperber, J. Mathieu, Y. Wang et al., "The metabolome regulates the epigenetic landscape during naive-to-primed human embryonic stem cell transition," *Nature Cell Biology*, vol. 17, no. 12, pp. 1523–1535, 2015.

[64] H. Zhang, M. G. Badur, A. S. Divakaruni et al., "Distinct metabolic states can support self-renewal and lipogenesis in human pluripotent stem cells under different culture conditions," *Cell Reports*, vol. 16, no. 6, pp. 1536–1547, 2016.

[65] C. B. Ware, A. M. Nelson, B. Mecham et al., "Derivation of naive human embryonic stem cells," *Proceedings of the National Academy of Sciences*, vol. 111, no. 12, pp. 4484–4489, 2014.

[66] Y. Takashima, G. Guo, R. Loos et al., "Resetting transcription factor control circuitry toward ground-state pluripotency in human," *Cell*, vol. 158, no. 6, pp. 1254–1269, 2014.

[67] J. M. Harris, V. Esain, G. M. Frechette et al., "Glucose metabolism impacts the spatiotemporal onset and magnitude of HSC induction in vivo," *Blood*, vol. 121, no. 13, pp. 2483–2493, 2013.

[68] N. Vannini, M. Girotra, O. Naveiras et al., "Specification of haematopoietic stem cell fate via modulation of mitochondrial activity," *Nature Communications*, vol. 7, article 13125, 2016.

[69] B. D. Macarthur, A. Ma'ayan, and I. R. Lemischka, "Systems biology of stem cell fate and cellular reprogramming," *Nature Reviews Molecular Cell Biology*, vol. 10, no. 10, pp. 672–681, 2009.

[70] T. Suda, K. Takubo, and G. L. Semenza, "Metabolic regulation of hematopoietic stem cells in the hypoxic niche," *Cell Stem Cell*, vol. 9, no. 4, pp. 298–310, 2011.

[71] P. Chaudhari, Z. Ye, and Y. Y. Jang, "Roles of reactive oxygen species in the fate of stem cells," *Antioxidants & Redox Signaling*, vol. 20, no. 12, pp. 1881–1890, 2014.

[72] Y.-Y. Jang and S. J. Sharkis, "A low level of reactive oxygen species selects for primitive hematopoietic stem cells that may reside in the low-oxygenic niche," *Blood*, vol. 110, no. 8, pp. 3056–3063, 2007.

[73] I. G. Winkler, V. Barbier, R. Wadley, A. C. W. Zannettino, S. Williams, and J. P. Levesque, "Positioning of bone marrow hematopoietic and stromal cells relative to blood flow in vivo: serially reconstituting hematopoietic stem cells reside in distinct nonperfused niches," *Blood*, vol. 116, no. 3, pp. 375–385, 2010.

[74] A. Ludin, S. Gur-Cohen, K. Golan et al., "Reactive oxygen species regulate hematopoietic stem cell self-renewal, migration and development, as well as their bone marrow microenvironment," *Antioxidants & Redox Signaling*, vol. 21, no. 11, pp. 1605–1619, 2014.

[75] M. Vlaski-Lafarge and Z. Ivanovic, "Reliability of ROS and RNS detection in hematopoietic stem cells – potential issues with probes and target cell population," *Journal of Cell Science*, vol. 128, no. 21, pp. 3849–3860, 2015.

[76] K. Takubo, N. Goda, W. Yamada et al., "Regulation of the HIF-1α level is essential for hematopoietic stem cells," *Cell Stem Cell*, vol. 7, no. 3, pp. 391–402, 2010.

[77] K. Takubo, G. Nagamatsu, C. I. Kobayashi et al., "Regulation of glycolysis by Pdk functions as a metabolic checkpoint for cell cycle quiescence in hematopoietic stem cells," *Cell Stem Cell*, vol. 12, no. 1, pp. 49–61, 2013.

[78] D. J. Rossi, C. H. M. Jamieson, and I. L. Weissman, "Stems cells and the pathways to aging and cancer," *Cell*, vol. 132, no. 4, pp. 681–696, 2008.

[79] L. Shao, H. Li, S. K. Pazhanisamy, A. Meng, Y. Wang, and D. Zhou, "Reactive oxygen species and hematopoietic stem cell senescence," *International Journal of Hematology*, vol. 94, no. 1, pp. 24–32, 2011.

[80] C. D. L. Folmes, P. P. Dzeja, T. J. Nelson, and A. Terzic, "Metabolic plasticity in stem cell homeostasis and differentiation," *Cell Stem Cell*, vol. 11, no. 5, pp. 596–606, 2012.

[81] K. Ito, A. Hirao, F. Arai et al., "Regulation of oxidative stress by ATM is required for self-renewal of haematopoietic stem cells," *Nature*, vol. 431, no. 7011, pp. 997–1002, 2004.

[82] K. Ito, A. Hirao, F. Arai et al., "Reactive oxygen species act through p38 MAPK to limit the lifespan of hematopoietic stem cells," *Nature Medicine*, vol. 12, no. 4, pp. 446–451, 2006.

[83] W. W. Wheaton and N. S. Chandel, "Hypoxia. 2. Hypoxia regulates cellular metabolism," *American Journal of Physiology-Cell Physiology*, vol. 300, no. 3, pp. C385–C393, 2011.

[84] K. Miyamoto, K. Y. Araki, K. Naka et al., "Foxo3a is essential for maintenance of the hematopoietic stem cell pool," *Cell Stem Cell*, vol. 1, no. 1, pp. 101–112, 2007.

[85] A. Shinohara, Y. Imai, M. Nakagawa, T. Takahashi, M. Ichikawa, and M. Kurokawa, "Intracellular reactive oxygen species mark and influence the megakaryocyte-erythrocyte progenitor fate of common myeloid progenitors," *Stem Cells*, vol. 32, no. 2, pp. 548–557, 2014.

[86] M. M. Juntilla, V. D. Patil, M. Calamito, R. P. Joshi, M. J. Birnbaum, and G. A. Koretzky, "AKT1 and AKT2 maintain hematopoietic stem cell function by regulating reactive oxygen species," *Blood*, vol. 115, no. 20, pp. 4030–4038, 2010.

[87] Q. Le, W. Yao, Y. Chen et al., "GRK6 regulates ROS response and maintains hematopoietic stem cell self-renewal," *Cell Death & Disease*, vol. 7, no. 11, article e2478, 2016.

[88] C. Li, L. Lu, J. Zhang et al., "Granulocyte colony-stimulating factor exacerbates hematopoietic stem cell injury after irradiation," *Cell & Bioscience*, vol. 5, no. 1, p. 65, 2015.

[89] D. Li, Z. Tian, W. Tang et al., "The protective effects of 5-methoxytryptamine-α-lipoic acid on ionizing radiation-induced hematopoietic injury," *International Journal of Molecular Sciences*, vol. 17, no. 6, p. 935, 2016.

[90] J. Zhang, X. Xue, X. Han et al., "Hydrogen-rich water ameliorates total body irradiation-induced hematopoietic stem cell injury by reducing hydroxyl radical," *Oxidative Medicine and Cellular Longevity*, vol. 2017, Article ID 8241678, 16 pages, 2017.

[91] Z. W. Ye, J. Zhang, D. M. Townsend, and K. D. Tew, "Oxidative stress, redox regulation and diseases of cellular differentiation," *Biochimica et Biophysica Acta*, vol. 1850, no. 8, pp. 1607–1621, 2015.

[92] D. Li, L. Lu, J. Zhang et al., "Mitigating the effects of Xuebijing injection on hematopoietic cell injury induced by total body irradiation with γ rays by decreasing reactive oxygen species levels," *International Journal of Molecular Sciences*, vol. 15, no. 6, pp. 10541–10553, 2014.

[93] C. R. Mantel, H. A. O'Leary, B. R. Chitteti et al., "Enhancing hematopoietic stem cell transplantation efficacy by mitigating oxygen shock," *Cell*, vol. 161, no. 7, pp. 1553–1565, 2015.

[94] T. Itkin, S. Gur-Cohen, J. A. Spencer et al., "Distinct bone marrow blood vessels differentially regulate haematopoiesis," *Nature*, vol. 532, no. 7599, pp. 323–328, 2016.

[95] S. Kumar and H. Geiger, "HSC niche biology and HSC expansion ex vivo," *Trends in Molecular Medicine*, vol. 23, no. 9, pp. 799–819, 2017.

[96] U. Harjes, C. Verfaillie, and P. Carmeliet, "Endothelial barrier and metabolism: new kids on the block regulating bone marrow vascular niches," *Developmental Cell*, vol. 37, no. 3, pp. 210–212, 2016.

[97] K. De Bock, M. Georgiadou, S. Schoors et al., "Role of PFKFB3-driven glycolysis in vessel sprouting," *Cell*, vol. 154, no. 3, pp. 651–663, 2013.

[98] S. Vandekeere, M. Dewerchin, and P. Carmeliet, "Angiogenesis revisited: an overlooked role of endothelial cell metabolism in vessel sprouting," *Microcirculation*, vol. 22, no. 7, pp. 509–517, 2015.

[99] M. Zhao, J. M. Perry, H. Marshall et al., "Megakaryocytes maintain homeostatic quiescence and promote post-injury regeneration of hematopoietic stem cells," *Nature Medicine*, vol. 20, no. 11, pp. 1321–1326, 2014.

[100] S. Yamazaki, H. Ema, G. Karlsson et al., "Nonmyelinating Schwann cells maintain hematopoietic stem cell hibernation in the bone marrow niche," *Cell*, vol. 147, no. 5, pp. 1146–1158, 2011.

[101] L. J. Bendall and K. F. Bradstock, "G-CSF: from granulopoietic stimulant to bone marrow stem cell mobilizing agent," *Cytokine & Growth Factor Reviews*, vol. 25, no. 4, pp. 355–367, 2014.

[102] F. Liu, J. Poursine-Laurent, and D. C. Link, "Expression of the G-CSF receptor on hematopoietic progenitor cells is not required for their mobilization by G-CSF," *Blood*, vol. 95, no. 10, pp. 3025–3031, 2000.

[103] M. Tesio, K. Golan, S. Corso et al., "Enhanced c-Met activity promotes G-CSF-induced mobilization of hematopoietic progenitor cells via ROS signaling," *Blood*, vol. 117, no. 2, pp. 419–428, 2011.

[104] A. Amara, O. Lorthioir, A. Valenzuela et al., "Stromal cell-derived factor-1α associates with heparan sulfates through the first β-strand of the chemokine," *The Journal of Biological Chemistry*, vol. 274, no. 34, pp. 23916–23925, 1999.

[105] J. J. Tsai, J. A. Dudakov, K. Takahashi et al., "Nrf2 regulates haematopoietic stem cell function," *Nature Cell Biology*, vol. 15, no. 3, pp. 309–316, 2013.

[106] T. L. Deem and J. M. Cook-Mills, "Vascular cell adhesion molecule 1 (VCAM-1) activation of endothelial cell matrix metalloproteinases: role of reactive oxygen species," *Blood*, vol. 104, no. 8, pp. 2385–2393, 2004.

[107] P. Ramirez, M. P. Rettig, G. L. Uy et al., "BIO5192, a small molecule inhibitor of VLA-4, mobilizes hematopoietic stem and progenitor cells," *Blood*, vol. 114, no. 7, pp. 1340–1343, 2009.

[108] N. Yanai, N. Matsui, T. Furusawa, T. Okubo, and M. Obinata, "Sphingosine-1-phosphate and lysophosphatidic acid trigger invasion of primitive hematopoietic cells into stromal cell layers," *Blood*, vol. 96, no. 1, pp. 139–144, 2000.

[109] H. Rosen and E. J. Goetzl, "Sphingosine 1-phosphate and its receptors: an autocrine and paracrine network," *Nature Reviews Immunology*, vol. 5, no. 7, pp. 560–570, 2005.

[110] S. Akunuru and H. Geiger, "Aging, clonality, and rejuvenation of hematopoietic stem cells," *Trends in Molecular Medicine*, vol. 22, no. 8, pp. 701–712, 2016.

[111] B. Dykstra, S. Olthof, J. Schreuder, M. Ritsema, and G. de Haan, "Clonal analysis reveals multiple functional defects of aged murine hematopoietic stem cells," *The Journal of Experimental Medicine*, vol. 208, no. 13, pp. 2691–2703, 2011.

[112] K. Sudo, H. Ema, Y. Morita, and H. Nakauchi, "Age-associated characteristics of murine hematopoietic stem cells," *The Journal of Experimental Medicine*, vol. 192, no. 9, pp. 1273–1280, 2000.

[113] G. de Haan, W. Nijhof, and G. Van Zant, "Mouse strain-dependent changes in frequency and proliferation of hematopoietic stem cells during aging: correlation between lifespan and cycling activity," *Blood*, vol. 89, no. 5, pp. 1543–1550, 1997.

[114] B. M. Moehrle and H. Geiger, "Aging of hematopoietic stem cells: DNA damage and mutations?," *Experimental Hematology*, vol. 44, no. 10, pp. 895–901, 2016.

[115] J. Flach, S. T. Bakker, M. Mohrin et al., "Replication stress is a potent driver of functional decline in ageing haematopoietic stem cells," *Nature*, vol. 512, no. 7513, pp. 198–202, 2014.

[116] Y. Liang, G. Van Zant, and S. J. Szilvassy, "Effects of aging on the homing and engraftment of murine hematopoietic stem and progenitor cells," *Blood*, vol. 106, no. 4, pp. 1479–1487, 2005.

[117] L. Shao, Y. Wang, J. Chang, Y. Luo, A. Meng, and D. Zhou, "Hematopoietic stem cell senescence and cancer therapy-induced long-term bone marrow injury," *Translational Cancer Research*, vol. 2, no. 5, pp. 397–411, 2013.

[118] H. Zhang, Z. Zhai, Y. Wang et al., "Resveratrol ameliorates ionizing irradiation-induced long-term hematopoietic stem cell injury in mice," *Free Radical Biology & Medicine*, vol. 54, pp. 40–50, 2013.

[119] A. V. Ergen and M. A. Goodell, "Mechanisms of hematopoietic stem cell aging," *Experimental Gerontology*, vol. 45, no. 4, pp. 286–290, 2010.

[120] Z. Tothova, R. Kollipara, B. J. Huntly et al., "FoxOs are critical mediators of hematopoietic stem cell resistance to physiologic oxidative stress," *Cell*, vol. 128, no. 2, pp. 325–339, 2007.

[121] K. Brown, S. Xie, X. Qiu et al., "SIRT3 reverses aging-associated degeneration," *Cell Reports*, vol. 3, no. 2, pp. 319–327, 2013.

[122] M. L. Porto, B. P. Rodrigues, T. N. Menezes et al., "Reactive oxygen species contribute to dysfunction of bone marrow hematopoietic stem cells in aged C57BL/6 J mice," *Journal of Biomedical Science*, vol. 22, no. 1, p. 97, 2015.

[123] H. Jung, M. J. Kim, D. O. Kim et al., "TXNIP maintains the hematopoietic cell pool by switching the function of p53 under oxidative stress," *Cell Metabolism*, vol. 18, no. 1, pp. 75–85, 2013.

[124] C. W. Cheng, G. B. Adams, L. Perin et al., "Prolonged fasting reduces IGF-1/PKA to promote hematopoietic-stem-cell-based regeneration and reverse immunosuppression," *Cell Stem Cell*, vol. 14, no. 6, pp. 810–823, 2014.

[125] C. Chen, Y. Liu, Y. Liu, and P. Zheng, "mTOR regulation and therapeutic rejuvenation of aging hematopoietic stem cells," *Science Signaling*, vol. 2, no. 98, article ra75, 2009.

[126] M. Mohrin, J. Shin, Y. Liu et al., "Stem cell aging. A mitochondrial UPR-mediated metabolic checkpoint regulates hematopoietic stem cell aging," *Science*, vol. 347, no. 6228, pp. 1374–1377, 2015.

[127] M. C. Florian, K. Dörr, A. Niebel et al., "Cdc42 activity regulates hematopoietic stem cell aging and rejuvenation," *Cell Stem Cell*, vol. 10, no. 5, pp. 520–530, 2012.

[128] H. Jung, D. O. Kim, J. E. Byun et al., "Thioredoxin-interacting protein regulates haematopoietic stem cell ageing and rejuvenation by inhibiting p38 kinase activity," *Nature Communications*, vol. 7, p. 13674, 2016.

Hindawi
Oxidative Medicine and Cellular Longevity
Volume 2018, Article ID 1823189, 17 pages
https://doi.org/10.1155/2018/1823189

Clinical Study

Influence of Dental Restorations on Oxidative Stress in Gingival Crevicular Fluid

Ervin Taso,[1] Vladimir Stefanovic,[1] Ivana Stevanovic,[2] Danilo Vojvodic,[2] Aleksandra Topic,[3] Aleksandra Petkovic-Curcin,[2] Kosovka Obradovic-Djuricic,[4] Aleksa Markovic,[5] Mirjana Djukic,[6] and Dragana Vujanovic[6]

[1]*Clinic for Stomatology, Military Medical Academy, Belgrade, Serbia*
[2]*Institute for Medical Research, Military Medical Academy, Belgrade, Serbia*
[3]*Department for Biochemistry, Faculty of Pharmacy, University of Belgrade, Belgrade, Serbia*
[4]*Department for Prosthetics, Faculty of Dental Medicine, University of Belgrade, Belgrade, Serbia*
[5]*Department for Oral Surgery, Faculty of Dental Medicine, University of Belgrade, Belgrade, Serbia*
[6]*Department for Toxicology, Faculty of Pharmacy, University of Belgrade, Belgrade, Serbia*

Correspondence should be addressed to Mirjana Djukic; mirjana.djukic.cipa@gmail.com

Received 1 February 2018; Accepted 25 March 2018; Published 24 July 2018

Academic Editor: Tomris Ozben

Biocompatibility of dental materials (DM) can be evaluated by gingival crevicular fluid (GCF) oxidative stress (OS) status. The goal of the study was to ascertain influence of dental caries degree, teeth position, and type and amount of applied DM on GCF OS profile. For this purpose, we tested six DMs that were sealed in one session: amalgam (Amg), composites: Tetric EvoCeram and Beautifil (BF), phosphate cement—zinc phosphate and polycarboxylate cements—zinc polycarboxylate cements, and glass ionomer cement (GIC). The study included 88 dental outpatients. Follow-up was scheduled at 7th and 30th day. Oxidative stress parameters (malondialdehyde (MDA) and glutathione (GSH) levels and total superoxide dismutase (tSOD) activity) were measured before (0th day) and after the treatment (7th and 30th day) in GCF. Control teeth were mirror-positioned healthy teeth. The DM accomplished the following effects (listed in descending order): increase of GSH in GCF was realized by ZPoC > BF > GIC > Amg; tSOD activity increase by ZPoC > BF > Amg; and MDA decrease by ZPoC > ZPhC > Amg > TEC. Dental caries provokes insignificant rise of OS in GCF. ZPoC and ZPhC showed the highest antioxidant effect, contrary to GIC. Restorations with antioxidant properties may reduce gum diseases initiated by caries lesion, what is of great clinical relevance in dentistry.

1. Introduction

Convincing evidence concerning oxidative stress- (OS-) associated dental pathologies (parodontopathy, oral cavity cancer, etc.) has been reported during recent decades [1–3]. Up-to-date studies on redox status in oral environment have referred mainly to peroxidase activity in saliva [2, 4–7]. Reports in 2017 turned researchers' attention to gingival crevicular fluid (GCF) as a diagnostic tool for oral diseases analysis and treatment outcome. The impact of oral environmental stressors (hygienic food and eating habits, smoking, etc.) on saliva is much more intense than on GCF, though it was reported that smoking instantly increases GCF flow [8, 9].

Leading by the fact that GCF is a very specific oral cavity fluid (a transudate of blood plasma placed in the gingival sulcus), less exposed to oral environmental stressors compared to saliva, which requires noninvasive sampling, we chose GCF as an appropriate oral matrix for this kind of testing [8]. Herein, we tested the influence of dental caries (a bacterial disease of the dental hard tissues, also defined as a final stage of local teeth immune response to oral pathogen invasion) as well as six dental fillings on GCF redox homeostasis [10].

Recently, it was documented that cell redox activity, that is, antioxidant defense against environmental stressors (including smoking, i.e., nicotine) has important implications on periodontal disease and is important [9]. It is well acknowledged that OS (or other type of stress) is an inability of antioxidative defense system in living organisms to cope with free radicals (FRs) overproduction that results in oxidative injury of all classes of biomolecules, including proteins, lipids, phospholipids, and deoxyribonucleic acid. Different classes of FRs (reactive oxygen, nitrogen, sulfur, or carbon species (ROS, RNS, RSC, or RCC)) can initiate corresponding type of stress, oxidative, nitrosative, thiyl, or carbonyl stress (OS, NS, TS, and CS), respectively [11]. Along with changed cell signalization and energy breakdown, the overall occurrences finally end up with a cell death, by apoptosis [12].

Overproduction of ROS (including superoxide anion ($O_2^{\bullet-}$), hydrogen peroxide (H_2O_2), hydroxyl radical ($HO^{\bullet}$), and hypochlorous acid (HOCl)) occurs in dental lesions (caries) during phagocytosis. Reactive species injure subcellular and/or cellular membranes of phagolysosomes and/or neutrophils during respiratory burst. Over time, oxidation products of polyunsaturated fatty acids (cell membrane ingredients) become converted into carbonyls, such as malondialdehyde (MDA), a reliable marker of lipid peroxidation (LPO) [13]. Together with myeloperoxidase and NADH-oxidase, they leak out of phagolysosomes into phagocyte cytosol and further at a site of infection or inflammation and damage phagocytes and injure tissue. Reports on exogenously present myeloperoxidase assume that it enhances bacterial phagocytosis and intracellular killing by macrophages.

Accordingly, total superoxide dismutase (SOD) (covers cytosolic and extracellular form (Cu/Zn-SOD) and mitochondrial (Mn-SOD), as well) converts $O_2^{\bullet-}$ into H_2O_2, which further becomes converted into H_2O, by catalase. These biochemical reactions can attenuate myeloperoxidase-induced bactericidal activity within or out of phagocytes and reduce myeloperoxidase-associated lipid peroxidation (LPO) [11, 14]. The role of SOD in dental pathologies has not been investigated until now.

In support of the possible redox interactions of the tested dental restoratives is the fact that some xenobiotics undergo redox metabolism and contribute to $O_2^{\bullet-}$ production [15]. Hitherto, testing of dental materials' pro or antioxidant activity has not been implemented in biocompatibility type of analysis *in vitro* and *in vivo*.

By measuring GSH, MDA, and tSOD in GCF, we studied its redox response to dental caries and six dental restorations, considering the dental lesion degree, teeth position, and placed amount into teeth.

2. Material and Methods

The study was carried out on dental outpatient from the Clinic for Stomatology at the Military Medical Academy, Belgrade, Serbia, for 30 days, in accordance with the International Ethical Guidelines and Declaration of Helsinki (1964/1975) and was approved by the Ethical Committee of the Military Medical Academy, Ministry of Defense, Serbia (Preference number VMA/10-12/A.1). The participants were introduced with the essence of the study and planned procedures, filled out a questionnaire dental record form related to general and oral health, and gave written consent to participate in this study.

Table 1: Patients' recruited criteria.

The inclusion criteria	Criteria related to teeth condition
	(i) The proximal caries on anterior and posterior teeth
	(ii) The existence of the same type of antagonistic teeth ("mirror"-positioned healthy teeth) used controls
	(iii) An absence of fresh postextractional or traumatic wounds in the restoration area or the area of restored surfaces
	(iv) An absence of infection in the area of restored surfaces
	Other influencing criteria
	(i) Patients with no bone-associated diseases or treatments
	(ii) Satisfactory oral hygiene
	(iii) Reliable and cooperative patients
The exclusion criteria	Criteria related to teeth condition
	(i) Endodontic and/or periodontal infections in the area of cervical filling
	(ii) Parodontopathy
	(iii) Prominent periodontal pockets
	(iv) Subgingival caries
	(v) Fillings that were prominent outside the cavity
	Other influencing criteria
	(i) Patients on radiation immunosuppressive therapy
	(ii) Patients bone-associated diseases and malignant diseases
	(iii) Addictive patients on drug/alcohol/cigarettes (>20 cigarettes per day)
	(iv) Bad oral hygiene
	(v) Unreliable and uncooperative patients

Inclusion criteria: criteria related to teeth condition. The proximal caries on the anterior and posterior teeth. The existence of the same type of antagonistic teeth ("mirror"-positioned healthy teeth) used controls. An absence of fresh postextractional or traumatic wounds in the restoration area or the area of restored surfaces. An absence of infection in the area of restored surfaces. Other influencing criteria. Patients with no bone-associated diseases or treatments. Satisfactory oral hygiene. Reliable and cooperative patients. Exclusion criteria: criteria related to teeth condition. Endodontic and/or periodontal infections in the area of cervical filling. Parodontopathy. Prominent periodontal pockets. Subgingival caries. Fillings that were prominent outside the cavity. Other influencing criteria. Patients on radiation immunosuppressive therapy. Patients' bone-associated diseases and malignant diseases. Addictive patients on drug/alcohol/cigarettes (>20 cigarettes per day). Bad oral hygiene. Unreliable and uncooperative patients.

2.1. Patients. The 88 dental outpatients, aged 18–70, were recruited by the tabular specified criteria (Table 1).

Table 2: Distribution of patients according to Black's Classification Criteria with defined teeth position and applied type of restoratives.

Dental restoratives	*K2* $n = 58$	*K3* $n = 10$	*K4* $n = 6$	*K5* $n = 14$
TEC	12 (21) 6/6	—	—	5 (36) 4/1
Amg	8 (14) 8/0	—	—	6 (43) 6/0
ZPoC	5 (8) 3/2	4 (40) 4/0	5 (83) 5/0	—
BF	15 (26) 8/7	—	—	—
GIC	11 (19) 9/2	2 (20) 2/0	—	1 (7) 1/0
ZPhC	7 (12) 5/2	4 (40) 3/1	1 (17) 1/0	2 (14) 2/0

The number of patients within the K groups were given in respect to the type of applied restoration and in bracket (the percentage of the patients treated with the certain restoration in respect to all patients within the appropriate K group). Also, the number of patients with posterior/anterior positioned teeth was indicated (P/A).

In respect to Black's Classification Criteria, patients were classified into four groups (K2–K5), and according to the type of the applied dental fillings, patients were divided into six groups: Amg, TEC, BF, ZPhC, ZPoC, and GIC. Position of the treated teeth were also presented (Table 2) [16, 17].

2.2. GCF Sampling Procedure. The GCF sampling was performed by the filter paper technique. After removing supragingival biofilm, the sampling area (with sterile cotton rolls) was gently air dried 1 min before the sampling procedure. A paper strip (Perio-paper, Pro Flow, Amityville, NY, USA) was inserted into the gingival/periodontal sulcus/pocket until mild resistance and left for 30 seconds [18]. Strips contaminated with blood or saliva were discarded. The volume of taken GCF was measured by Periotron 6000 (Interstate Drug Exchange, Amityville, NY, USA), previously calibrated. The GCF sampling paper strips were placed into microcentrifuge plastic tubes. Elution of GCF was performed with 500 μL phosphate-buffered saline by vortexing for 10 seconds and centrifugation at 3000 g for 5 min, to remove plaque and cellular elements. The supernatants were transferred into Eppendorfs and stored at −70°C until OS analysis.

The sampling of GCF adjacent to treated teeth was performed three times (prior and two times after the treatment (0th, 7th, and 30th day)), while GCF sampling from the corresponding healthy mirror-positioned, that is, antagonistic healthy teeth was done, once, at 0th day (Scheme 1).

2.3. Dental Restorations. Dental fillings (temporary and permanent) were sealed in one session, and placed mass refers to the range 0.07–2.03 g (Table 3).

Used dental fillings referred to temporary restorations: ZPhC (Cegal NV, Galenika, R Serbia) and ZPoC (Harvard, USA); permanent restorations: Amg (Extracap D caps, Galenika, R Serbia); and two nanohybrid composites that require UV light for binding in cavity: BF (the mixture of bisphenol-A-diglycidyl-dimethacrylate (BisGMA) 15–25%, triethyleneglycol-dimethacrylate (TEGDMA) 12–14%, aluminofluoroborosilicate glass 50–60%, aluminium trioxide (Al_2O_3)

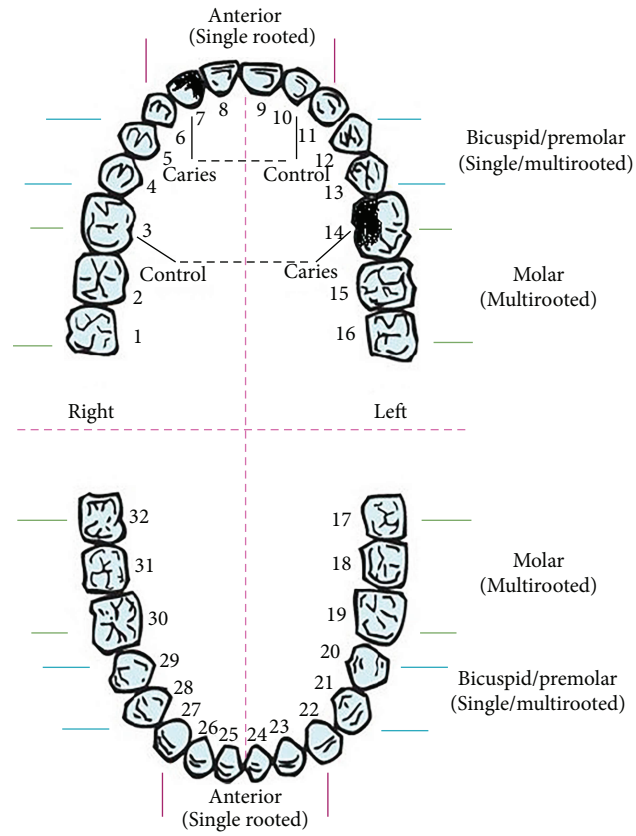

Scheme 1: Teeth diagram. Scheme taken form https://www.pinterest.com/pin/290763719669177256/ is modified by the illustration of teeth with caries and corresponding controls.

Table 3: The amount of sealed restoratives in regard to teeth position.

Type of restoration *Number of patients (P/A)*	*Posterior (Number of patients)*	*Anterior (Number of patients)*
Amg, $n = 14$ *(P/A 14/0)*	**1.32 ± 0.71** $n = 14$	/
ZPoC, $n = 14$ *(P/A 12/2)*	**0.23 ± 0.167** $n = 12$	**0.04 ± 0.025** $n = 2$
TEC, $n = 17$ *(P/A 10/7)*	**0.15 ± 0.159** $n = 10$	**0.03 ± 0.023** $n = 7$
BF, $n = 15$ *(P/A 8/7)*	**0.06 ± 0.042** $n = 8$	**0.03 ± 0.014** $n = 7$
GIC, $n = 14$ *(P/A 12/2)*	**0.17 ± 0.153** $n = 12$	**0.04 ± 0.015** $n = 2$
ZPhC, $n = 14$ *(P/A 11/3)*	**0.24 ± 0.145** $n = 11$	**0.08 ± 0.081** $n = 3$

1-2%, and DL-Camphorquinone) (Shofu, Japan)) and TEC (the mixture of 2.5–10% of BisGMA and 2.5–10% of urethane-dimethacrylate (UEDMA) and nonhazardous additions (Ivoclar Vivadent, USA)); GIC (GC Fuji PLUS®, Green Circle, USA) was used for both settings, stand-alone restorations and the base for nanohybrid composites (BF and TEC).

2.4. Measurement of Oxidative Stress Markers in GCF

2.4.1. Malondialdehyde Measurements. Malondialdehyde, LPO biomarker was measured spectrophotometrically by thiobarbituric acid reactive substances (TBARS) production method. In brief, MDA forms red-colored compound with TBA reagent (15% TCA and 0.375% TBA, water solution, pH 3.5) during the incubation at 95°C, measured at 532 nm. Data were expressed as nmol MDA/mg proteins [19].

2.4.2. Superoxide Dismutase Measurements. Superoxide dismutase (EC 1.15.1.1.; SOD) activity was measured spectrophotometrically, as an inhibition of epinephrine oxidation to colored product adrenochrome by $O_2^{\bullet-}$. Kinetics of SOD activity was measured at 480 nm after the addition of 10 mmol epinephrine into samples prepared in carbonate buffer (50 mmol, pH 10.2), containing 0.1 mmol EDTA [20]. Data were expressed as U SOD/mg proteins.

2.4.3. Glutathione Measurements. The reduced form of glutathione (GSH) reduces Elman's reagent [5,5′-dithiobis (2-nitrobenzoic acid), DTNB] (36.9 mg DTNB in 10 ml of methanol) in TRIS-HCl buffer (0.4 M, pH −8.9) into yellow colored 5-thio-2-nitrobenzoic acid (TNB) [21]. Produced TNB is proportional to the amount of depleted GSH (on the account of its oxidation) and was determined spectrophotometrically (at 412 nm), by the enzymatic recycling assay. The results were expressed as nmol TNB/mg proteins.

2.5. Protein Measurements. Total protein concentrations were estimated in supernatants of GCF samples according to Lowry et al. method [22].

2.6. Statistical Analysis. The appropriate statistical analysis for this type of results after determining the normality of data distribution is the analysis of covariance ANCOVA, since we compare teeth with the corresponding control. The ANOVA test is inappropriate since it excludes the individuality (the corresponding matches for single patient) and implies overall values.

In more details, the one-sample Kolmogorov-Smirnov normality test followed by nonparametric Wilcoxon signed-rank test for two related samples and two-tailed independent *t*-test were used to analyze the differences between OS parameters in GCF adjacent to control healthy teeth (healthy teeth mirror positioned) and untreated teeth with caries (K2–K5, 0th day). The impact of six applied restorations on the OS parameters was tested when data were analyzed in respect to both independent variables, degree of caries (K groups) and/or type of applied restorations, 2 × 2 between-group analysis of covariance (ANCOVA), and post hoc comparisons (least-significant difference (LSD)) were used.

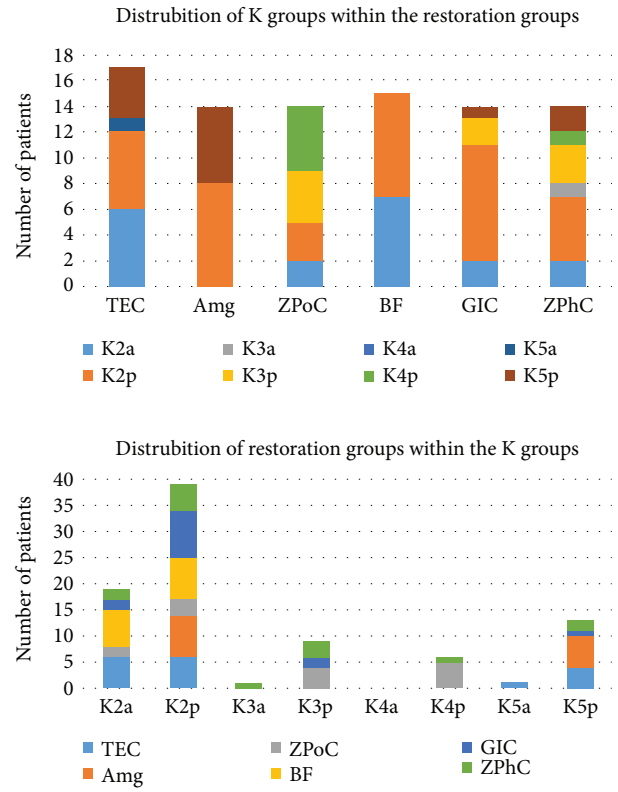

Figure 1: Distribution of patients across the groups obtained on the basis of two criteria: K2–K5 groups and six restoration groups. The representation of certain groups within the groups obtained on the basis of the other criteria. Suffixes a and p in the K groups' nomenclature indicate teeth position, anterior and posterior, respectively. Data corresponds to the data given in Table 2.

The influence of filling mass on OS parameter was estimated by nonparametric Spearman's correlation analysis, while association between teeth position and filling mass was analyzed by Pearson correlation 2-tailed test.

In all performed analyses, dependent variables were OS parameters in GCF from 7th to 30th day, while those on 0th day were used as a covariate to control individual differences in therapy outcome (A-set of analyses). Value $p \leq 0.05$ was considered statistically significant.

Two statistical programs SPSS 17.0 were used for the above analyses and Excel Microsoft program, version 2016, for graphical data presentation.

3. Results

Since we did not have enough patients within some of the formed groups (referring to the degree of dental caries—groups K2-K5, and the applied restorations—6 groups: Amg, TEC, BF, ZPhC, ZPoC, and GIC), we cross-examined GCF OS status before and after the applied treatments.

The number of patients treated with certain dental fillings within the K groups and opposite were presented in Figure 1. Percentages of that distribution (extracted from Table 2)

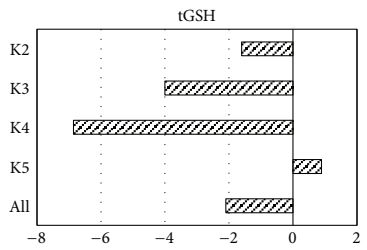

Paired samples	tGSH (nM/mg proteins)	p
C / $K2_{0th}$	21.6 ± 1.7/20.6 ± 1.6	0.386
C / $K3_{0th}$	24.7 ± 5.3/17.9 ± 4.7	0.285
C / $K4_{0th}$	30.3 ± 5.0/23.4 ± 4.2	0.043
C / $K5_{0th}$	10.8 ± 1.4/11.6 ± 1.5	0.646
C / All_{0th}	21.1 ± 1.5/18.9 ± 1.3	0.161

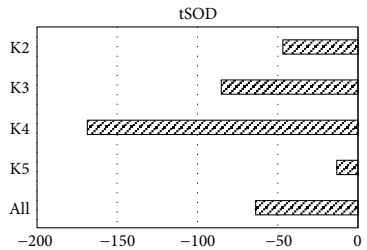

Paired samples	tSOD (U/mg proteins)	p
C / $K2_{0th}$	797.3 ± 65.1/750.4 ± 65.4	0.373
C / $K3_{0th}$	502.2 ± 96.1/417.0 ± 97.9	0.386
C / $K4_{0th}$	712.6 ± 82.1/544.0 ± 76.1	0.043
C / $K5_{0th}$	640.0 ± 78.6/628.8 ± 67.6	0.799
C / All_{0th}	733.5 ± 48.4/678.9 ± 48.4	0.188

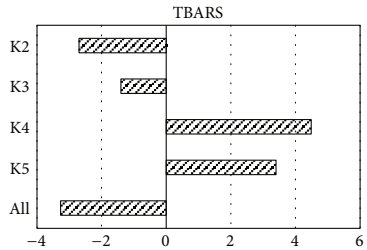

Paired samples	TBARS (nM/mg proteins)	p
C / $K2_{0th}$	21.9 ± 3.1/19.1 ± 2.7	0.707
C / $K3_{0th}$	17.9 ± 10.7/16.4 ± 8.1	0.678
C / $K4_{0th}$	14.4 ± 7.3/19.0 ± 6.9	0.345
C / $K5_{0th}$	6.8 ± 1.5/10.2 ± 2.5	0.074
C / All_{0th}	21.1 ± 3.1/17.6 ± 2.1	0.715

(a)

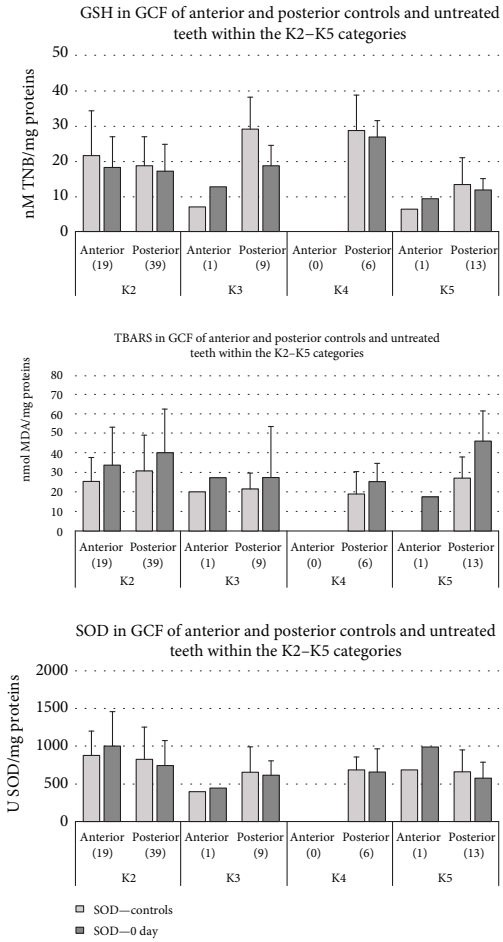

(b)

Figure 2: (a) The impact of caries degree on OS parameters. Differences in OS markers in GCF between controls and untreated teeth with caries (0th day) in respect to Black's classification (K2–K5): GSH was expressed as nmol TNB/mg proteins; LPO, that is, TBARS as nmol MDA/mg proteins and tSOD activity as U SOD/mg proteins. Zero line represents mean of the controls. Tables on the right show mean ± standard error of OS parameters obtained in two related samples and differences between them (p) from all patients. The number of patients within the K groups (0th day) was as follows: K2–58, K3–10, K4–6, and K5–14 (in Table 2). Nonparametric Wilcoxon signed-rank test for two related samples was used. $p \leq 0.05$ value was considered statistically significant. (b) GCF redox status in anterior and posterior controls and pretreated teeth within the K2–K5 categories. Groups K2–K follow the Black's Classification. Teeth position: separated posterior and anterior teeth. GSH was expressed as nmol TNB/mg proteins; LPO, that is, TBARS as nmol MDA/mg proteins and tSOD activity as U SOD/mg proteins. Controls: corresponding antagonistic "mirror"- positioned teeth; 0th day: pretreated teeth with caries.

were mentioned in descending order, where is appropriate, within this section.

Multiple estimation approaches were performed to test the influence of caries (four K categories) and restorations (six types of dental fillings) on OS status (tSOD, GSH, and TBARS) in GCF.

Initially, we determined differences of OS markers within the healthy controls (to reveal if teeth position affects GCF OS status) and then compared pretreated teeth (0th day) with corresponding health control teeth (to test if caries by itself affects redox status in tooth decay degree dependent manner) (Figure 2(a)). No significance was observed, except that GSH and tSOD activities were lower ($p = 0.043$, in both cases) within K4 group, compared to control teeth. Data were presented as histograms in Figure 2(b).

GCF OS status of pre- (0th day) and posttreatment period (7th and 30th day) within K2–K5 groups was presented in Figures 3 and 4(a)–4(f). The highest GSH and tSOD activities were documented in the K3 group, at 30th day: (K3: ZPhC 40%, ZPoC 40%, and GIC 20%); GSH was significantly higher in K3 than in K2 ($^{**}p = 0.001$) and K5 ($^{**}p = 0.001$), at 30th day) (K2: BF 26%, TEC 21%, GIC 19%, Amg 14%, ZPhC 12%, and ZPoC 8% and K5: Amg 43%, TEC 36%, ZPhC 14%, and GIC 7%). The lowest MDA was obtained in K4 group (K4 group: ZPoC 83% and ZPhC 17%) on 30th day, and it was significantly lower compared to K2 ($p = 0.026$), at 30th day for MDA (Figure 3).

Data were presented as histograms in Figures 4(a)–4(f).

Significant beneficial influence of the applied restorations on the certain OS markers in GCF mainly occurred at 30th

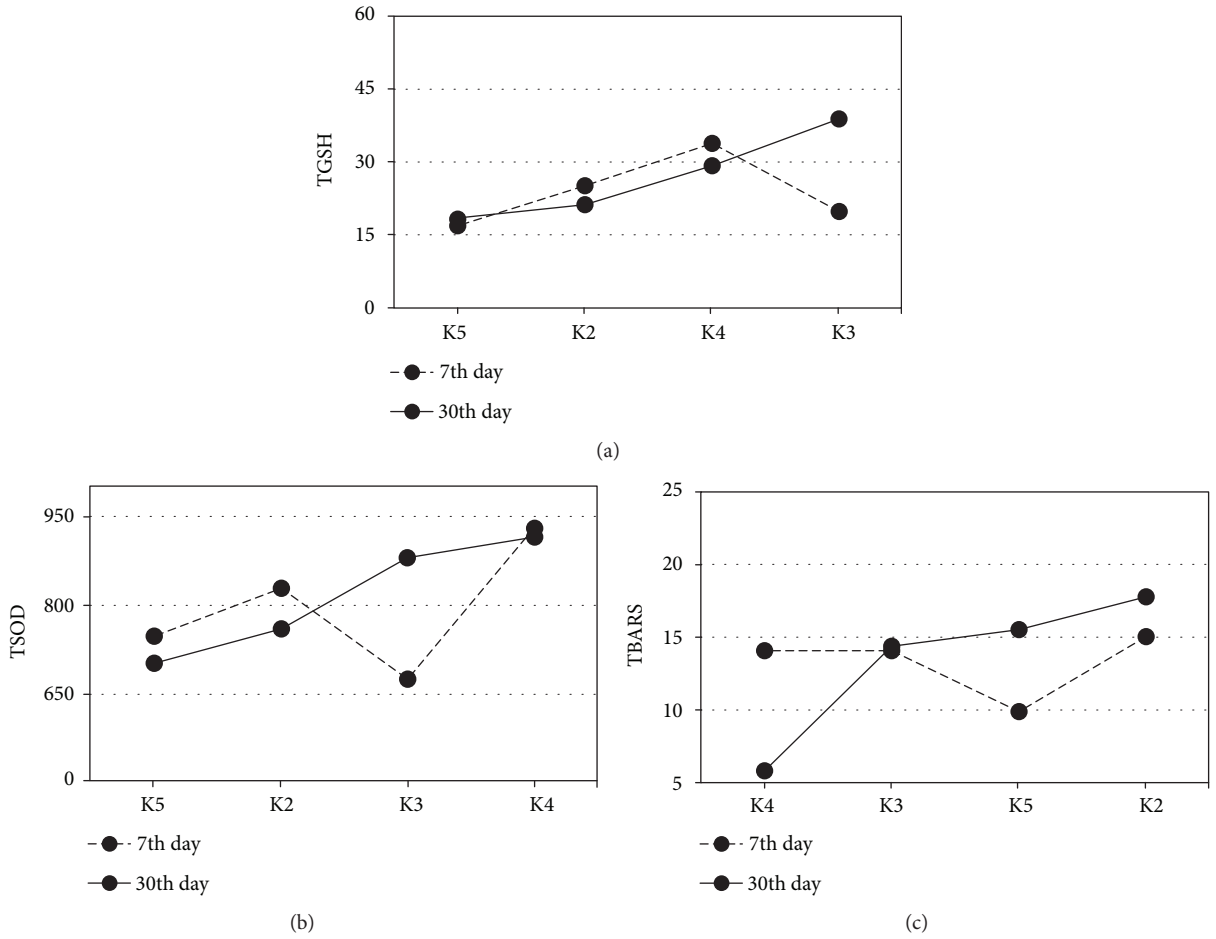

Figure 3: GCF redox status of pre- and posttreatment period within the K2–K5 groups. Estimated marginal means for OS parameters at 7th and 30th day were evaluated with 0th day, in regard to Black's classification (K2–K5): (a) GSH covariates at the 0th day was 18.4 nmol TNB/mg proteins; significant difference was found in 30th day between K2-K3 ($p = 0.001$) and K3–K5 ($p = 0.001$); (b) tSOD covariate at the 0th day was 675.8 U SOD/mg protein; (c) TBARS covariate at the 0th day was 18.1 nmol MDA/mg proteins; significant difference was found in 30th day between K2 and K4 ($p = 0.026$). The patients' distribution across the 4 K groups is tabulated (Table 2). 7th and 30th days were presented with a dash and solid line, respectively. 2×2 between-group analysis of covariance (ANCOVA) and post hoc comparisons (least-significant difference (LSD)) was used. $p \leq 0.05$ value was considered statistically significant.

day and are listed in descending order: elevated GSH was obtained by ZPoC > BF > GIC > Amg and tSOD activity by ZPoC > BF > Amg; while decreased MDA was gained by ZPoC > ZPhC > Amg > TEC (Figure 5).

Higher tSOD activity was accomplished in anterior, compared with posterior teeth, on 30th day ($p = 0.018$).

No association was confirmed for filling mass and OS parameters. Significant correlation was obtained between filling mass and teeth position (Table 3) (Pearson correlation: 0.307, $p = 0.004$).

4. Discussion

Current reports on OS-associated dental/periodontal pathologies have mainly been related to peroxidase activity in saliva. Redox profile differs across oral environmental compartments including hard dental tissue, saliva, and GCF [1, 23]. Herein, we tested the influence of dental caries and six dental fillings on GCF OS homeostasis, which recently has been recognized as reliable diagnostic fluids for periodontal diseases and drug analysis [8].

Hence, physiology of GCF depends on teeth position (anterior includes incisors and canines versus posterior includes premolars and molars), size, shape, root characteristics, function related to pressure at bite, and so on; herein, we compared OS status of GCF across controls and teeth with caries, before (0th day) and after the treatments (7th and 30th day) individually, for each patients, by using ANCOVA statistics [24, 25]. Adhering to the inclusion criteria (that also cover smokers that smoke less than one pack of cigarettes/day) (Table 1) and comparing individually the obtained results for the treated teeth with the control teeth (for each patient), the study was carefully designed to minimize bias.

We ascertained that OS status of GCF is not associated with teeth position, except that GSH was insignificantly

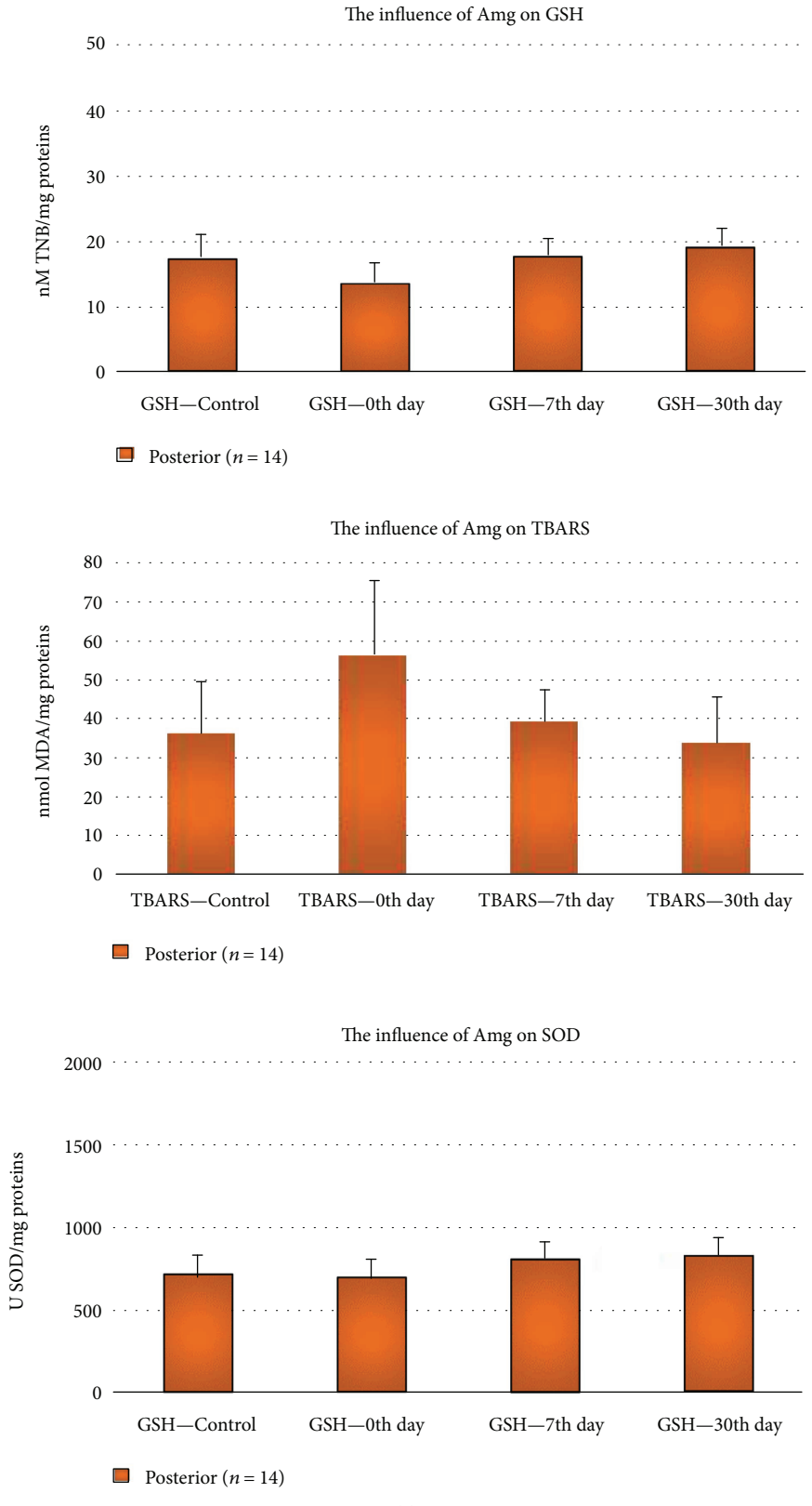

(a)

Figure 4: Continued.

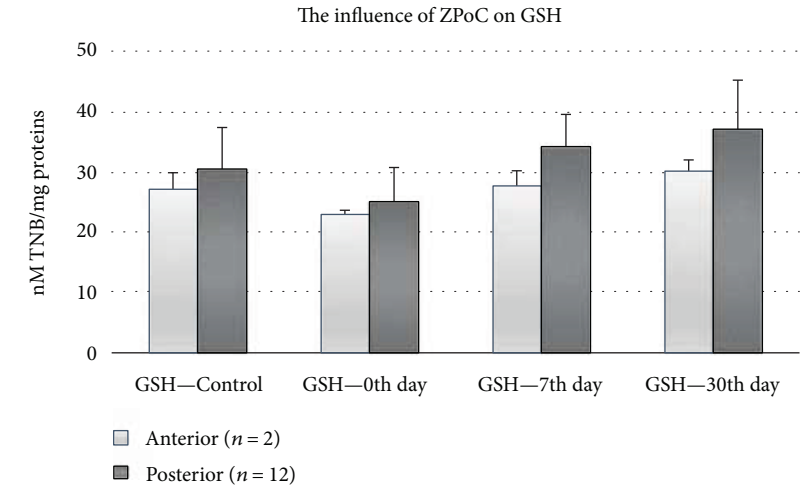

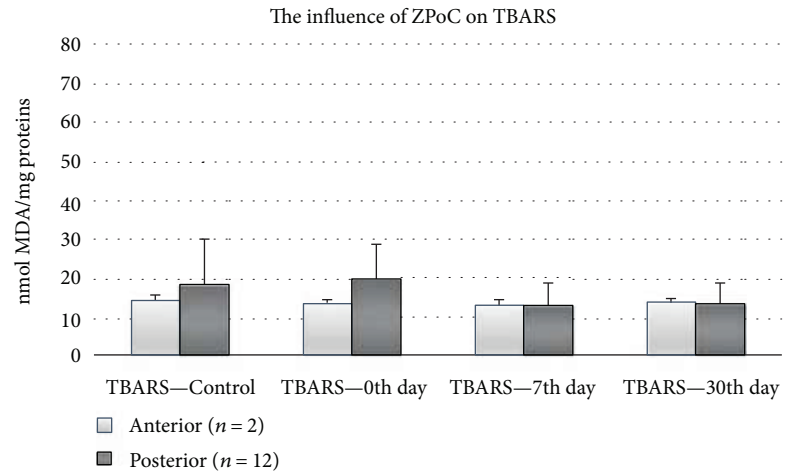

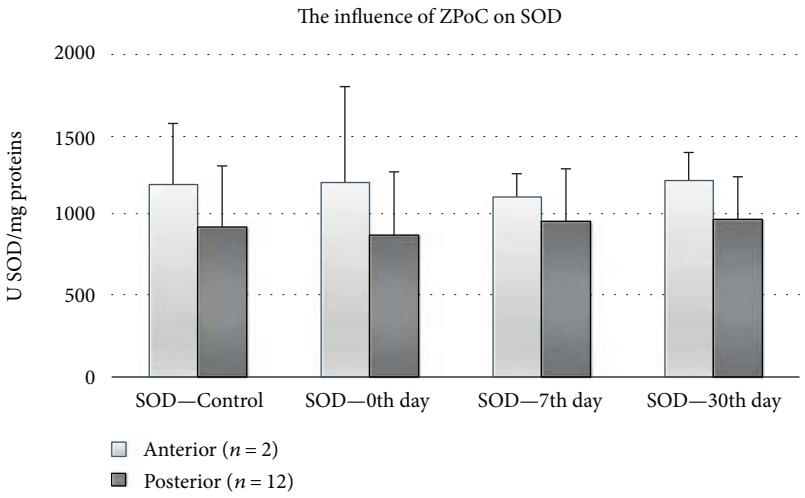

(b)

Figure 4: Continued.

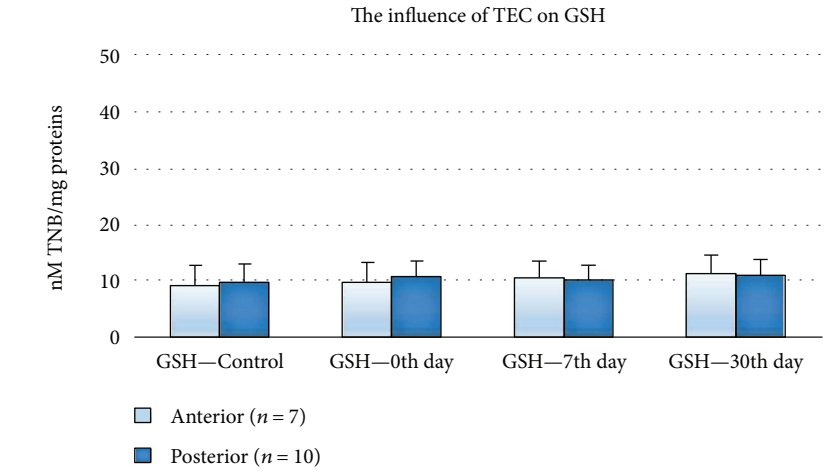

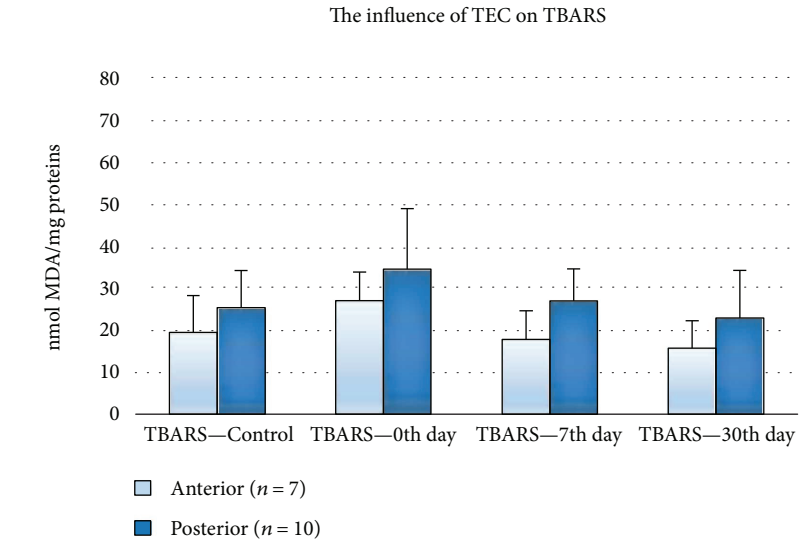

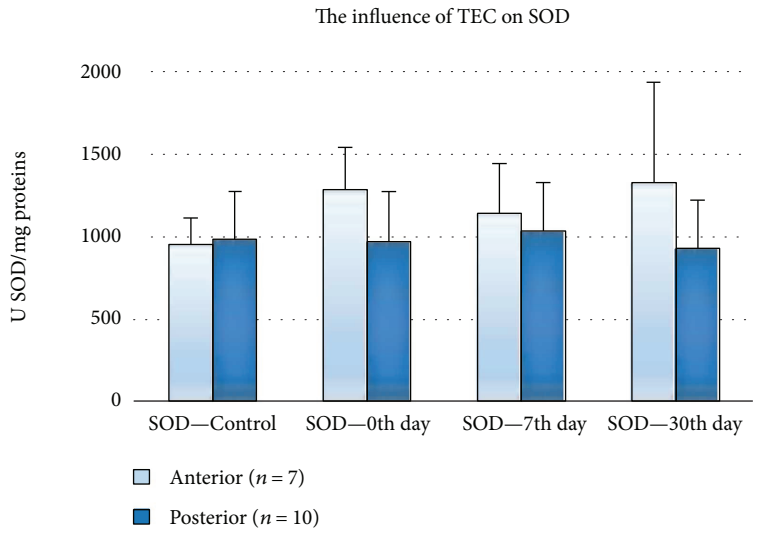

(c)

Figure 4: Continued.

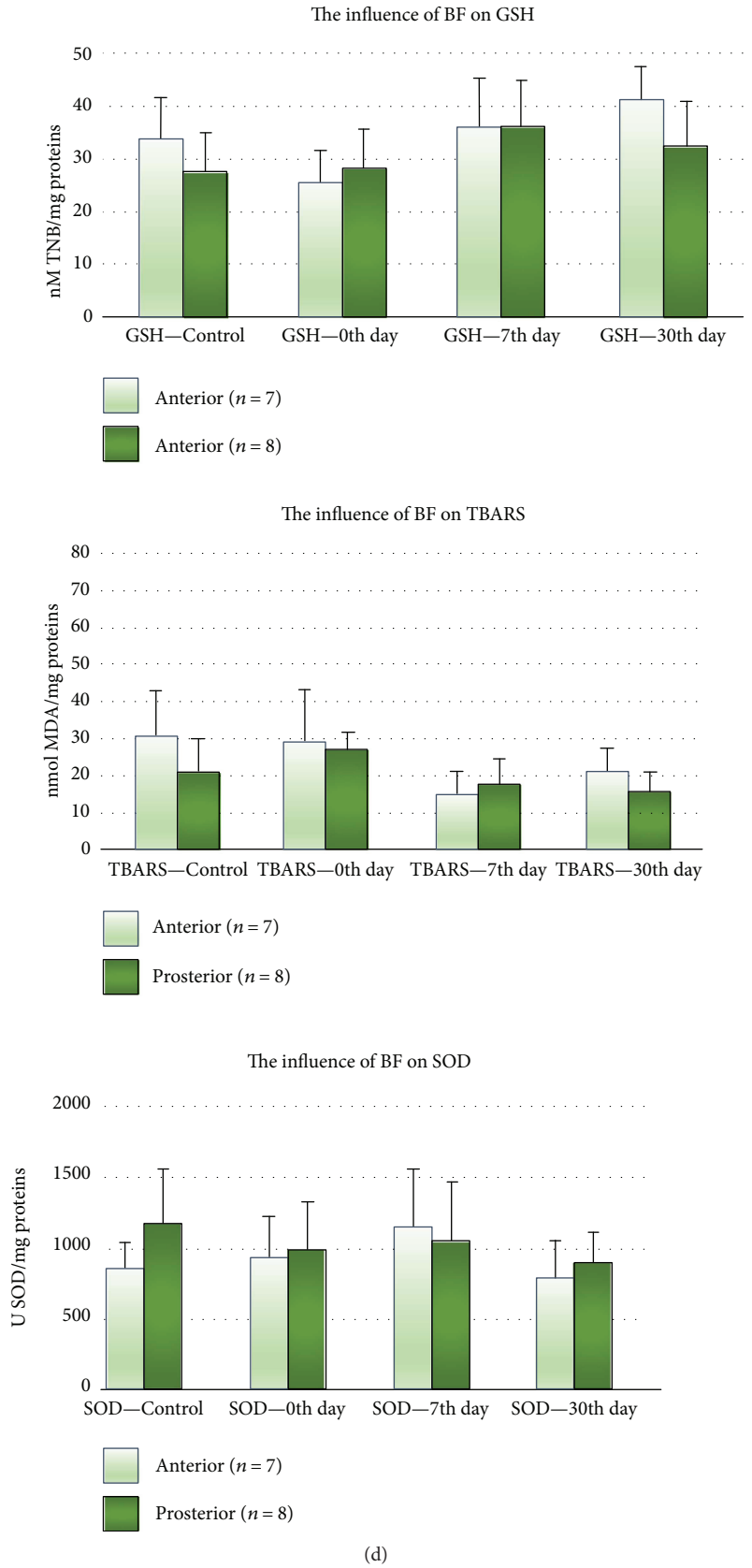

(d)

Figure 4: Continued.

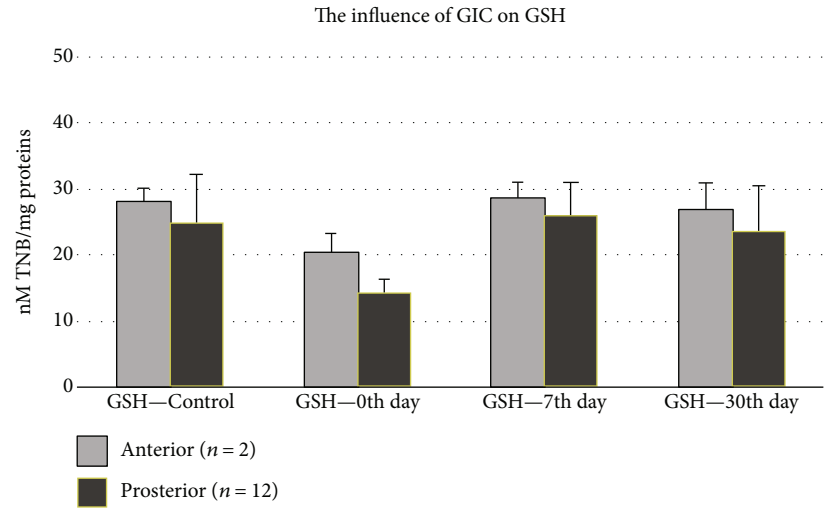

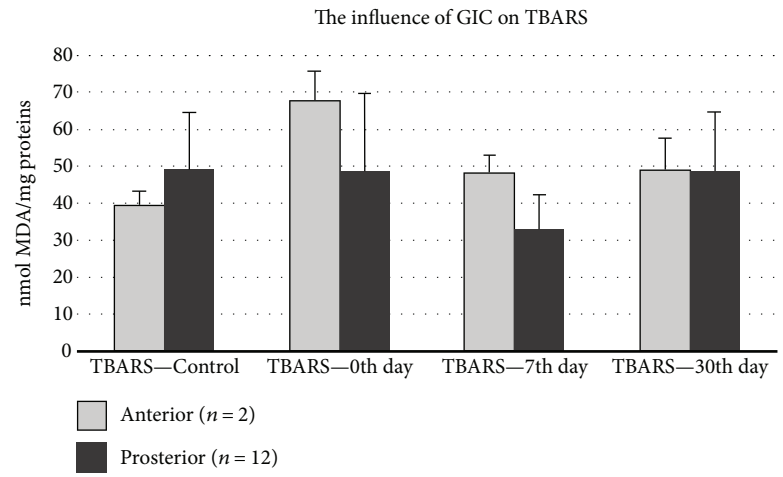

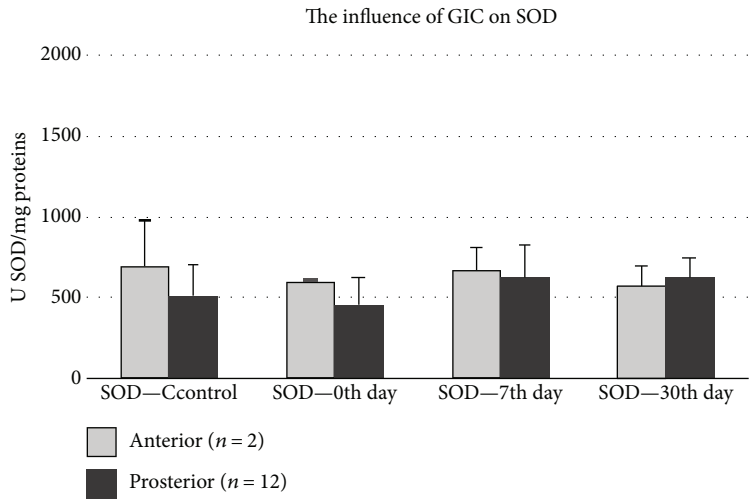

(e)

Figure 4: Continued.

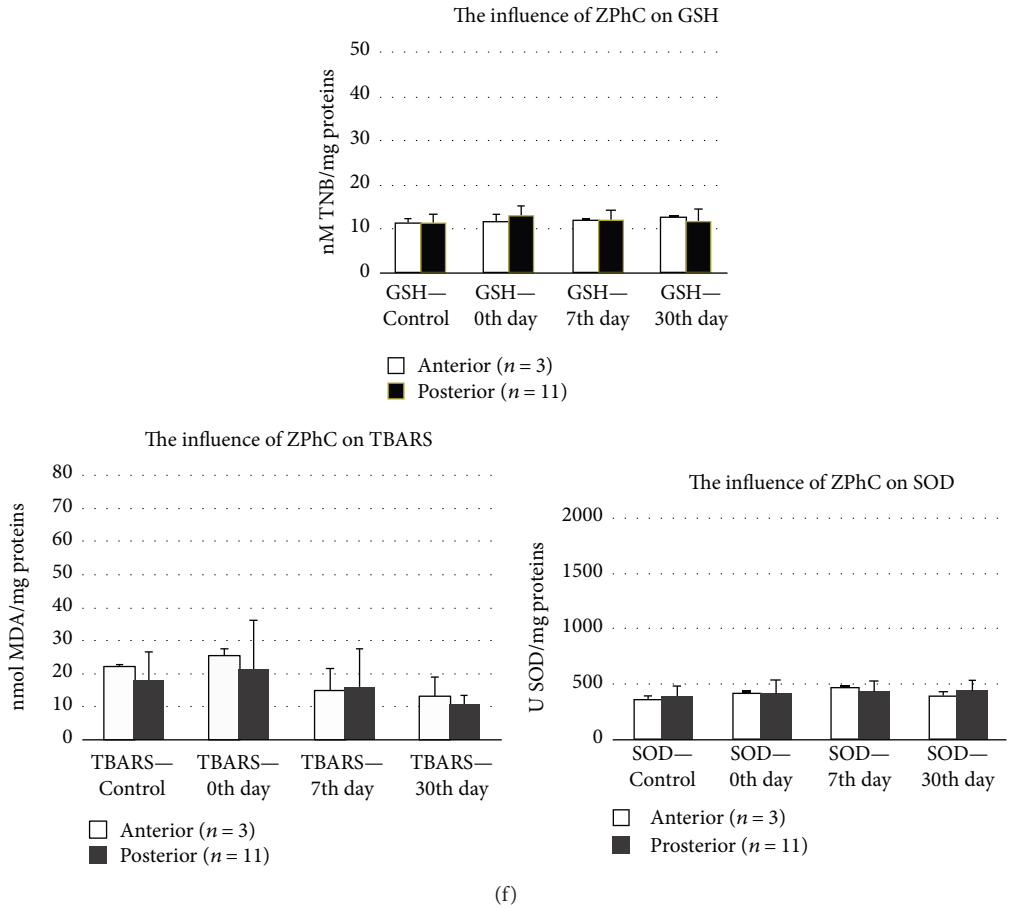

(f)

Figure 4: (a–f) The influence of tested restorations on GCF redox status of dental patients. OS parameters (GSH, MDA, and SOD) in GCF were presented in respect to teeth position (anterior and posterior) with given number of patients per posterior and anterior treated teeth. (a) The influence of Amg on GCF redox status of dental patients. Amg group: patients with posterior treated teeth only ($n = 14$ patients): 8 were from K2 and 6 from K5 group. The amount of sealed Amg: 1.318571 ± 0.71267 g. (b) The influence of ZPoC on GCF redox status of dental patients. Patients with posterior and anterior treated teeth ($n = 14$ patients): 12 patients with posterior treated teeth (3 from K2, 4 from K3, and 5 form K4 group) and 2 patients with anterior treated teeth (2 from K2 group). The amount of sealed ZPoC for anterior was 0.035 ± 0.025 g and posterior was 0.229 ± 0.167 g. (c) The influence of Tetric EvoCeram on GCF redox status of dental patients. Patients with posterior and anterior treated teeth ($n = 17$ patients): 10 patients with posterior treated teeth (6 from K2 and 4 from K5 group) and 7 patients with anterior treated teeth (6 from K2 and 1 from K5 group). The amount of sealed TEC for anterior was 0.029 ± 0.02253 g and posterior was 0.152 ± 0.159 g. (d) The influence of BF on GCF redox status of dental patients. Patients with posterior and anterior treated teeth ($n = 15$ patients): 8 patients with posterior and 7 with anterior treated teeth (all from K2 group). The amount of sealed BF for anterior: 0.029 ± 0.014 g and posterior 0.064 ± 0.042 g. (e) The influence of GIC on GCF redox status of dental patients. Patients with posterior and anterior treated teeth ($n = 14$ patients): 12 patients with posterior treated teeth (9 from K2, 2 from K3, and 1 from K5 group) and 2 patients with anterior treated teeth, from K2 group. The amount of sealed GIC for anterior was 0.035 ± 0.015 g and posterior was 0.168 ± 0.153 g. (f) The influence of ZPhC on GCF redox status of dental patients. Patients with posterior and anterior treated teeth ($n = 14$ patients): 11 patients with posterior treated teeth (5 from K2, 3 from K3, 1from K4, and 2 from K5 group) and 3 patients with anterior treated teeth (2 from K2 and 1 from K3 group). The amount of sealed ZPhC for anterior was 0.08 ± 0.081 g and posterior was 0.235 ± 0.145 g.

elevated in posterior teeth, though we should recall that the posterior teeth prevailed over the anterior in our patients (Table 2, Figures 2(a) and (b)). Contrary to the reports of Davis et al., we showed insignificant OS development with dental degree, from K2–K4, but accordingly, we obtained slightly lower OS in K5 group, what was probably a consequence of reduced central blood supply and teeth metabolic processes, thus diminished local antioxidant defense [26]. According to the literature, we showed that the lowest GSH and tSOD activities were in K4 group ($^*p = 0.043$) [17, 19, 27]. Slightly higher GSH level in K5 group may be explained by reduced metabolic activities, due to insufficient blood supply (Figure 2(a)).

The reason of reduced tSOD activity in K4 group ($^*p = 0.043$) (Figure 2(a) and 2(b)) may be prescribed to the lack of the substrate, $O_2^{\bullet -}$. Also, $O_2^{\bullet -}$ reacts easily with nitrogen monoxide to form harmful peroxynitrite anion (this reaction is three times faster than dismutation catalyzed by SOD). This last mentioned reaction is involved in the acetylation of amino acids, accomplished by gram-negative anaerobes

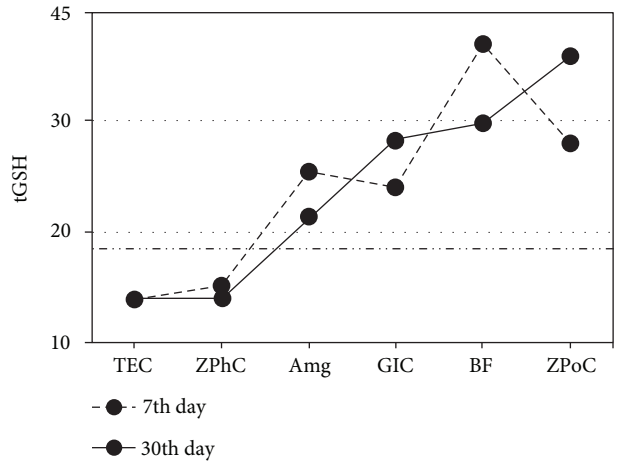

(a)

7th day	30th day
TEC versus Amg, GIC, BF, ZPoC	TEC versus GIC, BF, ZPoC
ZPhC versus Amg, GIC, BF, ZPoC	ZPhC versus GIC, BF, ZPoC
Amg versus BF	Amg versus ZPoC
GIC versus BF	–
F(5,72) = 4.80	F(5,72) = 4.45
$p = 0.001$	$p = 0.002$
pes = 0.250	pes = 0.268

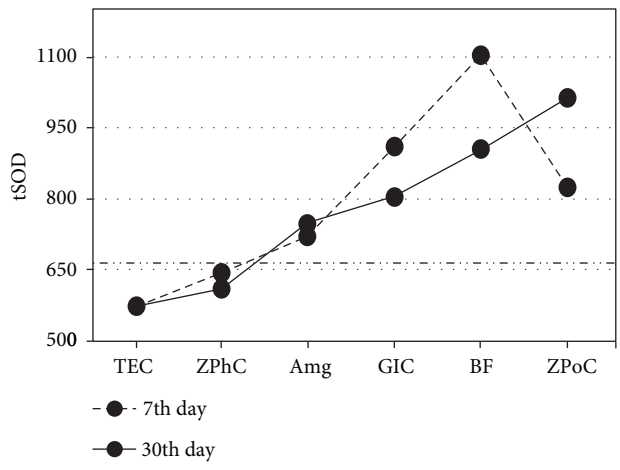

(b)

7th day	30th day
GIC versus Amg, BF	GIC versus Amg, BF, ZPoC
ZPhC versus Amg, BF	ZPhC versus BF, ZPoC
TEC versus BF	TEC versus BF, ZPoC
BF versus ZPoC	Amg versus ZPoC
F (5.72) = 4.07	F (5.72) = 4.90
$p = 0.003$	$p = 0.001$
pes = 0.225	pes = 0.277

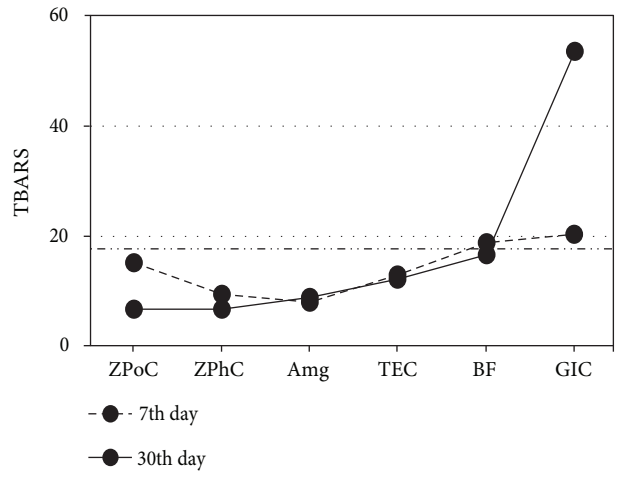

(c)

7th day	30th day
ZPoC versus Amg	ZPoC versus BF, GIC
ZPhC versus BF, GIC	ZPhC versus BF, GIC
Amg versusBF, GIC	Amg versus BF, GIC
–	TEC versus GIC
–	BF versus GIC
F (5.72) = 2,46	F (5.72) = 16.34
$p = 0.041$	$p < 0.001$
pes = 0.151	pes = 0.581

Figure 5: The influence of the restorations on OS parameters before and after the treatments. Estimated marginal means for OS parameters in GCF at 7th and 30th day were evaluated with 0th day (horizontal line: long dash dot dot). In regard to the applied restorative, (a) GSH covariate at the 0th day was 19.3 nmol TNB/mg proteins; (b) tSOD covariate at the 0th day was 665.6 U/mg proteins; (c) TBARS covariate at the 0th day was 17.8 nmol MDA/mg proteins. The patients' distribution across the K groups and restorative groups is tabulated (Table 2). 7th and 30th days were presented with a dash and solid line, respectively. Tables on the right show differences (p values) in OS parameters between restoratives' treatment groups. pes: partial eta squared. 2×2 between-group analysis of covariance (ANCOVA) and post hoc comparisons (least-significant difference, (LSD)) was used. $p \leq 0.05$ value was considered statistically significant.

(*Porphyromonas gingivalis, Prevotella nigrescens,* etc.) [28]. In accordance with the literature, we showed slightly increase of LPO in advanced dental lesion, confirming OS development with caries progression (Figure 2(a)). This notion is supported by ROS overproduction via NADPH oxidase and myeloperoxidase during phagocytosis of bacterial pathogens and their interactions with two main targets in membrane phospholipids, double bond between C-atoms and the ester linkage between glycerol and fatty acids [1, 29, 30]. Stick to dental caries is a bacterial inflammation accompanying with local immune response [10]. Placed within lysosomes (the azurophilic granules of phagocytes) of neutrophils, NADPH oxidase and myeloperoxidase produce ROS during so-called "respiratory burst." NADPH oxidase catalyzes superoxide anion ($O_2^{\bullet-}$) production through a large oxygen (O_2) consumption (when >80–90% of O_2 becomes converted into $O_2^{\bullet-}$), while myeloperoxidase catalyzes production of several reactive species, such as hypohalogenated acids (including hypochlorous acid (HOCl)) in reactions of hydrogen peroxide (H_2O_2) and halide ions (Cl^-, Br^-, and I^-); hypothiocyanous acid (HOSCN) from H_2O_2 and halide and pseudohalide ions; hydroxyl radical ($HO^{\bullet}$), via non-Fenton reaction between $O_2^{\bullet-}$ and HOCl; and nitrating intermediates, *in vivo* [31–34]. After being fused with lysosomes, phagosome (a vesicle formed around engulfed bacteria) matures into phagolysosomes, within the neutrophils. That is the point when intracellular killing of pathogens starts by ROS. Although ROS effects occur intracellularly, within phagolysosomes, they are diffusible and can react outside of phagolysosomes, within the neutrophils and surrounding tissues (for instance with GCF, in case of dental caries) [19]. The reactive species produced by myeloperoxidase are responsible for the oxidation, chlorination, and nitration of cytosolic proteins, glycoproteins, and lipoproteins in neutrophils or in nearby tissues (i.e., HOCl chlorinates amines and produces toxic chloramine, or HOSCN inhibits glycolysis and energy supply, etc.) and are responsible for the side effect of inflammation (death of phagocytes and tissue damage) [34–36].

Development of OS in GCF of teeth with caries was anticipated since immunoinflammatory-associated occurrences, such as caries, are characterized by ROS overproduction, depletion of reducing equivalent sources, such as NAD (P) H and GSH, and oxidative injure of biomolecules, including lipids (Figures 2(b)).

As to the effect of the restorations on OS profile of GCF, ANCOVA analysis of the data sorted by the Black's Classification Criteria (Figures 1 and 3) showed that the highest GSH and tSOD activities were documented in the K3 group (ZPhC = ZPoC > GIC), at 30th day, what was significant for GSH compared to K2 (BF > TEC > GIC > Amg > ZPhC > ZPoC) ($^{**}p = 0.001$) and K5 (Amg > TEC > ZPhC > GIC) ($^{**}p = 0.001$) and reduced LPO in K4 group (ZPoC> > ZPhC), what was significantly lower compared to K2 ($^{*}p = 0.026$), at 30th day for MDA. From this, we concluded that ZPoC and ZPhC, within the K3 group, have more (and equal) supportive role in increasing tSOD activity and GSH. To emphasize that, ZPoC notably reduced LPO within the K4 group.

Accordingly, ANCOVA analysis of the data arranged in respect to the applied restorations showed significant GSH increase by the following restorations listed in descending order: ZPoC > BF > GIC > Amg; and tSOD activity increase by ZPoC > BF > Amg; while MDA decrease was gained by ZPoC > ZPhC > Amg > TEC (Figures 4(a)–4(f) and 5). Consistent with the literature, we confirmed that ZPoC and ZPhC demonstrated profound antioxidant effect in comparison to the other used dental fillings, in terms of suppressed LPO and GSH regaining, contrary to GIC which demonstrated completely opposite, prooxidant effect, while composites, BF and TEC did not show noticeable effects on GCF OS status [37, 38].

According to the literature, the most profound antioxidant effect of ZPoC and ZPhC can be prescribed to hydrolysis of their acid components (itaconic and maleic acids versus phosphoric acid, resp.) [37, 39]. Dicarboxylic acids, such as itaconic and maleic acids, are used as monomers for biopolymers (resins or synthetic fibers). Lampropoulou et al. acclaimed itaconate as a major physiological regulator of the global metabolic rewiring and effector functions of inflammatory macrophages. It regulates succinate levels and function, mitochondrial respiration, and inflammatory cytokine production during macrophage activation [39]. Adhering to this, accomplished antioxidant role of ZPoC (especially in the suppression of LPO within GCF) probably comes from itaconic acid. On the other hand, phosphoric acid binds many divalent cations, including transient metals (iron, cooper, etc.). It is well known that transient metals (in low valent states) participate in Fenton reaction to produce the most potent ROS, $HO^{\bullet}$ (no enzymatic system exists in living organisms to scavenge it) [40]. It is used in dentistry as an etching, that is, corrosive solution. Corrosives kill pathogens and prevent locally bacterial diseases, including dental caries. The antioxidant effect of ZPhC was confirmed by all three OS markers.

From all applied restorations, only GIC accomplished prooxidant property (suppressed tSOD activity and elevated LPO). According to the literature, the explanation for such occurrences lies in fluoride anion (released from GIC) interactions with metal cations embedded in antioxidant metalloenzymes, such as SOD, catalase, and peroxidase. The obtained results are consistent with Yamaguti et al.'s study in which it was shown that low-dose fluoride treatment affects antioxidant enzymes, including SOD and catalase (CAT), and rises LPO in parotid and submandibular salivary glands of rats. Explicitly, they demonstrated that fluoride intoxication caused more pronounced OS in submandibular than in parotid salivary glands [38].

It is well known that prolonged leaching of small amount of unbound monomers (1.5–5%), such as TEGDMA for instance, is blamed for cytotoxic and other systemic effects of composites. The leaching of methacrylate monomers occurs because of the incomplete UV polymerizations of composites during sealing process [41]. Herein, the amount of the TEGDMA, present in the sealed composites (BF and TEC), was almost >300 times lower than its subtoxic dose (<4 mM), reported by Gul et al., thus adverse/toxic effects

(including disruption of redox homeostasis in GCF) were completely avoided [41–43]. Individual sensitivity of the patients with polymorphism of GSH to TEGDMA molecule was reported [44]. Additionally, low GSH levels in GCF of dental patients treated with TEC contrary to BF may relate to monomer UEDMA [45].

The low levels of GSH, tSOD activity, and MDA measured in K5 group before and after the dental restoration strengthening depraved influence of insufficient blood supply and metabolism on GCF profile.

Positive correlation between filling mass (0.07–2.03 g) and teeth position (Pearson correlation: 0.307, $p = 0.004$) was anticipated concerning the size of the anterior and the posterior teeth.

5. Conclusion

Taking into consideration the influential factors such as dental lesion degree, type of applied dental fillings, and teeth position, we made the following conclusions: (i) GCF OS status does not depend on teeth position and does not differ between healthy teeth; (ii) untreated teeth with caries do not differ significantly from corresponding controls (exclusion: elevated GSH in posterior teeth); (iii) reduced GSH and MDA were recognized as a more reliable and sensitive OS marker than tSOD; (iv) ZPoC and ZPhC achieved profound antioxidant effect; (v) none of the applied restorations accomplished complete antioxidant effect, while GIC realized prooxidant effect; and (vi) restorations with antioxidant properties may reduce gum diseases initiated by caries lesion.

To our knowledge, this is the first paper on this topic and performed with dental patient. Restorations with antioxidant properties may reduce gum diseases initiated by caries lesion, what is of great clinical relevance in dentistry. We showed and recognized that redox interactions may influence dental material biocompatibility; thus, evaluation of GCF OS status may be considered as a useful tool in biocompatibility testing of dental fillings.

Abbreviations

Al_2O_3: Aluminium trioxide
Amg: Amalgam
BF: Beautifil
BisGMA: Bisphenol-A-diglycidyl-dimethacrylate
DTNB – 5: 5-Dithiobis (2-nitrobenzoic acid)
GCF: Gingival crevicular fluid
GIC: Glass ionomer cement
H_2O_2: Hydrogen peroxide
LPO: Lipid peroxidation
MDA: Malondialdehyde
NS: Nitrosative stress
$O_2^{\bullet-}$: Superoxide anion
OS: Oxidative nitrosative stress
TBARS: Thiobarbituric acid reactive substances
TEC: Tetric EvoCeram
TEGDMA: Triethylene-glycol-dimethacrylate
TNB: 5-Thio-2-nitrobenzoic acid
GSH: Glutathione
tSOD: Total superoxide dismutase
UEDMA: Urethane-dimethacrylate
ZPhC: Zinc phosphate cement
ZPoC: Zinc polycarboxylate cement.

Data Availability

The data used to support the findings of this study are available from the corresponding author upon request.

Conflicts of Interest

The authors declare that they have no conflicts of interest.

Acknowledgments

This work was supported by grants from the Ministry of Education, Science and Technological Development of the Republic of Serbia (Project no. III 41018). The authors are also grateful to our reviewers for the contributive criticisms and suggestions.

References

[1] D. Uğar-Çankal and N. Ozmeric, "A multifaceted molecule, nitric oxide in oral and periodontal diseases," *Clinica Chimica Acta*, vol. 366, no. 1-2, pp. 90–100, 2006.

[2] R. Khanna, P. Thapa, H. Khanna, S. Khanna, A. Khanna, and H. Shukla, "Lipid peroxidation and antioxidant enzyme status in oral carcinoma patients," *Kathmandu University Medical Journal*, vol. 3, no. 4, pp. 334–339, 2005.

[3] J. Kundalić, University of Niš, Faculty of Medicine, PhD student, Niš, Serbia, D. Pavlović et al., "Oxidative stress in the pathogenesis of periodontal disease," *Acta Medica Medianae*, vol. 55, pp. 66–72, 2016.

[4] B. Mandić and T. Todorović, "Antioxidant status in oral cancer patients," *Oral Oncology*, vol. 8, pp. 38–42, 2002.

[5] D. Pavlica and T. Todorović, "Saliva–diagnostic fluid," *Stom Glas S*, vol. 48, pp. 137–141, 2001.

[6] M. Takane, N. Sugano, T. Ezawa, T. Uchiyama, and K. Ito, "A marker of oxidative stress in saliva: association with periodontally-involved teeth of a hopeless prognosis," *Journal of Oral Science*, vol. 47, no. 1, pp. 53–57, 2005.

[7] M. Khorsavi Samani, A. Poorsattar Bejeh Mir, M. Kashiri, and D. Gujeq, "Introducing cut-points for salivary nitric oxide to distinguish periodontitis from the normal periodontium," *Minerva Stomatologica*, vol. 61, no. 10, pp. 443–448, 2012.

[8] Z. Khurshid, M. Mali, M. Naseem, S. Najeeb, and M. Zafar, "Human gingival crevicular fluids (GCF) proteomics: an overview," *Dentistry Journal*, vol. 5, no. 1, p. 12, 2017.

[9] F. Tinti and M. Soory, "Mechanisms for redox actions of nicotine and glutathione in cell culture, relevant to periodontitis," *Scientific Reports*, vol. 2, no. 1, 2012.

[10] T. Todorovic, I. Dozic, M. Vicente-Barrero et al., "Salivary enzymes and periodontal disease," *Medicina Oral, Patología Oral y Cirugía Bucal*, vol. 11, pp. E115–E119, 2006.

[11] M. M. Djukic, M. D. Jovanovic, M. Ninkovic et al., "Protective role of glutathione reductase in paraquat induced neurotoxicity," *Chemico-Biological Interactions*, vol. 199, no. 2, pp. 74–86, 2012.

[12] M. Đukić, M. Ninković, and M. Jovanović, "Oxidative stress-clinical diagnostic significance," *Journal of Medical Biochemistry*, vol. 27, no. 4, 2008.

[13] H. Bayir and V. E. Kagan, "Bench-to-bedside review: mitochondrial injury, oxidative stress and apoptosis–there is nothing more practical than a good theory," *Critical Care*, vol. 12, no. 1, p. 206, 2008.

[14] J. A. Lincoln, D. L. Lefkowitz, T. Cain et al., "Exogenous myeloperoxidase enhances bacterial phagocytosis and intracellular killing by macrophages," *Infection and Immunity*, vol. 63, no. 8, pp. 3042–3047, 1995.

[15] B. Testa and S. D. Krämer, "The biochemistry of drug metabolism–an introduction," *Chemistry & Biodiversity*, vol. 4, no. 3, pp. 257–405, 2007.

[16] J. Sumitt, J. Robbins, R. Schwartz, and J. Santos, *Fundamentals of Operative Dentistry*, Quintessence Publishing Co, 2001.

[17] G. J. Mount and W. R. H. BDS, "A new cavity classification," *Australian Dental Journal*, vol. 43, no. 3, pp. 153–159, 1998.

[18] A. Guentsch, M. Kramesberger, A. Sroka, W. Pfister, J. Potempa, and S. Eick, "Comparison of gingival crevicular fluid sampling methods in patients with severe chronic periodontitis," *Journal of Periodontology*, vol. 82, no. 7, pp. 1051–1060, 2011.

[19] M. J. Girotti, N. Khan, and B. A. Mclellan, "Early measurement of systemic lipid peroxidation products in the plasma of major blunt trauma patients," *Journal of Trauma and Acute Care Surgery*, vol. 31, no. 1, pp. 32–35, 1991.

[20] M. Sun and S. Zigman, "An improved spectrophotometric assay for superoxide dismutase based on epinephrine autoxidation," *Analytical Biochemistry*, vol. 90, no. 1, pp. 81–89, 1978.

[21] M. Anderson, "The DTNB-GSSG reductase recycling assay for total glutathione (GSH+ 1/2GSSG)," *CRC Handbook of Methods for Oxygen Radical Research*, pp. 319–323, 1986.

[22] O. Lowry, N. Rosebrough, A. Farr, and R. Randall, "Protein measurement with the Folin phenol reagent," *The Journal of Biological Chemistry*, vol. 193, no. 1, pp. 265–275, 1951.

[23] A. P. Bejeh-Mir, H. Parsian, M. A. Khoram, N. Ghasemi, A. Bijani, and M. Khosravi-Samani, "Diagnostic role of salivary and GCF nitrite, nitrate and nitric oxide to distinguish healthy periodontium from gingivitis and periodontitis," *International Journal of Molecular and Cellular Medicine*, vol. 3, no. 3, pp. 138–145, 2014.

[24] A. B. Petković, S. M. Matić, N. V. Stamatović et al., "Proinflammatory cytokines (IL-1β and TNF-α) and chemokines (IL-8 and MIP-1α) as markers of peri-implant tissue condition," *International Journal of Oral and Maxillofacial Surgery*, vol. 39, no. 5, pp. 478–485, 2010.

[25] V. Stefanovic, E. Taso, A. Petkovic-Curcin et al., "Influence of dental filling material type on the concentration of interleukin 9 in the samples of gingival crevicular fluid," *Vojnosanitetski Pregled*, vol. 73, no. 8, pp. 728–734, 2016.

[26] M. S. Davis, S. W. Joseph, and J. F. Bucher, "Periapical and intracanal healing following incomplete root canal fillings in dogs," *Oral Surgery, Oral Medicine, Oral Pathology*, vol. 31, no. 5, pp. 662–675, 1971.

[27] C. F. Williams, N. Yarlett, M. A. Aon, and D. Lloyd, "Antioxidant defences of Spironucleus vortens: glutathione is the major non-protein thiol," *Molecular and Biochemical Parasitology*, vol. 196, no. 1, pp. 45–52, 2014.

[28] C. A. Butler, P. D. Veith, M. F. Nieto, S. G. Dashper, and E. C. Reynolds, "Lysine acetylation is a common post-translational modification of key metabolic pathway enzymes of the anaerobe Porphyromonas gingivalis," *Journal of Proteomics*, vol. 128, pp. 352–364, 2015.

[29] Y. Huang, M. Zhu, Z. Li et al., "Mass spectrometry-based metabolomic profiling identifies alterations in salivary redox status and fatty acid metabolism in response to inflammation and oxidative stress in periodontal disease," *Free Radical Biology and Medicine*, vol. 70, pp. 223–232, 2014.

[30] K. Das and A. Roychoudhury, "Reactive oxygen species (ROS) and response of antioxidants as ROS-scavengers during environmental stress in plants," *Frontiers in Environmental Science*, vol. 2, 2014.

[31] A. Sigel and H. Sigel, "Metal ions in biological systems," in *Interrelations between Free Radicals and Metal Ions in Life Processes*, vol. 36, CRC Press, 1999.

[32] J. P. Gaut, J. Byun, H. D. Tran et al., "Myeloperoxidase produces nitrating oxidants in vivo," *The Journal of Clinical Investigation*, vol. 109, no. 10, pp. 1311–1319, 2002.

[33] R. I. Handin, S. E. Lux, and T. P. Stossel, *Blood: Principles and Practice of Hematology*, Lippincott Williams & Wilkins, 2003.

[34] D. T. Love, T. J. Barrett, M. Y. White, S. J. Cordwell, M. J. Davies, and C. L. Hawkins, "Cellular targets of the myeloperoxidase-derived oxidant hypothiocyanous acid (HOSCN) and its role in the inhibition of glycolysis in macrophages," *Free Radical Biology and Medicine*, vol. 94, pp. 88–98, 2016.

[35] R. P. Wilkie-Grantham, N. J. Magon, D. T. Harwood et al., "Myeloperoxidase-dependent lipid peroxidation promotes the oxidative modification of cytosolic proteins in phagocytic neutrophils," *Journal of Biological Chemistry*, vol. 290, no. 15, pp. 9896–9905, 2015.

[36] M. C. M. Vissers and C. C. Winterbourn, "Oxidative damage to fibronectin: I. The effects of the neutrophil myeloperoxidase system and HOCl," *Archives of Biochemistry and Biophysics*, vol. 285, no. 1, pp. 53–59, 1991.

[37] A. McNaught and A. Wilkinson, *Compendium of Chemical Terminology*, Blackwell Science, Oxford, 1997.

[38] P. M. Yamaguti, A. Simões, E. Ganzerla, D. N. Souza, F. N. Nogueira, and J. Nicolau, "Effects of single exposure of sodium fluoride on lipid peroxidation and antioxidant enzymes in salivary glands of rats," *Oxidative Medicine and Cellular Longevity*, vol. 2013, Article ID 674593, 7 pages, 2013.

[39] V. Lampropoulou, A. Sergushichev, M. Bambouskova et al., "Itaconate links inhibition of succinate dehydrogenase with macrophage metabolic remodeling and regulation of inflammation," *Cell Metabolism*, vol. 24, no. 1, pp. 158–166, 2016.

[40] E. Pinto, T. C. S. Sigaud-kutner, M. A. S. Leitao, O. K. Okamoto, D. Morse, and P. Colepicolo, "Heavy metal-induced oxidative stress in algae1," *Journal of Phycology*, vol. 39, no. 6, pp. 1008–1018, 2003.

[41] S. Bouillaguet, "Biologicalrisks ofresin-basedmaterials to thedentin-pulpcomplex," *Critical Reviews in Oral Biology & Medicine*, vol. 15, no. 1, pp. 47–60, 2004.

[42] P. Gul, N. Akgul, H. H. Alp, and A. Kiziltunc, "Effects of composite restorations on oxidative stress in saliva: an in vivo study," *Journal of Dental Sciences*, vol. 10, no. 4, pp. 394–400, 2015.

[43] J. Volk, J. Engelmann, G. Leyhausen, and W. Geurtsen, "Effects of three resin monomers on the cellular glutathione

concentration of cultured human gingival fibroblasts," *Dental Materials*, vol. 22, no. 6, pp. 499–505, 2006.

[44] M. Goldberg, "In vitro and in vivo studies on the toxicity of dental resin components: a review," *Clinical Oral Investigations*, vol. 12, no. 1, pp. 1–8, 2008.

[45] M. Noda, J. Wataha, J. Lewis et al., "Dental adhesive compounds alter glutathione levels but not glutathione redox balance in human THP-1 monocytic cells," *Journal of Biomedical Materials Research Part B: Applied Biomaterials*, vol. 73, no. 2, pp. 308–314, 2005.

Hindawi
Oxidative Medicine and Cellular Longevity
Volume 2018, Article ID 4967318, 8 pages
https://doi.org/10.1155/2018/4967318

Research Article

Sodium Ferulate Attenuates Lidocaine-Induced Corneal Endothelial Impairment

Guojian Jiang and Tingjun Fan

Laboratory for Corneal Tissue Engineering, College of Marine Life Sciences, Ocean University of China, Yushan Road No. 5, Qingdao 266003, China

Correspondence should be addressed to Tingjun Fan; tjfan@ouc.edu.cn

Received 9 April 2018; Accepted 3 June 2018; Published 8 July 2018

Academic Editor: Luciano Saso

The introduction of intracameral anaesthesia by injection of lidocaine has become popular in cataract surgery for its inherent potency, rapid onset, tissue penetration, and efficiency. However, intracameral lidocaine causes corneal thickening, opacification, and corneal endothelial cell loss. Herein, we investigated the effects of lidocaine combined with sodium ferulate, an antioxidant with antiapoptotic and anti-inflammatory properties, on lidocaine-induced damage of corneal endothelia with *in vitro* experiment of morphological changes and cell viability of cultured human corneal endothelial cells and *in vivo* investigation of corneal endothelial cell density and central corneal thickness of cat eyes. Our finding indicates that sodium ferulate from 25 to 200 mg/L significantly reduced 2 g/L lidocaine-induced toxicity to human corneal endothelial cells, and 50 mg/L sodium ferulate recovered the damaged human corneal endothelial cells to normal growth status. Furthermore, 100 mg/L sodium ferulate significantly inhibited lidocaine-induced corneal endothelial cell loss and corneal thickening in cat eyes. In conclusion, sodium ferulate protects human corneal endothelial cells from lidocaine-induced cytotoxicity and attenuates corneal endothelial cell loss and central corneal thickening of cat eyes after intracameral injection with lidocaine. It is likely that the antioxidant effect of sodium ferulate reduces the cytotoxic and inflammatory corneal reaction during intracameral anaesthesia.

1. Introduction

In cataract surgery, traditional retrobulbar and peribulbar anaesthesia is associated with dangerous complications such as globe perforation, retrobulbar hemorrhage, optic nerve trauma, brainstem anaesthesia, and extraocular muscle injury [1, 2]. Topical anaesthesia has limitations, such as inadequate motor and sensory anaesthesia, insufficient analgesia, and increased intraoperative pain [3–5]. Intracameral anaesthesia acts directly on the iris and ciliary body, providing a significant decrease in pain and discomfort during intraocular procedures of cataract surgery [4]. Therefore, intracameral and topical anaesthesia when used in combination avoids the risks associated with retrobulbar and peribulbar blocks and provides another option for analgesia in ocular surgery [3–7].

Lidocaine (LD) has become a commonly used anaesthetic agent because of its inherent potency, rapid onset, tissue penetration, and efficiency [4]. However, intracameral LD causes adverse events such as corneal thickening, opacification, and significant corneal endothelial cell loss [8, 9]. In addition, increasing evidence shows that LD exerts cytotoxicity to corneal endothelial cells in a time- and dosage-dependent manner [9–13]. For example, higher concentrations cause necrosis by disruption of membranes, and lower concentrations induce apoptosis mainly by excessive reactive oxygen species (ROS) production via the mitochondrial pathway [10–17]. Methods to reduce the cytotoxicity, especially to relieve oxidative stress of LD, are important to protect the corneal endothelium and guarantee clinically safe administration during cataract surgery.

Sodium ferulate (SF), a sodium salt of ferulic acid (3-methoxy-4-hydroxy-cinnamate sodium), acts as a potent antioxidant by scavenging ROS and enhancing the cell stress response through the upregulation of cytoprotective systems, such as heme oxygenase-1, superoxide dismutase, catalase,

Table 1: HCE cells were treated with LD in combination with SF and recovered by SF ($n = 3$).

Groups	Control	I	II	III	IV	V	VI	VII	RSF I–V
LD con. (g/L)	0			2				0	
SF con. (mg/L)	0	0	25	50	100	200	200	50	50
Time of observation (h)	0, 4, 8, 12, 16, 20, 24								48
Medium	10% FBS-DEME/F12								

Note: the HCE cells in groups I–V were treated with 2 g/L LD in combination with different concentrations of SF for 24 hours, respectively, and subsequently were recovered by 50 mg/L SF correspondently for 24 hours. RSF I–V: the HCE cells in groups I–V were recovered by SF 50 mg/L.

and Hsp70 [18]. Furthermore, SF inhibits the expression and/or activity of enzymes, including inducible nitric oxide synthase, caspases, and cyclooxygenase-2, as well as the activation of JNK [18–23].

In the present study, both *in vitro* and *in vivo* experiments were designed to investigate the cytoprotective effects of SF on LD-induced corneal endothelial dysfunction and to determine if the clinical intracameral SF administration protects the corneal endothelia during anaesthesia.

2. Materials and Methods

2.1. Reagents. LD, dimethyl sulfoxide (DMSO), and 3-[4,5-dimethylthiazol-2-yl]-2,5-dipheny-l tetrazolium bromide (MTT) were purchased from Sigma-Aldrich (St. Louis, MO, USA). SF was the product of Qufu Hongly Chemical Industry Co. Ltd. (Shandong, China). Fetal bovine serum (FBS) was from Hyclone (Logan, Utah, USA). Dulbecco's modified Eagle media : Ham's nutrient mixture F-12 (1 : 1) medium (DMEM/F12) was obtained from Invitrogen (Carlsbad, CA, USA).

2.2. Cell Culture. Human corneal endothelial (HCE) cells at 120 passages established in our laboratory were maintained and cultured in DMEM/F12 media containing 10% FBS (10% FBS-DMEM/F12) at 37°C and 5% CO_2 [24].

2.3. Morphological Observation of HCE Cells. HCE cells were seeded onto a 24-well culture plate at a density of 5×10^4 cells per well and cultured in 10% FBS-DMEM/F12 at 37°C and 5% CO_2. To evaluate the effects of SF on LD-induced cytotoxicity, the HCE cells at a logarithmic phase were divided into seven groups and treated with LD and SF dissolved in 10% FBS-DMEM/F12 medium during which cell morphology was monitored for 24 h (Table 1). Subsequently, the growth medium was replaced with 10% FBS-DMEM/F12 containing 50 mg/L SF, and the HCE cells were observed 48 h later to determine if damaged cells can be recovered (Table 1). HCE cells at a logarithmic phase were also divided into three groups and treated with different combinations of LD and SF in 10% FBS-DMEM/F12 medium for 4 h (Table 2). Then, the growth medium was removed entirely, and 10% FBS-DMEM/F12 was supplemented (Table 2). The HCE cells were observed after 24 h to determine if 10% FBS-DMEM/F12 medium without SF allows the recovery of the damaged cells. Cell morphology and growth were monitored under an Eclipse TS100 inverted light microscope (Nikon, Tokyo, Japan).

Table 2: HCE cells were treated with LD in combination with SF and recovered by medium ($n = 3$).

Groups	Control	VIII	IX	X	RSF VIII–X
LD con. (g/L)	0		2		0
SF con. (mg/L)	0	0	50	100	0
Time of observation (h)		0, 4			24
Medium	10% FBS-DEME/F12				

Note: the HCE cells in groups VIII–X were treated with 2 g/L LD in combination with different concentrations of SF for 4 hours, respectively, and subsequently were recovered by 10% FBS-DEME/F12 correspondently for 24 hours. RSF VIII–X: the HCE cells in groups VIII–X were cultured in 10% FBS-DEME/F12 without SF.

2.4. Determination of Cell Viability by the MTT Assay. HCE cell viability was measured after treatment with LD and SF by using the MTT assay. Cells were seeded onto a 96-well cell plate at a density of 1×10^4 cells per well and cultured 48 h prior to treatments as described above. The growth medium was then removed, and 100 μL fresh medium containing 1.1 mM MTT was added prior to incubation for 4 h at 37°C in the dark. The medium was discarded, and 100 μL DMSO was added. Cell viability was determined by measuring the optical density values of samples using a microplate reader (Multiskan GO; Thermo Scientific, Waltham, MA, USA) at an absorption wavelength of 590 nm.

2.5. In Vivo Experimental Procedure. All of the animals in the present study were 5-year-old male domestic cats (*Felis catus*) weighing 3.6 ± 0.5 kg. Fifteen cats were acclimatized to the laboratory environment for 7 days; then, the health of their corneal endothelia was determined by ophthalmic examination including corneal endothelial cell density (CECD), mean cell area, coefficient of variation in cell size, percentage hexagonality, and central corneal thickness (CCT). Nine cats with healthy corneal endothelia were chosen and divided randomly into 3 groups. The anterior chamber of the eye was entered using a 30-gauge needle from the supero-temporal limbal area, and 150 μL of aqueous humor was aspirated and replaced with 150 μL of sterile solutions containing LD in combination with SF at the concentrations shown in Table 3. The drugs were prepared in fortified balanced salt solution (BSS) and BSS without drugs as control. CECD and CCT for each group were assayed at days 0, 5, 9, and 12 after injection of drugs. Before ophthalmic examination and intracameral injection, the cats were anaesthetized using Zoletil (Virbac France, 10 mg/kg, consisting of

Table 3: Cat eyes were intracamerally injected with LD and SF ($n = 3$).

Groups	XI		XII		XIII	
Eye	Right	Left	Right	Left	Right	Left
LD con. (%)	2	0	2	2	2	0
SF con. (mg/L)	0	0	0	100	0	100

Note: this table shows the concentrations of LD and SF. For example, in group XII, the left eye was intracamerally injected with 150 μL of sterile solution containing 2% LD and 100 mg/L SF. 2% LD is the clinical concentration of intracameral anaesthesia.

tiletamine and zolazepam) intramuscularly. Ophthalmic examination was carried out with noncontact specular microscopy (SP-3000P: Topcon Corporation, Tokyo, Japan). The individual differences in CECD and CCT amongst the cats were determined as percentage of CECD and percentage of CCT. The percentage of CECD was calculated as "CECD(%) = (CECD of experimental group/CECD of the same eye before exposure to drugs) × 100," and the percentage of CCT was calculated as "CCT(%) = (CCT of experimental group/CCT of the same eye before exposure to drugs) × 100." All procedures described in this study were conducted according to the guidelines in the Association for Research in Vision and Ophthalmology (ARVO) Statement for the Use of Animals in Ophthalmic and Vision Research and were approved by the institutional Ethics Committee of Animal Care and Experimentation (approval number SD-SYKY-2014-021).

2.6. Statistical Analysis. The results were presented as mean ± standard deviation (SD) from three independent experiments and analyzed by one-way analysis of variance (ANOVA) followed by post hoc test of Student's *t*-test with Bonferroni's correction. *P* values less than 0.05 were considered statistically significant ($^{*}P < 0.05$, $^{**}P < 0.01$).

3. Results

3.1. Drug-Induced Morphological Changes of HCE Cells. The use of LD at 2 g/L was determined previously [10]. Morphological changes evaluated were cell shrinkage, cell rounding, cytoplasmic vacuolization, and detachment from the culture matrix, which are all similar to changes that occur in apoptotic cells [10, 25–28]. The HCE cells in group I (Table 1) began shrinking at 4 h whereas group II, group III, group IV, and group V cells exhibited no obvious morphological changes (Figure 1(a)). At 16 h, HCE cells in group I exhibited clearer apoptotic characteristics than those in groups II–V. In addition, the cell density in group III and group IV was higher than that in groups I, II, and V (Figure 1(a)). At 24 h, most of the HCE cells in groups II–V became rounding and showed cytoplasmic vacuolization, whereas cells in group I which were at low density began to detach and float in the medium (Figure 1(a)). Twenty-four hours after the medium was replaced with 10% FBS-DMEM/F12 containing 50 mg/L SF, cells in groups II–V recovered to normal morphology and formed confluent monolayers. However, almost all of the cells in group I were floating in the medium (Figure 1(a)). 10% FBS-DMEM/F12 without SF did not prevent LD-induced apoptosis (Figure 1(b)). The cells in group VI, group VII, and control remained in a confluent monolayer, and their appearance was normal throughout the experiment indicating that SF concentrations of 200 mg/L and less were not toxic to HCE cells (not shown).

3.2. HCE Cell Viability. The viability of HCE cells in groups I to V treated with LD and SF was examined by MTT. From 0 to 4 h, variations in the viability of cells in groups I–V were not significant (Figure 2) ($P > 0.05$). However, the cell viability in groups I, II, IV, and V decreased significantly at 8 h postexposure ($P < 0.05$) but not in group III (Figure 2). From 16 to 24 h, the viability of cells in groups II, III, IV, and V was significantly higher than that in group I (Figure 2) ($P < 0.01$). At 24 h, the viability of cells in group I was significantly less than the viability of cells in groups II, III, IV, and V (Figure 2) ($P < 0.01$). At 48 h, which was 24 h after growth medium was replaced with 10% FBS-DMEM/F12 containing 50 mg/L SF, the viability of cells in groups II–V increased significantly ($P < 0.01$), but the cell viability in group I decreased significantly ($P < 0.01$) (Figure 2). During the experiment, the cell viability values in group VI, group VII, and control did not change significantly (not shown).

3.3. Variations of CECD and CCT of the Cat Cornea after Intracameral Injection. After intracameral injection of 2% LD, the percentages of CECD of the cat cornea decreased significantly from 100 ± 0.4% at day 0 to 94.2 ± 0.2% at day 12 ($P < 0.01$) (Figure 3(a)). In group XI, 2% LD treatment decreased the percentages of CECD significantly from day 0 to day 9 after which the percentages of CECD were stable from day 9 to day 12 (Figure 3(a)). The percentages of CECD of the left eye in group XII after intracameral injection of 2% LD combined with 100 mg/L SF and in group XIII after intracameral injection of 100 mg/L SF remained stable from day 0 to day 12 ($P > 0.05$), which were significantly higher than those of the right eye intracamerally injected with 2% LD at day 9 and day 12, respectively ($P < 0.01$) (Figures 3(b) and 3(c)).

After intracameral injection of 2% LD, the percentages of CCT in the right eye of group XI increased at day 5, decreased significantly at day 9 ($P < 0.01$), and then remained stable from day 9 to day 12 ($P > 0.05$) (Figure 4(a)). The percentages of CCT of the left eye in group XII after intracameral coinjection of 2% LD combined with 100 mg/L SF and in group XIII after intracameral injection of 100 mg/L SF remained stable from day 0 to day 12 ($P > 0.05$); these values were significantly lower than those of the right eye intracamerally injected with 2% LD at day 5 ($P < 0.01$) (Figures 4(b) and 4(c)).

4. Discussion

LD triggers apoptosis in several cellular models by impairment of respiratory chain functions resulting in reduced ATP production, depolarization of the mitochondria, loss of mitochondrial membrane potential ($\Delta\Psi$), and overproduction of intracellular ROS [10, 17, 29–34]. The increased

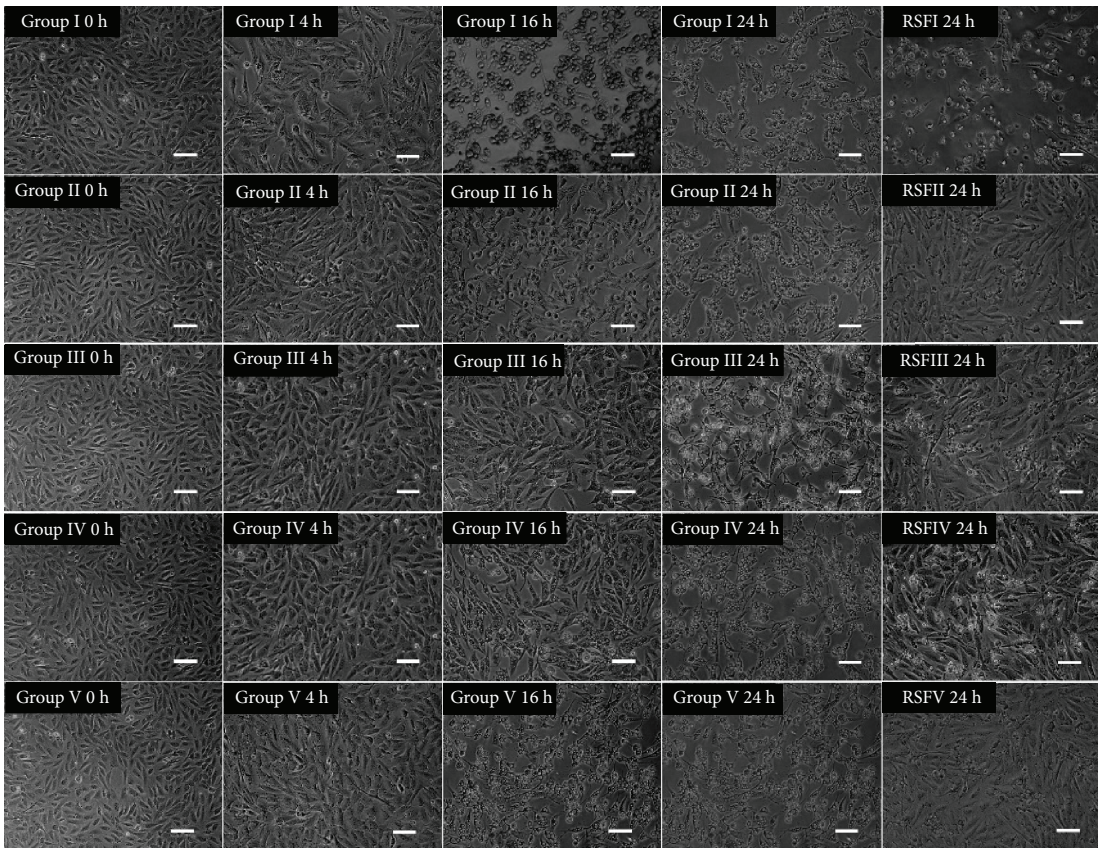

(a)

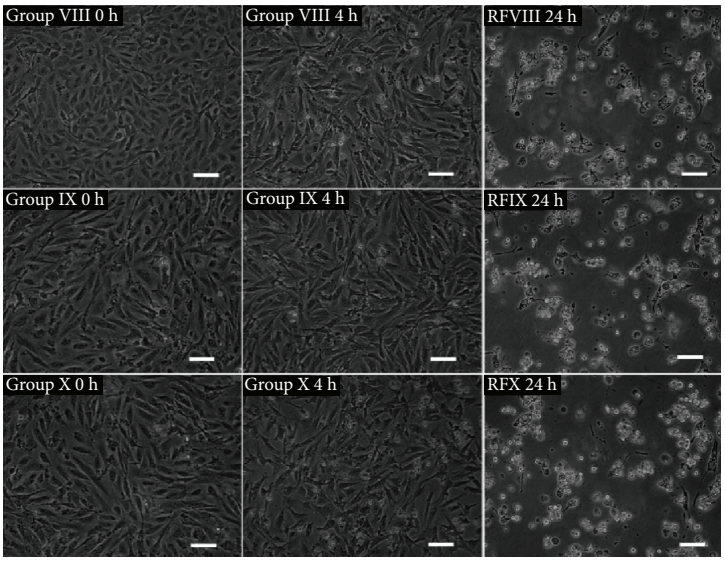

(b)

Figure 1: (a) Morphological changes in HCE cells after treatment with LD and SF for 24 h followed by incubation with 50 mg/L SF. The treatments and observation times are shown at the top left of each photograph. One representative photograph from three independent experiments is shown. Groups I–V: HCE cells were treated with 2 g/L LD in combination with 0, 25, 50, 100, and 200 mg/L SF, respectively. RSFI–RSFV: incubation of groups I–V for 24 h followed by treatment with 50 mg/L SF. Typical morphological features of HCE cells are shrinkage, rounding, cytoplasmic vacuolization, and detachment from substratum. Scale bar: 50 μm. (b) Morphological changes in HCE cells after LD and SF treatment for 4 h followed by incubation in 10% FBS-DMEM/F12. The treatment and observation times are shown in the top left of each photograph. One representative photograph from three independent experiments is shown. Groups VIII–X: HCE cells were treated, respectively, with 2 g/L LD in combination with 0, 50, and 100 mg/L SF in 10% FBS-DMEM/F12. RSFVIII–RSFX: treatment of GVIII–GX for 4 h followed by treatment with 10% FBS-DMEM/F12. Scale bar: 50 μm.

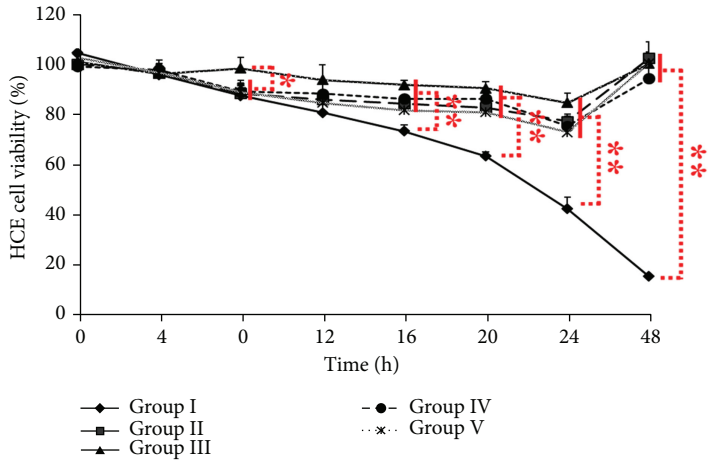

Figure 2: Viability of HCE cells cultured *in vitro* after treatment with LD and/or SF. ✦: group I: HCE cells were treated with 2 g/L LD alone for 24 h followed by treatment with 50 mg/L SF in 10% FBS-DMEM/F12 from 24 to 48 h; ■: group II: HCE cells were treated with 2 g/L LD in combination with 25 mg/L SF followed by treatment with 50 mg/L SF in 10% FBS-DMEM/F12 for 24 h followed by treatment with 50 mg/L SF in 10% FBS-DMEM/F12 from 24 to 48 h; ▲: group IIII: HCE cells were treated with 2 g/L LD in combination with 50 mg/L SF for 24 h followed by treatment with 50 mg/L SF in 10% FBS-DMEM/F12 from 24 to 48 h; ●: group IV: HCE cells were treated with 2 g/L LD in combination with 100 mg/L SF for 24 h followed by treatment with 50 mg/L SF in 10% FBS-DMEM/F12 from 24 to 48 h; ✳: group V: HCE cells were treated with 2 g/L LD in combination with 200 mg/L SF for 24 h followed by treatment with 50 mg/L SF in 10% FBS-DMEM/F12 from 24 to 48 h. $^{**}P < 0.01$, $^{*}P < 0.05$.

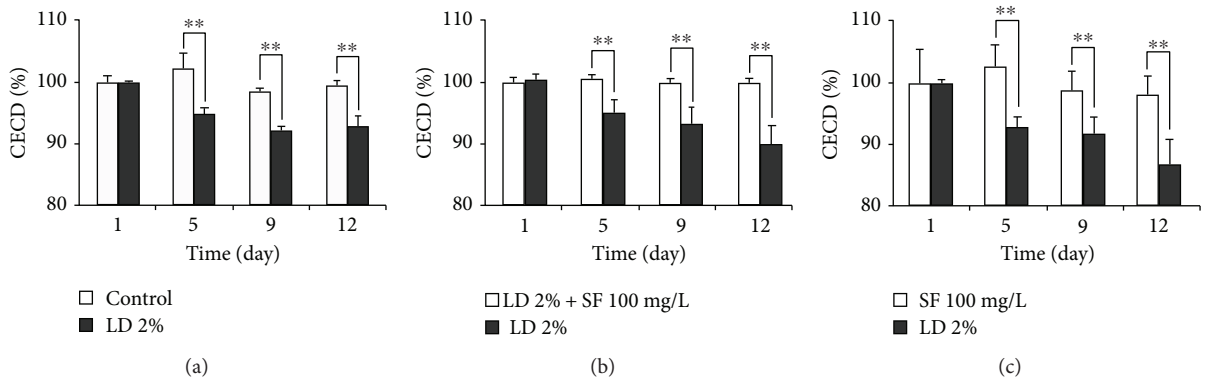

Figure 3: Variation in CECD of cat eyes after intracameral injection with LD and/or SF. (a) Comparison of CECD in group XI between the left eye intracamerally injected with BSS and the right eye intracamerally injected with 2% LD. (b) Comparison of CECD in group XII between the left eye intracamerally injected with 2% LD and 100 mg/mL SF and the right eye intracamerally injected with 2% LD. (c) Comparison of CECD in group XIII between the left eye intracamerally injected with 100 mg/L SF and the right eye intracamerally injected with 2% LD. $^{**}P < 0.01$.

production of ROS correlates with decreased cell viability after exposure to LD, and ROS plays a vital role in inducing apoptosis of corneal cells and corneal endothelial dysfunction [34–37]. Our previous studies indicated that LD exposure to HCE cells activates caspase-3, caspase-8, and caspase-9, suggesting that the LD-induced caspase-8/9/3 pathway is influenced by the production of ROS which involves the activation of caspase-8 [10, 38, 39].

Previously, the cell morphological changes and MTT were employed to determine the apoptosis of *in vitro* cultured HCE cells, and Halilovic et al. reported the relations of the morphology of the HCE cell with its apoptotic degree [10, 25–28]. Our present study showed that 2 g/L LD initiated damage in HCE cells at 4 h postexposure which is similar to the results of previous studies [10]. Therefore, in the present study, the antioxidant SF was tested for its ability to protect corneal endothelial cells from oxidative damage caused by LD. SF has a high antioxidant potential as it donates electrons to quench free radicals and induces upregulation of many phase-2 detoxifying and antioxidant enzymes which are mediated by the NF-E2-related factor (Nrf2) signaling pathway [18, 22, 40, 41]. Furthermore, SF binds to cytochrome c to prevent assembly of the apoptosome and downregulates caspase-8 and caspase-3 [22, 42]. The present study indicates that SF delays LD-induced shrinkage of HCE cells and limits LD-induced downregulation of HCE cell viability. Upon incubation with SF after LD exposure, cells recovered and formed confluent monolayers but this did not occur with

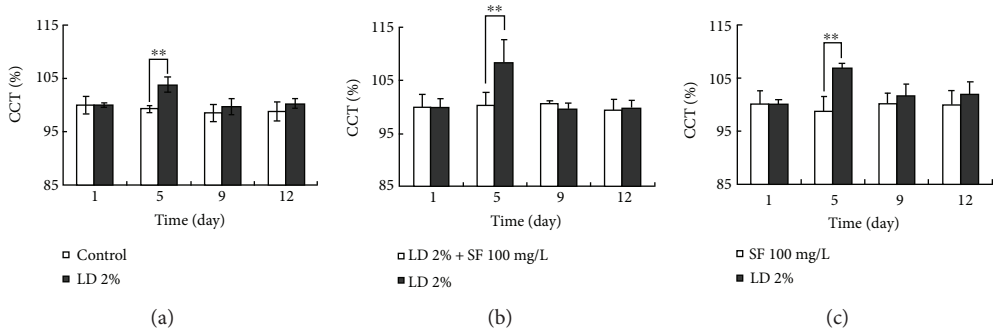

Figure 4: Central corneal thicknesses (CCT) of the cat eye after intracameral injection with LD and/or SF. (a) Comparison of CCT in group XI between the left eye intracamerally injected with BSS and the right eye intracamerally injected with 2% LD. (b) Comparison of CCT in group XII between the left eye intracamerally injected with 2% LD and 100 mg/mL SF and the right eye intracamerally injected with 2% LD. (c) Comparison of CCT in group XIII between the left eye intracamerally injected with 100 mg/L SF and the right eye intracamerally injected with 2% LD. $^{**}P < 0.01$.

cells exposed to LD alone. Moreover, incubation in growth medium without SF did not allow recovery of HCE cells exposed to either LD or LD and SF (Figure 1(b)). The results suggest that SF reduces the LD-induced damage in HCE cells thereby allowing time for cell recovery, growth, and monolayer formation. SF at 100 mg/L significantly reduced the cytotoxic effects of LD at 2 g/L on HCE cells *in vitro*. These *in vitro* data lead to the assumption that LD has similar effects *in vivo*. LD induces excessive ROS generation in the hippocampus and amygdala of adult rats and apoptosis in rabbit corneal endothelial cells after intracameral injections [9, 12, 33]. The *in vivo* studies in cat eyes described herein demonstrated that the endothelial cell densities of the cat cornea decreased significantly after intracameral injection of 2% LD. On the basis of these findings, 100 mg/L SF in combination with 2% LD was selected as a clinically relevant dosage for intracameral injection of cat eyes. The endothelial cell densities of the cat cornea after intracameral injection of LD and SF were significantly higher than those treated with LD alone, and SF had no adverse effect on cat corneal endothelial cells. Therefore, SF is likely to reduce LD-induced cytotoxicity in corneal endothelial cells because it offsets ROS generation. Additionally, SF probably employs its ROS-scavenging systems to inhibit the activation of caspase-8-, caspase-3-, and cytochrome c-induced apoptosis by binding and enhancing the stability of cytochrome to prevent assembly of the apoptosome.

CCT evaluation is becoming increasingly important in ophthalmic practice, providing information on eyes affected by corneal ectasia [43]. There were no significant differences in corneal thickness in dogs and New Zealand white rabbits after intracameral injection of preservative-free LD at 2% [44, 45]. Moreover, a preservative-free 0.5% solution of LD has no adverse effect on the corneal thickness of human eyes [46]. However, there is increasing evidence for a relationship between intracameral injection of LD and corneal thickening. For example, anterior chamber injection of unpreserved LD causes thickening of the cornea and opacification of eyes in pigmented rabbits [47, 48].

LD-induced CCT thickening is dose-dependent and differs with species. LD-induced CCT thickening is caused by oxidative stress arising from corneal edema inflammation by excessive generation of ROS. Schellini et al. demonstrated that intracameral injection of 2% LD caused rabbit corneal edema, and Kim et al. showed that LD causes a transient endothelial cell edema in the *in vitro* perfused endothelia of human and rabbit corneas [11, 49]. In the present study, LD significantly increased CCT of the cat eye after intracameral injection and then it gradually returned to normal. SF inhibits LD-induced corneal thickening in cat eyes, which may be due to the antioxidant activity of SF. Multiple studies have shown that SF relieves inflammation caused by oxidative stress through inhibiting the activity of NF-κB, the expressions of cyclooxygenase-2 and iNOS, and the contents of prostaglandin E2 and NO [22, 50]. In further study, we will firstly investigate the role of SF in the inhibition of the production of ROS, activation of caspases, and activation of NF-κB in LD-impaired HCE cells to explore the mechanism of SF rescuing the oxidative-damaged HCE by antiapoptosis and anti-inflammation.

5. Conclusion

This study demonstrated that SF prevents LD-induced cytotoxicity in *in vitro* cultured HCE cells and attenuates the loss of corneal endothelial cell and CCT thickening of the cat eye after intracameral injection with LD. Antioxidant therapy using SF may be effective in reducing the cytotoxic and inflammatory corneal reaction during topical and intracameral anaesthesia with LD.

Data Availability

The datasets used and/or analyzed during the current study are available from the corresponding author on reasonable request.

Conflicts of Interest

The authors have declared that no conflicts of interest exist.

Authors' Contributions

Jiang Guojian planned and executed the experiment, performed the data analysis and interpretation, and wrote the manuscript. Fan Tingjun planned the experiment, performed the data analysis and interpretation, and provided financial support. All authors have given their final approval of the version of the manuscript to be published.

Acknowledgments

This work was supported by the grants from the National Key Research and Development Program of China (2017YFE0103500). The authors deeply appreciate receiving advice from Professor Thomas H. MacRae (Department of Biology, Dalhousie University, Halifax, NS, Canada) who assisted in editing the paper.

References

[1] D. B. Davis II and M. R. Mandel, "Efficacy and complication rate of 16,224 consecutive peribulbar blocks. A prospective multicenter study," *Journal of Cataract & Refractive Surgery*, vol. 20, no. 3, pp. 327–337, 1994.

[2] D. H. W. Wong, "Regional anaesthesia for intraocular surgery," *Canadian Journal of Anesthesia*, vol. 40, no. 7, pp. 635–657, 1993.

[3] C. J. Anderson, "Combined topical and subconjunctival anesthesia in cataract surgery," *Ophthalmic Surgery*, vol. 26, no. 3, pp. 205–208, 1995.

[4] N. J. Anderson, W. D. Woods, T. Kim, D. E. Rudnick, and H. F. Edelhauser, "Intracameral anesthesia: in vitro iris and corneal uptake and washout of 1% lidocaine hydrochloride," *Archives of Ophthalmology*, vol. 117, no. 2, pp. 225–232, 1999.

[5] S. K. Pandey, L. Werner, D. J. Apple, A. Agarwal, A. Agarwal, and S. Agarwal, "No-anesthesia clear corneal phacoemulsification versus topical and topical plus intracameral anesthesia. Randomized clinical trial," *Journal of Cataract & Refractive Surgery*, vol. 27, no. 10, pp. 1643–1650, 2001.

[6] J. J. Dutton, S. A. Hasan, H. F. Edelhauser, T. Kim, C. L. Springs, and G. Broocker, "Anesthesia for intraocular surgery," *Survey of Ophthalmology*, vol. 46, no. 2, pp. 172–178, 2001.

[7] C. L. Karp, T. A. Cox, M. D. Wagoner, R. G. Ariyasu, and D. S. Jacobs, "Intracameral anesthesia. A report by the American Academy of Ophthalmology," *Ophthalmology*, vol. 108, no. 9, pp. 1704–1710, 2001.

[8] C. Liang, G. A. Peyman, and G. Sun, "Toxicity of intraocular lidocaine and bupivacaine," *American Journal of Ophthalmology*, vol. 125, no. 2, pp. 191–196, 1998.

[9] M. Borazan, A. Karalezli, S. Oto et al., "Induction of apoptosis of rabbit corneal endothelial cells by preservative-free lidocaine hydrochloride 2%, ropivacaine1%, or levobupivacaine 0.75%," *Journal of Cataract & Refractive Surgery*, vol. 35, no. 4, pp. 753–758, 2009.

[10] H. Z. Yu, Y. H. Li, R. X. Wang et al., "Cytotoxicity of lidocaine to human corneal endothelial cells in vitro," *Basic & Clinical Pharmacology & Toxicology*, vol. 114, no. 4, pp. 352–359, 2014.

[11] S. A. Schellini, M. C. Creppe, E. A. Gregório, and C. R. Padovani, "Lidocaine effects on corneal endothelial cell ultrastructure," *Veterinary Ophthalmology*, vol. 10, no. 4, pp. 239–244, 2007.

[12] Y. S. Chang, S. Y. Tseng, S. H. Tseng, and C. L. Wu, "Cytotoxicity of lidocaine or bupivacaine on corneal endothelial cells in a rabbit model," *Cornea*, vol. 25, no. 5, pp. 590–596, 2006.

[13] Y. Kamiya, K. Ohta, and Y. Kaneko, "Lidocaine-induced apoptosis and necrosis in U937 cells depending on its dosage," *Biomedical Research*, vol. 26, no. 6, pp. 231–239, 2005.

[14] N. Kitagawa, M. Oda, and T. Totoki, "Possible mechanism of irreversible nerve injury caused by local anesthetics and membrane disruption," *Anesthesiology*, vol. 100, no. 4, pp. 962–967, 2004.

[15] C. Cejka and J. Cejkova, "Oxidative stress to the cornea, changes in corneal optical properties, and advances in treatment of corneal oxidative injuries," *Oxidative Medicine and Cellular Longevity*, vol. 2015, Article ID 591530, 10 pages, 2015.

[16] M. N. Demir, Z. A. Demir, O. Yalcin Tok et al., "Oxidative stress of intracameral lidocaine and levobupivacaine on ocular tissues," *British Journal of Ophthalmology*, vol. 94, no. 8, pp. 1083–1087, 2010.

[17] R. Werdehausen, S. Braun, F. Essmann et al., "Lidocaine induces apoptosis via the mitochondrial pathway independently of death receptor signaling," *Anesthesiology*, vol. 107, no. 1, pp. 136–143, 2007.

[18] C. Mancuso and R. Santangelo, "Ferulic acid: pharmacological and toxicological aspects," *Food and Chemical Toxicology*, vol. 65, pp. 185–195, 2014.

[19] L. Tian, X. Q. Dang, C. S. Wang, P. Yang, C. Zhang, and K. Z. Wang, "Effects of sodium ferulate on preventing steroid-induced femoral head osteonecrosis in rabbits," *Journal of Zhejiang University SCIENCE B*, vol. 14, no. 5, pp. 426–437, 2013.

[20] Y. Jin, Y. Fan, E.-Z. Yan, Z. Liu, Z.-H. Zong, and Z.-M. Qi, "Effects of sodium ferulate on amyloid-beta-induced MKK3/MKK6-p38 MAPK-Hsp27 signal pathway and apoptosis in rat hippocampus," *Acta Pharmacologica Sinica*, vol. 27, no. 10, pp. 1309–1316, 2006.

[21] X. Pei, W. Wang, N. Miao et al., "The protective effects of the combination of sodium ferulate and oxymatrine on ethanol-induced liver damage in mice," *Environmental Toxicology and Pharmacology*, vol. 37, no. 1, pp. 423–430, 2014.

[22] J. Qin, L. Shang, A. S. Ping et al., "TNF/TNFR signal transduction pathway-mediated anti-apoptosis and anti-inflammatory effects of sodium ferulate on IL-1β-induced rat osteoarthritis chondrocytes in vitro," *Arthritis Research & Therapy*, vol. 14, no. 6, article R242, 2012.

[23] H. Y. Kim and S. M. Lee, "Ferulic acid attenuates ischemia/reperfusion-induced hepatocyte apoptosis via inhibition of JNK activation," *European Journal of Pharmaceutical Sciences*, vol. 45, no. 5, pp. 708–715, 2012.

[24] T. Fan, J. Zhao, X. Ma, X. Xu, W. Zhao, and B. Xu, "Establishment of a continuous untransfected human corneal endothelial cell line and its biocompatibility to denuded amniotic membrane," *Molecular Vision*, vol. 17, pp. 469–480, 2011.

[25] Y. H. Li, Q. Wen, T. J. Fan et al., "Dose dependent cytotoxicity of pranoprofen in cultured human corneal endothelial cells by inducing apoptosis," *Drug and Chemical Toxicology*, vol. 38, no. 1, pp. 16–21, 2015.

[26] Q. Wen, T. Fan, S. Bai, and Y. Sui, "Cytotoxicity of proparacaine to human corneal endothelial cells in vitro," *The Journal of Toxicological Sciences*, vol. 40, no. 4, pp. 427–436, 2015.

[27] S. B. Han, Y. J. Shin, J. Y. Hyon, and W. R. Wee, "Cytotoxicity of voriconazole on cultured human corneal endothelial cells," *Antimicrobial Agents and Chemotherapy*, vol. 55, no. 10, pp. 4519–4523, 2011.

[28] A. Halilovic, T. Schmedt, A. S. Benischke et al., "Menadione-induced DNA damage leads to mitochondrial dysfunction and fragmentation during rosette formation in Fuchs endothelial corneal dystrophy," *Antioxidants & Redox Signaling*, vol. 24, no. 18, pp. 1072–1083, 2016.

[29] J. Finsterer and S. Zarrouk-Mahjoub, "Mitochondrial toxicity of cardiac drugs and its relevance to mitochondrial disorders," *Expert Opinion on Drug Metabolism & Toxicology*, vol. 11, no. 1, pp. 15–24, 2015.

[30] S. Onizuka, T. Yonaha, R. Tamura, M. Kasiwada, T. Shirasaka, and I. Tsuneyoshi, "Lidocaine depolarizes the mitochondrial membrane potential by intracellular alkalization in rat dorsal root ganglion neurons," *Journal of Anesthesia*, vol. 25, no. 2, pp. 229–239, 2011.

[31] Y. Nishimura, A. Kanada, J. Yamaguchi et al., "Cytometric analysis of lidocaine-induced cytotoxicity: a model experiment using rat thymocytes," *Toxicology*, vol. 218, no. 1, pp. 48–57, 2006.

[32] B. Chazotte, G. Vanderkooi, and D. Chignell, "Further studies on F1-ATPase inhibition by local anesthetics," *Biochimica et Biophysica Acta - Bioenergetics*, vol. 680, no. 3, pp. 310–316, 1982.

[33] P. Dabadie, P. Bendriss, P. Erny, and J. P. Mazat, "Uncoupling effects of local anesthetics on rat liver mitochondria," *FEBS Letters*, vol. 226, no. 1, pp. 77–82, 1987.

[34] C. Fedder, B. Beck-Schimmer, J. Aguirre et al., "In vitro exposure of human fibroblasts to local anaesthetics impairs cell growth," *Clinical and Experimental Immunology*, vol. 162, no. 2, pp. 280–288, 2010.

[35] Y. L. Hsu, H. S. Yu, H. C. Lin, K. Y. Wu, R. C. Yang, and P. L. Kuo, "Heat shock induces apoptosis through reactive oxygen species involving mitochondrial and death receptor pathways in corneal cells," *Experimental Eye Research*, vol. 93, no. 4, pp. 405–412, 2011.

[36] C. Liu, D. Ogando, and J. A. Bonanno, "SOD2 contributes to anti-oxidative capacity in rabbit corneal endothelial cells," *Molecular Vision*, vol. 17, pp. 2473–2481, 2011.

[37] N. A. Vallabh, V. Romano, and C. E. Willoughby, "Mitochondrial dysfunction and oxidative stress in corneal disease," *Mitochondrion*, vol. 36, pp. 103–113, 2017.

[38] B. M. Kim and H. W. Chung, "Hypoxia/reoxygenation induces apoptosis through a ROS-mediated caspase-8/Bid/Bax pathway in human lymphocytes," *Biochemical and Biophysical Research Communications*, vol. 363, no. 3, pp. 745–750, 2007.

[39] J.-A. Pan, Y. Fan, R. K. Gandhirajan, M. Madesh, and W. X. Zong, "Hyperactivation of the mammalian degenerin MDEG promotes caspase-8 activation and apoptosis," *Journal of Cell Biology*, vol. 288, no. 5, pp. 2952–2963, 2013.

[40] B. C. Scott, J. Butler, B. Halliwell, and O. I. Aruoma, "Evaluation of the antioxidant actions of ferulic acid and catechins," *Free Radical Research Communications*, vol. 19, no. 4, pp. 241–253, 1993.

[41] Y. J. Surh, J. Kundu, and H. K. Na, "Nrf2 as a master redox switch in turning on the cellular signaling involved in the induction of cytoprotective genes by some chemopreventive phytochemicals," *Planta Medica*, vol. 74, no. 13, pp. 1526–1539, 2008.

[42] F. Yang, B. R. Zhou, P. Zhang, Y. F. Zhao, J. Chen, and Y. Liang, "Binding of ferulic acid to cytochrome c enhances stability of the protein at physiological pH and inhibits cytochrome c-induced apoptosis," *Chemico-Biological Interactions*, vol. 170, no. 3, pp. 231–243, 2007.

[43] N. Sorkin and D. Varssano, "Corneal collagen crosslinking: a systematic review," *Ophthalmologica*, vol. 232, no. 1, pp. 10–27, 2014.

[44] P. A. Gerding Jr, T. L. Turner, R. E. Hamor, and D. J. Schaeffer, "Effects of intracameral injection of preservative-free lidocaine on the anterior segment of the eyes in dogs," *American Journal of Veterinary Research*, vol. 65, no. 10, pp. 1325–1330, 2004.

[45] S. W. Liou, C. J. Chiu, and I. J. Wang, "Effect of intracameral injection of lidocaine and carbachol on the rabbit corneal endothelium," *Journal of Cataract & Refractive Surgery*, vol. 30, no. 6, pp. 1351–1355, 2004.

[46] L. P. Tutchenko, M. A. Znamens'ka, M. V. Dzhulaĭ, and I. M. Dzhulaĭ, "Investigation of the influence of intracameral injection of domestic lidocaine on the corneal thickness during phacoemulsification of cataract," *Likars'ka Sprava*, vol. 8, pp. 92–96, 2012.

[47] A. J. Judge, K. Najafi, D. A. Lee, and K. M. Miller, "Corneal endothelial toxicity of topical anesthesia," *Ophthalmology*, vol. 104, no. 9, pp. 1373–1379, 1997.

[48] M. Guzey, A. Satici, Z. Dogan, and S. Karadede, "The effects of bupivacaine and lidocaine on the corneal endothelium when applied into the anterior chamber at the concentrations supplied commercially," *Ophthalmologica*, vol. 216, no. 2, pp. 113–117, 2002.

[49] T. Kim, G. P. Holley, J. H. Lee, G. Broocker, and H. F. Edelhauser, "The effects of intraocular lidocaine on the corneal endothelium," *Ophthalmology*, vol. 105, no. 1, pp. 125–130, 1998.

[50] M. Srinivasan, A. R. Sudheer, and V. P. Menon, "Ferulic acid: therapeutic potential through its antioxidant property," *Journal of Clinical Biochemistry and Nutrition*, vol. 40, no. 2, pp. 92–100, 2007.